Eugenio Cavallo ·
Fernando Auat Cheein ·
Francesco Marinello · Kamil Saçılık ·
Kasiviswanathan Muthukumarappan ·
Purushothaman C. Abhilash   *Editors*

15th International Congress on Agricultural Mechanization and Energy in Agriculture

ANKAgEng'2023

Springer

Lecture Notes in Civil Engineering   **458**

Lecture Notes in Civil Engineering (LNCE) publishes the latest developments in Civil Engineering—quickly, informally and in top quality. Though original research reported in proceedings and post-proceedings represents the core of LNCE, edited volumes of exceptionally high quality and interest may also be considered for publication. Volumes published in LNCE embrace all aspects and subfields of, as well as new challenges in, Civil Engineering. Topics in the series include:

- Construction and Structural Mechanics
- Building Materials
- Concrete, Steel and Timber Structures
- Geotechnical Engineering
- Earthquake Engineering
- Coastal Engineering
- Ocean and Offshore Engineering; Ships and Floating Structures
- Hydraulics, Hydrology and Water Resources Engineering
- Environmental Engineering and Sustainability
- Structural Health and Monitoring
- Surveying and Geographical Information Systems
- Indoor Environments
- Transportation and Traffic
- Risk Analysis
- Safety and Security

To submit a proposal or request further information, please contact the appropriate Springer Editor:

– Pierpaolo Riva at pierpaolo.riva@springer.com (Europe and Americas);
– Swati Meherishi at swati.meherishi@springer.com (Asia—except China, Australia, and New Zealand);
– Wayne Hu at wayne.hu@springer.com (China).

All books in the series now indexed by Scopus and EI Compendex database!

Eugenio Cavallo · Fernando Auat Cheein ·
Francesco Marinello · Kamil Saçılık ·
Kasiviswanathan Muthukumarappan ·
Purushothaman C. Abhilash
Editors

15th International Congress on Agricultural Mechanization and Energy in Agriculture

ANKAgEng'2023

Springer

Editors
Eugenio Cavallo
National Research Council of Italy
Torino, Italy

Fernando Auat Cheein
Department of Electronic Engineering
Universidad Técnica Federico Santa María
Valparaíso, Chile

Francesco Marinello
Dipartimento TESAF (University of Padova,
TESAF Department)
Università di Padova
Legnaro, Italy

Kamil Saçılık
Department of Agricultural Machinery
and Technologies Engineering
Ankara University
Altındağ/Ankara, Türkiye

Kasiviswanathan Muthukumarappan
Department of Agricultural and Biosystems
Engineering
South Dakota State University
Brookings, SD, USA

Purushothaman C. Abhilash
Institute of Environment and Sustainable
Development
Banaras Hindu University
Varanasi, Uttar Pradesh, India

Preface

It is a great pleasure and honor for us to have your participation in the 15th International Congress on Agricultural Mechanization and Energy in Agriculture—AnkAgEng'2023 organized between October 29 and November 1, 2023, in Antalya, Türkiye, by Ankara University Faculty of Agriculture Department of Agricultural Machinery and Technologies Engineering. We are also honored to hold the 15th of our congress, the first of which was organized by Ankara University in 1980. Since the First International Congress on Agricultural Mechanization and Energy in Agriculture, we have continued our congress on a regular basis every three years. AnkAgEng'2023 congress was of great importance for us and the Turkish nation as 2023 is the "100th Anniversary of the Republic of Türkiye" and was held like a feast for the scientific world.

AnkAgEng'2023 offered a magnificent international platform for academics, researchers, engineers, industry participants, and students from all over the world to share their research results in the field of agricultural technology engineering. The main subjects of the congress are: Machinery and Energy Systems, Agriculture Information Technologies, Digital-Smart Agriculture, Ergonomics, Health & Safety, System Engineering, Postharvest Technologies & Process Engineering, Sustainable Agriculture, Natural Resources & Environmental Systems, Plant, Animal & Facility Systems, Agricultural Engineering Education, and Biosystems Engineering. The congress featured keynote speakers, oral and poster presentations, special sessions, and real-time discussions.

A total of 200 researchers from 30 different countries applied to participate in the congress by submitting abstracts. Participants were from the USA, Canada, Italy, England, Ireland, Spain, Portugal, Denmark, Belgium, Greece, China, Japan, Nigeria, Czechia, Pakistan, India, Iran, Russia, Sweden, Brazil, Bulgaria, Oman, Algeria, Poland, Finland, Malaysia, Romania, Sudan, Tanzania, and Türkiye. At the AnkAgEng'23 congress, 5 invited speakers and 8 online keynote speakers made oral presentations. In addition, 57 oral and 12 poster presentations were presented by researchers.

We would especially like to thank our invited/keynote speakers, session chairs, members of the Scientific Committee, authors, and colleagues for making their valuable contributions. We are thankful to Ankara University, Springer Nature, our main sponsor Türk Traktör, gold sponsor Ziraat Bankası, European Society for Agricultural Engineers, American Society of Agricultural and Biological Engineers, and International Commission of Agricultural and Biosystems Engineering for their kind support that enabled us to hold this congress.

Sincerely yours

On behalf of the Congress Organizing Committee

Ahmet Çolak

Organization

Reviewer List

Abdullah Sessiz
Bahattin Akdemir
Cengiz Karaca
Cevdet Sağlam
Claus Grøn Sørensen
Enrique Moltó Garcia
Eugenio Cavallo
Fernando Auat Cheein
George Papadakis
Hakan Kürşat Çelik
Hasan Ali İrik
Hasan H. Silleli
Havva Eylem Polat
İhsan Serkan Varol
İsmail Kavdır
Kâmil Saçılık
Kazım Çarman
Mahmut Kaplan
Metin Güner
M. Barış Eminoğlu
M. Metin Özgüven
Mustafa Özdemir
Necati Çetin
Onur Taşkın
Ömer Ertuğrul
Reza Ehsani
Sedat Karaman
Selçuk Arslan
Sema Kaplan
Serap Görücü
Thiago Romanelli
T. Göktürk Seyhan
Ufuk Türker
Yunus Emre Şekerli
Zeki Gökalp
Zeynep Ünal

Contents

Post-Harvest Technologies and Process Engineering

Natural Resources and Enviromental Systems in Agriculture

Plant, Animal and Facility Systems in Agriculture

Information Technologies, Sensors and Control Systems in Agriculture

Farm Management, Ergonomics, System Engineering, Health and Safety in Agriculture

Machinery Systems in Agriculture

Definition of Reference Models for Functional Parameters and Price for Mowers and Mowerconditioners

Daniele Pinna[1]([✉]), Cristina Pornaro[2], Giannantonio Armentano[3], Stefano Macolino[2], and Francesco Marinello[1]

[1] Department of Land, Environment, Agriculture, and Forestry, University of Padova, Via dell'Università 16, 35020 Legnaro, Italy
daniele.pinna@phd.unipd.it
[2] Department of Agronomy, Food, Natural Resources, Animals and Environment, University of Padova, Via dell'Università 16, 35020 Legnaro, Italy
[3] Edizioni L'Informatore Agrario srl, Via Bencivenga-Biondani 16, 37133 Verona, Italy
g.armentano@informatoreagrario.it

Abstract. At present, the management of different operations in agricultural production is rapidly evolving as an effect of increasing attention to the issues of sustainable development and intensification. The key components of sustainable agriculture are increased agricultural machinery productivity and efficiency. Different factors must be considered when defining the farm fleet (tractors and implements), as well as when planning and managing the machinery. Among them, the cost is important, but also their size, weight, working area, required power etc.

The objective of the current work is to determine the most important factors that affect the costs and effectiveness of mowing implements. To identify dependencies and extract reference models, the various parameters are analyzed in a correlation matrix. The study's methodology is based on linear regression analysis performed on approximately 250 mowers and 240 mowerconditioners, for a total amount of roughly 490 machines, among which both drum and disc apparatus were considered.

We were able to analyze the key significant parameters, calculate their impact, and develop forecasting models for price, power, mass, working width and number of mowing elements.

Relevant correlations were found between price and all the functional parameters.

According to these correlations, models have been proposed, which can be implemented to support the decision-making phases of the market stakeholders.

Keywords: Mowers · Mowers-conditioners · Price · Weight · Working-width · Required Power

1 Introduction

The challenges that farmers face managing natural resources while guaranteeing food production and achieving sustainable agriculture goals are becoming more and more complicated. Some of the most important management choices regarding farmers are

those related to purchasing agricultural machinery units. Even though the importance of the right machinery sizing is well-known, farmers often do not choose correctly according to their needs, thus leading to various adverse impacts [1].

In fact, farmers tend to overestimate farm machinery parameters, aiming to achieve greater efficiency and increase their productivity. But exceeding the dimensional and functional parameters of farm machinery can have harmful impacts on productive and economic performances. Among the negative effects that overestimated parameters such as mass and power can have on the farm [2, 3], some are affecting the environment as increased soil compaction and CO_2 emissions, while others affect the economy of the farm, raising the costs and requiring bigger investments [4].

To improve the decision-making process related to appropriate and proportionate choices of agricultural machinery units, there is an urgent need to develop regulatory mechanisms and measures [5, 6]. Nowadays, many farmers rely on new tools to organize their fleets, such as prediction models and optimized farm management software, improving their decision-making process and planning methodology [7, 8]. To simplify the decision-making process and optimize agricultural machinery' size selection, forecasting models are economically viable and environmentally sustainable solutions [9]. According to this concept, a large study has been carried out (5000 models of machinery included) on the development and implementation of reference models for main agricultural machinery groups [10–13]. Reference models predicting main functional parameters and price were developed for sowing, spraying, harvesting, and tillage operations. This study focuses on mowing implements, including mowing conditioners.

Unlike other farming implements, mowers are not of exclusive interest to farmers, as they are commonly used for riverbanks, roadsides, railways, public parks, and urban areas. Therefore, public, and private institutions managing green areas and infrastructure may also benefit from developing this reference model [14]. Even though the abovementioned use of mowers for non-agricultural activities exists, mower machines are essential devices for forage harvesting as the first step of the haymaking process.

Currently, mowers are divided into disc mowers, drum mowers, and reciprocating mowers, all of which can be furnished with a conditioning apparat. Even though reciprocating mowers are still present on the market, their number is very limited, thus in this study, we decided to focus only on disc and drum mowers, with and without conditioning apparat.

Disc mowers are mostly driven by a set of v-belts, a gearbox, and a gearcase driving a set of discs, they cut by rotating discs with attached knives, Fig. 1 shows an example of this kind of mowing apparat. Drum mowers are mostly driven by a set of v-belts, and meshing gears driving a set of drums, they are cut by knives attached to a set of drums.

The key elements that influence a mower's cutting performance are its structure and operating conditions. Even though the relationship between the functional parameters and machinery's costs has never been discussed, it is important to understand the relations between the different parameters and the final cost, to help the farmers avoid unnecessary investments.

The final aim of this study is to investigate how functional parameters such as minimum required power (CV), weight (Kg), working width (m), and number of mowing elements (n) relate among themselves and with the price of mowing machines among the

main categories on the market: disc, drum, and disc/drum mowers both with and without conditioning apparat. Together with the other studies carried out in this larger project [10–13], the path for the development of an innovative decision support system (DSS) able to consider complex relationships among functional factors and price of agricultural machinery has been laid.

2 Materials and Methods

The study is based on a statistical analysis of functional parameters and the price of implements for mowing and mowing-conditioning. To carry out the study, we created a large database based on machinery specifications and performance-related technical characteristics of mowing and mowing-conditioning implements available in the European market. Models from 12 top agricultural machinery manufacturers (BCS, Deutz-Fahr, Kverneland, CLAAS, Lely, etc.) served as the foundation for the data. In partnership with Informatore Agrario srl (Verona, Italy), data were gathered from agricultural machinery associations, open-source databases, and any available agricultural machinery producers. The database populated by 462 models includes mowers (247 machines) and mowerconditioners (215 machines), including discs and drums mowers. The analysis was centered around the mowing implements' minimum required power, weight, working width, number of mowing elements, and price.

Table 1 summarizes the ranges of maximum and minimum values of the functional parameters and price considered in the study. Both within the mowers and the mowerconditioners datasets, disc machines were the largest group, as shown in Fig. 2.

To model the relationship between variables and assess the applicability of the model parameters, linear regression analyses have been utilized to analyze the datasets of this research. The decision to use linear regression is justified by the desire for more straightforward models between the price and the predictors.

Fig. 1. Discs mowing apparat.

Even though other statistical techniques have better-predicting capabilities, linear models' ease of use is a critical component for practical decision-making applications, mainly if the goal is to gather rough preliminary estimations.

Statistical analyses were performed using Python (v. 3.11.3) packages Pandas, NumPy, matplotlib, seaborn, and scikit learn.
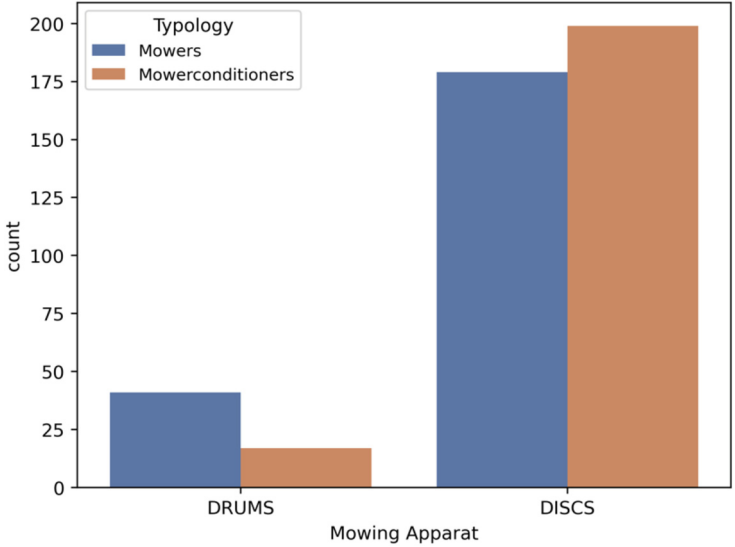
Fig. 2. Count plot of mowers and mowerconditioners by mowing apparat.

Table 1. Ranges of functional parameters and price among mowers and mowerconditioners grouped by mowing apparat.

Variable	Mowers		Mowerconditioners	
	Discs	*Drums*	*Discs*	*Drums*
Minimum Required Power, CV	26-175	25-100	36-228	60-100
Weight, kg	340-2860	190-1290	690-5200	680-1570
N. of mowing elements	4-20	2-4	5-24	4-4
Working width, m	1.60-11.20	1.05-3.26	2.00-10.05	1.85-3.15
Price, VAT excl., k€	4.32-39.7	2.51-20.1	8.95-90.46	9.19-24.4

3   Results

For each category of implements, the relations among the technical parameters and price are outlined below. Results of linear regression analyses are summarized reporting the determination coefficient R^2, the Root Mean Square Error (RMSE) and the equation representing the relation between the analyzed variables.

The corresponding inverted models (e.g., price as a function of working width and working width as a function of price) do not present the exact correlation (R^2 are similar but not identical). The reason for these differences is that for every regression analysis, the dataset has been randomly split into training and test set. The evaluation metrics reported in the tables refer to the performances of the models on the test sets. These differences are more evident in both groups with drums as mowing apparat, due to their significantly lower numerosity. In the paragraphs below, whenever commenting on a correlation between two parameters, the highest determination coefficient R^2 among the inverted models is reported.

Moreover, even if regression were evaluated always on the whole dataset, inverted models would not correspond to the non-inverted equation, due to the non-symmetrical behavior of linear regressions. The full collection of models is reported in the following paragraphs.

3.1 Disc Mowers

The linear analyses conducted on disc mowers (Table 2) showed interesting correlations. A high correlation is present between the price (k€) and weight (Kg) of the machines ($R^2 = 0.86$), price is also highly correlated with the number of working elements ($R^2 = 0.85$), minimum required power ($R^2 = 0.81$) and working width ($R^2 = 0.75$). Generally, the number of working elements shows a good correlation with all the considered functional parameters, since logically raising the of elements has an impact on the weight of the machine, also, increasing the working weight will generally require more working elements. Finally, a machine that has a larger working width and a higher number of working elements will require more power to work. The good correlations of functional parameters both among themselves and with price, give us the possibility of using these models in the building of decision-making tools.

Table 2. Linear Regression metrics of Disc Mowers functional parameters and price.

Disc Mowers			
Price Models (k€)	R^2	RMSE	Equation
Minimum Required Power (CV)	0.815	3.19	$Pr = -2.11 + 0.25 * Pw$
Working Width (m)	0.753	3.68	$Pr = -1.77 + 4.67 * Ww$
Weight (Kg)	0.858	2.79	$Pr = -0.48 + 0.02 * Wt$
Number of working elements (n)	0.846	2.90	$Pr = -5.08 + 2.45 * Ne$
Power Models (CV)			
Price (k€)	0.808	12.3	$Pw = 20.4 + 3.11 * Pr$
Working Width (m)	0.764	13.6	$Pw = 7.54 + 16.8 * Ww$

(*continued*)

Table 2. (*continued*)

Disc Mowers			
Price Models (k€)	R^2	RMSE	Equation
Weight (Kg)	0.816	12.0	Pw = 16.1 + 0.82 * Wt
Number of working elements (n)	0.769	13.5	Pw = 1.26 + 8.07 * Ne
Weight Models (kg)			
Minimum Required Power (CV)	0.844	139	Wt = 8.30 + 12.37 * Pw
Working Width (m)	0.626	136	Wt = 10.6 + 236 * Ww
Price (k€)	0.861	131	Wt = 154 + 46.4 * Pr
Number of working elements (n)	0.717	187	Wt = −70.2 + 112 * Ne
Working Width Models (m)			
Minimum Required Power (CV)	0.769	0.76	Ww = 0.21 + 0.05 * Pw
Weight (kg)	0.825	0.66	Ww = 0.69 + 0.01 * Wt
Price (k€)	0.760	0.77	Ww = 0.98 + 0.17 * Pr
Number of working elements (n)	0.810	0.69	Ww = −0.05 + 0.44 * Ne
N. of Elements Models (n)			
Minimum Required Power (CV)	0.763	1.59	Ne = 1.79 + 0.09 * Pw
Working Width (m)	0.802	1.46	Ne = 1.95 + 1.72 * Ww
Price (k€)	0.847	1.28	Ne = 2.85 + 0.35 * Pr
Weight (Kg)	0.704	1.78	Ne = 2.75 + 0.01 * Wt

3.2 Drum Mowers

The linear analyses conducted on drum mowers highlighted some correlations. A high correlation is present between price and working width ($R^2 = 0.84$), working width is also highly correlated with weight ($R^2 = 0.75$). Differently from what we have previously seen on disc mowers, within drum mowers, the number of elements is not a good predictor, as it shows very low correlations with all the other functional parameters and prices. The reason for this comes from the very low range on the number of working elements within the drum mowers group, in fact, these machines can only have 2 or 4 working elements. Generally, the strength of correlation models for drum mowers is lower than for disc mowers because of the low numerosity of the group. Table 3 shows the metrics of all the linear regressions performed over the group.

3.3 Disc Mowerconditioners

The analyses performed on disc mowerconditioners revealed high correlations among the parameters. The most correlated parameters are the number of mowing elements with working width ($R^2 = 0.87$), but working width is also highly correlated with power ($R^2 = 0.89$) and price ($R^2 = 0.71$).

Table 3. Linear Regression metrics of Drum Mowers functional parameters and price.

Drum Mowers			
Price Models (k€)	R^2	RMSE	Equation
Minimum Required Power (CV)	0.258	3.24	Pr = −0.67 + 0.17 * Pw
Working Width (m)	0.843	1.49	Pr = −5.79 + 6.76 * Ww
Weight (Kg)	0.627	2.29	Pr = −1.32 + 0.02 * Wt
Number of working elements (n)	0.194	3.37	Pr = −2.45 + 2.29 * Ne
Power Models (CV)			
Price (k€)	0.188	13.1	Pw = 28.9 + 3.42 * Pr
Working Width (m)	0.194	15.9	Pw = −1.55 + 27.6 * Ww
Weight (Kg)	0.101	13.8	Pw = 21.2 + 0.06 * Wt
Number of working elements (n)	0.017	14.5	Pw = 14.2 + 14.9 * Ne
Weight Models (kg)			
Minimum Required Power (CV)	0.289	216	Wt = 79.6 + 9.85 * Pw
Working Width (m)	0.751	128	Wt = −212 + 392 * Ww
Price (k€)	0.689	143	Wt = 163 + 53.9 * Pr
Number of working elements (n)	0.211	228	Wt = 230 + 143 * Ne
Working Width Models (m)			
Minimum Required Power (CV)	0.072	0.55	Ww = 0.82 + 0.02 * Pw
Weight (kg)	0.707	0.31	Ww = 0.89 + 0.01 * Wt
Price (k€)	0.785	0.26	Ww = 1.14 + 0.12 * Pr
Number of working elements (n)	0.163	0.52	Ww = 1.15 + 0.36 * Ne
N. of Elements Models (n)			
Minimum Required Power (CV)	0.370	0.75	Ne = 1.11 + 0.03 * Pw
Working Width (m)	0.021	0.65	Ne = 1.06 + 0.94 * Ww
Price (k€)	0.218	0.71	Ne = 2.20 + 0.11 * Pr
Weight (Kg)	0.177	0.69	Ne = 1.86 + 0.02 * Wt

Price shows high correlations with all the functional parameters (R^2 always above 0.7), thus suggesting the possibility that price-predictive models may be very accurate within this group of machines. Results of all the performed linear regressions are reported in Table 4.

Table 4. Linear Regression metrics of Disc Mowerconditioners functional parameters and price.

Disc Mowerconditioners			
Price Models (k€)	R^2	RMSE	Equation
Minimum Required Power (CV)	0.746	8.27	$Pr = -2.55 + 0.33 * Pw$
Working Width (m)	0.711	8.82	$Pr = 2.95 + 6.65 * Ww$
Weight (Kg)	0.848	6.39	$Pr = -3.15 + 0.02 * Wt$
Number of working elements (n)	0.780	7.69	$Pr = -6.60 + 4.14 * Ne$
Power Models (CV)			
Price (k€)	0.742	19.7	$Pw = 28.6 + 2.27 * Pr$
Working Width (m)	0.860	14.5	$Pw = 21.2 + 18.8 * Ww$
Weight (Kg)	0.535	26.5	$Pw = 22.1 + 0.04 * Wt$
Number of working elements (n)	0.772	18.6	$Pw = 1.24 + 10.9 * Ne$
Weight Models (kg)			
Minimum Required Power (CV)	0.564	580	$Wt = 297 + 14.9 * Pw$
Working Width (m)	0.522	608	$Wt = 596 + 284 * Ww$
Price (k€)	0.847	343	$Wt = 401 + 45.2 * Pr$
Number of working elements (n)	0.546	593	$Wt = 257 + 169 * Ne$
Working Width Models (m)			
Minimum Required Power (CV)	0.861	0.69	$Ww = -0.46 + 0.05 * Pw$
Weight (kg)	0.501	1.31	$Ww = 0.50 + 0.01 * Wt$
Price (k€)	0.700	1.01	$Ww = 0.66 + 0.11 * Pr$
Number of working elements (n)	0.873	0.66	$Ww = -1.12 + 0.58 * Ne$
N. of Elements Models (n)			
Minimum Required Power (CV)	0.773	1.41	$Ne = 2.49 + 0.06 * Pw$
Working Width (m)	0.869	1.08	$Ne = 3.06 + 1.41 * Ww$
Price (k€)	0.798	1.34	$Ne = 3.72 + 0.17 * Pr$
Weight (Kg)	0.577	1.94	$Ne = 3.71 + 0.01 * Wt$

3.4   Drum Mowerconditioners

The results of the analyses on the drum mowerconditioners group (Table 5) showed very variable results. While weight was highly correlated with price ($R^2 = 0.911$), all the other correlations were weak. The correlations with the number of elements were not investigated within this group of machines because they all have 4 mowing elements. Generally, the models were strongly influenced by the very small number of machines in the group, only 17, and predictive models may need a larger dataset to gain accuracy and precision.

Table 5. Linear Regression metrics of Drums Mowerconditioners functional parameters and price.

Drum Mowerconditioners			
Price Models (k€)	R^2	RMSE	Equation
Minimum Required Power (CV)	0.347	4.32	Pr = −3.48 + 0.24 * Pw
Working Width (m)	0.483	3.84	Pr = −4.84 + 7.63 * Ww
Weight (Kg)	0.911	1.59	Pr = 2.55 + 0.01 * Wt
Power Models (CV)			
Price (k€)	0.049	11.5	Pw = 40.1 + 2.49 * Pr
Working Width (m)	0.472	8.55	Pw = 16.6 + 23.3 * Ww
Weight (Kg)	0.019	11.7	Pw = 53.4 + 0.02 * Wt
Weight Models (kg)			
Minimum Required Power (CV)	0.032	319	Wt = 96.1 + 11.4 * Pw
Working Width (m)	0.259	278	Wt = −127 + 419 * Ww
Price (k€)	0.909	97.3	Wt = 59.9 + 59.9 * Pr
Working Width Models (m)			
Minimum Required Power (CV)	0.502	0.32	Ww = 0.37 + 0.03 * Pw
Weight (kg)	0.251	0.40	Ww = 1.49 + 0.01 * Wt
Price (k€)	0.273	0.39	Ww = 1.14 + 0.09 * Pr

4 Discussion and Conclusions

The decision-making process related to the acquisition of agricultural machinery is very important to reach the goal of sustainable farm management [6]. As well as other kinds of machinery, grass mowers play an important role for many farms, especially those working with livestock, being an essential tool for forage harvesting. Furthermore, their importance and potential for managing important ecosystems as riverbanks has been assessed [15].

Choosing the right dimension and functional parameters of mowers and mowerconditioners is not always an easy task for farmers and farm managers [13]. To help improve and to make more efficient this decision-making process, we modeled the relationships between the main functional parameters and the price of this machinery.

We divided the database into mowers and mowerconditioners, then we analyzed the machines divided by type of mowing apparat: discs and drums. The results we collected from the linear regression analyses we performed showed for disc mowers and mowerconditioners the correlations between functional parameters and price were good, revealing the potential of these models for practical applications. Both for mowers and mowerconditioners with drums as mowing apparat the strength of the correlation models was lower, showing weaker correlation metrics. For both mowers and mowerconditioners, the small number of machines in the database has influenced the poor results of the

analyses, another reason for the low strength of the models can be related to the relatively small range within the functional parameters.

Thus, it is important for the models to gain strength that the databases are populated with high numbers of machines with significant ranges of values both regarding functional parameters and prices.

In conclusion, with the help of these models, investments may be properly managed based on actual farm demands and the choice of the best machinery management strategy. Knowing and controlling the resources that are available will improve farm and production management.

References

1. Cavallo E, Ferrari E, Bollani L, Coccia M (2014) Attitudes and behaviour of adopters of technological innovations in agricultural tractors: a case study in Italian agricultural system. Agric Syst 130:44–54. https://doi.org/10.1016/J.AGSY.2014.05.012
2. Cillis D, Maestrini B, Pezzuolo A, Marinello F, Sartori L (2018) Modeling soil organic carbon and carbon dioxide emissions in different tillage systems supported by precision agriculture technologies under current climatic conditions. Soil Tillage Res 183:51–59. https://doi.org/10.1016/J.STILL.2018.06.001
3. Chamen T (2015) Controlled traffic farming - from worldwide research to adoption in Europe and its future prospects. Acta Technologica Agriculturae 18(3):64–73. https://doi.org/10.1515/ata-2015-0014
4. Guangnan C (2018) Advances in Agricultural Machinery and Technologies, 1st Editio, Boca Raton. https://doi.org/10.1201/9781351132398
5. Fountas S, Wulfsohn D, Blackmore BS, Jacobsen HL, Pedersen SM (2006) A model of decision-making and information flows for information-intensive agriculture. Agric Syst 87(2):192–210. https://doi.org/10.1016/J.AGSY.2004.12.003
6. European Agricultural Machinery Industry Association (CEMA). Advancing Agricultural Machinery and Solutions for Sustainable Farming. Brussels (2019)
7. Paraforos DS et al (2016) A farm management information system using future internet technologies. IFAC-PapersOnLine 49(16):324–329. https://doi.org/10.1016/J.IFACOL.2016.10.060
8. Bochtis DD, Sørensen CGC, Busato P (2014) Advances in agricultural machinery management: a review. Biosys Eng 126:69–81. https://doi.org/10.1016/J.BIOSYSTEMSENG.2014.07.012
9. Cavallo E, Ferrari E, Bollani L, Coccia M (2014) Strategic management implications for the adoption of technological innovations in agricultural tractor: the role of scale factors and environmental attitude. Technol Anal Strat Manag 26(7):765–779. https://doi.org/10.1080/09537325.2014.890706
10. Yezekyan T, Marinello F, Armentano G, Trestini S, Sartori L (2018) Definition of reference models for power, weight, working width, and price for seeding machines. Agriculture (Switzerland) 8(12):1–13. https://doi.org/10.3390/agriculture8120186

11. Yezekyan T, Marinello F, Armentano G, Sartori L (2018) Analysis of cost and performances of agricultural machinery: reference model for sprayers. Agron Res 16(2):604–614. https://doi.org/10.15159/AR.18.049

12. Yezekyan T, Marinello F, Armentano G, Trestini S, Sartori L (2020) Modelling of harvesting machines' technical parameters and prices. Agriculture (Switzerland) 10(6):1–12. https://doi.org/10.3390/agriculture10060194

13. Yezekyan T, Benetti M, Armentano G, Trestini S, Sartori L, Marinello F (2021) Definition of reference models for power, mass, working width, and price for tillage implements. Agriculture (Switzerland) 11(3):1–15. https://doi.org/10.3390/agriculture11030197

14. Boscaro D, Pezzuolo A, Grigolato S, Cavalli R, Marinello F, Sartori L (2015) Preliminary analysis on mowing and harvesting grass along riverbanks for the supply of anaerobic digestion plants in North-Eastern Italy. J Agric Eng 46(3):100–104. https://doi.org/10.4081/jae.2015.465

15. Boscaro D et al (2018) Evaluation of the energy and greenhouse gases impacts of grass harvested on riverbanks for feeding anaerobic digestion plants. J Clean Prod 172:4099–4109. https://doi.org/10.1016/j.jclepro.2017.02.060

Determination of the Effect of the Technical Parameters Which Affect the Tractor Energy Efficiency

İbrahim Ergül[1(✉)] [ID] and Ufuk Türker[2] [ID]

[1] Erkunt Traktör, OSB Batıhun Caddesi, No: 2, 06935 Sincan, Ankara, Turkey
ibrahim.ergul@erkunttraktor.com.tr
[2] Department of Agricultural Machinery and Technologies,
University of Ankara, Şht. Ömer Halisdemir Blv, 06110 Altındağ, Ankara, Turkey

Abstract. In this study, parameters which affect tractor energy efficiencies, such as wheel drive types, fuel injection systems, and transmission types were studied. There is much more data which are relating to tractor energy efficiency in OECD Code 2 tractor test reports. While the calculation of the total efficiency, specific fuel consumption, hourly fuel consumption and power data were measured on OECD Code 2 power take-off and drawbar tests. Results have been evaluated according to tractor technical specification separately and the effect of those specifications have been determined. As well as tractor energy efficiency depends on the engine, wheel drive system, soil type and characteristics, tyres, working pressures, tractor weight, compatibility between tractor and equipment and driving efficiency; The effect of the first two parameters was found to be between 60–70%. According to the results, the average total efficiency of 293 tractors was 28.2%. Among these tractors, the average total efficiency of 4WD tractors was the lowest at 27.7%, while the average total efficiency of tractors with CVT and CRD systems was the highest at 30.8%. While the effect of the CRD injection system on the total efficiency in tractors was 9.03%, this rate was 1.99% in the CVT transmission specific to tractors. The effect of both the CRD injection system and the CVT transmission on the total efficiency of the tractors was determined as 11.2%.

Keywords: tractor · energy efficiency · hourly fuel consumption · tractor efficiency · tractor testing

1 Introduction

Energy is the most important input of the economy, the thing of orient world politics and the most efficient determiner of social, economic, and geographic order of the world via climate change. The procurement of the sustainability and security of energy, efficient usage, reducing the effects of greenhouse gas, saving the environment, and passing from fossil fuel to new and renewable energy sources should be the most important topics of the world [1]. In many countries, during the past decade, there has been an increased interest in finding ways to save energy in the use of cars, appliances and all types of

machines including agricultural tractors. The tractor, which, is used as a power machine in agricultural works, can transmit power to non-self-propelled agricultural machines in different ways so that they can fulfil their functions. In addition, a significant portion of mechanization investments belong to the tractor. In the case of agricultural tractors and machinery, there is a similar interest in finding ways to save energy and this is the reason why many countries have launched specific programs to achieve this goal [2]. In recent years, the importance of energy efficiency in the agricultural sector has become increasingly apparent. As the world faces challenges such as climate change, resource scarcity, and population growth, the need for sustainable and efficient agricultural practices has intensified. Energy plays a crucial role in agricultural production, from powering machinery and irrigation systems to processing and transportation. Therefore, understanding the scientific advancements and collaborative efforts in the field of energy efficiency in agriculture is essential for devising effective strategies, promoting innovation, and achieving global sustainability goals [3]. There are significant technological advances in engines regarding the incorporation of electronic control units, in which algorithms and programs are stored, allowing self-diagnosis, the control of air and fuel feeding systems based on pollutant emissions under different operating conditions, and data transfer. Therefore, such advances improved combustion, performance, and thermodynamic efficiency, and reduced pollutant emissions [4]. Many tractor models are now available with both standard geared transmissions (GTs) and continuously variable transmissions (CVTs). Unlike traditional geared transmissions that operate using a series of fixed gear ratios, CVTs have the ability to operate over an infinite number of gear ratios within a certain range [5]. In addition to transportation, the main function of tractors is to drive agricultural machinery needed for agricultural production, which needs the transmission of tractors to provide constantly changing speed and torque to adapt to frequent external load changes. In this context, the use of a continuously variable transmission (CVT) for tractors has become a trend. The most common type of CVTs is hydraulic static transmission (HST) which mainly includes hydraulic pumps, hydraulic motors, and control mechanisms. In order to overcome the above shortcomings, the HST is connected in parallel with the mechanical components to form a hydromechanical continuously variable transmission (HMCVT). HMCVT transmits only part of the power through the HST; the remaining power is transmitted through the mechanical components, so the efficiency is much higher than HST. HMCVT can realize step-less speed regulation through the HST while relying on mechanical components to achieve high-efficiency transmission. In addition, the HMCVT can control the engine to operate on an optimal power curve or optimal economic curve, thus achieving optimum power performance or optimum fuel economy for tractors [6]. Modern common rail fuel systems use electronically controlled fuel injectors and high-pressure pumps to deliver precise volumes of fuel into the engine at precisely specified times to ensure the engine runs smoothly and efficiently. In more modern engines, the injectors may be electronically activated, allowing higher pressures to be reached, and to more accurately meter the amount of fuel injected. These advances have led to more efficient, more powerful, and also quieter engines [7]. The ever-stricter emission limits force the manufacturers of combustion engines to constantly develop more modern equipment in order for the engine to fulfil these criteria. One of the options, aside from catalytic systems and particle filters, is the use of high-pressure

injection equipment. As a result, higher pressures are reached, and a higher amount of heat is released in the cylinder. These two parameters are the basic prerequisite for higher engine efficiency – higher power output of the engine at lower fuel consumption and decreased production of harmful emissions [8]. OECD code 2 test reports give the farmer the only reachable, reliable, and comparable data by means of tractor performance in the worldwide [9].

2   Methods

The study is derived from the database used in the doctoral thesis and consists of three parts. First of all, the evaluation method was defined. Then, the operating periods of the tractor's Power Take-Off (PTO) work, and drawbar works were calculated as percentages respectively based on the literatures. Finally, tractor test results selected from OECD Code 2 [10] test reports were analyzed, and the results were evaluated.

2.1   Material

The distribution of the selected tractors according to technical specifications is given in Table 1. 293 tractors which were tested as per OECD Code 2 test reports between 2011–2014 were selected as material. OECD Code 2 test reports were published by the Directorate of Testing Centre of Agricultural Equipment and Machine (TAMTEST) which is the only official OECD Testing Stations in Türkiye. Technical specifications of the tractors were classified as 2WD, 4WD, type of the injection system and type of the transmission system. Nominal power tractors were between 9.5 kW and 168.6 kW. The emission levels of tractors were stage IIIA, stage IIIB and stage IV which had fitted some aftertreatment systems such as exhaust gas recirculation system (EGR), diesel oxidation system (DOC), and selective catalytic reduction system (SCR). 166 tractors were imported from 13 different countries, and they were produced by 24 different manufacturers. 127 domestic production tractors were produced by 10 different manufacturers in Türkiye. All the 2WD tractors were driven by geared transmission and had mechanical injection systems.

Table. 1. Distribution of the tractors according to the technical specifications

Production	2WD	4WD			Total
	Mechanic*	Mechanic	CRD*	CRD and CVT*	
Domestic	42	83	2	–	127
Import	6	117	34	9	166
Total	48	200	36	9	293

*Mechanic: Mechanical injection and geared transmission, CRD: common rail injection, CVT: Continuously variable transmission

2.2 Method

Total efficiencies of tractors were calculated as such dividing of the produced maximum power to the consumed thermal energy. Total efficiency was calculated as given formula [11].

$$\eta_t = \frac{P_t}{P_f} \qquad P_f = \frac{BxH_u}{860}$$

η_t: Total efficiency of tractor (%), measured and calculated
P_t: Maximum tractor power (kW), measured and calculated
P_f: Thermal power of fuel (kW), calculated
B: Hourly fuel consumption of tractor (kg/h), measured
H_u: Lower calorific fuel value, accepted as 10 200 kcal/kg

The OECD Organization for Economic Cooperation and Development Standard Codes for the Official Testing of Agricultural and Forestry Tractors allow participating countries to perform tractor tests according to harmonized procedures, and to obtain OECD official approvals which facilitate international trade [12]. Tractor power (P_t) and hourly fuel consumption (B) values were measured as per OECD Code 2 and taken from the OECD Code 2 test reports. In order to calculate the total tractor efficiency (η_t), related data which were maximum tractor powers (P_t) and hourly fuel consumptions (B) in the PTO and drawbar tests data were taken from the OECD code 2 test reports of tractors.

To determine the working percentage of agricultural works in pto works and drawbar works, two works of literature were considered which were studied by [13, 14]. Average values of their results were calculated and $K_\text{ç}$ for towing works accepted as 69%. K_pto for pto works accepted as 31%.

P_pto and $P_\text{ç}$ were obtained from the test reports, While $P_\text{ç}$ was the maximum drawbar power, and P_pto was the maximum PTO power, P_t was calculated as given formula.

$$P_t = (P_\text{ç}.K_\text{ç}) + (P_\text{pto}.K_\text{pto}) \qquad B = (B_\text{ç}.K_\text{ç}) + (B_\text{pto}.K_\text{pto})$$

$P_\text{ç}$: Maximum drawbar power (kW),
P_pto: Maximum pto power (kW),
$K_\text{ç}$: Percentage of drawbar&draught working hours, 0.69
K_pto: Percentage of pto working hours, 0.31
$B_\text{ç}$: Hourly fuel consumption at maximum drawbar power (kg/h),
B_pto: Hourly fuel consumption at maximum drawbar power (kg/h),

The measurements, and observations in Table 2 were considered and accepted during the calculation of the total efficiency of the tractor.

Table. 2. Data taken by OECD Code 2 test reports.

Data	Unit	Measurement/Observation
B_{pto}, Hourly fuel consumption	kg/h	Measured maximum pto power test (taken from OECD code 2 test report)
P_{pto}, Maximum pto power	kW	Measured maximum pto power test (taken from OECD code 2 test report)
$B_ç$, Hourly fuel consumption	kg/h	Measured maximum drawbar power test (taken from OECD code 2 test report)
$P_ç$, Maximum drawbar power	kW	Measured maximum drawbar power test (taken from OECD code 2 test report)
2WD/4WD	–	Observation (taken from OECD code 2 test report)
Injection system (CRD or mechanical)	–	Observation (taken from OECD code 2 test report)
Transmission system (CVT or geared)	–	Observation (taken from OECD code 2 test report)

3   Results

Total tractor efficiency (η_t) values according to the technical specifications of 293 tractors were calculated and given in Table 3. According to the results, while the average total efficiency of 293 tractors was 28.2%, the average total efficiency of 4WD tractors was the lowest at 27.7%, while the average total efficiency of tractors with CVT and CRD systems was the highest at 30.8%.

Table. 3. Average η_t values as per technical specifications of tractors

Technical specification of tractors	Average η_t values (%)
Whole tractors	28.2
2WD	28.5
4WD	27.7
4WD, CRD	30.2
4WD, CRD and CVT	30.8

There was not any tractor with CRD injection system and CVT transmission system in 2WD tractors, hence the effects of CRD injection system and CVT transmission system were studied for only 4WD tractors and including those systems. In Fig. 1, it is seen that the effect of the CRD injection system on the total efficiency of the tractors is 9.03%, while this effect is 1.99% for the tractors with only CVT gearboxes. It has been determined that both the CRD injection system and the CVT have an effect of

11.99% on the total efficiency of the tractors. According to the researchers [5] results indicated that the CVT-equipped tractor operated in automatic mode was more fuel efficient than the standard geared transmission tractor operated at full engine speed (GT: Geared transmission at FT: Full throttle).
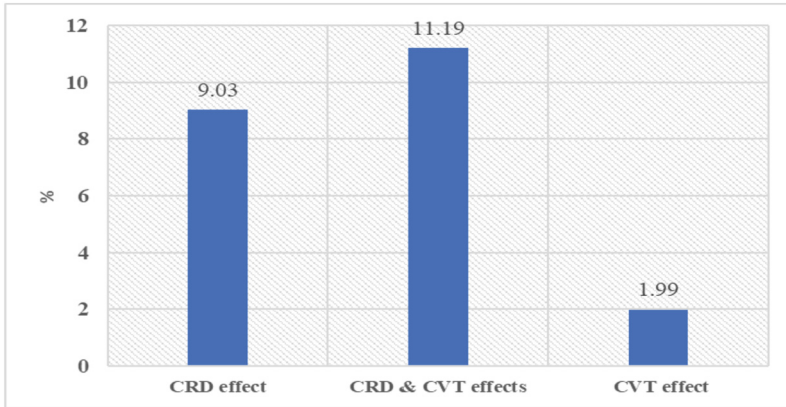
Fig. 1. The effects of CRD, CRD&CVT, and CVT on the total efficiency of tractors

   Among the evaluated tractors, the 4WD and 9.5 kW tractor had the lowest efficiency with 19.93%, while the 4WD and 61.5 kW CRD tractor had the highest efficiency with 32.86%. 2WD tractors were 2.9% more efficient than 4WD tractors. The reason for this may be; that 4wd tractors have more friction losses during motion transmission than 2wd tractors, and they also consume more fuel because they produce more traction power. The average efficiency values of domestic 127 tractors and imported 166 tractors were 28.2% and 28.3% respectively. The power ranges, number of tractors, average powers and average efficiencies are given in Table 4. Tractors with horsepower higher than 100 kW are 12.7% and 8.7% more efficient than tractors from 50 kW to 100 kW and less than 50 kW, respectively. All tractors over 100 kw have CRD injection systems so that the average total efficiencies of those tractors are higher than others.

Table. 4. Average η_t as per power ranges

Power Range (kW)	Number of tractors	Average power (kW)	Average η_t (%)
<50 kW	161	37.7	27.6
50–100 kW	118	62.0	28.8
>100 kW	14	126.9	31.1

4 Conclusion

This paper has highlighted the effect of the engine and wheel drive system of the tractor on the energy efficiency such as 2WD, 4WD, CRD, and CVT. Apart from the engine and wheel, other parameters such as drive system, soil type and characteristics, tyres, working pressures, tractor weight, compatibility between tractor and equipment, and driving efficiency should be analyzed. Generally speaking, the energy efficiency of a tractor depends on several factors, among which can be highlighted: 1. Engine. 2. Transmission. 3. Type of soil and characteristics of the working field. 4. Tires and working pressure used. 5. Ballast of the tractor. 6. Compatibility between tractors and implements. 7. Efficient driving. The efficiency of the first two factors (engine and transmission) is assessed by an energy efficiency index, and it would mean between 60–70% of the total energy efficiency of a tractor. In terms of efficient use of the tractor by a farmer, according to many authors, this can mean as much as 20–30% of the total energy efficiency [15]. Drivers & farmers should be trained with a special program about efficient driving and about correct selecting of compatibility between tractors and implement.

The economic life span of the tractor is 12000 h or 12 years. The number of tractor fleets in Türkiye reached 1.946.806 end of 2020, 49% of them are older than 24 years, and 500.000 tractors are older than 40 years [14]. If we consider that the stage IIIB emission standard implemented in 2018 and the stage IV standard implemented in 2019 in Türkiye, most of the emission levels of tractors used in Türkiye are stage IIIA or lower-level engines and they do not have CRD injection systems. According to the results of this research, it means that they work with a lower efficiency of 9.3%. According to the researchers, tractors that have completed their economic life cause to consume an average of 700 L more fuel and 100–150 h of workforce loss per year [16]. Based on the average of the exhaust emission measurements made with tractors older than 25, there is an additional CO_2 emission of 1,816 kg for the 250 h/year average operation foreseen for these old tractors [17]. Engine technologies improve the use of non-renewable fuels by adjusting the programming of the ECU, which controls the high-pressure injection system, and reduces pollutant emissions according to legislation [4]. Replacement of the inefficient and unsafe tractors that have completed their economic life should be supported by the governments.

References

1. Satman A (2007) Türkiye'nin enerji vizyonu. jeotermal enerjiden elektrik üretimi semineri, TESKON 2007, VIII. Ulusal Tesisat Mühendisliği Kongresi, 25–28 Ekim 2007, İzmir
2. Anonymous (2012) Energy efficiency indexes (EEI) applied to agricultural tractors. Background note/literature review. TAD/CA/T/WD (2012)3. OECD, Organization for Economic Co-operation and Development, Paris, France
3. Benedek A, Rokicki T, Szeberényi A (2023) Bibliometric evaluation of energy efficiency in agriculture. Energies 16:5942
4. Schlosser JF, Farias MS, Bertollo GM, Russini A, Herzog D, Casali L (2020) Agricultural tractor engines from the perspective of Agriculture 4.0. Revista Ciência Agronômica 51:1–12
5. Howard CN, Kocher MF, Hoy RM, Blankenship EE (2013) Testing the fuel efficiency of tractors with continuously variable and standard geared transmission. University of Nebraska – Lincoln, Biological Systems Engineering: Papers and Publications, p 297

6. Xu LY, Zhou ZL, Zhang MZ et al (2006) Research and design of hydro-mechanical continuously variable transmission for tractors. J Northeast Agric Univ 13(2):182–186
7. Yang B, Wei X, Zeng K, Lai M (2014) The development of an electronic control unit for a high pressure common rail diesel/natural gas dual-fuel engine. SAE Technical Paper 2014-01-1168
8. Tunca L, Polcar A (2016) The influence of common-rail adjustment on the parameters of a diesel tractor engine. Acta Universitatis Agriculturae Et Silviculturae Mendelianae Brunensis, 64(03)
9. Ergul I (2016) Türkiye'deki tarım traktörlerinin enerji verimliliği sınıflandırmasına yönelik bir sistem geliştirilmesi. Ankara Üniversitesi, Fen Bilimleri Enstitüsü, Tarım Makineleri ve Teknolojileri Mühendisliği Anabilim Dalı, Doktora tezi, 2016, 143 sayfa. Ankara
10. OECD (2023) OECD Code 2, OECD Standard Codes For The Official Testing Of Agricultural and Forestry Tractors. Organization for Economic Co-operation and Development, Paris, France
11. Saral A (1997) Tarım traktörleri (II. Baskı). Ankara Üniversitesi Ziraat Fakültesi Yayın No: 1471, Ders Kitabı: 436. Ankara
12. OECD (2023) Organization for Economic Co-operation and Development. https://www.oecd.org/agriculture/tractors/. Accessed 21 Aug 2023
13. Sayın S (2006) Amik ovasında mekanizasyon planlaması, tarım makinaları edinim olanaklarına ilişkin veri tabanı oluşturulması ve bunların değerlendirilmesi konusunda bir araştırma. Doktora Tezi, Çukurova Üniversitesi, Fen Bilimleri Enstitüsü, Tarım Makineleri Anabilim Dalı, Adana
14. Sağlam C, Polat R, Sağlam R (2006) Şanlıurfa ili kuru tarım işletmelerinde optimum makina boyutu ve traktör gücünün belirlenmesi. Tarım Makinaları Bilimi Dergisi 2(4):279–283
15. Anonymous (2012) Possibilities for harmonizing methodologies used to calculate energy efficiency indexes applicable to agricultural tractors using OECD code 2 tests. TAD/CA/T/WD(2012)4. OECD, Organization for Economic Co-operation and Development, Paris, France, 6–7 November 2012
16. Ünsal Y (2022) Türkiye'de tarımsal mekanizasyon düzeyi, sorunları ve çözüm önerileri, Tarımsal Ekonomi ve Politika Geliştirme Enstitüsü Müdürlüğü, Ankara
17. Evcim HÜ, Ulusoy E, Gülsoylu E, Tekin B (2010) Tarımsal mekanizasyon durumu, sorunları ve çözüm önerileri. ziraat mühendisliği VII. teknik kongresi, 11–15 Ocak, Ankara

Chopper System for In-line Small Square Balers

Sedat Kahraman[1], İbrahim Ethem Polat[1(✉)], Sinan Gökçe[1], and Ali Oral[2]

[1] Paksan Makina Sanayi ve Ticaret A.Ş., Akçapınar Mah, Akçapınar Cad, No: 271, Bandırma, 10202 Balıkesir, Turkey
ethempolat@paksanmakina.com.tr
[2] Department of Mechanical Engineering, Balıkesir University, 10145 Balıkesir, Turkey
a.oral@balikesir.edu.tr

Abstract. A small square baler is a piece of machinery used to compact, compress, and cut hay and other materials into square-shaped bales. These machines are usually pulled from the side of the tractor by the tractor and driven from the tractor PTO. These machines, which move next to the tractor, occupy a larger area in the field. In this project, a chopper system will be designed for in-line small square balers that will work center of the tractor track width. Chopper is a shredding system used to cut stem part of the grass into smaller pieces that has been harvested and spread on the field. The farmers prefer the bale system with chopper, stating that the small grass is eaten more easily by the animal. In-line small square balers with chopper system is used to produce bales with small grain sizes, while reducing time and labor costs during the feed preparation stage.

At regular small square balers, prong system which sends the grass to the bale chamber, carries the grass to the bale chamber by dragging it from the side, the gearbox works slower (output speed = 92 rpm), at in-line small square balers, the fork system will work faster (102 rpm) as it will work together with the rotor. This will reduce unit costs by producing approximately 10% more products at the same power value.

In the developed in-line small square baler, there is a movable counter under the rotor that can be opened and closed with hydraulic drive when necessary, enabling working with or without knives, and movable knives that can be removed and mounted inside the movable counter. The use of the machine with or without cutting blades is ensured by the up or down position of the blades in the moving contra. When this system is overloaded and clogged, the system is protected by a safety clutch to prevent any damage to the system.

In the system we have developed, the chopper system can be disassembled from the machine with the retracting of the pick-up system, the machine can also be used without chopper system. With this study, in-line small square baler with chopper system design will be developed and prototype production will be made after design verification studies. In-line small square baler with chopper system is not available in the national or international market. This machine, which will be developed by Paksan Makina R&D Center, is an innovation for our country and the world.

Keywords: Square baler · Chopper system

1 Introduction

Agriculture is one of the important links in the food chain, the other important link in this chain is animal husbandry. Agriculture and animal husbandry have a very important place in the adequate and balanced nutrition of people. However, unlike other sectors, these sectors are also very important for the country's economy as they include many sectors from the machinery sector to the software sector (1).

Roughages have an important place in cattle and sheep breeding in our country. One of the most important storage methods of roughages is baling. Balers collect plants such as grass, alfalfa, stalks and herbaceous plants from the field, turn them into prismatic or round bales of the desired size and desired tightness, then tie them with rope or net to prevent them from dispersing and leave them on the field surface.

Balers can be classified in 4 main groups according to their drive mechanisms, bale geometry, compression pressure and binding material (2).

In the baling sector, balers are divided into two classes as prismatic and round according to the geometric shapes of the bales. Prismatic balers are divided into two groups as large and small balers. Large balers usually make bales of 100 kg and above, while small balers usually make bales between 15–25 kg. The baler user prefers the machine that is suitable for their own conditions from the above classification of balers.

Balers can also be classified differently as off-line and in-line (Fig. 1). Off-line balers move along the side of the tractor and collect the barreled weed piles in the field and turn them into bales. In-line balers are small square balers that collect and bale the materials drawn by centering the wheel track of the tractor. Since these machines are towed on the tractor wheel track, they are highly maneuverable in narrow areas and between vineyards. In addition, in some forms, it offers the opportunity to collect and bale without the need to make lines and groups (3).

Since small balers do not have chopper units, they cannot shred and cut the grasses to be made hay, and they cannot turn them into small pieces. In this study, a chopper system will be added to the in-line baler that will be developed in order to shred the straw raw material into hay.
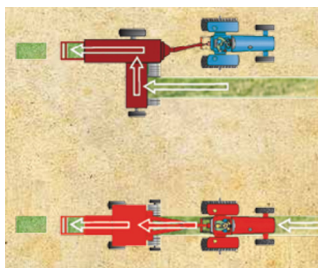
Fig. 1. Baling methods off-line and in-line balers (3)

2   Chopper System for In-line Small Square Balers

Grass, clover, stalks and herbaceous forage plants and other materials that can be baled are collected by the pick-up unit of the tractor-drawn baler and transferred to the chopper-cutter unit (Fig. 2).
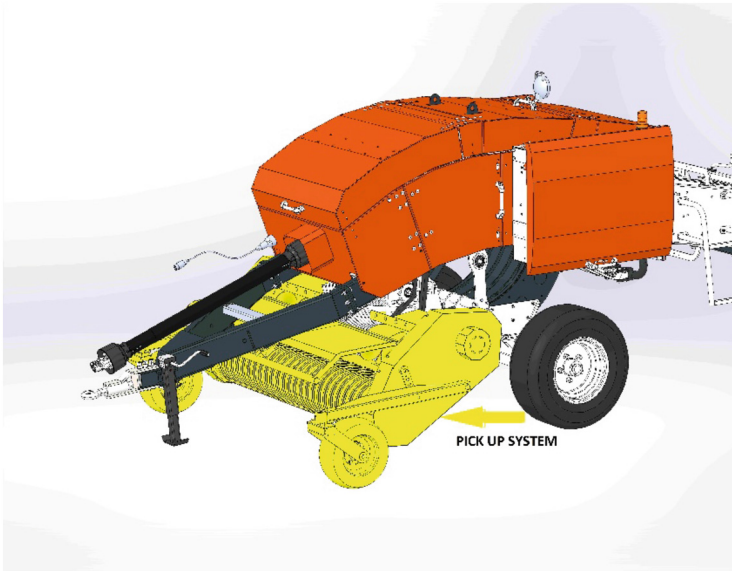
Fig. 2. Pick up system

In the chopper unit, they are cut into pieces of 4–10 cm in length and sent to the section with transfer prongs. From here, with the help of prongs, they are thrown in front of the plunger moving inside the compression unit above. The plunger, which operates at 102 strokes per minute, compresses the grass in the bale chamber. When the compressed materials reach the pre-determined and set bale length, the three-string tying device moves and the bale is formed (Fig. 3). Each formed bale is pushed out by the bale behind it.

In the chopper/cutter unit, instead of the existing gear system, there is a rotor (bator) consisting of four-cornered hypocycloid shaped similar sheets welded on a pipe in helical form with equal steps and angle difference. Underneath the rotor (bator) there is a moving contra-actuator, which is actually static only in the working state, which can be hydraulically opened and closed when necessary, enabling operation with and without blades. The movable contra and the movable blades can be opened and closed hydraulically when necessary for changing the movable blades, reducing the movable blades and removing blockages (Fig. 4).
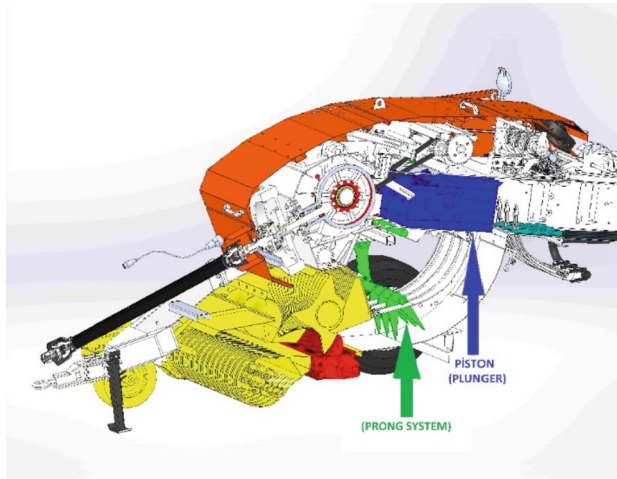
Fig. 3. Prong and Plunger system

The pick-up system convey grass, clover, stalks and herbaceous plants etc. to the rotor (bator). The rotor (bator) shreds grass, clover, stalks, woody and herbaceous plants and other materials that can be baled etc. into small pieces by passing them through the blades. The blades in the movable contra are in the up or down position and the machine is used with or without sizing (Fig. 5).
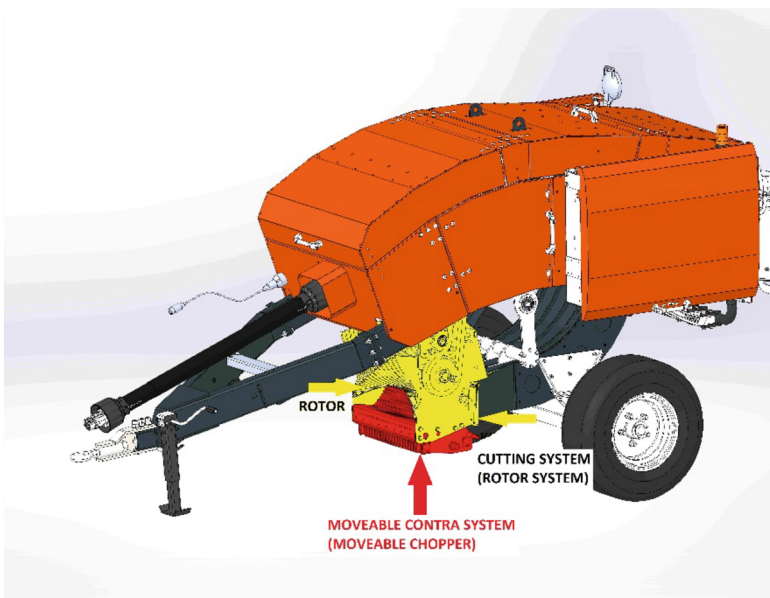
Fig. 4. Chopper unit
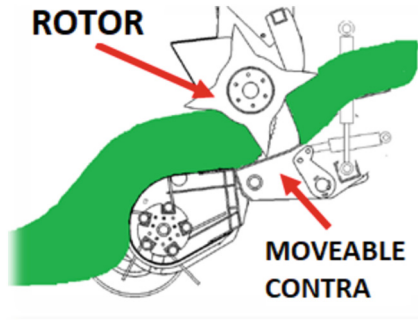
Fig. 5. Rotor and contra system

In-line machines developed by Paksan R&D Center, moist materials can be baled with the chopper system, while dry materials can be baled with or without chopper. At the same time, the machine can also be used without a bale by removing the pick-up system from the machine and moving the harrow (pick-up) system backwards.

3   System Design and Design Verification Studies

The general view of the in-line baler is given in Fig. 6. The design studies of the developed system were carried out with SolidWorks software. SolidWorks Simulation software was also used in design verification studies. The chopper system to be used in the in-line baler is given in Fig. 7 and the chopper rotor of this system is given in Fig. 8. In this study, the rotor connection shaft (Fig. 9.) is considered as the critical element of the system and finite element analysis is applied on this element.
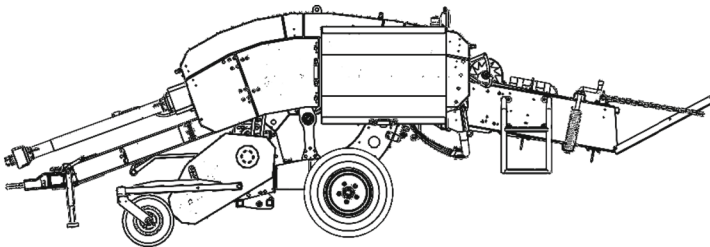
Fig. 6. In-line baler

The rotor connection shaft is driven by a chain gear mounted on it. In-line balers used in small bale making require tractors up to 70 HP. Assuming that 80% of the power generated by the tractor is transferred to the PTO, finite element analyses were performed on the rotor shaft and rotor discs. The moment on the tractor PTO shaft is
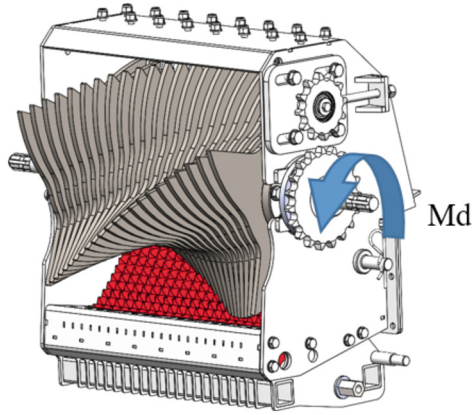
Fig. 7. Chopper System
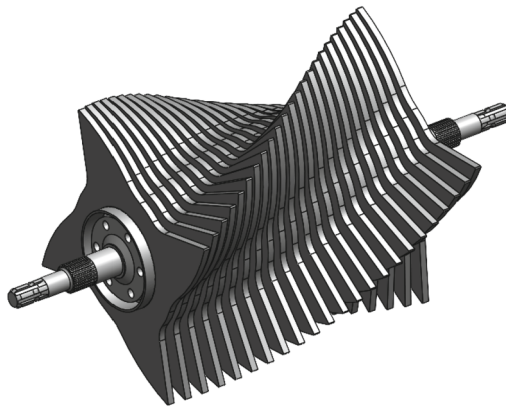
Fig. 8. Chopper rotor
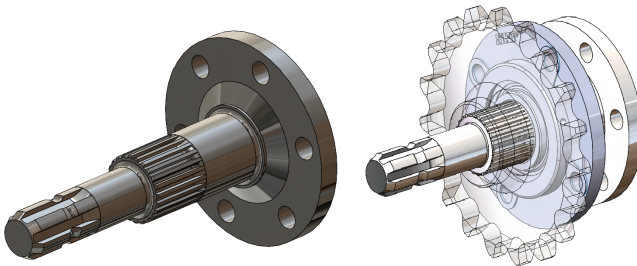
Fig. 9. Chopper system rotor connection shaft

730 Nm and this moment value is transferred to the Chopper rotor with a cycle ratio of $i = 5.29$. Chopper rotor is driven with a moment of approximately 3800 Nm. The rotor connection shaft material will be produced from AISI 1040 material and the mechanical values of the material are given in Table 1.

Table 1. AISI 1040 material mechanical properties (4)

Tensile Strength, Ultimate	620 MPa
Tensile Strength, Yield	415 MPa
Modulus of Elasticity	200 GPa
Bulk Modulus	160 GPa
Poissons Ratio	0,29

The rotor connecting shaft is connected to the rotor disks with bolts. As a boundary condition, the bolt holes are fixed and the housing is made on the rear side of the drive gear as shown in Fig. 9. The housing surface is defined as a cylindrical support surface. A moment of 3800 Nm is applied on the splined shaft to which the sprocket is connected. The mesh element was selected as "Solid-mesh - Blended curvature-based" in the mesh generation process. In the finite element model, the total number of nodes was 314089 and the total number of elements was 219759.

As a result of the analysis, it is seen that 400 Mpa values can be reached locally (Fig. 10a). In the calculations made by analytical methods, it is seen that the shaft is subjected to torsional stress of 154 Mpa. In the finite element analysis, it is seen that the stress distribution is around this value. The amount of strain was found to be within reasonable values with 0.13 mm (Fig. 10b).

(a)

(b)
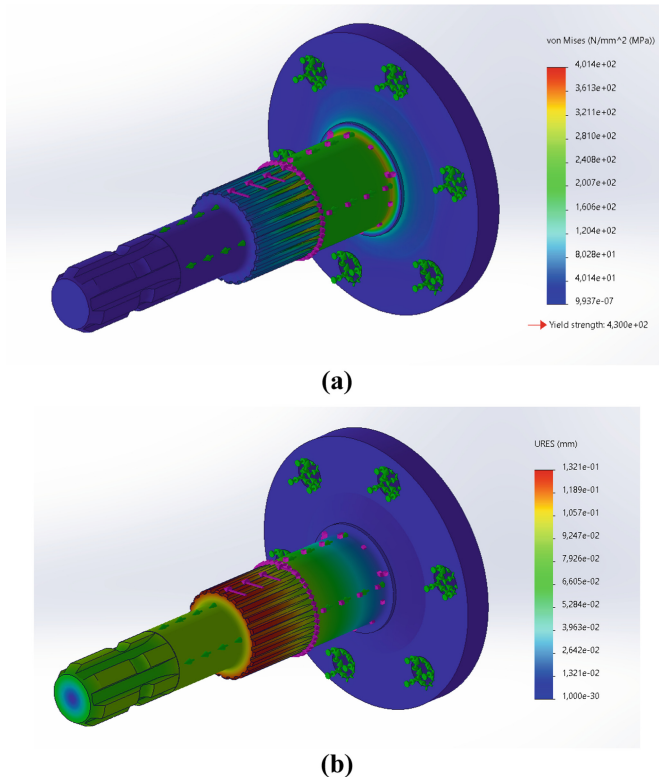
Fig. 10. (a) Stress distribution finite element analysis of rotor connecting shaft. (b) Amount of strain finite element analysis of rotor connecting shaft

4   Conclusion

In off-line systems, the gearbox operates slower due to the fact that the prong system, which sends the grass to the bale chamber, sends the grass to the bale chamber by dragging it from the side (output speed = 92 rpm.) In the in-line baling system, the prong system will be able to operate faster (102 rpm) since it will work together with the rotor. This will reduce unit costs by producing over 10% more product at the same power value.

With this study, in-line small square baler with chopper system design will be developed and prototype production will be made after design verification studies. In-line small square baler with chopper system is not available in the national or international market. This machine, which will be developed by Paksan Makina R&D Center, is an innovation for our country and the world.

References

1. Arslan M, Erdurmuş C (2012) Ülkemizde Hayvancılığa ve Kaba Yem Sorununa Genel Bir Bakış. Ziraat Mühendisliği Temmuz-Aralık 359:32–37
2. https://acikders.ankara.edu.tr/mod/resource/view.php?id=59585. Accessed Aug 2023
3. https://maplelanefarmservice.ca/resources/specsheets/massey-ferguson/balers/Massey_1800_Small_Square_Baler_Series_Brochure_NA.pdf. Erişim tarihi Ağustos 2023
4. https://www.paksanmakina.com.tr/Urunler/hammer/. Accessed Aug 2023
5. https://www.matweb.com/search/DataSheet.aspx?MatGUID=c8ada14779744d008a6c3e80f035c5d5&ckck=1

Determination of Suitable Shearing Conditions for Effective Pruning of Tree Branches

Saeid Minaei[1(✉)] , Mohamad Safvati[2] , and Alireza Mahdavian[1]

[1] Biosystems Engineering Department, Tarbiat Modares University, Tehran, Iran
minaee@modares.ac.ir

[2] Biosystems Engineering Department, University of Kurdistan, Sanandaj, Iran

Abstract. Pruning shears used for tree canopy management are manufactured in various sizes and blade curvatures. This paper reports on the selection of suitable blade curvature of manually-operated pruners for tree branch pruning. Various shears available on the market were examined and three with the highest, lowest and medium curvature radii were selected. These were mounted on a material testing machine and used for shearing tree branches (Morus alba) in a randomized complete block design experiment. Effects of blade curvature radius at three levels (42, 45 and 50.5 mm), cutting speed (200, 400 and 600 mm/min) and Mulberry branch diameter at three levels (thin, medium and thick) on the required cutting force and energy were studied. Analysis of covariance was used to remove the effect of branch moisture content. Statistical analysis of the data showed that the effect of blade-curvature on the required cutting force and energy was significant at the 1% level. Cutting force and energy, which are important in manual pruning due to the strain they place on the worker, significantly increased with blade curvature radius. The best cutting conditions for various branch diameters were found to be: blade-curvature radius of 45 mm for large branches and 42 mm for thin and medium branches all at cutting speed of 400 mm/min.

Keywords: Shears · Pruning Process · Cutting Force · Energy consumption

1 Introduction

Pruning is a method of caring for trees and shrubs that helps maintain their health and improve their quality by removing dead, diseased, or damaged wood. Fruit tree pruning is a horticultural practice used to regulate tree growth and performance, optimize tree size, and control branch density. This process helps to achieve a balance between vegetative and reproductive growth. Preventing damage and preserving the health and aesthetic appearance of the tree are the most important reasons for pruning. The timing and extent of pruning depend on the age, species, and growth stage of the tree. Trees should be pruned properly which requires skill and knowledge of pruning principles. Improper pruning can cause significant damage to the structure of the tree [15].

After careful pruning, tree growth will likely be optimal, resulting in higher quality wood compared to unpruned trees [14]. The effect of pruning on wood quality depends on several factors, including the pruning season, pruning method, tree species, and branch diameter. Growth of microorganisms, fungi, and bacteria may occur as a consequence of improper pruning. Regular pruning strengthens the fruit tree and is the most effective method for maintaining it. Sometimes, pruning is the best treatment for a diseased tree or shrub. Pruning at the wrong time can also cause significant damage to a tree and result in the production of small fruits and delayed fruiting [2]. Morus alba can be used to produce fodder, fruit, medicine, paper, and gas. Among its other uses, we can mention protection against fire in arid areas [5]. The Morus alba tree is very important in the silk industry, and due to its fast growth, it is pruned at least once a year [7]. The intensity of pruning will have a significant effect on the size and quality of the fruit [11] as well as the timing of fruit ripening.

In a study by Parish et al. [10], 9 manual pruning shears from 6 different manufacturers were tested to determine the manual force required to cut hardwood in different thicknesses. The test included measuring the force required to cut dry wood in 6 levels (diameters of 6.4, 7.9, 9.5, 12.7, 15.9, and 19.1 mm). The force was measured by a spring scale that applied force vertically to the end of one scissor handle. While the other handle was held horizontally by a clip. Statistical analysis showed a significant difference in the required force of different scissors [10]. From the studies conducted in Sicily and Lombardy regions, it can be seen that pruning with ordinary scissors was the most used in vineyards. Romano et al. [12] reported manual cutting force is a function of branch diameter and tree species. Also, Eliçin et al. [3] evaluated the cutting characteristics of grape cane using a material testing machine. According to their test results, a significant difference between the types of blades was observed at the 1% probability level. The best results were obtained in smooth blade, toothed type 2 and toothed type 1, respectively. While the lowest values of cutting force and strength were obtained for the smooth blade, so that the maximum values of cutting force, cutting strength, cutting energy and specific cutting energy for it were 234.5 N, 8.299 MPa, 1.783 J, and 0.06307 J.mm-2, respectively.

Mechanization of horticulture and agriculture in today's world is of great interest due to the importance of ensuring high quality and yield of fruit tree products. This study is dedicated to examining the impact of blade curvature radius, cutting speed, and branch diameter on cutting force and energy required which has not been reported for such shears before. The implications of these findings for optimizing pruning techniques and improving the efficiency and effectiveness of tree and shrub management will also be discussed.

2   Research Methodology

Finding the best way to cut branches is an important aspect in the development of pruning tools [6]. In order to achieve an optimal cut, especially in manual pruning, it is necessary to find the conditions that require the least amount of force and energy for cutting. By examining the curvature radius of the available models on the market, three bypass pruners with the lowest, average, and highest curvature radii were selected.

A coin with a diameter of 29.3 mm was used to calculate the curvature radius of the blades. By placing this coin on each of the blades, a vertical photo was taken. Then, using SolidWorks software, two circles on the coin and blade were matched, and their diameter values were recorded. As a result, the actual curvature radius of each blade was obtained by using the proportional ratio (Table 1). The blades were made of SK5 steel, and their sharpness angle was 12 ± 0.5 degrees. The curvature radii (CR) of the blades were determined to be 41.92 mm, 45.05 mm, and 50.56 mm which, for convenience, hereafter will be referred to as 42, 45, and 50.5 mm, respectively.

Table 1. Curvature radii of the pruner blades used in the study

Company/Model	Behco /8518	Behco /1	Behco /110–20
Radius of curvature	41.92 mm	45.05 mm	50.56 mm

Morus alba branches of various sizes (diameters) were obtained on November 9, 2020 from the college of agriculture campus of Tarbiat Modares University, Tehran. Subsequently, cutting tests were performed and moisture calculations were immediately carried out. The samples were divided into three size groups of: thin (5–7 mm diameter), medium (10–12 mm diameter), and large (15–17 mm diameter) branches. The experiments were repeated five times at three speed levels (200, 400, and 600 mm/min) and three blade-curvature levels using a material testing machine. To determine the moisture content of the samples, 2-cm portions were cut from each sample and subjected to drying in an oven at a temperature of 104 degrees Celsius for 24 h. It is desirable to obtain branches with similar moisture content and then eliminate the effect of the confounding variable through analysis of covariance (ANCOVA). This allows for a comparison of adjusted averages under a constant moisture content. After drying, the samples were weighed again, and the moisture content was determined on wet-basis [1].

In order to perform the shear test, the pruning shears were mounted on the material testing machine (Santam model STM-20) using appropriate fixtures such that before cutting, the loading speed was adjusted and the upper jaw of the machine was lowered to the point where the sample came in contact with the two blades. To remove the measurement error before starting the test, the force and displacement values were set to zero and the command to start the test was issued by the computer and continued until the samples were completely cut. The resulting force -displacement diagram was utilized to determine cutting force and energy (Fig. 1).
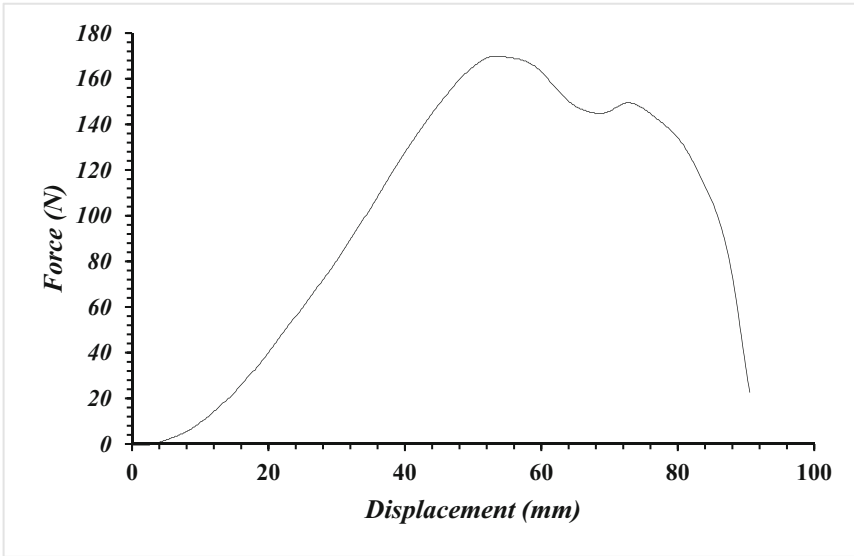
Fig. 1. A sample of force-displacement curve during shearing of Morus alba branch (11.05 mm diameter)

3   Results and Discussion

Statistical analysis based on a factorial test was conducted in the framework of completely randomized block design. The effect of moisture content was removed using covariance analysis. Comparisons of adjusted means at constant humidity of 41.2% were performed using Bonferroni test. Table 2 shows the results of ANCOVA on factors affecting Mulberry branch shearing.

Table 2. Analysis of covariance of force and energy (BD – branch diameter, CR – curvature radius, CS – cutting speed).

Factor	MSE_{force} (KN)	MSE_{energy} (KJ)
BD	209.372*	763.936*
CR	42.888*	107.214*
CS	0.116^{ns}	2.253^{ns}
BD × CR	8.120*	15.727*
BD × CS	0.561^{ns}	1.150^{ns}
CR × CS	0.834^{ns}	0.977^{ns}
BD × CR × CS	0.223^{ns}	0.323^{ns}
Moisture	0.042^{ns}	1.323^{ns}

(*continued*)

Table 2. (*continued*)

Factor	MSE_{force} (KN)	MSE_{energy} (KJ)
Block	5.887*	21.321*
Error	0.626	1.751

[ns] Non-significant difference at $\alpha = 0.01$
[*] Significant difference at $\alpha = 0.01$

Force and energy requirements for cutting Mulberry branches significantly increased with diameter. This is due to the fact that with increasing branch diameter, the cross-sectional area increases and the branch is harder to cut. The average value of cutting force for thin, medium and large diameter branches had a significant difference at the probability level of 1% and was determined to be 59.33, 157 and 253.49 N, respectively (Fig. 2).
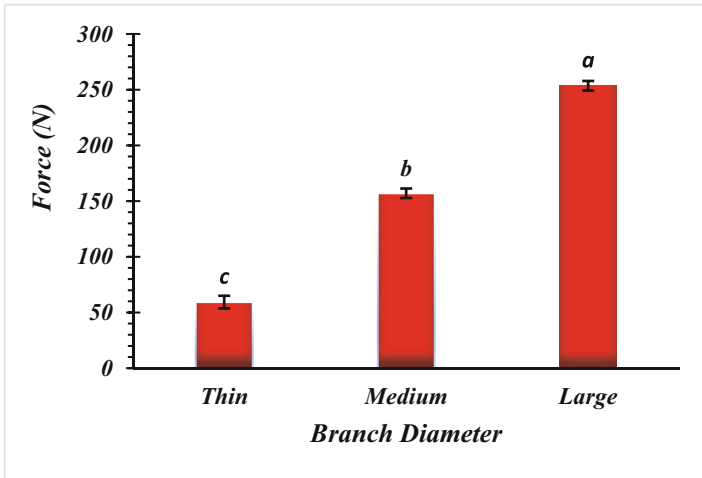
Fig. 2. The effect of mulberry branch diameter on shearing force at constant humidity (41.2% wb)

Energy consumption values for thin, medium, and thick branches were calculated as 2340.21, 7709 and 13797.88 mJ, respectively. These results are in agreement with those reported by Esgici et al. [4] in which the maximum cutting force and energy for shearing the branches of three grape varieties increased significantly with branch diameter. They furthermore reported a linear relationship. Similar results were also found by Khodaei and Akhijahani [9] for Rasa variety grapes. It is also consistent with the report by Ghahraei et al. [8] who showed that the maximum shear force and energy is directly proportional to the cross-sectional area of the cannabis stem. This information is valuable in choosing the right equipment to reduce the manual force and energy required for tree

pruning. This is because choosing the right cutting tool having the proper geometrical characteristics plays an important role in saving force and energy.

Results of this study indicate that, in general, more force is needed to make a complete cut with the largest radius blade, and the other two pruner blades do not differ significantly in terms of force requirement. The average values of the cutting force for the curvature radii of 42, 45 and 50.5 were equal to 139.60, 137.98 and 192.24 N, respectively. By increasing the curvature radius of the blade, the amount of energy consumed has increased. This result may be due to the fact that with the increase in the blade curvature radius, more vertical displacement is required for complete cutting, and as a result, with the increase of this displacement, energy consumption increases. The average values of this parameter were calculated as 6950.625, 7170.285, and 9727.178 mJ at the curvature radius of 42, 45, and 50.5, respectively (Fig. 3).
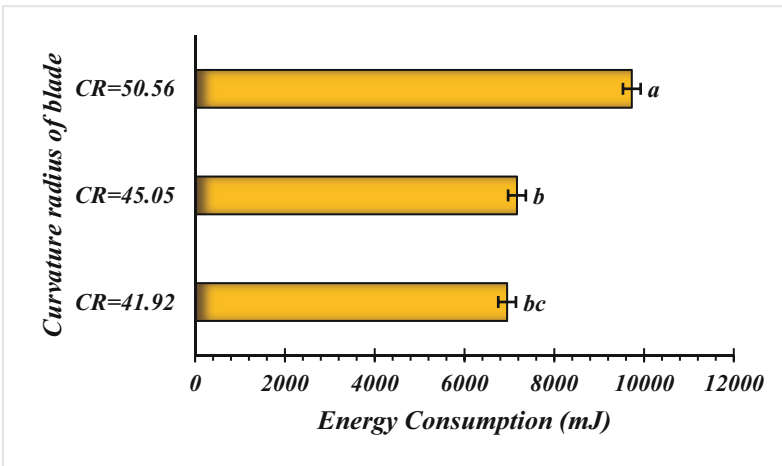
Fig. 3. The effect of curvature radius on energy consumption at constant humidity of 41.2%.

There is no significant difference between the first two levels of radius (42 and 45 mm) in terms of energy consumption. In a study by Sessiz et al. [13], where three blades with small teeth, with large teeth and smooth without teeth were used to cut thin grape branches, there was a significant difference between the three blades in terms of cutting force and energy at the probability level of 1%. The maximum force and energy were obtained for the blade with large teeth and the minimum force and energy were reported for the smooth blade.

The average values of force and energy consumed to make a complete cut of mulberry branches increased linearly with blade curvature radius (Fig. 4.). Force and energy had a high correlation with the curvature radius with coefficients of determination (R^2) equal to 0.85 and 0.92, respectively. At all three levels of the blade radius, force consumption increased with branch diameter. In cutting thin branches, the 42 mm blade performed better in terms of the required force, and its average value was 41.36 Newtons. For medium-size branches (10–12 mm diameter), the average values of the shearing force in both 42 mm and 45 mm blades were quite close (138.79 and 138.80 N, respectively).

Another point is the lower cutting force required by the 45 mm blade pruner for shearing large branches, the average value of which was 210.64 N. In general, the two mentioned blades performed better than the blade with the maximum curvature radius (50.5 mm) in terms of force requirement. The average amount of force used by the 50.5 mm-blade pruner to cut thin, medium and large diameter branches was equal to 72.16, 193.43 and 311.15 N, respectively. Compared to the other two curvature radii (42 and 45 mm), the less curved pruner (50.5 mm radius) requires more force to cut mulberry branches of all diameters. It is thus concluded that, in terms of force, for cutting thin, medium and large diameter branches, it is suitable to use pruners with curvature radii of 42 or 45 mm.
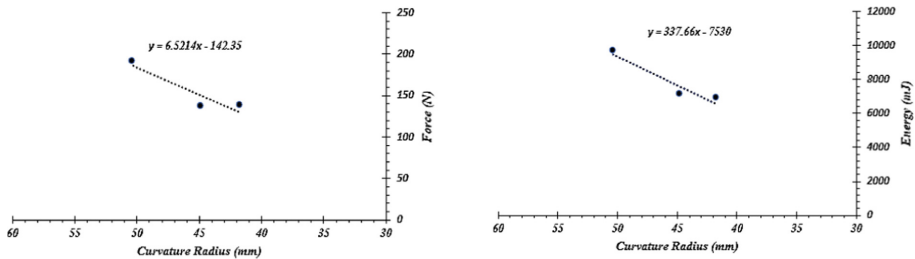
Fig. 4. Correlation between blade curvature radius and cutting parameters.

In cutting thin and medium branches, the blade with a radius of curvature of 42 mm performed better in terms of energy consumption with average values of 1661.26 and 6692.88 mJ, respectively. This is while for cutting thick branches, the average energy requirement is the least with the 45 mm-radius blade (12131.15 mJ). In terms of energy consumption, the 42- and 45-mm blades have performed better than the blade with the less curved pruner (50.5 mm). Thus, in terms of energy consumption, the best pruner is one with the most-curved blades i.e., 42 mm, for cutting thin and medium branches while the 45-mm-blade is more suitable for large branches.

4   Conclusions

Pruning is an important activity in horticultural management operations and any improvement in equipment utilization can positively affect performance and productivity. For cutting thin and medium branches, the most-curved shears (having blades with lower curvature radius i.e., 42 mm) and for cutting large branches, the pruner with medium curvature radius (45 mm) are more suitable in terms of force and energy requirements. The least-curved blade pruner (curvature radius of 50.5 mm) is not recommended for pruning mulberry branches. These results are useful in horticultural operations in terms of worker productivity and welfare by providing guidance for selecting the proper pruning shears.

References

1. ASAE (1999) Moisture measurement-ungrounded grain and seeds. ASAE Standard S3522:567–568
2. Dujesiefken D, Liese W, Shortle W, Minocha R (2005) Response of beech and oaks to wounds made at different times of the year. Eur J Forest Res 124(2):113–117
3. Eliçin AK, Sessiz A, Pekitkan FG (2019) Effect of various knife type, cutting angle and speed on cutting force and energy of grape cane. Avrupa Bilim ve Teknoloji Dergisi 15:519–525
4. Esgici R, Pekitkan FG, Ozdemir G, Guzel E, Sessiz A (2019) Cutting parameters of some grape varieties subject to the diameter and age of canes. Fresenius Environ Bull 28:167–170
5. Ferrandez-Villena M, Ferrandez-Garcia CE, Garcia-Ortuño T, Ferrandez-Garcia A, Ferrandez-Garcia MT (1806) Evaluation of fruit and vegetable containers made from Mulberry wood (Morus alba L.) waste. Appl Sci 9(9)
6. Franzen JB, Hirst PM (2014) Optimal pruning of apple and effects on tree architecture, productivity, and fruit quality. In: XXIX International Horticultural Congress on Horticulture: Sustaining Lives, Livelihoods and Landscapes (IHC2014) vol 1130, pp 307–310
7. García-Ortuño T, Ferrández-Villena M, Ferrández-García MT, Andreu-Rodríguez J, Ferrández-García CE (2013) Influence of the pre-treatment on the mechanical properties of medium density particleboards from mulberry. In: Vii Congress Ibérico De Agroingenieria and Horticultural Science
8. Ghahraei O, Ahmad D, Khalina A, Suryanto H, Othman J (2011) Cutting tests of kenaf stems. Trans ASABE 54(1):51–56
9. Khodaei J, Akhijahani HS (2012) Some physical properties of rasa grape (Vitis vinifera L.). World Appl Sci J 18(6):818–825
10. Parish RL (1998) Operating force requirements for manual pruning shears. Appl Eng Agric 14(4):349–352
11. Pawan SJ, Satpal B, Surinder S, Mukesh K (2017) Effect of the time and severity of pruning on growth, yield and quality in mulberry (Morus alba L.)
12. Romano E, Bonsignore R, Camillieri D, Caruso L, Conti A, Schillaci G (2010) Evaluation of hand forces during manual vine branches cutting. In: International Conference Ragusa SHWA, September, pp 16–18
13. Sessiz A, Eliçin K, Bayhan Y (2019) Cutting force and energy requirement of 'BOĞAZKERE' grape (Vitis vinifera L.) cane. Sci Papers-Ser B, Horticulture 63(1):265–270
14. Springmann S, Rogers R, Spiecker H (2011) Impact of artificial pruning on growth and secondary shoot development of wild cherry (Prunus avium L.). Forest Ecol Manag 261(3):764–769
15. Zhang L, Koc AB, Wang XN, Jiang YX (2018) A review of pruning fruit trees. IOP Conf Ser Earth Environ Sci 153(6), 062029. IOP Publishing

Shear Tests of Grapevine (*Vitis vinifera* L.) Canes

Abdullah Sessiz[1(✉)], Gültekin Ozdemir[2], and A. Konuralp Eliçin[1]

[1] Faculty of Agriculture, Department of Agricultural Machinery and Technologies Engineering, Dicle University, 21280 Diyarbakır, Turkey
asessiz@dicle.edu.tr

[2] Faculty of Agriculture, Department of Horticulture, Dicle University, 21280 Diyarbakır, Turkey

Abstract. In this study, shearing force, energy, strength and specific shearing energy values of the pruned branches of three local grape (*Vitis vinifera* L.) varieties (Öküzgözü, Boğazkere and Şire) were determined and compared. The aim of the study is to obtain appropriate data for the design of a machine that can be used in shredding vineyard pruning residues. In accordance with this purpose, the shear tests were carried out with three different knife shapes, two of them are serrated type (serrated 1 -knife-edge thick, serrated 2 -knife-edge thin) and flat (knife-edge flat) with five knife edge angles (50°, 60°, 70°, 80° and 90°). The shear tests were made by Instron Universal Materials Testing Machine, Lloyd LRX Plus. According to test results, maximum shearing force, strength and energy values were obtained at knife of serrated 1 (knife-edge thick) type, the lowest average value was observed at serrated 2 type knife as 382.77 N. The shearing force slowly decreased with increasing knife-cutting angle from 0° to 40°. The maximum shearing force was observed at 0° knife cutting angle as 426.90 N. The lowest values were obtained at 30° and 40° cutting angle. However, when all interaction of Duncan test results is considered, maximum shearing force was observed at serrated 1 knife, 10° shearing angle, and the cane of Öküzgözü grape variety as 669 N, the lowest value of cutting force was observed at Flat-edge knife type, 40° cutting angle and the Şire grape variety as 205.50 N.

Keywords: Grapevine cane · Shear test · Shear force · Shearing strength · branch shredding

1 Introduction

Turkey is situated between latitudes 36–42° north and longitudes 26–45° east, a favorable area for viticulture that has a long history in the cradle of civilization. Turkey is one of the top producers of grape in worldwide. It has 468.792 ha of vineyards and a production of approximately 4 million t. Over 77 million t of grapes are grown worldwide on more than 7.1 million ha area. Turkey ranks fifth in terms of growing area, after Spain, France, China, and Italy, and ranks sixth in production after China, Italy, USA, Spain and France.

Large variations in climatic conditions in Turkey allow for the production of table grapes, raisins and wine grapes. In total, 1.200 grape cultivars are grown in Turkey, mostly

belonging to the species Vitis vinifera L. [1]. Over 1.170 Vitis vinifera L. accessions are maintained at the Tekirdağ National Germplasm Repository Vineyard.

Öküzgözü, Boğazkere and Şire grape (Vitis vinifera L) varieties are widely grown in the Southeastern part of Turkey in Diyarbakir, Elazığ and Mardin provinces. Even though grape has always been a valuable and important product for human diet and economy in Turkey, pruning and harvesting processes in vineyards are still mainly performed by manually. Therefore, time-consuming and production costs are very high and labor efficiency is low in the vineyard pruning operations. Vineyard pruning residues are usually left in the vineyard and burned, or used of border vineyard. This creates a basis for both environmental pollution and the formation diseases and pests. Pruning residues that occur in large quantities as a result of pruning, maintenance and harvesting processes in vineyards and orchards become a problem for producers [2]. Instead of doing this, pruning residues can be shred and used as organic residue in the soil the using any machine/equipment. Evaluation in this way is important in terms of preventing environmental pollution and reintroducing the wastes to the soil. Thus, it will be of great benefit both economically and in terms of the implementation of recycling activities in agriculture. At the same time, sustainability in agriculture will be achieved by re-evaluating the vine residues ground in the branch shredder. As a result of the use of pruned branches as organic waste, the use of chemical fertilizers will also decrease.

To use machines successfully for shoot positioning, pruning, harvesting, and other grape production operations, trellis systems must be devised, and shoots positioned to accommodate precise mechanical movement [3, 4]. Pruning is made by worker with scissors in viticulture. Usually, flat-mouthed scissors are used, and this process is difficult and tiring. The same scissors are used for all types of vines. Power requirements are high. However, the cane cutting characteristics of each variety is different each other. Therefore, the mouth of the used scissors and the cutting angle are important to determine for reducing the energy requirement. Additionally, branch shredding machines are needed to avoid recycling the pruning residues. For a new design of shredder machine, above all, data on shearing and chopping of vineyard pruning canes are needed. The most important of these characteristics is cutting properties.

Labor requirement, time-consumption and production costs can be decreased by utilizing a mechanical pruner and shredder machine [5, 6]. The first stage for the design of an effective new pruner is to measure the cutting force and energy. The cutting strength and energy requirement depending on the species, variety, diameter, maturity, moisture content, cellular structure and the type of cutting blade used [7–9]. Knife edge angle, knife approach angle, shear angle, and knife rake angle are the most important knife angles that can directly influence the cutting force and energy [10].

Until now, many studies have been conducted on the mechanical, physical and cutting properties of canes for different grape varieties. Romano et al. [11] determined the cutting force such as Cabernet Sauvignon and Chardonnay at different regions in Italy. Sessiz et al. [5] determined the cutting properties end energy values for some local and international grape varieties in Turkey. Cutting properties and energy values were determined by Ozdemir et al. [12] depending on variety, moisture content and diameter of some local wine grape cultivars. Cutting properties of cutting force, cutting strength, cutting energy and specific cutting energy were measured in eight different wine grape

varieties. Canes of Tannat, Merlot, Cot, Chardonnay, Viognier, Cabernet Sauvignon, Shiraz and Cabernet Franc were profiled for their cutting properties during the dormant season. The results of data analysis showed that there was a significant difference between average values of cutting properties varying based on variety. The results demonstrated that the maximum cutting force, cutting strength and cutting energy for Cabernet Franc grape, the minimum cutting force, cutting strength and cutting energy were obtained at Tannat grape variety. Also, similar engineering properties of the Şire grape were determined by Esgici et al. [13]. Cutting properties of şire grape cane has been changed with harvesting time. Shearing force and energy requirement increased with increase internode diameter of canes. The maximum shearing force and energy requirement were determined the last harvesting time. Similar results were reported Pekitkan et al. [14] for cotton stalk. Cutting parameters of some grape varieties subject to the diameter and age of canes were determined by Esgici et al. [15]. From the above literatures study, there is limited information about the effect of knife type, knife edge angle and cutting speed of grape canes. So, we have felt to the need to conduct this study.

2 Methods

Grapevine canes of Boğazkere (wine), Öküzgözü (wine) and Şire (table) (Vitis vinifera L) grape cultivars (Fig. 1) belonging to the region were used were used for shear tests. Pruning canes were obtained from the vineyards of the grape producers at Diyarbakır province located in south-eastern part of Turkey. The test samples were randomly cut by hand from vineyards. The cut and collected grapevine canes (Fig. 1) were transported to the laboratory at the Department of Agricultural Machinery and Technologies Engineering. Then, the samples were kept in a 5 °C refrigerator for 2 months until started to cutting tests. Trial tests were carried out during the spring grape pruning season.

Fig. 1. View of grapevine canes of Öküzgözü, Boğazkere and Şire varieties.

The initial moisture content of grape canes samples was measured according to ASABE standards [16]. Before tests, four samples of 20 g cane stems were chopped, weighed and dried in an oven of 103 °C for 24 h which were then reweighed in order to determine the average moisture content for each variety. The average wet based moisture contents of canes samples were measured as 50.30% for Öküzgözü, 50.40% for Boğazkere and 50.90% for Şire grape, respectively. To compare and evaluate shear characteristics for all varieties, 8 mm diameter canes were used during the tests. The

cane diameters were measured using a digital caliper with an accuracy of 0.01 mm. The diameter of the canes (mm) was converted to cross-section area in 50.24 mm^2.

Shear force and energy values were measured using an Instron Universal Materials Testing Machine, Lloyd LRX Plus, as shown in (Fig. 2). The shear force was recorded as a function of displacement. Experiments were carried out with three various knife types (Fig. 2), two of them are serrated type (serrated 1 (knife-edge thick), serrated 2 (knife-edge thin) and flat (knife-edge flat) with five knife edge angles (50°, 60°, 70°, 80° and 90°). All cutting test was conducted 5 mms^{-1} constant loading speed in vertical loading direction. The cutting energy was calculated by measuring the surface area under the force-deformation curve by material testing machine [17–23]. A computer data acquisition system recorded all force-displacement curves during the cutting process by using a NEXYGEN computer program for each parameter.

(a)

(b)
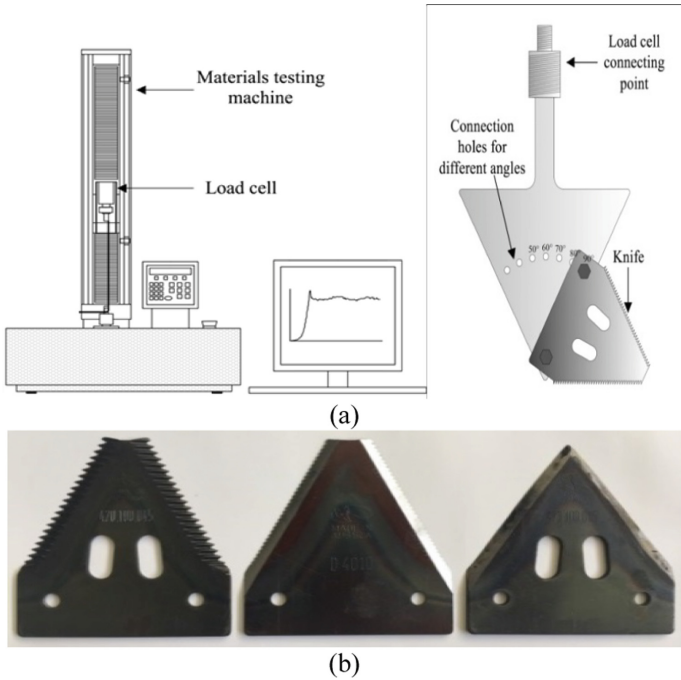
Fig. 2. Materials Testing Machine (a) and the cutting knives used in the experiments (b).

The maximum shearing strength, obtained from the force values by materials testing machine, was determined by the following equation [21, 22, 24–27]:

$$\sigma_s = \frac{Fmax}{A}$$

where: σ_s is the maximum shearing strength in (MPa), Fmax is the maximum shearing force in (N) and A is the cross-sectional area in (mm^2).

Specific shearing energy (E_{sc}) was calculated by:

$$E_{sc} = \frac{E_s}{A}$$

where: E_{sc} is the specific shearing energy (J mm^{-2}) and E_s is the shearing energy (J).

An analysis of variance (ANOVA) of the three-factor randomized complete block design with five replications was performed to detect significant differences in the observations due to the effect of grape variety, knife type, and knife edge angle of each factor using the MSTAT-C software. Means were compared at the 1% and 5% level of significance using Duncan's multiple range tests to identify the specific differences among treatments means.

3 Results

A typical force-deformation is given in (Fig. 3). As you seen in (Fig. 3), the first peak corresponds to the yield point (lower yield) at which branch damage was initiated. The second peak (upper yield) corresponds to maximum force (Fig. 3).
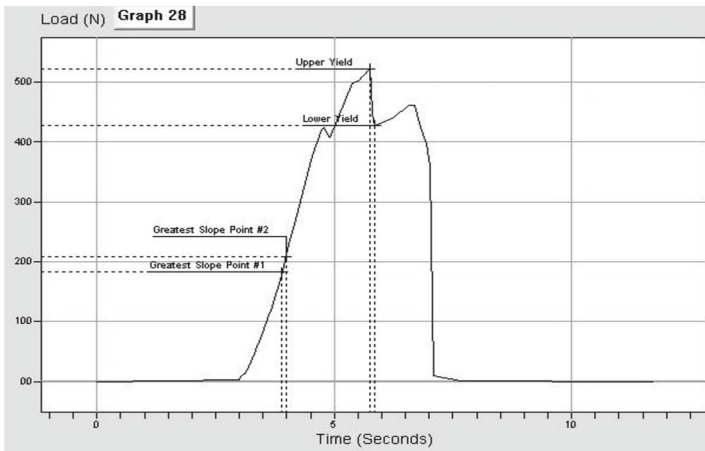
Fig. 3. Typical force-deformation curve.

The effect of knife type, knife cutting angle, and grape cane variety on shearing force are shown in (Fig. 4). The shear force was affected significantly ($P < 0.01$) by knife type, angle, and cane grape variety. The test results showed that the significant differences were found between the knife types at 1% probability level. While the maximum shear force values were measured at knife of serrated 1 (knife-edge thick) type as 429.14 N, there were no found significant differences between serrated 2 and flat-edge type knives. However, the lowest average value was observed at serrated 2 type knife as 382.77 N.

The effect of cutting angle also was found significant on the cutting force ($P < 0.01$). The cutting force slowly decreased with increasing knife-cutting angle from 0° to 40°.
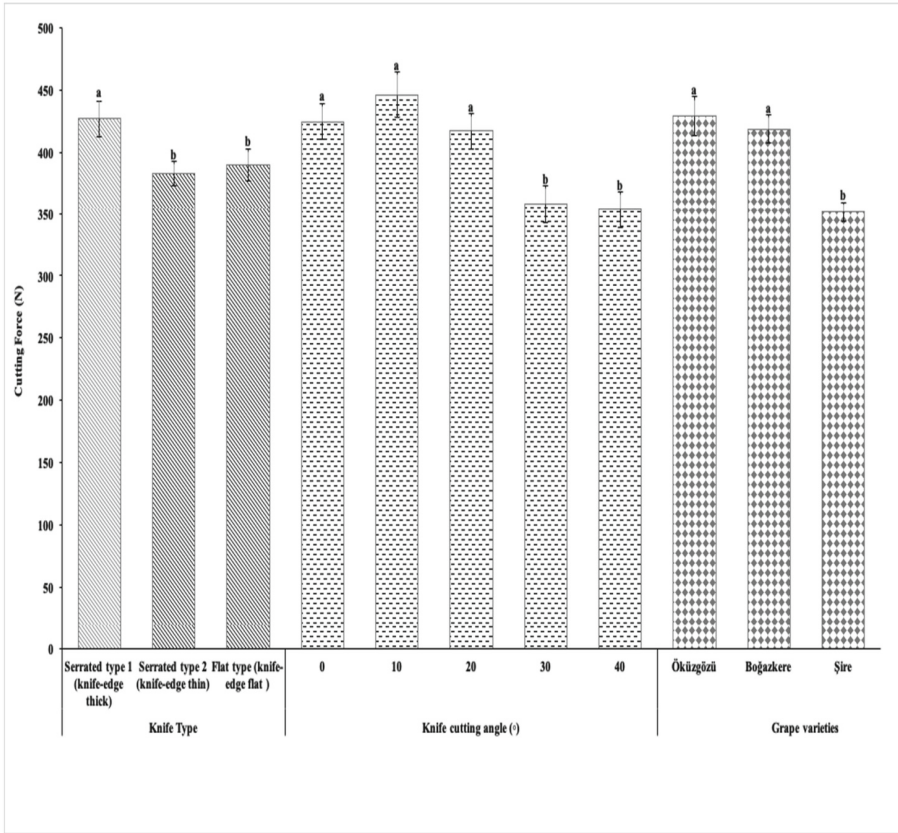
Fig. 4. The change of cutting force depend on knife type, knife cutting angle and grape variety.

The maximum cutting force was observed at 0° knife cutting angle as 426.90 N. The lowest values were obtained at 30° and 40° cutting angle. No significant differences were found among 20°, 30° and 40° cutting angle. The lowest values of cutting forces were obtained at 40° cutting angle as 353.30 N (Fig. 4). The similar results were observed by Kronbergs et al. [28], showing that the suitable knives bevel angle change between 25° and 45°. The decrease of cutting force and cutting energy depend on knife edge angle allows proper design of the cutting unit and cutting machine for grape cane and predicting the power requirements [9, 12, 13]. Our results consistent with result of Suryanto et al. [29], the knife edge angle has a significant effect on the cutting force and energy. Dowgiallo [30] also reported that besides the cutting edge, knife edge sharpness and knife speed are effect on cutting properties. Based on our results, the best results were obtained at 40° cutting angle. As a result, it can recommend and consider these values for a new design of shredding and construct a shear knife. This information is very valuable for selecting a suitable equipment design for reducing the energy requirement and consumption. Because, the selection of suitable cutting apparatuses and equipment

are playing an important role in economizing on cutting force and energy requirement [27].

In addition to these parameters, one of the important cutting parameters is the variety of biological materials. As seen in (Fig. 4), while there was not found a difference between Öküzgözü and Boğazkere variety, there was found significant differences between Şire variety and the other two varieties, Öküzgözü and Boğazkere. The highest cutting force requirement was obtained for Öküzgözü variety as 426 N at 50.24 mm^2 cross-section area and 50.30% moisture content, followed by Boğazkere and Şire variety.

When all interaction of Duncan test results is evaluated separately, the peak values of cutting force was observed at serrated 1 knife, 10° shearing angle and the cane of Öküzgözü grape variety as 669 N, the lowest value of cutting force was observed at flat-edge knife type, 40° cutting angle and the Şire grape variety as 205.50 N.

The values of the shearing strength are given in (Fig. 5) depending knife type, the cutting angle and varieties. As shown in the (Fig. 5), the effect of knife type, the cutting angle and variety were found significant on the cutting strength of grapevine canes (P < 0.01). The maximum cutting strength was obtained at serrated type 1 as 8.50 MPa. However, there was not found significant differences between the other knife types (Fig. 5). The cutting strength decreased with increasing knife-cutting angle from 0° to 40°. There were not found significant different statistically among 0°, 10° and 20°
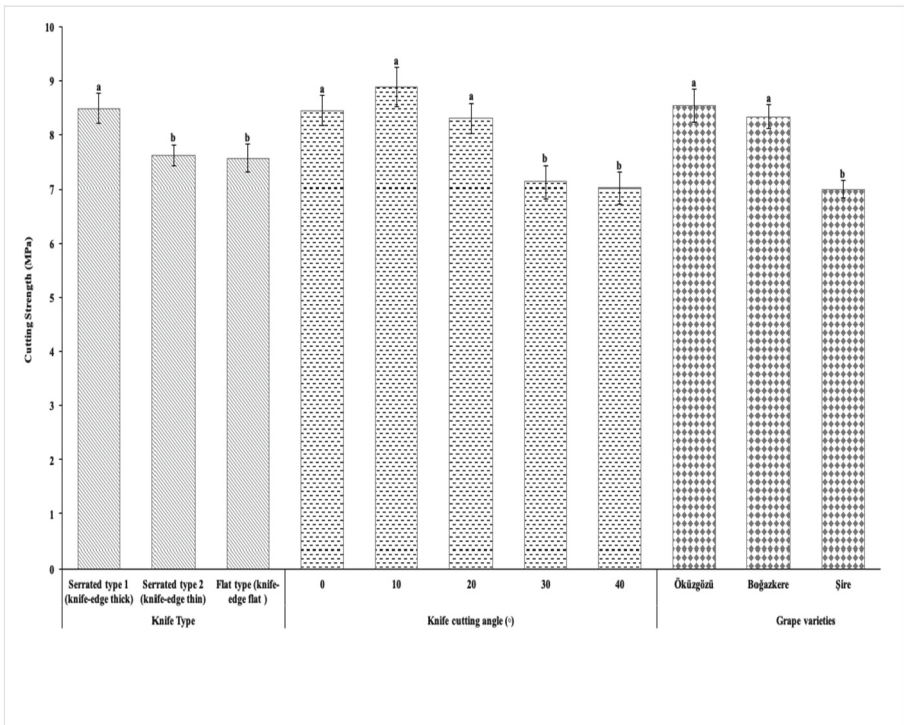
Fig. 5. The change of cutting strength depend on knife type, knife cutting angle and grape.

cutting angle. The maximum cutting strength were observed at 0°, 10° and 20° cutting angle as 8.45, 8.88 and 8.30 MPa, respectively. The lowest values were obtained at 30° and 40° cutting angle as 7.13 and 7.02 MPa, respectively (Fig. 5). When all interactions of statistical test results are evaluated together, the peak values of cutting strength were observed at serrated 1 knife, 10° cutting angle and the cane of Öküzgözü grape variety as 13.30 MPa, the lowest value of cutting force was observed at flat-edge knife type, 40° cutting angle and the Şire grape variety as 4.09 MPa.

Like the force values, while the maximum cutting strength dates was found the same at Öküzgözü and Boğazkere grape variety more than 8.00 MPa (Fig. 5), the lowest cutting strength values were obtained Şire variety as 7.00 MPa. As shown in the (Fig. 6), contrary to shearing force and shearing strength, when knife types are compared with each other in terms of cutting energy, the lowest energy values were obtained at serrated 1 type. However, there were not significant difference between serrated 1 and flat-edge type. The values were statistically the same. In terms of energy requirement, flat–edge type knife and serrated 2 (knife edge thin) knife type are more suitable than the serrated 1 (knife-edge thick) type. When the knife types are compared according to cutting energy, the flat edge type knife (shears) can be recommended than serrated type knife for a new design of pruning shears and pruning waste shredding machine for all variety grape
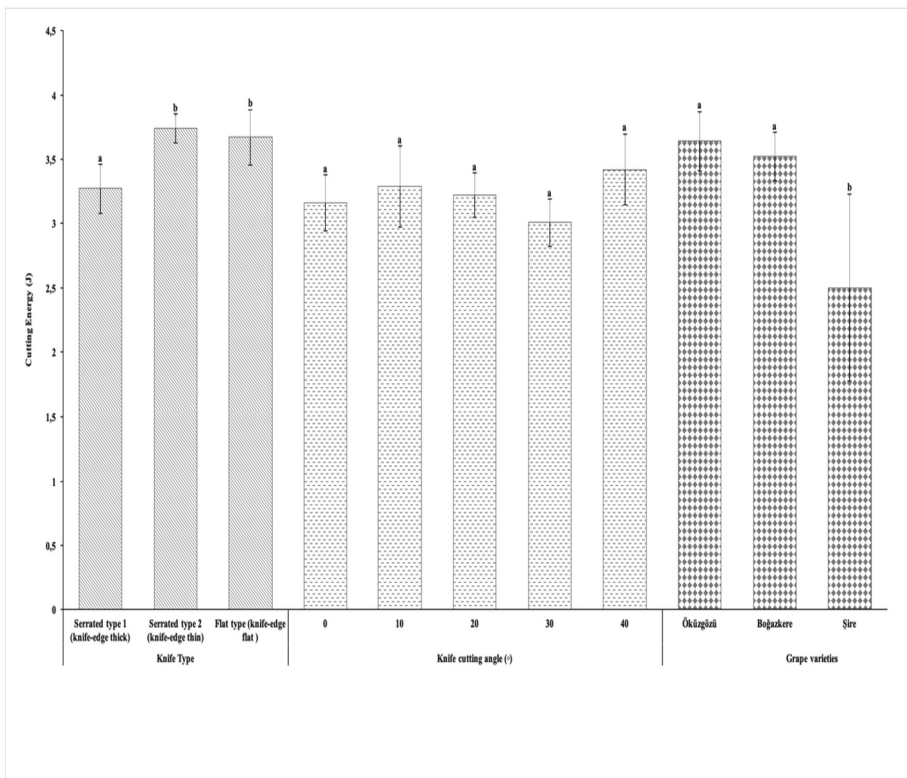
Fig. 6. The change of cutting energy depend on knife type, knife cutting angle and grape variety.

cane. The similar results were observed by Eliçin et al. [31], Sessiz and Ongoren [6]. Researchers have reported that blades with flat blades have lower energy consumption. In addition, they stated that energy consumption varies depending on the grape type and branch diameter. Besides that, the effect of cutting angle was found insignificant on cutting energy. The effect of all cutting angles was statistically the same.

When the specific energy requirement is compared according to variety, while the lowest specific energy value was obtained 2.50 J, there were not found differences between Öküzgözü and Boğazkere grape variety.

When all interactions of Duncan test results are considered, the peak values of cutting force were observed at serrated 1 knife, 10° shearing angle, and the cane of Öküzgözü grape variety as 669 N, the lowest value of cutting force was observed at Flat-edge knife type, 40° cutting angle and the Şire grape variety as 205.50 N.

The change of specific cutting energy depending on knife type, cutting angle and variety are shown in the (Fig. 7). As can be seen from figure, the lowest specific cutting energy value was observed at serrated types. The maximum specific cutting energy was obtained at flat-edge knife type. There were not found significant difference between
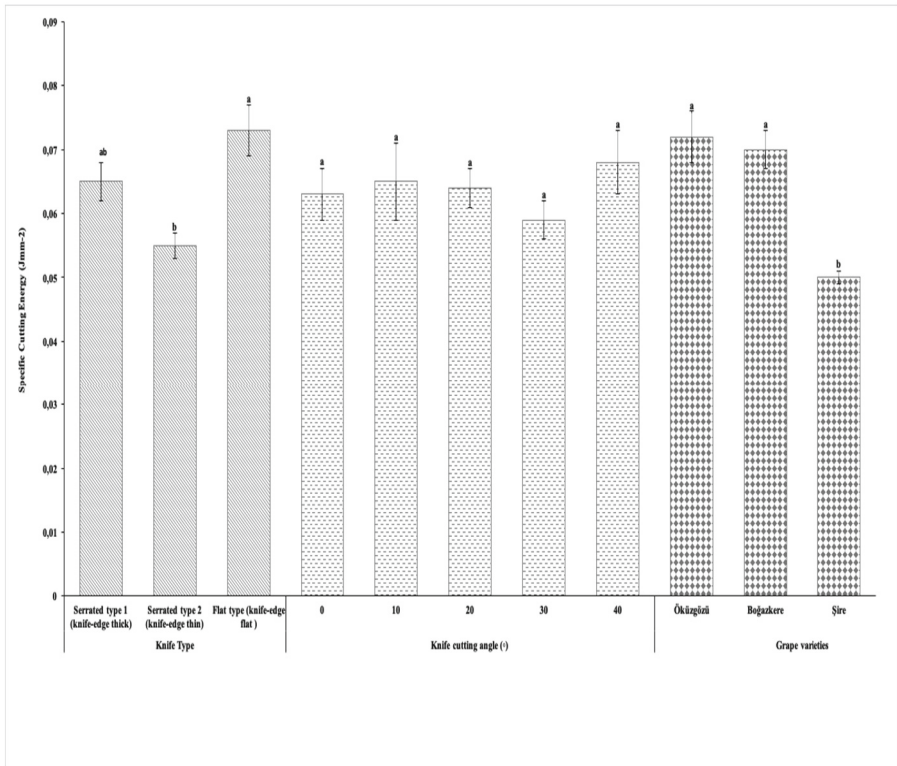
Fig. 7. The change of specific cutting energy depending on knife type, knife cutting angle and grape variety.

serrated 2 and flat-edge type knives. Also, the effect of cutting angle was not found significant on specific cutting energy. There were not found significant differences statistically among the all cutting angles. Also, there were not found significant differences between Öküzgözü and Boğazkere grape variety. While the lowest energy value was obtained 0.050 Nmm^{-2} at Şire grape, there were not found differences between Öküzgözü and Boğazkere grape.

According to all interaction of Duncan test results, the peak values of shearing force were observed at serrated 1 knife, 10° shearing angle, and the cane of Öküzgözü grape variety as 669 N, the lowest value of cutting force was observed at flat-edge knife type, 40° cutting angle and the Şire grape variety as 205.50 N.

4   Conclusion

The test results showed that there were significant differences between the knife types at 1% probability level. The maximum cutting force and strength values were obtained at knife of serrated 1 (knife-edge thick) type as 429.14 N and 8.50 MPa, respectively. The cutting force and strength decreased with increasing knife-cutting angle from 0° to 40°. The lowest values were obtained at 30° and 40° cutting angle. There were not found significant different statistically among 20°, 30° and 40° cutting angle. The highest force, strength, energy and specific energy requirement were obtained Öküzgözü variety, followed by Boğazkere and Şire variety. However, when all parameters were evaluated together, although there were some differences in terms of shear properties for all three varieties, similar results were obtained depending on selected parameters. Considering these data, it has been concluded that a suitable branch shredding machine can be designed for small-scale farmers and used for this purpose.

References

1. Uzun I, Bayır A (2010) Distribution of wild and cultivated grapes in Turkey. Not Sci Biol 2(4):83–87
2. Pekitkan FG, Çanakçı M, Esgici R, Sessiz A (2022) Determination of some cutting properties of different pruning wastes for use in the design of shredding machines. JOTAF/J Tekirdag Agric Faculty 19(2)
3. Morris JR (1993) Effects of mechanical pruning and mechanical shoot positioning on yield and quality of grapes. In: Proceedings of 2nd NJ Shaulis grape Symposium, Fredonia NY, pp 57–66
4. Morris JR (2000) Past, present, and future of vineyard mechanization. In: Proceeding ASEV 50 the Anniversary Annual Meeting, Seatle, WA, vol 51, pp 155–164
5. Sessiz A, Güzel E, Bayhan Y (2018) Bazı Yerli ve Yabancı Üzüm Çeşitlerinde Sürgünlerin Kesme Kuvveti ve Enerjisinin Belirlenmesi. Türk Tarım ve Doğa Bilimleri Dergisi (Turk J Agric Nat Sci) 5(4):414–423. https://doi.org/10.30910/turkjans.471203

6. Sessiz A, Ongören N (2022) Evaluation of the relationship between pruning waste shredding capacity and cutting properties for a shredder machine. Türk Tarım ve Doğa Bilimleri Dergisi 9(3):786–793
7. Persson S (1987) Mechanics of Cutting Plant Material. ASAE Publications, St Joseph
8. Taghijarah T, Ahmadi H, Ghahderijani M, Tavakoli M (2011) Shearing characteristics of sugar cane (Saccharum officinarum L.) stalks as a function of the rate of the applied force. AJCS 5(6):630–634
9. Nowakowski T (2016) Empirical model of unit energy requirements for cutting giant miscanthus stalks depending on grinding process parameters. Ann Warsaw Univ Life Sci – SGGW Agric (Agric Forest Eng) 67:63–70
10. Ghahraei O, Ahmad D, Khalina A, Suryanto H, Othman J (2011) Cutting tests of kenaf stems. Trans ASABE 54(1):51–56
11. Romano E, Bonsignore R, Camillieri D, Caruso L, Conti A, Schillaci G (2010) Evaluation of hand forces during manual vine branches cutting. In: International Conference Ragusa SHWA2010 - 16–18 September 2010. Ragusa Ibla Campus - Italy. Work Safety and Risk Prevention in Agro-food and Forest Systems
12. Ozdemir G, Sessiz A, Esgici R, Elicin AK (2015) Cutting properties of wine grape cultivars. Sci Papers Ser B, Hortic LIX:151–158
13. Esgici R, Ozdemir G, Pekitkan FG, Elicin AK, Ozturk F, Sessiz A (2017) Some engineering properties of the Sire grape (Vitis Vinifera L.). Sci Papers-Ser B-Horticulture 61:195–203
14. Pekitkan FG, Esgici R, Elicin AK, Sessiz A (2018) The change of shear force and energy of cotton stalk depend on knife type and shear angle. Sci Papers Ser A Agron LXI(1):360–366
15. Esgici R, Pekitkan FG, Ozdemir G, Guzel E, Sessiz A (2019) Cutting parameters of some grape varieties subject to the diameter and age of canes. Fresenius Environ Bull 28(1/2019):167–170
16. ASABE Standards (2008) S358.2. Moisture Measurement – Forages. American Society of Agricultural and Biological Engineers, St. Joseph, MI
17. Chattopadhyay PS, Pandey KP (1999) Mechanical properties of sorghum stalk in relation to quasi-static deformation. J Agric Eng Res 73:199–206
18. Yore MW, Jenkins BM, Summers MD (2002) Cutting properties of rice straw. In: Paper Number: 026154.ASAE Annual International Meeting/CIGR XVth World Congress
19. Chen Y, Gratton JL, Liu J (2004) Power requirements of hemp cutting and conditioning. Biosyst Eng 87(4):417–424
20. Kocabiyik H, Kayisoglu B (2004) Determination of shearing features of sunflower stalk. Int J Agric Sci 10(3):263–267
21. Ekinci K, Yilmaz D, Ertekin C (2010) Effects of moisture content and compression positions on mechanical properties of carob pod (Ceratonia siliqua L.). Afr J Agric Res 5(10):1015–1021
22. Zareiforoush H, Mohtasebi SS, Tavakoli H, Alizadeh MR (2010) Effect of loading rate on mechanical properties of rice (Oryza sativa L.) straw. Aust J Crop Sci 4(3):190–195
23. Voicu G, Moiceanu E, Sandu M, Poenaru IC, Voicu P (2011) Experiments regarding mechanical behaviour of energetic plant Miscanthus to crushing and shear stress. In: Engineering for Rural Development Jelgava, vol 26
24. Mohsenin NN (1986) Physical Properties of Plant and Animal Materials, 2nd edn. Gordon and Breach Science Publishers, New York, NY
25. O'Dogherty MJ, Huber JA, Dyson J, Marshall CJ (1995) A study of the physical and mechanical properties of wheat straw. J Agric Eng Res 62(2):133–142
26. Chandio FA, Changying J, Tagar AA, Mari IA, Guangzhao T, Cuong DM (2013) Comparison of mechanical properties of wheat and rice straw influenced by loading rates. Afr J Biotech 12(10):1068–1077
27. Sessiz A, Elicin AK, Esgici R, Ozdemir G, Nozdrovický L (2013) Cutting properties of olive cucker. Acta Technologica Agriculturae. Sci J Agric Eng J Slovak Univ Agric Nitra 16(3):80–84

28. Kronbergs A, Širaks E, Kronbergs AE (2011) Mechanical properties of hemp (cannabis sativa) biomass. In: Environment, Technology, Resources. Proceedings of the 8th International Scientific and Practical Conference, vol 1, pp 184–190
29. Suryanto H, Ahmad D, Yahya A, Akande FB, Syahrita K (2009) Cutting tests of oil palm empty fruit bunches. Trans ASABE (Am Soc Agric Biol Eng) 52(3):723–726
30. Dowgiallo A (2005) Cutting force of fibrous materials. J Food Eng 66(1):57–61
31. Eliçin AK, Sessiz A, Pekitkan FG (2019) Effect of various knife type, cutting angle and speed on cutting force and energy of grape cane. Avrupa Bilim ve Teknoloji Dergisi (Eur J Sci Technol) (15):519–525

The Effect of Different Tillage Methods on Plant Emergence Parameters for Wheat

Zeliha Bereket Barut and Serkan Ozdemir[✉]

Faculty of Agriculture, Department of Agriculture Machinery and Technologies, Cukurova University, Adana, Turkey
cansa.serkanozdemir@gmail.com

Abstract. Conventional tillage; it is an application where most of the plant residues are buried or burned under the ground, and the plant residues on the soil surface are less than 15% after planting. With the environmental awareness that developed after the 1970s, alternative methods have been developed that minimize the field traffic and soil tillage without overturning it. In this method, which is defined as conservation tillage, the main criterion is that the field surface is covered with at least 30% plant residue. Reduced tillage forms the subgroup of conservation tillage. In this system, chisel or disc tools are generally used for primary tillage, harrow disc or cultivators are used for secondary tillage and seedbed preparation. In tillage application, no-tillage is done before planting after the previous crop harvest. Sowing is done directly on the previous crop stubble without seedbed preparation. In this research; no-tillage (direct seeder), reduced tillage (rototiller) and conventional (moldboard plow + disc harrow + roller) tillage methods were tested in terms of plant distribution and plant emergence uniformity. The mean emergence date, emergence rate index and percentage of emergence values were calculated for that. In the research, the best mean emergence time value was determined in the reduced tillage method with 15.18 days, the highest emergence rate index and percentage of emergence value were determined in the conventional tillage method with 20.7 plants/day m^2 and 70.4%, respectively.

Keywords: Conventional tillage · Conservation tillage · Sustainable agriculture · No-tillage

1 Introduction

From past to present, the losses and problems of soil and water resources caused by human factors based on agriculture have led researchers to new searches all over the world. Many studies have been carried out by researchers for many years to protect and ensure the sustainability of these resources, which are of vital importance for future generations. [1–3]. Although there are different classifications in the world today, tillage methods are generally evaluated under two main headings: conventional tillage and conservation tillage, according to the previous crop plant residues left on the soil surface.

Conventional tillage: it is the soil tillage method with the highest field traffic. It is a tillage method in which a large part of the plant residues are buried underground

and the plow is often used (Fig. 1). Processing the soil by conventional methods by creating intense field traffic greatly triggers soil compaction and erosion [4]. Our soils are damaged by significant degradation in the short and long term. It is of great importance to develop and disseminate a conventional method instead of this unsustainable method, which consumes more time, labor and energy. Methods that minimize field traffic and tillage the soil without turning it over have been developed in this application [5–7]. The conservation tillage method is examined under five headings; strip tillage, plant-tillage, mulch-tillage, reduce-tillage and no-tillage are the methods.

Fig. 1. Conventional tillage application (all plant residues on the soil surface after sowing are buried)

Reduced tillage, which is a subgroup of conservation tillage; in this method, chisel or disc tools are generally used for primary tillage and disc tools or cultivators are used for secondary tilalge and seed bed preparation. It provides significant fuel and energy savings compared to conventional tillage due to less machine traffic (Fig. 2).

Fig. 2. Reduce tillage application (superficial is processed and the stubble remains on the soil surface)

No-tillage method, which will be compared as an alternative to conventional tillage in the research; In planting, after the harvest of the previous crop, no soil tillage is

done before planting. In other words, planting is done directly on the previous crop stubble without any seed bed preparation. No-tillage improves the structure of the soil and maintains soil moisture (Fig. 3). Plant residues on the soil surface are of great importance in terms of soil protection [8]. It largely prevents wind and water erosion even if there are very few plant residues on the soil surface.

Fig. 3. No-tillage application (plant residues on the soil surface after sowing are more than 80%)

Research was conducted to compare technically and economically the conservation tillage and planting systems applied in wheat agriculture in the Çukurova Region. As a result of the evaluations, the highest wheat yield was obtained in the reduced tillage method, while the lowest yield was obtained in the two-row sowing method. The lowest value in terms of time and fuel consumption among the methods; Additionally, the highest value in terms of work efficiency was obtained in the no-tillage method. The no-tillage method provides savings of approximately 81–86% compared to other methods in terms of time consumption, fuel consumption and work efficiency [9].

A study was conducted to compare the technical and economic aspects of conventional tillage and conservation tillage and planting practices for second crop silage corn in the Çukurova Region. In this research, the fuel consumption and work efficiency of the machines, percentage of emerge, emergence rate index and mean emerge date were tested. The best results in terms of emergence rate index (1.63 day/m^2) were observed with conventional tillage. The best results in terms of percentage of emerge (%100) were observed with conventional tillage. As a result, the highest corn green grass yield was obtained in the stubble tillage method. Among the applications, the lowest fuel consumption and highest work efficiency were obtained in the no-tillage method. The no-tillage method provides savings of approximately 85–92% in terms of fuel consumption and work efficiency compared to other methods [10].

No-tillage and conventional tillage methods have been investigated in second crop sunflower agriculture. As a result of the research, the shortest average germination time was 6.55 days in no-tillage, while the longest germination time was 7.87 days in the conventional method. While germination was lowest in the conventional method with 88.63%, it was highest in no-tillage with 96.29% [11].

In a study comparing reduced tillage and direct sowing techniques with conventional tillage methods in wheat (Tritucum aestivum L.) production. In order to determine the

effect of tillage systems on the soil, their effects on bulk denstiy, penetration resistance and organic matter were also determined. The results found that the effects of tillage methods on soil bulk weight, penetration resistance and organic matter content were significant [12].

In a study, three different applications were used in wheat production. These are conventional tillage, reduced tillage and no-tillage practice. The effects of the applications on the penetration resistance of the soil, total fuel consumption, plant output values and yield were evaluated. The highest total fuel consumption (5.15 l/da) was obtained in the conventional tillage application and the lowest (0.91 l/da) was obtained in the no-tillage application [13].

Six different tillage systems, including conventional tillage and conservation tillage, were tested in this research. Bulk density, aggregate stability, organic matter content and soil penetration resistance were evaluated as indicators of soil quality in this study. Accord¬ing to the results of the research, conservation tillage systems (no-tillage) improved soil organic carbon content and aggregation stability. Different tillage systems showed a significant effect on the amount of organic matter and aggregate stability in the soil. Organic matter values were lower (49–60%) in conventional applications and residue burning accelerated the loss of organic carbon content. The highest aggregate stability values were found for no-tillage (38%). Penetration resistance and bulk density of plowed soils were lower than that of uncultivated plots, while heap density was 1.26–1.32 g at all soil depths in conventional tillage. As a result of their experiments, it has been shown that conservation tillage practices can provide better soil characteristic values than conventional practices in soils of the Adana region [14].

In the studies reviewed, the advantages of reduced tillage and no-tillage compared to conventional tillage can be listed as follows;

- Prevents wind and water erosion
- Protects and increases the amount of organic matter
- Reduces moisture loss in the soil
- Field traffic is minimized
- Sustainable yield
- It saves time
- Less fuel consumption occurs and saves energy
- Better plant emergence parameters
- It prevents the fatal damage caused by burning stubble to living things [15].

The studies examined show that; global warming, which means the continuous increase in the Earth's temperature due to the greenhouse effect, has disrupted the agricultural ecosystem and caused unexpected changes in agricultural climate elements such as drought, temperature, precipitation, weather events and sunlight. In terms of agricultural production, these negative changes lead to a decrease in product yield and quality, a decrease in soil fertility, an increase in soil erosion due to heavy rainfall, and an increase in diseases and pests. It is an important known problem of today that climate change increases the fluctuation in agricultural production and harms agricultural production in general. Therefore, considering the food security of the ever-increasing world population, it is extremely important to create sustainable agricultural production systems that will reduce greenhouse gas emissions, are resistant and sensitive to climate change,

and develop technological and innovative agricultural production methods. The advantages of conservation tillage methods are quite obvious. Conservation tillage methods are essential to maintain sustainability.

In this research, the conventional tillage method, reduced tillage and no-tillage methods applied in wheat agriculture were compared in terms of emergence uniformity parameters.

2 Methods

A field study was performed at the Çukurova üniversity, in the Mediterranean coastal plain of Turkey between 2019 and 2020. The site is located near Adana. The Mediterranean region has hot and arid summers and mild, rainy winters. The average annual rainfall was 625 mm; average annual temperature, 19 °C and average annual humidity, 67% (from 46% in October to 80% in August). The experiment was carried out on a clay soil, which was classified as a Typic Haploxerert. The soil consisted of 47% clay, 30% silt and 23% sand. Winter wheat (Triticum aestivum L.) were planted in 12×40 m trial plots using a completely randomized block design with three replications. In the study, three different tillage methods consisting of conventional tillage, reduce tillage, no-tillage (Fig. 4). Equipment used in conventional tillage; moldboard plow, disc harrow (two times), roller (two times) and seeder. Equipment used in reduce tillage; rotatiller with roller and seeder. Equipment used in no-tillage; direct seeder.

Fig. 4. Trial plots

In field trials, daily plant emergence after wheat planting and the distance between successive plants in the same row were measured when emergence was fixed. Emergence uniformity was determined using a 1m2 iron circle in measurements made on random sample rows after planting (Fig. 5).

Plant counts started with the first plant emergence and continued at the same time every day until plant emergence stabilized. With these counts, mean emerge date (MED), emergence rate index (ERI) and percentage of emerge (PE) values were calculated. Mean emerge date is the average emergence time of emerging plants until plant emergence stabilizes. Emergence rate index is the number of plants emerging per day per unit length. Percentage of emerge is the ratio of the number of plants germinating per day per unit

Fig. 5. Taking samples for emergence uniformity

length to the number of seeds planted per unit length. These parameters were calculated with the following equations [16].

$$MED = \frac{G_1B_1 + G_2B_2 + \cdots + G_nB_n}{B_1 + B_2 + \ldots + B_n}, \quad PE = \frac{Nb}{N}, \quad ER\dot{I} = \frac{Nb}{MED}$$

MED: Mean emerge date (day)
ERI: Emergence rate index (plant/day)
PE: Percentage of emerge (%)
B: Number of young plants emerging since the previous census.
G: Number of days after planting
Nb: Number of plants per unit length (plant/m^2)
N: Number of seeds planted per unit length (seed/m^2).

3　Results

In the field trials of the research, the best mean emerge date (15.18 day) was observed in reduced tillage. The longest mean emerge date (16.53 day) was determined in the conventional tillage method with (Fig. 6). Since conservation tillage methods have more plant residue on the field surface than conventional tillage methods, they provide higher soil moisture and plant emergence is observed in a better time. These results agreed with those obtained by Bayhan [11].
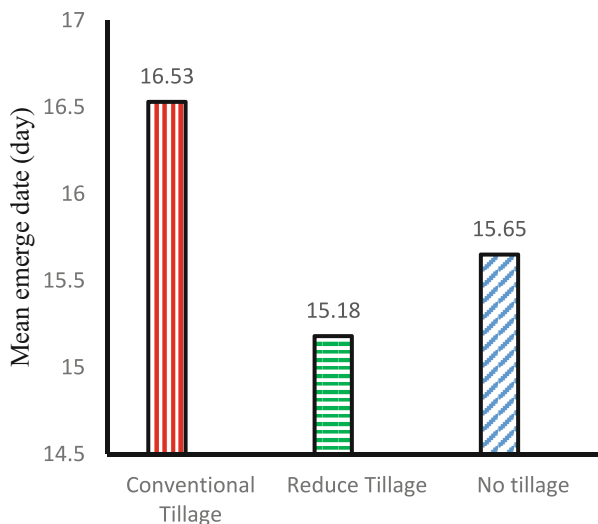
Fig. 6. Mean emerge date values (day)

The best results in terms of emergence rate index (20.7 day/m^2) were observed with conventional tillage (Fig. 7). Similar results were obtained with the research conducted by Karaağaç and Barut [10].
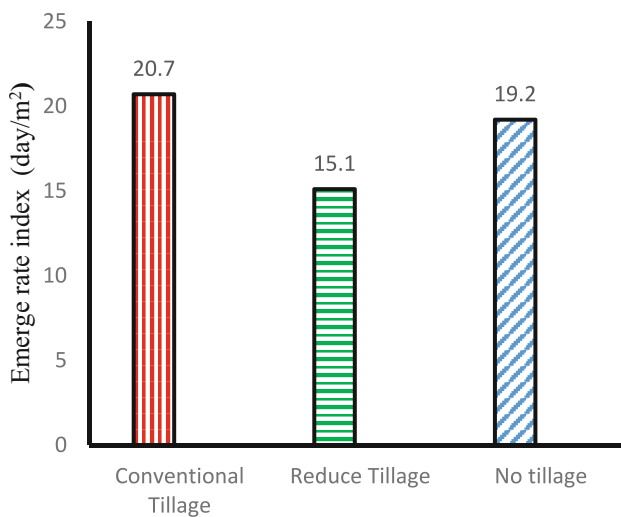
Fig. 7. Emerge rate index values (day/m^2)

When the percentage of emerge (70.4%) were examined in the research, the best results were determined in conventional tillage (Fig. 8). In conventional tillage, the field is tilled many times to prepare a good seed bed. This provides better plant emergence.

In the conservation tillage method, field traffic is minimal. Therefore, lower short-term outputs are achieved. In addition, intensive field traffic in conventional tillage increases input costs significantly, so the conservation tillage method is thought to be a more profitable application. Similar results were obtained with the research conducted by Karaağaç and Barut [10].
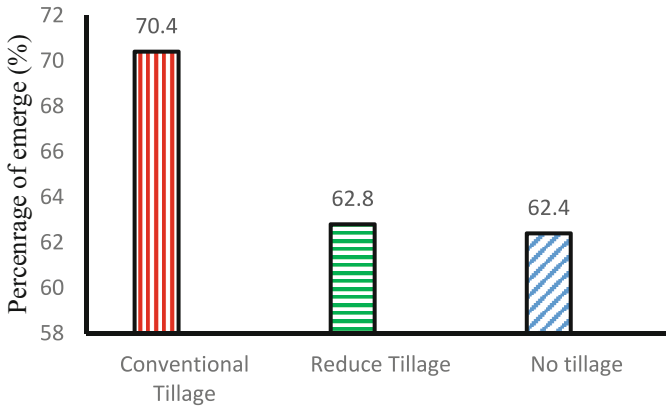
Fig. 8. Percentage of emerge values (%)

4   Conclusion

In this research, conventional tillage method, no-tillage and reduced tillage were tested in terms of emergence uniformity parameters. As a result of this trial, different tillage methods were compared by calculating the mean emerge date, emergence rate index and percentage of emerge values. In the research, the best mean emerge date was determined in the reduced tillage method, while the highest emergence rate index and percentage of emerge value were determined in the conventional tillage method. Soils damaged by intensive tillage applied in conventional tillage, reduce tillage can be an alternative treatment method compared to other tillage methods in wheat production, in terms of uniformity parameters and input costs. It is recommended to develop and investigate an efficient method that can be applied in reduced tillage method.

References

1. Barut ZB (2006) Ekim Makinaları, Ed. Serdar Öztekin Tarım Makinaları 2. Nobel Kitapevi. s.408, Adana
2. Barut ZB, Çelik İ (2009) Tillage effects on soil quality indicators in the semi- arid mediterranean coastal plain of Turkey. Philipp Agric Scientist 92(3):290–300
3. Choudhury SG et al (2014) Tillage and residue management effects on soil aggregation organic carbon dynamics and yield attribute in rice–wheat cropping system under reclaimed sodic soil. Soil Tillage Res 136:76–83

4. ASABE (2013) Terminology for Soil Engaging Components for Conservation. ASABE Standards S477:364–369
5. Köller K (2003) Conservation tillage-technical, ecological and economic aspects. Koruyucu Toprak İşleme ve Doğrudan Ekim Çalıştayı İzmir. Ss.9–34:23–24
6. Hobbs PR, Gupta RK (2004) Problems and challenges of no-till farming for the rice–wheat systems of the Indo-Gangetic plains in South Asia. Sustain Agric Int Rice-Wheat Syst
7. Özdemir S, Barut ZB (2022) Türkiye'de Şeritvari Toprak İşleme ve Ekim Uygulamalarının Durumu. Tarımsal Mekanizasyonlar ve Enerji Üzerine Güncel Araştırmalar. 2:173–185
8. Korucu T (2011) Anız Yakmaya Alternatif Çözüm: Korumalı Toprak İşleme. KSÜ Çiftçi Köşesi Web sayfası. http://www.gencziraat.com/Toprak-Bilgisi/Aniz-Yakmaya-Altarnatif-cozum-Korumali-Toprak-isleme-10.html
9. Aykanat S, Karaağaç HA, Barut H, Sevilmiş U (2019) Farklı Toprak İşleme ve Ekim Yöntemlerinin Buğdayda Bazı Agronomik Özellikler Üzerine Etkisi. Uluslararası Doğu Akdeniz Tarımsal Araştırma Enstitüsü Dergisi. 2(2):136–144
10. Karaağaç HA, Barut ZB (2007) İkinci Ürün Silajlık Mısır Tarımında Farklı Toprak İşleme ve Ekim Sistemlerinin Teknik ve Ekonomik Yönden Karşılaştırılması. Çukurova Üniversitesi Ziraat Fakültesi Tarım Makineleri Anabilim Dalı Adana. 3(1):33–40
11. Bayhan Y (2015) İkinci ürün ayçiçeği tarımında doğrudan ekim olanaklarının araştırılması. Tekirdağ Ziraat Fakültesi Dergisi. 12(1):110–118
12. Yalçın H et al (2010) Ege Bölgesi'nde buğday ve arpa üretiminde koruyucu toprak işleme ve doğrudan ekim sistemleri. Bitkisel Araştırma Dergisi. 2:8–16
13. Marakoğlu T, Çarman K (2008) Buğday üretiminde azaltılmış toprak işleme ve direk ekim uygulamaları. Selcuk J Agric Food Sci 22:46
14. Barut ZB, Celik I (2010) Different tillage systems affect plant emergence, stand establishment and yield in wheat-corn rotation. Philipp Agric Scientist 93(4):392–398
15. Kassam A, Friedrich T (2012) An ecologically sustainable approach to agricultural production intensification: global perspectives and developments. J Field Actions Sci Rep Special Issue (6):1–6
16. Erbach DC (1982) Tillage for continue corn and Soybean rotation. Trans ASAE 25(4):906–911

Design Approaches of One-Pass Strip-Till Machines

Zeliha Bereket Barut and Serkan Ozdemir[✉]

Faculty of Agriculture, Department of Agriculture Machinery and Technologies, Cukurova University, Adana, Turkey
cansa.serkanozdemir@gmail.com

Abstract. All over the world and in our country, the increasing awareness on the conservation of soil and water resources, together with the demands of reducing production costs, made it necessary for researchers to turn to alternative production ways in agriculture. As a result of these searches, it has been revealed that conservation tillage methods should become widespread as an alternative to traditional tillage method, where field traffic and fuel consumption are high, and environmental effects such as carbon emissions, soil degradation and air pollution. Despite years of research and government support, no-tillage, which is one of the sustainable agricultural practices and applied on an area of approximately 200 million hectares in the world, has unfortunately not been sufficiently adopted in Türkiye. Strip-tillage, which creates a soil environment that enhances seed germination, is a new alternative to no-tillage in areas where poorly drained soils are dominant. In this context, the strip tillage and sowing method is a combination of traditional and no-tillage methods and provides both environmental and economic benefits by saving time, labour and fuel as an alternative to the traditional method. Where soil moisture conditions are suitable, strip-tillage creates narrow-width tilled strips, traditionally in the fall, to increase early spring soil evaporation and soil temperature in the top 5 cm of the soil. When the previous studies on sowing with strip tillage are examined, it is seen that it is frequently applied in countries where agriculture is developed in the world, but there is not enough research and application area in Türkiye. In countries where agriculture is developed, it is seen that the strip tillage and sowing method is applied as a combination of two separate machines in a one-pass (tillage and sowing). In the studies carried out in Türkiye (strip tillage and sowing), it is applied separately in two stages. Both sowing application and strip-tillage can be performed in one-pass. The basic requirements for strip-tillage to be effective are accuracy in matching tillage equipment on the tool bar with the planter and placement of seeds in the tilled zones. In this study, an in-row of pneumatic spacing drill, mounted on a single chassis that can reduce the field traffic to a one-pass, is designed and simulated.

Keywords: Strip tillage · Conservation tillage · Sustainable agriculture

1   Introduction

Global warming, which means the continuous increase in the Earth's temperature due to the greenhouse effect, has disrupted the agricultural ecosystem and caused unexpected changes in agricultural climate elements such as drought, temperature, precipitation, weather events and sunlight. In terms of agricultural production, these negative changes lead to a decrease in product yield and quality, a decrease in soil fertility, an increase in soil erosion due to heavy rainfall, and an increase in diseases and pests. It is an important known problem of today that climate change increases the fluctuation in agricultural production and harms agricultural production in general. Therefore, considering the food security of the ever-increasing world population, it is extremely important to create sustainable agricultural production systems that will reduce greenhouse gas emissions, resistant and sensitive to climate change, and develop technological and innovative agricultural mechanization tools and machines. Moreover, the search for new sustainable production systems that protect natural resources such as soil, water and air in agricultural production has accelerated. As a result of these searches, alternative conservation tillage to traditional tillage and the development of new tools and machines to be used in this process come to the fore. Conservation tillage is a practice in which the soil surface is covered with at least 30% of the pre-plant residues after planting, in order to reduce water and wind erosion along with soil moisture loss [1, 2]. The main purpose of conservation tillage is to keep pre-crop residues on the field surface and reduce tillage intensity. The main problems of today's world are drought and limited water resources, so it is important to ensure the preservation of in-soil water and moisture. Since plant residues cover the soil surface and block sunlight, humidity rates are higher than in parcels without plant residues [3, 4]. In areas where the soil is intensively and continuously cultivated, soil degradation caused by soil preparation is clearly visible.

Strip tillage method is a conservation tillage method in which 30%-40% of the field surface is allowed to be cultivated before planting for seed bed preparation. In this practice, soil tillage is mostly done together with planting, but it is also known to be done before planting. A 10 to 40 cm wide band that overlaps the sowing row line is processed (Fig. 1). Apart from this, the remaining rows are left unprocessed, covered with stubble. Therefore, the method can be perceived as a mixture of reduced tillage and no tillage method [5].

In multi-year field experiment, the soil properties after application of one-pass strip tillage technology for 8 years were compared to those of soil under conventional tillage with the use of a moldboard plough to a depth of 20 cm, and equally deep loosened and reduced tillage. A field experiment of these three treatments was performed. A total of 44 features were examined that described the physical, chemical, biological, and biochemical soil properties in the 0–20 cm layer, and penetration resistance, bulk density and soil moisture in the 25–30 cm layer. The influence of the one-pass strip tillage technology on the yield of crops was also determined. Multivariate analysis shows that the one-pass strip tillage technology method, in terms of affecting the soil properties, differs considerably from reduce tillage and conventional tillage treatments. The soil after the one-pass strip tillage technology method contained two- to four-fold more earthworms, with a mass 2- to fivefold higher, than those in the soil following reduce tillage and conventional tillage respectively [6].

Fig. 1 Strip tillage system

In the study, Mzuri Pro-Til, a combined strip tillage planting machine, was tested. They made an evaluation of the effect of the strip tillage method on soil properties and the effects of crop cultivation. Scientific observations and field trials were carried out in Poland, Ukraine, Lithuania, the Czech Republic, Slovakia, the eastern states of Germany, Belarus, Serbia and Romania. Compared to traditional tillage, soil moisture, organic carbon content, infiltration, number of microorganisms and worms, and organic activity were found to be higher, especially during periods of lack of rainfall. It has been shown that the strip tillage method provides fuel savings of 20–30 L/ha compared to reduced and conventional tillage methods, respectively, and is successful in terms of plant emergence and product yield. Increasing tillage intensity increased soil CO_2-C fluxes and bacterial populations, but decreased fungal populations. In the research, they stated that strip tillage will be the key element in conservation agriculture [7].

It compared one-pass strip tillage (combined strip tillage plus seeder), conventional tillage and reduced tillage methods in an 8-year field trial. In this research, a total of 44 properties describing the physical, chemical, biological and biochemical properties of the soil in the 0–20 cm layer and the penetration resistance, bulk density and soil moisture in the 25–30 cm layer were examined. Statistically, significant differences were detected in the strip tillage method compared to the reduced and conventional method. In the strip tillage method, the phosphorus and available potassium content, the total number of bacteria, cellulolytic microorganisms and fungi, and the activity of phosphatases were significantly higher. It reduced and found two to four times more earthworms than conventional tillage. The yield of winter rapeseed and wheat grown with strip tillage was found to be higher than the conventional and reduced method [8].

Strip tillage applied in sugar beet (*Beta vulgaris* L.) production compares conventional tillage and dirno tillage methods. It was determined that strip tillage caused less soil erosion and retained more moisture than conventional tillage. Compared to the no tillage method, it has been shown that there is better seedbed preparation, optimum fertilizer placement, more carbon sequestration and less fuel consumption. It has been

stated that the strip tillage method is a more profitable alternative method compared to no tillage and the conventional method, considering efficiency and input costs [9].

In the research, three different strip widths were created by changing the connection of three different milling (rotor) blades on the flanges and were tested comparatively with the conventional tillage method. They compared three strip tillage methods and one conventional method with strip widths of 22.5, 30.0 and 37.5 cm on CO_2-C flux, bacterial and fungal populations during sunflower growth. They identified significant differences in CO_2-C fluxes, microbial populations, soil bulk weight and total porosity between different tillage systems. The highest CO_2-C fluxes during the flowering and harvest periods were in the conventional method, and the lowest values were observed in the 22.5 cm strip spacing [10].

When the studies on strip tillage are examined, the main reasons why strip tillage method is gaining more and more importance in agricultural production are as follows: It can be listed as providing a good seed bed preparation on stubble soil, providing in-soil water and moisture conservation, soil protection against erosion, reducing carbon dioxide emissions into nature, saving fuel consumption by limiting the number of tractor passes in the field, low cost and high yield potential [11–13]. It is seen that it is frequently applied in developed countries, but in our country, this method is not applied sufficiently on a producer basis and sufficient research has not been done. With this research, it is aimed to design and develop a lightweight one-pass strip tillage planting machine unit that can be applied under Türkiyeconditions.

2 Methods

The study was articulated in two parts. The first step consisted of reviewing the literature about strip tillage method, comparing one-pass and two-pass. Literature about one-pass strip tillage technology has been revised through a targeted search on scientific journals databases, such as Science Direct, Applied Engineering in Agriculture, Soil and Tillage Research, and Asabe. A keyword-based search was used to identify articles, using the following keywords: Strip tillage* OR one-pass technology* OR conservation tillage* OR reduce tillage*. In the second step of the research, the designs and simulation studies of the one-pass strip tillage planting machine unit planned to be developed were carried out at Çukurova University Faculty of Agriculture, Department of Agricultural Machinery and Technologies Engineering.

3 Results

Nowadays, strip tillage and planting practices are carried out in two different ways: one-pass and two-pass. In two-pass; first, strip tillage cultivation (Fig. 2) is carried out, and then the processed strips are planted with a normal planting machine (Fig. 3).

Fig. 2 Strip tillage machine

Fig. 3 Spacing drill

There are two types of strip tillage machines commonly used in two-pass strip tillage. These consist of different unit combinations that process the band on the planting line before planting. The strip tillage machine with chisel tines, which works by tearing the soil and forming a narrow band, is one of the most commonly used combinations of this combination (Fig. 4). Soil processor elements consist of stubble cutting disc, scratch cleaners, chisel tines and roller units.

Fig. 4 Strip tillage machine with Chisel tines unit

Another commonly used type of strip tillage is the machine that processes the soil by creating a wider band with the rototiller unit, the active parts of which consist of the soil milling machine (Fig. 5).

It is seen that in countries where agriculture is developed, strip-tillage and planting method is applied as a combination of two separate machines in a one-pass (tillage and planting) (Fig. 6 and Fig. 7). Compared to the two-pass method, field traffic is minimized, providing less fuel consumption and less soil compaction [6].
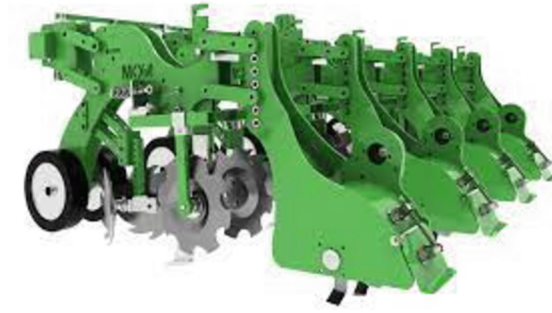
Fig. 5 Strip tillage machine with rototiller unit

Fig. 6 One-pass strip tillage machine combination

Fig. 7 Another one-pass strip tillage machine combination

Combined strip tillage machines used in a one-pass are very heavy types, have high production costs and require high traction power. A one-pass strip tillage planting machine unit suitable for use by farmers and producers in our country's conditions was designed in this research (Fig. 8). The designed unit consists of planter arrangement and soil processing organs (stubble cutting disc, chisel tines and roller) mounted on a single chassis.
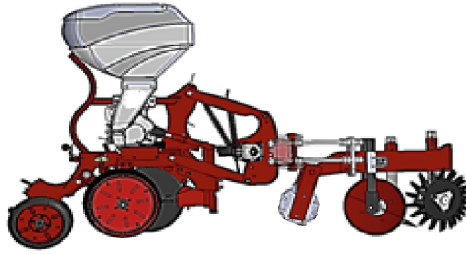
Fig. 8 Preliminary work of the designed one-pass strip tillage planting machine unit

Designed one-pass strip tillage planting machine unit may have toothed discs at the front that loosen the soil strip and break up the stubble on the surface. These discs can also be equipped with scratch removers. Chisel type tines, capable of deep processing, placed behind the stalk shredder and soil loosening discs, cut long plant residues after harvest and push them between the rows. Chisel tines with replaceable wings at the bottom prevent moist soil from drying out quickly, clumping and crusting by deeply loosening a narrow strip of soil without raising it to the field surface. Mineral fertilizer applicator can be mounted behind the chisel tines.

4 Conclusion

Research on conservation tillage methods shows that strip tillage methods are becoming increasingly important in agricultural production. In this research, one-pass and two-pass methods applied in strip tillage methods were examined. Although two-pass methods are common, tillage and planting in a one-pass will minimize field traffic. With this study, a strip tillage planting machine unit was designed to be applied in a one-pass, which will provide environmental, economic and social benefits to farmers, who are the end users within the scope of sustainable agricultural practices. As a result, the one-pass strip tillage unit will directly contribute to agriculture and the environment, and will benefit the country's economy with reduced fuel consumption, reduced input costs and reduced time consumption. It is estimated that this study will reduce the carbon footprint and prevent stubble burning, which is one of the important problems of the country. In the continuation of the research, it is recommended to evaluate, design and develop the strip tillage planting machine as a whole.

References

1. ASABE: Terminology for soil engaging components for conservation. ASABE Standards S477, pp. 364–369 (2013)
2. Barut, Z.B., Makinaları, E., (Ed.): Serdar Öztekin Tarım Makinaları 2. Nobel Kitapevi. s.408, Adana (2006)
3. Klocke NL, Currie RS, Aiken RM (2009) Soil water evaporation and crop residues. Trans of ASABE 52(1):103–110
4. FAO: http://www.fao.org/ag/ca/. Basic principles of conservation agriculture. Erişim tarihi: Kasım (2015)

5. Özdemir S, Barut ZB (2022) Türkiye'de Şeritvari Toprak İşleme ve Ekim Uygulamalarının Durumu. Tarımsal Mekanizasyonlar ve Enerji Üzerine Güncel Araştırmalar. 2:173–185
6. Jaskulska, I., et al.: Soil properties after eight years of the use of strip-till one-pass technology. Argonomy (2020)
7. Jaskulska I, Jaskulski D (2020) Strip-till one-pass technology in central and Eastern Europe: a Mzuri Pro-Til hybrid machine case study. Agronomy 10:925
8. Tabatabaeekoloor R (2011) Soil characteristics at the in-row and inter-row zones after strip-tillage. Afr J Agric Res 6:6598–6603
9. Overstreet FL (2009) Strip tillage for sugarbeet production. Int. Sugar J. 111:292–304
10. Bilen S, Çelik A, Altıkat S (2010) Effects of strip and full-width tillage on soil carbon IV oxide-carbon (CO2-C) fluxes and on bacterial and fungal populations in sunflower. African J. Biotechnol. 9(38):6312–6319
11. Farmaha BS, Fernández FG, Nafziger ED (2011) No-till and strip-till soybean production with surface and subsurface phos-phorus and potassium fertilization. Agron J 103(6):1862–1869
12. Benincasa P, Zorzi A, Panella F, Tosti G, Trevini M (2017) Strip tillage and sowing: is precision planting indispensable in silage maize. Int. J. Plant Prod. 11:577–588
13. Potratz DJ, Mourtzinis S, Gaska J, Lauer J, Arriaga FJ, Conley SP (2019) Effect of strip-till timing, fertilizer placement, and row spacing on soybean seed yield. Crop. Forage Turfgrass Manag. 5(1):1–5

Energy Systems in Agriculture

Coefficient of Dynamic Wall Friction for Hardwood Fuel Pellets

Aaron P. Turner(✉) , Ali Bulent Koc , and Ryan H. Dean

Department of Agricultural Sciences, Clemson University, Clemson, SC 29634, USA
apturne@clemson.edu

Abstract. The design of storage and handling systems for bulk materials requires an understanding of their frictional properties. While these properties are well-studied for many agricultural commodities, they need to be better defined for pelletized biomass, which present unique challenges due to their particle sizes and nontypical aspect ratios. This study evaluated the coefficient of dynamic wall friction for hardwood fuel pellets against two common handling surfaces (ultra-high molecular weight polyethylene (UHMW-PE) and galvanized steel). Effects of confining pressure and shear displacement were investigated using a direct shear wall friction tester, which allowed for up to 20 cm of displacement. Three confining pressures (5 kPa, 10 kPa, and 15 kPa), and two loading methods were evaluated. Fuel pellets against UHMW were most impacted by displacement, with friction decreasing up to 9.5% over the length of the test. Additionally, sequentially increasing the confining pressure over the length of a single test resulted in shear stress differences of up to 14.2%, compared to independent tests. The lowest confining pressure was most affected by these trends and showed higher friction values, relative to the higher confining stresses. Linear functions for stress-dependent friction were estimated, and the overall wall friction angle across methods was 13.2° for UHMW and 11° for steel. Overall, this study explored several factors that influence wall friction test methods, and the results can help improve the design of pellet storage and handling systems.

Keywords: Coefficient of friction · Wood fuel pellets · Physical properties · Direct shear testing

1 Introduction

The design of storage and handling systems for bulk materials requires an understanding of both their physical properties and handling characteristics. While frictional properties are well-studied for many bulk commodities, there is a need to better define these values for many pelletized biomass products, which present unique challenges because of their large particle sizes and nontypical aspect ratios [1]. Mandates to increase energy production from renewable sources, along with an overall trend of increasing fuel pellet production [1–3], show a need to better define these properties so facilities can operate reliably and efficiently.

Of specific interest to this study is the coefficient of dynamic (sliding) friction against wall surfaces commonly encountered in pellet handling systems. Sometimes presented as the wall friction angle, this value has practical applications in silo design, for both strength and flow [4, 5]. These values also have an impact on power requirements for handling equipment, and influence flowability. For bulk materials with relatively small particle sizes and uniform distributions, wall friction is commonly estimated from direct shear tests using a shear box (i.e., Jenike tester). However, test procedures for bulk agricultural commodities and biomass products need to be adapted to accommodate their large particle sizes and varying aspect ratios [6–8].

Due to their simplicity, direct shear tests are commonly used to estimate both internal and wall friction for bulk materials [8]. In the case of wall friction, a sample of the bulk material is sheared against a fixed surface and friction is estimated from the steady-state force required to slide the sample and the applied load or confining stress. Wall friction in general, and particularly values measured from direct shear tests can be influenced by several factors including shear displacement, wall surface, confining stress, wear-in period, and shear velocity. Wall friction values are estimated large enough displacements to assume the test has reached steady state [4, 5]; however, some works have shown shear displacement has an effect on friction and advocate for using longer displacements for more representative friction estimations [9].

The are few works which have evaluated wall friction for pelletized biomass materials often utilize a direct shear tester with increased displacement and/or surface contact area, relative to those commonly used for soils [2, 3, 10]. Wu et al. [10] evaluated three sizes of Canadian wood fuel pellets under confining pressure ranging from 0.1–4.2 kPa, and found wall friction angles that ranged from 11°-19° for common handling surfaces, however values for concrete ranged from 30° to 33°. Craven et al. [2] evaluated wall friction for wood pellets and showed the wall friction angle was relatively consistent for confining stresses between approximately 2–14 kPa. Wall friction angle values measured by Craven et al. [2] were similar to Wu et al. [10] for TIVAR 88 (a low friction lining material), but values for steel were higher (approximate range of 26° to 34°, depending on type). Stasiak et al. [3] evaluated pine pellets against steel and aluminum using confining stresses of 15 kPa & 30 kPa. The average coefficient of friction was 0.45, which is equivalent to a wall friction angle of approximately 24°. Following a different approach, Mattsson & Erik [11] measured the coefficient of static friction directly using a tilting table.

1.1 Objectives

In this study, dynamic wall friction was measured for hardwood fuel pellets using a direct shear wall friction tester. The stability of the friction values over a range of shear displacements (i.e. sliding path length) was evaluated, as were two loading methods. Specific objectives were to:

1. Determine the coefficient of dynamic wall friction and wall friction angle for hardwood fuel pellets using three confining pressures (5 kPa, 10 kPa, and 15 kPa), across two common handling surfaces (galvanized steel and UHMW).
2. Evaluate the effect of shear displacement on the measured friction value, specifically as related to the stability of the response and test procedure.

2 Methods

2.1 Pellet Properties

An example of the wood fuel pellets used in this study are shown in Fig. 1. These were premium hardwood fuel pellets (American Wood Fibers, Columbia, MD), which were designed for heating applications. Descriptive physical properties of the pellets are shown in Table 1. Bulk density was measured in triplicate using the Winchester test cup method [12], and particle geometry was estimated by measuring the length and diameter of a random sample of 20 pellets using calipers with a resolution of 0.001 mm (Mitutoyo CD-6" CSX, Mitutoyo America Corp. Aurora, IL). The moisture content was determined following ASABE Standard S269.5 [13]. Approximately 36 kg of fuel pellets were used in this study, and they were stored under lab conditions (approximately 21 °C and 65% relative humidity), in their original packaging.

Fig. 1 Example hardwood fuel pellets

Table 1 Pellet Physical Properties[a]

Moisture Content	Bulk Density	Average Diameter	Average Length
(% w.b.)	(kg m^{-3})	(mm)	(mm)
7.3	625 $\pm$ 3	6.8 $\pm$ 0.2	16.1 $\pm$ 5.1

[a] Values shown are means $\pm$ one standard deviation. n = 20 for pellet length and n = 3 for bulk density and n = 2 for moisture content.

2.2 Direct Shear Tester Specifications

The coefficient of dynamic wall friction was measured using the direct-shear test fixture shown schematically in Fig. 2. Samples of bulk pellets were placed against the target

surface within a High-Density Polyethylene (HDPE) container with a sample chamber 25.4 cm in diameter and 10.2 cm deep. Known confining pressures were provided by the varying normal loads placed on top of the sample, and shearing action was provided by a linear actuator with a 109 kg capacity and a 30 cm stroke length (Model FA-PO-240–12-12, Firgelli Automation, Ferndale, WA). The shear force was recorded using an in-line 226.8 kg S-beam load cell (LC103B-500, Omega Engineering Inc., Norwalk, CT), connected to load cell amplifier (model HX711, SparkFun Electronics, Niwot CO). Control of the actuator and data recording were handled by a microcontroller (Arduino Mega 2560 Rev3, Arduino, Monza Italy), and force and position data were recorded at a nominal 10 Hz using the Data Streamer Add-In in Microsoft Excel. The fixture could accommodate a maximum size surface sample of 51 cm X 30 cm, and the maximum useable stroke length was approximately 22 cm.
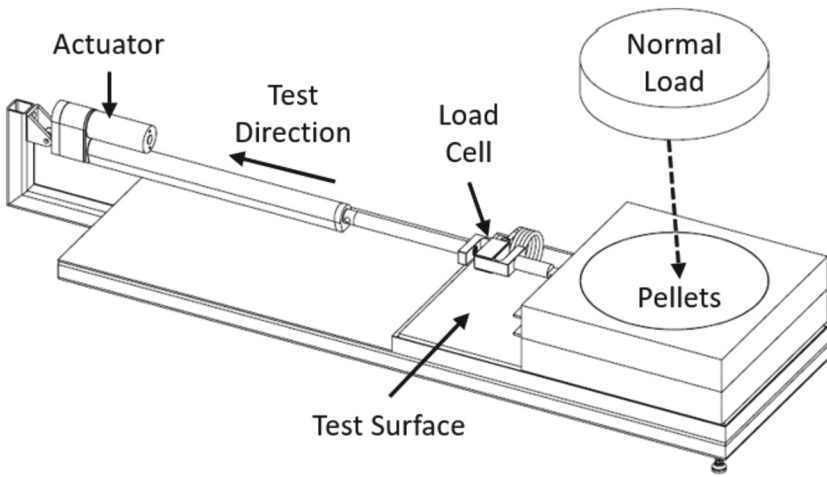
Fig. 2 Schematic of the developed direct shear test fixture

2.3   Test Procedure

Each test began with the linear actuator fully extended, and the sample container placed on cardboard shims. A funnel was used to add a consistent mass of 0.45 kg of pellets to the container, which were leveled with a brush before the appropriate amount of weight was added to reach the target confining stress (5 kPa, 10 kPa, or 15 kPa). Prior to testing, the shims were removed, and the lateral pressure exerted on the sample container by the pellets held the container slightly above the surface, ensuring no contact between sample container and wall surface during testing.

Two sample load procedures were evaluated as part of this work. The independent loading procedure was conducted by shearing the material over the full length of the wall sample (approximately 22 cm) with a single confining pressure. The fixture was then reset, and a new sample was loaded for each wall material/confining stress combination.

For sequential loading tests all three confining stresses were evaluated in a single test by progressively increasing the load after stopping every 7 cm. A minimum of three replications were performed for each test method/confining stress combination.

Before testing, the fixture was leveled, and the wall surface and linear actuator were confirmed to be within one degree of zero utilizing a digital angle finder with a resolution of 0.1° (Model 1886–0100, Johnson Level & Tool Mfg. Co. Inc, Mequon, WI). Tests were conducted at a nominal velocity of 0.152 cm/s, which is a sufficient speed to overcome stick–slip, similar to Wu et al. [10]. Initial testing showed the actual velocity remained within 11.8% of this value, even at the highest nominal load. To prevent differences in the friction attributed to material wear-in [14], wall surfaces were subjected to a breaking consisting of forty "shears" under a 10 kPa normal stress prior to testing.

2.4 Analysis

The changes in the coefficient of friction (COF) and shear stress over different displacement ranges and loading methods were used to evaluate the stability of the friction values. The instantaneous shear stress was determined from the force required to pull the pellets against the wall surface and the cross-sectional area of the pellet sample (Eq. (1)). The effective coefficient of friction at each point was also determined as the ratio of the shear force to the normal force applied (Eq. (2)). At low displacements, slack is taken out of the system, static friction is overcome, and the particles realign. These points were removed by trimming the first 0.95 cm from the data. Similarly, the final displacement was trimmed to reduce variation in where the test ended. This resulted in 20 cm of usable data for the independent loading method and 5 cm for each segment of the sequential loading tests. For the independent loading method, the response was compared using the overall average (1 cm – 20 cm), near average (3.8 cm – 5.1 cm), and far average (18.7 cm – 20 cm). Because of the shorter displacements, the overall average of the entire duration was taken for the sequential loading method.

$$\tau = \frac{F}{A} \tag{1}$$

where:

$\tau =$ Shear stress (kPa).
$F =$ force required to slide the material (kN).
$A =$ Area (m^2)

$$\mu = \frac{\tau}{\sigma} \tag{2}$$

where:

$\mu =$ Coefficient of wall friction (unitless).
$\sigma =$ Normal or confining stress (kPa).

Wall yield loci were produced using the overall average shear and confining stress pairs for each wall surface and loading method combination. A linear regression was used to evaluate the shear stress as a function of confining stress, the slope of the regression line was set equal to the tangent of the angle of wall friction (Eq. 3) [4, 10]. The regression

line was also combined with Eq. 2 to estimate friction as a function of confining stress [15]. All analysis was conducted using MATLAB (MATLAB 2019b, The MathWorks Inc. Natick, M.A., USA).

$$\varphi_{wall} = \tan^{-1}\left(\frac{\tau}{\sigma}\right) \tag{3}$$

where:

$\varphi_{wall} =$ Wall friction angle (degrees).

3   Results and Discussion

Typical curves of shear stress versus displacement for the independent loading procedure and sequential loading procedure can be seen in Fig. 3a and Fig. 3b, respectively. At low displacements, a rapid increase in shear stress is observed when slack is removed from the system. This increase corresponds to overcoming static friction and "hardening" as the particles reorient and increase contact with the wall surface [16]. The approximately horizontal portion at larger displacement represents the residual shear force required to overcome dynamic friction [5]. Changes in this range indicate that displacement influenced the coefficient of friction. The data was segmented into subsections, as indicated on Fig. 3, to evaluate this effect.

3.1   Response Stability

Figure 4a shows the coefficient of friction as a function of displacement against UHMW. There was a general trend of decreasing friction observed for all confining stresses. The trend was most pronounced at 5 kPa, which also exhibited the highest overall values. This decrease indicates either friction is changing, or the material is yet to reach steady state. Fuel pellets against the steel surface (Fig. 4b) showed gradually increasing values which peaked and then began to decrease. Again, friction was notably higher for the lowest confining pressure, indicating friction is not independent of the load, at least at low confining stresses. Preliminary tests using other bulk materials and a solid surface confirmed the response was not an effect of the test fixture [17].

Table 2 shows the wall friction coefficient and precent changes in friction obtained when sub-sampling different displacement distances. The values are expressed using the overall average (1 cm – 20 cm), near range (3.8 cm – 5.1 cm), and far range (18.7 cm – 20.0 cm) of displacement. For UHMW, the overall coefficient of friction was highest at the lowest confining pressure (0.27) and decreased to 0.22 at the highest confining pressure. The same trend was observed for steel, where the coefficient decreased from 0.25 to 0.19 as confining stress increased. In both cases, the largest changes occurred between 5 and 10 kPa, while the values at 10 kPa and 15 kPa were comparable. Other bulk materials have been shown to produce varying responses, especially at lower confining pressures [15]. However, this was inconsistent with Craven et al. [2] who showed relatively stable friction values for wood pellets for confining stresses between approximately 2–14 kPa. Thompson & Ross [14] observed similar trends to this study in grain (using notably higher loads), and suggested this behavior was consistent how contact
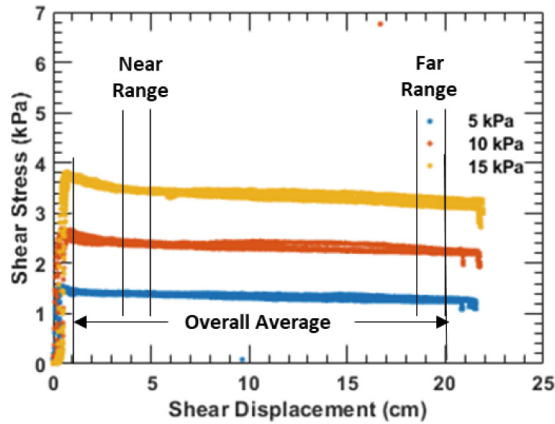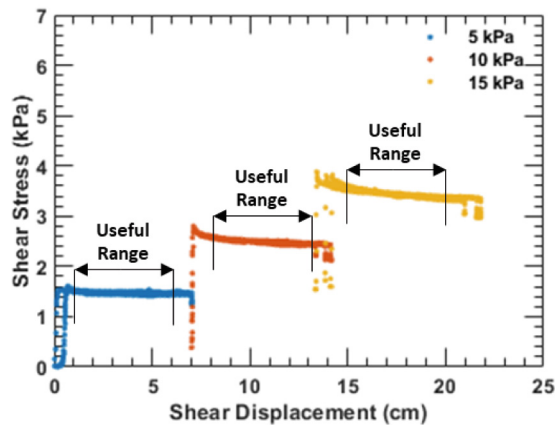
Fig. 3 Example shear stress versus displacement results for fuel pellets against UHMW using 5 kPa, 10 kPa, 15 kPa confining stresses. Includes data from all replications. (a) Independent loading method (b) sequential loading method

stresses are transferred in bulk materials. Another plausible explanation for this trend is an increase in contact points/area between the pellets and the surface. When the load is applied, the bulk density of the material increases as void space is removed and particles rearrange to support the load. This effect is most pronounced at low confining pressures, which would help explain why the largest differences occurred at low confining stress.

In terms of response stability, UHMW showed a general trend of decreasing friction with displacement. The coefficient of friction decreasing between 6.53% and 7.88% between the near and far sub-sampling range, depending on confining stress (Table 2, Fig. 4a). The response for steel was more consistent, with less pronounced differences. In this case, friction at the near sub-sampling range tended be lower, while the far sub-sampling range tended to be slightly higher compared to the average (Fig. 4b). The largest differences were observed between near and far sub-sampling ranges, where friction
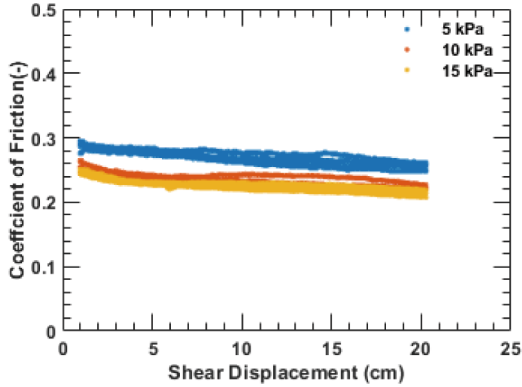
(a)
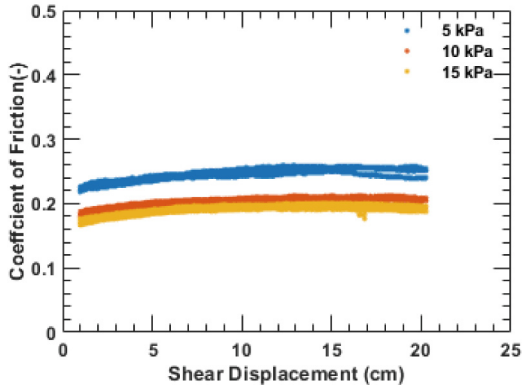
(b)

Fig. 4 Instantaneous coefficient of friction for fuel pellets using the independent loading method. Includes data for all replications. (a) UHMW, (b) steel

Table 2 Effects of confining stress and displacement on friction [a]

Material	Confining stress (kPa)	Coefficient of friction (-)			Percent differences (%)[b]		
		Overall	Near range	Far range	Near to Overall	Far to Overall	Near to Far
UHMW	5	0.27	0.28	0.26	3.60	-4.57	-7.88
UHMW	10	0.23	0.24	0.22	2.90	-4.49	-7.18
UHMW	15	0.22	0.23	0.22	2.38	-4.31	-6.53

<div align="right">(continued)</div>

Table 2 (*continued*)

Material	Confining stress (kPa)	Coefficient of friction (-)			Percent differences (%)[b]		
		Overall	Near range	Far range	Near to Overall	Far to Overall	Near to Far
Steel	5	0.25	0.24	0.25	-3.27	1.46	4.88
Steel	10	0.20	0.20	0.20	-2.71	0.87	3.68
Steel	15	0.19	0.19	0.19	-2.80	0.70	3.60

[a] Friction values are based on n=3 per treatment.
[b] Precent differences calculated relative to the overall estimate. Near & far refer to the sub-sampling ranges

increased from 3.6% to 4.88% over the length of the test. The trend was not consistent between the two surfaces, but at least some cases, larger displacements may be needed to produce realistic friction estimates. Bradley & Berry [9] showed several meters of sliding were required before steady state was reached for soda ash, when starting from a clean surface. In this study, the wall surface was preconditioned, but there could be a wear-in effect on the pellets themselves. Additionally, particle realignment could change contact area, which would produce results similar to what was described above.

3.2   Comparison with the Sequential Loading Procedure

The coefficient of friction over the range of displacements for sequential loading method are shown in Fig. 5a for UHMW and Fig. 5b for steel. The general trends observed here were consistent with the independent loading procedure (Fig. 4a and Fig. 4b). Utilizing the sequential loading method, testing time was sustainably reduced, but the impacts of displacement were much harder to investigate due to the shorter displacement range. The overall coefficient of friction for sequential tests and a comparison to results obtained using the independent method are shown in Table 3. The coefficient of friction values obtained using sequential loading were higher than those obtained using the independent loading method, regardless of confining stress, wall material, and sub-sampling range. The largest differences were observed for UHWM, which was the more variable of the two materials in the independent tests. In terms of confining stress, the lowest confining stress was most impacted, with differences of 9.5% and 6.8% for UHMW and steel respectively, when compared to the overall estimate from the independent loading method. The differences were even larger (up to 14.2%) when compared to the far sub-sampling range of the full-length test. This further supports that particle wear-in or realignment occurs over longer displacement, especially under lower confining stresses.

Table 3 Coefficient of friction for the sequential loading and comparison to independent loading method[a]

Material	Confining stress (kPa)	Coefficient of friction (-)	Percent differences (%)[b]		
			Sequential to Overall	Sequential to Near	Sequential to Far
UHMW	5	0.30	9.49	5.96	14.15
UHMW	10	0.25	6.59	3.74	11.18
UHWM	15	0.23	2.28	0.07	6.69
Steel	5	0.23	6.77	3.45	8.21
Steel	10	0.20	0.03	2.71	0.90
Steel	15	0.18	4.14	1.31	4.84

[a] Friction values are based on n=3 per treatment.
[b] Precent differences were calculated relative to the independent loading method. Overall, near, and far refer to the sub-sampling ranges from the independent tests.

3.3 Overall Wall Friction Angles

An example wall yield locus diagram obtained for galvanized steel using the independent loading method is shown in Fig. 6. If wall friction is independent of confining stress, the slope of the regression line is equal to the tangent of the wall friction angle, otherwise confining stress-dependent fiction values need to be determined [4]. In the stress dependent case, the intercept represents adhesion between the surface and the pellets. There was no clear reason to assume there was meaningful adhesion between the pellets and the wall surface, however the differences in friction observed between the lowest confining stress and the other two make the confining stress independence less clear (Table 2 and Table 3). Initial investigation into the statistical significance of the intercept showed mixed results and given the mixed results both and overall wall friction angle and stress-dependent function for friction are presented Table 4. Additional testing at other confining stress levels is needed to clarify which representation is the most appropriate [5]. The linear regression equation obtained from the wall yield loci were used to express friction as a function of confining stress as indicated in Table 4. The wall friction angles presented in Table 4 were determined based on a linear fit passing through the origin. These values were based on the overall average from the independent tests. The differences observed between loading methods did not translate to the overall wall friction angle, with the results for the two methods being within a degree of each other. The average wall friction angle observed for UHMW was 13.2°, which is similar to previously reported values for TIVAR 88, a formulation of UHMW-PE [10]. Both of which were lower than those reported by Craven et al. [2]. The average wall friction angle for galvanized steel was 11° and was lower than the previously reported values for both mild and stainless steel [2, 10].
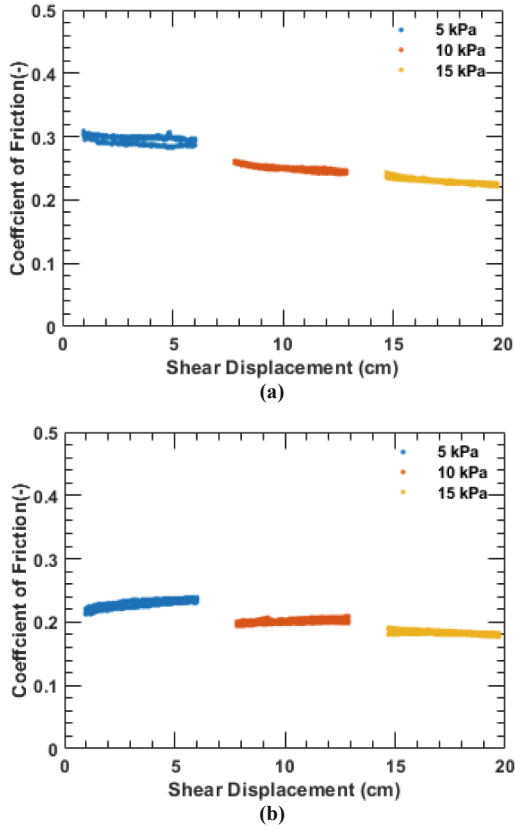
Fig. 5 Instantaneous coefficient of friction for fuel pellets using the sequential loading method and 5 kPa, 10 kPa, 15 kPa normal loads. Includes results for all replications. (a) UHMW, (b) steel

Table 4 Estimated wall friction angles and coefficient of friction equations

Material	Loading Method	Wall friction angle (°)[a]	Equation	R^2
UHMW	Independent	13.0	$\mu = 0.2030 + 0.3219/\sigma$	0.9999
UHMW	Sequential	13.5	$\mu = 0.1974 + 0.5016/\sigma$	0.9996
Steel	Independent	11.2	$\mu = 0.1646 + 0.3932/\sigma$	0.9994
Steel	Sequential	10.9	$\mu = 0.1610 + 0.3636/\sigma$	0.9979

[a] Estimated from regression without intercept, assuming independent of stress.

$\tau = 0.1646 * \sigma + 0.3932$
$r^2 = 0.999$
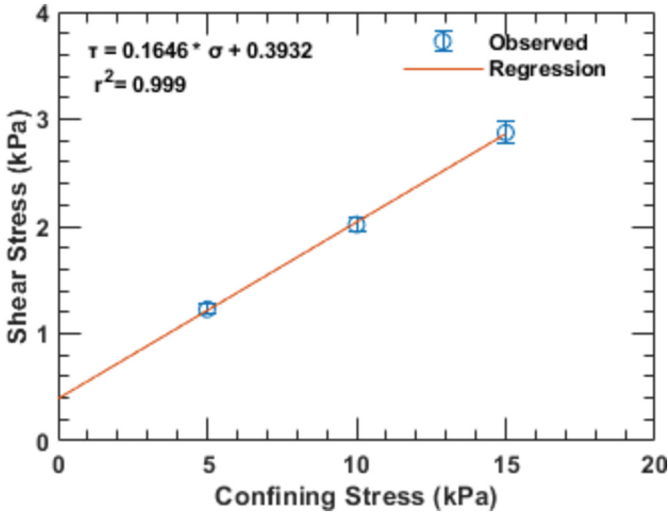
Fig. 6 Example wall yield locus using the independent loading method on a galvanized steel surface. Error bars represent standard deviations

4   Conclusions

The frictional properties of bulk materials are directly related to the handling characteristics and design of storage and handling systems. This study evaluated the coefficient of dynamic friction for hardwood fuel pellets against two common handling surfaces and examined several factors that influence the results of these tests. Shear displacement was shown to change friction, with UHMW being most impacted, resulting in friction changes of up to 9.5% over the length of the same test method. Variations of over 14.2% were observed between methods. The lowest confining stress was most affected by these trends, and showed higher friction values, relative to the higher levels. This highlights the need to use representative conditions when evaluating types of materials. Further investigation is needed to evaluate the required sliding distance before friction stabilizes, and to evaluate the dependence of friction on confining pressure, especially at lower levels. The effects discussed here were shown influence test results and actual friction, but practical applications should utilize conservative friction estimates to ensure reliability. Equations for the coefficient of friction as a function of confining stress were presented, and the overall wall friction angles for hardwood pellets against UHMW and galvanized steel were 13.2° and 11°, respectively. These values tended to be slightly lower than those reported for other pellet types against similar surfaces. Overall, these hardwood-specific friction estimates help to increase the robustness of the limited data available for wood fuel pellets and can help improve the design of pellet storage and handling systems.

Conflict of Interest.   The authors have no conflict of interest to disclose.

References

1. Dean, R.H., Turner, A.P., Koc, A.B., Karthikeyan, R.: Influence of moisture content and fine levels on angle of repose for pelletized materials. Appl. Eng. Agric. **39**(2), 141–152 (2023). https://doi.org/10.13031/aea.15141
2. Craven, J.M., Swithenbank, J., Sharifi, V.N.: Investigation into the flow properties of coarse solid fuels for use in industrial feed systems. J. Powder Technol (2015) https://doi.org/10.1155/2015/786063
3. Stasiak M et al (2020) Friction and shear properties of pine biomass and pellets. Materials 13(16):3567. https://doi.org/10.3390/ma13163567
4. Schulze, D.: Powders and Bulk Solids: Behavior, Characterization, Storage and Flow Second ed. Springer Nature, Cham, Switzerland (2021). https://doi.org/10.1007/978-3-540-73768-1
5. European Committee for Standardization: EN1991: Eurocode 1 - Actions on structures. Part 4. Actions on silos and tanks. Brussels, Belgium (2006)
6. ASTM: D6128–16 Shear testing of bulk solids using the Jenike shear tester. West Conshohocken, PA: ASTM International (2016)
7. Stasiak M, Molenda M, Gancarz M, Wiącek J, Parafiniuk P, Lisowski A (2018) Characterization of shear behaviour in consolidated granular biomass. Powder Technol 327:120–127. https://doi.org/10.1016/j.powtec.2017.12.037
8. Molenda M, Thompson S, Ross I (2000) PH—postharvest technology: friction of wheat on corrugated and smooth galvanized steel surfaces. J Agric Eng Res 77(2):209–219
9. Bradley, M., Berry, R.: Evolution of wall friction with realistic displacements wall" conditioning" and the need to measure wall friction over a long distance of travel. In: Proceedings of the 6th International Conference for Conveying and Handling of Particulate Solids (CHoPS), Brisbane, Queensland, Australia (2009)
10. Wu M, Schott D, Lodewijks G (2011) Physical properties of solid biomass. Biomass Bioenergy 35(5):2093–2105. https://doi.org/10.1016/j.biombioe.2011.02.020
11. Mattsson JE (1990) Basic handling characteristics of wood fuels: angle of repose, friction against surfaces and tendency to bridge for different assortments. Scandinavian J. For. Res. 5(1–4):583–597
12. USDA-FGIS: Grain inspection handbook. In: Book II Grain Grading Procedures. Grain Inspection, Packers and Stockyards Administration. Washington, DC (2020)
13. ASABE Standards. S269.5 Densified products for bulk handling- Definitions and methods. St. Joseph, MI: ASABE (2016)
14. Thompson SA, Ross IJ (1983) Compressibility and frictional coefficients of wheat Trans. ASAE 26(4):1171–1180
15. Molenda M, Montross MD, Horabik J, Ross IJ (2002) Mechanical properties of corn and soybean meal. Trans ASAE 45(6):1929
16. Rusinek R, Molenda M (2007) Static and kinetic friction of rapeseed. Res Agric Eng 53(1):14–19
17. Dean, R.H.: The physical properties and handling characteristics of pelletized biomass materials (M.S.), Clemson University Clemson, SC (2022)

Mapping Biomass Energy Potential
from Agricultural Residues in Tanzania

Geofrey Prudence Baitu[1(✉)] , Khaled Adil Dawood Idress[2] ,
Omsalma Alsadig Adam Gadalla[3] , and Yeşim Benal Öztekin[4]

[1] College of Agriculture and Food Technology, Department of Agricultural Engineering,
University of Dar es Salaam, P.O. Box 35091, Dar Es Salaam, Tanzania
prudencegeofrey@gmail.com

[2] Department of Agricultural Engineering, Al-Neelain University, P.O. Box 12702,
Khartoum, Sudan

[3] Department of Agricultural Engineering,
University of Khartoum, P.O. Box 321, Khartoum, Sudan

[4] Faculty of Agriculture, Department of Agricultural Machinery and Technologies Engineering,
Ondokuz Mayis University, Samsun, Turkey

Abstract. Tanzania, like many countries in sub-Saharan Africa, faces significant challenges in meeting its growing energy demands while simultaneously promoting sustainable development. Biomass energy, derived from agricultural residues, has emerged as a promising alternative to fossil fuels, offering a range of economic, social, and environmental benefits. This paper presents a comprehensive assessment of the biomass energy potential from agricultural residues in Tanzania. The analysis incorporates data on crop production and residue generation to estimate the potential contribution of agricultural residues to the national energy mix. GIS was utilized to map the spatial distribution of the biomass energy potential. The data were obtained from multiple sources, including national surveys and existing literature. Thirteen mostly grown crops in Tanzania (maize, paddy, sorghum, cassava, groundnut, sunflower, sesame, banana, cotton, tobacco, coffee, sugarcane, and coconut) were selected for this study. The results of the study indicate that Tanzania has significant untapped potential for biomass energy from agricultural residues of about 135PJ/year only from the selected crops. The highest potential is in the central and southern regions of the country. The study concludes with policy recommendations for promoting the sustainable utilization of agricultural residues for energy production. These include the development of appropriate technologies for small-scale farmers, the establishment of incentives for biomass production, and the promotion of public-private partnerships for the development of biomass energy projects. The research contributes to the growing body of literature on renewable energy in Africa and provides valuable insights for policymakers, researchers, and practitioners working in the energy and agricultural sectors.

Keywords: Biomass energy · Agricultural residues · GIS · Renewable energy · Sustainable development

1   Introduction

As the global demands for sustainable and renewable energy sources skyrocket, biomass has emerged as a significant contender in the quest for cleaner and more environmentally friendly alternatives [1]. In particular, agricultural residues present a promising resource for biomass energy production due to their abundant availability and potential to mitigate waste management challenges [2, 3]. Tanzania, a country gifted with ample agricultural lands and a diverse agricultural sector, stands to benefit greatly from the exploration and utilization of biomass energy emanating from agricultural residues [4]. In recent years, Tanzania has glimpsed impressive economic growth and rapid urbanization, resulting in a surge in energy consumption. However, this increased demand for energy has been predominantly met by fossil fuels, which not only contribute to greenhouse gas emissions but also make the nation heavily reliant on costly and non-renewable resources [5]. A study by [6] estimated that for every 1% increase in the level of urbanization, an estimated increase of 12%, 14%, and 14% would be expected in electricity, petroleum, and charcoal consumption respectively. Conceding the need for a sustainable energy transition, Tanzania has embraced the potential of biomass energy as an important solution to address these pressing challenges [7]. Agricultural residues encompass a broad range of byproducts generated from various agricultural activities, such as crop residues, agro-industrial residues, and animal waste [8]. Leaving these residues unused or treated just as waste leads to environmental problems and missing the opportunity for energy generation.

Harnessing the biomass energy potential from agricultural residues in Tanzania holds immense promise for several reasons. Firstly, Tanzania boasts a favourably diverse agricultural sector that encompasses staple crops, cash crops, agro-industrial activities, and livestock farming [9]. As a result, a noteworthy volume of agricultural residues is generated across the country. By mapping and quantifying these residues, researchers, policymakers, and energy stakeholders can identify the most viable sources of biomass energy, optimize resource utilization, and design suitable energy generation and distribution strategies.

Secondly, biomass energy from agricultural residues offers a sustainable alternative to fossil fuels, lessening the carbon footprint and fostering the transition towards a low-carbon economy [10]. It not only aids in mitigating greenhouse gas emissions but also promotes rural development by equipping energy access to remote areas, thereby improving the livelihoods of local communities.

Furthermore, the utilization of agricultural residues for biomass energy can contribute to waste management and environmental sustainability [11, 8]. Proper management of these residues can help reduce pollution, prevent the release of harmful gases during decomposition, and minimize the pressure on landfills [12].

[13] conducted a study to assess the potential of energy generation from biomass wastes in Tanzania, where four types of wastes were examined, which are agricultural residues, livestock wastes, forestry residues, and urban human waste. Agricultural residues were found to have the highest energy potential of all four wastes, accounting for more than 87% of the total energy potential. Another study by [14], demonstrated that the proper utilization of agricultural residue for energy generation can improve energy access in rural and urban areas and significantly reduce the consumption of fossil fuels.

[15] assessed the energy potential of agricultural residues from commercial crops grown in Tanzania and the study revealed that the use of these residues would improve and secure energy supply as well as enhance the sustainability of the land-use practices.

As summarized above, many studies have been done to explore the potential of biomass energy from agricultural residues in Tanzania. However, none of these studies explored the potential of biomass energy at the regional level in Tanzania and visually presented that potential distribution. In this article, we aim to explore and map the biomass energy potential from agricultural residues in Tanzania. By analyzing available data and utilizing advanced geospatial techniques, we identified and evaluated the key biomass energy sources and their geographical distribution. Ultimately, this research will contribute to the formulation of evidence-based strategies for biomass energy development in Tanzania, promoting sustainable and clean energy generation, rural development, and environmental conservation. By unlocking the untapped potential of agricultural residues, Tanzania can position itself as a regional leader in the biomass energy sector, paving the way for a more sustainable and resilient future.

2   Materials and Methods

2.1   Study Location

The study location, Tanzania, was carefully selected to probe the untapped potential of agricultural residues for biomass energy production. Situated in East Africa within the Great Lakes region and bordered by a mosaic of nations, including Kenya, Uganda, and Rwanda Re (Fig. 1). Its distinguishable regions, each marked by distinctive landscapes and cultural nuances, present a microcosm of diversity and complexity for agricultural activities. In the northern highlands, regions like Arusha and Kilimanjaro showcase fertile soils and temperate climates conducive to coffee, tea, and horticultural crops. Moving towards the coastal plains and valleys, Tanga and Morogoro experience a tropical climate, supporting a variety of crops including cashews, coconuts, and fruits. The central regions, including Dodoma and Singida, present a semi-arid climate, which has led to the cultivation of drought-resistant crops such as millet, sorghum, and pulses. The western regions, bordering Lake Victoria, are known for their rice and fish production. The semi-autonomous archipelago of Zanzibar, off the coast of Tanzania, focuses on spices like cloves and tropical fruits, leveraging its unique climate and historical trade connections. Lastly, the southern regions of Mbeya and Ruvuma exhibit agro ecological diversity, ranging from highlands to lowlands enabling farmers to engage in a mix of subsistence and cash crop agriculture, cultivating everything from maize and beans to tobacco and sugarcane. Tanzania's diverse agricultural landscape provides an ideal setting for investigating the viability of utilizing crop residues as a renewable energy source.
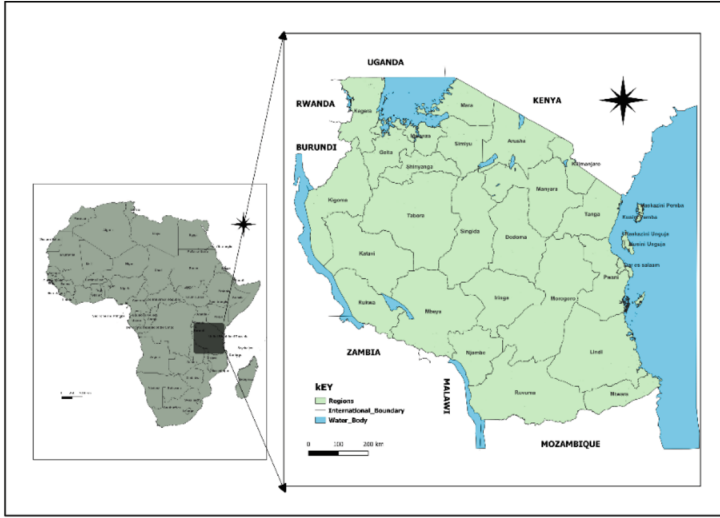
Fig. 1. Location of the study area (Tanzania) in the African map

2.2 Agricultural Residue Biomass Potential Assessment

In this study, 13 commonly grown crops grown in Tanzania were selected. The data of the yield of the selected crops for each region in the 2019/20 cultivating season was retrieved from the Tanzania National Bureau of Statistics (NBS) database in the National Sample Census of Agriculture 2019/20 report. From the yearly production for every crop, the amount of agricultural residues was estimated by using the residue-to-product ration (RPR) [16]. The RPR used in this study were average of different RPR values from different literatures Re (Table 1). The gross agricultural residues of the ith crop in tons per year was calculated using Eq. (1). Where $AR_{G(i)}$ is the gross amount of residue for the ith crop in tons per year, RPR_i is the residue product ratio of the ith crop, and TP_i is the total production of crop i^{th} in tons per year.

$$AR_{G(i)} = RPR_i \times TP_i \qquad (1)$$

Since agricultural residues have competitive uses including animal feed usage and fuel for cooking in rural areas [17], not all can be available for biomass energy production. Hence, the surplus availability factor was used to estimate the surplus agricultural residues available that can be used for energy production as shown in Eq. (2). Where $AR_{S(i)}$ is the surplus amount of residue for the ith crop in tons per year, and SF_i is the surplus residue availability factor. Table 1 shows the surplus factors for each crops.

$$AR_{S(i)} = AR_{G(i)} \times SF_i \qquad (2)$$

Furthermore, Table 1 shows the lower heating values retrieved from different literatures that were used to calculate the energy potential from agricultural residues as shown in Eq. (3). Where, $BE_{(i)}$ is the technical biomass energy potential for the ith crop

in MJ/year, and LHV$_{(i)}$ is the lower heating value of the ith crop in MJ/Kg.

$$BE = AR_{S(i)} \times LHV_{(i)} \tag{3}$$

2.3 Mapping the Biomass Energy Potential

Geographic Information Systems (GIS) were employed as a fundamental tool to analyze and visualize the potential of biomass energy derived from agricultural residues. After the technical biomass energy potential from agricultural residue for each region of Tanzania was evaluated and complied together, they were integrated with geospatial dataset including land use to create a comprehensive map that visually represents the spatial distribution of biomass potential.

Table 1. Residue type, residue-to-product ratio, surplus availability factor, and low heating value for the crops used in the study.

No	Crop	Residue type	RPR	SF	LHV (MJ/Kg)
1	Maize	Stalk	*1.65 [a,b]	0.6	5.25 [b]
		Cob	*0.24 [a,c]	0.8	*15.46 [a,c]
		Husks	0.2 [a]	0.8	1.5 [a]
2	Paddy	Straw	*1.19 [a,b,c]	0.43	*14 [a,b,c]
		Husk	*0.26 [a,c,d]	0.8	*15.77 [a,c,d]
3	Sorghum	Straw	1.25 [c]	0.6	12.38 [c]
4	Cassava	Stalks	0.062 [c]	0.6	17.50 [c]
5	Groundnut	Husks/Shells	0.477 [c]	0.8	15.66 [c]
		Straw	2.28 [a]	0.4	17.58 [a]
6	Sunflower	Stalk	3 [f]	0.3	*14.47 [f,g]
7	Sesame	Stalk	1.2 [f]	0.6	14.35 f
8	Banana	Peel	0.28 [e]	0.6	18.89 [e]
9	Cotton	Stalk	*3.14 [a,c]	0.6	*16.21 [a,c]
10	Tobacco	Stalk	2 [h]	0.4	15.5 [i]
11	Coffee	Husk	2.1 [c]	0.6	12.38 [c]
12	Sugarcane	Bagasse	*0.59 [a,b,c]	0.6	*11.69 [a,b,c]
		Tops/Leaves	0.18 [a]	0.6	16.61 [a]
13	Coconut	Husk	0.419 [c]	0.8	18.62 [c]
		Shell	0.12 c	0.8	18.09 [c, j]

* An average of different values obtained from various literatures [a] [16], [b] [18], [c] [19], [d] [20], [e] [21], [f] [22], [g] [23], [h] [15], [i] [24], [j] [25].

3   Results and Discussion

3.1   Agricultural Production and Residue Availability Status in Tanzania

The total agricultural production for the specific selected crops across all regions was almost 16 million tons, according to the National Sample Census of Agriculture 2019/20. Among these regions, Kagera emerged as the leading producer, contributing approximately 1.4 million tons, with a predominant production of banana. Dodoma followed closely with a production level of 1 million tons. Notably, there were substantial regional differences in agricultural output, with the Unguja Kusini Region recording the lowest output with only roughly 35,291 tons of the selected crops produced. These discrepancies are due to the issue of crop preference in different regions that can be attributable to regional differences in climate, soil types and farming methods.

3.2   Biomass Energy Potential

A thorough assessment of the biomass potential from agricultural residues was made using Eq. (3) and data gathered for each region. The findings show Tanzania's biomass resources to be a diversified environment. Tanzania's total biomass potential from agricultural residues of the selected crops was estimated to be around 135 PJ/year in th2019/20 farming season. This is a sizable renewable energy source that has the potential to considerably improve the country's sustainability and energy security.

The analysis shows that some areas have a very high potential for biomass than others. Notably, Dodoma emerged as a leader in biomass energy potential, with an estimated capacity of about 11 PJ/year, despite being behind Kagera Region in terms of agricultural production. This is attributed by the type of crops grown in these areas. About 70% of the total production in Kagera is banana, which has a RPR of 0.28, a surplus residue availability factor (SF) of 0.6, and a lower heating value (LHV) of 18.89 MJ/Kg. On the contrary, the production in Dodoma was not only distributed throughout a variety of crops, but Dodoma also held the top spot for producing a number of different crops including sorghum, sunflowers, and groundnuts. It may be understood why Dodoma, as opposed to Kagera, came up with the largest biomass energy potential by referring to the RPR, SF, and LHV of these crops from (Table 1). With projected values of almost 10 PJ/year, 8.7PJ/year, 8.6 PJ/year, and 8.2 PJ/year, respectively, Tabora, Simiyu, Morogoro, and Mbeya regions also rated well in terms of biomass energy potential. Likewise, the diversity of their agricultural practices and high levels of productivity benefit these areas. Geita, Shinyanga, Mwanza and Kagera regions also exhibit significant biomass energy potential, with estimated values of approximately 7.9 PJ/year, 7.9 PJ/year, 7.2 PJ/year and 6.8 PJ/year, respectively. Conversely, Unguja Kusini, Unguja Kaskazini, and Pemba Kaskazini regions show relatively limited biomass energy potential, with estimated values of about 0.1 PJ/year, 0.15 PJ/year, and 0.23 PJ/year, respectively.

3.3   Implications for Energy and Sustainability

The substantial biomass energy potential identified in different parts of the country holds significant promise for Tanzania's energy security and sustainability and reducing the country's dependence on non-renewable energy sources. The estimated 135 PJ/year of biomass energy is equivalent to 37,500 GWh, which would have a very significant contribution to the national grid, according to the national energy demand. The utilization of this potentialwould help to reduce the energy crisis in the country hence, improving the livelihood of the people especially in rural area (Fig. 2).
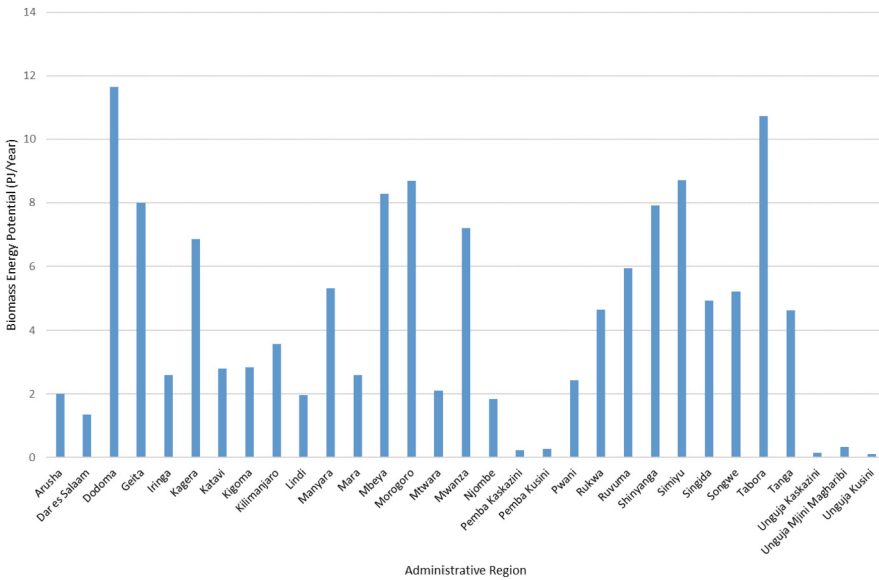
Fig. 2. Region wise biomass energy potential from agricultural residues in Tanzania.
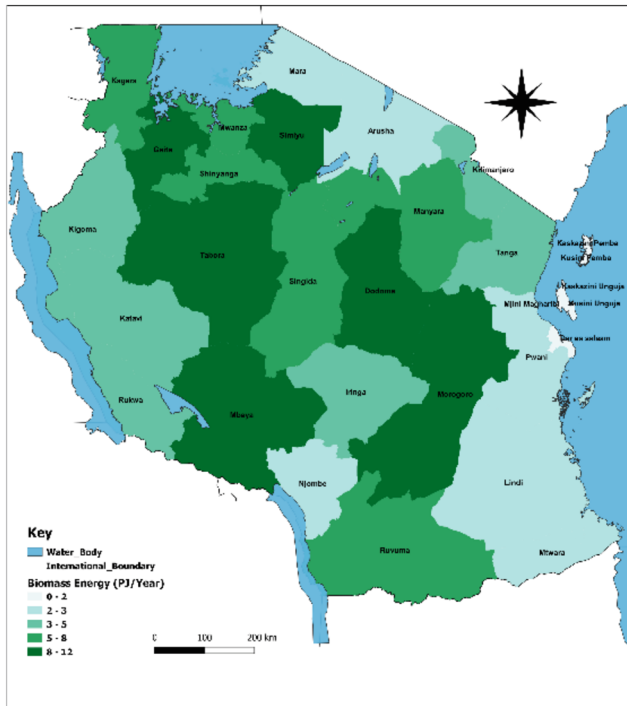
Fig. 3. Biomass energy potential from agricultural residues distribution in Tanzania.

4   Conclusion

In conclusion, this study successfully demonstrated the potential of biomass energy potential from agricultural residues in Tanzania. By leveraging the power of geospatial analysis, we have been able to visualize areas with significant potential for biomass energy production, thereby contributing to the country's renewable energy goals and sustainable development targets. The comprehensive map created through this methodology serves as a valuable resource for policymakers, investors, and local communities, offering insights into optimal locations for biomass energy projects while considering ecological, economic, and logistical factors (Fig. 3).

Moving forward, several recommendations emerge from this research. First and foremost, it is essential to continuously update and refine the dataset regarding agricultural activities, incorporating the latest land use changes, crop yields, and technological advancements. More research should be done to develop appropriate technologies to help small scale farmers in rural areas utilize biomass energy in a more sustainable way. Collaborative efforts between government agencies, research institutions, and private enterprises are crucial for sharing data, expertise, and resources to further refine the assessment of biomass energy potential.

Furthermore, a comprehensive cost-benefit analysis should be undertaken to assess the economic feasibility of biomass energy projects in the identified zones. This will aid

in attracting investments and ensuring the long-term viability of such ventures. Local capacity building and awareness campaigns are also recommended to engage local communities and stakeholders in the sustainable management of agricultural residues for energy production.

In conclusion, this study not only contributes valuable insights into Tanzania's biomass energy potential but also serves as a blueprint for other regions aiming to harness renewable energy from agricultural residues. By combining advanced geospatial techniques with on-ground efforts, the vision of a greener and more energy-independent Tanzania can be realized, fostering both environmental conservation and socio-economic growth.

Conflict of Interest Statement. The authors declare no conflict of interest.

References

1. Demirbas MF, Balat M, Balat H (2009) Potential contribution of biomass to the sustainable energy development. Energ. Convers Manag. 50(7):1746–1760
2. Ali M, Saleem M, Khan Z, Watson IA (2019) The use of crop residues for biofuel production. Biomass, Biopolymer-Based Materials, and Bioenergy. Elsevier, pp 369–395. https://doi.org/10.1016/B978-0-08-102426-3.00016-3
3. Babu S et al (2022) Exploring agricultural waste biomass for energy, food and feed production and pollution mitigation: a review. Bioresour Technol 360:127566. https://doi.org/10.1016/j.biortech.2022.127566
4. Kusekwa, M. A. (2013). Biomass conversion to energy in Tanzania: A critique. In H. Arman I. Yuksel (Eds.), New development in renewable energy (pp. 240–270). Intech Open. https://doi.org/10.5772/52956
5. Albiman MM, Suleiman NN, Baka OH (2015) The relationship between energy consumption, CO2 emissions and economic growth in Tanzania. Int J Energ. Sect Manag. 9(3):361–375
6. Hosier RH, Mwandosya MJ, Luhanga ML (1993) Future energy development in Tanzania. Energ. Policy 21(5):524–542. https://doi.org/10.1016/0301-4215(93)90039-I
7. Felix M, Gheewala SH (2011) A review of biomass energy dependency in Tanzania. Energ. Procedia 9:338–343. https://doi.org/10.1016/j.egypro.2011.09.036
8. Koul B, Yakoob M, Shah MP (2022) Agricultural waste management strategies for environmental sustainability. Environ Res 206:112285. https://doi.org/10.1016/j.envres.2021.112285
9. Acland, J. D. (1971). East African Crops. (An introduction to the production of field and plantation crops in Kenya, Tanzania and Uganda ed.). Longman [for the] Food and Agriculture Organization
10. Abbasi T, Abbasi SA (2010) Biomass energy and the environmental impacts associated with its production and utilization. Renew. Sustain Energ. Rev. 14(3):919–937. https://doi.org/10.1016/j.rser.2009.11.006
11. Daza Serna L, Solarte Toro J, Serna Loaiza S, Chacón Perez Y, Cardona Alzate C (2016) Agricultural waste management through energy producing biorefineries: The Colombian case. Waste biomass valorization 7:789–798
12. Foo K, Hameed B (2009) Utilization of rice husk ash as novel adsorbent: a judicious recycling of the colloidal agricultural waste. Adv Coll Interface Sci 152(1–2):39–47

13. Aslam HZ, HammertonLi J, Andrews G, Ross A, Lovett JC (2021) Increasing access to electricity: an assessment of the energy and power generation potential from biomass waste residues in Tanzania. Energies 14(6):1793. https://doi.org/10.3390/en14061793

14. Lyakurwa FS (2016) Assessment of the energy potential of crop residues and animal wastes in Tanzania. Independent J. Manag. Prod. 7(4):1227–1239

15. Terrapon-Pfaff J (2012) Linking energy- and Land-Use Systems: energy potentials and environmental risks of using agricultural residues in Tanzania. Sustainability 4:278–293. https://doi.org/10.3390/su4030278

16. Koopmans A, Koppejan J (1997) Agricultural and forest residues-generation, utilization and availability. Reg. consultation Mod Appl. Biomass energy 6:10

17. Prasad S, Malav MK, Kumar S, Singh A, Pant D, Radhakrishnan S (2018) Enhancement of bio-ethanol production potential of wheat straw by reducing furfural and 5-hydroxymethylfurfural (HMF). Bioresour. Technol. Rep. 4:50–56. https://doi.org/10.1016/j.biteb.2018.09.007

18. Strehler, A., Stutzle, W. (1987). Biomass residues in Biomass Regenerable Energy, ed. by Hall DO and Overend RP. In: John Wiley & Sons Ltd., Chichester

19. Bhattacharya, S., Pham, H., Shrestha, R., Vu, Q. (1993). CO2 emissions due to fossil and traditional fuels, residues and wastes in Asia. Workshop on Global Warming Issues in Asia, Asian Inst. of Technol., Bangkok,

20. Mahajan K, Mishra J (1992) Energy from paddy husks-An overview. Energy Manag. 16:5–14

21. Wilaipon P (2009) The effects of briquetting pressure on banana-peel briquette and the banana waste in Northern Thailand. Am J Appl Sci 6(1):167

22. Zabaniotou A, Ioannidou O, Antonakou E, Lappas A (2008) Experimental study of pyrolysis for potential energy, hydrogen and carbon material production from lignocellulosic biomass. Int J Hydrogen Energy 33(10):2433–2444

23. Maj, G., Szyszlak-Bargłowicz, J., Zając, G., Słowik, T., Krzaczek, P., & Piekarski, W. (2019). Energy and Emission Characteristics of Biowaste from the Corn Grain Drying Process. Energies, 12(22), 4383. https://www.mdpi.com/1996-1073/12/22/4383

24. Mijailovic I, Radojicic V, Ecim-Djuric O, Stefanovic G, Kulic G (2014) Energy potential of tobacco stalks in briquettes and pellets production. J Environ Prot Ecol 15(3):1034–1041

25. Tanko, J., Ahmadu, U., Sadiq, U., Muazu, A. (2021). Characterization of rice husk and coconut shell briquette as an alternative solid fuel. Adv. Energy Convers. Mater., 1–12

Effect of Different Drying Temperatures on CO$_2$ Emissions in Acorn Drying

Mahmut Kaplan[1(✉)] , Necati Çetin[2] , and Seda Günaydın[3]

[1] Department of Field Crops, Faculty of Agriculture, Erciyes University, Kayseri, Turkey
`mahmutkaplan5@hotmail.com`

[2] Department of Agricultural Machinery and Technologies Engineering, Faculty of Agriculture, Ankara University, Ankara, Turkey

[3] Department of Biosystems Engineering, Faculty of Agriculture, Erciyes University, Kayseri, Turkey

Abstract. Since the harvest period of acorns comes to rainy periods, it has a very high initial moisture content. For this reason, its nutrient content decreases during storage, and deterioration occurs. To prevent losses, it is necessary to ensure the preservation of the products with the drying process immediately after the harvest. The aim of present study is to determine and compare the effects of gradually increasing drying temperatures on CO2 emissions related to specific energy consumption in acorn drying. Drying processes were performed in a convective dryer at 40, 60, 80, 100 and 120 °C. The CO2 emissions of these temperatures were calculated for wind, solar, hydroelectric, and geothermal power plants. As a result, while the lowest CO2 emissions were obtained from the wind power plant, the greatest CO2 emissions were obtained from the geothermal power plant. In addition, it was observed that as the drying temperature and drying time increased, the amount of CO2 emissions also increased

Keywords: Acorn · CO2 emission · Air-convective Drying · Energy

1 Introduction

Acorns are a type of forage that is high in carbohydrates, vitamins, and minerals and plays a significant role in animal nutrition [1, 2]. The carbohydrates found in acorns are in the form of starch, and the starch content varies between about 58% and the crude protein content varies between 1.17 and 8.72% [3]. It has the ability to multiply rapidly due to its high crude protein content [4]. Besides providing animal nutrition, oak trees are commonly used in the furniture sector [5]. Besides, because of their bioactive qualities, which include antioxidant, antitumor, and antibacterial capabilities, eating acorns as a functional food has gained popularity recently [6].

Drying is the best method for keeping acorns fresh for an extended period of time [7]. Drying is the process of reducing microbial growth by reducing the dense moisture present in the structure of products [8]. Biochemical and structural deformations occur in products that are exposed to high temperatures for a long time during drying [9].

Shortening the drying time increases the nutritional value of the dried final product [10]. The convective drying technique is widely used because it is cheap and easy to use [11]. However, this method, which is widely used in drying agricultural products, has a large share of greenhouse gas emissions [12].

One of the most comprehensive operations in the consumption of energy is the drying process 13]. Electrical energy is the main input for post-harvest processing and drying [14]. Dryers used for drying agricultural products cause greenhouse gas emissions as well as high energy consumption [15]. Climate change is caused by pollutants released by power plants [16]. The consumption of fossil fuels produces pollution that causes greenhouse gases in the atmosphere of the earth [17]. High energy consumption spent during drying of agricultural products leads to greenhouse gas emissions [18]. The increase in greenhouse gas emissions from the energy consumed by dryers also increases fossil fuel consumption, causing negativities effects such as climate change, global warming, increased desertification, acid rain, and increased water levels [15–19]. This endangers human health [20]. For this reason, energy analysis and greenhouse gas emission calculations consumed during drying are important for sustainability [13].

The number of studies in the literature on the effect of agricultural drying systems on greenhouse gas emissions is very limited. In this study, greenhouse emission values for wind, solar, hydroelectric, and geothermal power plants based on the total energy use of different temperature applications in the convective drying method were determined and the results were compared. Present study is the first report in the literature to calculate greenhouse gas emissions from the convective drying of acorns.

2 Material and Method

2.1 Material

The study made use of Quercus Robur acorns that were procured from Kayseri. Acorns were collected during the ripening period, and the healthy ones were selected. Acorns were stored in a lab fridge at + 4 °C during the drying process. To finding the initial moisture content of the acorns, 100 gr samples were kept in an oven (Memmert UN55, Germany) for 24 h at 70 °C in 3 replicates. The acorn samples initial and post-oven weights were used to calculate the average moisture content [21].

2.2 Drying Method

Acorns used in the study were weighed at 115 ± 3 g for each trial, and they were dried at 40, 60, 80, 100 and 120 °C using the convective drying method. The products were dried until they reached moisture equilibrium. The acorns were dried in a vacuum oven (Miprolab Mve30, Turkey). The vacuum drying oven can operate at all temperatures between 40 °C and 280 °C. The oven has two trays and a perforated polyamide platform. All drying procedures were repeated three times. Until the drying process was completed, the weight reduction of the products was recorded at regular periods with the help of a precision scale (Ohaus Adventurer AX224, Australia) with an accuracy of 0.0001 g.

2.3 Energy and Greenhouse Gas Emission Calculations

The energy consumption values of the dryers were determined using a digital wattmeter (Tt Technic PM-001, Turkey) during the drying process [22]. Specific energy consumption was calculated following Eq. (1).

$$SEC = \frac{E_c}{m_w} \tag{1}$$

Here, Ec refers to the amount of energy consumed by the system, and mw refers to the weight of water loss from the crop (kg).

The energy required by distinct dryers was quantified using the total energy consumption equation. Electrical energy is provided by the transmission network, from power plants to consumption points. It should be remembered that in power supply networks and substations, a portion of the power generated is lost as heat. It is possible to determine the primary energy (fossil fuel) needed in a power plant to generate 1 kW of electricity by factoring in the entire share of losses in power consumption. The total share of losses in the network and substations is 14.2%. Furthermore, power plants typically have an internal consumption of about 3.5% [20]. The following formula can be used to determine the total power plant production needed for dryer applications. For all dryers combined, the value of η was determined to be 1.22 [14–20].

$$Total\ Energy = \frac{SEC}{\eta_{total}} = \frac{SEC}{\eta_{powerhouse} + \eta_{distribution}} \tag{1}$$

Greenhouse gas emissions per 1 kg of electricity generated were identified for various systems utilizing the greenhouse gas production factors determined by Kaveh et al. [15]. It should be noted that the indirect method of calculating greenhouse gas emissions is used, and the amount of electricity used in the drying process is used. To calculate the energy required for each experimental process, one must first ascertain the amount of energy required in various power plants to remove one kilogram of water during the drying of acorn grains. The energy requirements of the experimental procedures and the mechanical and thermal pre-treatments for drying were ascertained, and then the electrical transmission factor from the power plant to the consumption point was chosen. The total amount of electricity produced was calculated using the power plants' internal consumption factor. Next, it was applied to the computation of emissions of pollutants per 1 kWh of electricity used. Turkey is one of the nations with large greenhouse gas emissions, and power plants are generally of the wind, solar, hydroelectric cycle and geothermal types, and the average greenhouse gas emission values in the electricity generation systems of these sources are 10, 23, 26 and 38 gCO_2e kWh-1, respectively [15, 23]. Therefore, these values were considered in GHG emission estimates. Convective, area capacity is 0.12 m^2.

3   Results and Discussion

The specific energy consumption of the convective drying methods using different temperature applications in the drying of acorns are given in Fig. 1, and the drying times are given in Fig. 2. Accordingly, the highest energy value was obtained in convective

drying at 60 °C (63.07), followed by convective drying at 100 °C (62.06). However, the lowest energy values were obtained at an air temperature of 120 °C (27.85) and an air temperature of 40°C (40.52). According to Fig. 2, the convective drying process of acorn at 40, 60, 80, 100 and 120 °C, in the specified order, took 5760, 4800, 1170, 1170, and 480 min. It has been determined that the drying time is significantly shortened by increasing the ambient air temperature of the convective dryer. In this context, the drying time at 120°C, which is the highest drying air temperature, was 12 times shorter than at 40°C, where drying occurs the slowest. El-Mesery [25] reported that the drying time was shortened by raising the dryer temperature in convective drying of tomatoes at air temperatures of 40, 50 and 60 °C. Chasiotis et al. [25] dried jute using the convective drying technique at 40, 50 and 60 °C and noted that by increasing the heat level, the drying time was shortened and, accordingly, energy consumption decreased.

In the study, CO_2 emissions of convective dryers for wind and solar power plants, where different temperature applications were used to dry 1 kg of acorn, are given in Table 1. The greatest rate for the wind power plant was 630.75 g kg^{-1} at 60 °C air temperature. In addition, the lowest emission level of CO_2 for the wind power plant was recorded at 120 °C air temperature, with 278.51 g kg^{-1}. Within the scope of the study, the CO_2 emission value were obtained at 60°C air temperature for the wind power plant was found to be 2.26 times higher than the CO_2 emission value were obtained at 120°C. In other words, the CO_2 emission values for the wind power plant because of drying the acorn with the convective drying method at air temperatures of 40°C, 80°C and 100°C were determined as 405.21 g kg^{-1}, 442.08 g kg^{-1} and 620.59 g kg^{-1}. Similarly, the highest CO_2 emission value for the solar power plant was determined as 1450.72 g kg^{-1} in the convective drying method at 60°C, while the lowest CO_2 emission value was 640.56 g kg^{-1} at 120°C air temperature.
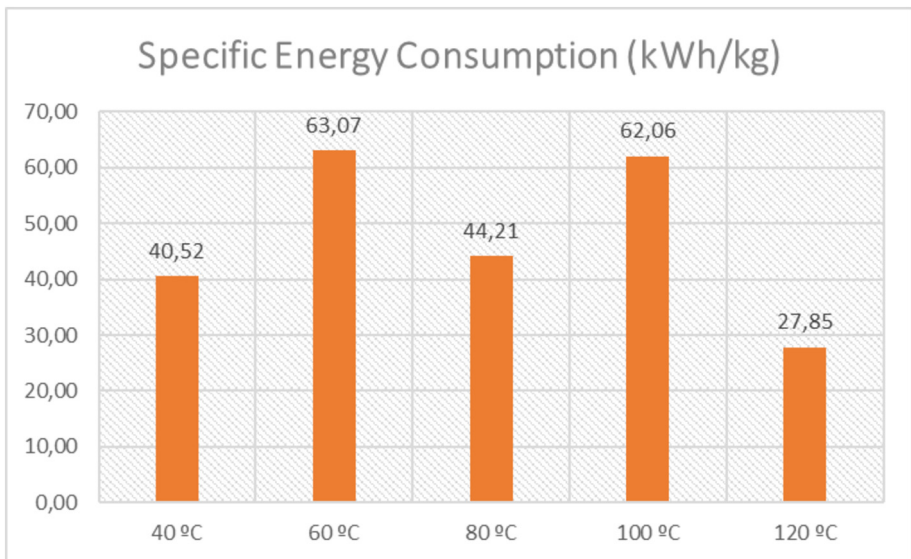
Fig. 1. Specific energy consumption for all drying methods
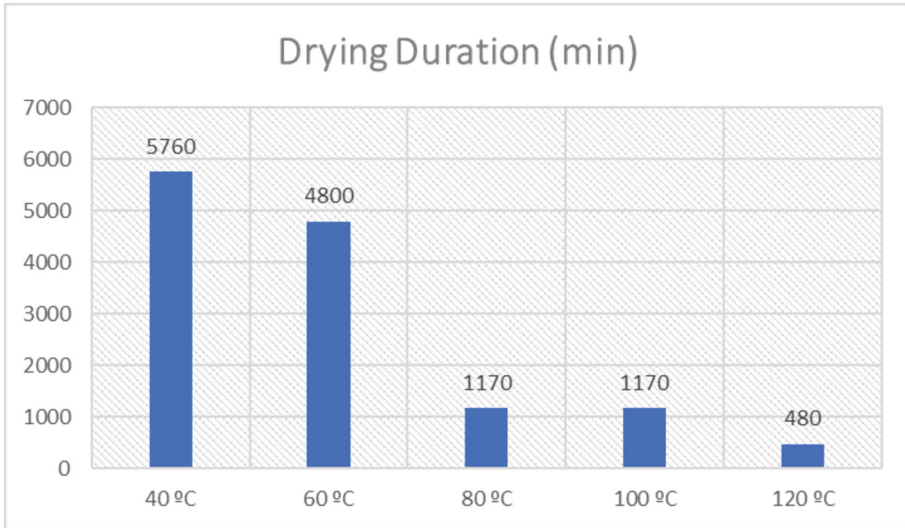
Fig. 2. Drying times for all drying methods

Table 1. Greenhouse gas emissions of the wind and solar power plants per kg of product ($g\,kg^{-1}$)

Drying Method	Wind	Sun
40 °C	405.21	931.99
60 °C	630.75	1450.72
80 °C	442.08	1016.78
100 °C	620.59	1427.36
120 °C	278.51	640.56

In the study, the highest and lowest CO_2 emissions of the convective dryer for hydroelectric and geothermal power plants, where different air temperatures are applied to dry 1 kg of acorn, are given in Table 2. Accordingly, the highest CO_2 emission value for the hydroelectric power plant in acorn drying was obtained at a 60 °C air temperature with 1639.95 g kg^{-1}, followed by 1613.54 g kg^{-1}, 1149.40 g kg^{-1}, 1053.55 g. kg^{-1}, respectively. Convective drying was followed at air temperatures of 100, 80 and 40°C. The lowest CO_2 emission value for the hydroelectric power plant was determined as 724.11 g kg^{-1} at 120°C drying temperatures. Similarly, for the geothermal power plant, the greatest CO_2 emission level was recorded at 60°C with 2396.85 g kg^{-1}, whereas the lowest CO_2 emission value was found to be 1058.32 g kg^{-1} at 120°C. It was noted that as the convective dryer air temperature increased, the drying time shortened and, accordingly, CO_2 emissions decreased. This situation is explained by the greater SEC score obtained during drying at low temperatures [20]. When all systems were evaluated in our study, the highest CO_2 emission value in the geothermal power plant was found to be 8.60 times higher than the lowest CO_2 emission value measured in the wind power

Table 2. Greenhouse gas emissions of the hydroelectric and geothermal power plants per kg of product (g kg^{-1})

Drying Method	Hydroelectric	Geothermal
40 °C	1053.55	1539.81
60 °C	1639.95	2396.85
80 °C	1149.40	1679.89
100 °C	1613.54	2358.25
120 °C	724.11	1058.32

plant. According to our findings, increasing the convective dryer air temperature in acorn drying reduced CO_2 emissions. In this regard, increasing the oven air temperature in convective drying may shorten the drying time and cause less greenhouse gas emissions. Our findings are similar to some studies in the literature. Kaveh et al. [26] found that in hot air drying of green peas at air temperatures of 35 and 50 °C, the CO_2 emission value decreased by higher the drying air temperature. Gökalp and Çetin [20] examined the CO_2 emissions for different power plants in the convective drying of orange slices at 50, 55 and 60 °C and reported that the lowest greenhouse gas emissions were obtained in wind power plants. Kaveh et al. [15] dried atlas gum convectively at 40, 55 and 70 °C stated that greenhouse gas emissions decreased by increasing the temperature level. Darvishi et al. [24] dried carrot slices with an initial moisture content of 89.5 ± 1.2% using microwave, convective, and hybrid drying methods and reported that the highest greenhouse gas emission values (CO_2, NOx, and SO_2) were measured in the convective drying method. Taghinezhad et al. [26] emphasized that in drying blackberries with ultrasound pretreatment (50, 60 and 70 °C infrared temperatures), CO_2 and NOx emission values decreased significantly because of increasing pretreatment application time and drying air temperature.

4 Conclusions

In the present study, CO_2 emission values for convective drying conditions where different temperature applications were used for drying acorn were determined. It was observed that the drying time was significantly shortened by increasing the dryer air temperature. However, according to our findings, it has been determined that CO_2 emissions decrease as the convective dryer air temperature increases. This situation is thought to be related to the high SEC value measured due to the long drying time in low temperature applications. It has been shown that high temperature applications give more reasonable results in terms of greenhouse gas emissions. The applications and analyses carried out in this study will contribute to the food processing sector, which produces high energy consumption in terms of greenhouse gas emissions, and to the possible studies of relevant researchers. For future studies, it may be recommended to try different drying systems and different power plants to determine the effect of drying techniques on greenhouse gas emissions. Present study is a preliminary study for large-scale forage crops drying

facilities. It is thought that the drying processes will be carried out more carefully and in an environmentally friendly manner, considering the greenhouse gas emissions caused by different temperature applications in the convective drying method. In addition, it is anticipated that studies on the design of different drying techniques and dryer systems that minimize greenhouse gas emissions will increase.

References

1. Karaman, M., Azize, TKM. (2019) The use of possibilities of oak acorn in diets of livestock. black sea j. Agric. 2(4): 230–232
2. Fkiri S et al (2021) Effect of geographic origin in mineral composition of zeen oak acorns (Quercus canariensis Willd). Thalassia Salentina 43:121–126
3. Zhang Z et al (2020) Effect of starch isolation method on structural and physicochemical properties of acorn kernel starch. Starch-Stärke 72:1–2
4. Zhao Y, Zeng W, Li W, Bi Y (2021) Complete chloroplast genome sequence of the drought and heat-resistant Chinese Alfalfa Landrace, Medicago Sativa 'Deqin.' Mitochondrial DNA Part B 6(4):1488–1489
5. Namicev P, Petrovski M (2019) The impact of the application of wood on the technological preparation for furniture manufacturing. J. Process. Manag.-New Technol. 7(3):1–9
6. Taib M, Bouyazza L (2021) Composition, physicochemical properties, and uses of Acorn starch. J Chem 2021:1–9
7. Çetin N, Ciftci B, Kara K, Kaplan M (2023) Effects of gradually increasing drying temperatures on energy aspects, fatty acids, chemical composition, and in vitro ruminal fermentation of acorn. Environ Sci Pollut Res 30(8):19749–19765
8. Mediani A et al (2022) A comprehensive review of drying meat products and the associated effects and changes. Front Nutr 9:1057366
9. Abraha B, Admassu H, Mahmud A, Tsighe N, Shui XW, Fang Y (2018) Effect of processing methods on nutritional and physico-chemical composition of fish: a review. MOJ Food Process. Technol. 6(4):376–382
10. An N-n, Lv W-q, Li D, Wang L-j, Wang Y (2023) Effects of hot-air microwave rolling blanching pretreatment on the drying of turmeric (Curcuma longa L.): physiochemical properties and microstructure evaluation. Food Chem 398:133925. https://doi.org/10.1016/j.foodchem.2022.133925
11. Stamenković Z et al (2020) Ranking and multicriteria decision making in optimization of raspberry convective drying processes. J Chemom 34(4):e3224
12. Motevali A, Minaei S, Banakar A, Ghobadian B, Khoshtaghaza MH (2014) Comparison of energy parameters in various dryers. Energy Convers Manage 87:711–725. https://doi.org/10.1016/j.enconman.2014.07.012
13. Kaveh M, Çetin N, Gilandeh YA, Sharifian F, Szymanek M (2023) Comparative evaluation of greenhouse gas emissions and specific energy consumption of different drying techniques in pear slices. Eur Food Res Technol 249(12):3027–3041. https://doi.org/10.1007/s00217-023-04346-2
14. Motevali A, Koloor RT (2017) A comparison between pollutants and greenhouse gas emissions from operation of different dryers based on energy consumption of power plants. J Clean Prod 154:445–461
15. Kaveh M, Chayjan RA, Taghinezhad E, Sharabiani VR, Motevali A (2020) Evaluation of specific energy consumption and GHG emissions for different drying methods (case study: Pistacia Atlantica). J Clean Prod 259:120963

16. Ahmed I, Rehan M, Basit A, Hong KS (2022) Greenhouse gases emission reduction for electric power generation sector by efficient dispatching of thermal plants integrated with renewable systems. Sci Rep 12(1):12380

17. Kocak E, Alnour M (2022) Energy R&D expenditure, bioethanol consumption, and greenhouse gas emissions in the United States: non-linear analysis and political implications. J Clean Prod 374:133887

18. Adnouni M, Jiang L, Zhang XJ, Zhang LZ, Pathare PB, Roskilly AP (2023) Computational modelling for decarbonised drying of agricultural products: sustainable processes, energy efficiency, and quality improvement. J Food Eng 338:111247

19. Kumari, S., Bains, G.: Agrifood and climate change: impact, mitigation, and adaptation strategies. Global Climate Change and Plant Stress Management 53–64 (2023)

20. Gökalp Z, Çetin N (2022) Evaluation of GGE of different process for drying orange slices. Curr. Trends Nat. Sci. 11(21):170–175. https://doi.org/10.47068/ctns.2022.v11i21.020

21. Kahraman O, Malvandi A, Vargas L, Feng H (2021) Drying characteristics and quality attributes of apple slices dried by a non-thermal ultrasonic contact drying method. Ultrason Sonochem 73:105510. https://doi.org/10.1016/j.ultsonch.2021.105510

22. Çetin N (2022) Comparative assessment of energy analysis, drying kinetics, and biochemical composition of tomato waste under different drying conditions. Sci Hortic 305:111405

23. Kaveh M, Chayjan RA, Taghinezhad E, Sharabiani VR, Motevali A (2020) Evaluation of specific energy consumption and GHG emissions for different drying methods (case study: Pistacia Atlantica). J. Cleaner Prod. 259:120963

24. Melikoglu M (2013) Vision 2023: forecasting turkey's natural gas demand between 2013 and 2030. Renew. Sustain. Energ. Rev 22:393–400

25. El-Mesery HS (2022) Improving the thermal efficiency and energy consumption of convective dryer using various energy sources for tomato drying. Alex Eng J 61(12):10245–10261

26. Chasiotis V, Tsakirakis A, Termentzi A, Machera K, Filios A (2022) Drying and quality characteristics of Cannabis sativa L. inflorescences under constant and time-varying convective drying temperature schemes. Therm. Sci. Eng. Prog. 28:101076. https://doi.org/10.1016/j.tsep.2021.101076

27. Kaveh M, Abbaspour-Gilandeh Y, Nowacka M (2021) Comparison of different drying techniques and their carbon emissions in green peas. Chem Eng Process 160:108274

28. Darvishi, H., Khodaie, J., Behroozi-Khazaei, N., Salami, P., Akhijahani, H.S.: Greenhouse gas emission reduction potential, energy and exergy analysis of combined microwave-convective dryer. Energy 128772 (2023)

29. Taghinezhad E, Kaveh M, Khalife E, Chen G (2021) Drying of organic blackberry in combined hot airinfrared dryer with ultrasound pretreatment. Drying Technol 39(14):2075–2791

Effect of Different OLR and Mixture Ratios on Biogas Production Using Goat Dung and Maize Silage

Aslı Ayhan Arslan[1(✉)], Şeniz Öziş Altınçekiç[2], Emine Budaklı Çarpıcı[3], Halil Ünal[1], Ufuk Alkan[4], and Kamil Alibaş[1]

[1] Faculty of Agriculture, Department of Biosystems Engineering, Bursa Uludağ University, Bursa, Turkey
aayhan@uludag.edu.tr
[2] Faculty of Agriculture, Department of AnimalScience, Bursa Uludağ University, Bursa, Turkey
[3] Faculty of Agriculture, Department of Field Crops, Bursa Uludağ University, Bursa, Turkey
[4] Faculty of Engineering, Department of Environmental Engineering, Bursa Uludağ University, Bursa, Turkey

Abstract. The aim of this study is to determine the effect of the use of goat excrement, which has not been used much in biogas research, and the use of maize silage on biogas production. The maize silage used does not contain cobs and maize kernels. It was studied under mesophilic conditions in a batch fermentation system with a hydraulic retention time (HRT) of 40 days. In the experiments, anaerobic fermenters with a total volume of 3 L each, with a heating and automatic mixing system were used. The amount of biogas produced was measured using the water displacement principle and the biogas content was measured with a biogas analyzer. Trials were carried out using two different mixing ratios at the same (0.5 grVS/l day) organic loading rate (OLR) and using the same mixing ratio at two different OLR values. The highest biogas production (approximately 40 L) was measured at an OLR value of 0.8 gVS/l d using 65% goat manure and 35% silage in the mixture. Also, the highest methane content was obtained in this application. Although increasing the amount of silage with a constant OLR resulted in a small increase in the biogas generation, the methane content decreased. It was concluded that goat excrement can be used to generate biogas as a substrate.

Keywords: Biogas · Goat dung · Maize silage · OLR · Mixture ratio · Renewable energy

1 Introduction

Biogas is an important renewable energy source in terms of today's energy needs, sustainability and clean production principles. The use of biogas reduces greenhouse gas emissions, one of the most important responsible for global warming. In addition, increasing

---

the use of biogas as a renewable energy source is an important part of the development of energy agriculture. Anaerobic fermentation must be environmentally friendly, environmentally beneficial, and economically efficient. Raw materials that can be used in biogas production, their effects on biogas yield, and the determination of optimum working conditions are important issues to be emphasized. The supply of high-quality raw materials is an indispensable prerequisite for obtaining optimum gas efficiency.

Agriculture and animal production are of utmost importance for the economy of Turkey. Nonetheless, the energy need is met by primary energy sources for agricultural enterprises. Thus, environmentally friendly energies, such as biogas, gain importance for these enterprises so as to reduce production inputs. This will both increase the efficiency of the enterprise and reduce the damage to the environment by reducing greenhouse gas emissions. Agricultural wastes, manure, and energy crops may be utilized as a source of biogas in agricultural enterprises [1–12].

Although agricultural wastes with lignocellulose content are low in nutritional and thermal value, they are used in animal nutrition, as fuel, and as animal bedding on farms. Some of them are left in the fields or burned. This causes nitrate loss, air pollution, and an increase in greenhouse gas emissions. In addition, animal wastes can be used as fuel in the form of dung, stored in vacant lots, or discharged to the nearest water source. It is stored in the manure pits in the enterprises under the best conditions. However, it is seen that these tanks do not have the sealing properties in the standards. These traditional ways of use and disposal cause many environmental pollutions such as water, air, image, and energy loss.

The raw materials used in biogas production and their properties have a significant effect on biogas yield. The production of methane from organic materials depends on substances that can decompose into methane (CH_4) and carbon dioxide (CO_2). The composition and decomposition of animal manure and plant wastes are key factors in methane yield. Crude protein, crude oil, fiber, cellulose, hemicellulose, starch, and sugar are significantly effective in methane formation [4].

OLR is the amount of organic matter that is supplied to the digester per unit volume of the digester, and is mostly related to anaerobic digestion determinants. The microbial population is influenced directly by OLR which stimulates the AD process. Organic loading matter may have a positive or adverse effect in biogas production [13].

The nutritional composition of anaerobic digestion substrates can be different due to the varying properties of biodigestible OM. If not managed appropriately, the discrepancies in the nutritional composition can pose hazards causing process instability and can vary the critical OLR point for each substrate as a result of microbial processes [13].

Co-digestion requires combining different raw materials having different nutritional compositions and the resultant mixture is used as the substrate in a digester. Co-digestion is necessary either to enable the dilution of the toxic substances in certain materials or, generally, to obtain the appropriate Carbon:Nitrogen (C:N) ratio in the mixture [13].

The biodegradable organic compounds such as proteins, fats, and carbohydrates determine the biogas yield under anaerobic conditions. For instance, biogas yields for proteins, fats, and carbohydrates were found to be 0.38, 0.53, and 1.0 m3/kg VS, respectively for biogas compositions (CH_4:CO_2) of 60:40, 70:30, and 50:50. Furthermore, high amounts of heavy metals (Ca, Li, Mg) are present in goat and chicken dung. In an

anaerobic digestion process for the wastes, cationic elements are needed for microbial growth, however, in high concentrations, microbial activity can be inhibitory [14].

OM content of the biomass and the total biogas production are also associated with DM and ODM [14]. Furthermore, water provides hydrogen ions to bond with carbon ions resulting in methane, implying that water contributes to biogas production as well [15].

It can be deduced from the previous studies that the characteristics of the crude materials and the operational factors need to be taken into account appropriately for biogas production under anaerobic fermentation.

According to Turkish Statistics Institution (TUIK) data, the area planted in maize was approximately 1.44 million ha in 2022 resulting in a total yield of 37.2 million tons. Turkey's total number of goats was approximately 11.6 million in 2022 [16]. It may be suggested that both the maize and goat are important entities in the countries' agricultural economy. The previous research has not focused much on the use of goat excrement in biogas studies.

The aim of this study is to determine the effect of the use of goat excrement, which has not been used much in biogas research, and the use of maize silage on biogas production. Unlike the corn silages used in most of the previous studies, materials other than the grain and cobs were used to make the silage for biogas production in this study, which differs from most of the previous studies. Silage from sweet corn residues was prepared using the corn husks and stalks. In addition to raw material availability, the effect of mixing ratio and OLR on biogas yield was also examined.

2   Methods

As the plant material, sugar corn plant (merit variety, MayAgro Seed Co.) was used. Merit variety is known to be a high-yielding and early emerging plant.

In the biogas trials, the plant wastes, remaining after the cobs were threshed, were used. The maize silage did not contain cobs and maize kernels. In order to reduce the particle size, the plant material was chopped with a laboratory blender. The material to be used as silage was filled into 1-L glass jars that were labeled and tared beforehand, allowing only gas escape, and the silage production process was carried out by closing the mouths. No additives were used in the silage production. The prepared silage jars were subjected to fermentation for 60 days in the darkroom and at the end of this period, the jars were opened and the silage material was subjected to biogas tests. Corn waste to be used as silage and goat manure was stored in a deep freezer at -20 °C in order to prevent any deterioration until the start of the trial.

Goat manure was used as animal waste in the research. Goat manure was supplied from 2–3-year-old Saanen cross goats raised in Bursa Uludağ University Faculty of Agriculture Agricultural Application and Research Center Farm. Goats are kept in shelters at night and taken to pasture during the day. During their stay in the shelter, the goats are given a ration prepared in the enterprise containing a mixture of wheat, corn, sunflower meal, vitamins, and minerals. There is always water and licking stones in front of them. Goat dung was collected and packed in air-tight plastic bags.

Prior to the analyses, an electrical blender was used to reduce the particle sizes of the goat manure and the maize silage. Then the samples were mixed thoroughly. Prior to

analysis, the specimens were kept at 4 ° C to prevent bacterial decomposition. Industrial inoculum was provided by a private biogas plant and was used as a catalyst for the anaerobic digestion process.

Prior to the experiment, substrates were analyzed for dry matter (DM), volatile solid (VS), ash (XA), and C:N ratio with standard analysis procedures [17]. pH measurement was made with a desktop pH meter.

At the beginning of the experiment, the C:N ratio of the mixtures was calculated and the initial pH was measured. While the carbon-nitrogen value of corn silage was higher than the limit value for biogas production, the value of goat feces was low, although it was within the limit values. By subjecting them to fermentation together, the optimum carbon-nitrogen value for anaerobic fermentation was obtained.

Experiments were carried out at mesophilic conditions in a laboratory-scale batch process. In the batch reactors, there were different sets of experiments carried out with two different compositions of feeding materials and two different OLRs. The details of the experimental design are shown in Table 1.

Table 1. The experimental design.

Reactor	Mixture Rate (M:S, %)*	Inoculum (L)	Hydraulic Retention Time (d)	OLR (gr VS/L*d)
R1	65:35	1.6	40	0.5
R2	65:35	1.6	40	0.8
R3	55:45	1.6	40	0.5

* M: Manure, S: Silage; OLR: Organic Loading Rate

In this study, two factors were examined to investigate their effects on biogas yield. The first factor was the mixing ratio of goat feces (M) and corn silage (S). M/S rates were 65% manure + 35% silage and 55% manure + 45% silage, respectively. The second factor was OLR with a mixture of %65 manure + %35 silage at 0.5 and 0.8 gr VS/L*d. Hydraulic Retention Time (HRT) was chosen as 40 days due to the presence of cellulosic structure.

Anaerobic fermenters were used in the experiment, which were specially designed and manufactured. Feed pipe, gas outlet line and mixer are placed on the upper flange of anaerobic fermenters with a total volume of 3 L and the main body made of heat-resistant glass material based on borosilicate. The leakage and ingress of air were prevented by using tight caps so as to create and maintain anaerobic conditions. There is a discharge port and thermocouple on the flange under the bottle. The temperatures of the bottles were automatically controlled using a heating system consisting of a temperature sensor insulated and inserted into the mixing chamber. The amount of biogas was measured daily according to the water displacement principle.

The gas outlet line was used for gas sampling from the digester for biogas analysis. The biogas was gathered in plastic gas bags to check the biogas composition. Biogas

quality (CH_4, CO_2, H_2S, O_2, other) was analyzed with a biogas analyzer (Model Biogas 5000, Geotechnical Instrument Ltd., England). Methane and carbon dioxide are measured by infrared absorption and oxygen and H_2S are measured by a chemical cell.

To examine gas production more closely during the 40-day hydraulic retention period, the process was divided into 10-day periods (P1, P2, P3, P4).

3   Results

The results of the preliminary analyses are given in Table 2, presenting some characteristic features of goat feces, waste corn silage, and inoculum at the beginning of the trial. Raw material properties in the current study were similar to the findings in other studies [18–22]. According to Schattauer and Weiland [23], a C:N range of 10–30 is required during anaerobic digestion, otherwise carbon conversion to CH_4 is not optimal, i.e., the potential to generate CH_4 is not maximized. In Table 2, while the carbon-nitrogen value of corn silage was higher (39.75) than the acceptable range (10–30) for biogas production, the value of goat feces was low, although it was within the limit values.

Table 2. The characteristics of the substrates.

Parameters	Goat Dung	Maize Silage	Inoculumn
DM	39.26	26.43	7.73
VS	72.23	76.58	53.48
XA	24.60	27.76	29.26
C:N	18.94	39.75	3.74
pH			8.57

Biogas production and methane efficiency are affected by the animal diet. It was reported that, during anaerobic digestion, higher methane levels could be obtained from manures containing higher levels of crude protein [4].

The presence of lignin in the crude materials is not preferred since lignin is known to be vigorously recalcitrant in AD process. Additionally, lignin prevents some nutrients from accessing the microorganisms. Therefore, to promote the release of biodegradables, further steps become necessary during the digestion of materials containing high levels of lignin [13]. According to Amon et al. [4], methane efficiency and biogas production are influenced by the type of maize, time of harvest, harvesting method, and ensilage operation. The methane yield, for instance, reduced when the crop was near full maturity.

In the current study, the maize was harvested at about maturity and had a C:N ratio lying outside the optimum range. Thus, the raw material did not have the potential to maximize methane production. Since a narrower C:N range was necessary to enhance biogas production [4, 23, 24], additional substrates were used to increase fermentation efficiency. In this study, the plant material was chopped to obtain the silage, and the shredding generated chemicals such as lactic and acetic acids, methanol, alcohols, formic

acid, H^+, and CO_2, which were reported to be significant precursors in methane formation [25]. Finally, the decomposition of the raw fibers during ensiling makes the nutrients available for methanogenic metabolism. As a result of utilizing substrates and ensiling the plant material in the current study, the C:N range was within the recommended limits to optimize biogas production.

Although the limits for C:N ratios of the raw materials were improper for biogas generation at the beginning of the experiment, the C:N ratios were brought to the acceptable limits for the mixtures, as shown in Table 3. The value of pH ranged from 9.48 to 8.63 in the six fermenters whereas C:N values were 23.19 in R1-R2 and 24.78 in R3.

Table 3. pH and C:N rate of the mixtures.

Treatments	R1	R2	R3
pH	8.62	8.57	8.63
C:N	2319		24.78

The measured daily biogas volumes for the 40-day experiment are shown in Fig. 1. Fermenters R1 and R2 had the same mixing ratio while R2 had high OLR and had a significant increase in gas production. R2 produced 40.29 L biogas in batch assay for a period of 40 days. R1's methane percentage was 64% whereas R2's methane percentage was 65.8%. It was concluded that R2 had better biogas efficiency in terms of both quantity and gas quality. Sowunmi et al. [26] also found that higher loading concentrations of goat dung resulted in greater amounts of bio methane production.
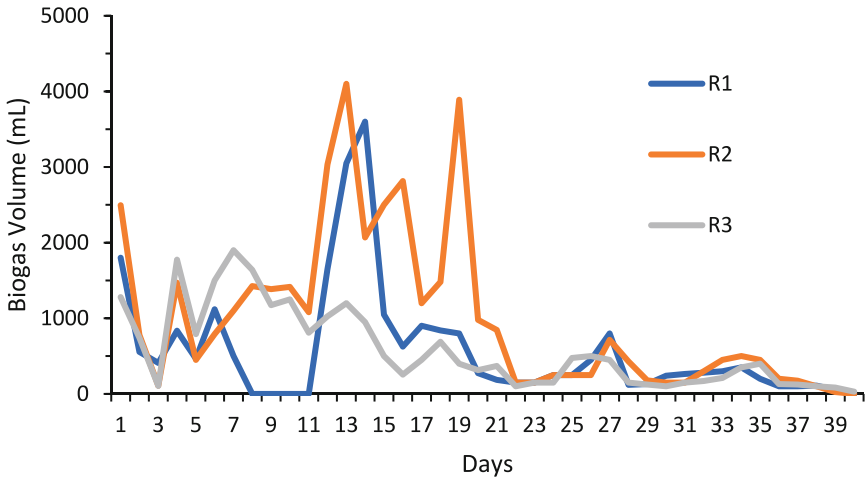
Fig. 1. Daily biogas production

The different mixtures of R1 and R3, with a higher amount of silage, produced some excess gas, but seems insignificant since R1 and R3 produced similar amounts of total

gases with 22.96 and 23.07 L, respectively. Methane percentages of R1 and R3 were measured to be 64% and 60%, respectively. In other words, although R3 produced more gas, its methane rate was lower. A similar result was found by Sowunmi et al. [26] using goat dung, stating that increasing the loading concentrations prevented from generating the highest methane gas. Pan-in and Sukasem [19] used a dry co-digestion method with goat dung and corn husks and obtained 46.13% methane, which was lower than the current study.

Daily gas measurements in Fig. 1 show that gas production fluctuated throughout the course of the experiment in all fermenters. The gas generation significantly increased in the second week of the HRT in the fermenters R1 and R2, still depicting large variations with time. R3, however, showed a tendency to reduce the gas generation. After day seven, R3 showed a general declining or low gas-yielding behavior until the end of the experiment.

The amount of biogas produced in 10-day periods was determined and depicted in Fig. 2. In P2, the gas production increased notably in fermenters R1 and R2 while R3 showed a large drop in biogas production. Figure 3 All fermenters yielded low and similar amounts of gas volumes in P3 and P4 compared to the first two periods.
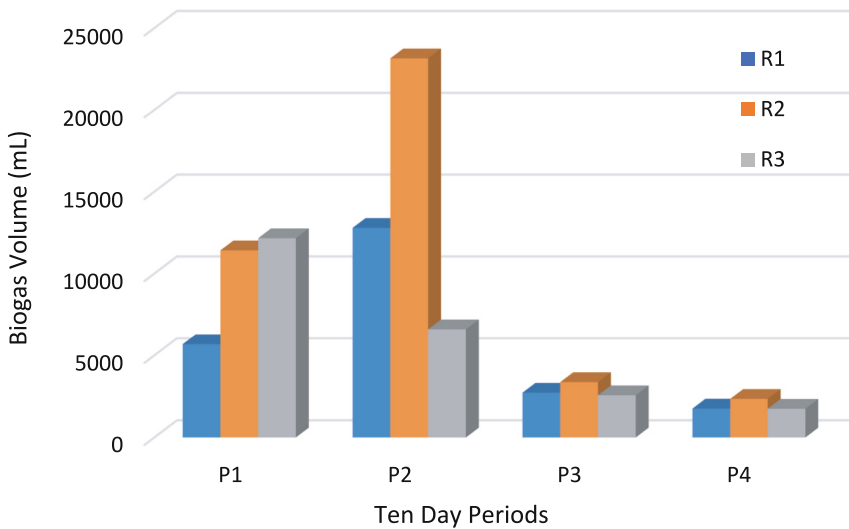
Fig. 2. Biogas production according to periods

In P2, the highest gas production was 23.15 L in R2. This value was approximately 25% higher than the total gas production of R1 and R3 in the first 20 days. It is understood that this result is related to the high OLR value. It was explained in other studies that high OLR value results in high gas production, however, the OLR value varies depending on the raw material properties used in anaerobic fermentation, HRT, etc., and hence the efficiency in biogas production may drop depending on the affecting factors [13–15, 27]. Hanafiah et al. [20] measured the biogas production in a mesophilic condition for

20 days and produced 2.141 L of biogas from the goat's dung, which was significantly low compared to the current study.

While the total gas production of R1 and R2 increased in P2, the gas production of R3 decreased (Fig. 2). When looking at the total of the first 20 days, these two mixtures with different mixture ratios, at a value of 0.5 g VS/L d OLR, produced approximately the same amount of gas (18.5 L).

In P4, the gas production of all fermenters decreased. Although the highest gas production was in R2 with 2.35 L of gas production, there was a decrease of approximately 69% compared to the previous period. For fermenters R1 and R3, the % decrease in the amount of gas compared to the previous period was approximately 64 and 68, respectively.

Figure 3 shows the cumulative volume of gas produced up to each period for each treatment. It was calculated that approximately 80, 86, and 81% of the total biogas volume was already produced at the end of P2 whereas 92, 94, and 92% were accumulated up to P3, respectively for R1, R2, and R3. At the end of the 20 days of fermentation, R1 and R3 treatments reached the same total volume of biogas production, but the cumulative gas production of R1 and R3 was much lower than that of R2. Longer HRT increased the total volume of biogas to be harvested, however at a much lower rate, especially in periods 3 and 4. As a result, the last period corresponding to 25% of the total time of HRT had a gas production of about 7–8%.
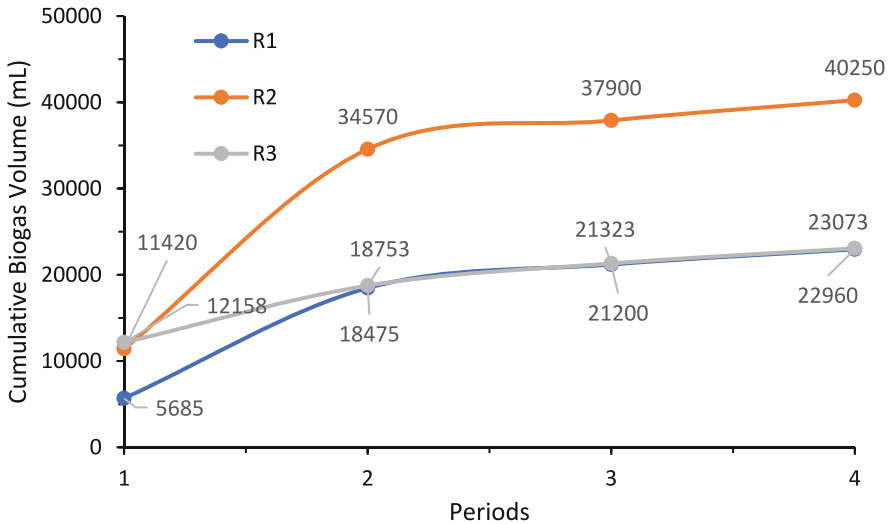
Fig. 3. Cumulative biogas volumes obtained from different treatments

4   Conclusion

This study focused on the effect of corn silage and goat dunk at different OLR values and mixture ratios (Manure:Silage, %) on biogas and methane productions for an HRT of 40 days. The treatments were 65:35% with 0.5 g VS/L*d in reactor R1, 65:35%

with 0.8 g VS/L*d in reactor R2, and 55:45% with 0.5 g VS/L*d in reactor R3. The biogas production fluctuated with time in all reactors throughout the experiments. The biogas yield was the greatest in P2 (the second period from 10th to 20th days of the experiment), followed by P1, P3, and P4. More than 80% of the total biogas production was accomplished at the end of P2. The biogas production continued until the end of the HRT with about 93% gas production at the end of P3. R2 produced the greatest amount of biogas (40.25 L) whereas R1 and R3 resulted in about 23 L of biogas, suggesting that a high OLR value promotes the gas production significantly. The effect of the mixture rate was less pronounced in the biogas production. Methane percentages in the gases were 65, 65.8, and 60%, respectively for R1, R2, and R3, implying that the methane rate was positively affected by the high OLR value in fermenter R2. By increasing the amount of silage in the mixture ratio, the increase in lignocellulosic structure must have resulted in a decrease in the methane value. Also, the silage containing a high mixture ratio of sweet corn should have contributed to the performance in biogas production, due to the lignin content of corn silage, which reduces microbial productivity. This study provided new data on biogas production using a mixture of goat dung and corn silage that was prepared without materials other than the grain and cobs. It can be concluded that, high OLR values can be used in order to increase the biogas production and methane rates when goat dung and corn silage are used in the mixture.

References

1. Al-Masri MR (2001) Changes in biogas production due to different ratios of some animal and agricultural wastes. Biores Technol 77:97–100
2. Alvarez R, Liden G (2009) Low temperature anaerobic digestion of mixtures of llama, cow and sheep manure for improved methane production. Biomass Bioenerg 33(3):527–533
3. Amon T, Amon B, Kryvoruchko V, Bodiroza V, Pötsch E, Zollitsch W (2006) Optimising methane yield from anaerobic digestion of manure: Effects of dairy systems and of glycerine supplementation. Int Congr Ser 1293:217–220
4. Amon T, Amon B, Kryvoruchko V, Zollitsch W, Mayer K, Gruber L (2007) Biogas production from maize and dairy cattle manure—Influence of biomass composition on the methane yield. Agr Ecosyst Environ 118:173–182
5. Biswas J, Chowdhury R, Bhattacharya P (2007) Mathematical modeling for the prediction of biogas generation characteristics of an anaerobic digester based on food/vegetable residues. Biomass Bioenergy 31:80–86
6. Chynoweth DP, Turick CE, Owens JM, Jerger DE, Peck MW (1993) Biochemical methane potential of biomass and waste feedstocks. Biomass Bioenergy 5(1):95–111
7. Gunaseelan VN (1997) Anaerobic digestion of biomass for methane production: a review. Biomass Bioenergy 13(1–2):83–114
8. Hammad M, Badarneh D, Tahboub K (1999) Evaluating variable organic waste to produce methane. Energ. Convers Manag. 40:1463–1475
9. Macias-Corral M et al (2008) Anaerobic digestion of municipal solid waste and agricultural waste and the effect of co-digestion with dairy cow manure. Biores Technol 99:8288–8293

10. Martin-Ryals A D (2012) Evaluating the potential for improving anaerobic digestion of cellulosic waste via routine bioaugmentation and alkaline pretreatment. Master Thesis. Agricultural and Biological Engineering in the Graduate College of the University of Illinois at Urbana-Champaign. http://hdl.handle.net/2142/34285, Accessed 20 Jan 2013

11. Tong X, Smith LH, McCarty PL (1990) Methane fermentation of selected lignocellulosic materials. Biomass 21:239–255

12. Weiland P (2003) Production and energetic use of biogas from energy crops and wastes in Germany. Appl Biochem Biotechnol 109:263–274

13. Nkuna R, Roopnarain A, Rashama C, Adeleke R (2022) Insights into organic loading rates of anaerobic digestion for biogas production: a review. Crit Rev Biotechnol 42(4):487–507

14. Abdul Aziz NIH, Hanafiah MM, Mohamed Ali MY (2019) Sustainable biogas production from agrowaste and effluents - A promising step for small-scale industry income. Renewable Energy 132:363–369

15. Spagni A, Casu S, Farina R (2010) Effect of the organic loading rate on biogas composition incontinuous fermentative hydrogen production. J Environ Sci Health Part A 45:1475–1481

16. Turkish Statistical Institute (2023) TUIK statistical database, Ankara

17. Association of Official Analytical Collaboration International (2000) Official methods of analysis of AOAC international. 17th edn. AOAC Int. Gaithersburg, MD., USA

18. Schievano A, D'Imporzano G, Adani F (2009) Substituting energy crops with organic wastes and agro-industrial residues for biogas production. J Environ Manag 90:2537–2541

19. Pan-in S, Sukasem N (2017) Methane production potential from anaerobic co-digestion of different animal dungs and sweet corn residuals. Energ. Procedia 138:943–948

20. Hanafiah MM et al (2017) Biogas production from goat and chicken manure in Malaysia. Appl Ecol Environ Res 15(3):529–535

21. Makki EK, Eljack BE (2003) Seasonal variation and production of biogas from three types of animal dung. Ahfad J. 20(2):18–25

22. Ayhan A, Qingyu L, Alibaş K, Ünal H (2013) Biogas production from maize silage and dairy cattle manure. J Anim Vet Adv 12(5):553–556

23. Schattauer A, Weiland P (2004) Handreichung Biogasgewinnung und – nutzung. Final Report. Förderkennzeichen 22027200. Fachagentur Nachwachsende Rohstoffe e.V. (Ed.), Gülzow

24. Amon T, Kryvoruchko V, Amon B (2011) Methane production from maize, grassland and animal manures through anaerobic digestion. http://www.ramiran.net/doc04/Proceedings%2004/T_Amon.pdf , Accessed 10 May 2012

25. Madigan MT, Martinko JM, Parker J (2000) Brock Mikrobiologie. Spektrum Akademischer Verlag, GmbH Heidelberg, Berlin

26. Sowunmi A, Mamone RM, Bastidas-Oyanedel JR, Schmidt JE (2016) Biogas potential for electricity generation in the Emirate of Abu Dhabi. Biomass Conversion Biorefinery 6:39–47

27. Yang S et al (2023) Biogas production of food waste with in-situ sulfide control under high organic loading in two-stage anaerobic digestion process: Strategy and response of microbial community. Biores Technol 373:128712

Exergy-Based Slow-City/Agriculture Mechanization with Circular Hydrogen and Renewable Energy Systems

Birol Kılkış[(✉)] [ID]

OSTIM Technical University, Ankara, Turkey
`birol.kilkis@ostimteknik.edu.tr`

Abstract. This paper presents a novel concept about an integrated, nearly-zero carbon agricultural and horticultural and animal farm complex, attached to a slow city. A Rational Exergy Management Model-based design concept has been developed to maximize land use effectiveness and minimize carbon dioxide emissions responsibility. The system involves a circular hydrogen approach and comprises the following primary features. 1- Deep wells, 2-Above-the-ground photo-voltaic-thermal solar collectors, 3-Artifical water basin/pool, 4-Water electrolysis system, 5- Hydrogen production and storage facility, 6- Closed water circuit between the pool and fuel cells that generate power and then return water, 7- Hydrogen cogeneration system, 8-Heat pumps and absorption cooling systems, 8-Thermal storage system, 8-Partial coverage of the lake surface with solar photo-voltaic-thermal panels with careful balance between marine life, surface evaporation, and power and heat generation, 9-Wind Turbines, 10-Geothermal energy system, 11-District Energy System, 12-Fishery, Agriculture and animal farm, 13-Light industry, 14-Advanced greenhouse system, 15-Irrigation system, 16-Hydrogen mobility and agricultural mechanization with electric and hydrogen fuel, 17-Food drying and cold warehouse complexes, 18-Dwellings and city infrastructure, 19-Biogas system, 20-Irrigation system, 21-Educational and agricultural research laboratories, 22-Milk industry. Sample calculations show that the net result will be nearly zero carbon complex with 100% renewables, such that nearly-avoidable carbon dioxide emissions responsibility is less than separate photo-voltaic and wind turbine systems by as much as seven times. A novel greenhouse concept and wind turbine-integrated solar photo-voltaic-thermal panel system are also introduced. The paper gives detailed information about this design and proves that a circular hydrogen economy is possible and economical.

Keywords: Circular hydrogen · Agriculture · Horticulture · Renewable energy · Slow-city and farm · Rational exergy management model

1 Introduction

Agricultural activities, covering crops and livestock, contribute to emissions in several aspects. Management of agricultural soils is one of them, which accounts for about 50% of the greenhouse gas emissions from the agriculture sector [1]. As a second example,

nitrous oxide emissions are the results of the application of fertilizers including organic ones, nitrogen-fixing crops, organic soil drainage, and irrigation methods. These few examples show that agricultural emissions are too complex to analyze, interrelated, often conflicting, and related to the level and type of mechanization. Therefore, agricultural mechanization may not be simply indexed to the number of tractors or the energy intensity per acre of land. Agricultural mechanization has two prongs, namely the CO_2 emissions due to the use of electromechanical systems and components, using fossil fuels or electricity, like electric tractors, and the potential decrease of emissions per agricultural yield due to increased productivity. The second prong is related to the trend of using more electric power over fossil fuels must be handled carefully because the added battery weight and the original source of electricity are important factors. The contradictory nature of these two prongs was explained by Kim, and et al. [2, 3]. See Fig. 1.

The annual contribution of hydro, solar, and wind energy to the energy budget of Turkey is around 30% as an actual figure. The installed capacity of renewables by 2022 in Turkey is 54%, which should not be confused with the actual annual contribution [4]. Furthermore, farm mobility like electric tractors needs to convert AC from the grid to DC first to charge their batteries and then re-convert to AC by inverters to run their electric motors for driving. Therefore, the share of on-site renewables, including solar, biogas, wind, and geothermal with the optimally available mix is an important issue, rather than relying on the central power plants, even if they are green to a certain extent. In addition, solar and wind energy systems come with their nearly avoidable CO_2 emissions responsibility, so-called ΔCO_2 due to their inherent exergy destructions. This concept is explained in the Appendix.

According to 2013 data shown in Fig. 2, by 11% share, the agricultural sector is the second emitter, following the energy sector concerning human-made greenhouse gas (GHG) emissions, excluding land-use change and forestry (LUCF) [5]. This share has risen to 12.72% (5.87 $GtCO_2eq$) by the year 2020 [6]. This marginal increase may be attributed to increased mechanization, especially the trend for total electrification in all sectors of the European Union.
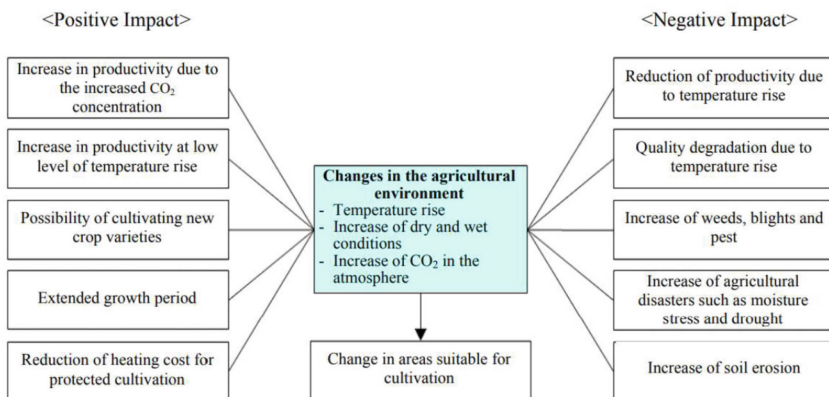
Fig. 1. Potential Impact of Farming on Global Warming [2]
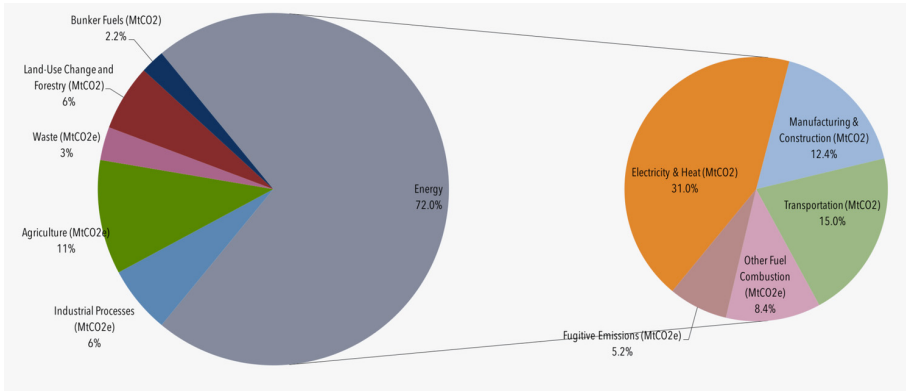
Fig. 2. Global Human-made Greenhouse Gas Emissions by Sector, 2013 [5]

Another trend is the smart farming concept, which must be grossly re-defined [7]. Figure 3 shows that the current understanding is simply computerization and electrification of the farming processes using big data, the cloud, and the internet of things as management and control tools with a main emphasis on the economy. Instead, a smart farming concept should focus on the environment, emissions, productivity, energy efficiency, exergy rationality, and water. Despite this fact, current metrics regarding agricultural mechanization are simply related to economics and productivity. Olaoye and Rotimi (2020) have measured the mechanization index and analyzed agricultural mechanization in Nigeria [8]. Their results in two states of southwestern Nigeria were such that the mechanization index was 31.3% and 28.6%, respectively and the total productivity ranged between 0.0115 ha/kWh and 0.0951 ha/kWh. This set of results confirms Fig. 4, such that productivity is somewhat proportional to mechanization. Yang and et. al. (2022) established dynamic linkages among climate change, mechanization, and agricultural carbon emissions in China [9]. They found a bidirectional causality relationship between rainfall, sunlight, agricultural mechanization, and carbon emissions. They found that rainfall and sunlight are Granger causes of agricultural mechanization. The method measures the ability to predict the future values of a time series using prior values of another time series. Yang and et. al. employed rainfall and sunlight data as Granger causes to predict the relationship among rainfall, sunlight, mechanization, and CO_2 emissions. They concluded that mechanization reduces emissions, which contradicts Fig. 4, while Fig. 1 indicates that mechanization may have both positive and negative impacts, such that the net impact depends on individual cases and causes.

Bagher and Almassi (2011) have reviewed parameters and indices affecting the decision-making process and concluded that sustainable development of agriculture can either be achieved by using simple manual farming or high technologies affected by parameters governing each case [10]. Bagher and Almassi defined theoretical and actual machine capacities in terms of machine speed and width (Theoretical), and field efficiency to determine the actual capacity. Their theoretical capacity approach resembles the method devised earlier by Kilkis, B. (1970), who correlated machine speed, harvesting efficiency, the width of single-pass harvesting, and geometry of the farmland [11].
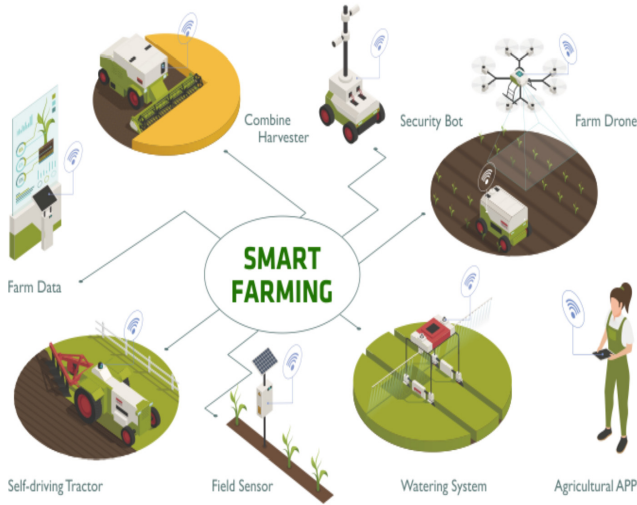
Fig. 3. The Current Understanding About Smart Farming [7]

Obaia and Ghazy (2017) reviewed different mechanization indices and applied them to farms in certain regions of Libya [12]. Obaia and Ghazy used the degree of mechanization index (kW/ha) or (kW/1000ha), which is defined as a ratio of the total power of tractors (kW) multiplied by a factor representing waste and useful equipment (less than one), and divided by the total cultivated area (ha). This definition and other definitions like ha/kW, which a reciprocal of the (kW/ha) definition, or the number of tractors per farmland area falls short of describing the degree of mechanization and their impact on the environment and global warming versus productivity and quality of production. For example, the type of fuel or the origin of the electric power, the type of tractor (like electric or hydrogen), utilization of wastes, and energy storage options are not considered. In addition, they used the definition, namely effective field capacity(ha/hour) as another index of mechanization Their mechanization definitions show another major gap in the literature, theory, and practice because these definitions do not refer to environment and emissions directly. In a similar approach, Akdemir [13] has related the mechanization index solely to the number of tractors per hectare cultivation (ha), and kW of mechanical power per ha, ha/tractor. Water use is not included in these definitions. Irrigation and water supply are also energy intensive and vaporization has an additional greenhouse effect.

This section concludes that there are gaps in theory and practice to lead agriculture to a truly environment-friendly nature, while productivity, economy, sustainability, and product resilience and quality are improved. The fundamental missing point is the Second Law of thermodynamics, which deals with the quality of energy, called exergy, E_X, which may be simply defined by the ideal Carnot cycle, as given in Eq. 1.

$$E_X = \left(1 - \frac{T_{ref}}{T_f}\right) \times E \qquad (1)$$

T_{ref} is the reference environment temperature, T_f is the energy source temperature. The term (E) is the amount of energy. For non-thermal energy sources like solar or wind energy, a Carnot cycle-based equivalent (virtual) temperature definition, T_f' is available:

$$T_f' = \frac{T_{ref}}{\left(1 - \frac{I_n \times 0.95}{TSI}\right)} \quad \{\text{Solar energy}\} \tag{2}$$

$$T_f' = \frac{T_{ref}}{(1 - 0.95 \times \eta_{IWT})} \quad \{\text{Wind turbine}\} \tag{3}$$

0.95 kW-h/kW-h is the unit exergy of electric power. TSI is the total solar irradiation. For further details see the Appendix.

2 Exergy-Based Model

To encompass all factors related to the environment and agricultural machinery, both laws of thermodynamics must be applied. Figure 4 relates the agricultural mechanization index to productivity, P, total CO_2 emissions responsibility, ΣCO_2 (Appendix 1), water consumption, W, and the new mechanization factor, MF given by Eq. 4. $LUEX$ is the exergy-based land use efficiency [14]. Water consumption is converted to CO_2 emission effect by considering irrigation and water supply ancillaries plus the greenhouse effect of water vaporization to the atmosphere. Therefore the unit of MF is ton of product/(kg CO_2/ton product). Figure 4 shows that in general, MF by definition decreases with the mechanization index, which is not desirable. To avoid this, sustainable measures must be collectively implemented and sustained, as given on the right-hand side of the figure. This requires novel designs with a wide horizon of thinking and creativity to minimize the emissions. It must be noted that the economy is not present in this analysis, because the economy has to come behind the actually sustainable and environmentally friendly agricultural activities requiring novel designs.

$$MF = \frac{P \times LUEX}{\sum CO_2 + W(CO_2)} \tag{4}$$
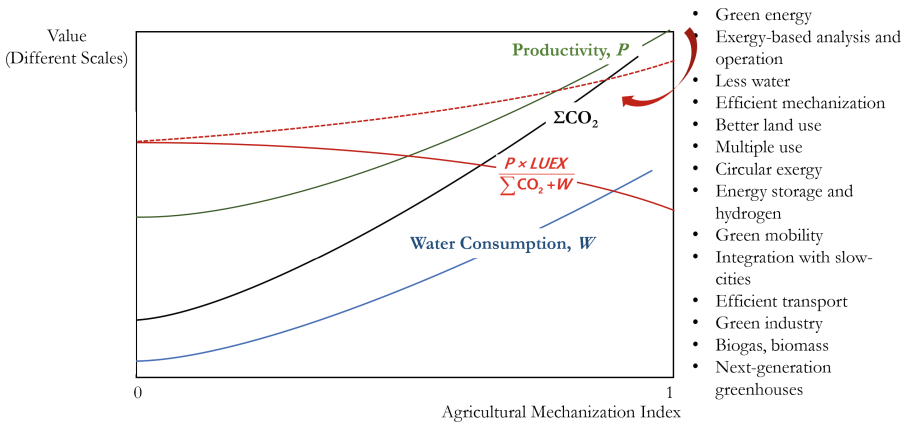
Fig. 4. Variation of Productivity, Emissions, Water Consumption, and the New Index

3 Novel Designs

This paper presents two novel designs, as given in Fig. 5 and Fig. 7. Figure 5 is a combined, renewable energy utilizing, hydrogen cycle, integrated farm with several components [15]. It starts with irrigation wells, driven by electric pumps, which are activated with raised solar PVT systems. The PV side generates electric power while the well water first passes through the thermal power generation side of the PV panel, which cools PV cells to maintain their rated efficiency during hot climatic conditions. The cold well water becomes a little warmer. The water flow rate is adjusted such that evaporation losses due to warmer air are minimized during irrigation. Part of the irrigation water goes to the electrolyzer unit first to generate hydrogen and oxygen. Hydrogen is stored and following the demand, electric power is re-generated in the fuel cell compartment. Water output is fed back to the water loop. Wind turbines are also employed on-site. Oxygen is stored and utilized in several applications on the farm. Greenhouses, farmer houses, light food industry, and husbandry follow the system in an integrated manner. Biogas is another source of energy. For cooling purposes, adsorption units (ADS) are used. Heat pumps with high *COP* values in two heat pumps in tandem are options. Water is also linked to an artificial pond of sufficient capacity for storing water and at the same time serving as a water collector during heavy rain and storms, to avoid flood. The pond also serves for fishery and aquaculture. Part of the pond may be devoted to additional PV panels. Hydrogen mobility for tractors and other farm mobility and industries completes the hydrogen cycle. Figure 6 shows how solar PVT panels and wind turbines may be integrated into a novel design [16, 17]. This arrangement utilizes the lower part of the wind turbine towers, which otherwise remain redundant. PVT panels are sun-tracking type in two axes. This system is the wind turbine PVT system shown in Fig. 5. If available, geothermal energy is appended to the system. Supplementary hydrogen production is possible.
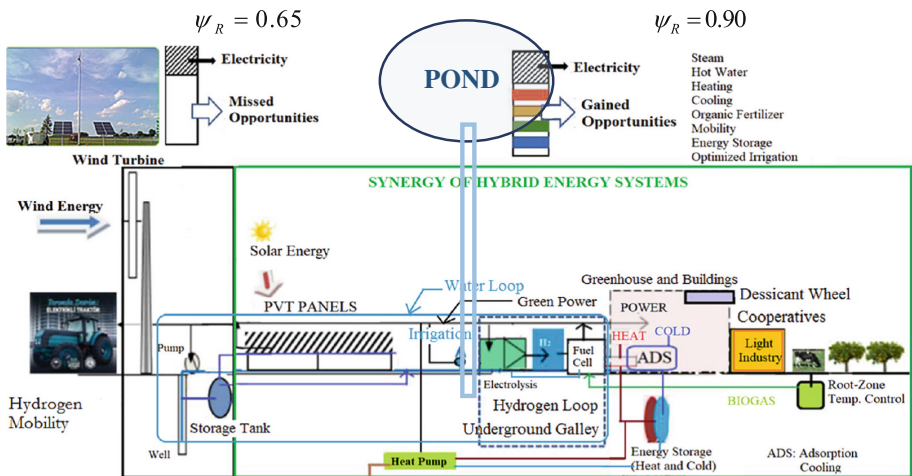
Fig. 5. Hydrogen Economy Based Integrated Farm [15].
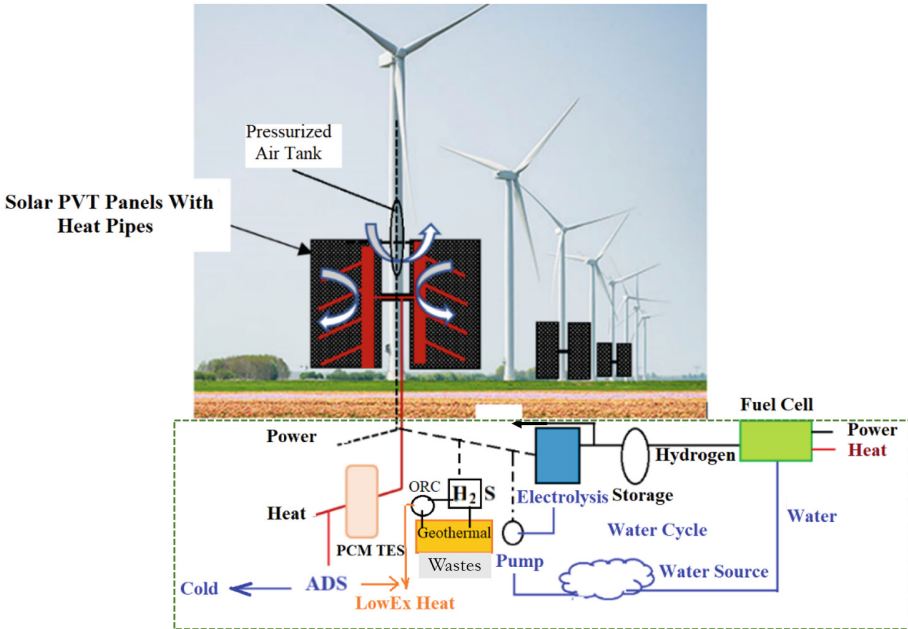
Fig. 6. Meeting of Wind and Solar on the Ground [16]
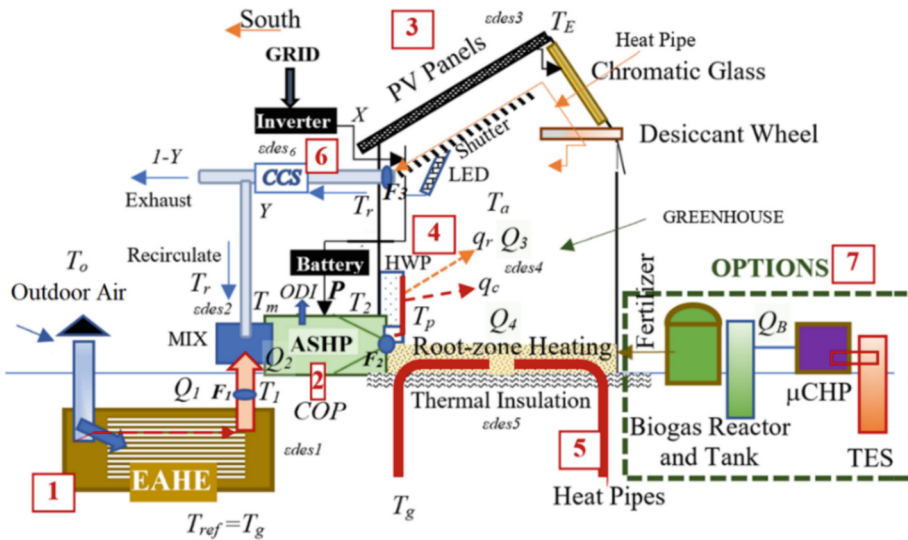
Fig. 7. Advanced Solar Greenhouse [18]

Figure 7 is an expanded view of the greenhouses indicated in Fig. 5. This system has earth-to-air heat exchanger (EAHE) designed with special care for negative carbon emissions (See the appendix). Electric power comes from the strategically positioned

PVT panels on the proper side of the greenhouse. An air-source heat pump system supplements heat or cold for the greenhouse. Root zone heating is applied with heat pipes. Heating radiators and cooling fan coils have low-enthalpy demand like 35 °C in heating and 19 °C in cooling. From agricultural waste, a mini biogas plant runs a micro-combined heat and power system (CHP). The greenhouse shown in Fig. 7 is heated by heat-piped radiators [16, 18]. Cooling and soil heating are also accomplished by heat pipes. The air-source heat pump (AHP) uses CO_2 for refrigeration gas, with a minimum ozone-depleting index (*ODI*), which is a combination of the ozone-depleting potential and global warming potential of a given refrigerant.

4 Conclusions

This paper presents a new approach to rate and compare agricultural mechanization by a combination of several factors, all based on the second law of thermodynamics. This new approach links mechanization with CO_2 emissions on different fronts, including exergy destruction-related nearly-avoidable emissions, land use effectiveness, direct emissions responsibility of the electricity used, and fuel spending. Most importantly, it permits to design and rate complex farms as shown in Fig. 5, and enhance creative thinking. For example, Fig. 5 shows that a standard way of utilizing solar and wind energy from separate PV panels and wind turbines has a rational exergy management efficiency, (ψ_R) of 0.65, where the integrated farm concept has a value of 0.95. Therefore, this novel system has about seven times less ΔCO_2 emissions responsibility than today's PV and wind turbine systems. This example shows the sustainable and proper way of decarbonization against global warming. The term ψ_R is a metric, which rates how rational any exergy source is utilized with minimum exergy destructions. At the same time, this metric is an indicator for nearly-avoidable CO_2 emissions responsibility (See Appendix). Other exergy-based metrics like *COPEX*, ΔCO_2, and *MF* are introduced, which collectively show the shortcomings of current mechanization indexes and provide ways of improving exergy-smart farms, interconnected with slow cities. In turn, a slow city when integrated with exergy-smart farms and horticulture, overall decarbonization efforts become positive.

This quadrilemma is non-linear and the Carnot cycle-based equivalence of the Pareto principle to a virtual temperature scale is only 110 °C, indicating that above this temperature today's green economy will not work. To avoid this drawback, the economy must first be separated from the other three components of the quadrilemma, those three solved first independently, and then the economy is transferred by Carnot cycle equivalence to a common temperature scale, and re-connected to the quadrilemma in a non-linearized format. By such an approach humanity will be able to find sustainable solutions and implement them for decarbonization to minimize global warming such that nature will be able again to manage the carbon balance of the globe. The application of this model to agriculture will be a role model to all other sectors related to energy, environment, and economy towards better human welfare and probably an ultimate peace.

Nomenclature

Symbols

c_k	Unit carbon dioxide content (of fuel, kg CO_2/kW-h)
CO_2	Carbon dioxide emissions, kg
COP	Coefficient of performance (of a heat pump)
COPEX	Exergy-based coefficient of performance
E	Energy, kW-h or electric (See Fig. 8 in Appendix)
E_X	Exergy, kW-h
I_n	Solar insolation, W/m^2
LUEX	Exergy-based Land use efficiency
MF	Mechanization factor, ton of product/(kg CO_2/ton product)
ODI	Ozone depleting index (For heat pump refrigerant)
P	Productivity, ton/acre
Q	Thermal power, kW
S	Solar power, kW
T	Temperature, K
T_f	Source temperature, K
T_f"	Virtual source temperature, K
T_{ref}	Reference temperature, K
TSI	Total solar irradiation, 1361 kW/m^2
W	Water consumption (CO_2 equivalent), kg CO_2/ton product

Greek Symbols

η_I	First law efficiency
η_{II}	Second law efficiency
ψ_R	Rational Exergy Management Model efficiency
ψ_{WT}	Wind Turbine efficiency (Limited by the Betz Law)
ΔCO_2	Nearly-avoidable emission due to exergy destruction
$\Sigma\, CO_2$	Total CO_2 emissions, kg

Subscripts

a	Air
B	Biogas (reactor and tank)
c	Cooling
dem	Demand (Exergy)
des	Destruction (Exergy)
eq	Equipment
g	Ground
in	Input (Energy or exergy)
o	Outdoor
PV	Solar photo-voltaic (panel)
r	Return
sup	Supply
WT	Wind turbine

Acronyms

AC   Alternating current
ADS   Adsorption cooling machine
ASHP   Air-source heat pump
CCS   Carbon capture and storage
CHP   Combined heat and power
DC   Direct current
E   Exhaust or leaving temperature
EAHE   Earth-air heat exchanger (Ground labyrinth)
GHG   Greenhouse gas
LUCF   Land use change and forestry
REMM   Rational Exergy Management Model
PVT   Solar-photovoltaic-thermal panel
TES   Thermal energy storage
μCHP   Micro CHP (Less than 50 kW capacity of power generation)

Appendix

Exergy Efficiency and Exergy Rationality.

Exergy efficiency and exergy rationality are two different concepts. The conventional definition of exergy efficiency is similar to the First Law efficiency, except the energy term is replaced by the exergy term.

$$\eta_{II} = \frac{\text{Inyput Exergy Utilized in UsefulWork(s)}}{\text{Input Exergy}} \qquad (5)$$

This term does not distinguish between how and where the exergy is utilized downstream. Neither does it distinguish where and how the input exergy is derived. In the contrary, the *Rational Exergy Management Model* efficiency, ψ_R not only concerns with how rational the exergy is utilized but at the same time concerns with the upstream and downstream of the system or process, or equipment. The definition has two levels:

1- System level, concerning mainly the primary energy conversion system, like a solar PVT or a gas boiler,
2- Equipment level, concerning about how the exergy is utilized downstream the system level, like a heat pump.

Example

A greenhouse utilizes the solar power directly converted from the solar energy, on site, by using photo-voltaic panels (PV). In the summer season the green house is precooled by directing the hot outdoor air through an underground labyrinth type of earth-to-air heat exchanger (EAHE) by forcing the air to the green house and exhausting it by electrically operated fan(s). The PV electric power generation capacity equals the fan power demand by its electric motor. See Fig. 8. In this example the PV panel array converts solar energy to electric power with a summer time (hot environment and without cooling) net conversion efficiency of $\eta_{IPV} = 0.15$. Let Q be 10 kW, $T_1 = 305$ K, $T_2 = 295$ K, $E = 1.2$ kW. $S = 8$ kW.

The two levels are mentioned below.
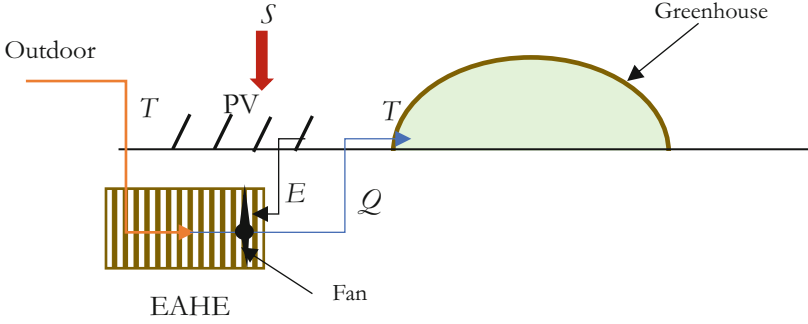
Fig. 8. Solar PV Panels and a Greenhouse Precooled by EAHE with a Fan

1- Energy Conversion System Level.

This is the PV array, which converts solar power, S, (Primary energy source) to electric power, E, consumed by the fan. PV panels do not recover the heat and release the thermal energy absorbed from the sun to the ambient, leading to local heat island. Outdoor air is precooled at a cooling power of Q_c. Figure 9 shows that this thermal energy loss means irreversible exergy destruction resulting in DCO$_{2\text{-system}}$ (Eq. 6). The REMM efficiency of the same system is noted in Eq. 7. In Eq. 6 the multiplier (1.1) is the proportionality constant linking the exergy destruction directly to in DCO$_{2\text{-system}}$ when major exergy destruction occurs downstream. The multiplier is (2.1) if the major exergy destruction is upstream like a flat plate solar collector or a gas boiler, both of which converts fuel to heat without generating power first. Figure 9 shows that although there are not any direct emissions from the PV array (except embodiments), it responsible for the offsetting of the thermal energy potential destroyed by someone, somewhere, sometime, possibly using some mix of fossil fuels. For example, an onsite gas boiler may be used, or solar flat-plate collectors, which this time misses the opportunity of generating electric power upstream its thermal power generation step. T_E is the temperature of the PV frame. In Eq. 7, the term 0.56 is the unit exergy of solar energy at an isolation level of 0.8 kW/m^2 on the PV panel surface.

$$\Delta CO_{2_{system}} = 1.1 \times S \times (1 - \eta_{IPV}) \times \left(1 - \frac{T_{ref}}{T_E}\right) = 1.65 \text{ kg CO}_2/\text{kW-h}_{ex} \quad (6)$$

$$\psi_{R_{system}} = 1 - \frac{S \times (1 - \eta_{IPV}) \times \varepsilon_{des}}{S \times \varepsilon_{solar}} = 1 - \frac{(1 - \eta_{IPV}) \times \varepsilon_{des}}{\varepsilon_{solar}}$$

$$= 1 - \frac{(1 - 0.15) \times \left(1 - \frac{283 \text{ K}}{363 \text{ K}}\right)}{0.56} = 0.66 \quad (7)$$

$$\Delta CO_{2_{eq}} = 2.1 \times \left[0.95 \times E - Q_c \times \left(1 - \frac{T_2}{T_1}\right)\right] = 1.7 \text{ kg CO}_2/\text{kW-h}_{ex} \quad (8)$$

$$\psi_{R_{eq}} = \frac{Q_c \times \varepsilon_{dem}}{E \times 0.95} = 0.29 \quad (9)$$

Electric power, $\eta_{IPV}=0.15$

$T_E=363$ K

ε_{des}

E

$T_{ref}=283$ K

Exergy Flow Bar of the PV Panel

ε_{des}

$T_1=305$ K

Therma power (Pre-cooling), Q_c

$T_2=295$ K
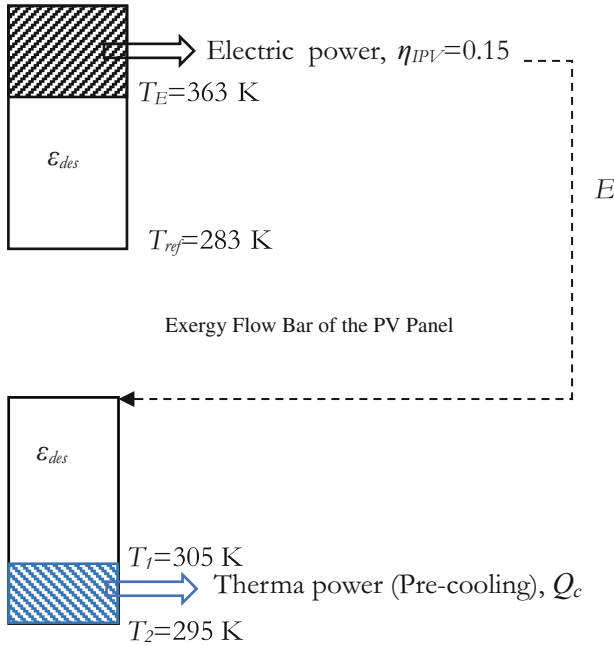
Fig. 9. Exergy Flow Bar of the UAHE System (Equipment) with Electric Fan

2- Energy Utilization (Equipment) Level.

This level comprises the UAHE and the green house. UAHE fan uses the electric power generated by the PV array (Fig. 9). The unit exergy of electric power is 0.95 (Fig. 9).

On the overall, emission responsibility terms are additive for calculating the total emission responsibility:

$$\sum \Delta CO_2 = \Delta CO_{2_{system}} + \Delta CO_{2_{eq}} = (1.65 + 1.75) \text{ Kg CO}_2/\text{KW-h}_{ex} \tag{10}$$

and the overall ψ_R is a multiple of individual efficiencies, while they are in series:

$$\overline{\psi}_R = \psi_{R_{system}} \times \psi_{R_{eq}} = 0.19 \tag{11}$$

For more than one different input exergy and more than one different equipment exergy, the general equation is:

$$\overline{\psi}_R = \frac{\sum\limits_{i=1}^{s} \psi_{R_{systemi}}}{\sum\limits_{i=1}^{s} S_i} \times \frac{\sum\limits_{j=1}^{e} \psi_{R_{eqj}}}{\sum\limits_{j=1}^{e} E_j} \tag{12}$$

An approximate relation between overall DCO_2 and $\overline{\psi}_R$ is obtained:

$$\Delta CO_2 = \left(\frac{E_{in} \times c_k}{\eta_I} \right) \times \left(1 - \overline{\psi}_R \right) \tag{13}$$

Furthermore, for the UAHE and the greenhouse system. Note that although *COP* in its conventional format may be greater than one, but the exergy-based *COP*, named *COPEX* is less than one.

$$COP = \frac{Q_c}{E} = \frac{10 \text{ kW}}{1.2 \text{ kW}} = 8.3 \tag{14}$$

$$COPEX = \frac{Q_c \times \left(1 - \frac{T_2}{T_1}\right)}{E} = COP \times \frac{\left(1 - \frac{295 \text{ K}}{305 \text{ K}}\right)}{0.95} = 0.29 \tag{15}$$

References

1. EPA. Sources of Gas Emissions <https://www.epa.gov/ghgemissions/sources-greenhouse-gas-emissions#agriculture>. Accessed 10 Oct 2023
2. Kim C-G, Lee S-M, Jeong H-K, Jang J-K, Kim Y-H, Lee C-K (2010) Impacts of climate change on Korean agriculture and its counterstrategies. KREI report, R593/English Edition, December 2010. <https://repository.krei.re.kr/bitstream/2018.oak/19577/1/Impacts%20of%20Climate%20Change%20on%20Korean%20Agriculture%20and%20Its%20Counterstrategies.pdf>. Accessed 10 Oct 2023
3. Kim C-G (2019) The impact of climate change on the agricultural sector: implications of the agro-industry for low carbon, green growth strategy and roadmap for the East Asian Region, Low Carbon Green Growth Roadmap for Asia and The Pacific. <https://www.unescap.org/sites/default/files/5.%20the-impact-of-climate-change-on-the-agricultural-sector.pdf>. Accessed 10 Oct 2023
4. MOFA (2023) Türkiye's International Energy Strategy, Ministry of Foreign Affairs. <https://www.mfa.gov.tr/turkeys-energy-strategy.en.mfa#:~:text=Furthermore%2C%20T%C3%BCrkiye%20has%20ranked%205th,at%20the%20end%20of%202022>. Accessed 10 Oct 2023
5. C2ES (2023) Global Carbon Dioxide Emissions 1850–2040, Center for Climate and Energy Solutions. <https://www.c2es.org/content/international-emissions/>. Accessed 10 Oct 2023
6. Climate Watch (2023) Agriculture <https://www.climatewatchdata.org/sectors/agriculture#drivers-of-emissions>. Accessed 10 Oct 2023
7. Indonesia Green Farm (2023) Smart Farming Technologies & System. <https://www.greenfarmina.com/smart-farming-technologies-system/>. Accessed 10 Oct 2023
8. Olaoye JO, Rotimi AO (2010) Measurement of agricultural mechanization index and analysis of agricultural productivity of farm settlements in Southwest Nigeria. Agric Eng Int CIGR J 12(1):125. Open Access at http://www.cigrjournal.org
9. Yang T, Huang X, Wang Y, Li H, Guo L (2022) Dynamic linkages among climate change, mechanization and agricultural carbon emissions in rural China. J Environ Res Publ Health 2022(19):14508. https://doi.org/10.3390/,ijerph192114508
10. Bagher ML, MortezaAlmassi M (2011) An analytical review of parameters and indices affecting decision making in agricultural mechanization. AJAE 2(5):140–146. ISSN 1836-9448
11. Kılkış B (1970) Corn Harvesting Machine, Graduation Project. Middle East Technical University, Mech. Eng. Dept., Ankara, Türkiye, 170 p
12. Obaia AR, Ghazy MI (2017) The study of agricultural mechanization indicators in Eastern Libya Misr J Ag Eng 34(2):567–580. Farm Machinery and Power
13. Akdemir B (2013) Agricultural mechanization in Turkey. In: 2013 International Conference on Agriculture and Natural Resources Engineering, IERI Procedia, vol 5, pp 41–44

14. Kilkis B (2022) Optimum urban land-use model for minimum CO2 responsibility under energy and exergy-based constraints. In: 5th SEE SDEWES Conference, 22–26 May, Vlore Albania

15. Kılkış B (2022) Green hydrogen: the common thread of the belt and road initiative. Belt Road Initiat Q (BRIQ) 3(3):6–20

16. Kılkış B, Çağlar M, Şengül M (2021) Energy benefits of heat pipe technology for achieving 100% renewable heating and cooling for fifth-generation, Low-temperature district heating systems. Energies 14(17):5398. https://doi.org/10.3390/en14175398

17. Kilkis B (2022) Exergy-rational utilization of solar energy with advanced PVT systems and heat pipe technology in 100% renewable cities. IOP Conf Ser Earth Environ Sci 1085:12029. https://doi.org/10.1088/1755-1315/1085/1/012029

18. Kilkis B (2022) Lessons learned from labyrinth type of air preconditioning in exergy-aware solar greenhouses. J Sustain Dev Energy Water Environ Syst 10(4):1100434. https://doi.org/10.13044/j.sdewes.d10.0434

Post-Harvest Technologies and Process Engineering

Optical Techniques for Automated Evaluation of Seed Damage

Mohammad Nadimi and Jitendra Paliwal(✉)

Department of Biosystems Engineering, University of Manitoba, Winnipeg, MB, Canada
j.paliwal@umanitoba.ca

Abstract. Cereal grains and oilseeds, fundamental components of global diets, face significant vulnerability to mechanical damage during various stages, including harvesting, transportation, and storage. Beyond immediate physical degradation, the repercussions of such damage extend to seed viability and consequent economic implications. Traditional assessment techniques, predominantly reliant on external visual inspections, face challenges of subjectivity and inefficiency, restricting evaluations to superficial seed alterations. To circumvent these shortcomings, this study presents a fusion of optical techniques, namely two-dimensional (2D) X-ray imaging and hyperspectral imaging (HSI) – all underpinned by machine learning and deep learning frameworks – targeting an automated, holistic assessment of flaxseed damages. Leveraging an expansive dataset of 3,600 flaxseed samples spanning varied moisture contents and impact energies, the findings underscore the amplified susceptibility of seeds to damage under heightened impact stress at minimal moisture levels. Remarkably, through the integrated approach, the study achieved classification accuracies surpassing 87% for all techniques. While X-ray imaging presented throughput limitations, Vis-NIR HSI can be considered an effective alternative. In summation, the study accentuates the profound potential harboured by optical techniques in seed damage assessments, advocating their capacity to replace conventional methods. By seamlessly integrating advanced imaging with computational intelligence, the study not only streamlines damage detection but also amplifies the possibility of curbing damage, promising heightened yields and minimized economic setbacks. Future endeavors should channel this foundational research towards broader crop varieties to ensure universal applicability and validation.

Keywords: Optical techniques · Flaxseeds · X-ray imaging · Mechanical damage

1 Introduction

As a cornerstone of global nutrition, cereal grains and oilseeds play a pivotal role in dietary sustenance. However, the journey of these crops, from field to consumer, is fraught with mechanical challenges. In particular, operations like harvesting, transportation, and storage have been recognized as key stages where these grains face potential damage [1]. This damage not only reduces the aesthetic appeal of the grain but also impinges upon its nutritional quality, viability, and overall market value.

Conventional methods to assess these damages have traditionally centred on visual examinations. While seemingly straightforward, such methods are inherently flawed. They are subjective, labor-intensive, and perhaps most critically, restricted in scope – capturing only the external damages while turning a blind eye to the nuanced, internal damages that could have long-term implications on the grain's shelf life, susceptibility to pests, and nutritional quality.

In an age where technology and agriculture are becoming inextricably linked, clinging to outdated methods feels like a squandered opportunity. Consequently, many researchers are delving into innovative tools and mathematical models to forecast the susceptibility of seeds to mechanical damage under varying moisture contents and impact energies [2–13]. Among the emerging techniques, optical methodologies, especially imaging and spectroscopy, have garnered significant attention, marking a paradigm shift in the research landscape [14, 15]. Riding this wave of innovation, our research pivots its focus on the comparative strengths and nuances of 2D X-ray imaging and hyperspectral imaging (HSI) in gauging seed damage, spotlighting flaxseeds for their global economic and nutritional footprint. Through this endeavor, we envision a confluence of state-of-the-art technology and agronomic expertise to craft a comprehensive, efficient, and robust system, capable of mapping both the seen and unseen damages in seeds, ensuring no facet of damage goes undetected.

2 Methods

Flaxseed samples were sourced from Arborg, Manitoba, Canada, and conditioned to moisture contents (MCs) of 6, 8, and 11.5% on a wet basis as described in detail elsewhere [16]. The seeds were then subjected to varying mechanical forces, using a drop weight impactor, at three distinct energy levels of 2, 4, and 6 mJ [17, 18]. These energy intensities were selected from preliminary tests to induce low, medium, and high levels of kernel damage to the flaxseed. In addition to the impacted samples, a set of control samples for each moisture content was incorporated, which were unexposed to any mechanical impact. The comprehensive experiment encompassed a total of 3600 seeds, spanning over 100 seeds for each of the 4 impact energies, three moisture contents, and with each combination replicated three times.

To ascertain the internal damages incurred by the seeds, a 2D X-ray imaging system (Model: MX-20, Faxitron Bioptics, LLC, Tucson, AZ) was utilized to render an internal view of the seeds. Furthermore, to garner hyperspectral imaging (HSI) data ranging from 400–1000 nm, a visible-near-infrared (Vis-NIR) HSI system from SPECIM Spectral Imaging Ltd., Oulu, Finland, was employed.

The X-ray data procured underwent rigorous analysis using the Matlab software suite (Mathworks Inc., Waltham, MA). Gray-level percentile scores provided an initial assessment [17], which was supplemented by the efficientNet-B0 model, a variant of convolutional neural network (CNN) [18]. Lastly, to classify seeds as sound or damaged based on the HSI data, a partial least squares discriminant analysis (PLS-DA) was carried out.

3   Results and Discussions

Figure 1 shows the digital image of flaxseeds with 8% MC under different impact stresses. It is apparent that inducing impact stress increases mechanical damage to seeds. Similar patterns were observed for other combinations of moisture contents and impact stress, as detailed in our earlier publications [17, 18]. The 2D X-ray images (Fig. 2) offer a more nuanced perspective, particularly highlighting the internal seed damages that are not always externally visible. In our preceding studies, we delved into the analysis of these 2D X-ray images. Leveraging gray-level percentile scores and the Support vector machine (SVM) classifier, flaxseeds were categorized into two primary groups: nil/low and medium/high damage with a classification accuracy of 87% [17]. Amplifying this process with convolutional neural networks (CNN) and transfer learning methodologies, particularly the EfficientNet-B0 model, catapulted the classification accuracy to a commendable 95% [18]. The confusion matrix of a test set (30% of the entire data), delineating the classification of seeds using CNN into the aforementioned groups, is outlined in Table 1.
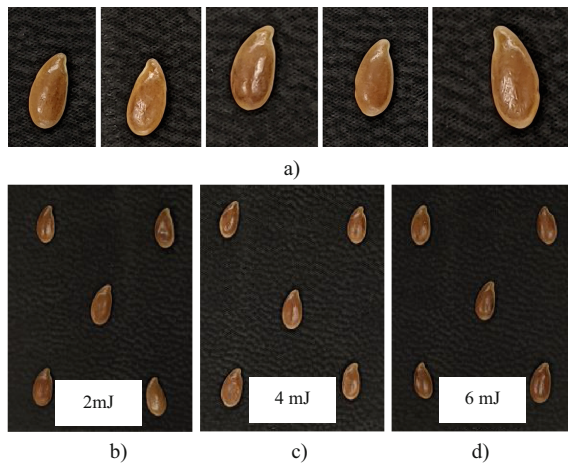
Fig. 1. Visuals of flaxseed with 8% moisture content, captured using a digital camera (model S20, Samsung Corp., Seoul, Korea) post-exposure to varied impact stresses: a) 0 mJ, b) 2 mJ, c) 4 mJ, d) 6 mJ.

Despite the undeniable prowess of X-ray systems in revealing detailed internal damages, their practical application in large-scale seed assessments is not without challenges. The first major obstacle is their constrained throughput performance; the time and resources required to scan extensive seed batches can be substantial. Secondly, the use of X-ray systems invariably introduces concerns regarding safety, especially in settings where continuous or prolonged use is necessitated. These inherent limitations of X-ray technology prompted us to seek out alternatives that could maintain a high level of accuracy while addressing these challenges.
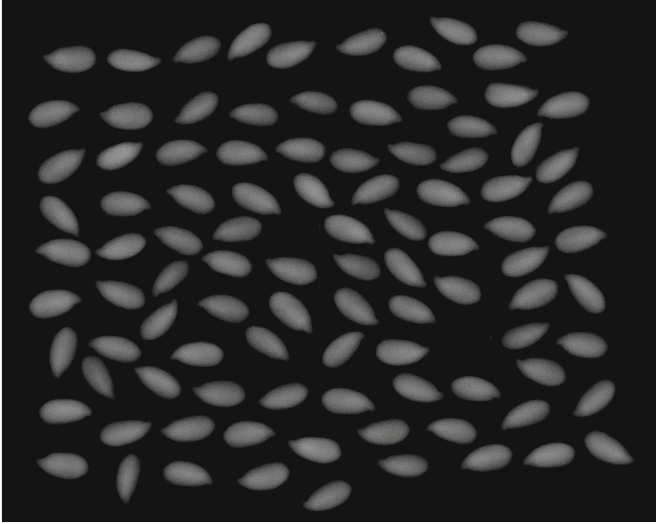
a)
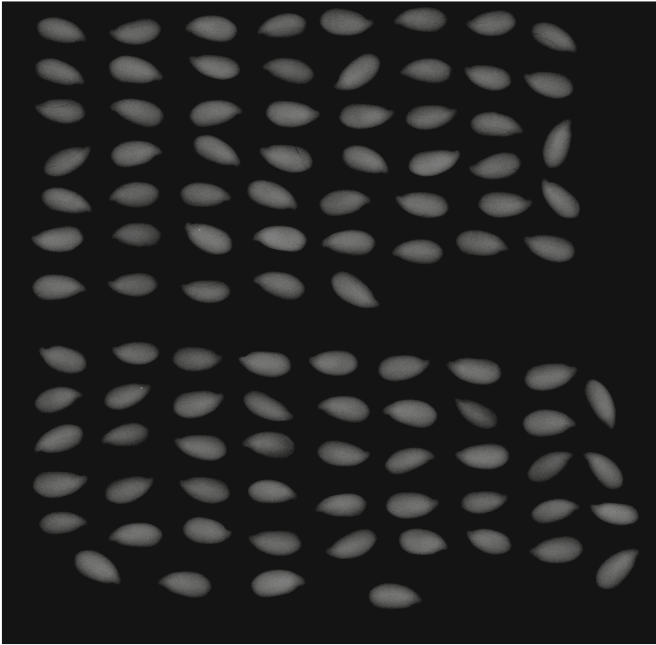
b)

Fig. 2. 2D X-ray images of flaxseeds with 8% moisture content, subjected to a series of impact energies: a) none (0 mJ); b) low (2 mJ); c) medium (4 mJ); d) high (6 mJ) (unpublished images from the following studies [17, 18]).
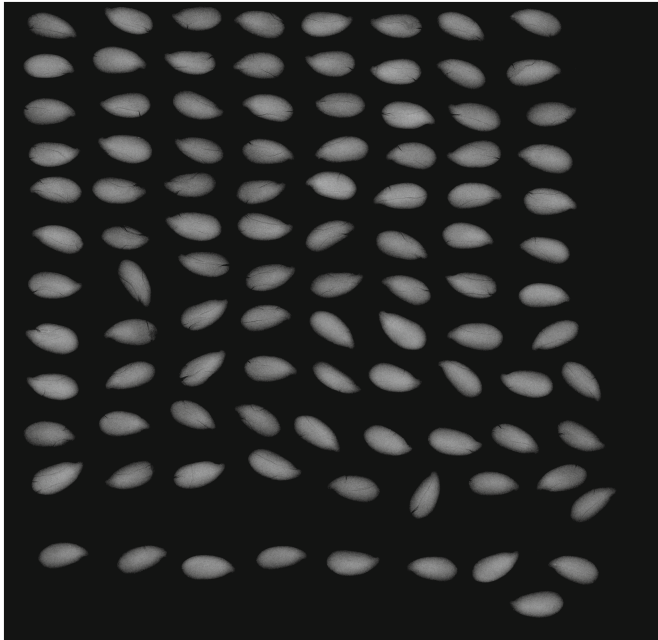
c)
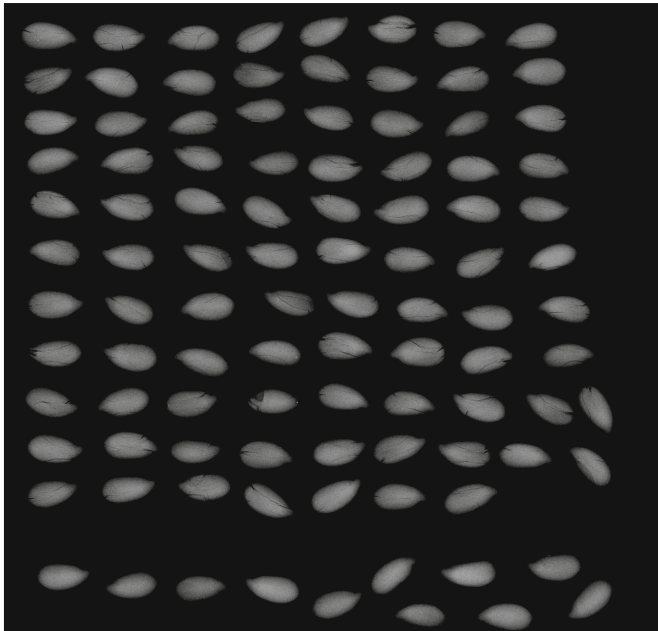
d)

Fig. 2. (*continued*)

Table 1. Classification outcomes using ANN classifiers [adapted from [18]]

Actual class/Predicted	Nil/low	Medium/high
Nil/low	707	6
Medium/high	44	274

In our quest for a suitable substitute, we turned our attention to the Vis-NIR HSI technique. This technology, renowned for its non-destructive and rapid analytical capabilities, emerged as a promising candidate. Our initial forays into Vis-NIR HSI involved processing the gathered data through mean centering, which aims to eliminate systematic biases. To further refine our data interpretation, PLS-DA model was tailored for supervised classification. Encouragingly, this approach yielded a classification accuracy of 89% under 5-fold cross-validation, positioning it competitively with the results achieved through X-ray systems.

While these preliminary findings showcase the potential of Vis-NIR HSI as a robust alternative to traditional X-ray imaging, they represent just the tip of the iceberg. The vast and intricate realm of possibilities proffered by Vis-NIR HSI beckons for more rigorous and comprehensive explorations to genuinely leverage its expansive capabilities in seed damage evaluations.

One should note that a challenge in implementing both the 2D X-ray and HSI systems lies in the complexity of analyzing large HSI datasets and the need for automating X-ray analysis for diverse seeds. While HSI systems typically come with a higher price tag compared to traditional spectroscopy systems, identifying key wavelengths can significantly minimize computational demands. This paves the way for multi-spectral systems, which are more cost-effective than full-fledged hyperspectral setups, streamlining analysis and reducing costs. As for X-ray imaging, automation would not only expedite the evaluation but also enhance its accuracy by mitigating human error and subjectivity. Exploring these areas further can potentially redefine seed evaluation, making it both more precise and economically viable.

In forthcoming research, we intend to delve into a meticulous analysis, prioritize wavelength selection, and undertake principle component analysis to further refine our approach and insights.

4   Conclusion

Overall, this study highlights the untapped potential of optical techniques in evaluating mechanical damage to seeds. The results suggest that implementing machine learning tools with optical techniques such as 2D X-ray imaging and HSI can provide a rapid and reliable alternative to the subjective and time-consuming visual inspection method. The outcomes of this research can contribute to developing new technologies for detecting and/or preventing damage, resulting in increased crop yields and reduced economic losses for stakeholders. However, to validate these findings, further testing should be performed on a wider range of crops.

References

1. Nadimi M, Hawley E, Liu J, Hildebrand K, Sopiwnyk E, Paliwal J (2023) Enhancing traceability of wheat quality through the supply chain. Compr Rev Food Sci Food Saf. https://doi.org/10.1111/1541-4337.13150

2. Shahbazi R, Shahbazi F (2022) Effects of cushion box and closed let-down ladder usage on mechanical damage during corn kernel handling: cracking. J Stored Prod Res 99:102006. https://doi.org/10.1016/J.JSPR.2022.102006

3. Shahbazi R, Shahbazi F (2022) Effects of cushion box and closed let-down ladder usage on damage to corn during handling: physiological deterioration. Plant Methods 18(1):1–11. https://doi.org/10.1186/S13007-022-00975-Y/TABLES/4

4. Shahbazi R, Shahbazi F (2023) Effects of cushion box and closed let-down ladder usage on impact damage to corn kernel during handling. Food Sci Nutr 11(5):2243–2253. https://doi.org/10.1002/FSN3.3137

5. Shahbazi F (2011) Impact damage to chickpea seeds as affected by moisture content and impact velocity. Appl Eng Agric 27(5):771–775. https://doi.org/10.13031/2013.39557

6. Shahbazi R, Shahbazi F, Nadimi M, Paliwal J (2023) Assessing the effects of free fall conditions on damage to corn seeds: a comprehensive examination of contributing factors. AgriEngineering 5(2):1104–1117. https://doi.org/10.3390/AGRIENGINEERING5020070

7. Shahbazi F, Dolatshah A, Valizadeh S (2014) Evaluation and modelling the mechanical damage to cowpea seeds under impact loading. Qual Assur Saf Crops Foods 6(4):453–458. https://doi.org/10.3920/QAS2012.0120

8. Shahbazi F, Dowlatshah A, Valizadeh S (2012) Breakage susceptibility of wheat and triticale seeds related to moisture content and impact energy. Cercetari Agronomice Moldova 45(3):5–13. https://doi.org/10.2478/v10298-012-0051-4

9. Shahbazi F, Valizade S, Dowlatshah A (2017) Mechanical damage to green and red lentil seeds. Food Sci Nutr 5(4):943–947. https://doi.org/10.1002/fsn3.480

10. Delfan F, Shahbazi F, Esvand HR (2023) Impact damage to chickpea seeds during free fall. Int Agrophys 37(1):41–49. https://doi.org/10.31545/INTAGR/156049

11. Khazaei J, Shahbazi F, Massah J, Nikravesh M, Kianmehr MH (2008) Evaluation and modeling of physical and physiological damage to wheat seeds under successive impact loadings: mathematical and neural networks modeling. Crop Sci 48(4):1532–1544. https://doi.org/10.2135/cropsci2007.04.0187

12. Shahbazi F, Sharafi R, Moomevandi SJ, Daneshvar M (2015) Influence of foliar iron fertilization rate on the breakage susceptibility of wheat seeds. J Plant Nutr 38(14):2204–2216. https://doi.org/10.1080/01904167.2015.1043379

13. Chen Z, Wassgren C, Kingsly Ambrose RP (2020) A review of grain kernel damage: mechanisms, modeling, and testing procedures. Trans ASABE 63(2):455–475. https://doi.org/10.13031/trans.13643

14. Gomes-Junior FG, Cicero SM, Vaz CMP, Lasso PRO (2019) X-ray microtomography in comparison to radiographic analysis of mechanically damaged maize seeds and its effect on seed germination. Acta Sci Agron 41(1):e42608. https://doi.org/10.4025/ACTASCIAGRON.V41I1.42608

15. Wang L, Huang Z, Wang R (2021) Discrimination of cracked soybean seeds by near-infrared spectroscopy and random forest variable selection. Infrared Phys Technol 115:103731. https://doi.org/10.1016/J.INFRARED.2021.103731

16. Mundhada S, Chaudhry MMA, Erkinbaev C, Paliwal J (2022) Development of safe storage guidelines for prairie-grown flaxseed. J Stored Prod Res 97:101965. https://doi.org/10.1016/J.JSPR.2022.101965

17. Nadimi M, Loewen G, Paliwal J (2022) Assessment of mechanical damage to flaxseeds using radiographic imaging and tomography. Smart Agric Technol 2:100057. https://doi.org/10.1016/j.atech.2022.100057

18. Nadimi M, Divyanth LG, Paliwal J (2023) Automated detection of mechanical damage in flaxseeds using radiographic imaging and machine learning. Food Bioproc Tech 16(3):526–536. https://doi.org/10.1007/S11947-022-02939-5/METRICS

Exploring Transfer Learning for Enhanced Seed Classification: Pre-trained Xception Model

Yonis Gulzar[1](✉) 📷, Zeynep Ünal[2] 📷, Shahnawaz Ayoub[3] 📷,
and Faheem Ahmad Reegu[4] 📷

[1] Department of Management Information Systems, College of Business Administration,
King Faisal University, Al-Ahsa 31982, Saudi Arabia
`ygulzar@kfu.edu.sa`
[2] Department of Biosystem Engineering, Niğde Ömer Halisdemir University, Central Campus,
51240 Niğde, Turkey
`zeynepunal@ohu.edu.tr`
[3] Glocal School of Science and Technology, Glocal University, Delhi-Yamunotri Marg (State
Highway 57), Mirzapur Pole, Dist - Saharanpur , U.P. 247121, India
[4] Department of Computer Science and Information Technology, Jazan University, Jazan 45142,
Saudi Arabia

Abstract. Seed classification plays a crucial role in various agricultural and industrial applications, such as crop breeding, seed quality assessment, and plant disease identification. This study presents a novel deep-learning model for seed classification. In this study, a dataset of 15 seeds has been created, containing around 3018 RGB images, with the objective of developing an accurate and efficient deep learning-based model capable of classifying seeds with high precision. In this study, we explore the effectiveness of two distinct approaches for seed classification: training the Xception model from scratch and leveraging transfer learning with the Pre-trained Xception model. The experimental results offer a comprehensive comparative analysis of training, validation, and testing outcomes. Notably, the Pre-trained Xception model showcases superior performance across various metrics. It achieves remarkable accuracy, attaining a perfect 1.0000 on both validation and test sets. Additionally, this model demonstrates significantly lower loss values throughout the training phases, highlighting its enhanced predictive capabilities. Impressively, convergence is reached with fewer epochs and in shorter training duration, further underlining the efficiency and effectiveness of the Pre-trained Xception model.

Keywords: Seed Classification · Deep Learning · CNN

1 Introduction

Seeds, the silent architects of biodiversity, hold within them the promise of life that spans across every corner of our planet. From the sun-soaked savannas of Africa to the misty rainforests of South America, seeds are nature's couriers of resilience and continuity. They carry with them the genetic blueprints of countless species, adapting and evolving to the unique challenges presented by each environment [1].

Seed classification is a vital aspect of plant science and agriculture, serving as a foundational framework for understanding plant diversity, evolution, and ecosystem dynamics [2]. It enables researchers, botanists, and farmers to categorize and organize seeds based on their characteristics, facilitating efficient study, conservation, and utilization of plant species. The classification process often involves assessing factors such as seed size, shape, color, texture, and germination mechanisms, leading to a deeper comprehension of plant relationships and ecological roles [2]. Seed classification provides insights into the evolutionary relationships among plant species, allowing scientists to reconstruct the evolutionary history of plants through their seed traits [3]. This aids in the development of accurate phylogenetic trees and contributes to our understanding of how various plant lineages have diverged and adapted over time.

Furthermore, seed classification is essential for conservation efforts. By identifying and categorizing seeds of rare, endangered, or economically valuable plant species, conservationists can prioritize their protection and preservation, ensuring that their genetic diversity is safeguarded for future generations[4]. In agriculture, seed classification plays a pivotal role in crop improvement and breeding programs. By understanding the genetic traits carried by different seed varieties, breeders can select and crossbreed plants to enhance desirable traits like yield, disease resistance, and nutritional content. This approach has led to the development of high-yielding crop varieties that contribute to global food security.

Recent advancements in artificial intelligence (AI) have reshaped industries, including personalized learning in education [5, 6], data analysis for finance [7, 8], precision farming in agriculture [9], and improved patient care in healthcare [10–14]. Particularly, deep learning, a subset of AI, has revolutionized seed classification using neural networks to identify diverse plant species accurately, offering the potential for advancing biodiversity studies and ecological understanding.

The literature shows that numerous scholars have endeavored to employ deep-learning techniques for seed sorting. As an illustration, a study by Hamid et al. [15] introduced a deep learning model aimed at classifying fourteen distinct seed species. The model demonstrated impressive testing accuracy, reaching 99%.

Hoai et al. [3] addressed essential rice seed classification. They evaluate hand-crafted descriptors, and CNNs, achieving 99.04% accuracy using the DenNet21 framework on the VNRICE dataset. Bao et al. [16] explored computer image analysis for morphological seed information. Deep learning, SVM, and random forest are tested on 150 aquatic plant seeds, achieving high accuracy: SVM 97.91%, random forest 97.08%, and deep learning 92.5%. This study enhances seed classification accuracy, favoring SVM and random forest for aquatic plant seed recognition. Kurtulmuş [17] developed a computer vision system using deep learning for sunflower seed identification. They test three architectures (AlexNet, GoogleNet, ResNet) on 4800 sunflower seeds, achieving 95% accuracy with GoogleNet. [18] addressed the challenge of plant species recognition via seed image analysis. They proposed SeedNet, a novel CNN, achieving promising results with accuracy values of 95.65% and 97.47% on two datasets. Xu et al. [19] addressed efficient maize seed sorting. Their method combined machine vision and deep learning using P-ResNet architecture. With 8080 seeds of five varieties, their model achieved 97.91% to 99.80% accuracy across different networks, excelling with P-ResNet.

Haung et al. [20] tackled precise soybean seed sorting using a pipeline combining Mask R-CNN for image segmentation and their lightweight network, SNet, with mixed feature recalibration modules for classification. SNet achieved 96.2% accuracy with 1.29M parameters, surpassing previous models. Ünal et al. [21] applied deep learning to distinguish hazelnut classes. Industrial dataset with 2094 images per class. EfficientNetB3 achieved 99.28% accuracy, excelling in "whole kernel" discrimination and economic loss reduction. Gulzar [22] exploits AI advancements for fruit classification. CNNs like MobileNetV2, and TL-MobileNetV2 (customized head), with transfer learning, achieve 99% accuracy, surpassing other models. The dropout technique minimizes overfitting. Sabanci K. [23] proposed a deep learning method to distinguish tomato seed cultivars. Images were taken, cropped, and augmented. MobileNetv2 achieved 93.44% accuracy in CNN classification, while BiLSTM reached 96.09%. The study innovatively enables accurate and rapid tomato seed cultivar classification.

Luo et al. [24] investigated weed seed classification using nondestructive image recognition. They compared six CNN models on a dataset of 47,696 samples from 140 weed species. AlexNet and GoogLeNet excelled, with AlexNet offering accuracy and efficiency, and GoogLeNet achieving the highest accuracy. Díaz-Martínez et al. [25] integrated hyperspectral imaging and deep learning for rice seed classification. Seed-based 3D-CNN achieved 91.33%, and pixel-based DNN achieved 94.83% accuracy, surpassing previous results. Wang et al. [26] used hyperspectral imaging and deep learning to identify sweet maize seed varieties. Various models were compared, with CNN-LSTM performing slightly better, achieving over 95% accuracy. The study highlights deep learning's potential for accurate seed variety identification. Zhang et al. [27] introduced an end-to-end trainable incremental learning (IL) framework for rapid and non-destructive maize seed variety classification. They employed one-class classifiers based on hyperspectral data, achieving over 91% accuracy in recognizing known varieties and rejecting unknowns. This method holds potential for both incremental learning and open-set recognition.

This paper highlights seed classification's importance in agriculture and industry, introducing a novel deep-learning model. It uses a dataset of 3018 RGB images containing 15 seed species to create a precise classification model. The contribution of the work is mentioned as follows:

- A new dataset has been created containing images of 15 distinct seed species.
- Thoroughly compareing the training of Xception model from scratch and using transfer learning with the Pre-trained Xception model, shedding light on transfer learning's advantages in seed classification applications.
- Demonstrating the Pre-trained Xception model's superiority through rigorous experiments.

2 Material and Methods

The methodology for creating a seed classification system is visually outlined in Fig. 1. The process encompasses several key steps, beginning with sample collection, followed by image acquisition. Subsequently, images are subjected to Image Rescaling to ensure uniformity. The dataset is then divided into training, validation, and testing subsets in a

ratio of 70/15/15, respectively [28, 29]. The core of the methodology involves training a selected model from scratch. Additionally, the model was selected but this time transfer learning was incorporated during training. The trained models are subjected to rigorous testing, and the results are systematically compared and evaluated to determine their performance characteristics and relative merits. This comprehensive approach ensures the robust development and assessment of the seed classification system.
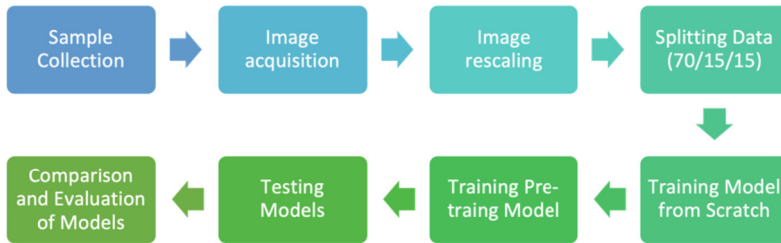
Fig. 1. Research Flow diagram

2.1 Dataset Description

In the initial phase, a diverse set of 15 distinct seed species, including black pepper, black-eyed peas, corn, white beans, jumbo red beans, lupin, coffee beans, oat seeds, wheat seeds, soya bean, pearl millet, red chori, lentil brown, black beans, and green peas, were meticulously gathered for the training of the seed classification model. These samples were methodically stored at room temperature, ensuring their integrity for subsequent image acquisition. To prevent any potential cross-contamination, each class of seeds was thoughtfully segregated into dedicated, well-organized containers. The containers, each with a one-liter capacity, accommodated varying seed quantities based on the seed type.

To facilitate the image acquisition process, a systematic approach was adopted. Each container was processed sequentially, with the seeds from the container being gently dispensed in measured portions onto a pristine white tray, meticulously positioned to optimize imaging. To capture a range of possible seed orientations, each portion of seeds was meticulously mixed and then photographed multiple times using a smartphone, capturing scenarios of diverse seed placements on the classification tray. The smartphone used offered a resolution of 4032 × 3024 pixels [29–31].

Maintaining consistency and accuracy during image capture was crucial. A tripod was employed to securely affix the smartphone at a fixed distance from the samples, minimizing any potential camera shake and ensuring uniformity across captured images. This strategic solution not only maintained a consistent distance but also eliminated the risk of image blurring due to inadvertent movement. A visual representation of captured image samples can be observed in Fig. 2, showcasing the meticulous approach employed in the seed classification project.

Captured images were labeled and saved in a dedicated folder for each class. Later saved images were rescaled according to model requirements which in our study was

Fig. 2. Samples of captured images

299×299. The resulting collection contains 3018 images, 70% of which were randomly selected and saved training folder. The remaining images were distributed equally and saved in validation and testing folders. The samples of images, and the number of images saved in the training, validation, and test folders are given in Table 1. The training was performed on 2108 images, validation was performed on 452 images and the test was performed on 458 images.

Table 1. Details of the obtained dataset

Class	Training	Validation	Test	Total
Black Pepper	148	32	32	212
Black-Eyed Peas	133	28	29	190
Corn	151	32	33	216
White Beans	135	29	30	194
Jumbo Red Beans	137	30	30	197
Lupin	141	30	31	202
Coffee Beans	140	30	30	200
Oat Seeds	141	30	31	202

(continued)

Table 1. (*continued*)

Class	Training	Validation	Test	Total
Wheat Seeds	140	30	30	200
Soya Bean	140	30	30	200
Pearl Millet	140	30	30	200
Red Chori	140	30	30	200
Lentil Brown	139	30	30	199
Black Beans	140	30	31	201
Green Peas	143	31	31	205
Total	**2108**	**452**	**458**	**3018**

2.2 Model Configurations and Experimental Settings

The model training process was conducted on a Windows 10 Pro operating system, utilizing hardware components including an Intel i5 processor, GeForce GTX 1660 Graphics Card, and 16 GB RAM. Python, along with essential libraries such as OpenCV and Keras, formed the core environment for constructing the models. Initially, the Xception model was trained from the ground up. To ascertain optimal parameters within this architecture, meticulous hyperparameter tuning was undertaken. The search for the optimal initial learning rate involved a systematic reduction by a factor of 10 for each trial, spanning from 0.1 down to 0.000001. From the results tabulated, the ideal learning rate emerged as 0.0001. The subsequent step involved pinpointing the optimal batch size; options 8, 16, 32, and 64 were explored, coupled with the established learning rate of 0.0001. Following thorough analysis, a batch size of 8 was determined to be optimal. A consistent epoch count of 100 was set, alongside the implementation of early stopping with a patience parameter of 20.

Given the balanced nature of the dataset, evaluation metrics like precision, recall, and F1-score closely mirrored accuracy. Consequently, the focus was placed solely on accuracy – the ratio of correctly predicted values to all values – as the reported metric. Beyond accuracy, model losses were pivotal for evaluation, denoting the extent to which the model's predictions aligned with actual data. Calculated as the deviation between actual and predicted classes, the loss value illuminated the model's predictive performance. These identical hyperparameters were seamlessly applied to the pre-trained model, ensuring consistency and rigor across the training regimen.

3 Results and Discussion

Figure 3a offers a visual insight into the evolving training and validation accuracy over the course of multiple epochs, while Fig. 3b delves into the corresponding training and validation loss trends. Analyzing Fig. 3a, it becomes evident that the accuracy trajectory of the Xception model, when trained from scratch on the seed dataset, embarked at around 60% and exhibited a gradual ascent, ultimately surging to an impressive 99% by the 15th

iteration, which it steadfastly maintained till the conclusion of the training regimen. In stark contrast, the journey of validation accuracy was less straightforward. Commencing at a modest 5%, it exhibited a wavering progression marked by fluctuations through subsequent iterations, highlighting the struggle of the Xception model's validation accuracy when built from the ground up. Transitioning to the discourse on training and validation loss, both aspects mirror the earlier trends. Training loss, relatively restrained, attested to the model's gradual learning, whereas validation loss exhibited a more volatile behavior, oscillating as training progressed. This intricately depicted similarity between the training and validation loss in Fig. 3b serves to corroborate the challenge observed in the model's validation accuracy. Collectively, Fig. 3 provides a comprehensive understanding that the Xception model encountered substantial loss variations during validation, underscoring limited learning and a shortfall in the model's grasp of the intricate nuances present within the seed dataset.
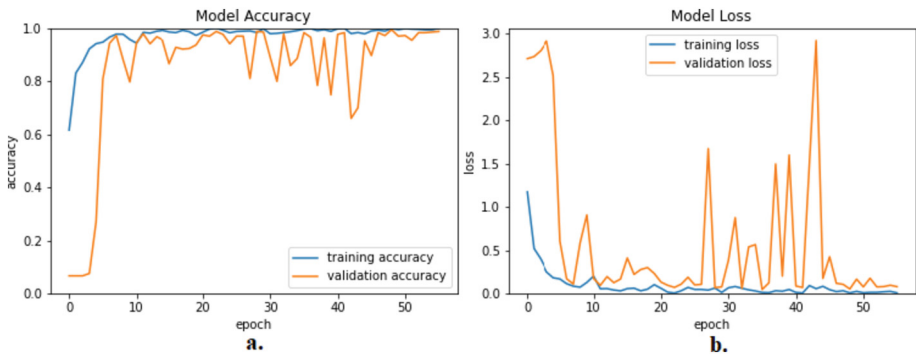
Fig. 3. Convergence curves of Xception Trained from Scratch **a.** Accuracy, **b.** Loss.

The insights garnered from Fig. 3 highlight a distinct pattern: training the Xception model from scratch incurred significant loss during the training phase. This observation led us to pivot towards the utilization of transfer learning. Acknowledging this pivotal shift, we transitioned to the subsequent phase, leveraging the pre-existing weights of the Xception model, originally trained on the expansive ImageNet dataset, and fine-tuning it on our specialized seed dataset. Figure 4 provides a comprehensive view of the Convergence curves of the Pre-trained Xception model, painting a vivid picture of its performance. In Fig. 4a, we examine the trajectories of both training and validation accuracy.

Figure 4a illustrates that the Pre-trained Xception model commenced its journey with an impressive 85% accuracy, which rapidly escalated to achieve full accuracy of 100% within the initial iterations. Remarkably, the validation accuracy exhibited an equally robust performance, beginning at 98% and swiftly converging to 100% over the ensuing two iterations, subsequently maintaining this peak accuracy throughout the training process.

Shifting our attention to Fig. 4b, the intricacies of training and validation loss are unveiled. In the case of the pre-trained Xception model, the training loss experienced

a higher magnitude at the outset, as the model initially encountered the novel nuances of the seed dataset. However, with a progressive decline, this loss diminished significantly, reaching less than 3 by the tenth iteration. Impressively, the trajectory continued its descent, ultimately reaching a state of minimal loss. Conversely, validation loss, as portrayed in Fig. 4b, embarked at 7% and exhibited a rapid decline, reaching an astonishingly low value of 0.0002 by the tenth iteration. This exceptional level persisted consistently until the validation phase concluded.

Cumulatively, the insights drawn from Fig. 4 underscore a resounding outcome: the Xception model showcased its zenith performance when underpinned by transfer learning. The model harnessed the richness of pre-existing knowledge while effectively adapting it to the intricacies of the seed dataset, yielding superior results when juxtaposed with the challenges associated with training from scratch on the specialized seed dataset.
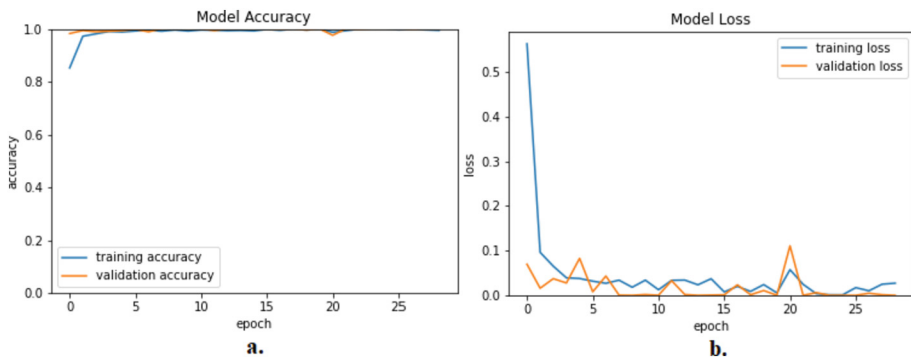
Fig. 4. Convergence curves of Pre-trained Xception **a**. Accuracy, **b**. Loss.

Table 2 provides a concise overview of the training, validation, and test Results for both the Xception model trained from scratch and the Pre-trained Xception model. Notably, the Xception Scratch model exhibited an impressive training accuracy of 0.9986 with a corresponding training loss of 0.0063. For validation, it achieved an accuracy of 0.9867 with a slightly higher validation loss of 0.0786. During the testing phase, this model maintained a strong accuracy of 0.9847, accompanied by a test loss of 0.0396. The training process for this model took approximately 1 h and 39 min, while the testing duration was notably brief at 5 s. The model underwent 56 epochs to reach these results.

On the other hand, the Pre-trained Xception model exhibited comparable performance. It achieved a training accuracy of 0.9943 with a training loss of 0.0273. This model's validation accuracy was a perfect 1.0000, coupled with an exceptionally low validation loss of 0.0002. During testing, the Pre-trained Xception model also demonstrated a flawless accuracy of 1.0000, accompanied by the same minimal test loss of 0.0002. The training duration for this model was notably shorter at 52 min, and the testing duration remained consistent at 5 s. The model converged to these results over 29 epochs.

Table 2. Training, Validation, and Test Results of Models

Values	Xception Scratch	Pre-Trained Xception
Training Accuracy	0.9986	0.9943
Training Loss	0.0063	0.0273
Validation Accuracy	0.9867	1.0000
Validation Loss	0.0786	0.0002
Test Accuracy	0.9847	1.0000
Test Loss	0.0396	0.0002
Training Duration	1 h 39 m	52 m
Test Duration	5 s	5 s
Epochs	56	29

4   Conclusion

The conducted study delved into the task of seed classification, employing two distinct approaches: training the Xception model from scratch and utilizing transfer learning with the Pre-trained Xception model. The results underscore a clear advantage in favor of the Pre-trained Xception model [32]. This model not only achieved remarkable accuracy levels but also demonstrated significantly lower loss values across the training, validation, and testing phases. Notably, the Pre-trained Xception model exhibited impeccable accuracy, achieving a perfect 1.0000 on both validation and test sets. Additionally, the model's convergence was achieved with a substantially reduced number of epochs and a shorter training duration, underscoring its efficiency and effectiveness. Given its promising performance, it is feasible to develop a mobile application intended for everyday users, enabling them to classify various seed species. While the Pre-trained Xception model has yielded impressive results, several avenues for further exploration and refinement exist:

1. Ensemble Approaches: Investigating ensemble methods that combine predictions from multiple models could potentially enhance classification performance even further.
2. Fine-tuning Strategies: Experimenting with different fine-tuning strategies for transfer learning, such as adjusting learning rates for specific layers, could lead to enhanced results.
3. Augmentation Techniques: Exploring advanced data augmentation techniques could contribute to a more robust model that generalizes better to unseen data.

Domain-Specific Pre-training: Considering domain-specific pre-training on related datasets could potentially yield models with an even greater understanding of seed-specific features.

References

1. Gao XL, Shao YH, Yang YH, Zhou WX (2022) Do the global grain spot markets exhibit multifractal nature? Chaos Solitons Fractals 164:112663. https://doi.org/10.1016/J.CHAOS.2022.112663
2. Gulzar Y, Hamid Y, Soomro AB, Alwan AA, Journaux L (2020) A convolution neural network-based seed classification system. Symmetry (Basel) 12:2018
3. Van Hoai DP, Surinwarangkoon T, Hoang VT, Duong H-T, Meethongjan K (2020) A comparative study of rice variety classification based on deep learning and hand-crafted features. ECTI Trans Comput Inf Technol 14:1–10. https://doi.org/10.37936/ecti-cit.2020141.204170
4. Romadanova NV, Kushnarenko SV (2023) Conservation of plant biodiversity by biotechnology methods. In: Proceedings on Applied Botany, Genetics and Breeding, vol 184
5. Sahlan F, Hamidi F, Misrat MZ, Adli MH, Wani S, Gulzar Y (2021) Prediction of mental health among university students. Int J Percept Cogn Comput 7:85–91
6. Hanafi MFFM, Nasir MSFM, Wani S, Abdulghafor RAA, Gulzar Y, Hamid Y (2021) A real time deep learning based driver monitoring system. Int J Percept Cogn Comput 7:79–84
7. Hamid Y, Elyassami S, Gulzar Y, Balasaraswathi VR, Habuza T, Wani S (2022) An improvised CNN model for fake image detection. Int J Inf Technol 2022:1–11. https://doi.org/10.1007/S41870-022-01130-5
8. Gulzar Y, Alwan AA, Abdullah RM, Abualkishik AZ, Oumrani M (2023) OCA: ordered clustering-based algorithm for e-commerce recommendation system. Sustainability 15:2947. https://doi.org/10.3390/SU15042947
9. Dhiman P, Kaur A, Balasaraswathi VR, Gulzar Y, Alwan AA, Hamid Y (2023) Image acquisition, preprocessing and classification of citrus fruit diseases: a systematic literature review. Sustainability 15:9643. https://doi.org/10.3390/SU15129643
10. Khan F, et al (2023) MRI-based effective ensemble frameworks for predicting human brain tumor. J Imaging 9:163. https://doi.org/10.3390/JIMAGING9080163
11. Anand V, et al (2023) Weighted average ensemble deep learning model for stratification of brain tumor in MRI images. Diagnostics 13:1320. https://doi.org/10.3390/DIAGNOSTICS13071320
12. Khan SA, Gulzar Y, Turaev S, Peng YS (2021) A modified HSIFT descriptor for medical image classification of anatomy objects. Symmetry (Basel) 13:1987
13. Alam S, Raja P, Gulzar Y (2022) Investigation of machine learning methods for early prediction of neurodevelopmental disorders in children. Wirel Commun Mob Comput 2022
14. Majid M et al (2023) Enhanced transfer learning strategies for effective kidney tumor classification with CT imaging. Int J Adv Comput Sci Appl 2023:14. https://doi.org/10.14569/IJACSA.2023.0140847
15. Hamid Y, Wani S, Soomro AB, Alwan AA, Gulzar Y (2022) Smart seed classification system based on MobileNetV2 architecture. In: Proceedings of the 2022 2nd International Conference on Computing and Information Technology (ICCIT). IEEE, pp 217–222
16. Bao F, Bambil D (2021) Applicability of computer vision in seed identification: deep learning, random forest, and support vector machine classification algorithms. Acta Bot Brasilica 35:17–21. https://doi.org/10.1590/0102-33062020ABB0361

17. Kurtulmuş F (2020) Identification of sunflower seeds with deep convolutional neural networks. J Food Meas Character 15(2):1024–1033. https://doi.org/10.1007/s11694-020-00707-7
18. Loddo A, Loddo M, Di Ruberto C (2021) A novel deep learning based approach for seed image classification and retrieval. Comput Electron Agric 187. https://doi.org/10.1016/j.compag.2021.106269
19. Xu P, Tan Q, Zhang Y, Zha X, Yang S, Yang R (2022) Research on maize seed classification and recognition based on machine vision and deep learning. agriculture (Switzerland) 12. https://doi.org/10.3390/agriculture12020232
20. Huang Z, et al (2022) Deep learning based soybean seed classification. Comput Electron Agric 202. https://doi.org/10.1016/j.compag.2022.107393
21. Ünal Z, Aktaş H (2023) Classification of hazelnut kernels with deep learning. Postharvest Biol Technol 197:112225. https://doi.org/10.1016/J.POSTHARVBIO.2022.112225
22. Gulzar Y (1906) Fruit image classification model based on MobileNetV2 with deep transfer learning technique. Sustainability 2023:15
23. Sabanci K (2023) Benchmarking of CNN models and MobileNet-BiLSTM approach to classification of tomato seed cultivars. Sustainability (Switzerland) 15. https://doi.org/10.3390/su15054443
24. Luo T et al (2023) Classification of weed seeds based on visual images and deep learning. Inf Process Agric 10:40–51. https://doi.org/10.1016/j.inpa.2021.10.002
25. Díaz-Martínez V, Orozco-Sandoval J, Manian V, Dhatt BK, Walia H (2023) A deep learning framework for processing and classification of hyperspectral rice seed images grown under high day and night temperatures. Sensors 23. https://doi.org/10.3390/s23094370
26. Wang Y, Song S (2023) Variety identification of sweet maize seeds based on hyperspectral imaging combined with deep learning. Infrared Phys Technol 130. https://doi.org/10.1016/j.infrared.2023.104611
27. Zhang L, Huang J, Wei Y, Liu J, An D, Wu J (2023) Open set maize seed variety classification using hyperspectral imaging coupled with a dual deep SVDD-based incremental learning framework. Expert Syst Appl 234. https://doi.org/10.1016/j.eswa.2023.121043
28. Gulzar Y, Ünal Z, Aktaş HA, Mir MS (2023) Harnessing the power of transfer learning in sunflower disease detection: a comparative study. Agriculture 13:1479. https://doi.org/10.3390/AGRICULTURE13081479
29. Ayoub S, Gulzar Y, Rustamov J, Jabbari A, Reegu FA, Turaev S (2023) Adversarial approaches to tackle imbalanced data in machine learning. Sustainability 15:7097. https://doi.org/10.3390/SU15097097
30. Ayoub S, Gulzar Y, Reegu FA, Turaev S (2022) Generating image captions using bahdanau attention mechanism and transfer learning. Symmetry (Basel) 14:2681
31. Malik I, et al (2023) Estimation of the extent of the vulnerability of agriculture to climate change using analytical and deep-learning methods: a case study in Jammu, Kashmir, and Ladakh. Sustainability 15:11465. https://doi.org/10.3390/SU151411465
32. Mamat N, Othman MF, Abdulghafor R, Alwan AA, Gulzar Y (2023) Enhancing image annotation technique of fruit classification using a deep learning approach. Sustainability 15:901

Classification of Pistachio Varieties Using Pre-trained Architectures and a Proposed Convolutional Neural Network Model

Khaled Adil Dawood Idress[1]([✉]), Yeşim Benal Öztekin[2],
Omsalma Alsadig Adam Gadalla[3], and Geofrey Prudence Baitu[4]

[1] Department of Agricultural Engineering, Al-Neelain University, P.O. Box 12702, Khartoum,
Sudan
adilkhaled850@gmail.com

[2] Faculty of Agriculture, Department of Agricultural Machinery and Technologies Engineering,
Ondokuz Mayis University, Samsun, Turkey

[3] Department of Agricultural Engineering, University of Khartoum, P.O. Box 321, Khartoum,
Sudan

[4] Department of Agricultural Engineering, College of Agriculture and Food Technology,
University of Dar es Salaam, P.O. Box 35091, Dar es Salaam, Tanzania

Abstract. Pistachio is a vital agricultural product native to the Middle East and Central Asia. The world's major pistachio producers, Iran, the USA, Turkey, and Syria, contribute close to 90% of the total production worldwide. In Turkey, there are eight primary domestic pistachio varieties, alongside five foreign varieties. Each produced kind has its unique market and pricing point for consumers to purchase. However, the existing method used to separate pistachio nuts is still carried out with basic knowledge, leading to a significant potential for errors in the classification process due to the virtually identical appearance of each pistachio variety. To address this challenge and enhance the efficiency of the packaging process, innovative technologies are required in the pistachio industry. This study focuses on the classification of three distinct pistachio varieties—Siirt, Tekin, and Uzun—using pre-trained VGG16 and Inception-V3 models, along with a proposed Convolutional Neural Network (CNN) model. The dataset used in the study was divided into three subsets, with 70% allocated for training, 15% for validation, and 15% for testing. Specifically, 1575 images were used for training, and 672 images were allocated for both validation and testing purposes. As a result of the performed classifications, test classification accuracies of 94.05%, 96.13%, and 97.02% were obtained from the pre-trained VGG16, Inception-V3 models, and the proposed CNN model, respectively. The pre-trained models and the proposed CNN model displayed impressive performance, but the proposed CNN model demonstrated a slight advantage with its higher test accuracy score. This suggests that it is more suitable and effective for the classification of the different varieties of pistachio compared to the pre-trained models.

Keywords: Pistachio · Classification · Convolutional neural network · Transfer learning

1   Introduction

Pistachio (*Pistacia vera* L.) is an agricultural product originally from the Middle East and Central Asia. Iran, the USA, Turkey, and Syria are the primary contributors, accounting for nearly 90% of global pistachio production. In Turkey, there are eight primary domestic pistachio types: Uzun, Kırmızı, Halebi, Siirt, Beyazben, Sultani, Değirmi, and Keten Gömleği. Additionally, five foreign varieties are cultivated: Ohadi, Bilgen, Vahidi, Sefidi, and Mümtaz [1]. Among these domestic and foreign pistachio varieties, the most preferred ones are Kırmızı, Siirt, and Halabi [2]. Pistachios rank second only to hazelnuts in terms of fat content. They are also abundant in essential minerals and vitamins, encompassing phosphorus, potassium, calcium, magnesium, and iron. Moreover, pistachios boast a vitamin-rich profile, including vitamins E, C, B1, and B2 [3].

Pistachio varieties exhibit considerable diversity, each catering to distinct markets and consumer preferences. Take, for example, the Kırmızı and Siirt varieties. Kırmızı stands out with its deep green hue, distinct flavor, and aromatic qualities, making it a favored choice in the confectionery and sweet pastry industries. On the other hand, Siirt's round shape and excellent cracking rate make it a popular snack option among consumers. [4]. Nonetheless, the method employed to differentiate between pistachio nuts continues to rely on fundamental techniques. Consequently, there exists a significant likelihood of errors during the classification procedure due to the nearly identical appearance of each pistachio variety. The introduction of innovative solutions is imperative to accurately identify the type of pistachio nuts, ensuring precise packaging for sales purposes [5].

In recent times, numerous research studies within the literature have focused on the classification of agricultural products by employing deep learning and machine learning methodologies. Nonetheless, the volume of research dedicated to the categorization of various pistachio types remains notably restricted. Specifically, there is a scarcity of investigations that leverage deep learning methodologies to address this concern. A study was conducted by Lisad et al. (2023) to classify two types of pistachio nuts using the transfer learning approach, namely AlexNet, VGG16, and VGG19. In this study, they used 2148 photos, 916 of the Siirt type and 1232 of the Kırmızı type. The dataset was split into training and testing sets with an 80:20 ratio. By applying transfer learning techniques using the AlexNet, VGG 16, and VGG 19 models, the classification results achieved were 94.42%, 98.84%, and 98.14%, respectively [5]. Ozkan et al. (2021) used an improved k-NN Classifier to classify open and closed pistachio nuts. In this study, shape and morphological features were extracted from images. These features were then used as inputs to train and test the machine learning algorithm. The results of the study showed that the proposed technique achieved a classification accuracy of 94.18% [4]. In their study, Farazi et al. (2017) utilized a combination of deep learning and machine learning approaches to distinguish between open-shelled pistachios and other types of pistachios with signs of deterioration. They initiated their work with an initial dataset containing 1000 images derived from both pistachio kernels and their shells. Employing data augmentation techniques, they subsequently enlarged this dataset to encompass a total of 20,000 images. The researchers then proceeded to extract relevant features from these images, employing the architectural frameworks of AlexNet and GoogleNet. Using Principal Component Analysis (PCA), they identified the 300 most influential features for subsequent analysis and classification purposes. Among these extracted features,

the top 300 were chosen using Principal Component Analysis (PCA). Subsequently, these selected features were used as input for a Support Vector Machine (SVM) classifier to carry out the classification tasks. Remarkably, the highest accuracy of 99% was achieved when utilizing features derived from the GoogleNet architecture [6]. Omid (2011) introduced an expert system that relied on an acoustic emission signal coupled with a fuzzy logic classifier to classify open and closed pistachio nuts. The evaluation of the sorting system using testing datasets yielded an impressive overall accuracy rate of 95.56% [7]. Abbaszadeh et al. (2019) employed deep auto-encoder neural networks to undertake the classification of pistachios into categories of defective and flawless. The results of their research yielded a classification accuracy of 80.3% in accurately identifying defective pistachios. [8]. Rahimzadeh and Attar (2022) introduced a computer vision system designed to differentiate between open and closed pistachios of various types. Their methodology encompassed the utilization of CNN-based models, including ResNet50, ResNet152, and VGG16, to extract pertinent features from pistachio images and perform classification. The average classification accuracies achieved through these models were 85.28%, 85.19%, and 83.32%, respectively [9]. In a study conducted by Dheir et al. (2020), CNN algorithms were employed for the classification of various types of nuts. The study encompassed the classification of five distinct nut types: chestnut, hazelnut, forest nut, pecan nut, and walnut. This classification was carried out utilizing a dataset consisting of 2868 images. The outcome of their work demonstrated an impressive accuracy rate of 98% achieved through the utilization of a pre-trained CNN [10]. Ataş and Doğan (2015) employed various classification techniques, including J48 Decision Tree, Naïve Bayes, and Multi-Layer Perceptron (MLP), to differentiate between open and closed pistachio nuts. Notably, the J48 decision tree was the primary classifier used in this study. The performance of the J48 decision tree was also compared to that of other classifiers such as Naïve Bayes and Multi-Layer Perceptron (MLP).The results of the study revealed that the proposed system utilizing the J48 decision tree not only provided a straightforward and easily interpretable classification model but also achieved a commendable classification accuracy rate of 94.5% [11]. In another study on the classification of defective and perfect pistachios, Dini et al. (2020) utilized pre-trained CNN algorithms. The outcomes derived from examining 958 images revealed that the GoogleNet, ResNet, and VGG16 models achieved classification accuracies of 95.8%, 97.2%, and 95.83% respectively [12].

Many studies have been conducted to improve the accuracy in categorizing various types of pistachio varieties and distinguishing between open and closed pistachio nuts by employing machine learning and deep learning techniques. However, most previous studies have concentrated on the classification of only two pistachio varieties, specifically Kırmızı and Sirrt. Furthermore, these studies primarily focused on differentiating between open and closed pistachio nuts, often employing traditional machine-learning techniques. This study aims to use pre-trained VGG16, inception-V3 models, and a proposed CNN model to classify three different pistachio varieties, including Siirt, Tekin, and Uzun. Then, we will compare the obtained results from the proposed CNN model with the pre-trained model.

2   Materials and Methods

2.1   Image Acquisition

This research was conducted at the laboratory of the Department of Agricultural Machinery and Technologies Engineering in the Faculty of Agriculture at Ondokuz Mayis University in Samsun. A total of 1911 samples from various pistachio varieties, namely Siirt, Tekin, and Uzun, were acquired from the Pistachio Research Institute of the Ministry of Agriculture and Forest in Gaziantep. These samples were examined and stored at room temperature. To ensure optimal image quality, a white surface was utilized as the background during the experiment. Adequate lighting is essential for capturing high-quality images; thus, two 8-W fluorescent lamps were employed as the light source within the image acquisition chamber. The images of the three different pistachio varieties were captured under identical conditions, including the same camera, position, and

Fig. 1. Image capturing system.
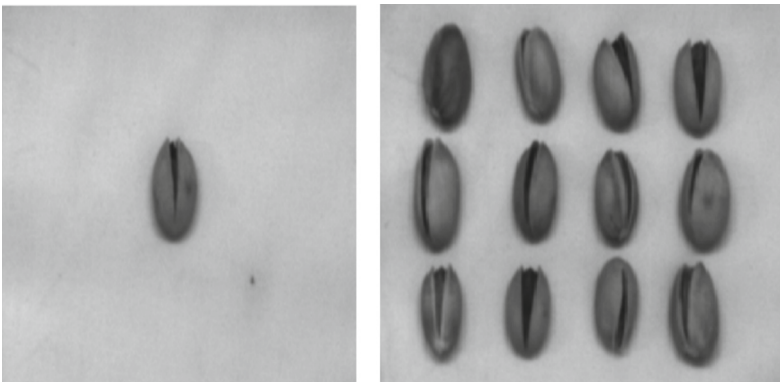
Fig. 2. Pistachio Siirt Type

background. The image capture system utilized in this study is depicted in Fig. 1, which consists of a camera connected to a computer equipped with an image capture card. Figure 2, Fig. 3, and Fig. 4 show samples of the various pistachio varieties used in this study.
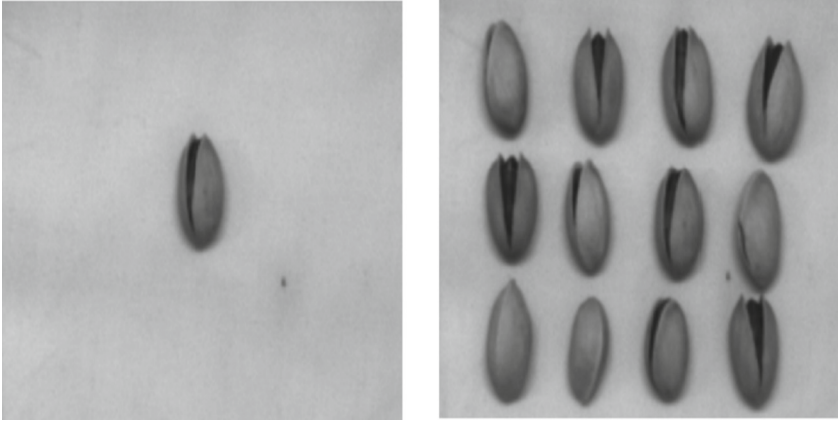
Fig. 3. Pistachio Tekin Type
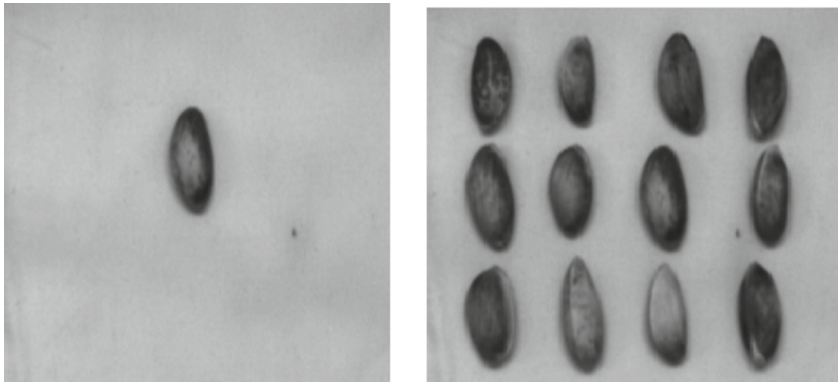
Fig. 4. Pistachio Uzun Type

2.2 Image Pre-processing

The pre-processing stage is essential to prepare the acquired dataset for utilization in pre-trained models such as VGG16, Inception-V3, and the proposed CNN model. This stage involves several operations to be performed on the dataset. These operations include image scaling, image array conversion, and dataset division, which will facilitate future classification processes. More detailed information about the pre-processing procedure that will be followed can be found in Fig. 5.
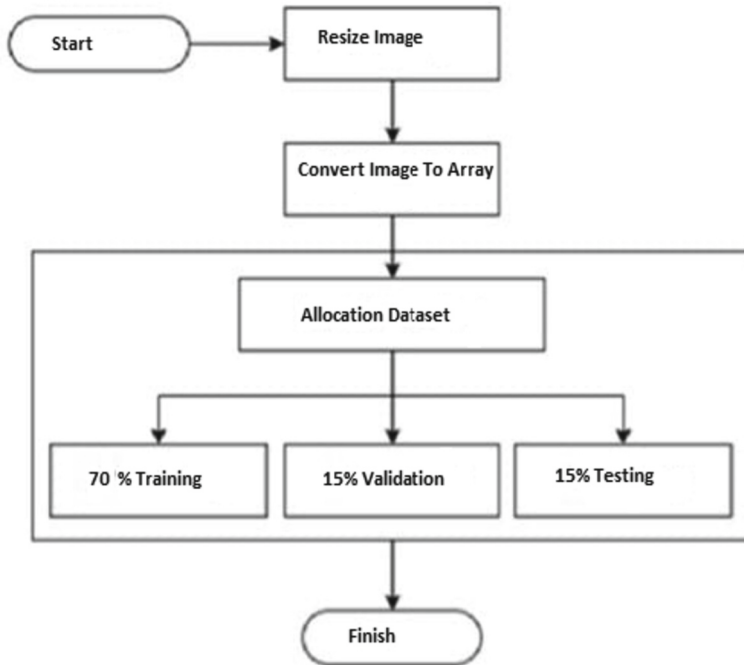
Fig. 5. Pre-processing Stages

2.2.1   Image Resize

Resizing involves adjusting the dimensions of an image to make it compatible with the model's input requirements. In the context of this study, image sizes were standardized to facilitate model processing. Specifically, the dimensions used were 150×150 pixels for the Inception-V3 model and 224×224 pixels for the VGG16 model. Consequently, during the subsequent training phase, images will be resized to these specific dimensions to match the input specifications of each respective model.

2.2.2   Dataset Allocation

During this phase, a random selection method is employed to split the existing dataset into two distinct subsets: training data and testing data. This process involves partitioning a designated library folder, allocating 75% of the data for training, and distributing 15% each for validation and testing purposes. The detailed distribution of the dataset is shown in Table 1.

2.3   Convolutional Neural Network-Based Model

Deep learning, a subset of machine learning, has gained significant attention and has been widely applied in various fields in recent years. In engineering applications, there is a growing emphasis on addressing complex object recognition problems, and CNN) has

Table 1. Allocation dataset

Pistachio Type	Allocation Dataset		
	Train (70%)	Validation (15%)	Testing (15%)
Siirt	525	112	112
Tekin	525	112	112
Uzun	525	112	112
Total	1575	336	336

emerged as the go-to deep learning algorithm for such tasks. The CNN architecture serves as the fundamental framework for deep learning, consisting of convolution, pooling, fully connected, dropout, and classification layers.

2.3.1 Convolution Layer

The convolutional layer plays a crucial role in extracting features from input data. It operates by convolving input vectors with filters, which involves performing a locally weighted sum aggregation. This process transforms the data into a feature space, allowing for the identification of significant patterns. In the context of image analysis, the initial convolutional layer primarily focuses on capturing fundamental attributes such as colors and edges [13].

2.3.2 Pooling Layer

The pooling layer is a crucial element within the CNN architecture, primarily serving two functions: diminishing processing load and reducing the number of parameters within the network [14].

2.3.3 Fully Connected Layer

In the fully connected layer, all the nodes or neurons are connected to the nodes of the preceding layer. Each node in this layer receives input from all the nodes of the previous layer. The number of nodes in the fully connected layer can vary between different network architectures. In this layer, the features extracted from the previous layers are preserved, and the learning process takes place by adjusting the weights and biases associated with each node. These weights and biases are updated during the training process using optimization algorithms like gradient descent to minimize the network's loss function [15].

2.3.4 Dropout Layer

During the training process, this layer employs a technique called selective connection removal to enhance the learning performance of the network. This technique involves selectively eliminating connections within the network. This process helps prevent over-fitting and improves the network's generalization capabilities. Once the input data is fed

into the CNN, the training process commences. Through multiple iterations and adjustments to the network's weights and parameters, the CNN gradually learns to recognize relevant patterns and features in the input data. The network's weights and parameters are updated to optimize its performance and improve its ability to make accurate predictions or classifications the CNN learns to identify relevant patterns and features [16].

In this study, pre-trained VGG16, Inception-V3, and a proposed CNN model were used to classify three different pistachio varieties, including Siirt, Tekin, and Uzun.

2.4 Pre-trained CNN Models

The literature encompasses a diverse range of CNN architectures. The selection of an appropriate architecture takes into account factors such as classification accuracy, model size, and computational speed. In this study, the choice of CNN models was made after conducting several experiments to assess their performance against these criteria.

2.4.1 VGG16 Model

VGG16 is a CNN architecture created by the Visual Geometry Group (VGG). It is an improvement over its predecessor, AlexNet, and is known for its high accuracy in image classification tasks. VGG16 focuses on using smaller filter sizes and strides in the first convolutional layer. While it achieves better accuracy compared to AlexNet, it requires a larger amount of memory due to its increased number of parameters. Unlike AlexNet, VGG16 employs smaller 3×3 dimensional filters in all convolution layers, with variable numbers of 64, 128, and 256 filters. VGG16 is a relatively straightforward CNN model with support for GPU acceleration. It consists of a total of 16 layers, including 13 convolutional layers, three fully connected layers, pooling layers, ReLU activation layers, dropout layers, and a softmax layer for classification. The input layer of VGG16 accepts images of size $224 \times 224 \times 3$ pixels, and the final layer is the classification layer that outputs the predicted class probabilities. The architectural structure of VGG16 is illustrated in Fig. 6 [17].
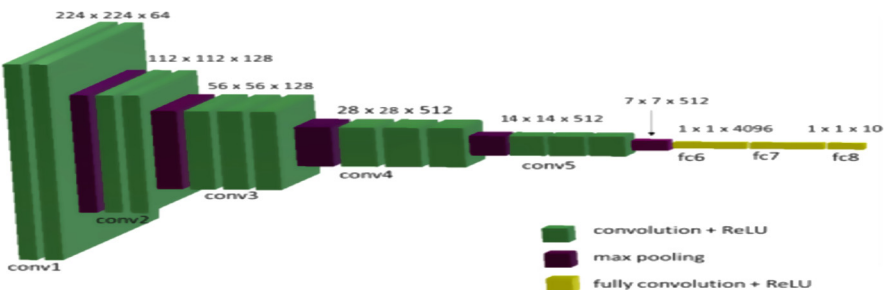
Fig. 6. VGG16 architecture

2.4.2 Inception-V3 Model

The Inception architecture typically consists of three different sizes of convolution layers, with the smallest one known as the unification layer. This architecture incorporates multiple layers, including the convolution layer, which divides the input into smaller subsets. This partitioning operation facilitates the processing of different features present in the input data, thereby improving computational efficiency and mitigating overfitting [18]. The concatenation layer serves as a link between the preceding module and the subsequent module. In the architecture, the fully connected layer includes all the neurons connecting the module layer to the fully connected layer. The activation function utilized in this Layer is SoftMax activation, which assists in addressing class categorization. The architecture of the Inception-V3 model is seen in Fig. 7.
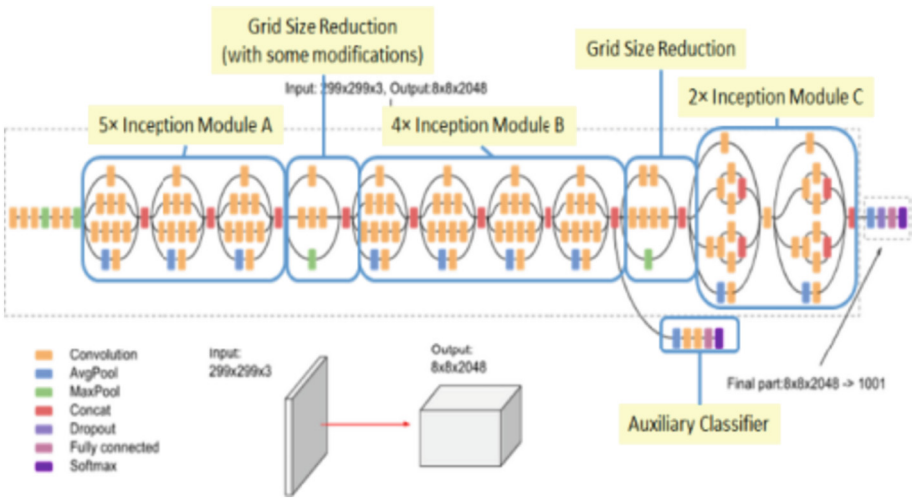
Fig. 7. Architecture of Inception-V3

2.5 The Proposed CNN Model

The proposed CNN model comprises five convolutional layers, MaxPooling, Batch Normalization, 2 Dense layers, and Dropout. Each CNN output estimate is activated using ReLU activation, while the output of the final sequential estimation model is activated using Softmax activation. Softmax activation is commonly employed at the end of a network for label estimation, particularly in multi-class classification tasks, as it enhances effectiveness and accuracy. The Adam model, a popular optimization algorithm, along with the Keras optimizer, was utilized in the training process with a learning rate of 0.0001. The model parameters and their corresponding values are summarized in Table 2.

Table 2. Proposed CNN model parameter

1. Conv2D Layer	2. Conv2D Layer	3. Conv2D Layer	4. Conv2D Layer	5. Conv2D Layer	Flatten Layer
output shape	output shape	output shape	output shape	output shape	output shape
248, 248, 32	122, 122, 64	59, 59, 128	27, 27, 128	11,11,128	21,632
MaxPooling2D	MaxPooling2D	MaxPooling2D	MaxPooling2D	MaxPooling2D	1. Dense and Dropout
124, 124, 32	61, 61, 64	29,29, 128	13, 13, 128	5, 5, 128	512
Activation function	Activation function	Activation function	Activation function	Activation function	Activation function
ReLu	ReLu	ReLu	ReLu	ReLu	Softmax
Total	Total parameters:	Trainable parameters:	Non-trainable parameters:		
	2,028,867	2,029,867	0		

In the first convolutional layer, the input dimensions are $32 \times 32 \times 3$. This is followed by the second convolutional layer with dimensions $64 \times 64 \times 3$, the third with dimensions $128 \times 128 \times 3$, the fourth with dimensions $128 \times 128 \times 3$, and finally, the fifth with dimensions $128 \times 128 \times 3$. The flatten layer is succeeded by two dense layers and a dropout layer.

2.6 Training- Validation-Testing Data and Model Evaluation

In this study, the dataset was split into three parts: 70% for training, 15% for validation, and 15% for testing. Specifically, 1575 images were used for training, and 672 images were allocated for both validation and testing. The model's performance was evaluated using metrics like true positive, false positive, false negative, and true negative, determining its accuracy. Besides accuracy, metrics such as precision, recall, and F1-score were employed to assess the CNN model. Precision measures correctly classified positive outcomes, showing the model's ability to identify positives accurately. Recall evaluates the correct identification of actual positive samples. The F1-score, derived from precision and recall, gives a balanced performance assessment. By using these metrics, the model's performance can be comprehensively evaluated [19]. There have been chosen particular parameters for the proposed CNN model (Table 3).

Table 3. Proposed CNN training parameter

Parameter	Value
Batch size	64
Epoch	20
Momentum	0.9
Learning rate	0.0001
Metric	Categorical cross-entropy
Optimization method	Adam

3   Result and Discussion

In this study, we employed three distinct models: a pre-trained VGG16, Inception-V3, and a CNN model proposed by us. The aim was to classify three different pistachio varieties, namely Siirt, Tekin, and Uzun. To ensure a robust and generalized model, we adopted hold-out cross-validation. This technique involves partitioning the data into training, validation, and test subsets. Specifically, 70% of the total data was allocated for training, 15% for validating the accuracy, and the remaining 15% for the test set. Given our utilization of the transfer learning approach, the model was initiated with pre-existing training weights. As the training progressed, these weights were updated with newly acquired features tailored to the specific classification task at hand. This methodology allowed us to build a model that can leverage the knowledge learned from previous tasks and adapt it for the accurate classification of the different pistachio varieties.
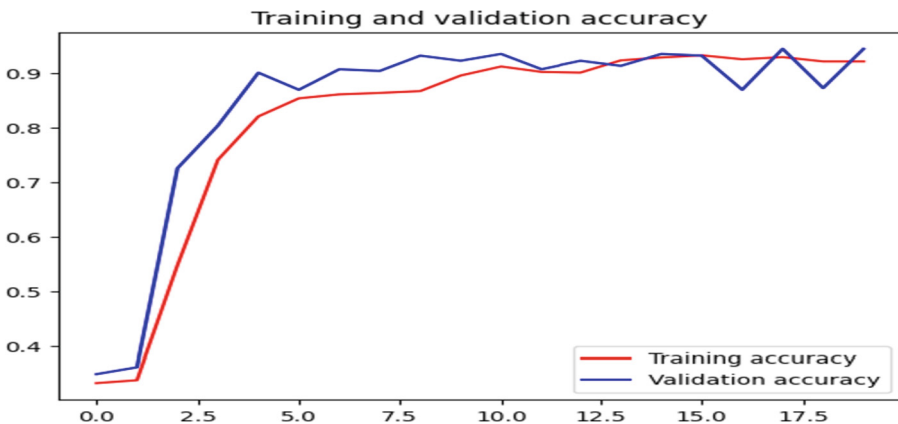
Fig. 8. Training and Validation Accuracy of proposed CNN model

The generalization of the model can be assessed by comparing the validation accuracy and training accuracy. Figure 8 shows that the validation accuracy is higher than
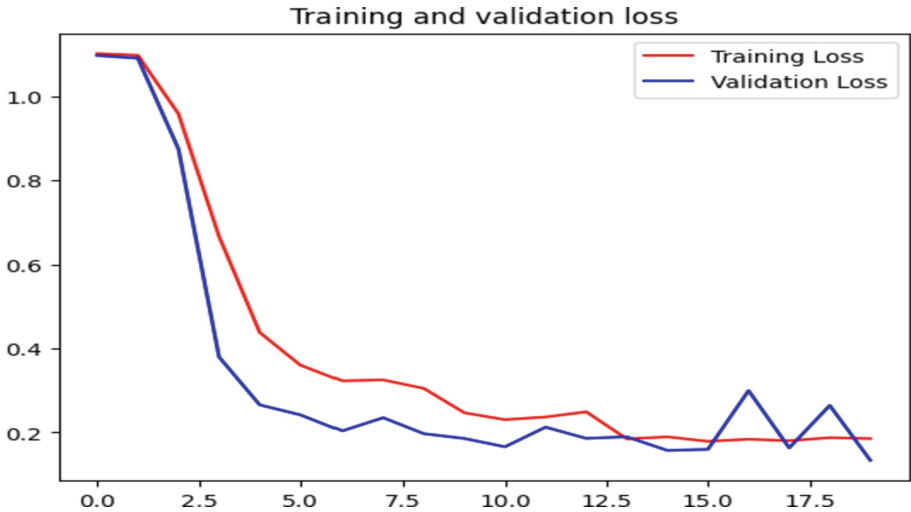
Fig. 9. Training and Validation Loss of CNN

the training accuracy. The training accuracy assesses the model's recognition capability with training samples after each training epoch. Subsequently, the model's performance on the validation set is evaluated during the training process. When the validation accuracy exceeds the training accuracy, it indicates that the model isn't overfitting and is performing effectively on previously unseen data. Figure 9 demonstrates that as training epochs increase, both training and validation loss decrease. The validation loss, in this case, is consistently lower than the training loss. This indicates that the proposed model is effectively learning from the training data and is able to generalize well to the validation data. Table 4 provides insights into the performance of the proposed model for the classification task at hand. It likely showcases metrics such as accuracy, precision, recall, or F1-score, which evaluate the model's performance in classifying the data accurately.

In this study, we employed pre-trained VGG16, Inception-V3 models, and a proposed CNN model to classify three distinct varieties of pistachios, namely Siirt, Tekin, and Uzun. The pre-trained VGG16 model achieved an impressive validation accuracy of 95.5% and a test accuracy of 94.05%. Similarly, the pre-trained Inception-V3 model achieved a validation accuracy of 98.21% and a test accuracy of 96.13%. These results highlight the effectiveness of the VGG16 and Inception-V3 models in accurately classifying the different pistachio varieties. Moreover, the proposed CNN model achieved even higher accuracy scores, with a validation accuracy of 98.8% and a test accuracy of 97.02%. These results indicate that the architecture, layers, and hyperparameters of the proposed CNN model were likely optimized for this specific classification task, leading to improved performance compared to the pre-trained models.

In Table 4, the proposed CNN model's performance on the test data was evaluated using precision, recall, and F1-score metrics, which were calculated for each individual class. The results demonstrate that the model achieved a high level of accuracy in classifying the data, as indicated by the average precision value of 98.07%. This implies that the model made a low number of false positive predictions. Furthermore, the model
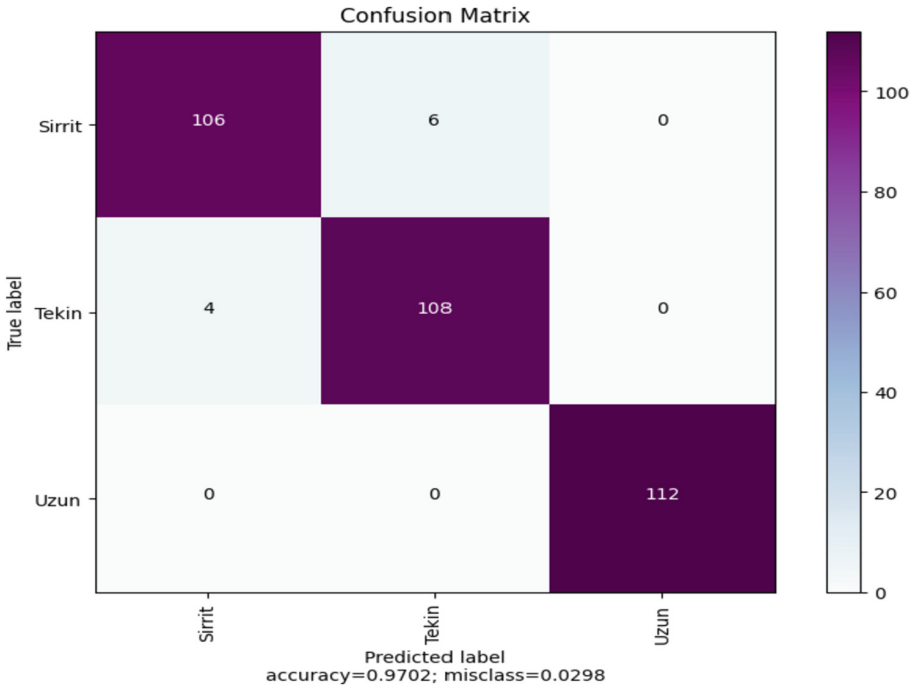
Fig.10. The confusion matrix of the classification task for the proposed CNN model

Table 4. Precision, recall, and f1-score for pistachio classification using the proposed CNN model

	Precision	Recall	F1-score
Siirt	0.9636	0.9464	0.9550
Tekin	0.9474	0.9643	0.9558
Uzun	1.000	1.000	1.000
Macro avg	0.9703	0.9702	0.9702
Weighted avg	0.9703	0.9702	0.9702

demonstrated a strong ability to correctly identify positive instances, as reflected by the average recall value of 98.05%. This indicates that the model had a low number of false negative predictions. The F1-score, which takes into account both precision and recall, also yielded impressive results with an average value of 98.05%. The high F1-score suggests that the model achieved a balanced performance between precision and recall. Overall, these results indicate that the proposed CNN model performed well in accurately classifying the test data across multiple classes, achieving high accuracy, precision, recall, and F1-score values.

Many studies have been conducted to improve the accuracy of classifying various types of pistachio varieties using machine learning and deep learning algorithms.

Table 5, provides a detailed summary of research specifically dedicated to classifying both open-closed pistachio nuts and distinguishing different pistachio varieties. It includes information such as the dataset size, classified varieties, employed models, and their corresponding accuracy rates.

Table 5. Comparison of accuracy rates of classifying open-closed pistachio nuts and different types of pistachio varieties using traditional machine learning and deep learning models.

Author/authors	Model architecture	Images numbers	Varieties	Accuracy
Hosseinpour-Zarnaq et al., (2022)	CNN model	1600	Akbari and Ahmad Aghaei (open or closed)	98.75%
Singh, Taspinar et al. (2022)	AlexNet, VGG16 and VGG19	2.148	Kırmızıı and Siirt	94.42%, 98.84%, and 98.14%
Lisad, kusrini et al. (2023)	Inception-V3 and ResNet50	2.148	Kırmızı and Siirt	96% and 86%
Rahimzadeh and Attar (2022)	ResNet50, ResNet152, and VGG16	3.927	different pistachio types (open-mouth or closed-mouth)	85.28%, 85.19%, and 83.32%
Ozkan, Koklu et al. (2021)	Improved k-NN	2.148	Kırmızı and Siirt (open or closed)	94.18%
Ataş and Doğan (2015)	J48 Decision Tree, Naïve Bayes, and Multi-Layer Perceptron (MLP)	200	different pistachio types (open – closed)	95.5%, 94.5% and 94.5%
Our study	VGG16, Inception-V3, and a proposed CNN	2.247	Siirt, Tekin, and Uzun	94.5%, 96.13%, and 97.02%

From the previous studies presented in Table 5, we have noticed that the highest classification accuracy for classifying different varieties of pistachios using deep learning algorithms was attained by Singh, Taspinar et al. (2022), who accomplished a high accuracy rate of 98.84%, which is close to the result that we have achieved with the proposed CNN model (97.02%) as presented in Fig. 10. Our proposed model was able to classify all Uzun variety correctly, and only four samples from the Tekin variety was misclassified as Siirt, and only six samples from the Siirt variety was misclassified as Tekin. These results indicate that the architecture, layers, and hyperparameters of the proposed CNN model effectively captured the distinctive patterns between the different classes, resulting in improving the performance of the classification. It's important to highlight that in comparison to previous studies, only the research conducted by Singh, Taspinar et al. (2022) attained higher accuracy rates than the CNN model proposed in this study. This underscores the effectiveness of the proposed CNN model in distinguishing

different pistachio varieties, making it a valuable tool for farmers and companies to classify various types of pistachios accurately.

From the previous studies, we have noticed that many studies focused only on classifying two or three distinct pistachio varieties. Further study should focus on classifying many varieties to test the capability of these models to classify them accurately.

4 Conclusion

The objective of this study was to classify three distinct pistachio varieties using two pre-trained models, VGG16 and Inception-V3, as well as a proposed CNN model. The dataset of the study includes a total of 2247 images of Siirt, Tekin, and Uzun pistachio types. The dataset was divided into segments: 70% of the entire data for training, 15% for validation to assess accuracy, and the remaining 15% reserved for the test set. The classification outcomes revealed that the pre-trained VGG16 model achieved a test accuracy of 94.05%, the Inception-V3 model obtained 96.13%, and the proposed CNN model exhibited the highest accuracy of 97.02%. These results indicate that the proposed model, fine-tuned for the classification of the different varieties of pistachio, successfully captured the unique patterns and characteristics associated with these classes. Overall, the pre-trained models and the proposed CNN model displayed impressive performance, but the proposed CNN model demonstrated a slight advantage with its higher accuracy scores. This suggests that it is more suitable and effective for the classification of the different varieties of pistachio compared to the pre-trained models. By implementing innovative technologies, such as the proposed CNN model, in the pistachio industry, the study emphasizes the potential to revolutionize the classification process. Precisely identifying the type of pistachio nuts will enable targeted packaging for sales, reducing errors and meeting consumer expectations. Moreover, maximizing yield productivity through improved classification methods will contribute to the well-being of farmers, ensuring their economic sustainability and prosperity.

References

1. Ak BE, Açar İ (1998) Pistachio production and cultivated varieties grown in Turkey
2. Singh D et al (2022) Classification and analysis of pistachio species with pre-trained deep learning models. Electronics 11(7):981
3. Aktaş H, Kızıldeniz T, Ünal Z (2022) Classification of pistachios with deep learning and assessing the effect of various datasets on accuracy. J Food Meas Character 16(3):1983–1996
4. Ozkan IA, Koklu M, Saraçoğlu R (2021) Classification of pistachio species using improved k-NN classifier. Prog Nutr 23:e2021044
5. Lisda L, Kusrini K, Ariatmanto D (2023) Classification of pistachio nut using convolutional neural network. Inform. Jurnal Ilmiah Bidang Teknologi Informasi dan Komunikasi 8(1):71–77
6. Farazi M, Abbas-Zadeh MJ, Moradi H (2017) A machine vision based pistachio sorting using transferred mid-level image representation of Convolutional Neural Network. In: 2017 10th Iranian Conference on Machine Vision and Image Processing (MVIP). IEEE
7. Hosseinpour-Zarnaq M, et al (2022) Acoustic signal-based deep learning approach for smart sorting of pistachio nuts. Postharvest Biol Technol 185

8. Abbaszadeh M, et al (2019) Deep learning-based classification of the defective pistachios via deep autoencoder neural networks. arXiv preprint arXiv:1906.11878
9. Rahimzadeh M, Attar A (2022) Detecting and counting pistachios based on deep learning. Iran J Comput Sci 5(1):69–81
10. Dheir IM, Abu Mettleq AS, Elsharif AA (2020) Nuts types classification using deep learning
11. Ataş M, Doğan Y (2015) Classification of closed and open shell pistachio nuts by machine vision
12. Dini A et al (2020) Designing a hardware system to separate defective pistachios from healthy ones using deep neural networks. Iran J Biosyst Eng 51:149–159
13. Chen H et al (2020) A deep learning CNN architecture applied in smart near-infrared analysis of water pollution for agricultural irrigation resources. Agric Water Manag 240:106303
14. Glorot X, Bordes A, Bengio Y (2011) Deep sparse rectifier neural networks. In: Proceedings of the Fourteenth International Conference on Artificial Intelligence and Statistics. JMLR Workshop and Conference Proceedings
15. Habib G, Qureshi S (2022) Optimization and acceleration of convolutional neural networks: a survey. J King Saud Univ-Comput Inf Sci 34(7):4244–4268
16. Gerdan D, Caner K, Vatandaş M (2023) Diagnosis of tomato plant diseases using pre-trained architectures and a proposed convolutional neural network model. J. Agric. Sci. 29(2):618–629
17. Simonyan K, Zisserman A (2014) Very deep convolutional networks for large-scale image recognition. arXiv preprint arXiv:1409.1556
18. Nour M, Cömert Z, Polat K (2020) A novel medical diagnosis model for COVID-19 infection detection based on deep features and Bayesian optimization. Appl Soft Comput 97:106580
19. Hossin M, Sulaiman MN (2015) A review on evaluation metrics for data classification evaluations. Int J Data Min Knowl Manag Process 5(2):1

Evaluation of Hydration State around Glycerol as a Humectant Using Microwave Dielectric Spectroscopy

Nao Takeuchi[1(✉)], Keiichiro Shiraga[1,2], Miho Morita[1], Yuichi Ogawa[1], and Naoshi Kondo[1]

[1] Graduate School of Agriculture, Kyoto University, Kitashirakawa Oiwake-Cho, Sakyo-Ku, Kyoto 606-8502, Japan
takeuchi.nao.34x@st.kyoto-u.ac.jp

[2] Japan Science and Technology Agency, PRESTO, Kawaguchi 332-0012, Japan

Abstract. Water in intermediate-moisture foods can be broadly classified into bound water, which is strongly bound to components, and free water, which can easily move or evaporate due to changes in surrounding environmental conditions. Free water is essential for the growth of microorganisms that can cause spoilage of foods. Glycerol, a humectant with high water retention capacity, has been used as an additive to reduce the free water content in processed foods because it is easily hydrated to form stable hydrogen bonds with water and has been thought to reduce the free water percentage in foods. Our research group used microwave dielectric spectroscopy and differential scanning calorimetry (DSC) to evaluate the hydration state around glycerol in comparison with several polyols with different water-holding capacity. Microwave dielectric spectroscopy showed that the dielectric spectra of the polyol aqueous solutions exhibited different molecular dynamics. Quantitative estimation of free water content for 10 mol% concentration aqueous solutions based on DSC results indicated that glycerol had significantly higher free water content. These results were consistent, suggesting that humectants with high water retention properties may not exhibit strong hydration. It was also suggested that the hydration state around the solute, with low hydration water content, may be a unique property of glycerol. In any case, the results overturn the conventional interpretation that hydration plays an important role in the water-holding capacity of humectants.

Keywords: Food additives · Humectants · Glycerol · Polyol · Hydration water

1 Introduction

Intermediate-moisture foods are attracting attention as foods with a long shelf life that can be stored without refrigeration while retaining the same nutritional content as fresh foods [1]. They are also considered new foods that require less energy for production and distribution due to new production technologies. Dried foods can be stored for long periods of time, but often lose their nutritional and sensory properties when water

is removed in conventional industrial dehydration processes that require long hours at high temperatures [2]. For this reason, intermediate-moisture foods have emerged as one of the effective solutions to the pressing future challenges of a growing world population and food supply needs [3].

In intermediate-moisture foods, food additives are used to extend shelf life by appropriately adjusting and maintaining the moisture content in foods [2, 4, 5]. The importance of the role of water in food preservation and food quality control in producing and storing of intermediate-moisture foods was recognized early in history [6]. Water in foods can be broadly classified into bound water, which is strongly bound to components such as proteins and starch, and free water, which can be easily transferred or evaporated by changes in surrounding environmental conditions. Free water is essential for the growth of microorganisms that can cause spoilage of agricultural products. Therefore, there is a need for additives that can reduce the amount of free water in foods and improve their storability.

Glycerol is used as an additive that can reduce the free water content in processed foods [7]. Glycerol is a highly water-holding capacity humectant, and is believed to reduce the free water content in processed foods. It is conventionally believed that hydration is related to the hygroscopicity of humectants, and it is assumed that the more hygroscopic a humectant is, the stronger its hydration effect is. In other words, highly hygroscopic humectants such as glycerol tend to hydrate by forming stable hydrogen bonds with water, and are used because they are thought to reduce the free water content by binding with water molecules in food products. Indeed, there have been many studies that have modelled and explained these phenomena based on these phenomena [8–10] (Fig. 1).
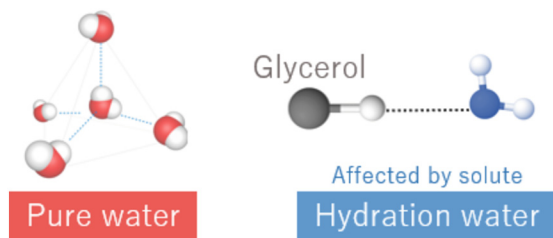
Fig. 1. The diagram of the conventional interpretation of the state of water molecules in pure water and those around glycerol, a highly hygroscopic humectant. The dotted lines represent hydrogen bonds.

In recent years, microwave dielectric spectroscopy has emerged as a technique to evaluate water dynamics. Microwave dielectric spectroscopy allows us to observe the oriented polarization of water under an alternating electric field. With this technique, water with a delayed orientation of water molecules compared to pure water due to hydrogen bonding with solutes can be distinguished from normal water (free water) as hydration water. In the microwave region, information about the hydration state can be read quantitatively due to dielectric relaxation caused by the orientation of water molecules. Hydration water is defined as a water molecule that is perturbed by the presence of a solute and

differs from free water in its properties. Hydration water dynamically bound by solutes has a significantly longer relaxation time than free water. Therefore, by using microwave dielectric spectroscopy, hydration water and free water can be observed separately based on the difference in their relaxation response, and the amount and dynamics of hydration water can be determined. If hydration water and free water also exhibit different relaxation times for humectants, it will be possible to separately observe each relaxation component of hydration water and free water in aqueous solutions of humectants.

We have performed microwave dielectric spectroscopy, which has not previously been used to study hydration water in aqueous solutions of humectants, on aqueous glycerol solutions and reported the possibility of observing the hydration state around glycerol [11]. Furthermore, our research group evaluated the hydration state around glycerol, which is known as a highly water-holding capacity humectant, and suggested that water-holding capacity humectants may not exhibit strong hydration. This result challenges the conventional interpretation that hydration plays an important role in the water-holding capacity of humectants. We have investigated the hydration state of water molecules surrounding glycerol.

Based on these findings, the objective is to develop a systematic understanding of the characteristics related to the water-holding mechanisms of glycerol and other humectants to clarify the relationship between water-holding capacity and hydration. We will compare glycerol with other humectants and verify whether this is a property unique to glycerol. If we can evaluate the dynamics of water molecules around glycerol and humectants, we may be able to determine the growth environment of microorganisms more accurately in processed foods. This is expected to become a new indicator of food safety and security.

In order to understand the characteristics of water-holding capacity humectants, low-molecular-weight alcohols are used as humectants. We used diglycerol (DiGL) and glycerol (GL), which are considered to have particularly high water-holding capacity, as well as propylene glycol (PG) and butylene glycol (BG), which also have water-holding capacity but less than DiGL and GL, as samples [12–14]. Dielectric spectra of each polyol are obtained. The dielectric spectra of each polyol are obtained and qualitatively discussed. Differential scanning calorimetry (DSC) is also performed to understand the state of water molecules around the polyol in more detail.

2 Methods

2.1 Sample Preparation

PG (99.5% purity; Fujifilm Wako Pure Chemicals Co., Ltd.), BG 99.5% purity; Fujifilm Wako Pure Chemicals Co., Ltd.), GL (99.5% purity; Fujifilm Wako Pure Chemicals Co., Ltd.) and DiGL (99.5% purity; Fujifilm Wako Pure Chemicals Co., Ltd.) were used as samples. The polyols/water mixtures were prepared by mixing deionized distilled water purified with WG250B (Yamato Scientific Co., Ltd.). We obtained a final polyol concentration of 0–60 mol % in 10 mol % intervals and 60–100 mol% in 20 mol% intervals.

2.2 Microwave Dielectric Spectroscopy

Among several methods for studying the hydration water around a solute, we performed dielectric spectroscopy in the microwave band. This technique observes the orientation relaxation of a material with respect to an electric field. The complex permittivity obtained from the measurement represents the dielectric loss in the imaginary part [15].

A vector network analyzer (VNA, Agilent Technologies, P5008B) with a coaxial reflection probe (N1501A) and an electronic calibration module (N4693-60001) mounted in a launch configuration as shown in Fig. 2 was used to measure the sample dielectric loss ε" in the frequency range 30 MHz ~ 20 GHz. The dielectric loss ε" of the sample was measured in the frequency range of 10 MHz ~ 20 GHz. Calibration was performed at three points with air, diethyl ketone, and pure water. 150 μL of sample was measured with a micropipette and placed in the measuring unit and each measurement was performed twice. The measurement intensity was −10 dBm, the intermediate frequency bandwidth was 30 Hz, and the temperature control Peltier (VICS, VPE-35) was set to 25.0 °C. The data were equally spaced on the frequency domain log scale.
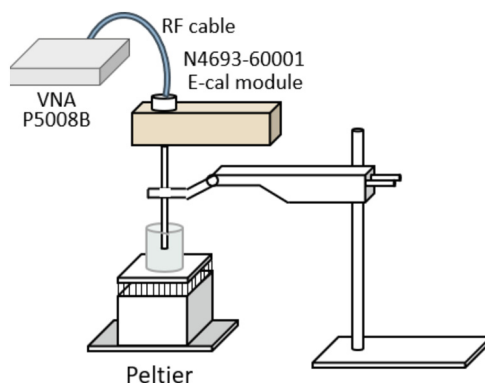
Fig. 2. The set up of the VNA experiment. The aqueous solution in the measuring section is temperature-controlled by a water-cooled Peltier with an error of ±0.04 °C.

2.3 Differential Scanning Calorimetry (DSC)

DSC is a powerful tool for exploring the microstructure and thermal behavior of a liquid humectant solution sample [16–18]. According to the criterion of freezing temperature, the microstructure of water in humectants can be classified into three types: nonfreezable water, intermediate water, and free water. Intermediate water and free water are also called freezable water because they can exhibit a phase transition [18]. In relation to microwave dielectric spectroscopy, nonfreezable water and intermediate water are bound waters that can be readily bound to the humectant by hydrogen bonding. The intermediate water and free water are called freezing water because they can exhibit a phase transition. In relation to microwave dielectric spectroscopy, nonfreezable water and intermediate water are bound waters that can be easily combined with the humectant by hydrogen

bonding. The intermediate water and free water are called freezing water because they can exhibit a phase transition. In relation to microwave dielectric spectroscopy, nonfreezable water and intermediate water are hydration water, which can be easily combined with the humectant by hydrogen bonding.

DSC measurements were performed by NEXTA DSC200 (Hitachi High-Tech). The melting process was observed after quenching from room temperature to -50 °C at 20 °C/min increasing the temperature to 15 °C at 5 °C/min. A blank aluminum pan was used as a reference temperature. Each polyol concentration was 10 mol% and measured twice.

3   Results

3.1   Microwave Dielectric Spectroscopy

As shown in Fig. 3, the dielectric loss spectrum of pure water exhibits a single broad peak at about 20 GHz. The dielectric loss spectrum of pure water showed a relaxation time of about 8.2 ps at 25.0 °C. The dielectric loss spectra of pure polyols are similar in that they have a single, broad peak, but the peak frequency is clearly lower than that of pure water. This indicates that the dielectric relaxation of pure polyols is slower than that of pure water, and the spectral shapes of PG, BG, and GL are in good agreement with previous studies [19–21]. Although the dielectric relaxation of DiGL has not been investigated in this range, the result that the relaxation peak is shifted to the lower frequency side than that of GL is consistent with the fact that the viscosity and molecular weight of DiGL are larger than those of GL.
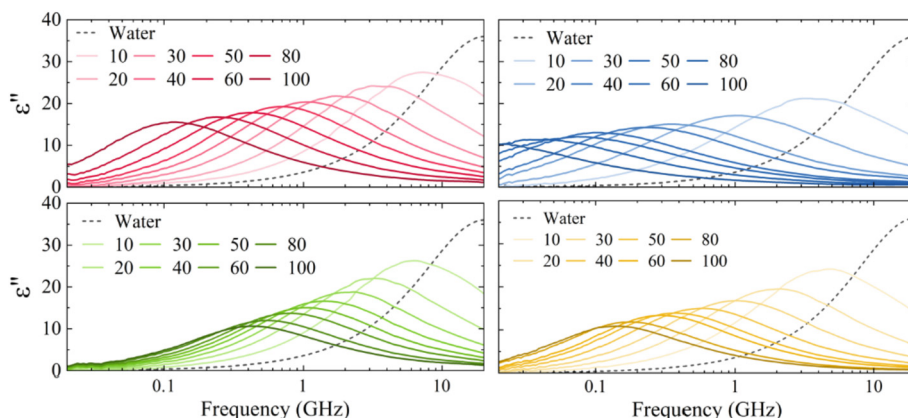
Fig. 3. Imaginary part of dielectric relaxation spectra of pure water and aqueous solution (mol%) of polyols. (a) GL solution, (b) DiGL solution, (c) PG solution, (d) BG solution.

Here, we want to see how much the peak frequency of the dielectric relaxation spectrum changes with concentration; by taking the difference between the peak frequency at 100 mol% and the peak frequency (Δ peak frequency) at each concentration, we can see in Fig. 4 how the amount of change varies among the samples.
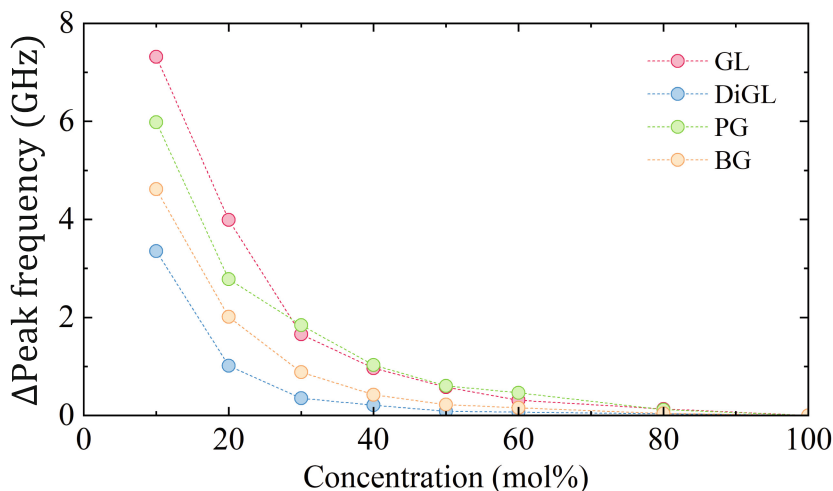
Fig. 4. The comparison of Δ peak frequency at each concentration when the peak frequency at 100 mol% polyol concentration is set to 0.

The peak frequency change with respect to the 100 mol% concentration showed a linear decrease at low concentrations and a gradual change toward higher concentrations for all samples. Roughly up to the 20–30 mol% boundary, the respective relaxation spectra were expected to be increasingly affected by the solute. The largest change was observed for GL. Given that the peak of pure water is around 20 GHz, this suggests that the free water effect of GL is greater at low concentrations than for other humectants. In other words, the discussion of the concentration dependence of the peak frequency transition suggests that GL is more affected by molecular dynamics due to free water than other polyols. On the other hand, the relaxation spectrum of DiGL, which is said to have more water-holding capacity than GL, shows that the molecular dynamics of the aqueous solution seems to be less affected by free water than that of the other polyols. Based on conventional understanding, the dynamics of aqueous polyol solutions should be significantly affected by the solute even at low concentrations because the higher the water-holding capacity, the more the polyol is hydrated with the surrounding water molecules. Here, however, GL did not follow this understanding. These results suggest that the water-holding capacity of not all humectants correlates with the molecular dynamics of water in the aqueous solution, and that GL has special properties. In other words, the results suggest that the water retention of GL is not due to hydration of the solute and its surrounding water molecules, different from the conventional perception.

3.2 Differential Scanning Calorimetry (DSC)

The characteristics of molecular dynamics in hydration were interpreted from the relaxation spectra obtained by microwave dielectric spectroscopy. Here, we would like to further evaluate the hydration status by quantitatively evaluating the specific amount of hydration water in aqueous polyol solutions. The heat flow of polyols during the melting process is shown in Fig. 5. Below the phase transition temperature, the temperature of

the sample increases at a constant rate [22]. When the phase transition temperature is reached, thermal energy is consumed by the phase transition and endothermy occurs. In other words, more energy is used for freezing for those with greater heat absorption, indicating more freezable water per gram of aqueous solution. In fact, if we take a base-line and integrate to obtain the enthalpy of aqueous solution, we obtain that the amount of freezable water per gram of solution is GL > BG > PG > DiGL.
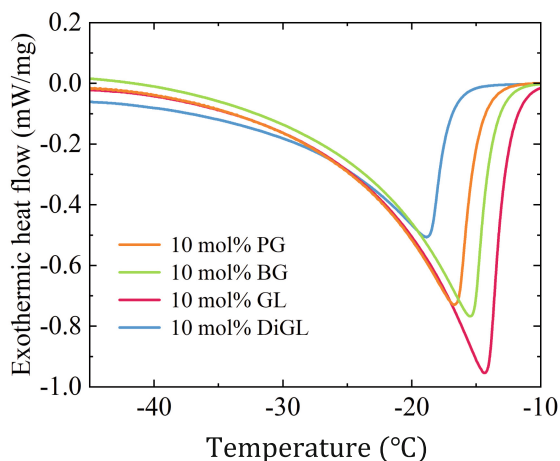
Fig. 5. The heat flow of 10 mol% polyol solution during melting process.

In addition, to evaluate the hydration state around the polyol in detail, the number of unfreezable and freezable water molecules per solute molecule was calculated (Fig. 6). Compared to other polyols, GL has a particularly low number of unfreezable water molecules per solute molecule and a high number of freezable water molecules per solute molecule. This result is consistent with the microwave dielectric spectroscopy results; the molecular dynamics of GL aqueous solutions are less affected by solute dynamics at low concentrations compared to other polyol aqueous solutions. These two results indicate that GL has a particularly low hydration water content and a high free water content, which is a property unique to GL, regardless of the water-holding capacity of the humectant, since DiGL does not show any outstanding characteristics when compared to other polyol aqueous solutions.
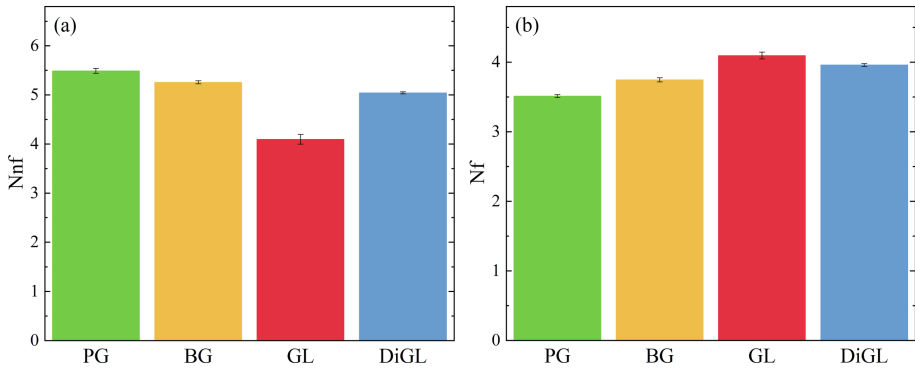
Fig. 6. The number of water molecules per solute molecule in the melting process of polyols. (a) Nnf: Number of nonfreezable water molecules per solute molecule, (b) Nf: Number of freezable water molecules per solute molecule.

4   Conclusion

The results of microwave dielectric spectroscopy and DSC, respectively, reveal the heterogeneous nature of GL among humectants. Microwave dielectric spectroscopy showed that the dielectric relaxation spectra were different between humectants with at least different water-holding capacities. These differences were not only in the spectral shape at 100 mol% solute, but also in the spectral change with concentration. It is suggested that it may be possible to distinguish the state of water molecules around the solute. The number of freezable and nonfreezable water molecules per solute molecule was estimated from the endothermic reaction during the melting process of a 10 mol% aqueous humectant solution obtained from DSC. These results indicate that at least GL has less antifreeze water per solute molecule than the other three humectants. This result supports the microwave dielectric spectroscopy results, which show the specificity of GL.

More detailed analysis of these results in the future may provide a detailed understanding of the water-holding mechanism of the GL and humectants at the molecular level. Elucidating the mechanism of GL's water retention could be used to better manage the water content in intermediate-moisture foods.

References

1. Liu X, Zhou P, Tran A, Labuza PT (2009) Effects of polyols on the stcapacity of whey proteins in intermediate-moisture food model systems. J Agric Food Chem 57(6):2339–2345
2. Qiu L, Zhang M, Tang J, Adhikari B, Cao P (2019) Innovative technologies for producing and preserving intermediate moisture foods: a review. Food Res Int 116:90–102
3. Carocho M, Barreiro M, Morales P, Frreira I (2014) Adding molecules to food, pros and cons: a review on synthetic and natural food additives. Compr. Rev. Food Sci. Food Safety 13(4):377–399
4. Finn S et al (2015) Exposure of Salmonella enterica Serovar Typhimurium to three humectants used in the food industry induces different osmoadaptation systems. Appl Environ Microbiol 81(19):6800–6811

5. Schmidt FC, Carciofi BAM, Laurindo JB (2008) Salting operational diagrams for chicken breast cuts: hydration–dehydration. J Food Eng 88(1):36–44
6. Taoikis P, Richardson M (2020). Principles of Intermediate-Moisture Foods and Related Technology. John Wiley & Sons, Ltd.
7. Troller JA, Christian JHB (1981). [Food and Water Activity] Syokuhin to suibun kassei (in Japanese). Gakkai Publishing Center
8. Hayashi Y, Puzenko A, Ryabov I, Feldman Y (2005) Relaxation dynamics in glycerol–water mixtures. 2. mesoscopic feature in water rich mixtures. J Phys Chem B 109:9174–9177
9. Kataoka Y, Kitadai N, Hisatomi O, Nakashima S (2011) Nature of hydrogen bonding of water molecules in aqueous solutions of glycerol by attenuated total reflection (ATR) infrared spectroscopy. Appl Specectrosc 65:436–441
10. Towey JJ, Dougan L (2012) Structural examination of the impact of glycerol on water structure. J Phys Chem B 116:1633–1641
11. Morita M, Fmatsumura TS, Ogawa Y, Kondo N, Shiraga K (2022) Hydrogen-bond configurations of hydration water around glycerol investigated by HOH bending and OH stretching analysis. J Phys Chem B 126(47):9871–9880
12. Umare SS, Chandure AS, Pandey RA (2007) Synthesis, characterization and biodegradable studies of 1,3-propanediol based polyesters. Polym Degrad Stcapacity 92(3):464–479
13. Steele JR (1987) Use of polyols to measure equilibrium relative humidity. Int J Food Sci Technol 22(4):377–384
14. Crowther M (2021) Understanding humectant behaviour through their water-holding properties. Int J Cosmet Sci 43(5):601–609
15. Grant HE, Sheppard JR, Shouth PG (1987). Dielectric Behaviour of Biological Molecules in Solution. Oxford University Press
16. Chen HJ et al (2022) Moisture retention of glycerin solutions with various concentrations: a comparative study. Sci Rep 12(1):10232
17. Sambale A, Kurkowski M, Stommel M (2019) Determination of moisture gradients in polyamide 6 using StepScan DSC. Thermochim Acta 672:150–156
18. Lin CP, Tsai SY (2019) Differences in the moisture capacity and thermal stability of Tremella fuciformis polysaccharides obtained by various drying processes. Molecules 24:2856
19. Hayashi Y, Puzeko A, Feldman Y (2006) Slow and fast dynamics in glycerol–water mixtures. J Non-Cryst Solids 354(42):4696–4703
20. Lux A, Stockhausen M (1993) A dielectric relaxation study of some liquid dihydric alcohols and their mixtures with water. Phys Chem Liq 26(1):67–83
21. Köhler M, Lunkenheimer P, Goncharov Y, When R, Loidl A (2010) Glassy dynamics in mono-, di- and tri-propylene glycol: from the α- to the fast β-relaxation. J Non-Cryst Solids 356(11):529–534
22. Saito K, Morikawa J (2012). [Practical Series in Analytical Chemistry Instrumental Analysis Part 13: Thermal Analysis] Bunsekikagaku jitsugi kiki bunseki hen 13 netsu bunseki (in Japanese). The Japan Society for Analytical Chemistry

Natural Resources and Enviromental Systems in Agriculture

Development of Fertigation System for Hose Reel Irrigation Machines

Turgay Polat[1(✉)] and Ahmet Çolak[2]

[1] Central Research Institute of Field Crops, 06170 Ankara, Turkey
turgayplt71@gmail.com.tr

[2] Department of Agricultural Machinery and Technologies Engineering, Faculty of Agriculture, Ankara University, 06110 Ankara, Turkey

Abstract. Hose reel irrigation machines irrigate with linear motion and sprinkler method. In this study, an integrated fertigation system was developed for a 110 mm × 400 m hose reel irrigation machine manufactured by SEZERMAC. In the developed system, together with an hose reel irrigation machine, a volumetric dosing pump with a microprocessor, a fertilizer tank manufactured in special dimensions, a pair of symmetrical consoles for the fertilizer tank and solar system components were used. In order to determine the working performance of the developed system, pH, EC, TDS values were measured in irrigation water mixed with liquid chemical fertilizer. At the same time, necessary analyzes were made to determine the total nitrogen and total phosphorus values. The Christiansen uniformity coefficient (CUC) was calculated to determine the working performance of the system developed using the values obtained as a result of measurement and analysis. CUC values calculated for pH, EC and TDS parameters were determined to be between 95.0% and 99.9%. The CUC values calculated for the total nitrogen and total phosphorus amounts were found to be between 83.79% and 96.42%. The developed fertigation system could be used successfully with hose reel irrigation machines.

Keywords: Dosing pump · Fertigation · Hose reel irrigation machine · Solar system components

1 Introduction

With the use of advanced technology systems in agriculture, savings can be achieved in inputs such as energy, biological materials, labor, spare parts, fertilizer, feed, various chemicals and irrigation water required for production. Due to global warming and climate changes seen in recent years, efficient use of inputs and circular economy are prominent paradigms. One of the important stages of plant production in field agriculture is irrigation and the other is fertilization. A researcher reported that the systems to be designed in the near future will be advanced equipment that mixes plant nutrients into irrigation water according to the need in order to increase product yield, called the fertigation technique [1]. Farmers dealing with field agriculture make fertilization at

least twice in many plants, especially in the cultivation of cool climate cereals. Combined sowing machines are generally used for the first fertilization. The second fertilization in the spring is done with rotary plate fertilizer spreaders used by hanging on the tractor or with trailed type universal fertilizer spreaders.

Miller et al. revealed in their study that the efficiency of fertilizer use is higher in nitrogen applications made by mixing fertilizer into the irrigation water with the drip irrigation method than nitrogen applications made by adding fertilizer to the plant row with the furrow irrigation method [2]. One of the modern irrigation equipment used in recent years is hose reel irrigation machines. Hose reel irrigation machines have high water usage efficiency. Also, it is quite easy to use. The machines make irrigation in the form of sprinkler using pressurized water.

The basic principle in agricultural production is to obtain the maximum amount of product from the unit area by using optimum inputs and protecting the agricultural environment. Optimum use of inputs and protection of the agricultural environment is possible by using technological innovations in agriculture. In addition, the use of technological innovations in agriculture reduces the unit product cost and enables the producer to compete in domestic and foreign markets. For these reasons, various studies have been realized to design a fertigation system that mixes fertilizer into irrigation water for hose reel irrigation machines. Bortolini and Bisol compared traditional fertilizer distribution systems and fertigation systems used with hose reel irrigation machines in the distribution of cattle manure used for corn plant production [3]. They pointed out that nitrogen losses in the form of nitrate were less in the water and air samples taken from the area where the fertigation application was made.

The lack of access to the electricity grid everywhere, especially in field conditions, is an obstacle to the use of electrically powered dosing pumps during irrigation. Recently, renewable energy sources such as solar or wind are used in many agricultural areas where there is no electricity grid. Solar and wind energy from these sources is converted into electrical energy with photovoltaic batteries and wind turbines and used for charging accumulators. The accumulators, which store the electricity produced from renewable sources, enable the devices that need electrical energy to be used integrated with agricultural machinery in agricultural areas where there is no electricity network. Another important point is that the tank to be used to store the liquid chemical fertilizers required to be mixed into the irrigation water is integrated into the hose reel irrigation machine. Otherwise, another trailer or carrier vehicle should be used for the tank that will carry the liquid chemical fertilizers. In this study, a fertigation system that will mix fertilizer into the irrigation water during irrigation using hose reel irrigation machines has been designed and its prototype has been manufactured. Before this study, images of fertigation systems designed for hose reel irrigation machines are given in Fig. 1 [4, 5]. A trailer is needed for these systems. In addition, there are no norm setting units. In one of the systems, an electrically powered pump-motor couple is used. Therefore, it is dependent on the electricity grid. In the other system, a proportional dosing pump was used to mix the fertilizer. Therefore, the fertilizer norm cannot be adjusted precisely.

The innovative aspect of our work is the development of a fertigation system that is integrated into hose reel irrigation machines, has a norm adjustment unit and produces its own electrical energy.

Fig. 1. Images of fertigation systems designed for hose reel irrigation machines.

2   Material and Method

In our study, an hose reel irrigation machine with 10 atm * 110 mm * 400 m pipe manufactured by SEZERMAC was used together with the boom. One of the most important components of fertigation systems is the fertilizer tank. The fertilizer tank has been sized considering the maximum work area of the hose reel irrigation machine and the maximum amount of fertilizer that should be applied to this work area in one irrigation. At the same time, attention was paid that the sized fertilizer tank volume should not be more than the reserve space volume on the machine. Another component that is sized according to the reserve volume on the machine is the console that will carry the fertilizer tank. By using the added constructions, the basic geometric dimensions of the hose reel irrigation machine have not changed. At the same time, after the addition of the console that will carry the fertilizer tank, "maneuver tests" were carried out by pulling it with a tractor.

Liquid chemical fertilizers with nitrogen (UAN-32) and phosphorus (Cleanphos) were used in fertigation experiments. Therefore, there is no need to prepare any solution for the fertilizer to be mixed with the irrigation water. The feeding of the hose reel irrigation machine was used by pressurizing the water supplied from the pond with a high-tech irrigation system working with the principle of constant pressure and variable flow. The measurement of the working performance of the developed fertigation system was carried out on a field with barley stubble on it without slope and large enough for hose reel irrigation machine trials. The manufacturing images of the construction of the developed machine are given in Fig. 2.

Kramer et al. stated in their study that electromagnetically driven dosing pumps are suitable for sensitively measuring and pumping any liquid in motor vehicles [6]. A 25 W Nova-D model electromagnetic dosing pump manufactured by "ENELSA-AnTech" has been supplied to apply fertilizer to the water inlet pipe of the hose reel irrigation machine. The LCD screen, touch buttons and suction pipe air release valve on the supplied dosing pump provide comfort. In addition, with its solenoid drive technology, it can automatically adapt to networks with different voltages between 95–260 V. The

Fig. 2. The manufacturing images of the construction of the developed machine

flow rate of the dosing pump changes according to the pressure in the water inlet pipe. The amount of fluid (L/h) pumped by the dosing pump with a stroke volume of 0.555 ml per unit time can also be expressed as the number of pulses (frequency) per unit time due to its intermittent operation [7]. The image of the dosing pump used in the study and the nomogram of its characteristics are given in Fig. 3.
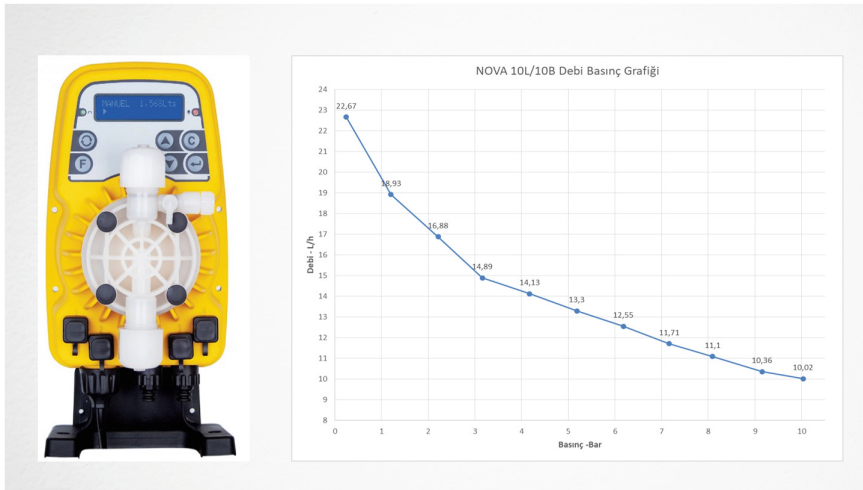
Fig. 3. Image of the dosing pump and nomogram of its characteristics

An accumulator (d) that can provide 12 V voltage and 65 Ah current was used to provide the electrical energy required for the dosing pump and lighting tools used in the study. Solar power system components were used to charge the accumulators used in field conditions. One of these solar power system components is a 190 Wp monocrystalline photovoltaic panel (a), which produces electrical energy with 24% efficiency. In order to charge the accumulator, a 130 W charge controller (b) and an inverter (c) with 300 W output power that produces the voltage required to operate the dosing pump were used. The images of the solar power system components used in the study are given in Fig. 4.

(a) Monocrystalline photovoltaic panel   (c) Inverter   (d) Accumulator

(b) Charge controller and its label
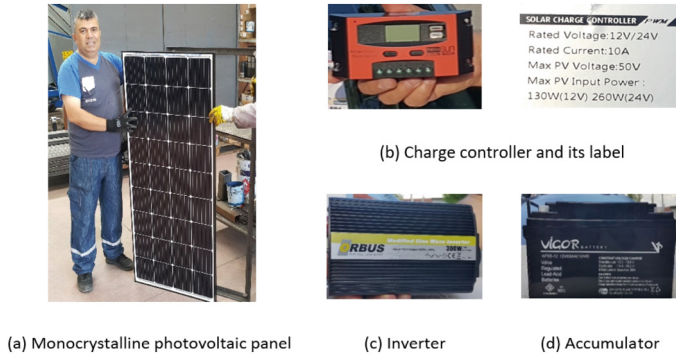
Fig. 4. Images of the solar power system components

The dosing pump used in the study, the charge controller, the inverter and the group socket controlled by automatic fuse were installed in an IP 65 board since it is not possible to operate them in atmospheric conditions. The solar panel and the accumulator, which cannot fit into the board, are placed in a cabinet made of metal material. However, the photovoltaic panel was the cover of the cabinet, which was manufactured by fitting it into a frame made of metal material. The images of the cabinet (a) and the board (b) used in the study are given in Fig. 5.

(a) Cabinet   (b) Board

Fig. 5. Images of cabinet and board

3   Results

After the components were installed on the hose real irrigation machine, field trials were carried out in the "randomized plots trial and factorial order" to measure the working performance of the designed fertigation system. In order to determine the working performance of the hose reel irrigation machine equipped with a fertigation system,

measurements were made for pH, EC and TDS parameters in irrigation water mixed with liquid chemical fertilizers. The specified measurements were carried out immediately under field conditions with a HANNA brand HI 9811-5 model portable device. The amounts of total nitrogen and total phosphorus mixed with irrigation water were determined by analyzing in Ankara University laboratories. The mixture of fertilizer and irrigation water used for measurement and analysis was obtained with plastic containers placed under the boom during irrigation. The images of the water collection and sampling containers are given in Fig. 6.

Fig. 6. Images of water collection and sampling containers

Hribik reported that the nutrient distribution uniformity mixed with the irrigation water is at the same rate as the water distribution uniformity [8]. He explained that water distribution uniformity is a unique and special value that determines the work quality of hose reel irrigation machines. Jobbagy et al. reported that the most common method used to determine the water distribution uniformity in sprinkler irrigation is to calculate the CUC coefficient [9]. In the fertigation application carried out in this study, Christiansen's uniformity coefficient was used to calculate the homogeneity of the fertilizers mixed with the irrigation water. The equation used in the calculation of the Christiansen's uniformity coefficient is given below [10, 11].

$$CUC = 100.(1 - \frac{\blacktriangle q0}{q0})$$

CUC: Christiansen uniformity coefficient (%).

▲q0: The average of the absolute deviations from the average of the fertilizer amount in the water collection containers (ppm)

q0: Average amount of fertilizer in water collection containers (ppm)

The trials were carried out at two different irrigation water pressures, 5 bar and 2.5 bar. Similarly, the dosing pump was operated at two different frequencies, 150 pulse/min and 300 pulse/min. The pH, EC (μS/cm) and TDS (ppm) values measured in the samples taken from the irrigation water mixed with fertilizer in the 4 combinations of fertigation

Table 1. pH, EC, TDS, average and CUC values in fertigation with nitrogen

Parameters	5 bar 150 Pulse/min		5 bar 300 Pulse/min		2.5 bar 150 Pulse/min		2.5 bar 300 Pulse/min	
	avg	CUC	avg	CUC	avg	CUC	avg	CUC
pH	8.58	99.9	8.58	99.6	8.59	99.7	8.40	99.9
EC	602	97.3	690	98.7	694	95	915	99.5
TDS	294	97	339	98.8	341	95.1	451	99.6

application with nitrogen liquid chemical fertilizer (UAN-32) and the mean (avg) and CUC (%) values calculated by using these values are given in Table 1.

The pH, EC (μS/cm) and TDS (ppm) values measured in the samples taken from the irrigation water mixed with fertilizer in the 4 combinations of fertigation application with phosphorous liquid chemical fertilizer (CLEANPHOS), and the average (avg) and CUC (%) values calculated by using these values are given in Table 2.

Table 2. pH, EC, TDS, average and CUC values in fertigation with phosphorous

Parameters	5 bar 150 Pulse/min		5 bar 300 Pulse/min		2.5 bar 150 Pulse/min		2.5 bar 300 Pulse/min	
	avg	CUC	avg	CUC	avg	CUC	avg	CUC
pH	8.03	96	7.53	99.1	7.58	98.2	7.13	99.1
EC	519	96.8	503	98.6	504	97.6	485	98.1
TDS	252	96.7	244	97.7	244	97.6	236	97.7

The average amount of nitrogen and uniformity coefficient were calculated by analyzing of the samples taken from irrigation water in four combinations of fertigation application with nitrogen liquid chemical fertilizer (UAN-32). Calculated values are given in Table 3.

Table 3. The average nitrogen and uniformity coefficient

5* 150**	Total Nitrogen %	5* 300**	Total Nitrogen %	2.5* 150**	Total Nitrogen %	2.5* 300**	Total Nitrogen %
avg	0.0031	**avg**	0.0049	**avg**	0.0058	**avg**	0.0090
CUC	83.79	**CUC**	90.03	**CUC**	91.8	**CUC**	91.19

[*] bar ** pulse/min

The average amount of phosphorus and the coefficient of uniformity were calculated by analyzing the samples taken from the irrigation water in four combinations of fertigation application with phosphorus liquid chemical fertilizer (P_2O_5). Calculated values are given in Table 4.

Table 4. The average phosphorus and uniformity coefficient

5* 150**	Total P2O5 %	5* 300**	Total P2O5 %	2.5* 150**	Total P2O5 %	2.5* 300**	Total P2O5 %
avg	584	**avg**	471	**avg**	445	**avg**	439
CUC	89.81	**CUC**	96.42	**CUC**	95.30	**CUC**	94.83

* bar ** pulse/min

The average and CUC values calculated for the amount of nitrogenous water (AONW) collected in the containers placed under the boom in the 4 combinations of fertigation application made with nitrogen liquid chemical fertilizer (UAN-32) are given in Table 5.

Table 5. The average and CUC values calculated for the amount of nitrogenous water

5** 150*	AONW (kg)	5** 300*	AONW (kg)	2,5** 150*	AONW (kg)	2,5** 300*	AONW (kg)
avg	5.40	**avg**	5.39	**avg**	4.35	**avg**	4.27
CUC	88.91	**CUC**	85.30	**CUC**	83.88	**CUC**	84.95

* bar ** pulse/min

The avg and CUC values calculated for the amount of phosphorus water (AOPW) collected in the containers placed under the boom in the 4 combinations of fertigation application with phosphorus liquid chemical fertilizer (P_2O_5) are given in Table 6.

Table 6. The average and CUC values calculated for the amount of phosphorus water

5** 150*	AOPW (kg)	5** 300*	AOPW (kg)	2,5** 150*	AOPW (kg)	2,5** 300*	AOPW (kg)
avg	5.75	**avg**	5.69	**avg**	4.41	**avg**	4.43
CUC	85.35	**CUC**	88.38	**CUC**	86.69	**CUC**	80.06

* bar ** pulse/min

As a result of the calculations made to determine the working performance of the developed fertigation system, the minimum and maximum CUC values of the parameters measured and analyzed in all combinations are summarized in Table 7.

Table 7. The minimum and maximum CUC values of the parameters

CUC %	pH	EC (μS/cm)	TDS (mg/L)	Total Nitrogenous (mg/L)	Total Phosphorus (mg/L)
Minimum	96	95	95.1	83.79	89.81
Maximum	99.9	99.5	99.6	91.80	96.42

When Table 7 is examined, it is seen that the CUC values, which are an indicator of the working performance of the developed fertigation system, were at least 83.79% and at most 99.9% in all combinations in the trial. Although no mixer mechanism is used in the system that ensures homogeneous mixing of liquid chemical fertilizers with the irrigation water, the reason for obtaining a high level of homogeneity is that the integrated turbine-gearbox mechanism, which moves the drum of the machine, has a mixing effect.

4   Conclusion

In this study, an integrated fertigation system (TURPO CLK FS) for hose reel irrigation machines was designed and prototype was manufactured. In order to determine the working performance of the developed fertigation system, field trials were carried out independent of vegetation. Measurements, analyzes and calculations were made using fertilizer mixed water samples obtained from the field trials. Two different liquid chemical fertilizers were used in the experiments. These fertilizers were mixed into the irrigation water with two different dosage pump frequencies at two different irrigation water pressures.

The following objectives have been achieved with the fertigation system developed in this study.

1. A fertigation system that mixes fertilizer with irrigation water with high uniformity has been obtained.
2. The advantages of fertigation, which is mostly applied in horticultural agriculture, are also transferred in field agriculture.
3. Compared to conventional fertilizer applications, field traffic has also been reduced.
4. An effective and synergistic application was realized by using water and fertilizer together.
5. Combined Hose Reel Irrigation Machine was obtained by integrating the fertigation system.
6. There is no need to use another trailer for the tank that will carry the liquid chemical fertilizers and the other components used in the fertigation system.
7. By using an irrigation machine with a fertigation system, there is no need to apply fertilizer with conventional machines, especially in grains in the spring. In other words, field traffic has also been reduced.
8. Just like liquid chemical fertilizers, liquid pesticides can also be applied with the developed system.

9. A platform that can be used for variable rate fertilizer applications has been obtained.
10. There is a boom behind the standard hose reel irrigation machines and a gearbox on the left side. There is no hardware on the front and right side of the machine. The fertilizer tank in the fertigation system is replaced in the front of the machine, and the solar system components are installed on the right side. Therefore, the balance of hose reel irrigation machines with fertigation system is higher than standard machines.

Cavero et al. investigated the effects of day and night irrigation on plant growth and yield using sprinkler heads on corn plants [12]. They explained that the evaporation losses seen in daytime irrigation are twice the evaporation losses seen in night irrigation. Another issue they reported was that corn grain yield was 10% less in daylight irrigation due to the decrease in biomass production. Biswas stated that 20–60% increase in yield is achieved with fertigation in many plants, while 20–70% savings can be achieved in water usage [13]. He explained that the fertigation application is the most suitable method for wetting the root zone of the plant, and it increases the efficiency of fertilizer use at least twofold. For this reason, he recommended the farmers to do fertilization and irrigation effectively, in other words, to meet with fertigation.

Wind turbines should be used to charge the accumulators used in the fertigation system developed in this study, even during night irrigation. The fertigation system developed for hose reel irrigation machines in this study has high working performance. It will enable farmers to save time and energy.

References

1. Burt CM (1995) Fertigation- the next frontier. Irrig Bus Technol 3(4), 16–19. http://www.itrc.org/papers/fertig/fertigationnextfrontier.pdf. ITRC Paper 95–004. California Polytechnic State University
2. Miller RJ, Rolston DE, Rauschkolb RS, Wolfe DW (1976) Drip application of nitrogen is efficient. California Agriculture
3. Bortolini L, ve Bisol T (2008) A low environmental impact system for beef cattle manure distribution on maize. In: Innovation Technology to Empower Safety, Health and Welfare in Agriculture and Agro-food Systems" International Conference: September 15–17, 2008 Ragusa – Italy
4. Demircioğlu M, ve Çelen İH (2020) Design of a fertilizer system that can be used in the hose reel irrigation machines. Int J Innov Eng Sci Res 4(3). ISSN: 2581-4591
5. Anonymous (2021) Website. https://www.sezermac.com/otomatik-dozajlamauniteleri/elektrikli-otomatik-dozajlama-unitesi.html. Accessed 13 Feb 2021
6. Kramer T, Petzold M, Weber J, Ohligschläger O, Müller A (2016) SMART control of electro-magnetically driven dosing pumps. In: 10th International Fluid Power Conference—Dresden. Group 13- Actuators and Sensors—Paper 13-1
7. Anonymous (2019) ENELSA-AnTech. AnTech "Water Control Technologies" Product Catalogue
8. Hribik J (2009) Synergicke učinky zavlažovania špecialnych plodin. Dostupne na intrnete. http://www.zahradaweb.cz/projekt/clanek.asp?pid=2&cid=2014
9. Jobbagy J, Michlian N, Dacanin P, Rigo I (2019) Application and evaluation of performance quality of hose-reel irrigation machine. Acta Technologica Agriculturae 4 Nitra, 109-114. Slovaca Univesity of Agriculture in Nitrae

10. ASAE (2003) Field evaluation of micro irrigation systems. EP458, pp 760–76. American Society of Agricultural Engineers, St. Joseph
11. Chiristiansen JE (1942) Hydraulic of springling system for irrigation. Trans ASCE 107:221–239
12. Cavero J, Jimenez L, Puig M, Faci JM, Cob AM (2008) Maize growth and yield under daytime and nighttime solid-set sprinkler irrigation. Agron J 100(6)
13. Biswas BC (2010) Fertigation in high tech agriculture a success story of a lady farmer. Fertiliser Marketing News October 2010

Developing a Data-Driven Model for Predicting Water Stress in Pistachio Trees

Azar Alizadeh[1] , Mohsen Farajijalal[1] , Zeinab Rezvani[2] , Arash Toudeshki[1] , and Reza Ehsani[1(✉)]

[1] University of California Merced, Merced, CA 95343, USA
rehsani@ucmerced.edu
[2] Shahid Bahonar University of Kerman, Kerman, Iran

Abstract. Drought and water shortage are major concerns in California and many parts of the world, and efficient water use is critical for growers. Water stress refers to the condition where the water demand exceeds the available water for a plant. The immediate goal of this research was to enhance existing water stress monitoring systems and develop a better irrigation scheduling system for pistachio trees in California. Currently, existing strategies for detecting water stress are either model-based or sensor-based, and each approach has limitations. In this project, we developed a data-driven model that combines model-based and sensor-based approaches and a system that takes advantage of both techniques. The test site was a pistachio orchard in Central California. During the growing season, extensive amounts of data were collected. Local environmental data such as ambient temperature, relative humidity, and pressure, were collected using sensors. Besides these, other collected data included multi-spectral aerial images, thermal images, sap flow, stem water potential data, and local. Aerial images were used to construct several vegetative indexes. A feature selection method was used to determine the most relevant input data. All the selected data was fed into different AI models. This paper discusses the results and shows the best approach for water stress detection in a pistachio orchard.

Keywords: Sensor · Irrigation scheduling · AI model

1 Introduction

Due to major issues of increasing water scarcity and drought, efficient water use is crucial for growers in California and many other parts of the world [1]. In response to these challenges, farmers are gradually adopting innovative irrigation practices and technologies to maximize water efficiency [2]. These include precision irrigation systems that supply water directly to the roots of plants [3], as well as the use of measuring devices and data analytics to optimize irrigation schedules based on crop needs and real-time climate conditions [4].

To detect water stress, model-based approaches use mathematical models [5, 6] to simulate how plants respond to water availability [7]. Although generating, analyzing, and understanding model-based or sensor-based techniques are simple, these approaches

are currently the most common methods for detecting water stress, and each has its drawbacks [8]. Therefore, improved techniques are continually in demand.

On the other hand, inputting precise and reliable data is crucial to ensure accurate modeling. It also needs to be considered that the models may not work correctly in all real-world complexities. The quality of the data utilized for modeling significantly influences the accuracy of the forecasts and results [9]. To eliminate biases or mistakes that might reduce the dependability of the results, it is critical to carefully test and clean the data before feeding it into the models [10].

Nowadays, machine learning (ML) and artificial intelligence (AI) are widely used in data analysis in many sectors, including agriculture [11, 12]. In a study, using deep learning and digital images to classify different levels of water stress with high accuracy was proposed [13]. An AI-based approach was utilized to automatically detect water on the Earth's surface using GNSS-R sensors onboard UAVs [14]. Using the AI technique in this study diminished the calibration limitation of a threshold setting for water detection. This approach indicated that the demonstrated unsupervised ML algorithm improved the traditional manual-based threshold-setting technique for water detection. These computer science-based methods have transformed the way data is collected, processed, and used in agriculture [11]. Based on these technologies, farmers can now make better decisions about crop yield prediction, pest control, and irrigation management [15, 16].

Based on the findings, neither model-based nor sensor-based approaches can properly predict water stress in trees. Therefore, other alternative procedures should be investigated to improve both methods. A potential strategy would be to use AI and ML, changing them depending on the features acquired from these models.

The objective of this study was to develop a data-driven model that combines both model-based and sensor-based approaches, as well as a system that takes advantage of both techniques.

2   Methods

In 2022, during the pistachio kernel development season in California, which is normally between May and August [17, 18], large amounts of data were collected from a Pistachios orchard located in the Central Valley in California ($37°15'58.9''$N, $120°25'16.4''$W). The pistachio shell and kernel growth stages in Central Valley, California, are shown in Fig. 1. These data were collected from the field using several types of sensors and equipment. Local weather stations collected the ambient temperature, relative humidity, and pressure as the local environmental data. Besides these, thermal images, multispectral aerial images, sap flow, and stem water potential data were also gathered.

Several ultra-low power, low-cost, and small weather sensor nodes were installed in different rows of the pistachio orchard. These sensor nodes included a BME680 (Bosch Sensortec GmbH, USA) and were equipped with ESP8266 (Espressif Systems, China) for wireless sending weather data to the server.

Leaf surface temperatures were measured using a Melexis infrared thermometer for the non-contact temperature sensor. These sensors recorded the canopy's internal temperature every 15 min. Data was saved on the device's MicroSD card.

Fig. 1. Pistachio shell and kernel growth stages in Central Valley, California right at the beginning of (a) June, (b) July, (c) August, and (d) September [17, 18].

A DJI P4 drone with a multiband camera module was used for collecting aerial images. This module consists of 1 RGB and a multispectral camera array. The multispectral array with five cameras covers two megapixels of Red, Blue, Green, Red Edge, and Near Infrared bands. The spectral peaks of Red, Blue, Green, Red Edge, and Near Infrared camera lenses are 650, 450, 560, 730, and 840 nm, respectively. The spectral accuracy of each camera is ± 16 nm. Aerial images were taken from an altitude of 76.2 m using DJI Phantom 4 Pro drone. The total data flight time for each aerial orchard photograph was about 10 min.

The sap flow sensor system [8] was equipped with a wireless module that allowed measured raw information to be sent to an internet-connected cloud. The ESP8266 (ESP-01) module was used as a low-cost Wi-Fi module. Thermocouples' temperature differences were measured every ten minutes. To improve the quality of data before modeling [9], the following steps were applied to the raw sap flow sensor data. First, the values of the sap flow density every 10 min were extracted from the values of the recorded temperature difference (ΔT) and the average temperature difference between midnight and 7:00 morning (ΔT_m) using the improved Granier's sap flow density equation [19]. The daily peaks of calculated sap flow density as analytical features were statistically analyzed.

The stem water potential of 18 selected pistachio trees was measured manually in the field with a typical PMS Instrument pressure bomb (Model 615). Sap flow and trunk moisture sensors were installed on 6 of these 18 trees. At about noon, several leaves on different sides of a pistachio tree were covered using dark and reflective zipped plastic bags for a duration of approximately 30 min. The covered leaf stems were then cut with a sharp blade and inserted into the pressure chamber according to instructions in the device handbook. Pressurized air was gradually introduced into the chamber until the sap was visible to the naked eye. At this moment, the air pressure gauge's value was recorded.

The stochastic decision tree (SDT) was used as an ML method for a site-specific calibration of aerial images based on the massive time series data collected from ground sensors. In addition, the support vector machines (SVM) and k-nearest neighbors (KNN) algorithms were used beside SDT for this purpose. The achieved prediction accuracy was used for comparison and evaluate the result of these AI and ML-based methods.

3   Results

The local weather station recorded a massive amount of ambient data of temperature (Fig. 2), relative humidity (Fig. 3), and barometric pressure (Fig. 4) every 15 min during the growing season. The collected data covered four important pistachio shell and kernel growth months. Based on data from June, the difference in temperature between the minimum temperature in the morning and the maximum in the warmest time in the afternoon was changing very much. In July, this fluctuation reduced, and it was almost constant. During August, just a few days less temperature difference was observed, and the other days were like the previous month. In the first ten days of September, the temperature difference was like July and August. But it significantly reduced during the second ten days and returned to the amount that was observed in the first ten days in the last ten days of September.
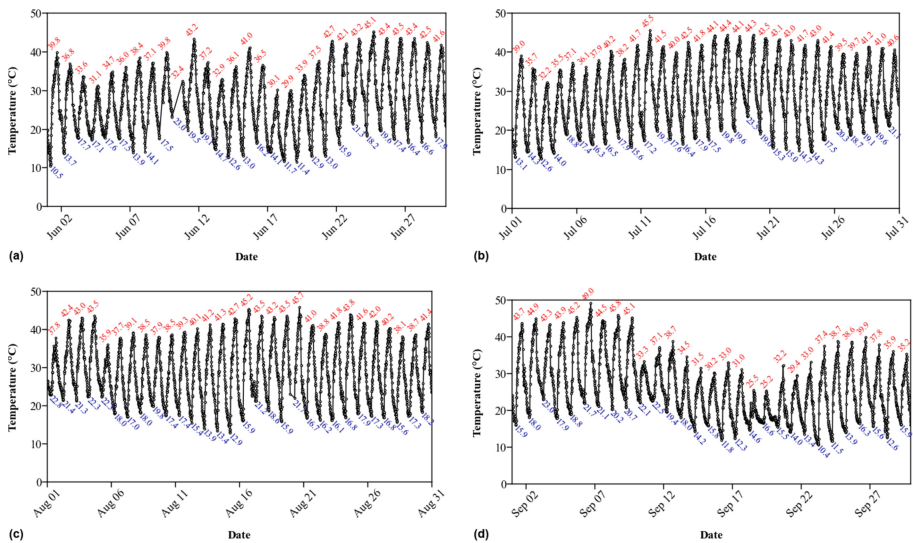
Fig. 2. Temperature changes in the pistachio field during (a) June, (b) July, (c) August, and (d) September.

It was observed that the minimum relative humidity always occurred when the temperature was at maximum level in the afternoon. The peak of the relative humidity also happened around 6:00 AM when the temperature was at its daily minimum value. Relative humidity fluctuations were observed on all days during the pistachio nut growth season. However, the average humidity increased significantly in the second half of September.

The barometric pressure was behaving the same between June and August. A notable drop was observed on September 9th. After this drop, the pressure increased to a level higher than what it was in the last three months.

Several aerial multispectral images were recorded from the pistachio field. Sample aerial NDVI images during the growth season are shown in Fig. 5. It was observed that
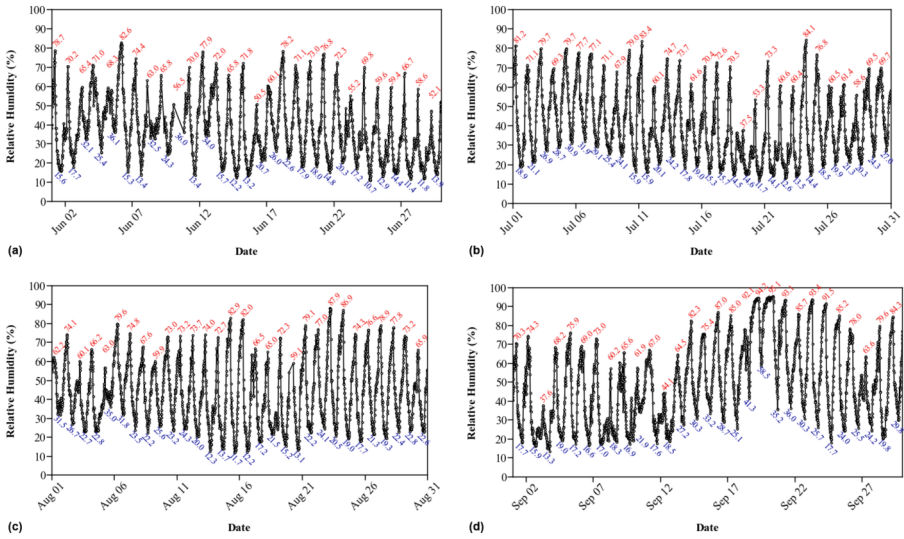
Fig. 3. Relative humidity changes in the pistachio field during (a) June, (b) July, (c) August, and (d) September.
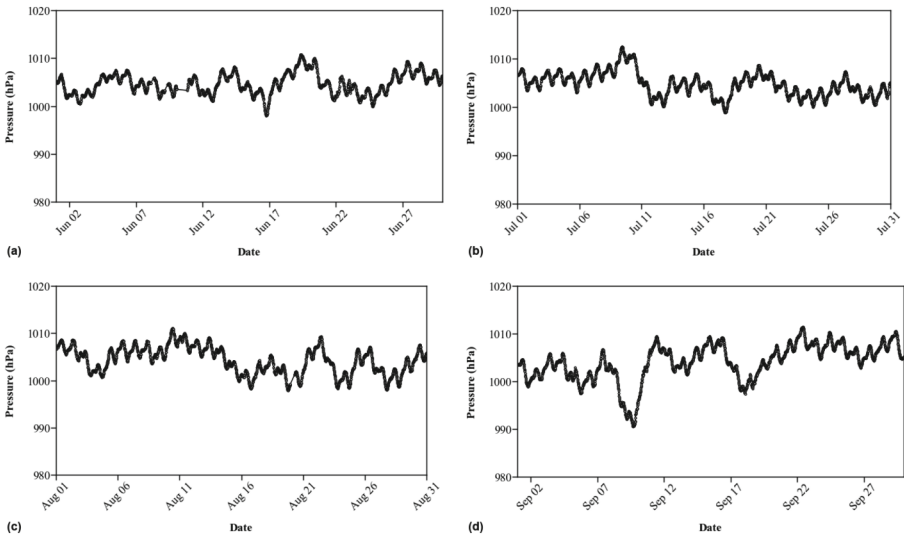
Fig. 4. Barometric pressure changes in the pistachio field during (a) June, (b) July, (c) August, and (d) September.

the ground vegetation index level decreased as time passed. However, the vegetation index slightly increased over the tree area from the beginning of June until mid-July. It almost remains at the same level in August and a little bit decreased in September. Some error was in analyzing the aerial NDVI images due to the undesirable increase in

vegetarians under the tree canopy. It was found that the cause of this issue was the fault in the irrigation system that made data uneven for precise analysis.
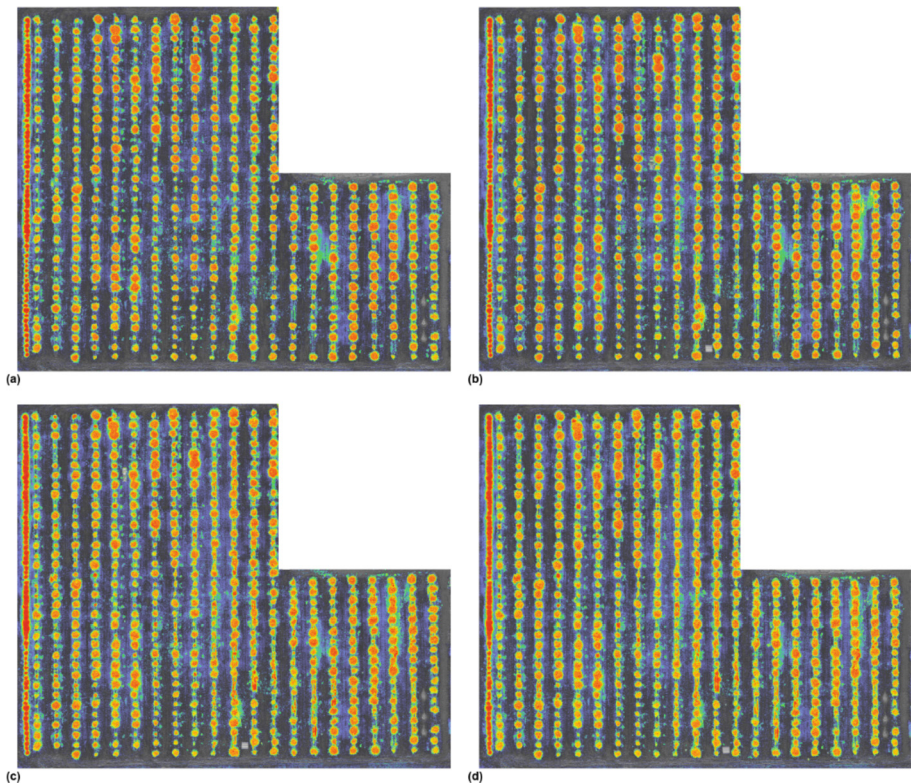
Fig. 5. NDVI changes in the pistachio field during (a) June, (b) July, (c) August, and (d) September.

The sap flow data during the four important pistachio growth months is shown in Fig. 6. Simply examining this time streaming data does not uncover what happened during these months. However, as this is obvious, the sap flow density patterns were not similar every day. Therefore, a feature of daily sap flow density peaks was chosen as the input of the statistical analysis algorithm.

Figure 7 shows the daily peak values of the sap flow density during the four important pistachio growth months. The peak values were also varying every day. It was found that following the peak values pattern was still complicated and could not be directly related to the growth stages of the pistachio shell and kernel.

On the other hand, the result of statistical analysis for the peaks of sap flow density is shown in Table 1. Based on these results, the maximum value of the daily sap flow density peaks increasing from 36.15 in June to 43.70 $\frac{mL}{m^2 s}$ in September. The rate of this growth was slow during June and July. Between July and August, this rate became about ten times faster. And finally, between August and September, this rate became one-third
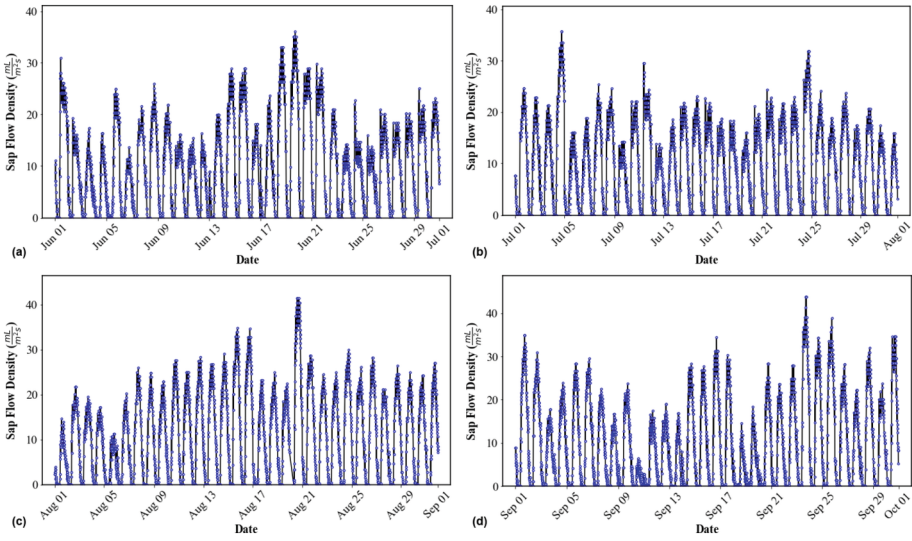
Fig. 6. Changes of the sap flow density of a pistachio tree during (a) June, (b) July, (c) August, and (d) September.
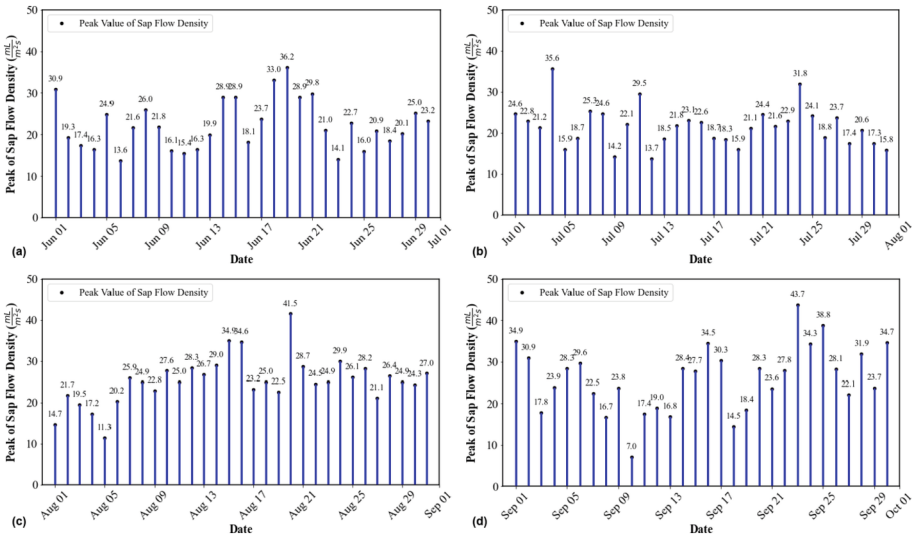
Fig. 7. Daily peaks of the sap flow density of a pistachio tree during (a) June, (b) July, (c) August, and (d) September.

of what it was during the last month. The same phenomena occurred for the median and mean values of the daily sap flow density peaks.

An interesting correlation was found between the histogram for daily peaks of the sap flow density of a pistachio tree during the growing season which is shown in Fig. 8.

Table 1. Statistical values for the daily peaks of sap flow density

Month	Peak values of the sap flow density ($\frac{mL}{m^2 s}$)				
	Minimum	Mean	Median	Maximum	Standard Deviation
June	13.61	22.28	21.60	36.15	5.84
July	13.74	21.51	21.62	35.64	4.81
August	11.35	25.25	25.01	41.49	5.68
September	7.04	25.99	27.84	43.70	7.86

The number of days that the peak of the sap flow density was greater than 25 $\frac{mL}{m^2 s}$ was 13 days in June. This number remained the same in the month of July. It became 21 and 22 days in August and September, respectively. This clearly indicates that a sap flow sensor can be used to monitor the developing stages of the shell and kernel of pistachios. In the early stages, less sap was transmitted from the root system toward the young pistachio nut. However, the rate of sap flow increased when the kernel started to grow larger during the months of August and September.
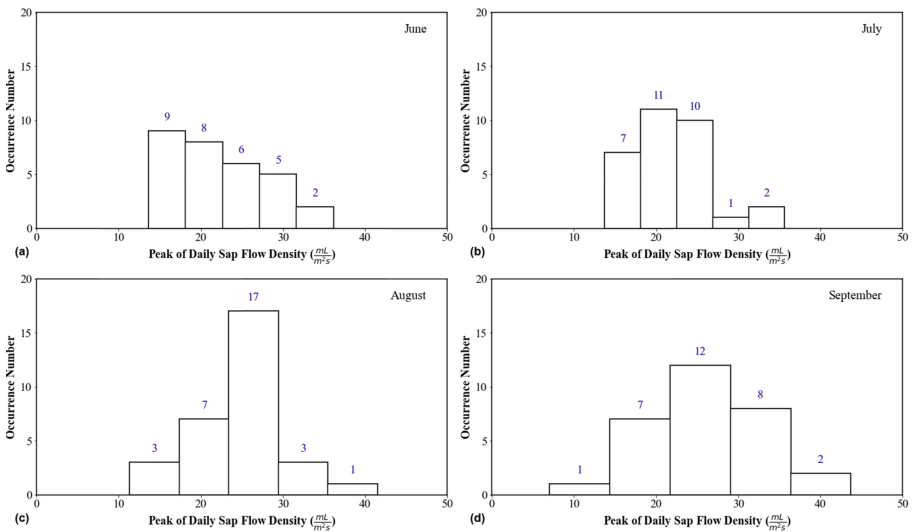
Fig. 8. Histogram for daily peaks of the sap flow density of a pistachio tree during (a) June, (b) July, (c) August, and (d) September.

In another study, the pistachio trunk's relative moisture was monitored. The changes in the pistachio trunk's relative moisture between the months of June and September are shown in Fig. 9. It was observed that the relative moisture increased by about 6% during the month of June. It was raised approximately 2% in July. It remains the same during the first two weeks of August but slightly decreased in the last two weeks of this month.

This reduction continued during the next month. The relative moisture content declined by nearly 5% during September.
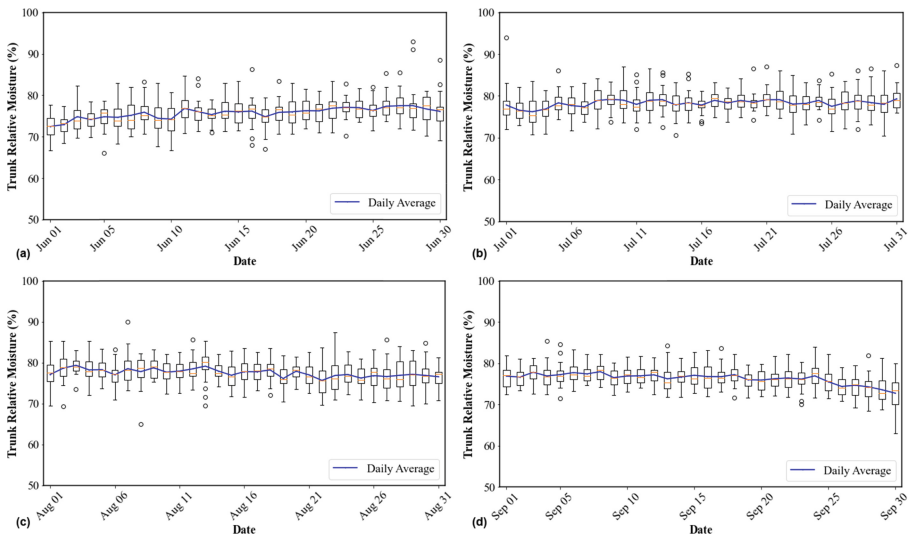
Fig. 9. Changes of the trunk's relative moisture of a pistachio tree during (a) June, (b) July, (c) August, and (d) September.

The result of reading pressure values and measured canopy temperature are shown in Fig. 10. At the beginning of June, the leaves were young and wetter in comparison with the situation of leaves at the end of September. At the beginning of June, the water in the stem was extracted using lower pressure, unlike in September when higher-pressure Nitrogen gas was injected into the chamber to be able to observe water coming out of the leaf's stem. The canopy temperature over time behaved in the same pattern as the stem water potential did. Correlating the variation of average pressure with canopy temperature remains complex and more data needs to be analyzed.

Based on the findings, it was discovered that statistical analysis of sap flow density daily peaks had a stronger link with each stage of pistachio nutshell and kernel development. As a result of this research, sap flow sensors could be utilized in future studies to monitor pistachio nut growth and determine the best time to harvest the yield. However, it was discovered that the changing rate of the stem water potential and aerial NDVI were the same. Due to the high standard deviation, it did not exhibit as strong an association with kernel growth as the sap flow density daily peaks did. During the pistachio growing season, a similar relationship was seen between the tree canopy temperature and the stem water potential increase. The trunk relative moisture is a helpful indication for detecting the need for tree irrigating significantly sooner than the stress being noticed from the stem water potential data.

The SDT results indicate that the applied model was able to provide about 90% accuracy in estimating the stem water potential even feeding the vegetation indices and sap flow data to the AI algorithm. Using only ambient temperature, relative humidity,
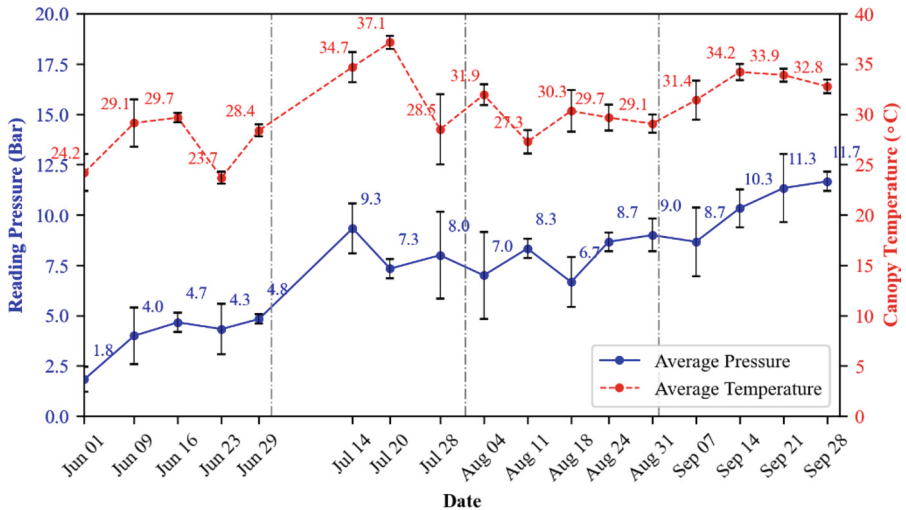
Fig. 10. Graphs related to leaf stem water potential based on chamber pressure reading and recorded canopy temperature on different sides of a pistachio tree.

barometric pressure, and thermal image data was enough for this ML-based prediction. Moreover, in separate trials, SDT found that can perform at least 8% more precisely than SVM and 20% more accurately than the K-NN technique for predicting stress.

4   Conclusion

This research integrated model-based and sensor-based methods, as well as AI and ML that use both approaches. A massive quantity of data was collected, processed, and evaluated from the beginning of June to the end of September, which were key months for the growth of the shell and kernel of pistachio nuts. Ambient temperature, relative humidity, barometric pressure, canopy thermal image, aerial hyperspectral images, sap flow, tree trunk relative moisture content, and stem water potential were the collected data. Based on the acquired data, the data behavior was modeled. These data were cleaned before being given into the AI and ML-based SDT, SVM, and K-NN algorithms. SDT, SVM, and K-NN techniques obtained prediction accuracy of 90%, 82%, and 70%, respectively.

References

1. Yaddanapudi R, Mishra AK (2022) Compound impact of drought and COVID-19 on agriculture yield in the USA. Sci Total Environ 807:150801
2. Deligios PA et al (2019) Climate change adaptation and water saving by innovative irrigation management applied on open field globe artichoke. Sci Total Environ 649:461–472
3. Wanyama J, Bwambale E (2023) Precision water management. In: Zhang Q (eds) Encyclopedia of digital agricultural technologies. Springer, Cham. https://doi.org/10.1007/978-3-031-24861-0_213
4. Alizadeh A, Toudeshki A, Ehsani R, Migliaccio K, Wang D (2021) Detecting tree water stress using a trunk relative water content measurement sensor. Smart Agric Technol 1:100003
5. Kizer EE et al (2017) Continuous, proximal leaf monitoring system to assist with precision irrigation implementation using a wireless mesh network of and controllers in almonds. Paper presented at the 2017 ASABE annual international meeting
6. Elbeltagi A et al (2023) Forecasting vapor pressure deficit for agricultural water management using machine learning in semi-arid environments. Agric Water Manag 283:108302
7. Robbins NE, Dinneny JR (2018) Growth is required for perception of water availability to pattern root branches in plants. Proc Natl Acad Sci 115(4):E822–E831
8. Alizadeh A, Toudeshki A, Ehsani R, Migliaccio K (2018) Potential sources of errors in estimating plant sap flow using commercial thermal dissipation probes. Appl Eng Agric 34(6):899–906
9. Jain A et al (2020) Overview and importance of data quality for machine learning tasks. In: Proceedings of the 26th ACM SIGKDD international conference on knowledge discovery & data mining
10. Jesmeen MZH et al (2018) A survey on cleaning dirty data using machine learning paradigm for big data analytics. Indonesian J Electr Eng Computer Sci 10(3):1234
11. López-Andreu FJ, López-Morales JA, Erena M, Skarmeta-Gómez AF, Martínez JA (2022) Monitoring system for the management of the common agricultural policy using machine learning and remote sensing. Electronics 11(3):325
12. Pallathadka H, Mustafa M, Sanchez DT, Sekhar Sajja G, Gour S, Naved M (2021) Impact of machine learning on management, healthcare and agriculture. Mater Today Proc 80:2803–2806
13. Soffer M, Hadar O, Lazarovitch N (2021) Automatic detection of water stress in corn using image processing and deep learning. In: CSCML 2021: Proceedings of the 5th international symposium on cyber security cryptography and machine learning, Be'er Sheva, Israel, vol 5, pp 104–113
14. Favenza A, Imam R, Dovis F, Pini M (2019) Detecting water using UAV-based GNSS-reflectometry data and artificial intelligence. In: 2019 IEEE International workshop on metrology for agriculture and forestry (MetroAgriFor), pp 7–12
15. Orn D, Duan L, Liang Y, Siy H, Subramaniam M (2020) Agro-AI education: artificial intelligence for future farmers. In: Proceedings of the 21st annual conference on information technology education
16. Dharmaraj V, Vijayanand C (2018) Artificial intelligence (AI) in agriculture. Int J Curr Microbiol Appl Sci 7(12):2122–2128
17. Allan CA (2014) Pistachio nut phenology and development in five cultivars as a function of heat units. Report to the California Pistachio Research Board
18. Fichtner E, Ferguson L, Mahvelati NM, Zhang L (2017) Pistachio nut phenology: California studies address crop development as a function of heat unit accumulation, West Coast Nut, JCS Marketing, July 2017, pp 16–19
19. Lundblad M, Lagergren F, Lindroth A (2001) Evaluation of heat balance and heat dissipation methods for sapflow measurements in pine and spruce. Ann For Sci 58(6):625–638

Plant, Animal and Facility Systems in Agriculture

Evaluation of Air Conditioning Parameters in Semi-closed Greenhouses under Turkey's Climatic Conditions

Mohammed Hassan and Hasan Hüseyin Silleli[✉]

Department of Agricultural Machinery and Technologies Engineering, Faculty of Agriculture, Ankara University, Dışkapı, Ankara, Turkey
engmhdtahr07@gmail.com

Abstract. Due to climate change and increasing energy prices worldwide, it has become necessary to use greenhouses more efficiently and to spread production throughout the year. The aim of this study is to investigate the possibilities of using semi-enclosed or fully enclosed greenhouse technologies that can replace traditional modern greenhouses. In line with this goal, greenhouse technologies that could provide a solution between traditional greenhouses and semi-closed greenhouse concepts are being explored in Turkey. Given that Turkey's climatic conditions are much more favorable compared to many other countries, controlling traditional modern greenhouses using semi-closed techniques is seen as a viable solution under desired conditions. This technique, especially applicable to plastic greenhouses, could extend the production process in greenhouses to 345 days. In addition to designing greenhouses with a semi-enclosed technology during the installation phase, it is also important to adapt existing greenhouses to meet this concept. Data related to the creation of necessary parameters and the determination of transition phases to formulate control algorithms for domestically developed systems with multi-climate or poly-climate techniques in Turkey are being evaluated within the scope of this study. The effects of energy efficiency and product quality of the greenhouse operating with the Multi climate technique, which was installed in the province of Mersin (covering an area of $5000\,\text{m}^2$), have been evaluated under both classical greenhouse and semi-closed greenhouse conditions. The establishment of an appropriate climate for plant growth and development in greenhouses is achieved by controlling variables such as temperature, relative humidity, and sunlight within the greenhouse. In traditional greenhouses, the climate is constantly changing due to external factors like sunlight, temperature, humidity, rain, and more. Excess energy accumulation is managed to a limited extent through strategic activation of ventilation or cooling systems. Semi-closed greenhouses exhibit significant differences in control methods and operational techniques. Particularly, the positive pressure within the greenhouse is the most distinctive feature that alters the control approach. Positive pressure inside the greenhouse is achieved using electronically controlled fans. Additionally, heating-cooling coils coupled with these fans allow for climate control within the greenhouse. Another key distinction of semi-closed greenhouses is that they require a smaller area for roof ventilation windows compared to traditional greenhouses. These significant differences also offer important advantages in greenhouse control techniques. Controlled air exchange between the interior of the greenhouse and the climate

corridor also facilitates energy savings. Controlled air inlet and outlet allow for homogeneous profiles of horizontal and vertical temperature, humidity, and CO_2 concentration to be obtained.

Keywords: Semi-closed greenhouse · Climate control · Coolers · Chiller · AHU

1 Introduction

The main objective of greenhouse cultivation, in its simplest sense, is to provide a homogeneous temperature higher than the average temperature of the region and to protect the plants from environmental influences such as wind, rain, hail, etc. To this aim, in order to be able to grow plants successfully, it is necessary to regulate the climate in the greenhouse in a way that is close to natural. When adjusting climate control, it is important to avoid high temperatures that can stress the plants, while at the same time preventing the humidity level in the greenhouse from fluctuating between maximum and minimum limits, adjusting the carbon dioxide level and thus controlling the risk of diseases that can jeopardize production. In this sense, an industrial greenhouse should aim to find the appropriate value point between the ergonomic capacity of greenhouse production systems, investment and operating costs, including climate control, and the capital resources of the grower. In the greenhouse, temperature is the most important variable to control. The majority of the plants grown are temperate climate plants and their general temperature requirements are between 17–27 °C on average. The lower upper limit temperature values are 10–35 °C. In general, greenhouses should be heated when the average outside temperature is below 12–13 °C. When the average outside temperature is below 27 °C, natural ventilation will prevent the temperature inside the greenhouse from reaching extremes. When the temperature rises above this value, it is important to use artificial cooling methods (fog, fan-pad, shading, and chiller) to maintain product quality. The temperature inside the greenhouse should not reach 30–35 °C in the long term.

The second parameter to be controlled in the greenhouse is relative humidity. Generally, a change in relative humidity between 60–85% does not have a great effect on plants. However, humidity levels below 60% can cause water stress on the fresh leaves of young plants, especially when ventilation is also done. On the other side, if the relative humidity in the greenhouse exceeds 95% in the long term, fungal diseases spread rapidly, especially at night. Adjusting the vapor pressure balance in the greenhouse regulates transpiration and reduces disease problems.

At night, if the greenhouses are not heated, the inside and outside temperature is almost equal and it is not easy to reduce the humidity inside the greenhouse if the outside humidity is high. Light, or more specifically PAR (Photosynthetically active radiation) is another important parameter for production in greenhouses. But this need can only be supplied by solar radiation [1]. A shading system, on the other side, is used when the light intensity outside the greenhouse is too high or when it is desirable to slow down the growth process by reducing the light intensity.

Another parameter that needs to be controlled in the greenhouse and directly affects the amount of production is the CO_2 concentration. Although natural ventilation during

the day provides CO_2 transfer into the greenhouse, the rate inside the greenhouse is always lower than outside due to the plants' constant need for CO_2 for photosynthesis. In a well-insulated greenhouse, the highest concentration is around 200 μmol mol^{-1}, while in the outside atmosphere it is 360 μmol mol^{-1}. Due to the high plant density in greenhouses, the CO_2 ratio should be 2–3 times that of the atmosphere [1].

In an industrial greenhouse, the aim should be to find the appropriate value point between the agronomic capacity of the production systems, the investment and operating costs, including climate control, and the capital resources of the grower. Today, 95% of greenhouse areas are located in regions such as Antalya, Adana, Mersin and Izmir, which have very hot summers. In these regions, production stops until the end of August due to the increasing temperature and rising humidity as of the end of June and greenhouses remain empty for 60–80 days. The fact that greenhouses remain empty during this period when solar radiation is intense creates great economic losses for the producer and the country's economy. Therefore, there is a need for new technologies that can include the summer months in production. Within the scope of this study, the control parameters and algorithm will be developed by testing the semi-closed greenhouse technologies, which can be used in the local and international market, different from the classical type greenhouses, which are accepted as the new generation in the world, under humid region conditions. Although the new generation of closed and semi-closed greenhouse systems require higher initial investment and technological know-how, in the long term, up to 30% reduction in energy use, 80% reduction in chemical use, 50% reduction in irrigation water use and a 2-fold increase in crop yield compared to conventional greenhouses can be achieved [3]. The greenhouse climate with the positive pressure obtained through the closed system provides significant advantages in terms of energy use and cultivation. In this type of greenhouses, energy, climate and nutrient management can be carried out more effectively.

In addition, while fuel economy benefits can be achieved in the winter months, production, which is terminated due to high temperatures in the summer period, can be extended to the whole year thanks to the controlled and economical cooling. In greenhouse cultivation, the most important obstacle to production in the summer months is that the temperature inside the greenhouse cannot be controlled under night conditions, and it rises higher than the limits required by the plant. In the semi-closed greenhouse technique, the cooling process that starts in the daytime will continue at night and it will be possible to create suitable climatic conditions. In these conditions, the most important success criterion is to ensure the continuation of production in the greenhouse, which is left empty in the summer months, and to ensure that the product to be obtained during the periods when the field crop has not yet emerged and greenhouse production is significantly reduced, is given to the market with a price above the market averages or exports are realized. On the other side, by ensuring that the plant enters the fall with its healthy, strong and adult structure, it will be possible to catch the increasing prices and increase profitability during the period when the field crop is over and the general greenhouse crop does not come out. For this purpose, it is extremely important to determine the parameters that will ensure the transition between the classical and semi-closed technique of the greenhouse (Fig. 1).
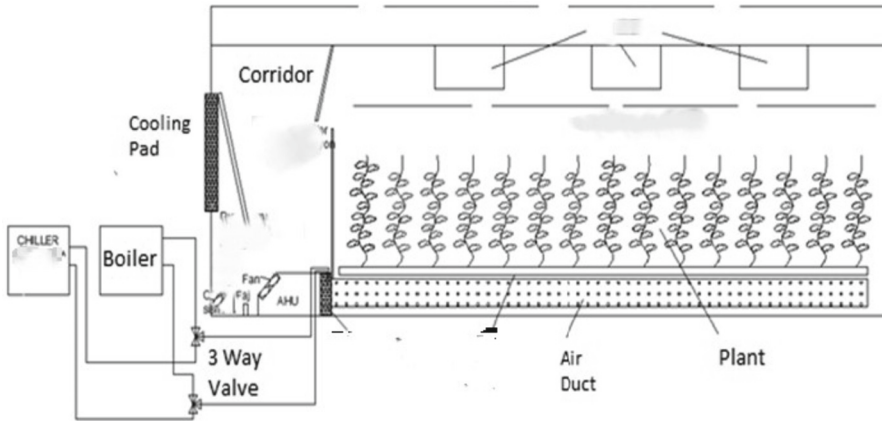
Fig. 1. Equipment of the Semi-Closed Greenhouse Climate Corridor.

Today, 95% of the greenhouse areas in Turkey are located in regions such as Antalya, Adana, Mersin and Izmir, where the summer months are very hot. In these regions, production stops until the end of August due to the increasing temperature and rising humidity as of the end of June and greenhouses remain empty for 60–80 days. In this period when the solar radiation is high, empty greenhouses cause great losses for the producer and the country's economy. Therefore, there is a need for new technologies that can include the summer months in production. Semi-closed greenhouses can be managed according to the outside climate [4]. With a decision mechanism that works according to the temperatures inside and outside the greenhouse, the greenhouse can switch between a classic and a semi-closed greenhouse. Thus, the outdoor climate is utilized in the most appropriate way. In this type of greenhouses, control is realized as a result of the interaction of all factors such as outdoor relative humidity and temperature, indoor relative humidity, temperature, wind direction and speed, solar radiation, evaporation, etc. with each other. In these respects, the automation system is extremely important [5]. The system should be able to perceive and evaluate this interaction well and should have a structure that can draw a correct conclusion. The air temperature inside the greenhouse, which rises with the effect of the sun in the summer months, can be kept within the desired limits in different ways with automation systems.

2   Materials and Methods

In a $5000\,\mathrm{m}^2$ semi-closed greenhouse established in Mersin province, tomato production was carried out in soilless agriculture using the system known by the trade name POLY-CLIMA. As is known, the climate of Mersin is very hot in summer and the humidity is high. The high temperature problem in the greenhouse was solved with a cooling system (chiller+Cooling-pad). However, when the heat was avoided, the relative humidity increased. In the semi-closed (POLYCLIMA) system, both temperature and humidity could be controlled according to the outside climate [6]. The temperature and humidity

values could be reduced by using the ventilation system together with the cooling system. When the outside climate changes, the ventilation window and interior windows are opened and closed proportionally. Conditioned water is used in the chillers used in the cooling of the greenhouse. The system consists of chiller unit, compressors, electrical control unit, pumps, buffer tank, normal - solenoid valves, strainers, gas and water pipelines. Coal is used to heat the water. It works in the same pipeline with the chiller. After the water is heated, it is sent to the climate corridor with the pump group, sent into the greenhouse and Air Handling Units (AHU) as in the chiller system, and returns to the boiler again after the task is completed. AHU and air ducts are used to send the air returning from outside or from the greenhouse into the greenhouse using the climate corridor. Air Handling Units (AHU) consists of fan and coil. The fan pushes the air from the climate corridor inside.

At the same time, as the air passes through the coil, it is conditioned, heated or cooled according to the situation. After the AHU, the air is homogeneously distributed inside the greenhouse with the help of the holes on the ducts. When the design of the AHUs was finished and before they were put in place, they were tested and the results of the test are shown below. A cooling by fogging system was used when the humidity was low. A heat curtain was used to break the sunlight in the greenhouse and to save energy, especially at night. Fans were provided to circulate the air inside the greenhouse. All devices are under control using the climate control system (Fig. 2).
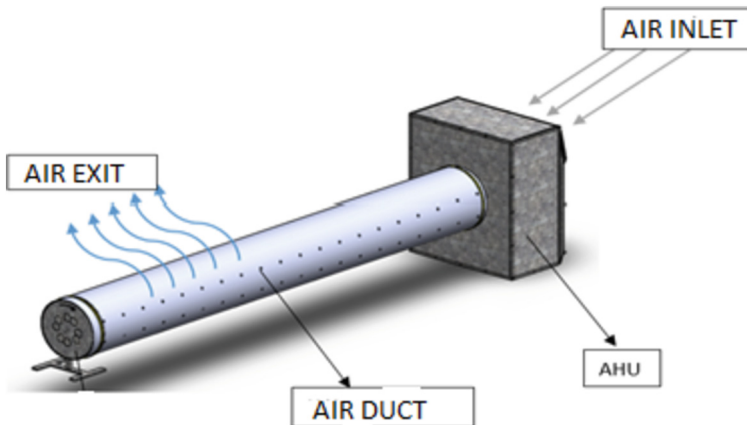
Fig. 2. AHU (Air Handling Unit) and Air Distribution system.

3 Results

The basic design parameters of the Air Handling Units (AHU) system include the number of greenhouse air changes and the energy values required for cooling and heating. At this point, the cooling capacity of the coil in the AHU is determined by considering the climatic data of the region and the critical temperatures to be reached in the greenhouse (Figs. 3, 4, 5, 6, 7, 8 and Tables 1, 2, 3, 4, 5, 6).

Table 1. AHU, duct is not connected.

Frequency Hz	velocity m/s	Current A	Voltage V	diameter mm	Area m2	Flow rate m3/h	Power (W)
50	20	3.9	395	500	0.19625	14130	2132.052
45	16	3.7	361	500	0.19625	11304	1848.609
40	15	3.5	322	500	0.19625	10598	1559.768
35	13	3.3	283	500	0.19625	9185	1292.518
30	11	3.2	244	500	0.19625	7772	1080.627
25	9	3	205	500	0.19625	6359	851.16
20			167				
15			128				
10			90				
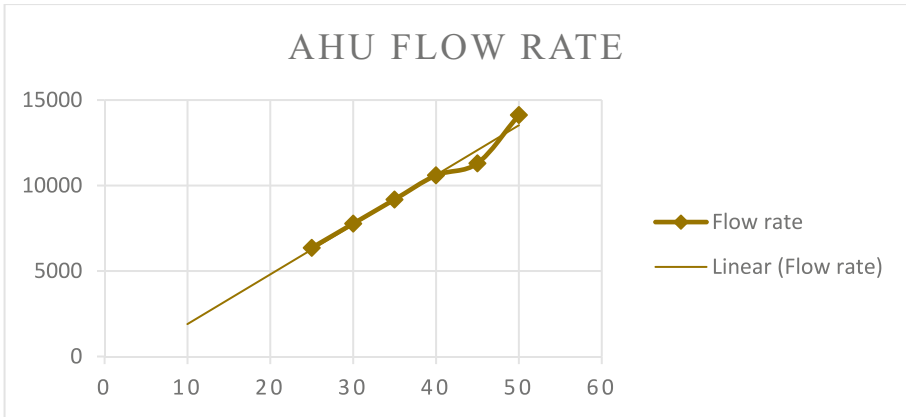
Fig. 3. AHU values, duct is not connected.

Table 2. AHU, duct connected - no holes.

Frequency Hz	Velocity m/s	Current A	Voltage V	Diameter mm	Area m^2	Flow rate m^3/h	Power (W)	Speed (min-1)
50	9.5	3.9	395	630	0.311567	10656	2132.05	1500
45	8.5	3.7	361	630	0.311567	9534	1848.61	1350
40	8	3.5	322	630	0.311567	8973	1559.77	1200

Table 2. (*continued*)

Frequency Hz	Velocity m/s	Current A	Voltage V	Diameter mm	Area m^2	Flow rate m^3/h	Power (W)	Speed (min-1)
35	6.5	3.3	283	630	0.311567	7291	1292.52	1050
30	5.5	3.2	244	630	0.311567	6169	1080.63	900
25	5	3.1	205	630	0.311567	5608	879.53	750
20	3.5	3.1	167	630	0.311567	3926	716.50	600
15	2	3.2	128	630	0.311567	2243	566.89	450
10	1	3.5	90	630	0.311567	1122	435.96	300
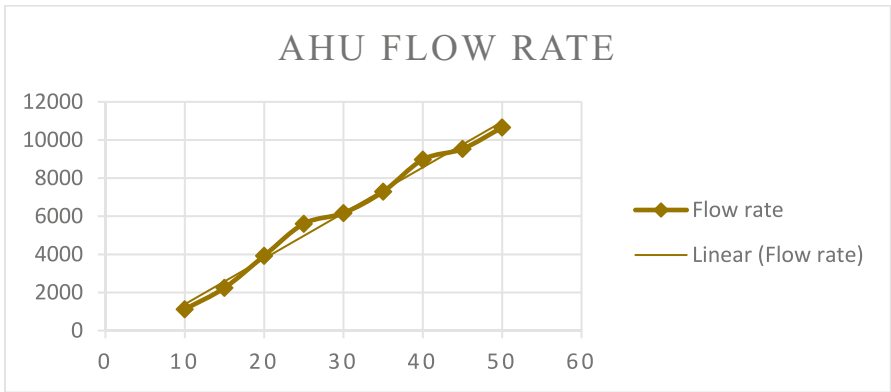
Fig. 4. AHU values, duct connected - no holes.

Table 3. AHU, duct connected - 2 holes every 5 MT 36 holes

Frequency Hz	Air velocity m/s	Diameter mm	Area m2	Flow rate m3/h
50	10	630	0.311567	11216
45	9	630	0.311567	10095
40	8.5	630	0.311567	9534
35	7.5	630	0.311567	8412
30	6.5	630	0.311567	7291
25	5.7	630	0.311567	6393

(*continued*)

Table 3. (*continued*)

Frequency Hz	Air velocity m/s	Diameter mm	Area m2	Flow rate m3/h
20	4.5	630	0.311567	5047
15	3	630	0.311567	3365
10	1.5	630	0.311567	1682
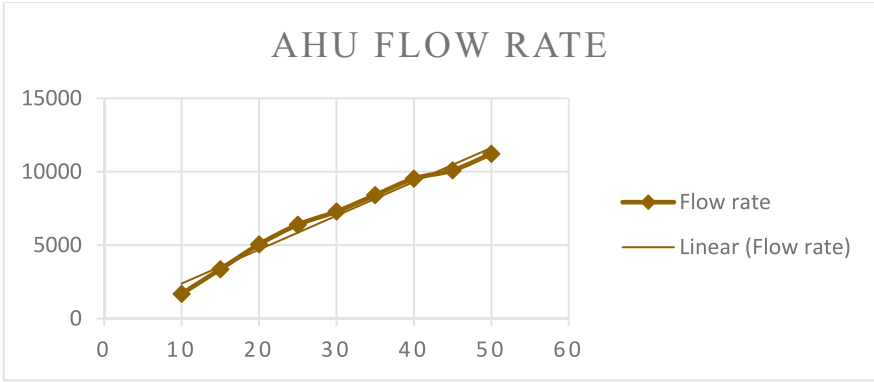
Fig. 5. AHU values, duct connected - 2 holes every 5 MT 36 holes.

Table 4. AHU, duct connected - 2 holes every 1 MT.

Frequency Hz	Air velocity m/s	Diameter mm	Area m2	Flow rate m^3/h
50	9	630	0.311567	10095
45	8	630	0.311567	8973
40	7	630	0.311567	7851
35	6	630	0.311567	6730
30	5	630	0.311567	5608
25	4	630	0.311567	4487
20	3	630	0.311567	3365
15	2	630	0.311567	2243
10	0.5	630	0.311567	561
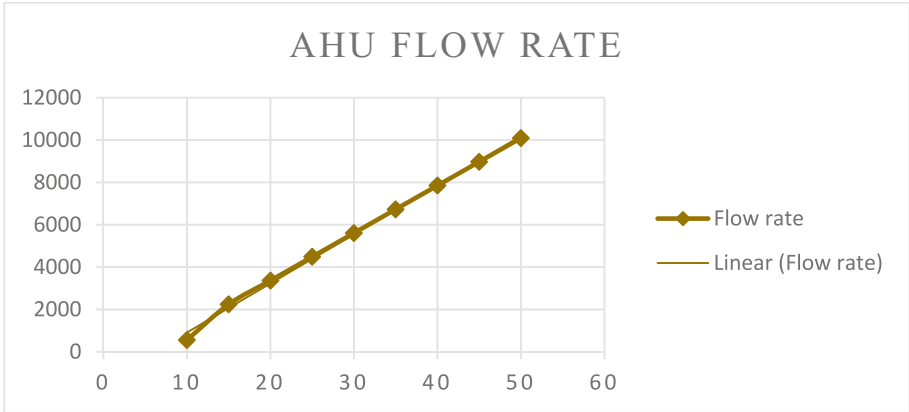
Fig. 6. AHU values, duct connected - 2 holes every 1 MT.

Table 5. AHU, duct connected - 4 holes every 1 m total number of holes 107x4.

Frequency Hz	Air velocity m/s	Diameter mm	Area m^2	Flow rate m^3/h
50	8	630	0.311567	8973
45	7	630	0.311567	7851
40	6.25	630	0.311567	7010
35	5.25	630	0.311567	5889
30	4.25	630	0.311567	4767
25	3.5	630	0.311567	3926
20	2.2	630	0.311567	2468
15	1.5	630	0.311567	1682
10	0.5	630	0.311567	561
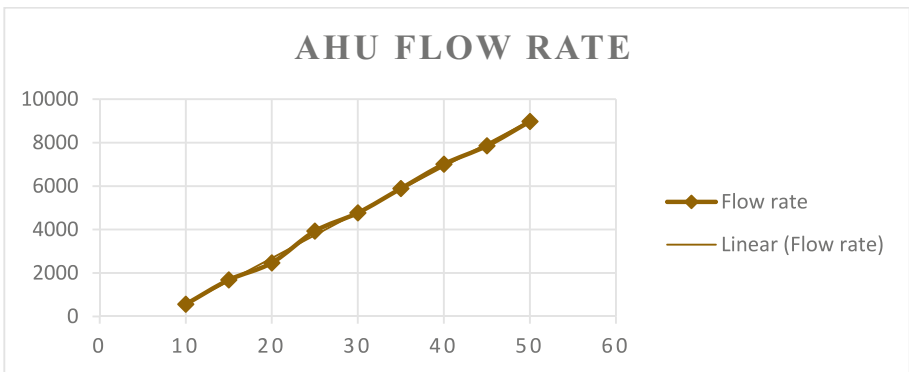
Fig. 7. AHU data, channel connected - 4 holes every 1 m.

Table 6. AHU, duct connected - 8 holes every 1 MT 107x8.

Frequency Hz	Air velocity m/s	Current A	Diameter mm	Area m^2	Flow rate m^3/h
50	7	3,8	630	0.311567	7851
45	6.25		630	0.311567	7010
40	5.25		630	0.311567	5889
35	4.75		630	0.311567	5328
30	4		630	0.311567	4487
25	3.5		630	0.311567	3926
20	3		630	0.311567	3365
15	1		630	0.311567	1122
10	0.5		630	0.311567	561
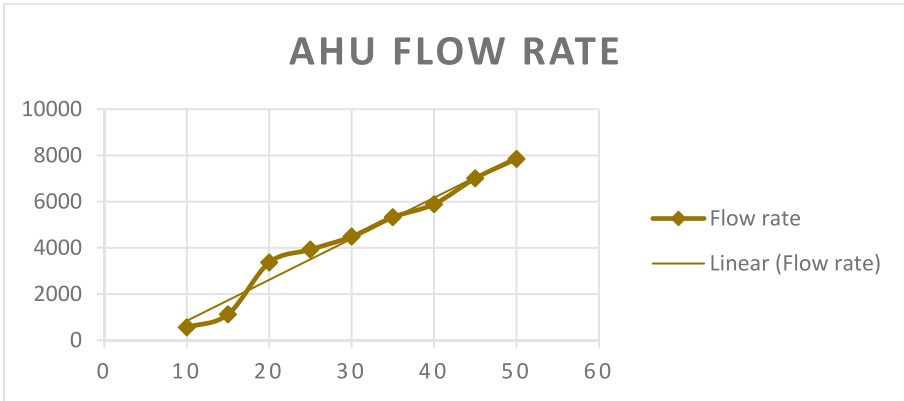
Fig. 8. AHU data, channel connected - with 8 holes every 1 m.

In the tables above, the results of the tests carried out to determine the appropriate number of holes are given. With 105 m duct, fan current and power values for different air flow rates obtained at different speeds and different frequency values were observed (Fig. 9 and Table 7).

Table 7. 01.08.2016 Climatic Data.

Time	T out	T in	RH out	RH in	T Duct	T Corridor	RH Corridor	T Pad	Frequency Hz
10:00:00	35.00	31.00	68.00	64.00	23.20	30.50	77.00		25.00
11:00:00	37.00	31.00	68.00	59.00	24.50	32.20	77.00		30.00
12:00:00	38.00	32.00	70.00	58.00	25.10	31.50	77.00	28.00	30.00
13:00:00	38.00	32.00	70.00	58.00	26.10	31.00	78.00	27.90	30.00
14:00:00	38.00	32.70	70.00	58.00	26.20	31.20	73.00	28.00	35.00
15:00:00	37.00	32.00	66.00	55.00	26.50	31.30	72.00	28.20	35.00
16:00:00	36.00	30.00	66.00	59.00	26.20	30.60	72.00	27.60	35.00
17:00:00	35.00	28.00	70.00	64.00	26.00	30.00	71.00	27.00	35.00
18:00:00	35.00	26.00	72.00	64.00	25.20	29.30	74.00	27.00	35.00
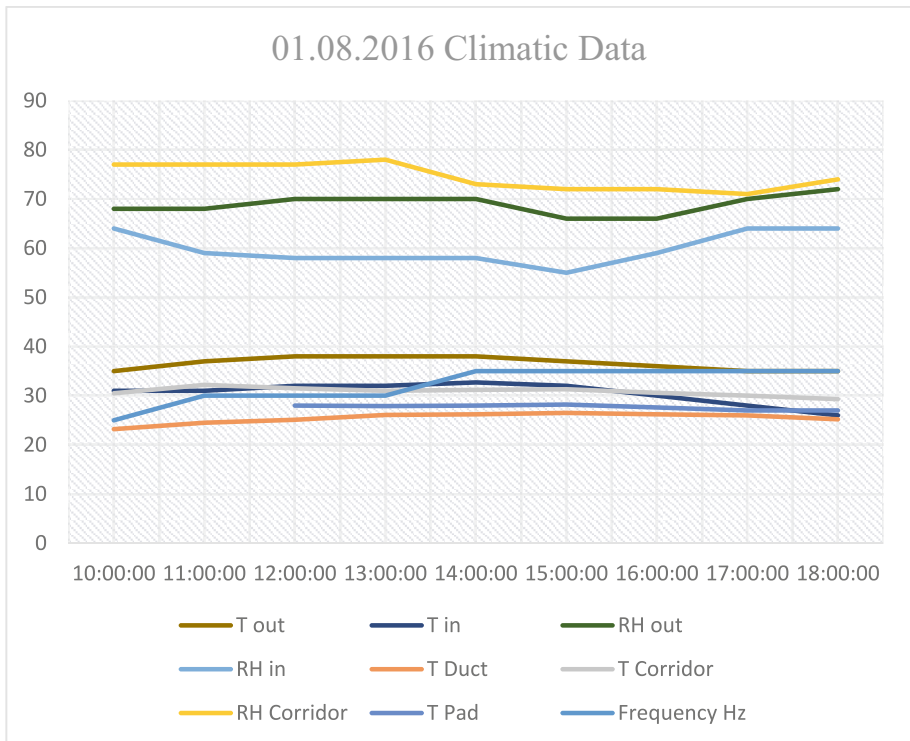
Fig. 9. 01.08.2016 Greenhouse climatic data; due to cooling and heating, the temperature difference between outside and inside is always approximately constant.

The system started with chillers and Air Handling Units (AHU) at 10 am in the morning. As the temperature increased over time, the temperature was reduced by operating the cooling pad system, and when the outside temperature dropped in the evening, the cooling pad system and chiller were turned off and continued with AHUs until the humidity decreased (Fig. 10 and Table 8).

Table 8. 09.08.2016 Climatic Data.

Time	T out	T in	RH out	RH in	T Duct	T Corridor	RH Corridor	T Pad	Frequency Hz
09:00:00	34.00	30.70	71.00	76.00	28.70	30.70	66.00		5.00
10:00:00	34.00	31.70	71.00	75.00	28.70	31.30	65.00		35.00
11:00:00	36.00	32.50	69.00	70.00	28.60	30.50	72.00	27.00	35.00
12:00:00	37.00	32.50	69.00	69.00	28.60	30.50	69.00	26.90	35.00
13:00:00	35.00	32.70	66.00	67.00	28.70	31.20	68.00	26.80	35.00
14:00:00	33.50	32.90	72.00	67.00	28.40	32.00	66.00	26.80	35.00
15:00:00	33.00	32.50	72.00	67.00	28.00	32.00	67.00	27.20	35.00
16:00:00	35.00	32.20	73.00	69.00	27.80	31.20	74.00	27.20	35.00
17:00:00	35.00	29.60	73.00	78.00	27.60	30.60	76.00	26.40	35.00

When the day started with Air Handling Units (AHU) and the temperature started to rise, chillers were turned on. During the day, the temperature was reduced by opening the Cooling Pad and increasing the speed of the AHUs, the circulation fan and ventilation window were opened to reduce humidity. In the evening, when the interior window was opened and the pad window and ventilation window were closed, the air was returned from the greenhouse to the climate corridor and then back to the greenhouse with the help of AHUs (Fig. 11 and Table 9).

Since the temperature was low in the morning, only AHUs were turned on and air was sent to the greenhouse, when the temperature started to rise, both the chiller and Cooling Pad were turned on while the heat curtain was closed and the ventilation window was proportionally open by controlling the humidity. In the evening, the humidity and temperature were kept under control by rotating the air inside the greenhouse without taking it from the outside air (Fig. 12 and Table 10).

Since the outside temperature did not differ from the values of the previous days, the temperature and humidity were kept below the desired values using the same method (AHUs in the morning, chiller and cooling pad during the day). As mentioned in the semi-closed greenhouses, all climate parameters (temperature, humidity, CO_2 and light) are automatically controlled by the automation system together with the cooling, heating and ventilation system. Therefore, the greenhouse can produce throughout the year (both in summer and winter when the temperature and humidity are high).
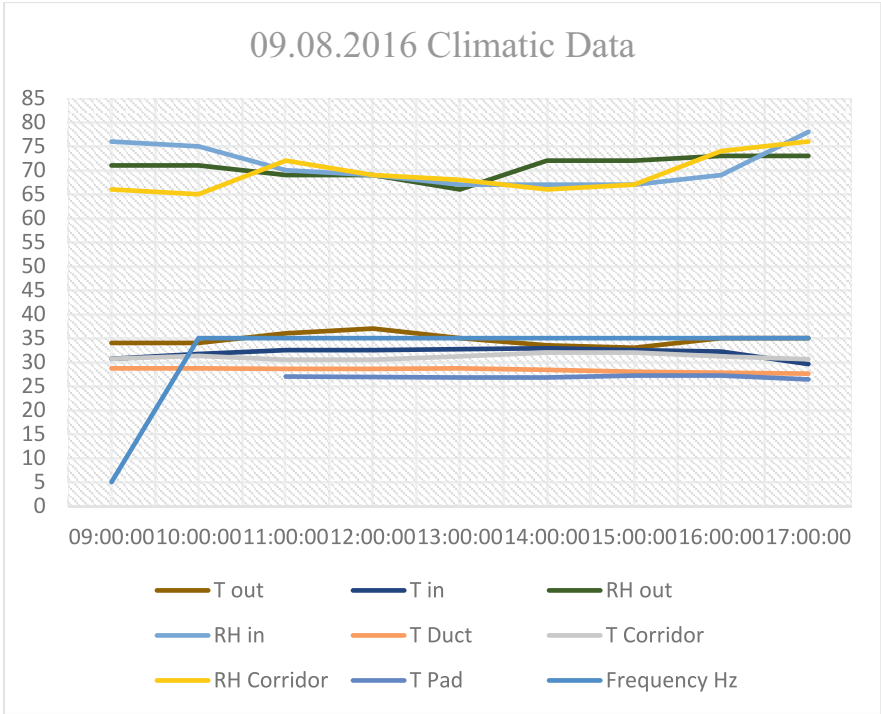
Fig. 10. 09.08.2016 Greenhouse climatic data.

Table 9. 20.08.2016 Climatic Data.

Time	T out	T in	RH out	RH in	T Duct	T Corridor	RH Corridor	T Pad	Frequency Hz
09:00	33.00	28.40	68.00	73.00	24.50	29.90	72.00		25.00
10:00	35.00	29.20	68.00	72.00	25.70	32.00	63.00		25.00
11:00	35.00	31.20	70.00	68.00	26.50	31.00	69.00	27.40	35.00
12:00	36.00	31.50	69.00	67.00	26.50	30.00	78.00	28.60	35.00
13:00	37.00	32.70	68.00	66.00	26.70	30.80	73.00	28.20	35.00
14:00	37.00	32.80	64.00	64.00	27.20	30.60	69.00	27.90	35.00
15:00	36.00	31.50	79.00	66.00	26.50	30.00	72.00	27.80	35.00
16:00	36.00	31.00	71.00	68.00	26.70	29.60	78.00	27.80	30.00
17:00	34.00	29.00	73.00	70.00	26.40	28.70	81.00	27.40	30.00
18:00	33.00	28.50	74.00	72.00	25.20	30.00	84.00	27.20	30.00
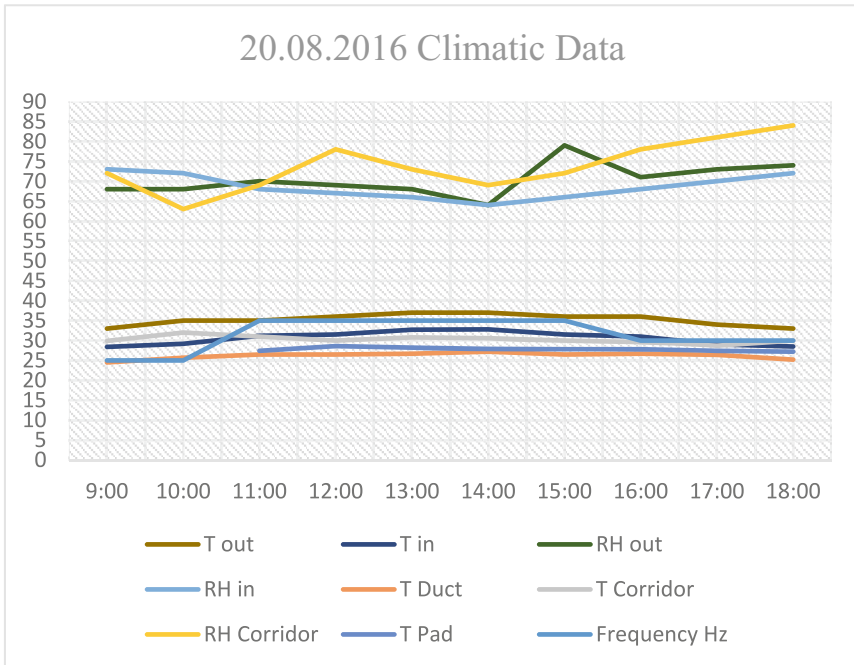
Fig. 11. 20.08.2016 Greenhouse climatic data.

Table 10. 22.08.2016 Climatic Data.

Time	T out	T in	RH out	RH in	T Duct	T Corridor	RH Corridor	T Pad	Frequency Hz
09:00:00	32.00	26.10	65.00	68.00	22.00	30.90	47.00		25.00
10:00:00	34.00	27.70	65.00	70.00	23.80	32.90	56.00		30.00
11:00:00	35.00	30.20	68.00	69.00	25.30	28.70	80.00	26.20	30.00
12:00:00	36.00	31.20	69.00	63.00	25.40	29.60	69.00	25.80	35.00
13:00:00	36.00	32.00	70.00	63.00	26.50	31.20	59.00	27.10	35.00
14:00:00	37.00	32.50	64.00	61.00	26.50	31.90	64.00	27.40	35.00
15:00:00	37.00	31.30	68.00	66.00	26.70	31.40	65.00	27.40	35.00
16:00:00	36.00	30.20	70.00	68.00	26.40	31.10	68.00	27.50	35.00
17:00:00	35.00	29.80	70.00	70.00	26.00	30.70	69.00	27.40	35.00
18:00:00	33.00	28.20	72.00	73.00	25.10	29.80	72.00	26.90	30.00

The aim of the greenhouse is not only to produce in summer but also to increase yields. For the evaluation of chillers and fan-pad, the difference between the outside temperature and the inside temperature of the greenhouse is calculated (Fig. 13).
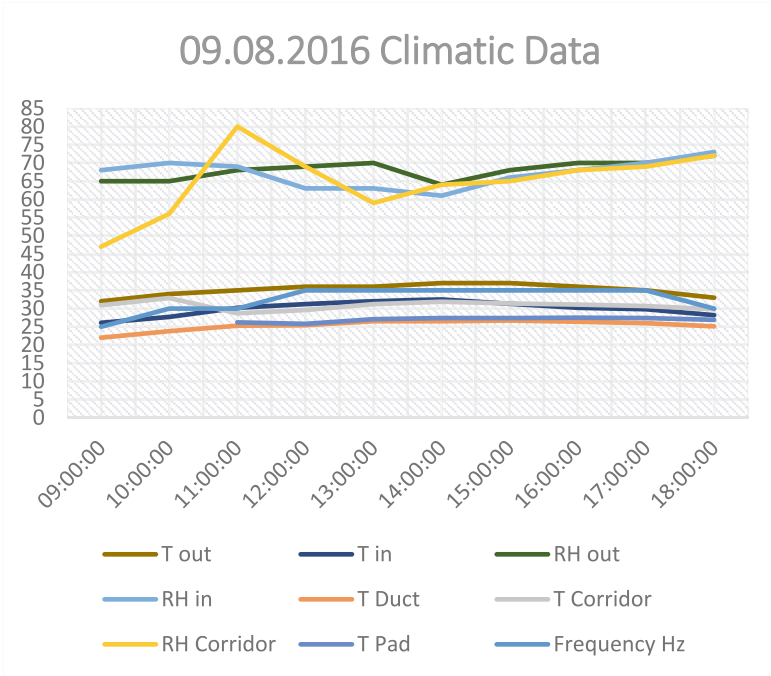
Fig. 12. 22.08.2016 Greenhouse climatic data.
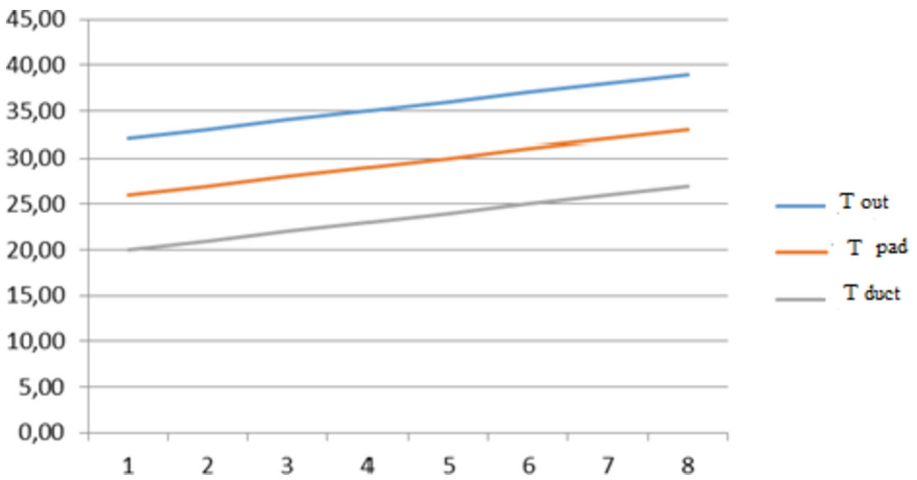
Fig. 13. Outside, pad and duct temperature.

The difference between the outside temperature and the pad temperature shows how much the pad reduces the temperature. The difference between pad temperature and

duct temperature shows how much the chiller+AHU system reduces the temperature (Figs. 14 and 15).
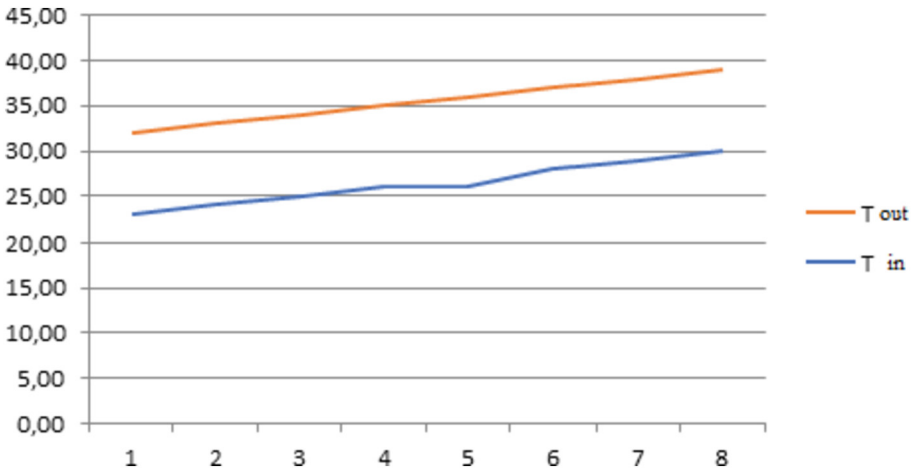
Fig. 14. Outside and inside temperature.

In the figure, the difference between the outside temperature and the inside temperature shows the efficiency of the system.
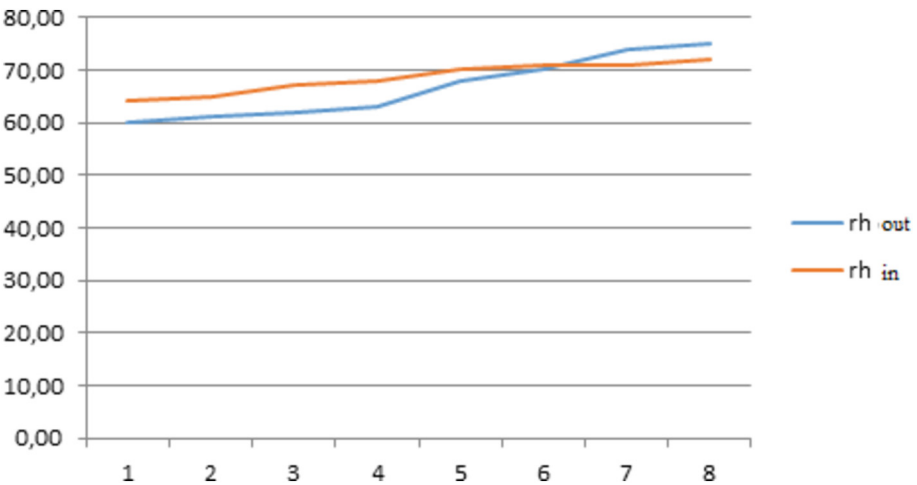
Fig. 15. Outside and inside humidity.

In summer, the aim of the system is not only to reduce humidity but also to keep it at the desired level. Therefore, when the outside humidity is high, it is lowered and when it is low, it is raised.

T out = Outside Temperature °C T In = Inside Temperature °C RH out = Outside Humidity RH In = Internal Humidity.
T Duct = Duct Temperature °C T corridor = Corridor Temperature °C
RH corridor = Corridor humidity T Pad = Pad Temperature °C

4 Conclusion

On normal days, the highest air temperature was 38 °C and the highest humidity was 90%. Inside the greenhouse, the temperature was kept between 24–28 °C and humidity between 60–85%. The number of holes in one meter of channel was determined as 12 pieces (Ø 16 mm). It was determined that 6 channels (Ø 600 mm) were suitable in each tunnel. AHU speed was started with 25 Hz and activated as 50 Hz.

Although new generation closed and semi-closed greenhouse systems require higher initial investment and technology knowledge, in the long term, up to 30% reduction in energy use, 80% reduction in chemical use, 50% reduction in irrigation water use and a two times increase in crop yield compared to conventional greenhouses can be achieved. Thanks to the positive pressure obtained through the closed system, the climate inside the greenhouse provides significant advantages in terms of energy use and cultivation. In this type of greenhouses, energy, climate and nutrient management can be carried out more effectively.

Even in a country like Turkey where energy costs are high, it is very suitable for investment in terms of feasibility. Because it is a system that can amortize itself in a few years. It is also very suitable for countries where energy is cheap and tomato prices are high (such as Azerbaijan, Turkmenistan, Kazakhstan, Russia, Ukraine, Iran, Saudi Arabia, Kuwait, Qatar).

A modern greenhouse has to meet many requirements. The first requirement for a grower is to have a greenhouse that is mostly energy efficient. With PolyClima, advances have been made towards the greenhouse of the future. It is a greenhouse that combines all the needs of modern growers: higher yields, maximum food safety, minimum energy and water consumption, minimum CO_2 emissions and better returns.

PolyClima improves the greenhouse climate by providing full control over climatic conditions. The greenhouse can, for example, be ventilated from the inside and outside, or a combination of the two, allowing more sunlight in and significantly increasing CO_2 levels. In short, a favorable value is the best growing environment for photosynthesis. PolyClima has the potential for higher returns compared to other greenhouses.

The PolyClima concept is based on semi-enclosed cultivation using positive pressure and filtered air inlet and outlet. This ensures effective pest control, lower disease levels and residue-free cultivation. The result is maximum food safety.

References

1. Albright LD, Behler ML (1984) An air-liquid-air heat exchanger for greenhouse humidity control. Trans ASAE 27(5):1524–1530
2. Albright LD, Seginer I, Marsh LS, Oko A (1985) In Situ thermal calibration of unventilated greenhouses. J Agric Eng Res 31(3):265–281

3. Campen JB, Kempkes FLK (2009) Climatic evaluation of semi-closed greenhouses. Acta Hort 893:495–502
4. Heuvelink E, Bakker M, Marcelis LFM, Raaphorst M (2008) Climate and yield in a closed greenhouse. Acta Hort 801:1083–1092
5. Silleli H, Dayıoğlu MA, Yılmaz C (2013) Seralarda Otomasyon ve Kontrol Teknolojileri Otomatik Kontrolde Üniversite-Sanayi İşbirliğine Örnek Ankara Üniversitesi-Elimko. Tarım Türk, sayı: 3, 79–84, Temmuz-Ağustos
6. Lee WF (2010) Cooling Capacity Assessment Of Semi-Closed Greenhouses. Graduate Program in Food, Agricultural and Biological Engineering the Ohio State University, Ohio, p 114

Criteria of Ecological Pressure on Agricultural Systems

Valentin B. Sapunov[(✉)]

Medical and Social Institute, St. Petersburg, Russia
sapunov@rshu.ru

Abstract. The article is suggestion on cheap and effective monitoring of agricultural systems under modern ecological state. Article include both mathematical algorithm for assay quality of agrocenosis and example of its use basing on indicating species. The current global environmental situation leads to significant environmental disturbances in agricultural systems. Quantitative and qualitative assessment of the state of agrocenosis is necessary to ensure efficient agricultural production and ensure environmental cleanliness of products. There is a need for effective and inexpensive methods of regular monitoring of agricultural systems. Such methods can be based on the achievements of fundamental science, especially ecology. These methods were developed for a number of years by the ecological scientific schools of Russia. The methods of assessing the state and forecasting are static and dynamic. Dynamic methods are based on the assessment of trends in the development of the system using methods of applied mathematics. In static approaches, the method of phenogenetic indication based on the measured parameters of the population, such as sex ratio, sexual dimorphism, quantitative and qualitative variability, is important. At the same time, the types of indicators of the quality of the ecological situation are determined, the populations of which are subject to assessment and survey. Biological species that may be used as indicator are proposed. The species must be wide spread and useful for phenogenic study. Such tree as a *Betula* is proposed.

Keywords: Ecological control · Phenogenic indication

1 Introduction

Article deals with express control of state of agricultural systems. Some innovate methods founded on records of theoretical ecology and genetics are proposed. Humanity is currently producing more agricultural products than in the past. At the same time agrarian area per person is minimal during history. This is due to scientific and technological progress and intensification of agrarian producing adding by biotechnology. Accordingly, reports and ideology of agrarian crisis and overpopulation of the planet are groundless. But social progress is taking place against the backdrop of accumulated environmental problems [8]. Pests are attacking agrocenoses [5]. In the beginning of 20th century, pests eat and destroyed about 10 percent of crops. Now this value has

increased to 15%. There is an accumulation of a large number of environmental problems. The current global environmental situation is characterized by: 1. The increase of anthropogenic pressure. Applied chemistry if perspective part of world industry and it produces millions of new chemical compounds every year, and some of them has toxic and mutagenic effect. 2. The growth of climate instability due to unknown reasons. The number of natural catastrophes and extremal ecological disasters from begin of XXI increased 2 times [8]. Human effect is not so big as natural disasters. But progress of chemical technology got new form of pollutions. This leads to significant environmental disturbances in agricultural systems. Quantitative and qualitative assessment of the state of agrarian ecological systems is necessary to ensure efficient agricultural production and ensure environmental cleanliness of products. There is a need for effective and inexpensive methods of regular monitoring of agricultural systems. Such methods can be based on the achievements of fundamental science, especially ecology. The corresponding approaches described below have been worked out on the assessment of agricultural systems in the North-Western region of Russia and can be applied to other regions of the globe, in particular, to the Mediterranean Sea region. The most significant projected trends are the growth of specific agricultural production in conditions of population stabilization and increased instability of the ecological situation. This suggests needful of permanent control and monitoring basing on records of fundamental science such as ecology and genetics [3, 4 etc.].

2   Ecological Monitoring of Agricultural Area

Present work has aim to develop methods of ecological monitoring. That is a system of regular repeated observations and assessments of the biotic components of the natural environment. Like any scientific research, monitoring has two main goals: 1. The ability to predict the development of environmental processes, 2. More importantly, the ability to control environmental processes. Nowadays, the importance of regular monitoring for science and the national economy was increased. Monitoring of agricultural objects is of particular importance among all forms of monitoring. Monitoring allows to create a database on the basis of which you can build predictive models. The latter can be divided into dynamic and static. Dynamic ones are based on the analysis of tempo and mode of ecological systems development, a time series of observations with the identification of the direction of further development of the process. Static ones are based on a one-time assessment of the state of the object and a forecast of the further path of the system development. Static ones are less accurate and require more science-intensive processing methods. But the lack of data on the dynamics of systems in some cases and the serious groundwork achieved in the field of fundamental ecology leads to the necessity and possibility of the active use of static models [1, 5]. This is becoming especially relevant today due to insufficient funding for monitoring work. This paper analyzes the perspective use of the suggested methods of phenogenetic monitoring carried out under conditions of lack of information and synthesizes several approaches.

3   Phenogenetic Indication as Effective Variant of Monitoring

Author of the article used hard methods of monitoring based on both genetic and ecological data. Let us consider the method of static analysis of the state of agrarian ecological systems. The method of phenogenetic indication has been developed since the last century [3, 7] and is used in the study of terrestrial and aquatic ecological systems [2]. The practical application of most mathematical models of natural populations requires the knowledge of many variables that can only be measured through long and expensive studies in nature. Such observations are not always possible and have not been made for most species and ecosystems. Compensation for the lack of initial data can be carried out on the basis of a knowledge-intensive approach, taking into account the achievements of environmental science. Is it possible, on the basis of a short-term or even one-time analysis of the state of populations, to determine which of the possible categories it belongs to, what is its further fate, and what is the minimum information required to predict the fate of a population and ecological system? An ecological system includes interacting populations and their environment. The population is characterized by the following features. Number dynamics. It is difficult to draw conclusions based on its absolute value. A more significant characteristic is the law of change in the number (N_t) over time (t). Unlimited population growth is described by the equation:

$$N_t = N_0 e^{kt}$$

where N_0 is the initial number, k is the coefficient reflecting the reproductive potential of the population. Periodic fluctuations in the number are possible, described by the dependence.

$$N_t = k \sin t$$

In this case, the population can be considered as relatively stable.

Variation in Quantitative Characteristics. It is usually estimated using the standard deviation, the coefficient of variation. The issue of a comprehensive assessment of variability for a number of quantitative traits has already been considered in the literature [3, 6]. However, to date, all available algorithms are cumbersome and require the use of high-speed computers. We propose the following simple algorithm. For each feature, all organisms are divided into three groups. In the first one, the quantitative measure of the trait (let's denote x) is less than 0.9 μ. The second group includes organisms in which the trait is within μ (1 ± 0.1), in the third "x" is more than I, I μ. Then the quantitative variability in terms of a set of features is described by the formula:

$$W_{Qn} = \frac{\left[\sum_{i=1}^{n}\left(\sqrt{P_{i1}} + \sqrt{P_{i2}} + \sqrt{P_{i3}}\right)\right]^2}{n} \tag{1}$$

where:

$$pi_1 = p(x < 0.9\mu), \quad pi_2 = p(0.9\mu \le x \le 1.1\mu),$$

$$pi_a = p(x > 1.1\mu)$$

Qualitative Variability can be assessed in two ways. If one wild type predominates and anomalous forms occur as an exception, the proportion of such forms in the population can be estimated:

$$P_{af} = \frac{n_{af}}{N} \tag{2}$$

where n_{af} is the number of abnormal specimen. If the wild type is not so clearly distinguished in the population and there is polymorphism, then the intrapopulation diversity can be estimated by the formula:

$$W_{QL} = \left(\sum_{i=1}^{m} \sqrt{p_i} \right)^2 \tag{3}$$

The next characteristic is asymmetry according to bilateral signs. On its basis, the state of the population is traditionally assessed [3]. Asymmetry is characterized by the indicator:

$$S_{d^2} = \frac{\sum (ar - al)2}{N - 1} \tag{4}$$

where ar and al are the feature values on the right and left sides, respectively. The question of the evolutionary role of sexual dimorphism was considered in detail by Geodakyan [2]. He found that the male-female line corresponds to the direction of the evolutionary process. The degree of sexual dimorphism can be estimated using the coefficient:

$$S_{sd} = (X_{\male} - X_{\female})/X_{\male} \tag{5}$$

A positive value of the coefficient indicates the tendency of the attribute to increase, a negative value indicates a decrease. The sex ratio is an easily measured and informative indicator. It is estimated as the proportion of individuals of one, more often male:

$$P_{\male} = n_{\male}/N \tag{6}$$

wherein $N = n_{\male} + n_{\female}$. Sexual dimorphism in terms of the degree of quantitative variability, which is important for adaptation at the population level [2, 6]. With the use of all these parameters, it is possible to characterize the population and approximately estimate its fate in the future. The most favorable case is when there is at least a limited number of consecutive observations. However, it is possible that there is only a single sample of animals. How can the results of this analysis be interpreted? Data on the absolute size of the population, if available, are usually not very informative, but they allow some conclusions to be drawn. If for dioecious species the number is reduced by 150–200 individuals, it can be concluded that the population is "near death" because of genetic inbreeding.

An essential characteristic is variability in quantitative characteristics. When controlling the population analysis data for quantitative variability, one can proceed from the fact that in the norm, for most morphological traits, the coefficient of variation is within 0.1 [6–8]. A significant excess of this value may indicate a genetic imbalance. If we are talking about a set of features (formula 1), then for the threshold value we can

take the figure obtained on the basis of the previous figure 2.67. Exceeding this value suggests that the population is destabilized.

The proportion of anomaly forms is within 5% in most cases under favorite conditions. It is no coincidence that biological statistics are based on an empirically found significance level of 0.95. 0.05 individuals are atypical. It is this proportion of anomalous forms that is observed in many biological populations [3, 6]. Based on this, it can be said that the appearance in the population of atypical forms with frequencies greater than 5% indicates that the state of the population is unfavorable.

When analyzing population polymorphism (formula 2, 3), we will assume that atypical forms are rare with recorded deviations from the wild type. As a threshold value for the indicator of intrapopulation diversity, one can take the value I.4 (formula 3). Morphological asymmetry and the degree of sexual dimorphism are important not only in comparison with the species norm. Sexual dimorphism in variability (formula 5, 6) in a stable population is close to I, at the initial stage of adaptation it significantly increases [2].

As for the sex ratio, despite some deviations, it is usually close to I:I, i.e. the proportion of males is 0.5. The shift towards females indicates the limiting stabilization and conservation of the gene pool, while towards males it indicates the adaptation of the population to unfavorable conditions. The excessive predominance of males indicates that the adaptive potencies have been exhausted, and the population is on the verge of extinction. Those species where females are rare can be considered as evolutionarily conserved. Such are aphids, stick insects. In progressive species there is some predominance of males. This is the majority of mammals, including humans. The predominance of males several times indicates that the species is toward dying out.

To make it more obvious, methods for assessing the state of the population, based on a small number of quantitative and qualitative assessments, they are summarized in Table 2. It is clear that it is difficult to draw conclusions about the state of the population based on one parameter. A comprehensive study of a possibly large number of the listed parameters is required. But in practice, sometimes you have to limit yourself to only a small number of them. All the mentioned characteristics are correlated with each other. However, the degree of correlation can vary widely depending on what specific features are being studied, the biology of the object, and environmental conditions. The degree of connection between all characteristics is also a sign subject to individual variability. Therefore, the algorithm-formula should describe the parameters in total, based on the following considerations.

1. The formula should take into account all 6 characteristics, but at the same time, it should work even if there are only a part of the characteristics.
2. The proportion of functions that reflect each of their variables should be approximately the same.

The data are summarized in Table 1.

As noted above, in populations under unfavorable conditions, variability increases, primarily in males, and the proportion of males increases. For most species, the degree of change in these characteristics is close in order of magnitude. Here are the threshold values, the excess of which indicates an unfavorable condition:

Table 1. Population character and sense

Character	Mean	Sence
1. Quantitative variability	$W_{Qn} < 2.67$	Ecological stability
	$W_{Qn} > 2.67$	Genetic disbalance
2. Mode of distribution	Symmetrical	Stable or under stress
	Assymetrical	Adaptation for new environment
	Extremal assymetry	Adaptive resources are over
	Bimodal	Disruptive selection
3. Quality diversity	$W_{QL} < 1.4$	Stable population
	$W_{QL} > 1.4$	Destabilisation
4. Ratio of males	$P\male = 0.5$	Stability
	$P\male < 0.5$	Super stability
	$P\male > 0.5$	Adaptive progress
	$P\male >> 0.5$	Close to suffocation
5. Quota of atypical forms	$P_{af} < 0.05$	Stability
	$P_{af} > > 0.05$	Destabilisation

$$W_{Qn} = 2.67.\ Wq1 = 1.4,\ S_d = \frac{P_{af\male}}{P_{af\female}} = 1.\ S_r = 0.5.\ P_{af} = 0.05$$

4 From Theory to Practice. Folia Variability of Tree *Betula* as Ecological Indication

The innovative part of modern work is suggestion of perspective method for monitoring available for both Russia and Mediterranean Sea area keeping in mind fact that ecological and genetical processes have the same basis within all the world. The growth of the anthropogenic load and the permanent pollution of the natural and agrarian environment require the availability of effective methods for monitoring the ecological quality of territories. Priority should be given to simple, cheap and knowledge-intensive methods. These are the methods of phenogenetic indication and assessment of morphological variability of widespread plants, considered above [7]. Pollutants can be divided into 4 categories: toxins, teratogens, carcinogens and mutagens. Toxins inhibit the development of organisms, but do not affect their genetic program. Teratogens disrupt the implementation of the genetic program. Mutagens and carcinogens disrupt the very genetic program, and these disruptions can be passed on to the next generation. A convenient object of express monitoring is the tree *Betula pubescens (alba)* L, widespread in Eurasia both in Russia and Turkey. Toxic emissions inhibit its growth. This increases the variability in the linear parameters of the leaves. Teratogens increase the proportion of trees with dichotomy and trichotomy [2, 3].

This paper presents estimates of the indicators of morphological variability of birch leaves in different places of the Leningrad region. The methodological basis was an express method for assessing the variability of a white birch or warty birch leaf. Previous work has shown that the level of morphological variability can be a criterion for the ecological burden on a population [3]. Of particular importance may be such an indicator as fluctuating asymmetry, which can be correlated not only with the general level of environmental load, but specifically with mutagenic pollution. The geometrical parameters of the leaf and their variability were measured, see Fig. 1. Data on width (L) and asymmetry at the widest point were processed in detail. The mean value, the standard deviation, the coefficient of variation and the nature of the distribution were determined. The latter approached normal or Gaussian in most cases. Correlation coefficients between the considered parameters were estimated. The fluctuating asymmetry coefficient was determined by formula (4), where l1 and l2 are linear asymmetry indices.
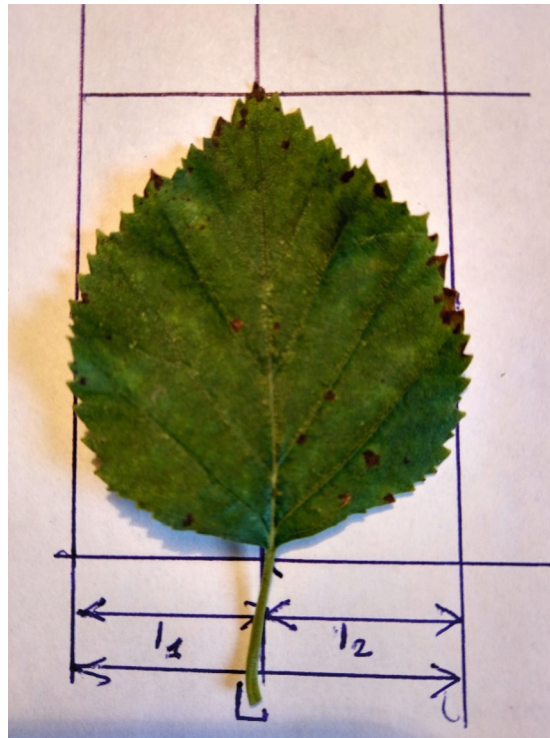
Fig. 1. Check of folia.

Estimates and measurements were made in a number of districts of the Leningrad region, the coordinates of which are indicated in the table. Places were taken for which there were estimated environmental data on the degree of pollution, as well as places where there is a possible increase in radiation - near the Leningrad Nuclear Power Plant, on the trail of the Chernobyl disaster of 1986, [5], on the Karelian Isthmus in the area

of exits granites, which create a certain radiation background (up to 50 micro roentgen per hour).

5   Results

The main purpose of the work is suggestion of theoretical approach toward biological indication of agrarian ecological systems. Let us make some example of use such a method. A certain level of variability is always maintained in a population as material for natural selection and for adaptation at the population level. Variability indicators in this case corresponded to those for other species [6]. With increasing pressure from the environment, they increased. In other words, there was a population stress that activated adaptation. The correlation between the level of fluctuating asymmetry and the general indicators of variability is average and amounts to 0.6. Consequently, these values to a certain extent reflect different processes in the environment. Fluctuating asymmetry is associated with mutagenic pollution of the environment. General variability - with pollution by toxins and teratogens. The greatest morphological variability is in large leaves that have been exposed to environmental factors for a longer time. The closer to the freeway, the stronger the overall variability index became. The correlation coefficient between distance from the freeway and morphological variability was 0.75. Those. There was a high correlation. Therefore, this parameter can be used as an indicator of teratogenic and toxic pollution.

The variability of the morphological parameters of white birch leaves can be used, along with other methods, as a means of rapid assessment of the state of the environment.

The obtained data are presented in Table 2. The correlation between the general level of variability and fluctuating asymmetry is within 0.5–0.6. Those. we are talking about the average means of biological traits, these indications can reflect both general and different characteristics of the environment.

Table 2. Dependence of CV and Ka on distance from trace

Distance, м	CV	Ka
10	0.32	0.17
100	0.15	0.24
200	0.22	0.06
300	0.22	0.08
500	0.20	0.01
1 000	0.07	0.20
4 000	0.08	0.16

6 Conclusions

1. The correlation between the level of fluctuating asymmetry and general indicators of variability is small and amounts to 0.25. Consequently, these values reflect different processes in the environment.
2. Fluctuating asymmetry is associated with mutagenic pollution of the environment. General variability - with pollution by toxins and teratogens.
3. The greatest morphological variability in large leaves that have been exposed to environmental factors for longer.
4. The variability of morphological parameters of white birch leaves can be used along with other methods as a means of rapid assessment of the state of the environment.

7 General Conclusions

The development of agricultural territories and the intensification of agriculture require constant monitoring of the ecological quality of agrocenoses. The differences and coincidence of local ecological satiation must be kept in mind [9, 10]. The coincidences are more significant. Biological indication is a promising monitoring method that does not require large expenditures and is supported by mathematical algorithms. For each territory, it is possible to select indicator species available for study and evaluation by agricultural and environmental control workers. As example for Turkish ecology may be recommended palms and other big folia plants that are wide spread at north bench of Mediterranean Sea. Future is development of green economy in accordance with UN policy of sustainable development basing on fundamental sciences records.

References

1. Chapron B, Dikinis A, Karlin L, Sapunov V (2012) Toward modeling of ecological dynamics of deep levels of Baltic sea basing on satellite monitoring data. XIII Int Environ Forum "Baltic Sea Day", 364–365
2. Геодакян ВА (1983) Эволюционная логика дифференциации полов и долголетие. Природа, №1, с. 70–80. (Geodakyan VA (1983) Evolutionary logic of sex differentiation and longevity. Nature 1:70–80 (1983)
3. Mather K (1953) Genetical control of stability in development. Heredity 7:297–310
4. Карта радиоактивного загрязнения Ленинградской области. Мин. Сельхоз. РФ, С-Пб, Ленлес, 30 листов (1992). (Radiation pollution map of St. Petersburg district, S-Pb, Lenles, 30 pages (1992)
5. Сапунов ВБ (2018) Развитие сельских территорий в условиях глобальных социально-экологических реалий XXI века. Качественный рост российского агропромышленного комплекса: возможности, проблемы и перспективы. Материалы деловой программы XXVII международной агропромышленной выставки «АГРОРУСЬ – 2018» (21–24 августа 2018 года, конгрессно - выставочный центр «ЭКСПОФОРУМ», Санкт-Петербург, с. 43–46 (2018). (Sapunov V (2018) Development of agriculture areas under modern situation within 21 centuries. Mater Congress Agrorus, 43–46
6. Sapunov V (1998) Quantitative approach to species variability of insects. VI Eur Congr Entomol Ceske Budeevice, Ac. Sci Czech Rep, 309

7. Сапунов ВБ (2007) Феногенетическая индикация как метод оценки состояния агроценоза. История науки и техники, т. 6, с. 11–12. (Sapunov V. Phenogenetic indication as method of agrocenosis assay. History Sci Techniks 6:11–12

8. Sapunov V (2019) Clean ecological methods for sustainable development of urban area under pressure of urban pests. In: Geophysical research abstracts, vol 21, EGU2019 – 225. EGU General Assembly

9. Cociasn A, Varga L, Lazar L, Vasilin D (2009) Recent data concerning evolution of the eutrophical level indicators in Romanian seawater. J Environ Prot Ecol 10(3):701–731

10. Lomborg B (2002) The skeptical environmentalist. measuring the real state of the world. Cambridge Univ Press, Cambridge. 515 p.

Discharge Coefficients for Adjustable Slot Inlets Used to Ventilate Animal Production Buildings

John P. Chastain[(✉)] [iD]

Department of Agricultural Sciences, Clemson University, Clemson, SC 29634, USA
jchstn@clemson.edu

Abstract. The purpose of this study was to empirically determine discharge coefficients (C_d) for inlets with an adjustable baffle and to compare the results with published C_d values and equations for airflow per m of slot length. Two types of baffled inlet were included in the study. One was built so as to direct the air jet across the ceiling, and the other was oriented to direct the air jet down the wall. Experiments were conducted using a model ventilation system that contained the two inlets and several fans to vary the airflow rate. The inlet velocity was measured with a hot wire anemometer and the pressure drop across the inlet was measured using a manometer. The airflow per m (Q/L) was calculated from the data and compared with published equations. In addition, the discharge coefficients were determined for 20 inlets with aspect ratios (w/L) ranging from 0.008 to 0.030. It was found that jet orientation did not influence values of Q/L or C_d as has been accepted for many years. The average discharge coefficient for the baffled inlets was 0.50 for aspect ratios of 0.018 or less and was not significantly different from the literature. For aspect ratios between 0.018 to 0.030 the value of C_d increased from 0.50 to 0.62 based on regression analysis. The results of this study will provide better discharge coefficient estimates for inlet sizing for new buildings and to develop better recommendations for retrofitting existing buildings.

Keywords: Mechanical Ventilation · Inlets · Air Velocity · Animal Environment · Energy

1 Introduction

A well-designed ventilation system for an animal production building requires energy efficient fans to provide the required ventilation rates, and properly sized inlets to provide the desired inlet velocity and airflow rate for each stage of ventilation [1–3]. The required airflow rates vary by the season of the year (winter vs summer), and the number and stage of growth of the animals.

For a ventilation system to function properly the inlet area must be controlled to match the airflow rate of the fans while providing a velocity high enough to provide proper air distribution and mixing. In general, slot inlets work best for inlet velocities in the range of 2.5 to 5 m/s depending on the season of the year and inlet orientation [1–3]. If inlet velocities are too low during winter, the heavy cold air will quickly fall

to animal level with detrimental impacts on animal health and performance. Provision of sufficiently high inlet velocities near the ceiling will promote turbulent mixing of the warm air in the building with the cold fresh air to prevent cold air from reaching the animals. The general recommendation is to provide well distributed inlets that are sized to provide the required airflow rate with ceiling inlet velocities in the range of 4 to 5 m/s [1–3]. During hot weather, ventilation rates are often 10 to 12 times greater than the minimum ventilation rate used during winter [1–3] and air movement past animals is desirable to promote animal cooling. Larger inlet areas are needed and inlet velocities in the range of 2.5 to 4 m/s can be used and will often reduce the total static pressure difference (ΔP) across the inlets and the fans. Operating at a lower ΔP typically increases the airflow delivered by the fans (Q).

The adjustable baffled slot inlet was first developed by Millier [4], and the most recent detailed treatment of ventilation has been provided in a monograph by Albright [2]. Adjustable baffled inlets were originally built into animal housing structures to bring fresh air into the building from a screened opening below the eaves [1, 5]. The most common type of baffled inlet was constructed so as to cause the air jet to form along the ceiling as shown in Fig. 1a. Such an inlet was called a ceiling jet inlet and it provided the best method to ventilate animal structures during cold weather because warm building air was drawn into the cold air jet reducing the possibility of chilling animals with cold drafts. The second type of inlet studied by Albright [2, 5] was installed to direct the air jet down the wall and it was called a wall jet inlet (Fig. 1b). A wall jet inlet was only a viable option during winter if animals were not kept along the outside walls of the barn and the recommended range of inlet velocities was 2.5 to 4 m/s [2]. As a result, wall jet inlets were typically used in dairy or beef cattle barns with layouts that allowed air to be directed toward an alley along the outside walls. A common recommendation was to install a continuous ceiling or wall inlet along both sidewalls of a building [1–3]. Such a configuration provided excellent air distribution and mixing within the ventilated space [1, 2]. Baffled inlets are typically not installed along the end walls since they would interfere with the air jets of the sidewall inlets.
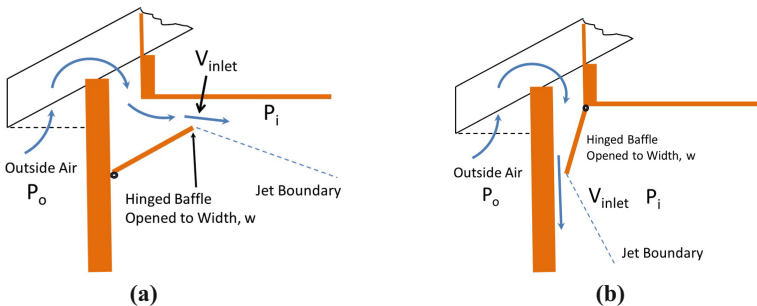
Fig. 1. Sketches of ceiling jet (a) and wall jet (b) inlets

Manufactured baffled inlets are readily available that are most often installed along the sidewall or in the ceiling and they and work under the same principles of fluid mechanics as the inlets shown in Fig. 1. Many of the available ceiling inlets are composed

of one or two baffled inlets, similar to Fig. 1a, with a slot length (L) in the range of 0.3 to 1.5 m. However, the original baffled inlet design is still widely used.

One of the recommended ways to determine the airflow rate for baffled ceiling and wall jet inlets was the use of empirical correlations for the airflow per meter of slot length (L) developed by Albright [2, 5]. The prediction equation for Q/L for a ceiling jet inlet was:

$$Q/L_{ceiling} = 0.00071 \ w^{0.98} \Delta P^{0.49}, \text{ and} \tag{1}$$

the corresponding correlation for a wall jet inlet was:

$$Q/L_{wall} = 0.0012 \ w^{0.98} \Delta P^{0.49}. \tag{2}$$

The units for the slot opening width, w, in the Eqs. (1) and (2) are in mm and not m and the conversion factor was included in the coefficients. The units for the static pressure drop across the inlet (ΔP) were Pa, and the units for Q/L were m^3/s/m. The larger coefficient in Eq. (2) indicated that the wall jet inlet used to develop the equation provided more airflow than the ceiling jet inlet at the same inlet opening width (w) and ΔP. Information concerning the dimensions and aspect ratio of the wall jet inlet used by Albright [5] was not presented in the original publication, thus the aspect ratio (w/L) of the inlet used was unknown.

The more fundamental approach is to predict the inlet velocity (V_{inlet}) by application of Bernoulli's energy equation to the airflow through the inlet assuming that air behaves as an ideal fluid, and the air velocity outside the building is zero. The results indicated that the ideal inlet velocity (V_{ideal}) was a function of the static pressure drop across the inlet and the density of the air flowing through the inlet, ρ, and was given as:

$$V_{ideal} = (2 \ \Delta P/\rho)^{0.5}. \tag{3}$$

The details of the derivation were given by Chastain and Massey [6] and are also provided by Hellickson and Walker [1], Albright [2], and most textbooks on fluid mechanics.

The actual inlet velocity has been observed to be lower than the ideal velocity due to the effects of fluid friction and restrictions related to inlet geometry [1, 5–7]. The resistance associated with the flow of a real fluid was represented by an empirically determined discharge coefficient, C_d, which yields the following equation for the inlet velocity:

$$V_{inlet} = C_d(2 \ \Delta P/\rho)^{0.5}. \tag{4}$$

The total length of the baffled inlets used in an agricultural building (L) will vary depending on the length of the building or the length of the manufactured inlet. As a result, comparison of the airflow rates between two slot inlets has often been made on an airflow per unit length basis. The relationship for airflow per meter of slot length, L, (Q/L) using the relationship for the inlet velocity was:

$$Q/L = w \ C_d(2 \ \Delta P/\rho)^{0.5}. \tag{5}$$

Previous experimental work has shown that the average C_d for a ceiling jet inlet (Fig. 1a) was 0.50 for very long slim inlets that are commonly used in animal facilities [1, 5]. The value of C_d for the wall jet inlet (Fig. 1b) was observed to vary from 0.72 to 0.86 with an average of 0.78 [5]. The most commonly recommended value of C_d for the wall jet was 0.80 [1, 5]. Several ventilation design texts suggest that a C_d of 0.60 should be used for general inlet design [1–3]. However, a simple sensitivity analysis on Eqs. (4) and (5) indicated that small errors in the value of C_d resulted in large errors in the prediction of the inlet velocities that could lead to poor ventilation system performance. Therefore, a better method to predict the C_d for the actual type of inlet used in a building will allow more precise sizing of inlet openings which would be expected to improve ventilation system performance and has the potential to reduce electrical energy requirements [8].

In modern, mechanically ventilated swine and dairy barns a common inlet system combines baffled ceiling inlets and long sidewall inlets that are formed by lowering the top of a wall curtain to form a long rectangular slot along the sidewalls. The ceiling inlets are used during the late fall, winter, and early spring with two stages of ventilation and can provide good velocity and airflow control if the inlets are adjusted properly. The ceiling inlets are locked closed during the warm and hot months of the year and the curtains are lowered from the top to provide a slot width, w, and area (w x L) that will provide the desired range of velocities and airflows for the mild and hot weather stages of ventilation. The common difficulty that many encounter when using such a system is that the wrong value of discharge coefficient is either used explicitly by selecting a value of 0.60, or by just lowering the curtain so as to provide the total inlet area that is calculated by dividing the airflow rate by an assumed velocity. Many times, the static pressure drop that is measured across the building envelop falls below the minimum desirable value of 10 Pa and if the slot width is decreased to a practical minimum value of 6 mm the ΔP measured may never reach the preferred value of 25 to 30 Pa [1–3]. Chastain et al. [7] measured the discharge coefficient for a large variety of rectangular and circular inlets and demonstrated that the flow length, z, of a rectangular slot as well as the aspect ratio ($\alpha = w/L$) had a large impact on the value of the discharge coefficient. For long rectangular slots with flow lengths of 38 mm or less the discharge coefficient averaged 0.79 and is the value that should be used for a simple rectangular inlet created by opening a curtain or adjusting a slider across a rectangular slot. Such an inlet will be referred to as a rectangular slot or curtain inlet in this paper.

The objectives of this study were to: (1) collect V_{inlet} versus ΔP data for a range of opening widths for ceiling jet and wall jet inlets, (2) calculate the Q/L for each inlet setting, (3) compare the Q/L data with the equations provided in the literature, (4) empirically determine the discharge coefficients for each inlet setting, w, and (5) compare the impact of the values of C_d on design inlet velocities.

2   Methods

A model ventilation system was designed and constructed that included a baffled ceiling jet inlet (Fig. 1a) and a baffled wall jet inlet (Fig. 1b). The external dimensions of the model were 1.22 m × 1.22 m × 1.22 m. The walls were constructed of 12.7 mm plywood, that provided a smooth interior surface, and were supported by a wooden external frame

(3.8 cm × 3.8 cm). The ceiling and wall inlets were built into the structure of the model using baffles made from 12.7 mm plywood, The baffles of the two inlets were attached to the wall and ceiling of the model using 112 cm long hinges. Rubber strips were attached to the inside edge of the baffles to allow the inlet that was not in use to be sealed shut. Two long bolts with nuts were used to fabricate a simple clamping mechanism on each end of the two baffles. The bolts were used to hold the inlet at the desired slot width (w), and to provide the necessary force to press the baffle to the interior plywood wall to form a seal when not in use. Rectangular wooden strips of varying thickness were cut to lengths of about 10 cm to allow the slot width, w, to be set to a known value. The thicknesses of the wood strips were measured 6 to 8 times using a digital caliper. The mean of the 6 to 8 measurements was used as the thickness of the wood strips. The width, w, of the slot inlet opening was set by clamping two wooden strips of the same thickness on each end of the slot. The slot length, L, was the distance between the inside edges of the wooden strips. The range of slot widths, w, ranged from 8.18 to 32.6 mm and the slot lengths, L, ranged from 1.022 to 1.097 m. This provided data for 20 baffled inlets with aspect ratios, $\alpha = w/L$, from 0.008 to 0.030. Five of the data sets were for wall jet inlets and 15 were for ceiling jet inlets. The complete details concerning the model construction was provided by Chastain and Massey [6].

Five tube axial fans were selected to provide a variety of airflow rates for inlet testing. The fans had rated airflow rates ranging from 0.010 to 0.067 m^3/s at a ΔP of 25 Pa based on data provided by the manufacturers. Elastic plastic covers were placed on fans that were not in use to prevent airflow from entering the model through the unused fans. For example, when fans 1 and 2 were operated together to provide the desired airflow rate the plastic covers were placed on fans 3, 4 and 5 to prevent air from entering the model through those fans. The velocities that were provided ranged from 0 to 4.67 m/s with values of ΔP ranging from 0 to 59.8 Pa by varying the number and combination of fans.

2.1 ΔP, Velocity, and Air Temperature Measurements

The static pressure drop across the inlets was measured using a liquid filled manometer (Dwyer MARK II 25®) that could be read to the nearest 2.49 Pa and was mounted to the exterior framing of the model. The low-pressure inside the model was measured using a surface-mounted pressure tap installed in the wall near the inlet openings. The high-pressure tap was mounted in a shielded location on the outside of the model. The taps were constructed from 9.5 mm brass fittings that had pipe thread on one end to facilitate mounting and a barb to secure the tubing on the other. The pipe thread of the low-pressure tap was screwed into a pre-drilled hole in the plywood wall until the fitting was at the wall surface. A small piece of plywood was fixed to the framing on the outside of the model structure. The brass fitting for the high-pressure tap was screwed into the plywood so as to have the tap open in the space between the framing and the outside of the model wall.

Velocity and air temperature measurements were taken using a digital hot-wire anemometer that included a thermistor in the probe tip (ALNOR CompuFlow® Thermo Anemometer, model 8525). Velocity measurements were made by inserting the velocity probe into holes at the desired distance from the inlet. One of the most critical aspects of this experiment was the placement of the velocity probe at the exit of the inlet baffle.

Texts on the fluid mechanics of a wall jet [1, 2] indicated that at this point the velocity in the air jet was constant. Therefore, care had to be taken to position the probe vertically by moving away from wall and observing the velocity. As the probe was moved from near the wall to the center of the air jet the velocity would increase quickly to a maximum value. If the probe was extended from the wall too much the velocity would fall quickly indicating that the probe was outside the air jet. The probe was positioned correctly when it was held at a point perpendicular to the air jet in the region of maximum velocity. The probe was held in the correct position using a laboratory clamp and stand. A rubber laboratory stopper, with a hole cut to fit around the probe, was pressed into the ceiling of the model to form a seal between the wall of the model and the probe.

Once the thermistor anemometer probe was correctly positioned all fans were turned off and the fan or fans to be used to collect a velocity and ΔP data point were uncovered and turned on. The flow was allowed to equilibrate for about one minute prior to taking a set of velocity readings. While the flow was stabilizing, the air temperature was measured using the thermistor. The air temperature that was recorded was the average of 10 readings. Finally, the ΔP was measured and the velocity was measured and recorded. Each velocity measurement was the average of 10 readings. This general procedure was followed for as many fan combinations as possible. The number of data points for each inlet opening ranged from 6 for the largest value of w (32.6 mm) to 11 for the smallest w (8.18 mm). Additional information concerning the procedures used to collect these data was provided by Chastain and Massey [6].

The density of the air in the laboratory (kg/m^3) was calculated from the air temperature (T) using the following correlation that was developed from a standard table of air properties [9, Table A-5]:

$$\rho = 1.293 - 0.0046\,T + 0.00001\,T^2, \ \ 0\,°C \le T \le 40\,°C. \tag{6}$$

2.2   Comparison of Measured Q/L with Previous Work

The airflow per m was calculated for each of the measured inlet velocities and the inlet width (w in m) as:

$$Q/L_M = w\,V_{inlet}. \tag{7}$$

These results were compared with the predications from the ceiling and wall jet inlet equations, Eqs. (1) and (2), developed by Albright [5] using the ΔP data and w-values for each of the inlets. The flow data (Q/L_M) were compared with the predictions from the equations (Q/L_P) by correlating the data versus the predictions using the following simple relationship:

$$Q/L_M = b\,Q/L_P. \tag{8}$$

An analysis of variance of the regression, ANOVAR, was used to calculate the 95% confidence interval about the slope, b, and the value of the slope was compared to 1.0 which would indicate perfect agreement.

2.3   Determination of the Discharge Coefficient

The discharge coefficient of an inlet was determined by plotting the measured inlet velocities (V_{inlet}) versus the ideal velocity (V_{ideal}) derived from Bernoulli's equation as given in Eq. (3). Comparison with the equation for the actual inlet velocity, Eq. (4), indicated that the slope of the regression line was the empirically determined C_d. Preliminary data indicated that this method was very reliable with R^2-values on the order of 0.971 to 0.998 [6]. A sample analysis for a wall jet inlet is provided in Fig. 2.
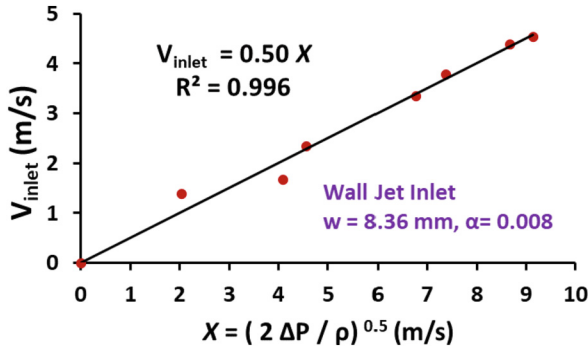
Fig. 2. Sample regression analysis used to determine the discharge coefficient for a baffled wall jet inlet ($C_d = 0.50$).

The measured discharge coefficients for the 20 inlets were compared with the published values of 0.50 for the ceiling jet inlet and 0.80 for the wall jet inlets [1, 5]. Preliminary results [6], and data provided by Chastain et al. [7], indicated that geometric parameters such as the aspect ratio (w/L) had more influence on the value of C_d than did inlet orientation. Correlation analysis was used to determine if the value of C_d for baffled inlets was significantly related the aspect ratio.

The values of C_d from this study for adjustable baffled inlets and the value for long rectangular slot inlets ($C_d = 0.79$ [7]) were used with Eq. (4) to compare the inlet velocities that could be used for inlet system design over a wide range of static pressure differences. Particular emphasis was placed on the inlet velocities that could be realistically used for ΔP values of 10 to 30 Pa and the practical range of inlet velocities for winter (4 to 5 m/s) and summer (2.5 to 4 m/s) ventilation of animal facilities [1–3].

3   Results

The inlet velocity versus pressure drop data for the ceiling and wall inlets was used to calculate the airflow rates (Eq. (7)) and were compared with the values predicted using the ceiling jet and wall jet equations published by Albright [2, 5]. The Q/L_M data were divided into two groups based on aspect ratio namely $\alpha \le 0.018$ and $\alpha > 0.018$. These two groups were further divided by inlet orientation (ceiling jet vs wall jet). The results for all of the relevant comparisons are provided in Table 1.

Table 1. Comparison of the measured airflow rates (Q/L_M) with the predictions (Q/L_P) using the ceiling jet and wall jet equations presented by Albright [2, 5].

Comparison	$b \pm$ C.I	n	SEy	R^2
$Q/L_M = b$ [Q/L_P using Eq. (1)] ceiling jet				
Ceiling jet inlets only, $\alpha \leq 0.018$	1.012 ± 0.012	60	0.0020	0.998
Wall jet inlets only, $\alpha \leq 0.018$	0.979 ± 0.025	21	0.0020	0.997
All inlets, $\alpha \leq 0.018$	1.005 ± 0.011	81	0.0020	0.997
All inlets, $\alpha > 0.018$	$1.159 \pm 0.035^*$	42	0.0063	0.991
$Q/L_M = b$ [Q/L_P using Eq. (2)] wall jet				
Wall jet inlets only, $\alpha \leq 0.018$	$0.687 \pm 0.087^*$	21	0.0096	0.931
All Wall jet inlets, $\alpha > 0.018$	$0.670 \pm 0.030^*$	13	0.0045	0.995

* Slope was significantly different from 1.0.

The results summarized in Table 1 indicated that all Q/L_M data collected for ceiling and wall jets inlets with $\alpha \leq 0.018$ were not significantly different from the predictions for a ceiling jet inlet provided by Eq. (1) since the slope of the regression line, $b = 1.005$, was not significantly different from 1.0. This result agreed with the preliminary data used to verify the efficacy of the ventilation model [6]. Furthermore, the Q/L_M for the inlets with $\alpha > 0.018$ were significantly different from the predictions using the ceiling jet equation, Eq. (1), as indicated by a slope of 1.159 that was significantly greater than 1.0. The data for all inlets with $\alpha \leq 0.018$ are compared in Fig. 3 showing the near perfect agreement. Therefore, the preliminary observation by Chastain and Massey [6] that jet orientation was not a factor for baffled slot inlets was confirmed.

Lastly, the wall jet equation consistently overpredicted Q/L for all wall inlets as indicated by a slope of 0.670 ± 0.030. The Q/L data for all inlets with $\alpha > 0.018$ are compared with the lines of perfect agreement for the ceiling and wall jet equations in Fig. 4. Given that the ceiling jet equation, Eq. (1), corresponds to a C_d of 0.50, and the wall jet equation, Eq. (2), corresponds to a C_d of 0.85 indicated that the discharge coefficients of these inlets were greater than 0.50 but less than 0.85.

3.1 Variation of C_d with Aspect Ratio ($\alpha = w/L$)

The discharge coefficients were determined for all 20 inlets using the regression method demonstrated in Fig. 2. The values of the R^2 ranged from 0.971 to 0.999. Fourteen of the inlets had aspect ratios less than or equal to 0.018. The mean for these 14 inlets was 0.502 ± 0.010 (95% C.I.) which was not significantly different from the value of 0.50 reported by Albright [2, 5]. As the value of α increased above 0.018 the values of C_d ranged from 0.52 to 0.68. Correlation analysis indicated that C_d was significantly, positively correlated with the aspect ratio. All 20 values of C_d are compared to the equation of
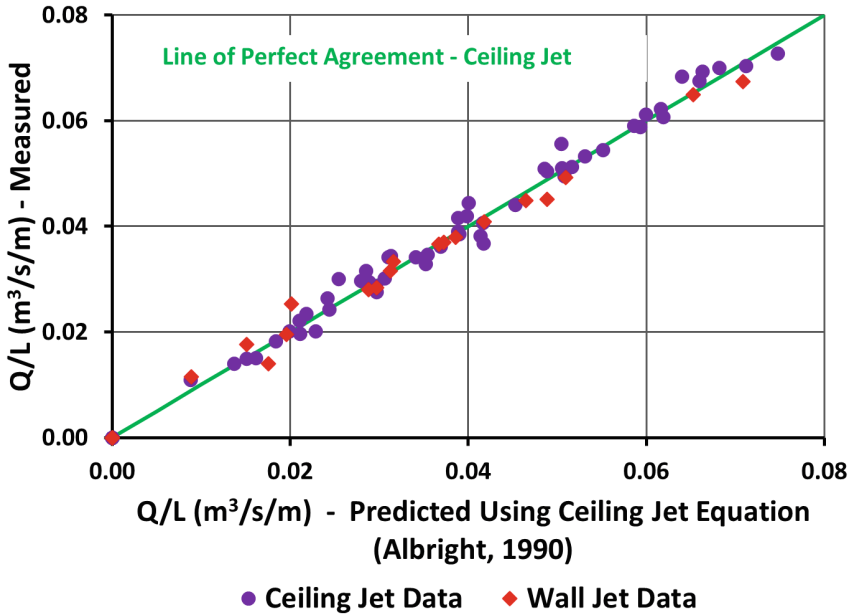
Fig. 3. Comparison of Q/L data for wall and ceiling jet inlets with $\alpha \leq 0.018$ with the ceiling jet equation (Eq. (1)).

best fit in Fig. 5. The results indicated that the y-intercept of 0.526 ± 0.069 was not significantly different from the mean of 0.502 for the 14 inlets with $\alpha \leq 0.018$. It was concluded that a C_d of 0.50 should be used for inlet system design when the aspect ratio for all baffled inlets is known to be less than 0.018. The correlation equation provides the best estimate for $\alpha > 0.018$ but ≤ 0.030 based on the data in this study.

3.2 Impact of C_d on Design Inlet Velocities

The recommended range for inlet velocities is 4 to 5 m/s during cold weather and 2.5 to 4 m/s during hot weather [1–3]. The corresponding static pressure differences range from 10 Pa during hot weather to 30 Pa during cold weather. The maximum recommended ΔP for propeller fans is 37 Pa. Centrifugal or tube-axial fans are recommended if a ΔP greater than 37 Pa is needed to meet inlet velocity requirements.

The impact of the discharge coefficient on inlet velocities and static pressure differences for baffled inlets ($0.50 \leq C_d \leq 0.62$) and a rectangular slot inlet ($C_d = 0.79$, [7]) is provided in Fig. 6. The horizontal dashed lines in the figure indicate the minimum recommended inlet velocity for summer ventilation of 2.5 m/s, and the other two dashed lines correspond to the range of velocities recommended for winter ventilation (4 to 5 m/s). The maximum ΔP recommended for propeller fan operation, $\Delta P = 37$ Pa, is shown by the bold, purple vertical line.

At a ΔP of 30 Pa the inlet velocities for the adjustable baffled inlets ranged from 3.4 m/s for a C_d of 0.50 to 4.3 m/s for a C_d of 0.62. Many design texts [1–3] recommend a C_d of 0.60 for inlet sizing calculations. The ΔP is typically assumed to be 30 Pa with
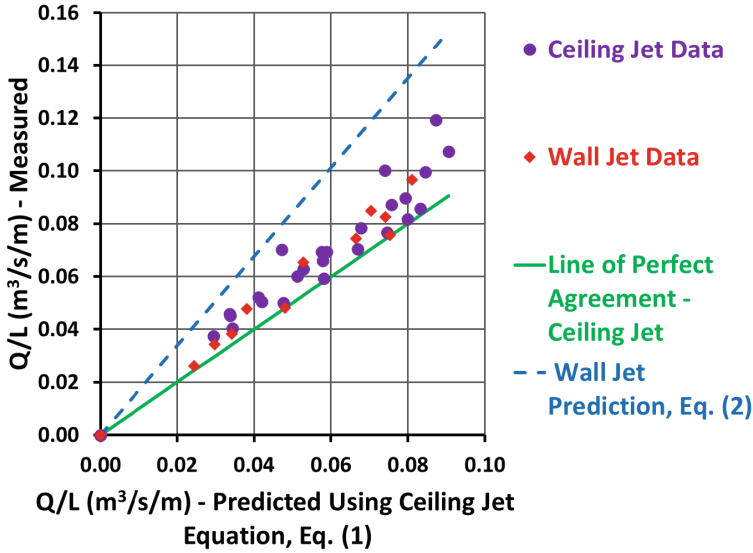
Fig. 4. Comparison of Q/L data for wall and ceiling jet inlets with $\alpha > 0.018$ with the ceiling jet equation and wall jet equations (Eqs. (1) and (2)) presented by Albright [2, 5].
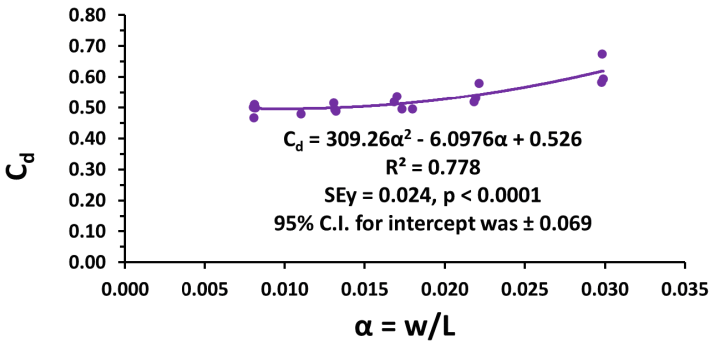
Fig. 5. Correlation of discharge coefficient with respect to aspect ratio for all 20 baffled inlets included in this study.

an inlet velocity of 4 m/s. Then using fan data, the value of Q provided by the fans at 30 Pa is divided by the assumed inlet velocity (4 m/s) and the required inlet area, width, w, and length, L, are determined. If the actual C_d of the inlet is truly 0.60 then V_{inlet} will be about 4.2 m/s which is in the desired range for winter ventilation (4 to 5 m/s). However, if the C_d of the baffled inlet is 0.50 the velocity will actually be 3.4 m/s which is 15% below the target of 4.0 m/s, and 19% below the V_{inlet} of 4.2 m/s calculated using a C_d of 0.60. Such an error in the discharge coefficient will result in velocities below the recommended values and possible underventilation of the building that may lead to higher moisture, ammonia, and CO_2 concentrations in the animal housing area. By
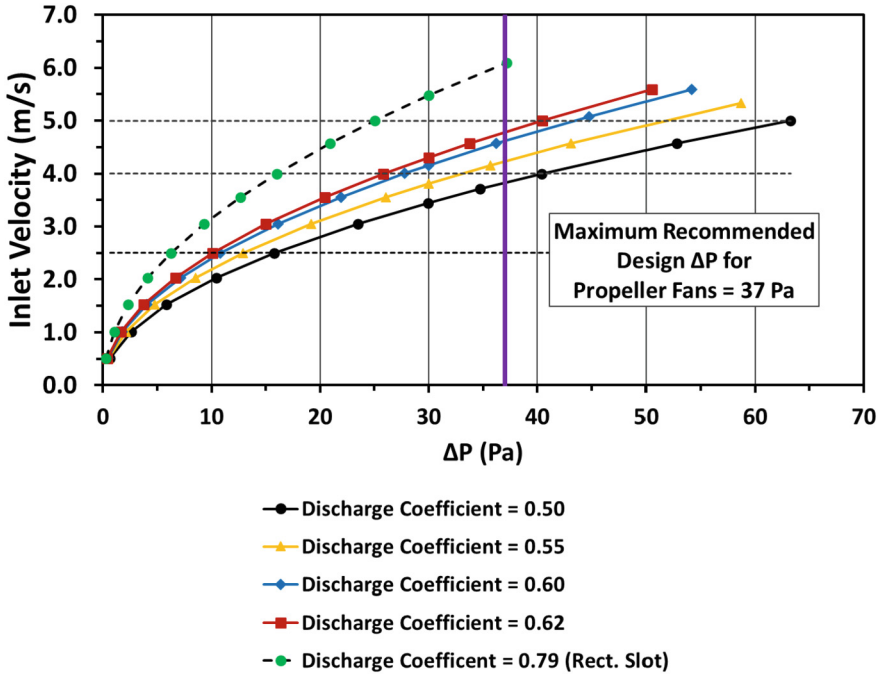
Fig. 6. Impact of the value of C_d on inlet velocities for ventilation of animal facilities (T = 10 °C, $\rho = 1.248$ kg/m^3).

iteration, it was determined that the minimum C_d that could be used to provide a V_{inlet} of 4.0 m/s at a ΔP of 30 Pa was 0.576 which corresponded to an aspect ratio of 0.026.

Another result that can be observed in Fig. 6 is that none of the baffled inlets with a C_d in the range of 0.50 to 0.62 can provide an inlet velocity of 5 m/s at $\Delta P = 30$ Pa or at the maximum practical ΔP of 37 Pa for propeller fans. It was determined that the inlet would require a C_d of 0.72 to provide a V_{inlet} of 5 m/s at $\Delta P = 30$ Pa. Some manufactured inlets with relatively high aspect ratios may be able to meet these requirements.

A rectangular slot inlet or curtain inlet ($C_d = 0.79$) would be advantageous for summer ventilation since an inlet velocity of 3.1 m/s can be provided at 10 Pa of pressure drop and 4.0 m/s at a ΔP of 16 Pa. Using lower operating ΔP values at high airflow rates will increase the airflow delivered per fan and increase the total airflow delivered per W of electricity used (Q/W) [8]. However, a C_d of 0.79 must be used to size the inlets and not a C_d of 0.60 as is commonly recommended [1–3].

The results observed from Fig. 6 clearly point out that using a better C_d estimate for sizing inlets will allow more precise control of the inlet velocity during winter ventilation and will allow for more energy efficient operation during summer. These results also clearly show that no single value of ΔP can be used in design and evaluation of the performance of a ventilation system. Instead of relying only on a ΔP measurement across the building envelop to estimate the inlet velocity, the system evaluator should

also measure the inlet velocity provided by the inlets for each stage of ventilation using a high-quality hot wire anemometer.

This brief discussion did not include the interaction between the fan curves of the equipment selected and the inlets. The reader is referred to Albright [2] or Hellickson and Walker [1] for a detailed treatment of methods to determine the actual operating point of inlets and fans for each stage of ventilation. Consideration of the fan and inlet interaction is mostly beneficial for sizing inlets for the minimum ventilation rate.

4   Conclusions

A model ventilation system that had a ceiling jet and wall jet inlet was used to collect 20 sets of inlet velocity versus pressure drop data. The opening widths (w) ranged from 8.18 to 32.6 mm and the aspect ratios (α = w/L) ranged from 0.008 to 0.030. The airflow per m (Q/L) values were calculated for each data point and the results were compared with published equations for ceiling and wall jet inlets. The results indicated that inlet orientation did not impact measured values of Q/L and all inlets with $\alpha \leq 0.018$ agreed with the published equation for the ceiling jet inlet. Furthermore, the empirically determined discharged coefficient (C_d) for all baffled inlets with $\alpha \leq 0.018$ was 0.502 ± 0.010 (95% C.I.) which was not significantly different from the value of 0.50 reported by Albright [5]. In addition, the value of C_d for baffled inlets was significantly correlated with respect to the aspect ratio of the inlet and a highly significant regression equation (Fig. 5, p < 0.0001) was developed from the data that can be used to predict C_d-values for α up to 0.030. None of the data obtained in this study agreed with the Q/L prediction equation or C_d values for the wall jet inlets reported in the literature.

The impact of using the correct value of C_d for inlet sizing was demonstrated for baffled slot inlets with C_d values ranging from 0.50 to 0.62 and a rectangular slot inlet with a C_d of 0.79. It was concluded that closer estimates of the C_d for the type of inlets installed in an animal production facility are needed to allow more precise inlet sizing during ventilation system design. The results also indicated that measuring the static pressure drop across the building envelop (ΔP) is not sufficient for setting the correct inlet velocity if the actual C_d of the installed inlet is unknown. In such a case, a ventilation system evaluator should measure the inlet velocity and ΔP for each stage of ventilation to precisely develop recommendations for retrofitting a ventilation system.

The results from this study will allow practitioners to calculate inlet velocities more accurately in many cases which will enhance overall system performance to provide the optimal environment for animal health and use fan energy more efficiently. Additional work is needed to empirically determine the discharge coefficients for the wide range of manufactured inlets that are available.

References

1. Hellickson MA, Walker JN (1983) Ventilation of Agricultural Structures. ASABE, St. Joseph, MI
2. Albright LD (1990) Environmental Control for Animals and Plants. ASABE, St. Joseph, MI
3. MWPS (1990) Mechanical ventilating systems for livestock housing (MWPS-32). MidWest Plan Service, Iowa State University, Ames, IA
4. Millier WF (1950) The ventilation of dairy stables with electric fans. Ph.D. diss., Cornell University Libraries, Itaca, NY
5. Albright LD (1976) Airflow through hinged baffle slot inlets. Trans ASAE 19(4):728–732,735
6. Chastain JP, Massey HF (2020) A model for teaching slot inlet theory for ventilation of animal housing structures. J Agric Syst Technol Manage 21:9–25
7. Chastain JP, Colliver DG, Winner PW (1987) Computation of discharge coefficients for laminar flow in rectangular and cylindrical openings. ASHRAE Trans 93(2B):2259–2283
8. Chastain JP, Anderson PT, Vassalos M (2017) Analysis of available efficiency and performance data for axial flow agricultural ventilation fans. Paper No. 1700116. ASABE, St. Joseph, MI. https://doi.org/10.13031/aim.201700116
9. Holman JP (1976) Heat transfer, 4th edn. McGraw-Hill Book Company, New York, NY

Using Composted Cow Manure to Improve Nutrient Content, Aeration Porosity, and Water Retention of Pine Bark-Based Potting Media

Tom O. Owino[1(✉)] , John P. Chastain[2] , and Hunter F. Massey[2]

[1] Department of Environmental Engineering and Earth Science, Brackett Hall, Clemson University, Clemson, SC 29634, USA
`towino@clemson.edu`

[2] Department of Agricultural Sciences, McAdams Hall, Clemson University, Clemson, SC 29634, USA

Abstract. Composted cow manure (CCM) was used as a potting media amendment. A common base mix of 8 parts pine bark and 1part sand was compared with 3 other mixes that contained 20%, 30%, and 40% compost (v/v). The plant nutrient concentrations of the base mix and the three CCM-base mix blends were compared with major plant nutrient concentrations provided by fertilizing the base mix with a common granular fertilizer. It was found that adding compost to the mix could replace a portion of the P_2O_5, all of the K_2O and about half of the nitrogen. The aeration porosity, total porosity, volumetric water holding capacity and bulk density of the four mixes were measured. The results indicated that mixing CCM with the base mix made a substantial improvement in the aeration porosity, total porosity, water holding capacity, and density. Water retention curves (WRCs) were developed using the dewpoint method for the four mixes with high levels of correlation. The R^2 values for the four fitted curves ranged from 0.87 to 0.94. The results indicated that the 40% CCM mix provided the best amount of readily available water for a plant. It was concluded that mixing CPM with a bark-sand base mix has the potential to reduce the need for non-renewable ingredients, such as peat moss, and to reduce fertilizer costs for a commercial nursery. The study delivers a template to prepare and analyze soil-like substrates regarding their WRCs using the dew point method**.**

Keywords: Compost · Potting Media · Water Retention Curve · Dew Point · Porosity

1 Introduction

Urban gardening is on the increase as an effective adaptation option for climate change. In addition, many commercial producers of container vegetables and ornamental plants are looking for natural, renewable potting mix ingredients to replace or reduce the need to add sphagnum of peat moss to improve aeration porosity and water holding capacity. Such potting media are usually amended with commercially produced slow-release granular

fertilizers to add major and minor plant nutrients. There is also interest in replacing or reducing the amount of commercial fertilizer needed to provide the nutrients needed for urban container gardening and commercial plant production. Therefore, the demand for natural, fertile potting media is on the increase in many parts of the world.

Many of our current cropping systems deplete the soil of organic matter, N, and P and require replenishing on an annual basis to ensure productivity. Organic producers typically add organic, N and P by adding organic material such as cow manure, which can in part mineralize and release N and P for plant uptake. However, federal and state regulations on animal farms have caused many in the animal industries to consider composting as an alternative manure treatment option. The resulting compost product could be used to enhance soil structure and provide nutrients for fruit and vegetable production, and container ornamental production [1]. Mixing composted cow manure with soilless media may provide a natural, more climate friendly alternative to commercial fertilizers for many of the nutrients needed to grow healthy plants.

Composting is considered a good way for recycling the surplus of manure as a stabilized and sanitized end product for agriculture [2]. It has been evaluated as an alternative to peat moss in pine bark media because it offers the advantages of supplying nutrients and improving the physical properties of the media [1, 3]. Disadvantages of including compost in the growing media include possible high total soluble salts and fine particle size [3].

Screened pine bark is a common primary ingredient for soilless potting mixes in the USA [1, 4–6]. Traditionally, the advantages of pine bark were good availability and low price. It has also been shown to contain enough phosphorus, potassium, calcium, magnesium, zinc, iron, and boron for production of plants in containers [4, 5]. The primary disadvantages of pine bark are its high bioavailable carbon content and low pH. Bioavailable carbon can cause immobilization of soluble nitrogen in the container resulting in a reduction of nitrogen that can be taken up by the plant [1, 7]. Low pH, on the order of 5.0, requires addition of lime to raise media pH if plants require a pH of 6.0 or more to grow efficiently.

Limited information is available that relates amount of compost added to a potting mix to the chemical and physical properties of the mix. The chemical properties of interest included pH, and concentrations of major plant nutrients (organic-N, soluble-N, P, K), secondary and minor plant nutrients (Ca, Mg, S, Zn, Cu, Mn, Fe), sodium, carbon, and organic matter. The physical properties that were important in evaluating a potting media were the aeration porosity (AP), water holding capacity (WHC), total porosity (TP), and dry bulk density (BD). The ideal amount of compost to add to potting mix would be the amount that adds plant nutrients that are similar to fertilized media blends used in the nursery industry while providing enhance aeration porosity and water holding capacity to maximize plant performance.

The other important physical characteristic investigated in this study is the potting media matric potential (PMP). PMP represents the forces that bind water molecules to solid particles and to each other in potting media pores, thus restricting the movement of water through the potting media matrix. Plants must apply a force greater than PMP to be able to extract water from the potting media. PMP is a negative pressure (suction) and the values have a negative sign. However, in his study the negative sign will not be

included in reporting PMP. A water retention curve can be used to graphically display the relationship between volumetric water content and PMP for a particular potting mix. The water retention curve is an important characteristic for describing water storage in potting media and water availability to plants. Knowledge of the water retention characteristic of a potting media may make it possible to reduce the loss of nutrients from potted plants through excessive watering. This curve can also be used for converting volumetric water content to PMP and vice versa.

A commercially available composted cow manure was used as a potting media amendment. Four potting media mixes were formulated that contained 0%, 20%, 30%, and 40% compost on a volume basis. The base mix (0% compost) was composed of 8 parts screened pine bark (PB) and 1 part sand on a volume basis. A common base mix of 8 parts pine bark and 1part sand was compared with 3 other mixes that contained 20%, 30%, and 40% compost (v/v). The remaining fraction of these three mixes was the base mix (bark and sand).

The primary objective of this study was to observe the impact of blending 0%, 20%, 30%, and 40% (v/v) of composted cow manure (CCM) with a standard bark-sand mix on the concentrations of major, secondary, and minor plant nutrients, sodium, carbon, organic matter, and key physical properties including aeration porosity, total porosity, water holding capacity, and bulk density. The second objective was to compare the plant nutrient and mineral composition of the three blends of CCM and base mix with the nutrient contents of the base mix blended with a commercially available slow-release granular fertilizer. The third objective was to develop water retention curves for the three CCM and base-mix blends with the pine bark and sand base mix.

2   Methods

Two bags of a blend of pine bark and forest by-products was obtained from a potting media manufacturer. The pine bark was sun dried for two days to prepare the materials for screening. For most nursery container mixes, 70% to 80% (by volume) of the particles should be in the range of 0.61 to 9.54 mm [3]. To achieve this specification, the pine bark mix was initially sifted with a 2.0 mm screen to reduce the very fine particles in the mix. The pine bark was screened again with a 6.35 mm screen to exclude particles greater than 6.35 mm. The arithmetic mean particle size of the screened pine bark used to make the base mix in this study was 4.18 mm.

Three bags of composted cow manure (CCM) were purchased from a local garden supply retailer. Based on information from the manufacturer the compost was made from dairy cow manure and wood waste in open, turned windrows.

Four potting mixes were formulated by mixing 0%, 20%, 30%, and 40% of the composted cow manure with a bark-sand base mix on a volume basis. The base mix selected was a mixture of 8 parts screened pine bark and 1 part builder's sand [6]. The ingredients not included, but would normally be added by a nursery producer, were lime for pH adjustment, and a granular slow-release fertilizer (SF) to provide a base-level of N, P_2O_5, and K_2O fertility for the base mix. Previous studies have shown that screened pine bark often provides sufficient concentrations of secondary and minor plant nutrients so that additional mineral products are often not needed [1, 5]. These additional ingredients

were not included because an objective of this study was to determine if adding CCM to the base mix would provide the required improvements in media pH and add amounts of N, P_2O_5, K_2O like adding granular fertilizer.

2.1 Plant Nutrients Measured

The composted cow manure was stored in a covered, plastic storage bin and the screened pine bark (PB) was stored in a separate plastic bin. Three well-mixed, samples were taken of each of these materials, CCM and PB, were collected to provide three replicate samples for analysis. The volume of each of the samples was about 500 mL and each sample was placed in a sealable plastic bag and transported to the Agricultural Services Laboratory at Clemson University for analysis. Each of the CCM and PB samples were analysed to determine the concentrations of total nitrogen (TN), total ammoniacal nitrogen (TAN = NH_4-N + NH_3-N), nitrate-N (NO_3-N), total phosphorous, total potassium, calcium (Ca), magnesium (Mg), sulphur (S), zinc (Zn), copper (Cu), manganese (Mn), iron (Fe), sodium (Na), and aluminium (Al). The total P and total K were reported as P_2O_5 and K_2O to correspond with commercial fertilizer specifications. Other characteristics measured included: moisture content (MC), total carbon content (C), organic matter content (OM), pH, electrical conductivity (EC_5), and dry bulk density.

Standard laboratory procedures were used for all analyses and details are summarized online by the laboratory director of the Agricultural Services Laboratory at Clemson University [8, 9]. The concentrations of TN and C were determined from a dried and ground sub-samples using the Elementar procedure. The TAN concentrations were measured by mixing a representative 2 g sub-sample in a flask containing 20 mL of KCl (2 M) followed by standard digestion and acid titration techniques. This method included the small amount of NH_3-N that was present in the samples. As a result, it provided a measurement of the total ammoniacal nitrogen content (TAN). The NO_3-N concentration was determined using the cadmium reduction method for solid manures. The organic-N concentration (Org-N) was calculated as:

$$[\text{Org-N}] = [\text{TN}] - [\text{TAN}] - [\text{NO}_3\text{-N}]. \tag{1}$$

All other elements (P, K, Ca, Mg, S, Zn, Cu, Mn, Fe, Al, and Na) were measured using ICP Mass Spectrometry [9]. The moisture content of all replicate samples was determined by drying a sub-sample in an oven maintained at 105 °C for 2.5 to 3 h and determining the weight of the dry matter fraction (DMF). The moisture content (%) was calculated as: MC = 100 (1-DMF). The organic matter (OM) was determined by burning a dry sample in a 360 °C furnace for 2.5 h. The OM was expressed as the percent of the dry matter and was calculated as the difference between the dry weight and the ash weight divided by the dry weight. The pH was measured after mixing a 15 mL sub-sample with 15 mL of deionized water and soaking for 30 min. The pH of the resulting solution was measured using a pH analyser.

The electrical conductivity (EC_5) was determined by making a 1:5 dilution of the sample with deionized water [8]. After allowing the slurry to equilibrate, an electrical conductivity meter was used to measure the conductivity in mmhos/cm.

2.2 Physical Properties

The physical properties included in this study were the total solids (TS), volatile solids (VS), bulk density (BD), aeration porosity (AP), water holding capacity (WHC), and total porosity (TP). The aeration porosity, water holding capacity, and total porosity were measured using a chamber that was designed for that purpose as described by Massey, et al. [10]. The procedures used to measure the WHC included the antecedent moisture content of the media prior to saturation.

Total solids (TS) and fixed solids (FS) of the compost, pine bark, and builders' sand were measured using standard oven-drying techniques [11]. Three replicate samples for each of these ingredients were dried in an oven at 105 °C for 24 h. Total solids content was determined by the difference in the wet and dry masses of the samples after cooling in a desiccator. Fixed solids content (ash) was determined by incinerating the dried solids in a furnace at 550 °C for 24 h, allowing the sample to cool, and determining the sample mass. Volatile solids were calculated as the difference between the total and fixed solids. The moisture content was calculated as 100 – TS (%). The fraction of the TS that was VS (VS/TS) was calculated from the data to describe the composition of the dry matter. A high value of VS/TS indicated the lack of soil and minerals in the material and would be indicative of a soilless media ingredient (*i.e.*, PB and CCM). A very low value of VS/TS would indicate that a media ingredient was low in organic matter and contained mostly minerals or soil.

Bulk Density. The density of the composted poultry litter, pine bark, sand, and each potting media mix was measured using a calibrated aluminium container (323 ± 1.71 mL). The density of each media ingredient and mix was determined by filling the calibrated container with a well-mixed sample, measuring the mass of the sample, and dividing the sample mass by the container volume. Three replications were performed for each material. The dry bulk density (g DM /cm^3) was calculated as the wet bulk density (g sample/cm^3) divided by the dry matter fraction (g DM /g sample).

Aeration Porosity, Water Holding Capacity, Total Porosity. The aeration porosity, water-holding capacity and total porosity of a potting media, or individual ingredient, is typically measured and reported on a wet volume basis. The aeration porosity is defined as the percentage of saturated media which is occupied by air after completely draining water from the media by gravity. The volume of the water drained ($V_{DRAINED}$) was measured and represents the volume of the pores occupied with air at 100% water holding capacity. The aeration porosity (AP, %) was calculated as [12]:

$$AP = (V_{DRAINED}/MV)\ 100. \tag{2}$$

The total porosity is defined as the percentage of the media that is occupied by open pores on a volume basis at saturation. The defining relationship for the total porosity (TP, %) was [12]:

$$TP = (PV/MV)\ 100, \tag{3}$$

where PV is the water added to saturate media and fill pore volume (mL), and MV is the volume of solid media and pores (mL).

The water holding capacity is defined as the percentage of the media and pore volume that is occupied by water at saturation. The suggested water holding capacity (WHC) equation given by BCMA [12] was: WHC = TP - AP. However, Calculation of WHC as the difference between TP and AP did not account for the antecedent moisture content prior to adding water to reach saturation and fill the pore volume. To account for the antecedent moisture, the defining equation for the water holding capacity was rewritten as:

$$WHC = (V_{TW}/MV)\ 100. \tag{4}$$

The total water volume (V_{TW}) was the amount of water contained in the media plus the amount of water required to bring the media to saturation and fill the pore volume. The total water volume was calculated based on the antecedent moisture content and the volume required to reach saturation as:

$$V_{TW} = 1/\rho_w(MC_I/100) \times M_{PM}) + V_{WR}, \tag{5}$$

where ρ_w was the water density (1g/ mL); MC_I was the initial moisture content of media (wet basis, %); M_{PM} was the mass of potting media before adding water (g); and V_{WR} was the volume retained by media after draining (mL). The volume of water retained was defined as the difference in the volume of water added (VA_{DDED}) to fill the total pore space and the volume of water drained. The water volume retained (V_{WR}) was calculated as:

$$V_{WR} = V_{ADDED} - V_{DRAINED}. \tag{6}$$

The total porosity was calculated using Eq. (2) for AP and Eq. (4) for WHC as:

$$TP = AP + WHC. \tag{7}$$

A test chamber was designed and constructed to facilitate the measurement of the aeration porosity, and water holding capacity [10]. The chamber was constructed from a section of acrylic pipe with an inside diameter of 14.6 cm and a height of 8.25 cm. The bottom was a round, 0.635 cm thick piece of acrylic sheet that was chemically welded to the pipe to form a water-tight seal. Three holes were drilled in the bottom of the chamber and were fitted with rubber stoppers that were flush with the inside surface of the bottom of the chamber when fully inserted. A circular piece of plastic window screen (1.27 mm openings) was placed in the bottom of the test chamber to retain the media while water was allowed to drain from the pore volume. The chamber was placed on a level metal rack that facilitated the collection of water drained from saturated potting media in a container. The chamber was calibrated to a volume of 1364.7 mL which corresponded to the volume of media contained in commonly used 15 cm diameter pots.

The test chamber was used to determine the aeration porosity and the water holding capacity of screened pine bark, the base mix (8 parts PB and 1 part sand), and the three mixes that contained 20%, 30%, and 40% CCM using the following procedure.

1. The media to be tested was placed into a large plastic container and water was added to increase the moisture content. It was determined that if extremely dry media was

used the pine bark would float and it would take a prohibitively long time to saturate the media. After water was added to the media a tightly fitting cover was used to minimize evaporation between replications.

2. A large sample of the moistened potting media was removed from the storage container and the moisture content was measure using standard oven drying techniques (105 °C oven for 24 h). This provided a measure of the initial or antecedent moisture content and was used in Eq. (5).

3. The test chamber was filled with media to the 1364.7 mL mark. This was the value used for media volume (MV) in Eq. (2) and (4). The chamber was dropped onto a hard surface from the height of 7.6 cm four times and additional media was added to re-fill the container to the 1364.7 mL mark. This was done to ensure consistent compaction for all replications of all four potting mixes.

4. The test chamber full of media was placed on a level rack and a plastic container was placed below the rack.

5. Water was slowly added to the media using a graduated cylinder until the solids were completely saturated and the pore volume was full. When this had been achieved, no air bubbles were present in the media and the surface of the media glistened. The total volume of water added (V_{ADDED}) was recorded and was used in Eq. (6).

6. The three rubber stoppers were removed, and water was allowed to drain from the pore space of the media until all dripping stopped (approximately 1 h per replication). The total amount of water that drained from the test chamber was measured using a graduated cylinder and was recorded. The volume drained ($V_{DRAINED}$) was used in Eq. (2) and (6) and the calculation of the AP and WHC was completed.

This procedure was followed for three replications of each of the four potting mixes.

2.3 Calculation of Chemical and Physical Properties of the Potting Mixes

The plant nutrient, sodium, carbon, and organic matter concentrations, bulk density, and pH were measured for screened pine bark and the composted cow manure. The only properties measured for the sand that was used to make the base mix were the moisture content and the bulk density. The pH of the sand was not measured; however, the pH of sand was about 7.0 according to the literature [13]. The concentrations of all the elements and compounds (% d.b.) contained in the four potting mixes were calculated using the mean values for two ingredients using the following formula:

$$[C_{j\,MIX}] = \left[(\Pi_{j1}BD_1V_1 + \Pi_{j2}BD_2V_2)/(BD_1V]_1 + BD_2V_2)\right] \times 100, \quad (8)$$

where [$C_{j\,MIX}$] was the concentration of nutrient C_j of the mixture of the two ingredients (% d.b.); Π_{j1} was [C_{j1}]/100 (g C_{j1}/g DM_1); BD_1 was the bulk density of ingredient 1 (g DM/cm^3); V_1 was the volume of ingredient 1 (cm^3); Π_{j2} was [C_{j2}]/100 (g C_{j2}/g DM_2); BD_2 was the bulk density of ingredient 2 (g DM/cm^3); and V_2 was the volume of ingredient 2 (cm^3).

The chemical composition of the base mix was calculated first using the concentration data and measured BD for the screened pine bark (ingredient 1) and the BD of the sand (ingredient 2). It was assumed that the sand did not contribute plant nutrients to the base

mix. The volume of the pine bark was 800 cm^3 (V$_1$) and the volume of the sand was 100 cm^3 (V$_2$). The bulk density of the base mix was calculated based on total mass of dry matter in the mix and the total volume of the mix (V$_T$ = V$_1$ + V$_2$) as:

$$BD_{MIX} = (BD_1V_1 + BD_2V_2)/V_T. \tag{9}$$

The pH and moisture content of a mix of two ingredients was calculated as a weighted average based on the volumes of the two ingredients as:

$$pH_{MIX} = pH_1(V_1/V_T) + pH_2(V_2/V_T), \text{ and} \tag{10}$$

$$MC_{MIX} = MC_1(V_1/V_T) + MC_2(V_2/V_T). \tag{11}$$

After the chemical concentrations ([C$_{jMIX}$]), BD$_{MIX}$, pH$_{MIX}$ and MC$_{MIX}$ of the base mix were calculated the composition of each of the three mixes that contained 20%, 30%, and 40% CCM were calculated using Eq. (8) through Eq. (11) using the base mix results as the first ingredient and the data for the composted poultry litter as the second ingredient. The total volume of mix used in the calculations (V$_T$) was 1000 cm^3. The 20% CCM mix used 800 cm^3 for the pine bark (V$_1$) and 200 cm^3 for the CCM (V$_2$). The volumes for the other two mixes were V$_1$ = 700 cm^3 and V$_2$ = 300 cm^3 for 30% CCM, and V$_1$ = 600 cm^3 and V$_2$ = 400 cm^3 for 40% CCM.

A common practice in commercial woody ornamental production is to add slow-release pellet fertilizer (SF) to large volumes of container media to provide base-levels of TN, P$_2$O$_5$, and K$_2$O fertility prior to filling pots with media [4, 14]. After planting, additional fertilizer is provided either through irrigation water or by surface application of granules to meet the specific needs of the plants being produced. Many fertilizer formulations are available, but a commonly used product contained 14% TN, 14% P$_2$O$_5$, and 14% K$_2$O. Recommended fertilizer application rates for general fertilization of media range from 2 to 5 kg m^{-3} of media [4]. Some producers also add fertilizers that provide secondary and minor plant nutrient (*e.g.*, Ca, Mg, Mn, Zn). However, pine bark often provides enough of these nutrients [1, 5].

Mixing CCM with the base mix used in this study was expected to provide P$_2$O$_5$, K$_2$O, and many secondary nutrients that would typically be added to media via application of commercial fertilizers. In order to compare the nutrient contents of the three mixes containing CCM with a typical fertilized base mix the concentrations of plant nutrients that would be achieved by blending 2 and 5 kg of slow-release fertilizer (SF) per m^3 of base mix were calculated using Eq. (8) and Eq. (9) assuming a SF analysis of 8.2% NH$_4$-N, 5.8% NO$_3$-N, 14% P$_2$O$_5$, and 14% K$_2$O with a BD of 1.205 g/cm^3 (data obtained from product specifications). This allowed comparison of the nutrient composition of the unfertilized base mix, the base mix blended with 2 kg SF m^{-3}, the base mix blended with 5 kg SF/ m^3, the 20% CCM mix, the 30% CCM mix, and the 40% CCM mix. The nutrient concentrations of all six of these blends were converted to a volume basis ([VC$_{j\,MIX}$]; g C$_{j\,MIX}$/m^3) using the following formula:

$$[VC_{j\,MIX}] = 1,000,000\, BD_{MIX}[C_{j\,MIX}]/100. \tag{12}$$

Not all the organic nitrogen contained in pine bark or compost will be mineralized during the first growing season. Several publications have indicated that bark-based soil

amendments tend to immobilize soluble-N requiring increased N fertilization to achieve good plant performance [1, 5, 7, 14]. Franklin et al. [7] measured the release of organic-N for fourteen soil amendments that included un-composted pine bark soil conditioners and several types of compost. They reported the following correlation to estimate the mineralization factor (m $_{fCS}$, g N released /g Org-N applied) for the range of products included in their study [7]:

$$m_{fCS} = 0.139 - 0.0036 \text{ C:N}, \ R^2 = 0.84. \tag{13}$$

The correlation provided by Franklin et al. [7] was used to estimate the amount of Org-N that would be released during a growing season based on the C:N of the four potting mixes. The plant available nitrogen was estimated for each mix using the following relationship:

$$[\text{PAN-est}] = m_{fCS}[\text{Org-N}] + [\text{TAN}] + [\text{NO}_3\text{-N}]. \tag{14}$$

The phosphorus contained in compost and bark-based soil amendments is also not all available to a plant during the first growing season [7, 15]. Franklin et al. [7] observed the release of P after mixing a soil conditioner that contained chopped pine bark and forest by-products with soil in a laboratory incubation study. Their results indicated that soil amended with such a product would experience immobilization of P, release of P, and re-immobilization of P over a full growing season (214 d). Therefore, none of the P_2O_5 contained in un-composted pine bark could be relied upon to fertilize a plant. The fraction of P released for pine bark (PR_f, g P released/ g P applied) was zero for practical estimation. The full-season P release for manure-based compost products mixed with soil ranged from 24% to 64% which was similar to the range of 25% to 40% reported by Rynk et al. [15]. The value of PR_f used to estimate the availability of P_2O_5 contained in the composted cow manure was 0.40 which was about the average observed for manure-based compost [7, 15]. The general relationship that was used to estimate the available P_2O_5 (AP_2O_5-est) contained in the mixes was:

$$[\text{AP}_2\text{O}_5-\text{est}] = 0.40 \ f_{CCM}[\text{P}_2\text{O}_5]_{MIX} + [\text{P}_2\text{O}_5]_{SF}, \tag{15}$$

where f_{CCM} was the fraction of the $[P_2O_5]$ in the mix ($[P_2O_5]_{MIX}$) supplied by CCM on a volume basis, and $[P_2O_5]_{SF}$ was the $[P_2O_5]$ supplied by granular fertilizer and was calculated as $[P_2O_5]_{MIX} - [P_2O_5]_{Base\ Mix}$.

The volumetric concentrations of all of the measured plant nutrients, as calculated from the data using Eq. (12), the C:N ratios, and the estimates of available N and P_2O_5 contained in the three mixes that contained CCM were compared with the nutrient composition and C:N ratios of the base mix and the base mixed fertilized at the rates of 2 kg SL/m^3 and 5 kg SL/m^3. These results would indicate if the CCM could replace a portion, or all the fertilizer needed to prepare a mix prior to filling pots and planting.

2.4 Water Retention Curves for Compost Mixes

Water retention curves (WRC) for four potting media mixes were determined using the WP4C dew point method. The WP4C measures water potential by determining the

relative humidity of the air above a sample in a sealed chamber. Once the sample comes into equilibrium with the vapor, relative humidity is determined using the chilled mirror method.

Water Retention Curves Developed using Dew Point Method. The dew point apparatus used was the WP4C meter (Decagon Devices, WP4C Dewpoint PotentiaMeter) and is shown in Fig. 1.

Fig. 1. Image of the WP4C on left shows the front side view with headspace closed. On right is the WP4C with headspace open showing location of sample cup.

The water potential of a solid or liquid sample using the dew point method can be found by relating the sample water potential reading to the vapor pressure of air in equilibrium with the sample. The relationship between the sample's water potential (Ψ) and the vapor pressure of the air is [16]:

$$\Psi = (RT/V) \times \ln (P/P_0).   \tag{16}$$

where P was the vapor pressure of the air (MPa); P_0 was the saturation vapor pressure at sample temperature; R was the gas constant (8.31 J/mol K); T was the Kelvin temperature of the sample (K); and V was the molecular volume of water (m^3/mol). The vapor pressure of the air was measured by a chilled mirror, and P_0 was computed from the sample temperature.

The WP4C measured water potential by equilibrating the liquid water phase of the sample with the vapor phase in the headspace after closing the chamber. Water potential was then determined by measuring the vapor pressure of the headspace. Each sample was placed in a sample cup, which was sealed against the sensor block. There was a fan, a dew point sensor, a temperature sensor, and an infrared thermometer inside the sensor block. The dew point sensor measured the dew point temperature of the air, and

the infrared thermometer measured the sample temperature. The purpose of the fan was to speed equilibrium and to control the boundary layer conductance of the dew point sensor.

From these measurements, the vapor pressure of the air in the headspace was computed as the saturation vapor pressure at dew point temperature. When the water potential of the sample and the headspace air were in equilibrium, the measurement of the headspace vapor pressure and sample temperature (from which saturation vapor pressure was calculated) gave the water potential of the sample.

In addition to equilibrium between the liquid water phase in the sample and the vapor pressure, the internal equilibrium of the sample itself was also important. If the sample was not at internal equilibrium, one would measure a steady-state vapor pressure (over the period of measurement) which was not the true water potential of the sample.

The WP4C was calibrated prior to measurement for each media mix. Verification standards were specially prepared salt solutions of known specific molarity and water potential. The acceptable range of water potential reading was ± 0.05 MPa. If the value was over the range, the equipment was cleaned and recalibrated until the value was within the acceptable range.

The WP4C continuously provided accurate water potential measurements if its internal sensors were not contaminated. Careful preparation and loading of samples lengthened the time between cleaning but minimized downtime and repairs. The procedure used with the WP4C is provided below [17].

1. Six 500 mL plastic bottles were prepared with each containing 100 g of oven dry base mixture. 10 g, 20 g, 30 g, and 40 g of water were added to the bottles separately. This resulted in a media mass wetness θ_m of 0.1, 0.2, 0.3, and 0.4.
2. Sealed bottle containing media and water was then shaken for approximately two minutes to ensure thorough mixing before transferring sample to a plate. This sample was then transferred to the WP4C disposable plastic cups.
3. The sample cup was filled with the mix to the half full mark. Overfilled cups can contaminate the sensors in the chamber (more was not necessarily better).
4. The sample cups were placed in the chamber for matric potential measurement.
5. Steps 2 to 4 was repeated for 20%, 30%, and 40% mixtures to obtain respective sample matric potential values.

3   Results

The chemical and physical properties of the screened pine bark, composted cow manure and sand used to formulate the four potting mixes are compared in Table 1. The values shown are the means of three observations along with the standard deviations (s) for each characteristic. The only measurements that were included for the sand were the bulk density, moisture content, and VS/TS.

Comparison of the concentrations of the major plant nutrients indicated that CCM contained 2.6 times more TN than screened pine bark. The TN in pine bark was composed of 94% Org-N with only a small amount of soluble TAN. By comparison, 98% of the TN in CCM was organic with the same TAN content as PB. The composted cow manure contained 11.7 times more P_2O_5 and 4.6 times more K_2O than the pine bark. While the

Table 1. Chemical and physical properties of the screened pine bark (PB), composted cow manure (CCM), and sand used to make the four potting mixes.

	Screened Pine Bark - PB		Composted Cow Manure - CCM			
	Mean (% d.b.)	s (% d.b.)	Mean (% d.b.)	s (% d.b.)		
TAN	0.02	0.040	0.02	0.035		
Org-N	0.34	0.050	0.90	0.040		
NO_3-N	0.000	0.00	0.002	0.0002		
TN	0.36	0.064	0.92	0.020		
P_2O_5 [A]	0.06	0.023	0.70	0.017		
K_2O [B]	0.12	0.029	0.55	0.025		
Ca	0.22	0.021	3.97	0.221		
Mg	0.03	0.006	0.25	0.010		
S	0.03	0.006	0.32	0.015		
Zn	0.0019	0.0002	0.0155	0.0005		
Cu	0.0007	0.0003	0.0084	0.0013		
Mn	0.0059	0.0004	0.0129	0.0003		
Fe	0.0362	0.0074	0.3728	0.0830		
Na	0.0062	0.0037	0.0953	0.0030		
Al	0.0667	0.0083	0.6985	0.0525		
C	54.94	0.267	17.00	0.283		
OM	97.20	0.557	26.13	0.252		
					Sand	
					Mean	s
C:N	153	30.8	18.5	0.51	NM [C]	NM
EC_5 (mmhos/ cm)	0.20	0.010	1.84	0.053	NM	NM
pH	4.57	0.058	8.20	0.000	7.0 [D]	NM
Moisture (%)	17.45	0.480	46.47	1.155	3.7	0.328
BD (g DM/cm^3)	0.164	0.002	0.348	0.007	1.143	0.010
VS/TS	0.994	0.0014	0.310	0.003	0.0028	0.0003

[A] To convert P_2O_5 to total P divide by 2.29.
[B] To convert K_2O to total K divide by 1.21.
[C] NM = not measured.
[D] pH of sand [13].

pine bark contained significant, but small amounts, of the secondary and minor plant nutrients, the CCM contained 18.0 times more Ca, 8.3 times more Mg, and 2.2 times more Mn than pine bark.

Pine bark contained more C and OM than CCM resulting in a much higher C:N ratio for the pine bark. The C:N of the pine bark was 153:1 as compared to 18.5:1 for the composted cow manure. The high C:N of the pine bark would be expected to immobilize a large portion of the soluble N provided by any type of N fertilizer [7]. Addition of a lower C:N compost to a potting mix would be expected to lower the C:N and may improve N availability.

The most potentially harmful element to plants measured in this study was sodium since it is typically in a non-nutritive salt form (NaCl). Composted cow manure contained about 15.3 times more Na than the pine bark indicating that the amount of Na applied to the mix may be a limiting factor in selecting the optimum blend of the base mix and CCM. However, the electrical conductivity (EC_5), which is a general indicator of total soluble salts, was not excessively high for either mix ingredient [1].

The high value of VS/TS for the pine bark, 0.994, indicated that it contained very little soil. The very low VS/TS of the sand indicated that it was clean and not contaminated with organic matter.

Finally, the pH of the pine bark was very low at 4.57 and agreed with other published values [1, 5]. The higher pH of the CCM (8.20) would be expected to improve the pH of the mix when blended with pine bark and sand.

As expected, the bulk density of the sand was the greatest and the MC of the sand was the lowest. The BD of the pine bark was essentially the same as published values provided by Baumscha et al. [5] and BCMA [12]. The extreme variation in ingredient moisture contents mandated that all blending calculation be performed on a dry matter basis.

3.1   Comparison of the Nutrient Concentrations of the Base Mix and the Mixes Fertilized with Compost or Slow-Release Fertilizer

The dry matter concentrations of all the measured nutrients and elements were calculated for the base mix (8 parts PB:1 part sand), the base mix fertilized with 2 and 5 kg of slow-release fertilizer per m^3, and the three CCM blends using the data shown in Table 1 with Eqs. (8) and (12). Also, the weighted mean values of BD, pH, and MC were calculated using Eqs. (9), (10), and (11). These results, along with estimates of the available nitrogen and P$_2$O$_5$ (Eqs. (14) and (15)) are provided in Table 2.

Comparison of the Base Mix with the CCM Blends. As expected, blending CCM with the base mix resulted in substantial increases in the concentrations of in the TN. The TN concentration was increased by a factor of 2.0 to 3.0 as the percentage of CCM was increased from 20% to 40%. Also, adding CCM added a small amount of nitrate-N. Adding CCM to the base mix decreased the carbon content from 80237 g/m^3 for the base mix to 71823 g/m^3 for the 40% CCM mix. The increase in TN and small decrease in C provided a large decrease in C:N that would be expected to improve the availability of the Org-N [7]. The best improvement in C:N was the 70% decrease provided by using CCM for 40% of the potting mix.

Table 2. Comparison of plant nutrient contents, C:N, pH, and BD of the pine bark and sand base mix (B-M) blended with 2 to 5 kg/m^3 of a commercially available slow-release fertilizer with the mixes blended with 20%, 30%, and 40% composted cow manure (CCM).

	B-M	B-M + 2 kg SF/m^3	B-M + 5 kg SF/m^3	20% CCM	30% CCM	40% CCM
	(g/m^3)	(g/m^3)^A	(g/m^3)^A	(g/m^3)	(g/m^3)	(g/m^3)
TAN	34	198	442	41	45	48
Org-N	497	496	495	1023	1286	1549
NO$_3$-N	0	116	289	2	2	3
TN	531	809	1226	1065	1333	1600
m $_f$ CS	−0.41	−0.22	−0.10	−0.12	−0.06	−0.02
PAN-est	−167	206	684	−78	−31	16
PAN-est/TN	−32%	25%	56%	−7%	−2%	1%
P$_2$O$_5$	93	372	789	562	796	1031
AP$_2$O$_5$-est	0	279	695	45	96	165
AP$_2$O$_5$-est/P$_2$O$_5$	0%	75%	88%	8%	12%	16%
K$_2$O	170	450	867	517	691	864
Ca	316	316	315	3021	4373	5726
Mg	49	49	48	213	295	378
S	49	49	48	264	372	480
Zn	3	3	3	13	18	23
Cu	1	1	1	7	9	12
Mn	9	9	9	16	20	23
Fe	53	53	53	302	426	551
Na	9	9	9	74	106	138
Al	97	97	97	565	798	1032
C	80237	80104	79906	76030	73926	71823
OM	141964	141729	141378	131777	126683	121589
pH	4.8	4.8^B	4.8^B	5.5	5.8	6.2
C:N	151	99.0	65.2	71.4	55.5	44.9
BD (g DM/cm^3)	0.273	0.275	0.277	0.288	0.296	0.303
MC (%)	20.7	20.7^B	20.7^B	25.8	28.4	31.0

^{A} Slow-release granular fertilizer (SF) contained 8.2% NH$_4$-N, 5.8% NO$_3$-N, 14% P$_2$O$_5$, and 14% K$_2$O with BD = 1.205 g/cm^3.
^{B} Actual values unknown. However, the mixture with SF was expected to be similar to the base mix

The PAN estimates given in Table 2 (using Eq. (14)) indicated that the large amount of bioavailable carbon in the base mix would be expected to immobilize N at the rate of - 167 g N/m^3 greatly inhibiting plant growth. Blending the base mix with 20% to 40% CCM resulted in a decrease in C:N which yielded PAN estimates ranging from -78 g PAN/m^3 at 20% CCM to 16 g PAN/ m^3 at 40% CCM. These results indicate that the minimum amount of CCM needed to overcome the PAN-deficit caused by immobilization of N was 40% CCM on a volume basis.

Blending the CCM with the base mix provided a large increase in the P_2O_5 and K_2O fertility of the soilless media. Using Eq. (15) to estimate the available P_2O_5, indicated that none of the P_2O_5 contained in the pine bark would be expected to be available to grow a plant. Addition of CCM to the mix provided 45 to 165 g AP_2O_5/m^3 with the 40% CCM blend providing the most benefit. The potash (K_2O) contained in the pine bark and the compost provided a substantial amount of K fertility. Addition of CCM to the soilless media increased the K_2O content by a factor of 3.0 for the 20% CCM mix and a factor of 5.1 for the 40% CCM mix.

The addition of CCM to a pine bark and sand mix will most likely eliminate the need to purchase secondary or minor plant nutrients since the values were much larger than provided by the PB alone. The most undesirable increase was for Na. However, the Na content of all the CCM blends was lower than for the CCM alone which was 332 g/m^3 after converting the mean concentration provided in Table 1 to a volumetric concentration using Eq. (12). These results indicate that using a compost product similar in composition to the one used in this study would eliminate the need to purchase a secondary and minor nutrient product to blend with potting media.

The weighted mean values of pH in Table 2 indicated that the base mix had a pH of 4.8 and was below the preferred range of 5.5 to 6.4 [4]. At high values of pH (greater than 6.5) the availability of Fe and other minor plant nutrients will typically be reduced and is to be avoided [4, 14]. Addition of 20% to 40% CCM to the base mix increased the pH to 5.5 to 6.2 which was in the range that would be suitable for growing many plants. These results indicate that blending CCM with a bark-sand mix may provide the required pH adjustment and reduce or eliminate the need for adding lime to the mix.

Addition of CCM to the base mix provided a slight improvement in MC simply because the CCM was wetter than the PB. If wetter material were used to make the blends the MC would be higher.

Comparison of the Fertilized Media with the CCM Blends. Most nursey managers add slow-release granular fertilizer (SF) to soilless media to provide a base level of N, P_2O_5, and K_2O fertility. Typical application rates are 2 to 5 kg of SF per cubic meter of media. The plant nutrient concentrations resulting from mixing 2 to 5 kg SF/m^3 with the base mix are also shown in Table 2.

Addition of 2 to 5 kg slow-release fertilizer per m^3 to the base mix overcame the N-deficit to provide 206 to 684 g PAN per m^3. The proportion of the TN that was estimated to be available ranged from - 32% for the unfertilized base mix to 56% after adding 5 kg SF per m^3. By comparison, CCM would need to be blended at 40% by volume to provide a small amount of available N. The primary advantage of using CCM in the mix would be to reduce the amount of slow-release fertilizer needed to achieve the desired N fertility for soilless media. If the mix contained 60% base mix and 40% CCM the N

added from the fertilizer would become about 100% available. The N fertilization rates using slow-release fertilizer were 808 and 1226 g TN/m^3. Blending 40% CCM with the base mix prior to fertilization would reduce the rates needed to provide the equivalent amounts of plant available-N by 75% if the desired rate was 200 g PAN/m^3 and by about 44% if the desired rate was 680 g PAN/m^3. Therefore, blending CCM with the base mix has the potential to significantly reduce the need for N fertilizer,

The estimates of available P$_2$O$_5$, Eq. (15), given in Table 2 indicate that none of the CCM blend provided enough AP$_2$O$_5$ to eliminate the need for addition of granular fertilizer. However, the 40% CCM mix would be able to provide 59% of the AP$_2$O$_5$ provided by the fertilizer applied at the 2 kg SF/m^3 rate and 24% of the AP$_2$O$_5$ provided by the fertilizer applied at the 5 kg SF/m^3 rate. Therefore, blending CCM with the base mix at the rate of 40% by volume may reduce the amount of granular P$_2$O$_5$ fertilizer needed to provide a target fertility value for container media.

The most valuable major plant nutrient in the compost was K$_2$O. The 20% CCM mix provided 15% more K$_2$O than adding SF at the 2 kg/m^3 rate and the 40% CCM mix provided about the same K$_2$O fertility as the blending the base mix with 5 kg SF/m^3.

The results from this study suggest that blending CCM with a bark and sand base mix could supply the K$_2$O fertility that would normally be provided by granular fertilizer, and significant amounts of the P$_2$O$_5$ needed to grow plants. The small available nitrogen added by CCM may only be sufficient to overcome the N-deficit caused by immobilization of N to decompose the bioavailable carbon contained in the pine bark. Instead of blending a 14-14-14 granular fertilizer in the media the use of at 40% CCM by volume may allow the use of smaller amounts of 14-14-0 fertilizer. The other benefit may be the elimination of the need to add lime to the base mix to raise the pH to the desired range.

These results only apply directly to the materials used in this study. However, another type of compost could be evaluated in a similar manner by having samples of the soilless media and compost analysed for plant nutrients, carbon, and bulk density and following the calculation procedures described with Eqs. (8) through (15). If the compost being considered contained more nutrients than the CCM used in this study, then the percentage of compost in the optimal mix may be less than 40% compost by volume.

3.2 Impact of Blending Compost with the Base Mix on WHC, AP, TP, and BD

Proper plant growth is affected by the physical properties of the potting media. A good media must retain adequate water and air. As a result, the aeration porosity (AP) and the water holding capacity (WHC) are of great importance. A media that does not retain enough water at saturation will also tend to lose excessive amounts of soluble nutrients via drainage water resulting in a decrease in the efficiency of fertilizer use. The AP and WHC were measured for the for potting mixes using the previously described procedure with Eqs. (2), and (4), and the total porosity (TP) was calculated from the results, Eq. (7). The bulk density of each of the mixes was measured for each of the mixed as described previously (Methods). The means of these physical properties are compared in Table 3.

The water holding capacity (WHC) increased as the percentage of CCM in the mix increased. However, only the 40% CCM blend had a WHC within the desirable range of 45% to 65% [3].

Table 3. Mean water-holding capacity (WHC), aeration porosity (AP), total porosity (TP), and bulk density (BD) of the base mix and the three composted cow manure (CCM) blends.

	Base Mix	20% CCM	30% CCM	40% CCM
WHC (%)	41	41	43	45
	Desirable range for WHC = 45% to 65%[B]			
AP (%)	32	29	27	25
	Desirable range for AP = 10% to 20% [B]			
TP (%)	73	70	70	70
	Desirable range for TP = 50% to 70% [B]			
BD (g $_{DM}$/cm^3)[A]	0.21	0.26	0.28	0.28

[A] These bulk densities were measured after formulating the base mix and the three mixes that were blended with CCM as described in Methods.
[B] Robbins and Evans [3]

The desirable value for aeration porosity is in the range of 10% to 20% [3]. The high AP value of 32% for the base mix indicated that a significant amount of sphagnum or peat moss or another ingredient would be required to improve aeration. Mixing CCM with the base mix made a substantial improvement in the AP. The 40% CCM had an AP of 25% indicating that it was still higher than desired. Therefore, a small amount of an organic or synthetic bulking material would be needed to provide an AP of 20%. Increasing the amount of CCM used to 45% may provide the needed improvement in AP. However, adding too much CCM would have the potential to increase the pH too much.

The total porosity was the sum of WHC and AP. The total porosity (TP) of the base mix was too high when compared to the desirable range of 50% to 70% [3]. Addition of 40% CCM to the base mix lowered the TP to 70%. However, additional CCM or another material would still be needed to improve aeration.

A pot should be heavy enough to prevent tipping due to plant weight or wind. Addition of CCM resulted in an increase in the dry bulk density of potting media and would be expected to reduce pot tipping.

3.3 Water Retention Characteristics of the Mixtures Using the Dew Point Method

The trend in the moisture release curves for the four mixes was best described by a power function. A sample water retention correlation is shown with the data for the 40% CCM mix in Fig. 2. All the fitted power equations, bulk densities, and values of R^2 for the four mixes using the dew point method are summarized in Table 4. The value of the R^2 ranged from 0.87 for the 20% CCM mix to 0.94 for the 30% CCM mix indicating a high level of correlation between the data and the equations for all four mixes.

Water potential measurements represent the amount of water that can be extracted by a plant. Whereas volumetric water content measurements only indicate the amount of water in the soil. A soil with a low volumetric water content can have plenty of plant-available water and a soil with a high-water content can have almost none.
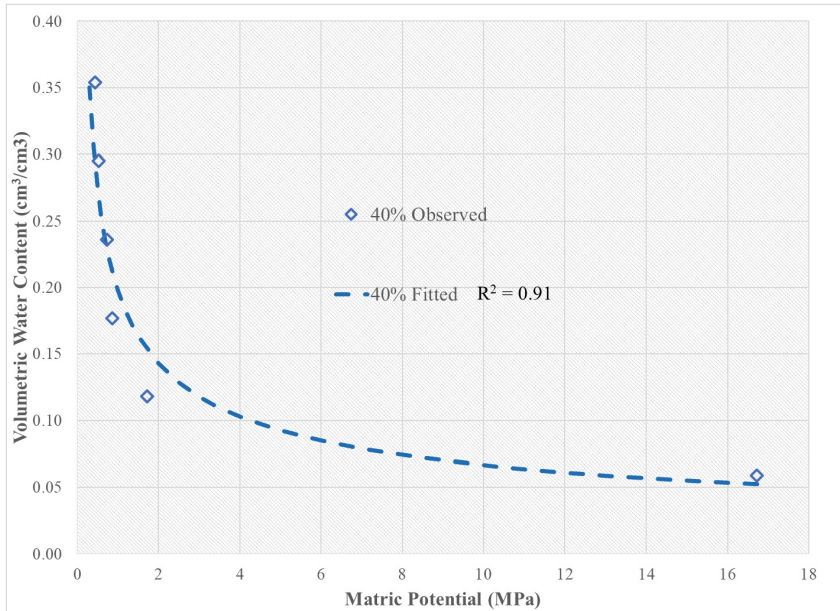
Fig. 2. Sample correlation using the observed water retention data and the fitted water retention curve for 40% CCM using the dew point method (WP4C).

Table 4. Power equations, R^2- values, and bulk densities of the four potting mixes.

Mix	Bulk Density (g/cm^3)	R^2	Equation	PWP, 100 θ_V at $\Psi = 1.5$MPa
Base Mix	0.44	0.91	$\theta_v = 0.1303\ \Psi^{-0.335}$	11%
20% CCM	0.54	0.87	$\theta_v = 0.1666\ \Psi^{-0.464}$	14%
30% CCM	0.58	0.94	$\theta_v = 0.1844\ \Psi^{-0.499}$	15%
40% CCM	0.59	0.91	$\theta_v = 0.1981\ \Psi^{-0.335}$	17%

Most plants will reach the permanent wilting point (PWP) at a matric potential of 1.5MPa. The PWP was calculated for all for mixes using $\Psi = 1.5$MPa in the four equations provided in Table 4. The value of PWP was 11% for the base mix. However, the PWP increased to 14% after adding 20% CCM to the mix. The PWP continued to increase as the fraction of CCM in the mix increased. The highest PWP was 17% for the mix that contained 40% CCM. These results clearly indicated that adding CCM to a bark-sand mix enhanced the PWP.

The bulk density of the base mix was 0.44 g/cm^3 dry basis and adding CCM to the mix yielded an increase in the bulk density to 0.54 g/cm^3 for the 20% CCM mix to 0.59 g/cm^3 for the mix that contained 40% CCM. A higher dry matter bulk density is desirable to reduce the movement or tipping of containers during high winds.

Pot water capacity, PWC refers to the maximum amount of volumetric wetness (%) a potting media can hold after drainage. It is the sum of θ_v at PWP plus WHC as a percentage. Refill Point (RP) marks the point at which the plant has used all readily available water which typically occurs at 50% of the WHC. Plants will stay out of stress and yield more when kept within this water potential comfort range. This is the range of readily available water, RAW [17]. The calculated values of PWC, WHC, PWP, and RP are compared for the four mixes in Table 5.

Table 5. Calculated values of pot water capacity, water holding capacity, permanent wilting point, and refill point for the four mixes using the Dew Point Method.

	Base Mix	20% CCM	30% CCM	40% CCM
PWC (%)	52	55	58	63
WHC (%)	41	41	43	46
PWP (%)	11	14	15	17
RP (%)	32	35	37	40

Table 5 shows that the pot water capacity (PWC) increased as the percentage of compost increased in the mixes. The 40% CCM mix had the highest PWC value of 63%. The addition of compost increased the water holding capacity of mix by increasing the number of micropores in the mix either by "gluing" mix particles together or by creating favorable living conditions for soil organisms. The refill point (RP) of the base mix (PWC – 0.5 WHC) was the lowest at 32%. Adding CCM to the mix increased the refill point to 35% for the 20% CCM mix, and it increased further to 40% for the mix containing 40% compost. Overall, the data indicated that adding CCM to a bark-sand mix increased the pot water capacity with a corresponding increase in the refill point. The practical result is that adding 30% to 40% CCM to the base mix will require less irrigation water to maintain a container at a high level of readily available water. The reduced plant stress and lower water cost may improve profits for a producer of container plants.

The water retention data were used to calculate the values of the matric potential (Ψ) that corresponded with water contents on a mass basis (θ_m) ranging from 0.1 to 0.6 g_{water}/g_{mix}. A one-way analysis of variance [18] was used to calculate the means values of Ψ, the pooled variance (S_P^2), and the least significant difference for each level of θ_m. The LSD was calculated as $t_\alpha \times (2\,S_P^2/r)^{0.5}$ and the level of probability selected was 95%. The number of replications per treatment was 3 (r) and the error degrees of freedom was 8. The LSD values used to test for differences between treatment means are provided for each value of θ_m in Table 6. Means with the same letter in Table 6 were not significantly different.

Table 6 values shows that the LSD (0.05) decreased as the θ_m increased. This was due to the decrease in variance (S_P^2) as the water content increased. At low water potentials, flow restriction within the sample and loss of hydraulic contact between mix

and measuring cup possibly resulted in the higher observed variance. Generally, we can say that the base mix's values were different from the mixtures with compost. Adding compost changed the ability of the potting media to retain the water and made the water contained in the media easier to extract for values of θ_m of 0.2 g $_{water}$/g $_{mix}$ or less which would be expected to reduce plant stress during sub-optimal water contents. Adding at 30% CCM to the mix made the greatest impact.

Table 6. Significant difference between treatment means for all mixes at each θ_m.

θ_m (g$_{water}$/g$_{mix}$)	Base Mix (MPa)	20% CCM (MPa)	30% CCM (MPa)	40%CCM (MPa)	Mean Square Error (S$_P^2$)	LSD $_{(0.05)}$
0.1	19.34**a**	13.47**b**	10.97**b**	16.72**a**	2.0648	2.71
0.2	5.56	1.63b	2.52	1.73**b**	0.0465	0.41
0.3	0.42	0.58	0.89**c**	0.87**c**	0.0035	0.11
0.4	0.40**a**	0.45**a**	0.49**a**	0.73	0.0038	0.12
0.5	0.20	0.51b	0.47**b**	0.53**b**	0.0010	0.06
0.6	0.23	0.50	0.36	0.44	0.0007	0.05

While we believe that the information presented in this work is important as a methodology for selecting the optimal mix of CCM with bark-sand base mix, it should also be recognized that this procedure can be used to optimize any potential mix such as poultry litter and or another type of organic ingredient. Also worthy of note is the fact that under field conditions there can be many other variables (beyond those presented in this study) that can vary water retention characteristics and of plant-available N and P of a mix. Past studies indicate that laboratory N mineralization data of manures and composts are strongly related to field N mineralization and plant-available N [7]. This indicates that laboratory work may be helpful to growers who wish to use or are using composts and base mixes to better select optimal composts and base mixes that maximize plant nutrients and water retention.

4   Conclusions

Sample analyses and experiments were conducted to determine if composted cow manure (CCM) could be used to fertilize a base mix that was formulated by mixing 8 parts of screened pine bark with 1 part sand. The compost product was mixed with the base mix at the rates of 20%, 30%, and 40% on a volume basis. The plant nutrient concentrations of the base mix and the three CCM-base mix blends were compared with common plant nutrient concentrations provided by fertilizing the base mix with a 14-14-14 granular fertilizer at the rate of 2 to 5 kg per m^3. If was found that the 40% CCM mix could replace granular fertilizer for a portion of the P_2O_5, and all of the K_2O, secondary, and minor plan nutrients included in the study. The CCM blends could also replace about 44% to 75% of the N fertilizer needed to fertilize a potting media. Additional N fertilizer

could be added after filling and planting the containers based on plant needs. The higher pH of the CCM may also allow a commercial producer of woody ornamentals to greatly reduce lime requirements since adding CCM to the base mix increased the pH from 4.8 to 5.5 for the 20% CCM mix to 6.2 for the 40% CPL mix.

Measurements of the aeration porosity (AP) indicated that the base mix in this study did not meet the recommended values. The water holding capacity (WHC) increased as the percentage of CCM in the mix increased. Mixing CCM with the base mix made a substantial improvement in the AP. The 40% CCM had an AP of 25% indicating that it was still higher than the desired value of 20%. Therefore, a small amount of an organic or synthetic bulking material would be needed to achieve an AP of 20%. Only the 40% CCM blend had a WHC within the desirable range of 45% to 65%. Therefore, CCM has the potential to reduce the amount of sphagnum or peat moss needed to mix with the media to improve these physical characteristics.

Water retention curves developed using the dewpoint method represented the water retention curves of the four mixes accurately with R^2 for the fitted curves for base mix, 20% CCM, 30% CCM and 40% CCM being 0.91, 0.87, 0.94 and 0.91 respectively. The water retention curve generated for each mix can be used to accurately convert volumetric water content to PMP for use in irrigation scheduling. Adding 30% to 40% CCM to the bark-sand based mix used in this study also increased the pot water capacity and the refill point. This would be expected to reduce the amount of irrigation water needed to maintain good plant growth.

It was concluded that mixing CPM with a bark-sand base mix has the potential to greatly reduce the need for non-renewable ingredients, such as peat moss, and to reduce the cost for fertilizer for a commercial nursery. The use of other types of compost can be evaluated using the measurements and procedures provided in this study. The final decision concerning the use of a compost mix product should be made after growing some trial pots of the plant that is to be produced.

References

1. Marble SC et al (2010) Evaluation of composted poultry litter as a substrate amendment for wholetree, clean chip residual, and pinebark for container grown woody nursery crops. J Environ Horticult 28(2):107–116
2. Bernal MP, Alburquerque JA, Moral R (2009) Composting of animal manures and chemical for compost maturity assessment, a review. Biores Technol 100(22):5444–5453
3. Robbins J, Evans M (2005) Growing media for container production in a greenhouse or nursery, part I – components and mixes, FSA6097. University of Arkansas Cooperative Extension Service, Little Rock, AR USA. https://www.uaex.uada.edu/publications/pdf/fsa-6097.pdf. Accessed 15 Aug 2010
4. Warncke DD, Krauskopf DM (1983) Greenhouse growth media: testing and nutrition guidelines, E-1736. Cooperative Extension Service, Michigan State University, St. Joesph, MI, https://archive.lib.msu.edu/DMC/extension_publications/e1736/e1736-1983.pdf. Accessed 10 July 2023
5. Buamscha G, Altland JE, Sullivan DM, Horneck DA, Cassidy J (2007) Chemical and physical properties of Douglas fir bark relevant to the production of container plants. HortScience 42(5):1281–1286

6. Polomski RF (2010) Personal communication on common pine bark and sand mixes used to produce woody ornamentals. Associate Extension Specialist–Horticulture/Arboriculture, Plant and Environmental Sciences Department, Clemson University, Clemson SC, USA

7. Franklin D, Bender-Özenç D, Özenç N, Cabrera M (2015) Nitrogen mineralization and phosphorus release from composts and soil conditioners found in the southeastern United States. Soil Sci Soc Am Jo 79:1386–1395. https://doi.org/10.2136/sssaj2015.02.0077

8. ASL (2023a) Summary of procedures for determination of ammonium-N, total-N, nitrate-N, total carbon, organic matter, EC_5, and pH. Agricultural Service Laboratory, Clemson University. https://www.clemson.edu/public/regulatory/ag-srvc-lab/compost/procedures/index.html. Accessed 27 Apr 2023

9. ASL (2023b) Summary of wet ashing procedure for determining P, K, Ca, Mg, Zn, Mn, Cu, Fe, Na, S and Al. Agricultural Service Laboratory, Clemson University. https://www.clemson.edu/public/regulatory/ag-srvc-lab/feed-forage/procedure6.html. Accessed 27 Apr 2023

10. Massey HF, Chastain JP, Owino TO, Polomski RF, Moore KP (2011) Chemical and physical properties of potting media containing varying amounts of composted poultry litter. Presented at the 2011 ASABE annual international. Meeting. Paper No. 1110935. ASABE, 2950 Niles Rd., St. Joseph, MI, pp 49085–9659

11. APHA (1995) Standard methods for the examination of water and wastewater. In: Eaton AD, Clesceri LS, Greenberg AE (eds) 19th edn. American Public Health Association, Washington

12. BCMA (2015) Importance of Aeration in Container Media. British Columbia Ministry of Agriculture, Victoria, BC, Canada. https://www2.gov.bc.ca/assets/gov/farming-natural-resources-and-industry/agriculture-and-seafood/animal-and-crops/crop-production/importance_of_aeration_in_container_media_2015.pdf. Accessed 10 July 2023

13. FM&T (2017) Understanding ADV and pH testing for mold, core sand. Foundry Management & Technology. https://www.foundrymag.com/ask-the-expert/article/21930175/understanding-adv-and-ph-testing-for-mold-core-sand. Accessed 10 July 2023

14. Yeager T, Million J, Larsen C, Stamps B (2010) Florida nursery best management practices: past present, and future. HortTechnology 20(1):82–88. https://rngr.net/publications/fnn/2011-winter/new-nursery-literature/florida-nursery-best-management-practices-past. Accessed 11 July 2023

15. Rynk R, et al (1992) On-farm composting handbook (NRAES-54) Natural Resource, Agriculture, and Engineering Service, Ithaca

16. WP4C-METER Group (2021) Operator's Manual. https://library.metergroup.com/Manuals/20588_WP4C_Manual_Web.pdf. Accessed 20 Oct 2023

17. Hillel D (2013) Fundamentals of soil physics. Academic Press

18. Steel RGD, Torrie JH (1980) Principles and procedures of statistics: a biometric approach, 2nd edn. McGraw-Hill Book Company, New York

Impact of Building Geometry, Window Types, and Materials on Daylighting Performance of Livestock Buildings

Sheikh Rishad Ahmmad[1(✉)] ⓘ, Maria Vilain Rørvang[1] ⓘ, Niko Gentile[2] ⓘ,
Knut-Håkan Jeppsson[1] ⓘ, and Marie-Claude Dubois[1,2] ⓘ

[1] Department of Biosystems and Technology, Swedish University of Agricultural Sciences,
Sundsvägen 16, 230 53 Alnarp, Sweden
`sheikh.rishad.ahmmad@slu.se`

[2] Division of Energy and Building Design, Lund University, Sölvegatan 24, 221 00 Lund,
Sweden

Abstract. The availability and quality of natural light in livestock buildings affect the welfare and productivity of animals and their caretakers, while affecting the energy performance of the buildings. This study investigated the impact of different building properties on daylight conditions of livestock buildings. The study was conducted via parametric daylight simulations in Climatestudio. Firstly, building geometries with different facade orientations, width-to-length ratios, and roof pitches were simulated. Secondly, different glazing types, sizes, and locations were considered for their respective daylight performance. Finally, the use of different materials for the facade, floor and roof of the buildings were simulated and comparatively analysed. The study analysed the simulation results to assess daylight availability in relation to different building properties. The results provided insight that can help determine building geometry, window properties, and material selection during the design process. Overall, the study highlighted the importance of further research and development of design guidelines and standards that incorporate these factors to improve the daylighting performance of these buildings, while ensuring animal welfare and productivity.

Keywords: Daylighting performance · Livestock buildings · Cattle · Parametric study · Lighting · Simulations

1 Introduction

Cattle have been domesticated in the course of human history. However, their ancestors used to live outdoors under natural light. Therefore, keeping the stable's light environment as close to the natural daylight as possible is important for the animals' health and welfare. A crucial aspect to ensuring a good indoor animal and human environment is by optimising daylighting in the livestock building. The Animal Welfare Act (2018:1192) sheds light on the importance of keeping animals in suitable environments that promote their wellbeing. A study by Dahl, Tao and Thompson (2012) shows that proper daylight

in cattle stable can increase milk production. Another study by Shinde and Gupta (2016) indicates that longer light exposure can increase milk production by 7–10%. Studies show that due to day length, energy use for lighting is reduced during summer months compared to winter months (Houston, Gyamfi and Whale, 2014). It is obligatory in Sweden to ensure that cattle stay outdoors around summer time with at least 60 days for Northern Sweden, 90 days for Middle Sweden, and 120 days for Southern Sweden (Swedish Board of Agriculture, 2022). However, they are kept indoors during the winter months when cold weather and the lack of sufficient light can negatively affect them. Poorly lit stables do not always have an even light distribution, as shown in Fig. 1, which may be harmful for cattle as they are especially sensitive to high contrasts (Harner et al., 2008). According to a study in Sweden by Sundahl (1974), the recommended lighting for cow barns is 75 lx while night-time lighting should be 5 lx. Furthermore, Swedish Institute for Standards (2012) recommends between 100–150 lx in cattle houses and 5 lx during night-time. However, the milking area requires 300 lx of illuminance (Haraldsson and Henrysson, 2011).

Fig. 1. A cattle stable located in Southern Sweden with poor lighting conditions (Photograph: Sheikh Rishad Ahmmad). Buildings such as these are not representative of the existing building stock in Sweden.

In addition, it is also extremely important to create a suitable environment in the stable for the human caretakers. Work in cattle environments represents 87% of work-related accidents for humans involved with animal husbandry (P. M. Layde et al., 1996). Many of the existing cattle stables have poor lighting conditions, which may lead to a dangerous or unsuitable work environment. Swedish National Board of Housing, Building and Planning (2021) recommends a 1% Daylight Factor for buildings in general, which is the ratio between the illuminance measured at a specific point in a room and the illuminance under an unobstructed overcast sky (Lewis, 2017). Health and safety executive (2023) in United Kingdom suggests adequate, suitable and flicker-free lighting, natural light without glare as well as well-lit exterior areas for the workers. On the other hand, Swedish

Board of Agriculture (2022) suggests lighting for animals that does not cause discomfort and supports their circadian rhythm and behavioral needs.

Due to the undeniable impact of daylighting on energy efficiency and animals' and workers' welfare, it is a crucial consideration in the building design process. However, it is often overlooked in reality, which causes animal buildings to end up with suboptimal daylighting or poor electric lighting. Cattle can keep a normal body temperature without using any additional energy to heat or cool their body between 5 °C and 25 °C (Hulsen, 2005). Therefore, it is possible to increase the window surface area without compromising the thermal environment for the animals. However, careful considerations must be taken as excessive cold or heat can cause adverse effect on dairy production (Dy, 2021). In recent practice, cattle stables with open or translucent facades and roof can be observed in contrast to the practice of designing stables with smaller windows. These stables invite more daylight into the buildings that can benefit both animals and humans. Two projects located in Quebec, Canada, exhibit such design principles (Fig. 2). Quebec has slightly more daylight in the winter and slighting less in the summer than Southern Sweden (Fig. 3), which is the primary study area for this research.

Fig. 2. A cattle stable designed by La Shed Architecture in Montérégie, Quebec (Carlson, 2020) on the left (Photograph: Virginie Gosselin), and a cattle stable in Quebec on the right (Photograph: Marie-Claude Dubois).
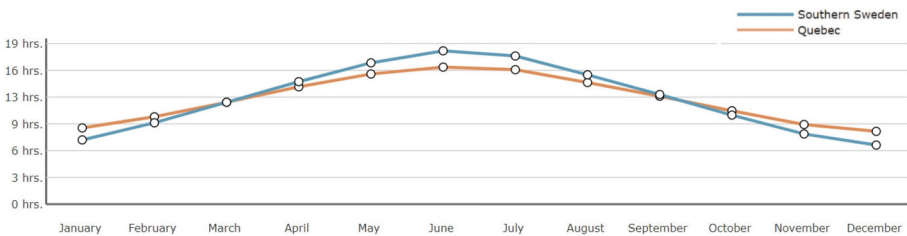
Fig. 3. Comparison of monthly average daylight hours between Southern Sweden and Quebec (Worlddata, 2023).

Southern Sweden exhibits particularly gloomy weather conditions during winter due to overcast sky, fog, and a thick layer of cloud. As Southern Sweden does not experience much snow compared to Northern Scandinavia, it cannot utilize the property of snow

as a natural light reflector to compensate for low daylight levels (Dubois et al., 2019). Therefore, it is extremely important to study the impact of daylighting on buildings in such a climate. This study made use of computer-based modelling and simulations to predict the impact of different building properties on the daylighting performance of the cattle stables. The objective of the study was to understand the impact of different building properties such as geometry, window types, and materials on the daylighting performance in a simulated environment.

2 Method

The overall study followed a process of optimizing a built form primarily based on its daylighting performance. Different building constraints were tested and simulated, and the best performing options were tested in the next phase of the study. The geometrical models used in this study were created using Rhinoceros 3D computer program (Robert McNeel & Associates, 2023). The simulations were conducted with Climatestudio (Solemma, 2023), which uses Radiance (Larson and Shakespeare, 1998) as the lighting simulation tool. Several metrics gathered from the simulation results were analysed. The general methodology of this study is illustrated in Fig. 4. The metrics used are described below:

1. Spatial Daylight Autonomy (sDA): sDA is the percentage of the analysis area meeting a minimum horizontal daylight illuminance for a specified fraction of time. The illuminance is set at 300 lx for office spaces with a time period corresponding to 50% of occupancy (Dubois et al., 2019). Although the cattle need 75 lx of light, the requirement for milking parlours is set at 300 lx (Haraldsson and Henrysson, 2011), the same for working environments for humans. Therefore, the standard of 300 lx for 50% of the occupied time was considered in this study. The purpose of using this metric was to evaluate the effectiveness of daylight distribution in the stable when electric lighting was switched off.
2. Annual Sunlight Exposure (ASE): The ASE is used to quantify the amount of direct sunlight that enters the space to assess the risk for glare, overheating, and higher energy demand. It is defined as the percentage of analysis points receiving at least 1000 lx for at least 250 h per year. Spaces with more than 10% ASE have unsatisfactory visual comfort in spaces for humans (U.S. Green Building Council, 2023).
3. Daylight Factor (DF): The DF is the ratio between the illuminance within a room at a certain horizontal plane and the illuminance under an unobstructed overcast sky (Lewis, 2017). The Median Daylight Factor was used for evaluation in this study as it informs on the spatial distribution of the Daylight Factor (Dubois et al., 2019).

2.1 Simulation Setup

The study area of the project was located in Southern Sweden and the climate file for the simulations was set to Copenhagen. The data for the location was collected from Kastrup Airport, which is one of the closest international airports and likely to provide the most reliable dataset from previous experience. For the initial simulations, a default
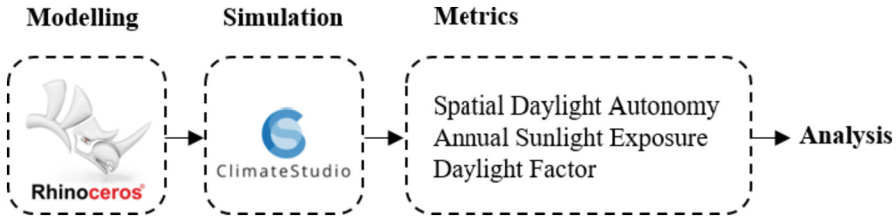
Fig. 4. A diagram explaining the general methodology of this study.

matte white material was used for all modelled surfaces. A simple clear glass material with Visible Solar Transmittance (T_{vis}) of 87.7% was used for all window surfaces, which corresponds to a single clear glass. A standard grass surface was used as a ground plane with a reflectance of 7.38%. It is to be kept in mind that the purpose of this phase of the study was to create a comparative analysis and real-life measurements in similar buildings can differ due to use of different materials, components, and amount of soiling (Diéguez et al., 2016). The last phase of the simulations dealt with different materials and interior components, which was likely to provide results closer to reality. The simulation parameters and conditions used in this study are described in Table 1.

Table 1. Simulation parameters and conditions used in the study

Location	Data type		Latitude	Longitude
Copenhagen-Kastrup	TMYx.2004-2018		55.6	12.6
Sensor spacing	Workplane offset		North offset	
1000 mm	850 mm		0°	
Samples per pass	Max. Number of passes	Ambient bounces	Weight limit	
64	100	6	0.01	

2.2 Geometry Study

In the first phase, the impact of different building geometries on daylighting performance was studied (Fig. 5). Three tests were performed:

1. A simple square building with windows on opposing two sides was used to determine the most optimal building orientation. Each building form had a length and width of 20 m, occupied floor area of 400 m^2, and a three-meter clear height. There were 10 square shaped 1 m^2 windows on each side placed at an equal distance, 20 windows in total. Four iterations of the same built form were used for this study: windows oriented towards North and South, East and West, North-west and South-east with a 45° rotation, and finally North-east and South-west with a 45° rotation.

2. Different building shapes with same occupied floor area (400 m^2) were studied to determine the optimum shape, keeping the best performing orientation in the previous study unchanged. Three iterations were analysed: a square building with 20 m in length and width, a rectangular building with 25 m length and 16 m width, and finally, a rectilinear building with 40 m length and 10 m width. The number of windows was the same as in the previous phase, with 10 windows placed on each of the two elongated facades at an equal distance.
3. Different sloped and flat roofs were tested, keeping the best performing shape in the previous study unchanged. The fours iterations were: a flat roof building, a building with a 10° roof slope, a building with 30° slope, and a building with an inverted roof slope of 30° on each side from the central ridge.
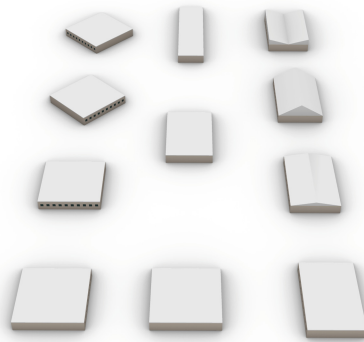
Fig. 5. Different geometries were modelled to determine the best orientation (left), shape (middle), and roof angle (right).

2.3   Window Type

In the second phase, different window sizes, shapes and locations were studied (Fig. 6). The simulations were performed in two stages:

1. Five window and opening options were considered in this stage: square windows at regular interval (1 m^2 each), corner windows in the meeting point of wall and roof (2.3 m^2 each), roof openings (1.5 m^2 each), open facades (6.3 m^2 each), and windows along the ridgeline of the roof (3.2 m^2 each). The open facade was included in this study due to its potential to provide natural ventilation to the building.
2. The best performing cases from the previous stage were used in different combinations to determine the best performing option.
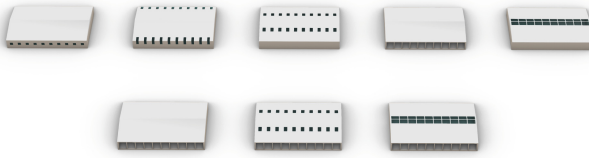
Fig. 6. Different window options simulated for the study (top) and combination of the best performing options (bottom).

2.4 Material Use

In the final phase, different materials such as white reflective panels, wood, metal, and concrete were compared to assess their impact on daylighting performance (Table 2). The best performing geometry and window combination was used for this study. Interior materials and components such as stalls, straw, partitions, the animals, etc., were added in this phase to make the simulations closer to reality (Fig. 7). The animals were placed in the model as a simplified rectangle to reduce geometric complexity.

Table 2. Materials used for simulations

Name of the material	Reflectance (%)	Specular (%)	Diffuse (%)	R	G	B
Matte White Wall	80.69	0.98	79.71	0.81	0.79	0.77
Wooden interior wall cladding Wooden parquet floor	16.94 19.78	0.60 2.05	16.34 17.73	0.28 0.32	0.13 0.14	0.05 0.03
Aluminium metal cladding Light grey interior metal partition	64.79 74.27	5.33 4.69	59.46 69.59	0.59 0.66	0.60 0.70	0.58 0.77
Concrete support	43.00	0.16	42.84	0.47	0.42	0.32
Dirty leather (cow skin)	59.66	0.00	59.66	0.64	0.59	0.47
Straw	29.03	0.00	29.03	0.38	0.27	0.09
Metallic hand rail (fence)	46.31	11.31	35.00	0.36	0.35	0.34
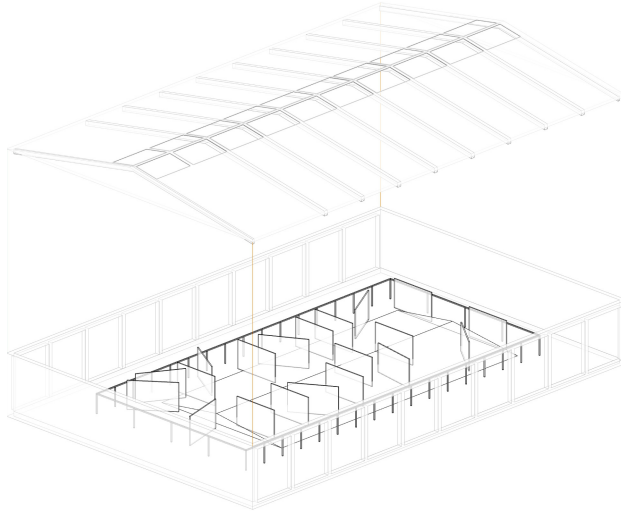
Fig. 7. An exploded isometric view of the 3D model illustrating the interior building components used for the simulations.

3   Results

3.1   Geometry Study

The results indicated that all studied building orientations performed similarly (Table 3). However, windows oriented towards North and South seemed to provide slightly better sDA but higher ASE, thus a higher risk for glare. The high sDA value for all cases indicated that the spaces had high level of daylight distribution.

Table 3. Simulation results for the orientation study.

	North-South	East-West	North-west and South-east	North-east and South-west
Spatial Daylight Autonomy (sDA), (%)	97.7	96.6	97.7	97.5
Annual Sunlight Exposure (ASE), (%)	4.3	3.9	3.4	3.4
Median Daylight Factor (DF$_{med}$), (%)	1.4	1.4	1.4	1.4

The building shape study demonstrated that the sDA was higher for rectangular and rectilinear shapes in comparison with the square shape (Table 4). Rectangular shape provided slightly lower ASE.

Table 4. Simulation results for the building shape study.

	Square (20 m × 20 m)	Rectangular (25 m × 16 m)	Rectilinear (40 m × 10m)
Spatial Daylight Autonomy (sDA), (%)	97.7	100	100
Annual Sunlight Exposure (ASE), (%)	4.3	3.4	3.5
Median Daylight Factor (DF$_{med}$), (%)	1.4	1.6	1.7

All the tested roof configurations performed similarly in terms of sDA and ASE (Table 5). The flat roof and roof with a lower slope had better DF$_{med}$. Although both roofs performed similarly, a slightly sloped roof can give more structural stability to carry snow load while providing a more effective drainage system.

Table 5. Simulation results for the roof configuration study

	Flat roof	10° slope	30° slope	Inverted roof
Spatial Daylight Autonomy (sDA), (%)	100	100	100	100
Annual Sunlight Exposure (ASE), (%)	3.4	3.4	3.4	3.4
Median Daylight Factor (DF$_{med}$), (%)	1.6	1.6	1.4	1.4

3.2 Window Type

Results from window location study showed that windows placed on corner, roof slope, and ridge as well as open facades performed significantly better than square windows on the wall in terms of DF$_{med}$ (Table 6). However, as the ASE increased above 10%, it rose concerns about visual discomfort for human occupants according to Illuminating Engineering Society (2012). A study by Abboushi (2020) recommended increasing current ASE limits of 10%–20% with careful consideration for its effects on energy, thermal comfort, and visual comfort.

A comparison between different window and opening options are illustrated in Fig. 8. Daylight Factor (DF) comparison for different window options.

As the open facade system proved to be providing most daylight to the building, its combination with two different roof windows were investigated (Table 7). Although ASE still posed a risk that needed to be addressed, DF$_{med}$ values indicated an exceptionally well daylit environment. It is to be noted that these values were simulation results of a simplified geometry with a single default material with high reflectance. Moreover, the presence of animals and loss of reflectance due to soiling were not considered. Therefore, the results are not representative of similar real buildings and can only be used for comparative analysis.

Table 6. Simulation results for the window location study.

	Wall	Corner	Roof slope	Open facade	Ridge window
Spatial Daylight Autonomy (sDA), (%)	100	100	100	100	100
Annual Sunlight Exposure (ASE), (%)	3.4	14.7	14.3	21.5	31.1
Median Daylight Factor (DF$_{med}$), (%)	1.6	7.1	10.9	10.7	17.9

Wall openings

Corner windows

Roof openings

Open façade

Ridge opening

Daylight factor scale
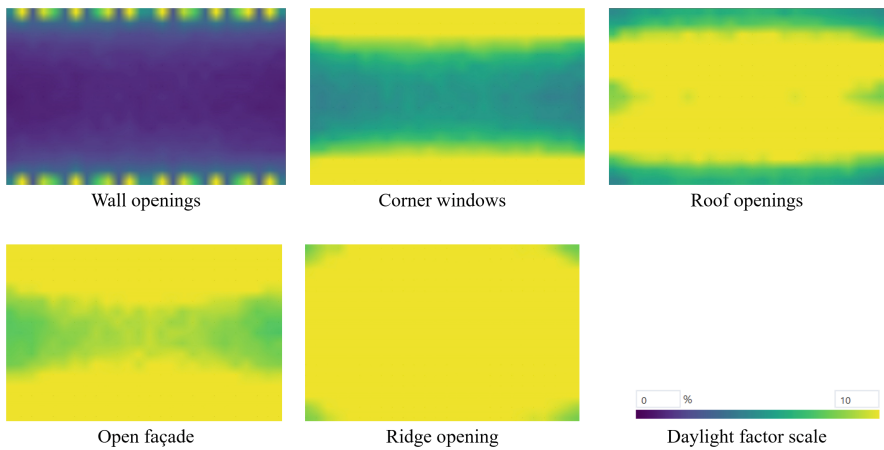
Fig. 8. Daylight Factor (DF) comparison for different window options.

Table 7. Simulation results for combined window placement study.

	Open facade only	Open facade + slope window	Open facade + ridge window
Spatial Daylight Autonomy (sDA), (%)	100	100	100
Annual Sunlight Exposure (ASE), (%)	21.5	43.2	56.6
Median Daylight Factor (DF$_{med}$), (%)	10.7	22.7	32.8

3.3   Material Use

sDA and ASE were not influenced by change in materials (Table 8). The highest DF$_{med}$ were obtained for a stable with reflective white materials in roof and wall as well as white floor surface, which is not realistic in an animal stable. However, it indicated

the importance of using light coloured materials and regular cleaning and maintenance. It is to be noted that, due to adding structural members and other interior building components, the values were lower in this case compared to previous tests. The use of metal as primary building material created the second best daylit environment, with concrete and wood coming second and third respectively.

Table 8. Simulation results for the material use study

	White	Wood	Metal	Concrete
Spatial Daylight Autonomy (sDA), (%)	98	98	98	98
Annual Sunlight Exposure (ASE), (%)	47.1	47.1	47.1	47.1
Median Daylight Factor (DF_{med}), (%)	23.7	14.4	20.9	15.7

4 Discussion and Conclusions

The study was conducted to understand the impact of different building properties such as geometry, window types, and materials on the daylighting performance of animal stables in a simulated environment. The simulations performed in this study indicated the intricate relationship between building properties and daylighting performance. The study on different geometric properties of the building such as orientation, shape and roof configurations showed that it is possible to make informed design decisions based on the simulation results to improve the stable environment for cattle and humans. A rectangular building oriented towards North-South with a gentle roof slope proved to be the most appropriate built form among those tested, but other aspects such as e.g., natural ventilation and function also have to be considered in the planning. Although there were some possible complications regarding sunlight exposure, glare and overheating, large windows created a highly daylit cattle environment. The best performing combination of roof ridge windows and open facade could bring in a lot of light as well as natural ventilation. Further investigation into material use showed that light coloured materials with reflective surfaces performed better than dark coloured absorbing materials such as wood. Wood could probably not be used due to moisture considerations as well.

The results of the study was not validated in comparison to a real building, which is a major limitation of the study. Further study is needed to address Useful Daylight Illuminance (UDI) as a metric. Moreover, multi-objective optimization can provide a broader understanding of the aspects studied.

In conclusion, this study provided information to architects, engineers and other stakeholders involved in livestock building design. Utilizing the full potential of daylight can reduce the reliance on electric lighting, thus leading to considerable energy savings, which contributes to more sustainable livestock buildings. It is important to note that design guidelines and standards must be updated to incorporate daylighting considerations to enhance both animal wellbeing and energy-efficiency. Current guidelines and rules regarding daylighting focus more on buildings predominantly occupied

by humans. Further research and development in this area will undoubtedly refine these insights and promote more sustainable design practices for future livestock buildings.

References

Abboushi B (2020) The case for multicriteria annual sunlight exposure guidelines. In: 2020 building performance analysis conference and SimBuild, Chicago. ASHRAE and IBPSA-USA, Chicago

Carlson C (2020) La Shed Architecture creates translucent barn to give cows "a better quality of life". Dezeen. https://www.dezeen.com/2020/08/16/la-shed-architecture-translucent-barn-cows-quebec/. Accessed 24 Aug 2023

Dahl GE, Tao S, Thompson IM (2012) Lactation biology symposium: effects of photoperiod on mammary gland development and lactation1. J Anim Sci 90:755–760. https://doi.org/10.2527/jas.2011-4630

Diéguez AP, Gentile N, Wachenfelt HV, Dubois M-C (2016) Daylight utilization with light pipe in farm animal production: a simulation approach. J Daylight 3:1–11. https://doi.org/10.15627/jd.2016.1

Dubois M-C, Gentile N, Laike T, Bournas I, Alenius M (2019) Daylighting and lighting under a Nordic sky, 1st edn. Studentlitteratur AB

Dy SS (2021) The hot and cold cow: a stochastic production frontier analysis of the effect of temperature and income diversification in Swedish dairy farms. Swedish University of Agricultural Sciences, Uppsala

Haraldsson L, Henrysson H (2011) Lighting in stalls for dairy cows (in Swedish), Självständigt arbete vid LTJ-fakulteten, SLU. Swedish University of Agricultural Sciences, Alnarp, Sweden

Harner JP, Smith JF, Janni K (2008) To see, or not to see, that is the question. Lighting Low Profile Cross Ventilated Dairy Houses, Housing of the future. Sioux Falls, South Dakota, USA

Health and safety executive (2023) Workplace safety and welfare. https://www.hse.gov.uk/agriculture/topics/welfare.htm. Accessed 12 Aug 2023

Houston C, Gyamfi S, Whale J (2014) Evaluation of energy efficiency and renewable energy generation opportunities for small scale dairy farms: a case study in Prince Edward Island, Canada. Renew Energy 67:20–29. https://doi.org/10.1016/j.renene.2013.11.040

Hulsen J (2005) Cow signals: a practical guide for dairy farm management. Roodbont Publishers, The Netherlands

Illuminating Engineering Society (IES) (2012) Approved Method: IES Spatial Daylight Autonomy (sDA) and Annual Sunlight Exposure (ASE) (No. LM-83-12). Illuminating Engineering Society of North America

Larson GW, Shakespeare R (1998) Rendering with radiance: the art and science of lighting visualization. Morgan Kaufmann Publishers Inc., San Francisco

Legal Secretariat, Ministry of Enterprise and Innovation (2018) Animal Welfare Act (2018:1192)

Lewis A (2017) The mathematisation of daylighting: a history of British architects' use of the daylight factor. J Archit 22:1155–1177. https://doi.org/10.1080/13602365.2017.1376342

Layde PM, Nordstrom DL, Stueland D, Wittman LB, Follen MA, Olson KA (1996) Animal-related occupational injuries in farm residents. J Agric Saf Health 2:27–37. https://doi.org/10.13031/2013.19439

Robert McNeel & Associates (2023). Rhinoceros. Rhinoceros. https://www.rhino3d.com/. Accessed 4 Oct 2023

Shinde KP, Gupta SK (2016) Role and importance of light in farm animals and birds. AJBS 11:317–320. https://doi.org/10.15740/HAS/AJBS/11.2/317-320

Solemma (2023) Climatestudio. Climatestudio. https://climatestudiodocs.com/index.html. Accessed 4 Oct 2023

Sundahl A (1977) Lighting in agricultural buildings (in Swedish) (No. 243), Aktuellt från Lantbrukshögskolan. Swedish University of Agricultural Sciences, Uppsala, Sweden

Swedish Board of Agriculture (2022) Care and stable environment for cattle (in Swedish). Swedish Board of Agriculture. https://jordbruksverket.se/djur/lantbruksdjur-och-hastar/notkreatur/skotsel-och-stallmiljo#h-Beteochutevistelse. Accessed 12 Aug 2023

Swedish Institute for Standards (2012) Outbuildings - Applications to the Swedish Housing Agency's and the Swedish Agency for Agriculture's rules regarding the design of outbuildings for agriculture, forestry and horticulture as well as horse operations (in Swedish). Swedish Institute for Standards. https://www.sis.se/en/produkter/agriculture/farm-buildings-structures-and-installations/general/sists372012/. Accessed 6 Oct 2023

Swedish National Board of Housing, Building and Planning (2021). Boverket's building regulations – mandatory provisions and general recommendations, BBR. Swedish National Board of Housing, Building and Planning. https://www.boverket.se/en/start/publications/publications/2019/boverkets-building-regulations--mandatory-provisions-and-general-recommendations-bbr/. Accessed 29 Sept 2023

U.S. Green Building Council (2023) Daylight: Indoor Environmental Quality. U.S. Green Building Council. https://www.usgbc.org/credits/healthcare/v4-draft/eqc-0. Accessed 4 Oct 2023

Worlddata (2023) Climate comparison. Worlddata.info. https://www.worlddata.info/climate-comparison.php?r1=ca-quebec&r2=se-southern-sweden. Accessed 24 Aug 2023

Estimation of Vitamin A Concentration in Cattle Blood Based on Fluorescence With/Without Blood Cell Separation by Plasma Filter

Mizuki Shibasaki[1], Tetsuhito Suzuki[2(✉)], Nanding Li[1], Moriyuki Fukushima[1], Tateshi Fujiura[1], Takahiko Ohmae[3], Norio Nishiki[3], Yuichi Ogawa[1], and Naoshi Kondo[1]

[1] Graduate School of Agriculture, Kyoto University, Kitashirakawa-Oiwakecho, Sakyo-ku, Kyoto-shi, Kyoto 606-8502, Japan

[2] Graduate School of Bioresources, Mie University, 1577 Kurimamachiya-cho, Tsu-shi, Mie 514-8507, Japan
`t-suzuki@bio.mie-u.ac.jp`

[3] Tajima Agricultural High School, 300-1, Takayanagi, Yoka-cho, Yabu-shi, Hyogo 667-0043, Japan

Abstract. "Japanese Black" is a breed of beef cattle endemic to Japan and has a propensity to produce marbled meat, which requires the regulation of the blood vitamin A, retinol. To control retinol levels in a healthy way, the fluorescence of whole blood, plasma and plasma with a blood cell separation filter of cattle was measured by Excitation Emission Matrix (EEM) fluorescence spectrophotometry to develop a blood retinol estimation technique that is simpler and faster than conventional chemical analysis. Actual blood retinol concentrations were determined by HPLC methods. The EEM of each sample was measured in the excitation 300–400 nm and fluorescence 320–550 nm range and the retinol concentration was estimated by PLS regression. R^2Pred, and RMSEP for the whole blood were 0.91, 9.12, for plasma 0.94, 7.58, and for plasma with glass filter 0.92, 11.1, respectively.

Keywords: Japanese black cattle · Fluorescence · Retinol · EEM · PLS

1 Introduction

Japan has an endemic breed of meat cattle called the Japanese Black Cattle. In terms of fat content in loin meat, the Japanese Black Cattle has a higher value of 39.6% compared to 3.6% for the Angus breed. Meat with high Beef Marbling Standard (BMS) is produced by lowering blood Vitamin A (VA) levels during the middle part of the fattening period. This VA is mainly present in the blood as retinol, and it is the used for the blood VA evaluation. Then, from around 13 months of age, generally called the mid-fattening period, the composition and quantity of roughage are changed to cut off the supply of retinol precursors in the diet and thus, the blood retinol concentration falls to around 30 IU/dL [1]. This practice of limiting blood retinol concentrations is mostly done by

experience and intuition of livestock farmers and requires observing behavioral changes in cows, such as loss of appetite and loss of energy, as signs of retinol deficiency status. However, as some individuals don't show any signs of retinol deficiency, relying solely on human senses may not be sufficient to adjust blood retinol concentrations, which can sometimes lead to livestock deaths and accidents. Defects such as myxedema and liver disease can be found in cattle carcasses in the slaughterhouses, where sometimes as many as 40% of their animals with liver disease have been linked to retinol deficiency [2]. Since visual impairment and anorexia are also observed in the deficiency state, and parts with lesions are discarded at meat inspection stations, excessive retinol restriction is problematic from two perspectives: animal welfare and profitability.

The way to prevent retinol deficiency is through regular blood test monitoring, and vitamin supplements are administered when blood retinol levels are low. The usual blood test involves a blood sample taken by a veterinary surgeon, followed by measurement of blood retinol by high-performance liquid chromatography (HPLC). This is highly accurate but also requires blood collection process and subsequent delivery to a laboratory analysis. Therefore, it takes several days to obtain the results and costs around 2000 yen per cow. Some feedlot farmers don't test it until a clear deficiency symptom occurred. Such retinol deficiency could well be prevented through early treatment, if farmers have a technology that allows them to assess blood retinol levels readily on the farm site. All of these necessitates a simpler and quicker measurement for blood retinol.

As a technique for quantifying retinol in blood, a kit for simple determination is now available for practical use. It differs from the usual HPLC measurement in that retinol is extracted by reagent mixing and other pre-treatments and measured using its fluorescence and absorption properties. In addition, previous studies have shown that it is possible to estimate plasma retinol concentration based on the fluorescence properties of blood by measuring the excitation fluorescence matrix (EEM), which consists of excitation wavelength, fluorescence wavelength, and fluorescence intensity [3]. In general, the presence of blood cells significantly reduces light transmission. This is why blood samples without blood cell components, such as plasma, are used. However, obtaining plasma requires mixing reagents and centrifugation, which is difficult for farmers to handle routinely. Therefore, we considered if a correlation between EEM fluorescence intensity and blood retinol concentration could be obtained even from whole blood containing all components without any pre-treatment, and thus enables the blood retinol concentration estimation. As an alternative approach, we then extracted plasma using a plasma filter, which can remove blood cell components easily, and measured samples absorbed on a glass filter. This study examines two methods for the rapid estimation of retinol: one method that does not require any pre-treatment, and another method that requires a single pre-treatment but enables more accurate estimation.

2 Methods

(1) Sample Collection

Tajima fattening cows aged between 7 and 32 months were used in the experiment, were fattened at the Hyogo Prefectural Tajima Agricultural High School. Approximately 32

cows are kept in the fattening barn, and the diet consists of concentrate and roughage (wheat straw, Italian grass, and Sudan grass), with the composition and quantity of the roughage adjusted according to the stage of growth.

10 mL Blood samples were collected from the jugular vein in blood collection tubes containing sodium heparin discs (10 mL) for fluorescence measurements of whole blood and plasma and in blood collection tubes containing serum separator coagulation enhancing film (9 mL) for HPLC measurements, respectively, for a total of 160 animals throughout six experiments conducted every two months. Blood samples were obtained from a total of 160 animals in six experiments carried out every two months. The blood samples were collected from the jugular vein of 160 animals at two-month intervals for a total of six experiments. In the last sixth experiment, 600 μL of the whole blood was applied to a plasma filter (Plasma Filter, WATSON) which separates the blood cells from the plasma and absorbs the plasma on glass filter paper. As a result, 22 samples were obtained.

(2) Measurement of Samples
Based on the fact that the fluorescence of retinol in plasma is 330 nm excitation and 470 nm fluorescence [4, 5], the measurement wavelength range was set to 300–400 nm excitation and 320–550 nm fluorescence. Fluorescence was measured on 7 μL of whole blood within approximately 30 min of blood sampling to construct a model for estimating blood retinol concentrations. Plasma was extracted from the supernatant of whole blood centrifuged (3,000 rpm, 10 min) and measured in the same way. A single-drop measuring unit (SAF-851, JASCO) was attached to a spectrofluorometer (FP-8300, JASCO), and surface fluorescence was measured by irradiating excitation light from the bottom of a drop of whole blood on a quartz window at an angle of incidence of 45°. The measurement wavelength range was 300–400 nm for excitation, 320–550 nm for fluorescence, and 10 nm for bandwidth. The glass filter with plasma was fixed to a solid material measuring device and fluorescence was measured using the front-face method, in which excitation light was irradiated at an angle of incidence of 30° and fluorescence on the surface of the material was measured. The measurement range was not changed.

(3) Estimation of Blood Retinol Concentration Using PLS
MATLAB software (R2021a, MathWorks Inc., USA) and PLS Toolbox (version 8.8.1, Eigenvector Inc., USA) were used for analysis. Auto-scale was used for data pre-processing [6]. The dataset was split so that each cow's individual data set was present only in the Training or Test sets, resulting in 128 and 32 data sets, respectively. 10-fold cross-validation was applied to the Training set and the number of latent variables in the PLS analysis was determined by minimizing the error relative to the Test set (RMSECV). The number of glass filters with plasma samples obtained was 22, all of which were used as Training sets. The number of latent variables was selected to minimize RMSECV in the PLS analysis.

3   Results

3.1   Comparison of Each Sample's EEM

In all EEM of samples, the fluorescence peak in the white circle in Fig. 1(a) increases in intensity with increasing blood retinol concentration as shown in Fig. 1(b). Since the fluorescence of retinol in plasma is 330 nm for excitation and 470 nm for fluorescence in previous studies, this fluorescence peak may be a trend related to retinol in blood. On the other hand, the diagrams of whole blood EEMs shown in Fig. 2(c) and (d) show that the overall fluorescence intensity of EEMs is lower than that of plasma EEMs and that it is difficult to discriminate the position of the retinol fluorescence peak. This indicates that the influence of blood components do not present in plasma, such as blood cells, is significant. However, as the fluorescence intensity near the peak position increases with blood retinol concentration, it can be expected that the estimation of blood retinol concentration is possible if analysis is carried out using multiple wavelengths. In the comparison of EEMs of plasma (Fig. 2 (e), (f)) and glass filter with plasma (Fig. 2(g), (h)), the fluorescence range of 400–500 nm was zoomed to exclude areas where the fluorescence of amino acids [7] was strongly visible. The EEM of glass filter & plasma shows that it is easier to identify the peak that seems to be the fluorescence peak of blood retinol than the figure of whole blood (Fig. 1 (c), (d)), showing that the fluorescence intensity increases as the concentration of blood retinol increases. The reason for the difference in EEM visibility between plasma and glass filters with plasma, even in the same individual cow, may be due to the characteristics of the glass filter. The glass filter is made of glass fibers and doesn't fluoresce like filter paper, while still has properties that cause strong light scattering.
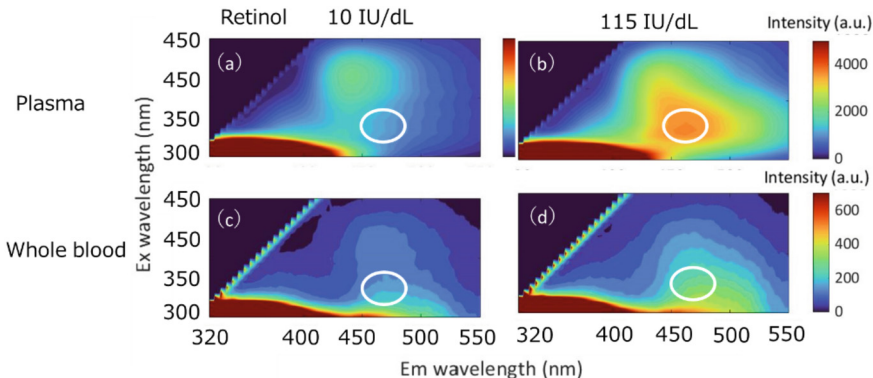
Fig. 1. EEMs of plasma, at a retinol concentration is 10 IU/dL(a), 115 IU/dL (b), EEMs of whole blood, at a retinol concentration is 10 IU/dL(c), 115 IU/dL (d)
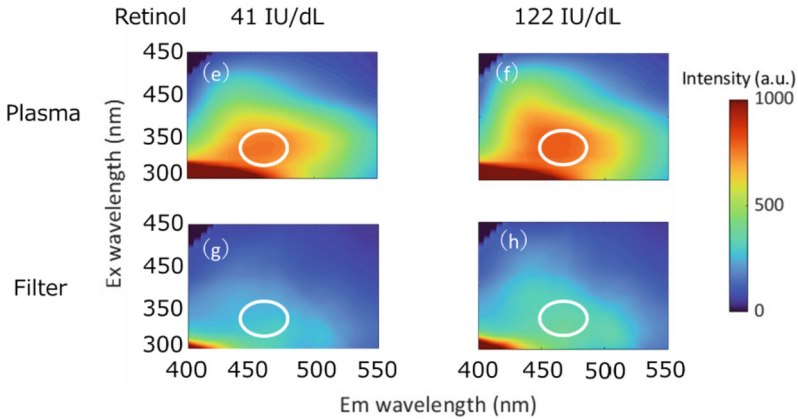
Fig. 2. EEMs of plasma, at a retinol concentration is 41 IU/dL(e), 122 IU/dL (f), EEMs of glass filter with plasma, at a retinol concentration is 41 IU/dL(g), 122 IU/dL (h)

3.2 Results of Retinol Concentration in Blood by PLS Analysis

First, the relationship between the number of each latent variable and RMSECV in a 10-fold cross-validation was tested using data from plasma. The results showed that RMSECV was lowest when there were three latent variables, which led to the conclusion that three latent variables were the appropriate number for this study. PLS analysis with the plasma data as explanatory variables and the actual blood retinol concentration measured by HPLC as the objective bias resulted in a coefficient of determination (R^2_{CV}) was 0.94, a root mean square error of cross-validation (RMSECV) was 7.58 and a ratio of standard deviation to standard error of prediction (RPD) was 4.17.

Next, a similar 10-fold cross-validation was carried out using the whole-blood training set, and the optimal number of latent variables was 3. The data from the Test set were applied to the model constructed by using the Training set, and the estimation results were as follows (Fig. 3). The results showed R^2_{Pred} was 0.91, RMSEP was 9.12 and RPD was 3.36, which can be evaluated as useful accuracy in practical terms [8]. And it turned out to be only about 1.5 difference from the error in the plasma data. The RMSEP in the high-retinol zone above 51 IU/dL was 10.22, in contrast to the RMSEP of 7.03 in the low-retinol zone below 50 IU/dL, which is important for preventing blood retinol deficiency, and thus has good accuracy that is useful in practical applications. The reason for the lower prediction accuracy in the high-retinol zone than in the low-retinol zone is that the distribution of retinol concentrations in the data obtained in this experiment was 19% above 80 IU/dL, 42% between 79 and 29 IU/dL and 39% below 30 IU/dL. This suggests that the reason for the lower prediction accuracy in the high retinol zone than in the low retinol zone may be a bias in the sample data.

The glass filter with plasma data was also tested in the same way as for the plasma data, with a 10-fold cross-validation, and the results showed that 3 was the optimal latent variable. The results showed $R^2{}_{CV}$ was 0.92, RMSECV was 11.1 and RPD was 2.88, which can be evaluated as semi-practical accuracy (Fig. 4). It was expected that glass filter with plasma data would provide more accurate estimates than whole blood data because of the absence of red blood cells and other hematological components, but the opposite was true. A possible reason could be insufficient glass filter with plasma samples. Whole blood data was sampled in every experiment, resulting in 160 samples, whereas glass filter & plasma data was obtained only in the last experiment, resulting in only 22 samples. The number of data points in the EEM is very large (3171) and 22 samples may not be sufficient to fully explain the information contained in the EEM. If more data is collected and re-analyzed, it can be expected that estimates can be made with a high degree of accuracy.
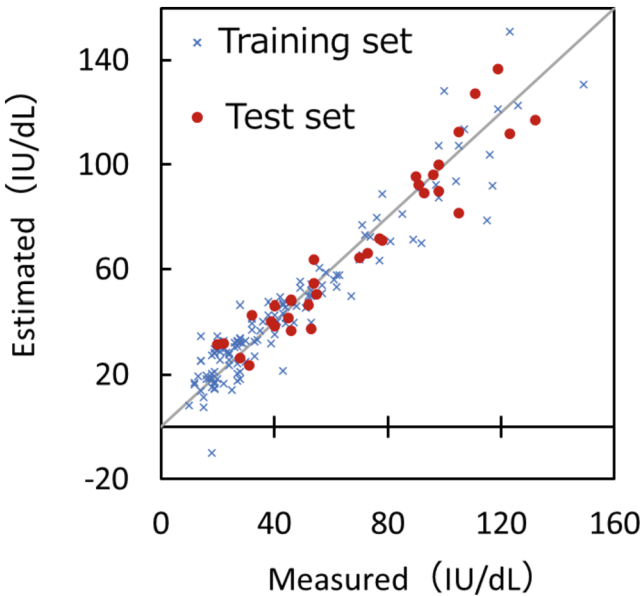
Fig. 3. Relationship between estimated and measured blood retinol concentrations by PLS regression analysis when using data from whole blood.
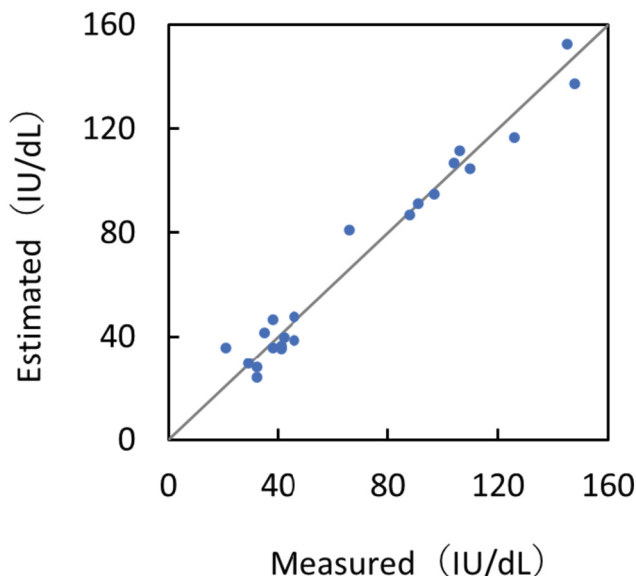
Fig. 4. Relationship between estimated and measured blood retinol concentrations by PLS regression analysis when using data from the glass filter with plasma.

4   Conclusion

This study aimed to develop a rapid, simple, and practical test method for the determination of retinol concentration in blood, which is faster and simpler than the HPLC method, a conventional method for measuring retinol concentration. As a result, two methods were proposed: whole blood without any pre-treatment after blood collection, and plasma absorbed by a glass filter, which is extracted by a plasma filter that separates blood cells by simply dropping a small amount of whole blood. From EEM of all samples. The excitation peak 300 nm and the fluorescence peak between 320 and 400 nm are thought to be amino acid peaks. Retinol fluorescence peaks were visible in plasma, but no clear fluorescence peaks could be seen in whole blood and plasma-absorbed glass filters. In whole blood, this may be due to absorption and scattering of light by the presence of blood cells. And in the plasma-absorbed glass filter, its white scattering body is a factor. PLS regression analysis was performed using the excitation range of 300–400 nm and the fluorescence range of 400–550 nm to avoid the influence of the amino acid fluorescence peak and three latent variables were used. As a result of the PLS regression analysis with each sample, R^2_{Pred}, RMSEP, and RPD are as follows. Whole blood results were 0.91, 9.12, and 3.36, plasma results were 0.94, 7.58, 4.15, and plasma with glass filter results were 0.92, 1.11. 2.88. All RPD value shows these measurement methods have the possibility to estimate retinol levels in blood with accuracy in practical sense. It was thought that glass filters & plasma could provide more accurate estimates than whole blood, but it turned out differently. This could be due to the small number of samples, and better results can be achieved with more samples and are-analysis in the future.

The results suggest that in the future development of techniques for measuring blood VA levels, a variety of test methods may be selected depending on the required measurement accuracy and the complexity of the pre-treatment.

References

1. Oka A (1999) Kurogewasyuhiikugyu no siyougijutsu to vitamin A (feeding techniques and vitamin A for Japanese black fattening cattle). Rinsyo Jui (Clinical Veterinarian) 17(11):16–18
2. Kubo H, Hirose T, Takahira R (2013) Hiikusyukkagyu no kanhaiki to edaniku seiseki oyobi syuueki no mondai (relationship between liver wastage and carcass performance and earnings of fattening shipping cattle.). Bull. Livestock Res. Inst. Toyama Prefectural Agric. Forest. Fish. Res. Cent. 3:17–24
3. Tamura Y, Inoue H, Takemoto S, Hirano K, Miyaura K (2021) A rapid method to measure serum retinol concentrations in Japanese black cattle using multidimensional fluorescence. J Fluoresc 31:91–96
4. Futterman S, Heller J (1972) The enhancement of fluorescence and the decreased susceptibility to enzymatic oxidation of retinol complexed with bovine serum albumin, β-lactoglobulin, and the retinol-binding protein of human plasma. J Biol Chem 247:5168–5172
5. Peterson PA, Rask L (1971) Studies on the fluorescence of the human vitamin a transporting plasma protein complex and its individual components. J Biol Chem 246:7544–7550
6. van den Berg RA, Hoefsloot HC, Westerhuis JA, Smilde AK, van der Werf MJ (2006) Centering, scaling, and transformations: improving the biological information content of metabolomics data. BMC Genomics 7:142
7. Wolfbeis OS, Leiner M (1985) Mapping of the total fluorescence of human blood serum as a new method for its characterization. Anal Chim Acta 167:203–215
8. Williams, P., Norris, K.: Near-Infrared Technology in the Agricultural and Food Industries. American Association of Cereal Chemists, St. Paul, p. 330 (1987)

Determination of Operating Parameters in Milking Robots with Milk First Cow Traffic

Hasan Kuraloğlu[1] and Halil Ünal[2(✉)]

[1] Sürü Yönetimi Hayvancılık Paz. Danış. İth. İhr. San. Tic. Ltdi. Şti., OSB. Mah.,
21 Sk. No: 7/A Kemalpaşa, İzmir, Türkiye
[2] Faculty of Agriculture, Department of Biosystems Engineering, Bursa Uludağ University,
Bursa, Türkiye
hunal@uludag.edu.tr

Abstract. The most important development among technological products has been the realization of milking processes with robotic systems. The main purpose is to reduce the labour, increase animal welfare and improve the quality of life of farmers with the use of robotic systems. Milking robots, which have been used for 30 years in developed countries, entered Turkey about 10 years ago. Robotic milking technology, which has become popular in our country in a short time, will be the most common technological development of dairy cattle enterprises in the future. In this study, it was aimed to determine the parameters and milking values for increasing the efficiency of robotic milking systems, which were acquired with high investment costs, by monitoring the operation in a commercial farm. The farm where the research was carried out was planned according to "milk-first cow traffic" and there are a total of 500 Holstein Friesian breed dairy cows in the farm. Some of the main parameters examined are; number of cows milked per robot, daily milking frequency per cow, daily milking distribution, hourly milking distribution of robots, daily milk yield, milking yield, milk flow, cow's milking time interval, rejection number and duration, robot's daily milking number, robot's milking loading rates in cleaning, idle and non-milking processes, etc. In the two-year trials comparing 8 robots in four barns, the average number of milkings per cow was found to be close to each other across the herd (2.66, 2.70 units/cow, day). In the first year of the trials, the average daily milk yield, yield per milking and time spent on the robot were 32.6 kg, 12.1 kg and 7.41 min, respectively, while in the second year these values were 37.2 kg, 13.9 kg and 7.63 min. Minutes are set. Grouping of animals according to their yield in the second year can be shown as a reason for this change. While the average daily milking number of the robots in the farm was 148.5 times in the first year, this number decreased to 138.3 in the second year, while the daily milking intervals of the cows increased from 8.56 h to 8.72 h.

Keywords: Dairy cows · Robotic milking · Cow traffic · Milking frequency · Robot loading · Milk yield

1 Introduction

Based on the experiences of the countries where dairy farming is developed, "Automation" will make the mechanization that has left its mark on the 21st century independent from the labour. The extensive use of sensors to collect data from animals, the interpretation of information, the addition of external factors to these data, and practical and profitable individual animal management have given a new direction to dairy cattle development. A better understanding of animal feeding has been made possible by mechanization and individual care in farms. The high labor costs also cause the development of individual maintenance-oriented technology and new tool equipment within the system [1].

A conventional dairy farm is managed on the basis of the farmer's observations. The herd is observed several times a day and each animal is checked 2–3 times a day during milking. The overall increase in average farm size leaves farmers less time for individual animals [2]. Data recording and management system in farms; The data collected with the help of sensors, pedometers, scales and other equipment are processed and analysed on the computer. It is mixed with external information (manually entered, cooperative or national animal registration systems data) and compares it with reference intervals (cow's previous performance, expected yield, current period performance, seasonal condition, etc.). The results are reported to the authority with decision suggestions or transmitted to the equipment (feeding system, doors, milking system, etc.) as a claim. All these processes can be done individually for each cow and are fully automatic according to the size of the investment [3].

In order to use resources more effectively on dairy farms, it is necessary to explore the full potential of each individual dairy cow. While herd management is applied in traditional milking farms, the basic logic in sensitive dairy farms is that each cow should be evaluated as an individual and each cow should be managed individually. The most interesting of the precision dairy farming technologies is milking robots. The use of milking robots has increased in the United States, Canada and Australia, especially in European countries. In our country, the use of this technology is new; Since the pros and cons of milking robots compared to traditional milking systems are not fully known by the operators, they are adopted slowly [4, 5].

There are three types of traffic regulations proposed by robot manufacturers in farms. The first is free cow traffic. When the animal leaves the cubicles, it is free to go to the robot or to the feed table. Without any separating cages, gates or directions, the cow can go wherever it wishes entirely of its own accord. Secondly, milk first cow traffic which the feed area and the rest areas are separated from each other. When the animal leaves the cubicles, it uses smart gates located close to the robot to switch to the feed table. If the cow doesn't have milking permission has not come, the smart gate directs the animal to the feed table. If there is a milking permit, the animal is sent to the waiting area in front of the robot to be milked. The cow, whose milking is completed, is directed to the feed table. The animal can pass from the feed lane to the resting area through one-way gates. The third type of traffic is the feed first cow traffic. In this traffic, cows provide free access to the ration feed area with one-way doors. When the cows return from the feeding area, they are controlled by a selection gate and directed to the robot if there is milking permission, and to the resting area if there is no permission [6–9].

There are many international studies on robotic milking systems. However, in Turkey, there are mostly survey-based studies that reveal the statistical figures in the enterprises, and compilation-weighted publications that examine the economic situation and reveal the differences of the system with the existing milking systems [4, 10, 11]. There are almost no studies that reveal the situation of commercial enterprises in the field and contribute to the performance of robotic systems. In this study, it was aimed to determine the 2-year performance of milking-related parameters to increase robot efficiency by following the studies of robotic milking systems in a commercial farm.

2   Material and Methods

2.1   Material

This study was carried out on a commercial farm, which was planned according to the 'milk first cow traffic' type. The main building, where the milking cows are located, consists of four barns of the same size, divided independently from each other, under the same roof. There are 8 robotic milking units in total, two in each barn.

The layout of a barn on the farm and the animal movements in the barn are given in Fig. 1. Accordingly, when the cows want to pass from the resting area (A) to the feeding area (C), they are selected at a pre-selection gate (5) and if there are milking permissions, with the guidance of the separation gate, the robot located in the milking room (B) (1) enters the waiting area (E) to be milked. Otherwise it is sent to the feed area where the partial mixed ration (PMR) is given. The animal that is milked in the robot is left in the exit area (F). Afterwards, it is directed to the separation area (G) if special care or treatment is required, and to the feeding area if it is not required, through another intelligent separator door (5). The transition from the feeding area to the resting area where the cubicles are located is provided by three one-way doors (6). The plans of the four barns on the farm are the same and they are positioned as symmetry of each other [12].

In the first year of the research, milk yield grouping of the cows was not made in the four milking barns in the farm. In other words; the cow that needed to be milked once a day and the cow that was milked four times a day were both included in the same barn group. However, the cows whose teats were not fully suitable for the robotic system were collected in Barn 1 section. The cows in this barn are followed by a worker during the day and attach the milking cups when necessary. In Barn 4, cows that will dry out and pregnant heifers that are close to calve (to get used to the robot) are housed. In the second year of the research, yield grouping was made and medium milk yield group cows were collected in Barn 2 and high milk yield group cows in Barn 3.

In Barn 1, cows that are delayed in milking (more than 8 h after the last milking) are found and fetch from the barn every 2 h. In the other three barns, cows that are delayed in milking are fetch back and 4 times in a day at 09:00, 15:00, 21:00 and 03:00. PMRs are distributed on the farm twice a day, at 08:30 in the morning and at 17:00 in the evening. In addition to PMR, concentrated feed is given from the feed station in the robotic system according to the individual needs of the animal. The ration in the feed line is pushed 3 times a day. In the milk room, there is a bulk milk cooling tank and a buffer tank that serves during the cleaning and milk discharging process. Robots

are automatically washed three times a day (at 03:00, 12:00 and 21:00) with alkaline detergent 3 times and acid detergent once, respectively. A cleaning time of a robot takes an average of 20 min.
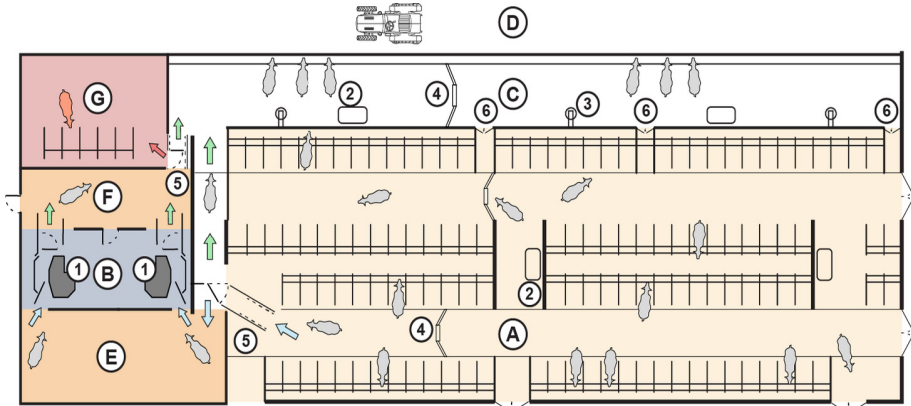
Fig. 1. Layout and animal movements of a barn on the farm. A-Resting area, B-Milking room, C-Feeding area, D-Feeding line, E-Waiting area, F-Exit area, G-Separation area, 1-Robotic Milking System (AMS), 2- Trough, 3-Brush, 4-Manure scraper, 5-Smart gate, 6- One-way gat

The herd management program (DelPro 4.5) used in the farm presents the information coming from all units (robotic system, automatic concentration feed station, smart gates, electronic tags, activity meters, etc.) in the form of a report on the computer. Necessary reports in the herd program, feeding, milking, device, activity, cow and herd monitoring etc. on the "Design Tree" selective time levels. Headers can be created by the user. In this research, the report named "Group Milking" presented under the "Animal" tab of the herd management program was used. In this report, group-based data were selected between certain dates with the "User Defined" tab, and the start date and time of the visit of each animal, its group, the number of the robot on which it was milked, the name of the operation (milking, feed only, rejection, exit without milking), the total milk yield of the cow in one visit, milking time (min:h), number of milking per day, unfinished operations, amount of milk, average milk flow amount (kg/min) were recorded.

2.2 Methods

In this study, two-year performances of the robots in the four barns of the farm were examined. In order for the robot data to represent homogeneous results in the trials, 20 February-20 April of each year was taken as a basis and 60-day data were used. The milking system performance results are not individual for each robot but are given as the average of two robots in the barns. The common waiting area of the two robots is the main reason for averaging. The research period could have been kept longer, but there has been a lot of animal movement in the barns. In addition, drying, sending to the infirmary due to illness, slaughtering, etc. For reasons, it becomes difficult to work with

the same animals in the same barn. The following basic parameters were investigated in each barn on the farm [12]:

– Number of cows milked in a robot (no./2 robots),
– Daily milking frequency per cow (no./day, cows),
– Hourly milking number distribution of the two robots during the day (#/h),
– Daily milk yield per cow (kg/day, cow),
– Cow milk yield per milking (kg/milking, cow),
– Milk flow per cow (kg/min, cow),
– Cow's daily milking time interval (h/cow, day),
– Percent distribution of cow's daily milking time interval (%),
– Time spent on the robot during milking (min),
– Number of rejections per day (number) and rejection times (min/day),
– Number of milking per day per robot (no./day, robot),
– Loading rates of the robot in milking, cleaning, idle and non-milking processes (%),
– Daily labour requirement per cow (man hour/cow, day).

While the above basic parameters can be directly taken from the herd management program, some of them are calculated with linked equations [13–15].

The research data were transferred daily from the herd program and analysed in MS Excel program and analysed in Minitab 17 program. The comparison of barns on the farm was analysed using ANOVA and compared using the LSD test ($P < 0.05$). The mean and standard errors of the data were calculated.

3   Results and Discussion

The milking characteristics of 2 years, obtained from two robots in each of the four barns of the farm, are given in Table 1. As seen in the table, the number of cows milked in the barns varies between approximately 96–122 and 48–61 cows are milked per robot. The number of cows per robot can be expected to be higher (approximately 65 units) in farms with mandatory milk-first cow traffic [14]. Therefore, it can be said that the optimum number of herds could not be reached in other barns except Barn 1 in the farm.

In the first year of the study, the daily milking frequency per animal was found to be higher in Barn 3 and Barn 4 with the values of 2.84 and 2.85 compared to the other two barns (Barn 1: 2.50; Barn 2: 2.59) ($P < 0.05$). In the second year of the study, the milking frequency in Barn 3 increased even more and became the highest barn with a value of 3.06. This barn was followed by Barn 2 with 2.73. As in the first year, Barn 1 had the lowest milking frequency. These values in all barns in the farm were similar to the limit values (2.5–2.9) of the farms applying milk-first cow traffic given in the literature [13, 16–18]. Since the Barn 1 was the lowest and the animals whose udder structure is not suitable for the robot were collected in this barn, the robotic arm was closed and the milking cups were attached manually, reducing the milking frequency. On the other hand, in the first week after the 3–5 days infirmary period, milking of heifers that gave calve for the first time in the second year is done manually in this barn. Thus, the regularity of milking frequency is controlled by the milker until the swelling in the udders of the animal decreases after calving.

Table 1. Two-year milking characteristics of the four barns on the farm (±SE)

Parameter	Unit	Year	Barn 1	Barn 2	Barn 3	Barn 4
Number of milked cows	no./2 robots	1st y.	119.7 ± 0.7a	110.7 ± 0.4b	110.9 ± 0.8b	101.5 ± 1.6c
		2nd y.	124.9 ± 0.9a	102.9 ± 0.7b	100.3 ± 0.7b	90.9 ± 1.7c
Number of days in milk	no.	1st y.	159.6 ± 1.3	141.9 ± 0.9	153.4 ± 1.0	114.8 ± 1.2
		2nd y.	148.6 ± 1.1	123.8 ± 0.9	195.1 ± 1.4	109.4 ± 1.9
Daily milking frequency	no.	1st y.	2.3 ± 0.01	2.1 ± 0.01	2.2 ± 0.01	2.2 ± 0.01
		2nd y.	2.6 ± 0.01	2.6 ± 0.01	2.8 ± 1.01	2.4 ± 1.02
Daily milking frequency	no.	1st y.	2.50 ± 0.02c	2.59 ± 0.02b	2.84 ± 0.02a	2.85 ± 0.02a
		2nd y.	2.40 ± 0.03c	2.73 ± 0.02b	3.06 ± 0.03a	2.44 ± 0.02c
Daily milk yield	kg	1st y.	30.4 ± 0.1c	32.80.2b	33.6 ± 0.3a	33.5 ± 0.2a
		2nd y.	32.9 ± 0.3c	44.2 ± 0.4b	46.6 ± 0.4a	25.1 ± 0.2d
Milk yield per milking	kg	1st y.	12.2 ± 0.1b	12.7 ± 0.1a	11.8 ± 0.1c	11.8 ± 0.1c
		2nd y.	13.8 ± 0.1c	16.2 ± 0.1a	15.3 ± 0.1b	10.3 ± 0.1d
Average milk flow rate	kg/min	1st y.	1.7 ± 0.01a	1.6 ± 0.01c	1.7 ± 0.01a	1.6 ± 0.01b
		2nd y.	1.9 ± 0.01b	1.9 ± 0.01b	2.0 ± 0.01a	1.4 ± 0.01c
Time spent on the robot during milking	min	1st y.	7.2 ± 0.03c	8.1 ± 0.04a	7.0 ± 0.03d	7.3 ± 0.03b
		2nd y.	7.2 ± 0.06c	8.5 ± 0.04a	7.7 ± 0.03b	7.1 ± 0.05c
Number of rejections per day	no.	1st y.	4.7 ± 0.29a	5.1 ± 0.61a	5.5 ± 0.44a	4.3 ± 0.40a
		2nd y.	3.1 ± 0.24c	5.9 ± 0.64a	2.0 ± 0.22c	4.7 ± 0.43b
Daily rejection duration	min	1st y.	2.6 ± 0.5b	5.4 ± 0.8a	4.9 ± 0.6a	4.8 ± 0.5a
		2nd y.	2.3 ± 0.3b	3.0 ± 0.4b	1.9 ± 0.3b	6.2 ± 0.9a
Number of milking per day of the robot	no.	1st y.	149.6 ± 1.1b	142.9 ± 1.0c	157.1 ± 0.8a	144.4 ± 2.1c
		2nd y.	149.4 ± 1.6a	140.6 ± 1.2b	153.0 ± 0.9a	110.1 ± 1.5c
Daily milking interval	h	1st y.	8.7 ± 0.03	8.7 ± 0.03	8.2 ± 0.02	8.6 ± 0.04
		2nd y.	9.7 ± 0.03	8.7 ± 0.02	8.3 ± 0.02	8.2 ± 0.04
Daily labour requirement	man h /day cow	1st y.	0.027	0.006	0.006	0.007
		2nd y.	0.024	0.007	0.007	0.007

[*] Average values shown with lowercase letters (a,b,c,d) on the same line show the differences between years ($p < 0.05$)

When the daily milk yields of the first year in Table 1 are examined, the highest yield was obtained in Barn 3 and Barn 4 with 33.6 and 33.5 kg/cow-day, while Barn 1 with 30.4 kg/cow-day had the lowest barn. It can be thought that the number of cows in Barn 1 is slightly higher than the other barns (120), hand-attached disrupts the milking rhythm, and the profile of the newly born heifer trying to get used to milking in the robot reduces the milking frequency per cow in this barn, resulting in a decrease in milk yield. In the second year on the farm, animals with medium milk yield were collected in Barn 2 and animals with high milk yield were collected in Barn 3. Cows with unproper udder structures were taken to Barn 1, and cows with feed acclimation and low yielding cows were taken to Barn 4 by the farm management. Daily milking averages per cow were low in these two barns and there was no statistical difference between them ($P >$ 0.05). In the second year, the barns with the highest daily milk yield were determined in Barn 2 and Barn 3 with 44.2 and 46.6 kg/cow. The lowest milk yield is in Barn 4 with 25.1 kg/cow-day. Although the number of animals in Barn 3 decreased by 10 in the second year compared to the first year, the daily milk yield of the second year increased by 39% compared to the first year. This amount has been reached thanks to the fact that animals with high milk yield throughout the farm are taken to this barn in the second year. It is an important issue to know how much milk will be given in addition to animals that are milked more than twice a day. When the milk amounts of cows milked 3x times a day and cows milked 2x are compared, the amount of milk can increase by 20% on average at 3x milking. If milking 4x times, an extra increase of 5–10% can be achieved. The additional increase in milk yield through stimulation of milk producing cells is associated with better feeding and better management on the farm that is milked 3x times [7]. With the grouping strategy made in the second year on the farm, feeding was done according to the expected yields in Barn 3, where the high-yielding cows were housed, and the highest milk yield was obtained.

The increase or decrease in the daily milk yield of the cows according to the years similarly increased or decreased the milk yield per milking. Accordingly, the milking yield, which was 11.8 kg in the first year in Barn 3, increased by 30% in the second year and rose to 15.3 kg, while the milking yield, which was 11.8 kg in Barn 4, decreased by 13% in the second year and decreased to 10.3 kg. (Table 1). While milking frequencies and daily milk yields in Barn 3 and Barn 4 were the highest in the first year compared to other barns, milk yields per milking were found to be the lowest (11.8 kg/milking). High-yielding cows are milked more frequently in these two barns. It can be said that this causes the total milk yields per day cow to be higher, but the milk yields per milking to be lower than the other two barns. On the other hand, while milking frequencies and daily milk yields in Barn 2 and Barn 3 were found to be the highest in the second year compared to other barns, milk yields per milking were also found to be high (16.2 and 15.3 kg/milking), unlike the first year. In these two barns, high-yielding cows were milked more frequently, increasing milk yields per milking. The fact that the farm collects the cows with high milk yield in these two barns and feeds them with a focus on yield reveals that the milk-based strategy is applied correctly. Milk yield increases showed that the cows were accustomed to the robot system. Controlling the robot operation from the manager to the workers in the barn, increasing the milking efficiency of the cows with

increasing lactation age and adapting to the environment and knowing the system, and herd grouping provided this improvement.

Another factor affecting the yield per milking is the milk flow rate. This value, which is related to the genetics of the animal, is also affected by environmental conditions, the care and settings of the milking system and the training of the cows. Stress is low in any animal that is well fed and has welfare conditions, and if milking is done at the right time with the right conditions and equipment, the milk flow rate will increase. Since no grouping was made in the first year of the study, the milk flow rates in the 4 barns were close to each other (1.6–1.7 kg/min) (Table 1). In the second year, thanks to cow grouping, milk flow rates reached the highest levels with 1.9–2.0 kg/min in Barn 2 and Barn 3. As expected, it was determined at the lowest level (1.4 kg/min) in Barn 4, where animals in the low yield group were housed. Although there are cows with unsuitable udder structure in Barn 1, milk flow rate values (1.9 kg/min) are high when it is considered that high-yielding cows are housed in this barn. The average milk flow rate values obtained in the farm both in the first year and in the second year were found to be higher than the data in the studies of other researchers [13], 1.44 kg/min; [19], 1.5 kg/min).

The time spent by the cows on the robot; daily milking frequency, milk yields per day and per milking, and milk flow rates are closely related. In the first year in which grouping was not done, the time spent by the cows in the robot in other barns, except Barn 2, was close to each other and at lower times (between 7.0 and 7.3 min). With the grouping made in the second year, the daily milk yields (44.2–46.6 kg) in Barns 2 and Barn 3 are 35–39% compared to the first year, and the milk yields per milking (16.2–15.3 kg) are in the first year. While it increased by 29% compared to the previous year, the time spent in the robot did not increase at the same rates (Table 1). The time spent in the robot in Barn 2 and Barn 3 in the medium and high yield groups increased slightly (between 5–10%) thanks to the increase in daily milking frequency and average milk flow rates. The fact that the time spent on the robot does not increase much is a desired situation for the entire herd to use the robot effectively.

When the daily rejection numbers of cows in the robot are examined, in the first year there were 4.3–5.5 rejections in the barns, while in the second year the rejection numbers decreased in Barn 1 and Barn 3 (3.1–2.0), and in Barn 2 and Barn 4. It increased in (5.9–4.7 units) (Table 1). While the rejection times in the robot were between 2.6–5.4 min in the first year, in the second year they increased in Barn 4 (6.2 min) and decreased in the other barns (1.9–3.0 min). When the rejection times of the first year are examined, the lowest rejection period was realized in Barn 1 with 2.6 min. Since the milking of the cows housed in this barn is controlled by the milker, the acceleration of the removal of the cows from the robot has reduced the rejection time. When the second-year rejection periods were examined, the longest period was found in Barn 4 with 6.2 min. Castro et al. [13] determined the daily rejection period to be 13.2 min. The rejection times found for all barns in this study were well below the study of Castro et al. [13]. Since the smart gates that select the animals before the waiting area are used in the farms where the milk-first cow traffic type is applied, the cow that has not received milking permission should not come to the robot. That is, the number and duration of rejections in the robot must be zero. However, after milking, the cows that are allowed

to be caught in the research farm are taken to the separation area (preliminary infirmary area). After the process in this area, the animal that needs to be sent to the feed area is left to the waiting area of the robot again because the ground structure in the farm does not allow this (code difference between the feed area and the separation area). Thus, the newly milked animal enters the system in a short time and leaves the feed area without milking. The system registers such cows as "rejection". In the second year, the ground level difference between the separation area and the feed area was eliminated. When the robotic system malfunctions, the cows are herded collectively to the waiting area. In such cases, the choice is left to the robot. This reduces the performance of the robotic system.

The maximum number of milking performed by a robot during the day was 157.1 units in Barn 3 in the first year data. The lowest milking number was 110.1 in Barn 4 in the second year (Table 1). This situation can be primarily associated with the number of animals in the barn in those years (110.9 cows in Barn 3 in the first year, 90.9 cows in Barn 4 in the second year). On the other hand, although the number of animals in Barn 1 was the highest in both years (119.7 and 124.9), the robot milking numbers were not as high as expected. The reason for this situation can be shown as insufficient milker performance due to manual milking of animals whose udder structure is not suitable for the robot in Barn 1. In Barn 3, although the number of animals in the second year was 100.3, the second lowest barn, it reached the highest robot milking rate. The grouping of high-yielding animals on the farm in this barn for the second year increased the robot loading rate.

When the daily milking intervals of the cows were examined, values close to each other were found between 8.6–8.7 h in the other barns except Barn 3, which was the lowest in the first year (Table 1). In the second year, milking intervals increased in Barn 1, remained at the same time in Barn 2 and Barn 3, and decreased in Barn 4. It can be said that the manual attachment of the milking heads of the cows in Barn 1 and the difficulties associated with it, the inability of the milker to catch and bring the cows whose milking time has come, and accordingly the low desire of the cows to come to the robot unit cause the milking interval time to increase. In Barn 3, which is in the high milk yield group, the fact that the cows fetching is decreased the milking interval time.

Among the barns, the highest labour requirement was in Barn 1 (average 0.025 worker h/day cows). In this barn, the attaching the udders is done with human labour and one person undertakes this task in each shift. In the other three barns, the labour requirement was found to be very low (average 0.007 worker h/cow day) since the people working in shifts only did routine work (bed cleaning, etc.). It can be said that the adaptation of the cows to the robotic system has decreased the labour over the years (Table 1).

The ratios of the time spent by two robots in each barn in milking, idle, cleaning and non-milking operations are given in Fig. 2. As seen in the figure, the highest percentage of loading of robots in milking in the first year was found in Barn 2 and Barn 3 with 79.8% and 76.7%, and the lowest rates were found in Barn 4 and Barn 1 with 73.4% and 74.7%. Leaving the milking routines completely to the robots in Barn 2 and Barn 3 increased the loading percentages. Manual attachment in Barn 1 and first practice of feed in Barn 4 decreased the percentage of milking time. Although the process of bringing animals back and forth in Barn 1 is higher than in other barns, the individual

performance inadequacy of the workers reduced the loading rate of the robots in milking. In the second year, thanks to the yield grouping of the barns, milking time percentages increased to 82.9% and 83.8% in Barn 2 and Barn 3. Barn 1 maintained the same rate (74.0%) in the second year, but the milking percentage decreased significantly (54.3%) in Barn 4, where low-yielding cows were taken.

When the idle time of the robots in the barns for the first year was examined, it was seen that it ranged from 14.9% (Barn 2) to 20.3% (Barn 1). In the second year, the percentages of idle time in Barn 2 and Barn 3 decreased significantly (9.8%-10.7%) thanks to yield grouping (Fig. 2). Idle percentage decreased slightly in Barn 1, but increased significantly (37.1%) in Barn 4. The most influential factor on idle time is the number of animals. On the other hand, wrong strategies in animal traffic, not supporting the type of traffic and not training the animals can be the reasons for this. Thanks to the yield grouping made in the second year, the loading rates of Barn 2 and Barn 3 increased and the percentage of idle times decreased.
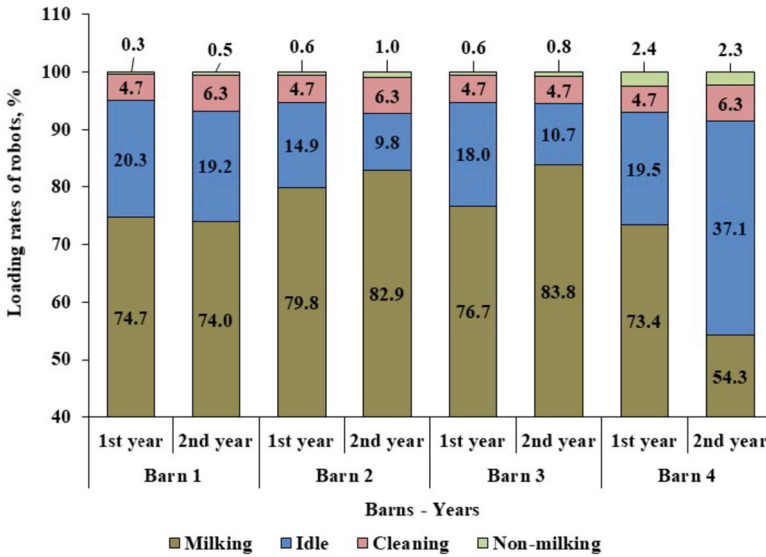
Fig. 2. Rates of time spent by robots in milking, idle, cleaning and non-milking operations

In general, increasing the number of cows in the barn can reduce idle time. However, increasing the number of cows is not the only factor that will increase the performance of the robot. Cow traffic management is also important. In other words, in order to reduce the idle time in robots, animals that have not been milked should be trained instead of bringing them [20]. Laurs et al. [17] found the rate of idle time to be 19% in a study they conducted in a guided type barn with 88 cows. Idle time rates found in this study Laurs et al. The research values stated in [17] were found at similar rates, and even lower rates in the second year in two barns (Barn 2 and Barn 3).

The times spent in cleaning in the barns were taken the same in all barns. In the first year, three main washes were carried out at 04:00, 12:00 and 20:00 for 20–25 min each.

In the second year, the number of cleanings was increased to 4 by adding 08.00 h in other barns except Barn 3. Therefore, excluding Barn 3, cleaning time percentages were 4.7% in the first year and 6.3% in the second year (Fig. 2). When the idle time of the robot exceeds 30 min, the system performs a short rinse. Cleaning processes such as cleaning and rinsing can be changed in the system. If the number of cows that are not milked on maintenance-repair day increases, the cleanings can be cancelled. In the second year in Barn 3, detergent washing was not increased in this barn as highly productive cows kept the robots busy.

When the processes other than milking were examined, Barn 4 was found to be different from other barns with an average rate of 2.4% (Fig. 2). Rejection, exit without milking and manual milking are included in the external milking header. Apart from these features, the prenatal training of pregnant heifers to the robot by using the "only feed" function in Barn 4 increased the non-milking rate.

The milking rates according to the number of milking per day in the barns are given in Fig. 3. When the figure is examined, the distribution of milking numbers per cow in both years is concentrated in 2x, 3x and 4x. In 1x milking, cow milking rates, which were 0.5% (Barn 3) and 3.8% (Barn 2) in the first year, decreased significantly in the second year except Barn 4 (Barn 3–0.3% and Barn 2–1.0%). In the second year when yield grouping was made, 4x milking increased significantly in Barn 2 and Barn 3, reaching 14.3% and 20.8%. When the 1x and 2x milking in Barn 2 and Barn 3 were examined, it was determined that these milking decreased in the second year and increased 3x and 4x milking. Especially in Barn 3, 2x and higher milking are 99.8%, which corresponds to almost all cows. It is mostly milking 3x times and above. With the purchase of low milk yielding cows in barn 4 in the second year, the percentage of cows milked 1x times increased significantly in this barn, from 1.9% to 7.6%. In addition, in Barn 4, the rate of
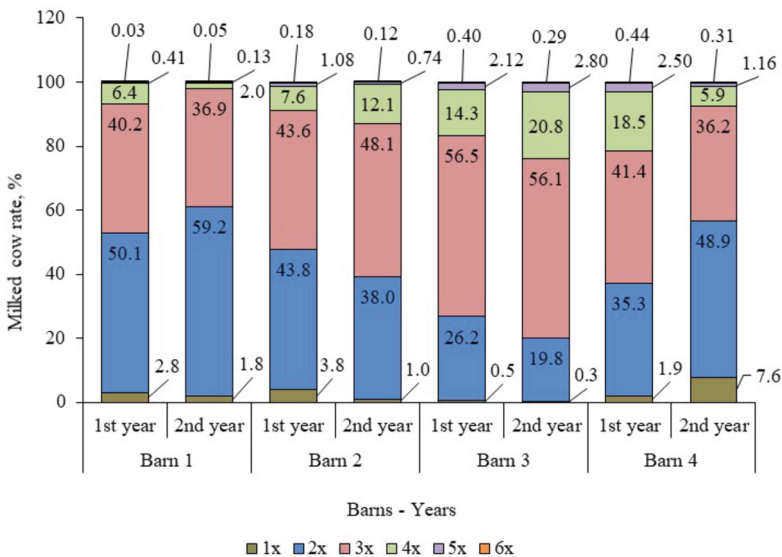
Fig. 3. Milking rates of cows in barns according to daily milking numbers

cows milked 4x times decreased by 68%, the rate of cows milked 3x times decreased by 28%, while the percentage of 2x milking increased by 38.5%. Thanks to the grouping created in the farm in the second year, the number of milking was increased especially in Barn 2 and Barn 3, and this contributed positively to yield. In Barn 4 and Barn 1, where the averages are low, robot visits can be improved with the feeding strategy of the cows, their training, and the routine fetching operations of those who are not milked.

When the hourly milking numbers of the two robots in the barns are examined in a 24-h period, the lowest and highest milking numbers in the first year were found in Barn 1 with 4.6 and 15.4 milking (Table 2). The cleaning times of the robots in the barns were made three times in the first year at 04:00, 12:00 and 20:00, and in the second year it was increased to four by adding 08:00 h. Only in Barn 3, no changes were made in the second year. In the first year average, visits to robots in Barn 3 were found to be the highest with 13.1, followed by Barn 1 with 12.5. Barn 4 and Barn 2 averaged 12.0 units. The hours when robotic units are cleaned have the lowest milking counts. The milking numbers in Barn 2, Barn 3 and Barn 4, where milking is completely left to the robots, match the flow of animal traffic, but because the teats of the animals in Barn 1 are crossed and close, the udder insertion process was done manually. Although there was no cleaning especially in the morning (08:00–09:00) and evening (15:00–16:00), the milking numbers decreased a little more in Barn 1. It can be said that the shift change of the caregivers in the farm during these hours hinders the manual intervention. On the other hand, in the robot cleaning at 12:00, the number of milking in Barn 1 was found to be less than in other barns. Here too, the fact that the caregivers who need to intervene manually are on a lunch break, may be the reason for this decrease. The high milking numbers in other barns except Barn 1 indicate that these barns are not dependent on labour.

Table 2. Distribution of hourly robot milking during a day (total of two robots)

Daily time intervals	Barn 1		Barn 2		Barn 3		Barn 4	
	1styear	2ndyear	1styear	2ndyear	1styear	2ndyear	1styear	2ndyear
(00)-(01)	14.58	13.83	13.50	13.02	14.05	13.42	12.58	10.53
(01)-(02)	14.78	15.15	13.18	12.87	14.13	13.47	12.80	10.15
(02)-(03)	14.18	15.22	12.90	12.82	13.72	13.85	12.73	11.12
(03)-(04)	14.02	15.60	12.62	12.72	13.82	14.15	12.57	11.95
(04)-(05)	6.03	7.32	6.40	9.20	6.82	9.45	7.10	7.68
(05)-(06)	9.55	11.93	9.05	10.53	12.47	11.95	11.02	9.10
(06)-(07)	15.25	16.13	12.40	11.65	13.15	11.60	12.05	10.80
(07)-(08)	13.33	11.53	12.45	10.57	12.47	10.18	12.73	8.70
(08)-(09)	10.13	9.87	12.47	11.45	12.68	12.80	11.47	4.68
(09)-(10)	14.72	13.80	13.70	12.00	14.05	13.72	12.80	10.23

Table 2. (*continued*)

Daily time intervals	Barn 1		Barn 2		Barn 3		Barn 4	
	1st year	2nd year	1st year	2nd year	1st year	2nd year	1st year	2nd year
(10)-(11)	15.38	13.33	13.58	12.45	15.17	13.53	13.88	11.38
(11)-(12)	14.47	13.85	12.83	12.78	13.95	13.50	13.05	8.70
(12)-(13)	4.62	8.90	6.53	9.27	6.55	10.12	6.58	5.43
(13)-(14)	10.18	11.30	9.35	11.10	12.43	12.90	11.50	7.28
(14)-(15)	12.88	13.60	12.97	11.90	13.90	13.12	12.98	8.50
(15)-(16)	10.68	12.43	13.25	12.60	14.55	13.48	13.03	10.50
(16)-(17)	14.68	13.17	12.92	12.33	15.13	14.03	13.47	11.33
(17)-(18)	14.60	14.38	13.50	12.85	15.23	14.30	13.03	11.07
(18)-(19)	15.12	14.60	13.63	13.12	14.88	14.42	12.72	10.85
(19)-(20)	13.78	14.00	13.47	12.98	14.22	13.77	12.60	9.58
(20)-(21)	7.08	5.52	7.82	7.38	8.08	8.28	7.78	5.05
(21)-(22)	11.35	10.95	10.58	10.18	14.05	13.30	13.30	8.78
(22)-(23)	14.12	13.40	13.10	12.45	14.17	13.43	13.48	8.32
(23)-(24)	13.68	8.93	13.68	12.88	14.58	13.28	13.48	8.50
Smallest	4.6	5.5	6.4	7.4	6.6	8.3	6.6	4.7
Biggest	15.4	16.1	13.7	13.1	15.2	14.4	13.9	12.0
Average	12.5	12.4	11.9	11.7	13.1	12.8	12.0	9.2
(00)-(08)	12.7	13.3	11.6	11.7	12.6	12.3	11.7	10.0
(08)-(16)	11.6	12.1	11.8	11.7	12.9	12.9	11.9	8.3
(16)-(24)	13.1	11.9	12.3	11.8	13.8	13.1	12.5	9.2

In the second year average; the highest number of visits to robots was found in Barn 3 with 12.8, followed by Barn 1 with 12.4, Barn 2 with 11.7 and Barn 4 with 9.2. The lowest milking counts were again realized during the hours when the robots were cleaning. In the second year, unlike the first year, one more wash was added and the daily wash was increased to four. In the second year, the number of milking decreased during the cleaning periods. The decrease in milking numbers continued during shift changes and lunch breaks. Except for Barn 3, the addition of one more cleaning and the change of shifts in the other barns at 08:00–09:00 in the morning decreased the milking habits and rhythm.

When the daily milking intervals of the cows were examined, values close to each other were found between 8.6–8.7 h in the other barns except Barn 3, which was the lowest in the first year (Table 1). In the second year, milking intervals increased in Barn 1, remained at the same time in Barn 2 and Barn 3, and decreased in Barn 4. It can be said that the manual attachment of the milking heads of the cows in Barn 1 and the difficulties associated with it, the inability of the milker to catch and bring the cows

whose milking time has come, and accordingly the low desire of the cows to come to
the robot unit cause the milking interval time to increase. In Barn 3, which is in the high
milk yield group, the fact that the cows fetching is decreased the milking interval time.

It was stated in Table 1 that there was no significant difference between the visit
times of the 2-year-old cows to the milking robot in the four barns in the farm, except
for Barn 3. In the second year, milking intervals increased in Barn 1, remained at the
same time in Barn 2 and Barn 3, and decreased in Barn 4. One of the features of robotic
milking is that cows can voluntarily visit the milking robot. This causes a significant
variation in the frequency of visits to the milking robot and therefore milking intervals
can result in high variation. For this, the milking time intervals of the cows in the robot
visit were examined proportionally (Fig. 4). As seen in the figure, the highest rate of
milking between 4–12 h in the first year was found in Barn 3 (89.4%). Barn 4 followed
this with 88.7%. Although Barn 3 decreased a little after the second year yield grouping,
it was still found to have the highest percentage (88.8%) in the 4–12 h milking interval.
Barn 1 and Barn 4 were found to have the lowest milking interval percentages close to
each other at these time intervals in the second year (81.3–81.5%).
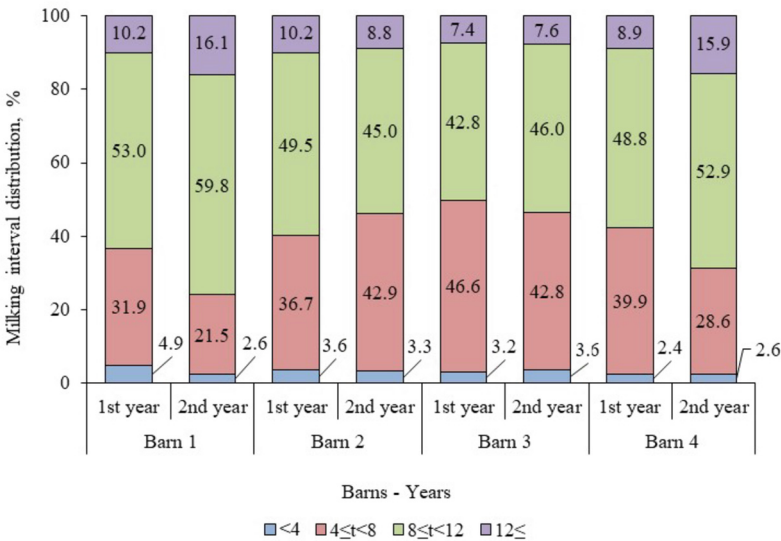
Fig. 4. Distribution rates of cows in the milking interval

On the other hand, the fact that the rates of milking over 12 h in Barn 1, which is
10.2%, and Barn 4, which is 8.9%, increased by 58% and 79%, respectively, compared
to the first year, may pose a problem for animal health. Since milking routines are largely
left to the robot in the second year, it makes it difficult to follow up cows that are delayed
in milking. In this case, human labor and initiative cause delays in the transportation of
the animal. On the other hand, milking visits under 4 h is another problem that reduces
robot performance. Because arrivals to the robot under 4 h cause rejections. In both years,
milking in all barns averaged 3% in less than 4 h. Hogeveen et al. [21] investigated the

relationship between the milking interval of the milking robot, milk production and milk flow rate on 66 cows. They found that 9.7% of milking were shorter than 6 h and 17.6% were longer than 12 h. The researchers reported that the average daily milking frequency of 6% of all cows was less than two, and this was due to the cow factor and the time of the day affecting the change in the milking interval. In addition to the cow factor, the authors found that milking interval length also had a significant effect on milk production and milk flow rate. They found that the effect of milking interval on milk production per hour was greater in high-yielding cows than in low-yielding cows. It can be said that the findings of the researchers are similar to the results of this study.

4 Conclusion and Suggestions

The priority of this study was to determine the performance of the robots in the processes of the commercial farm, including the first years of its establishment, to determine the factors affecting the performance and to propose solutions. The results obtained from this study can be summarized as follows.

– The daily milking frequency in the barns varied between 2.50–2.85 in the first year, and the number of 3.06 in Barn 3 was reached in the second year thanks to the grouping made throughout the farm. This showed that it is beneficial to classify animals according to yield groups for more effective use of robot performance.
– The daily milk yield in the farm increased by 35% in Barn 2 and 39% in Barn 3 in the second year. There was a slight increase in yield in Barn 1 where cows with bad udder structure were present, and it decreased by 25% in Barn 4 where cows with low milk yield were dried. It can be said that over time, the employees' mastery of the use of robots, the increase in the lactation age of the cows and the recognition of the system by adapting to the environment have increased the efficiency. Especially the yield grouping of the herd also provided this improvement.
– The fact that the farm collects the cows with high milk yield in Barn 2 and Barn 3 and feeds them with a focus on yield reveals that the milk-focused strategy is applied correctly. Milk yield increases showed that the cows were accustomed to the robot system.
– After the efficiency grouping of the barns, the loading percentages of the robots in Barn 2 and Barn 3, where medium and high yielding cows are located, were 80% and 77% in the first year, while increasing this to 83–84% in the second year is a significant improvement. This increase in milking has also significantly reduced the idle time of robots in existing barns (from 15–18% to 10–11%). The biggest reason for potential improvement seems to be using milking management strategies to increase the percentage of time each robot milks cows. It can be said that leaving the milking routine completely to the robot in farm management and especially the length of time spent in milking of high-yielding cows contribute to this improvement.
– Milking rates according to the number of milking per day in the barns were concentrated in 2x, 3x and 4x times milking across the farm. After the yield grouping in Barn 2 and Barn 3, a significant increase was achieved especially in 3x and 4x milking rates. This contributed positively to the yield. In Barn 4 and Barn 1, robot

visits can be improved by the feeding strategy of the cows, their training, and the routine fetching of the unmilked.

– The number of cows milked by the double robots in the barns during the day was the lowest during the cleaning of the robots. However, since certain time intervals where no cleaning is done coincide with the shift change of the caregivers or the lunch break, the milking visits in Barn 1 and Barn 4, which require manual intervention, have decreased. Yield grouping in Barn 2 and Barn 3, milking frequency of cows, milk yield etc. It has been observed that the robot performance can be maximized due to the improvement of the robots.

– Cow grouping can be done on farms that do not have capacity problems and have more than one robot. When creating groups, the number of cows with milking numbers suitable for robot loading should be taken into consideration.

– Idle time must be created for robots. In this way, non-dominant cows are not turned away during robot visits and the desired daily milking numbers can be achieved in the robots.

– Cows whose teat structure is not suitable for robot milking should be removed from the herd. Solutions that are contrary to robot operation, such as manual tooling, should be avoided.

– Cow traffic within the barn should be planned correctly. Interventions that will negatively affect the robot's performance should be avoided.

References

1. Rodenburg, J.: Success factors for automatic milking. In: Precision Dairy Conference, Mayo Civic Center, Rochester, Minnesota, June 26−27, 2013. pp. 22−34 (2013)
2. Hogewerf, P.H., Lokhorst, C., de Koning, C.J.A.M., Ipema, A.H., Bleumer, E.: Smart dairy farming: care for individual cows. In: ICAR 2012 38th Conference, pp. 28–05. Cork Ireland (2012)
3. Katz G et al (2007) Current and near term technologies for automated recording of animal data for precision dairy farming. J Anim Sci 85:377
4. Örs, A., Oğuz, C.: Milking robots, is it worth it to buy? Süleyman Demirel University, Faculty of Agriculture, Depart. of Agricultural Economics, 12th Agricultural Economics Congress, March 25–27, 2016, Isparta, pp. 1605–1614 (2016)
5. Örs A, Oğuz C (2018) Comparison of the economic performance of robotic milking system and conventional milking system. Manas J. Agric. Vet. Life Sci. 8(2):35–51
6. Kuraloğlu, H., Kulaç, S., Ünal, H.: Operating parameters in milking robots with forced cow traffic. In: ISPEC 12. International Conference on Agriculture, Animal Science & Rural Development, Ordu, Türkiye, 6–8 July 2023, pp. 801–819 (2023)
7. Hobbis, M.J.: Planning the right robotic system for the cow. In: Precision Dairy Conference, Mayo Civic Center, Rochester, Minnesota, June 26–27, 2013, pp. 123−126 (2013)

8. Rodriguez, F.: Choosing the right cow traffic system for your robotic dairy. Progressive Dairyman Magazine (2012). http://www.progressivedairy.com/index.php?option=com_content&view=article&id=9447:choosing-the-right-cow-traffic-system-for-your-robotic-dairy&catid=51:cow-comfort&Itemid=77

9. Rodriguez, F.: On guided cow traffic and feeding strategies in robotic dairies (2014). http://blog.delaval.com/dairy-farming/guided-cow-traffic-in-robotic-dairies/

10. Gonulol E (2016) Evaluating of robotic milking performance in Turkey. J. Emerg. Trends Eng. Appl. Sci. 7(1):31–34

11. Akar Çıkrıkçı, C.: Determination of herd management performance values of dairy farms that used robotic milking system in Turkey, Master's Thesis, Tekirdağ Namık Kemal University, Graduate School of Natural and Applied Sciences, Dept. of Biosystems Engineering, p. 32 (2019)

12. Kuraloğlu, H.: Determination of the parameters and milking values relating to increasing robot efficiency in robotic milking systems, Ph. D. Thesis, Bursa Uludağ University, Graduate School of Natural and Applied Sciences Department of Biosystems Engineering, p. 137 (2022)

13. Castro A, Pereira JM, Amiama C, Bueno J (2012) Estimating efficiency in automatic milking systems. J Dairy Sci 95:929–936

14. Priekulis, J., Laurs, A.: Research in automatic milking capacity. In: 11th International Scientific Conference, Engineering for Rural Development, May 24–25, 2012, Jelgava, Latvia, pp. 47−51 (2012)

15. Ünal H, Kuraloğlu H (2016) Determination of optimum cow capacity in robotic milking systems. J. Agric. Mach. Sci. 12(2):149–156

16. Ipema AH (1997) Integration of robotic milking in dairy housing systems: review of cow traffic and milking capacity aspects. Comput Electron Agric 17:79–94

17. Laurs, A., Priekulis, J., Purins, M.: Studies of operating parameters in milking robots. In: 8th International Scientific Conference, Engineering for Rural Development 28–29.05.2009, pp. 38–42 (2009)

18. Sitkowska B, Piwczynski D, Aerts J, Waskowicz M (2015) Changes in milking parameters with robotic milking. Arch. Anim. Breed. 58:137–143

19. Heringstad, B., Kjøren Bugten, H.: Genetic evaluations based on data from automatic milking systems. In: 39th ICAR Session, May 19–23. Berlin (2014)

20. Devir S, Ketelaar-deLauwere CC, Noordhuizen JPTM (1999) The milking robot dairy farm management: operational performance characteristics and consequences. Am. Soc. Agric. Biol. Eng. Trans. ASAE 42(1):201–213

21. Hogeveen H, Ouweltjes W, de Koning CJAM, Stelwagen K (2001) Milking interval, milk production and milk flow-rate in an automatic milking system. Livest Prod Sci 72:157–167

Fine-Tuning Growth Conditions: Leaf-Level Vapor Pressure Deficit Control for Optimized Photosynthesis

Temuçin Göktürk Seyhan(✉) 🆔 and Sinem Seyhan 🆔

Faculty of Agriculture, Department of Agricultural Machinery and Technologies Engineering, Ankara University, 06135 Ankara, Turkey
seyhan@ankara.edu.tr

Abstract. The optimization of plant growth conditions plays a crucial role in enhancing photosynthetic efficiency, which ultimately impacts crop productivity and resource utilization. Among various environmental factors, vapor pressure deficit (VPD) has gained considerable attention due to its significant influence on stomatal conductance and water loss in plants. This paper presents a comprehensive study on the fine-tuning of growth conditions through precise control of leaf-level VPD to optimize photosynthesis. To investigate the difference between constant relative humidity condition and constant leaf-level VPD, a series of controlled experiments were conducted. Humidifier, air conditioning and exhaust fan were used to control relative humidity, thus VPD. For the first experiment, temperature and relative humidity were set to 21.0 ± 1 °C and $65 \pm 5\%$, respectively. For the second experiment, temperature and VPD were set to 21.0 ± 1 °C and 1.2 ± 0.2 kPa. Relative humidity was changed according to calculated VPD value.

Under controlled leaf-level VPD conditions, a distinct optimization of photosynthesis, with a notable increase in biomass production and overall plant quality were observed, highlighting the significance of precise control over this environmental parameter. Experiments indicated that VPD control affects stomatal regulation, leading to improved water-use efficiency and reduced water loss. These findings emphasize the potential of optimizing growth conditions through VPD control to achieve sustainable water management and resource conservation in agricultural systems. Based on the obtained results, we propose practical strategies for implementing leaf-level VPD control in controlled environment agricultural practices. By fine-tuning growth conditions to maintain an optimal VPD range, farmers and researchers can optimize photosynthetic efficiency, reduce water consumption, and enhance crop productivity. This approach has the potential to address the challenges posed by climate change and limited water resources while ensuring sustainable and efficient agricultural production.

In conclusion, this paper highlights the importance of leaf-level VPD control for optimizing photosynthesis and improving resource utilization in plant growth. The findings contribute to the understanding of plant-environment interactions and offer valuable insights for agricultural practices aimed at achieving sustainable and efficient crop production.

1 Introduction

The optimization of plant growth conditions is crucial in vertical farming [1]. The conditions in which plants grow have a profound impact on their overall health, productivity, and resource usage [2]. By fine-tuning these growth conditions, it is possible to enhance photosynthetic efficiency, ultimately leading to increased crop yields and more sustainable agricultural practices. Among the various environmental factors that influence plant growth, vapor pressure deficit (VPD) has gained significant attention for its role in regulating stomatal conductance and water loss in plants [3]. This paper delves into a comprehensive study on the importance of fine-tuning growth conditions by controlling leaf-level VPD to optimize photosynthesis and, in turn, improve crop productivity and resource utilization.

Vapor Pressure Deficit (VPD) is a crucial environmental parameter that characterizes the relationship between air temperature and humidity. It is typically calculated as the difference between the saturation vapor pressure and the actual vapor pressure in the atmosphere. VPD holds immense significance in plant physiology and agriculture due to its direct influence on various plant processes. VPD is a key determinant of stomatal conductance, with higher VPD values generally leading to increased transpiration rates as plants open their stomata to release water vapor [3]. This parameter plays a vital role in regulating plant water-use efficiency, which is essential for sustainable water management in agriculture [4]. Additionally, VPD significantly affects photosynthesis by influencing the rate of carbon assimilation in plant tissues. Moreover, VPD is intimately tied to how plants respond to environmental stressors, making it a critical factor in understanding plant-environment interactions and developing strategies to optimize plant growth conditions. A VPD of 1.20 kPa promotes stomatal opening, reduces the CO_2 diffusion resistance from the atmosphere to the into the leaves and provides sufficient substrates for photosynthesis [4]. Authors of [5] found that VPD has a significant effect of leaf size, leaf mass per area, leaf dry matter content and relative water content.

Leaf-level VPD is a measure of the difference in vapor pressure between the inside of a plant leaf and the surrounding air [6]. Leaf-level VPD is more important because it is the driving force for transpiration, which is the process by which plants lose water vapor through their leaves [7]. Leaf-level VPD is a better indicator of plant water status than air VPD because it considers the plant's ability to regulate its own transpiration rate [8]. For example, if the air is very dry, plants will close their stomata (pores on the underside of leaves) to reduce water loss. This will result in a lower VPD_{leaf}, even if the air VPD is very high [8]. In ferns, for instance, it has been observed that hydraulics regulates stomatal responses to changes in leaf water status [9]. In [10], authors state that the temperature of leaves plays a direct role in controlling the rate of photosynthesis, the relative humidity of the air surrounding the leaves has an indirect effect on plant growth and development by influencing processes like transpiration, uptake of CO_2,

and exchange of O_2. Stomatal apertures, which are affected by various environmental conditions including humidity and light, determine the rate of exchange of water vapor, CO_2, and O_2.

The primary purpose of this study is to comprehensively investigate the role of vapor pressure deficit (VPD) in fine-tuning plant growth conditions to optimize photosynthesis. The significance of this research lies in its potential to significantly enhance our understanding of plant-environment interactions and its practical applications in agricultural practices. We aim to address several key objectives, including assessing the impact of controlled VPD conditions on photosynthesis, biomass production, and overall plant quality. By comparing constant relative humidity conditions with constant leaf-level VPD conditions, we seek to provide valuable insights into the benefits of precise VPD control. This study also intends to shed light on how VPD control affects stomatal regulation, leading to improved water-use efficiency and reduced water loss. In doing so, we aim to propose practical strategies for implementing leaf-level VPD control in controlled environment agricultural practices, offering a path toward optimized photosynthetic efficiency, reduced water consumption, and enhanced crop productivity. The goal is to contribute to more sustainable and efficient agricultural production, addressing the challenges posed by climate change and limited water resources.

2   Materials and Methods

2.1   Plant Material and Propagation

'Benefine' lettuce variety was chosen for this study because it is a hybrid seed and has a high germination rate. On the seed planting dates, we soaked 60-cell Oasis Horticubes with distilled water with a pH of 5.0. The pH was adjusted with 10% sulfuric acid (H_2SO_4). We planted 60 seeds in the growing medium then placed the growing medium under a PPFD of 195 $\mu mol \cdot m^{-2} \cdot s^{-1}$ delivered from LED lights for 20 h·day^{-1} for 14 days. We watered the seedlings every two days with modified Hoagland nutrient solution: 2.7 mM $NO_3{}^-$, 5.5 mM K^+, 1.6 mM P, 1.9 mM $Mg_2{}^+$, 4.7 mM $Ca_2{}^+$, 2.5 mM S, 71.6 μM Fe, 1.5 μM Zn, 46.3 μM B, 1.6 μM Cu, 1.6 μM Mo, 9.1 μM Mn and 0.6 mM $NH_4{}^+$, with a target electrical conductivity of 1.5 dS·m^{-1} and pH of 6.5. EC was adjusted using Hanna HI-98304 EC meter and pH was adjusted using Hanna HI-98107 pH meter. We grew the lettuce in a temperature and humidity-controlled growth room (the Vertical Farming Automation, Research and Mechanisms Laboratory) for 2 consecutive cycles. In the first experiment (Experiment – I), the temperature was set to 21.0 °C and the relative humidity was set to 65%. In the second experiment (Experiment – II), the temperature was kept at 21.0 °C and the relative humidity was adjusted according to the measured VPD$_{leaf}$ value. We used an ultrasonic fogger to increase the relative humidity. To reduce the humidity, we expelled the moist air with an exhaust fan. Ultrasonic fogger and exhaust fan were controlled by automation system.

2.2   Sensors

Temperature and relative humidity in the growth room were measured using SHT-35. Tolerance values of the sensor are in a usable range for this study (Fig. 1) [11]. The sensor was placed inside a sensor shield (Fig. 2).
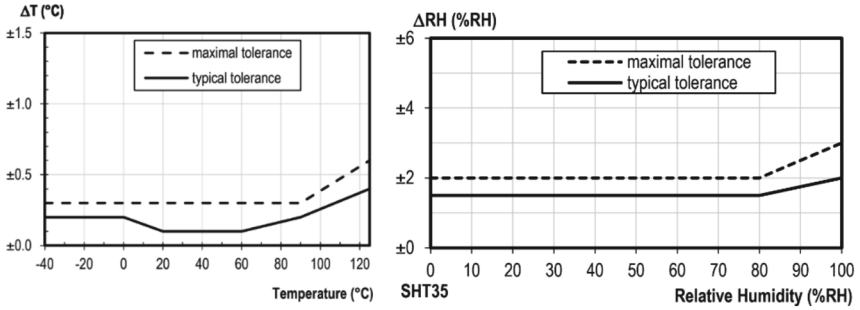
Fig. 1. SHT35 temperature and relative humidity tolerance charts

Fig. 2. Sensor shield and electronic control box

The MLX90614ESF-BCC was used to measure plant canopy temperature. The sensor measures the surface temperature by identifying the energy and wavelength distribution of infrared radiation [12]. A special sensor holder was designed, and 3D printed to hold the sensor. The sensor holder was glued to a flexible nozzle that can be pointed at the plant canopy (Fig. 3Hata! Başvuru kaynağı bulunamadı.). Emissivity value of the sensor was adjusted to 0.98, as recommended in [13].

VPD$_{leaf}$ was calculated with Eqs. 1, 2 and 3 using leaf temperature, air temperature and relative humidity.

$$Saturated\ Vapor\ Pressure(kPa) = \frac{610,7 * 10^{((7,5*T_{leaf}/(237,7+T_{leaf})))}}{1000} \qquad (1)$$
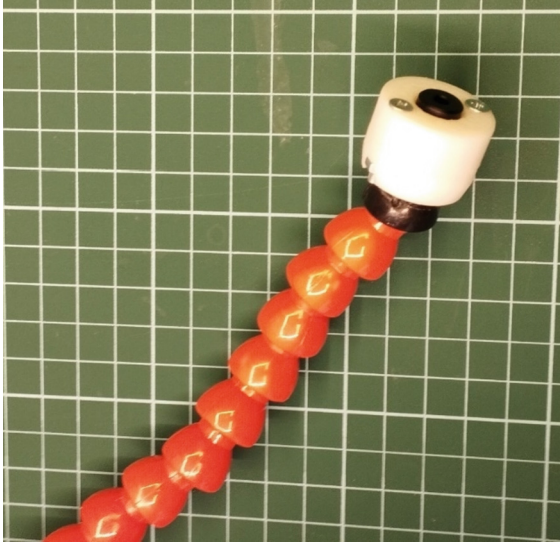
Fig. 3. MLX90614ESF-BCC sensor and 3D printed sensor holder, glued to a flexible nozzle

$$Actual\ Vapor\ Pressure(kPa) = \frac{610,7 * 10^{((7,5*T_{air}/(237,7+T_{air}))}}{1000} * (H_r) \qquad (2)$$

$$VPD(kPa) = SVP - AVP \qquad (3)$$

2.3 Experimental Design

We transplanted 42 seedlings out of 60 and placed them under a PPFD of 210 μmol·m^{-2}·s^{-1} light in a NFT plant production rack with 4 layers. Plants were grown for 28 days in every cycle (Table 1). We arranged the experiment as a randomized complete block design with two replications in time. Statistical analysis was performed using JMP 16 Pro. We conducted analysis of variance (ANOVA) and Tukey's Honestly Significant Difference (HSD) test (p = 0.05).

Table 1. Sowing, transplanting, and harvesting dates of experiment I and II.

| | Dates | | | |
| | Experiment – I | | Experiment – II | |
	Replication 1	Replication 2	Replication 1	Replication 2
Sowing	28.11.2022	16.01.2023	06.03.2023	24.04.2023
Transplanting	12.12.2022	30.01.2023	20.03.2023	08.05.2023
Harvesting	09.01.2023	27.02.2023	17.04.2023	05.06.2023

Experiment 1: Constant Relative Humidity Conditions:

In this experiment, temperature and relative humidity were set at 21.0 ± 1 °C and $65.0 \pm 5\%$, respectively. This condition served as a baseline for the study.

Experiment 2: Constant Leaf-Level VPD Conditions:

For this experiment, temperature was maintained at 21.0 ± 1 °C, and VPD was set to 1.2 ± 0.2 kPa. Relative humidity was adjusted to match the calculated VPD value.

2.4   Data Collection

We collected morphological data from 10 randomly selected plants on the day 28 after transplantation. We cut the lettuce at the root collar and weighed each one using an analytical balance (WL-303L, Weightlab, İstanbul, Türkiye). We measured the width and height of these plants. We counted fully expanded leaves (>2 cm in length) and obtained the leaf number. We then dried samples of these leaves for 7 days and weighed them using the same balance to calculate the dry matter content.

Water use efficiency (WUE) was calculated using total produced biomass versus total used water.

3   Results

Plant quality metrics, including leaf health and appearance, were notably enhanced under constant VPD conditions. Leaves exhibited greater vitality, and the overall appearance of the plants was more robust and marketable. This improvement in plant quality suggests that VPD control positively influences the health and aesthetic attributes of plants (Table 2).

Table 2. Plant quality metrics

	Experiment – I	Experiment – II
Fresh mass (g)	124.04 b	135.59 a
Dry matter (%)	4.7 b	5.35 a
Plant height (cm)	23.6 a	23.4 a
Plant width (cm)	26.7 a	27.6 a
Leaf number	24.0 a	24.5 a

Under constant relative humidity conditions (Experiment 1), the total biomass production was 5209.68 g. In contrast, under constant leaf-level VPD conditions (Experiment 2), the total biomass production increased to 5694.78, representing a 9.3% improvement. This significant difference underscores the importance of precise VPD control in optimizing plant growth and biomass production.

Controlled VPD conditions led to a substantial reduction in stomatal conductance and transpiration rates, indicating improved water-use efficiency. Stomata were less open,

resulting in less water loss, which has significant implications for resource conservation and sustainable water management in agriculture. WUE of Experiment – I was 0.14, Experiment – II was 0.179.

The experiments demonstrated that leaf-level VPD control reduced water consumption by %27.9, illustrating the potential for resource utilization optimization. This finding highlights the practical relevance of VPD control in addressing environmental challenges and improving the sustainability of agricultural practices.

These results provide valuable insights into the benefits of fine-tuning growth conditions through VPD control, offering promising prospects for enhanced crop productivity, resource conservation, and sustainable agriculture.

4   Discussion

The observed improvements in photosynthesis, biomass production, and plant quality under controlled vapor pressure deficit (VPD) conditions can be attributed to several key mechanisms. The reduction in stomatal conductance under constant VPD conditions led to decreased water loss, resulting in enhanced water-use efficiency. The combination of reduced transpiration rates and optimal stomatal regulation allowed plants to maintain a more favorable water status, which positively influenced photosynthetic activity and biomass production. These findings highlight the critical role of VPD in modulating plant responses to environmental conditions and the importance of precise VPD control for optimizing plant growth.

The implications of this study extend to sustainable agriculture in multiple ways. By optimizing VPD through controlled growth conditions, agricultural practices can achieve enhanced water-use efficiency, reduced water consumption, and improved resource utilization. This approach aligns with the need to address the challenges of climate change and water resource constraints, offering a pathway to more sustainable and environmentally friendly farming. Furthermore, by reducing the environmental impact of agriculture, these findings have the potential to contribute to broader efforts in mitigating climate change and promoting sustainable land use.

The results of this study provide practical strategies for implementing leaf-level VPD control in controlled environment agricultural practices. Farmers and researchers can achieve optimal photosynthetic efficiency by maintaining an ideal VPD range, which requires precise environmental control. This approach not only enhances crop productivity but also conserves water resources, making it a valuable addition to sustainable farming techniques. Moreover, the implementation of VPD control is adaptable to various agricultural contexts, including greenhouses and controlled environments, allowing for widespread adoption of this approach to enhance the sustainability and efficiency of crop production.

5   Conclusions

In conclusion, this study serves as a significant contribution to the field of plant science and agriculture by highlighting the importance of controlling vapor pressure deficit (VPD) in optimizing plant growth conditions and, subsequently, photosynthesis. The

key findings of this study underscore the substantial impact of VPD control on biomass production, plant quality, stomatal regulation, and water-use efficiency. These findings demonstrate the potential for a new approach to sustainable agriculture that prioritizes precise environmental control.

This research significantly advances our understanding of plant-environment interactions, with a particular focus on the influence of VPD. By shedding light on the practical benefits of maintaining an optimal VPD range, this study provides valuable insights for researchers and farmers alike. The ability to fine-tune growth conditions and control VPD offers a pathway to sustainable crop production that can address the challenges posed by climate change and limited water resources. This approach aligns with the broader efforts to ensure the sustainability and efficiency of agriculture, making it a crucial development in the field.

In summary, the optimization of plant growth conditions, with a specific emphasis on leaf-level VPD control, represents a promising strategy for achieving enhanced photosynthetic efficiency and improving resource utilization in plant growth. These findings have the potential to revolutionize agricultural practices, making them more sustainable and efficient, and thus contributing to a more sustainable and resource-conscious future in agriculture.

References

1. Seyhan S, Seyhan TG, Silleli H, Yılmaz H (2022) Bitki fabrikalarında kontrol edilen parametreler ve kontrol yöntemleri. Dicle Üniversitesi Mühendislik Fakültesi Mühendislik Dergisi 13(2):153–159. https://doi.org/10.24012/dumf.1058651
2. Lue, A.C.: Effects of water supply and vapor pressure deficit on leaf stomatal conductance and photosynthetic water use efficiency in alternative aridland crop species. Master's Thesis (2012)
3. Yu X, Zhang Y, Zhao X, Li J (2023) Systemic effects of the vapor pressure deficit on the physiology and productivity of protected vegetables. Vegetable Res 3(1). https://doi.org/10.48130/VR-2023-0020
4. Zhang D, Du Q, Zhang Z, Jiao X, Song X, Li J (2017) Vapour pressure deficit control in relation to water transport and water productivity in greenhouse tomato production during summer. Sci. Rep. 7(1):43461. https://doi.org/10.1038/srep43461
5. Amitrano C, Rouphael Y, De Pascale S, De Micco V (2022) Vapour pressure deficit (VPD) drives the balance of hydraulic-related anatomical traits in lettuce leaves. Plants 11(18):2369. https://doi.org/10.3390/plants11182369
6. Pasqualotto G, Carraro V, Huerta ES, Anfodillo T (2021) Assessment of canopy conductance responses to vapor pressure deficit in eight hazelnut orchards across continents. Front. Plant Sci. 12:767916. https://doi.org/10.3389/fpls.2021.767916
7. Ranawana SRWMCJK, Siddique KHM, Palta JA, Stefanova K, Bramley H (2021) Stomata coordinate with plant hydraulics to regulate transpiration response to vapour pressure deficit in wheat. Funct. Plant Biol. 48(9):839–850. https://doi.org/10.1071/FP20392
8. Grantz DA, Zinsmeister D, Burkhardt J (2018) Ambient aerosol increases minimum leaf conductance and alters the aperture–flux relationship as stomata respond to vapor pressure deficit (<scp>VPD</scp>). New Phytol. 219(1):275–286. https://doi.org/10.1111/nph.15102
9. Cardoso AA, Randall JM, McAdam SAM (2019) Hydraulics regulate stomatal responses to changes in leaf water status in the fern athyrium filix - femina. Plant Physiol. 179(2):533–543. https://doi.org/10.1104/pp.18.01412

10. Gates RS, Zolnier S, Buxton J (1998) Vapor pressure deficit control strategies for plant production. IFAC Proc. Vol. 31(12):271–276. https://doi.org/10.1016/S1474-6670(17)360 76-7
11. Sensirion (2015) Datasheet SHT3x-DIS. Accessed 16 Oct 2023. https://sensirion.com/media/ documents/213E6A3B/63A5A569/Datasheet_SHT3x_DIS.pdf
12. Melexis (2007) MLX90614 family Datasheet Single and Dual Zone Infra Red Thermometer in TO-39. Accessed 16 Oct 2023. https://www.melexis.com/en/documents/documentation/ datasheets/datasheet-mlx90614
13. López A, Molina-Aiz FD, Valera DL, Peña A (2012) Determining the emissivity of the leaves of nine horticultural crops by means of infrared thermography. Sci. Hortic. 137:49–58. https:// doi.org/10.1016/j.scienta.2012.01.022

Investigation of the Compliance of the Milking Routine and the Pulsator's Working Characteristics to Them Milking Technique in the Bozanönü District of Isparta Province

Mwiinga Micheal Milimo[(✉)], Zekeriya Görkem Güngör, and Ahmet Kamil Bayhan

Agriculture Faculty, Department of Agricultural Machinery and Technologies Engineering,
Isparta University of Applied Sciences, Isparta, Türkiye
mwiingamicheal01@gmail.com

Abstract. The number of dairy cows in Turkey increased from approximately 5 million to 7 million, while annual raw milk production rose from 8.7 million tons to 21.8 million tons between 2000 and 2020. However, despite these improvements, the average milk yield per cow still falls below ideal levels. Improving the milking routine and ensuring that milking machines meet standardized technical parameters can further enhance the average lactation milk yield. Enhancing the milking routine and aligning the technical parameters of milking systems with internationally recognized standards can increase the average yield per cow from the current 3,500–4,000 L per year to 5,000–6,000 L per year, representing a 25–30% increase in milk yield. This study was carried out in the Bozanönü District of Isparta province, involving 20 dairy enterprises. The evaluation of the milking system's components was based on pulsation tests conducted on the milking units. Additionally, the adherence of milkers (milking personnel) to the key components of the milking routine during machine milking was determined through the stopwatch method, relying on the work and time study technique. The objective of this study was to assess the compliance of milking machine configurations and the milking routine to internationally established standards (ISO standards), with the shared aim of improving udder health, milk yield, and quality. The findings of this study indicate that the use of properly configured milking machines in conjunction with appropriate milking routines significantly increases the quantity and quality of milk that can be obtained per cow.

Keywords: Milking Machines · Milking Routine · Udder Health · Milk Yield · Pulsation Test

1 Introduction

While 8.72 million tons of raw cow milk were produced annually in Türkiye from 5.28 million milked cows in 2000, in 2010, this number increased to 12.42 million tons. In 2020, it reached up to 21.75 million tons from approximately 7 million dairy cows. According to 2023 data, the raw milk production forecast, which was 23 million 200

thousand 306 tons in 2021, decreased by 7.1% in 2022 to 21 million 563 thousand 492 tons [1]. The main reasons for this nearly 3-fold increase in productivity in the last 20 years can be pointed to: Investments in better cattle genetics aimed at improving yields as well as through government support, especially in the interventions to offset rising feed prices and through its annual support payments [2]. However, this annual yield of approximately 3100 kg per dairy cow is very low according to the milk yield that can be achieved. Because according to their genetic performance, they should be able to produce at least 5 tons of milk per year [3]. Issues with functionality of the milking machine and improper milking practices can account for a substantial portion, ranging from 16% to 45%, of the differences in udder health observed between different herds. This emphasises the undeniable influence of both milking machinery and milking techniques on the overall health of the udder [4]. Over time, if these issues are not rectified, they can lead to a deterioration in udder health, subsequent individual udder losses, and eventually the necessity to cull dairy animals that no longer hold economic value. This, in turn, results in significant economic losses [5].

Errors occurring in milking machines can be attributed to a range of factors, such as irregular milking vacuum levels, pulsation rate, pulsator ratio, pulsation cycle phases (b, d), minimum massage phase duration, and differences in milking speed between the right and left udder quadrants (referred to as limping). The evaluation in this research mainly focused on these parameters.

Studies and practical observations have shown that maintaining a vacuum level with an average value ranging from 32 kPa to 42 kPa during the peak milking period for cows results in a quicker, gentler, and more thorough milking process. The pulsation rate is typically between 50 cycles/min and 65 cycles/min for cows and should not deviate more than ±5% from the given values. The pulsator ratio is typically between 60% and 70% for cows. The pulsator ratio of all pulsators in an installation should not vary from each other by more than 5 units of percentage. Limping, on the other hand, should not be more than 5 units of percentage, except where the milking unit is designed to provide different ratios between the fore- and hindquarters. For cows the liner-open phase/suction phase (b-phase) should not be less than 30% of a pulsation cycle while the massage phase (d-phase) should be not less than 15%. The minimum massage phase duration should not be less than 150 ms [6–8]. The working vacuum of a milking system varies according to the height of the milkline from the cow platform: Appropriate vacuum levels for each milkline are shown as follows: highline of 1.8 m ~ 48 kPa, highline of 1.6 m ~ 46–48 kPa, midline of 1.4 m ~ 44–46 kPa, midline of 1.2 m ~ 42–44 kPa, and lowline ~ 40–42 kPa [9]. Deviations from these standards in pulsation characteristics, encompassing factors like frequency and intensity, can, through damaging the teat, contribute to the development of mastitis [10].

When the established milking routine is not adhered to, several consequences can arise, mainly acute stress. Acute stress during milking reduces milk yield through a central inhibition of oxytocin secretion and through the increase in catecholamines (adrenaline and noradrenaline). Oxytocin, which is a hormone secreted by the central nervous system into the blood stream, is the main mediator of the milk ejection reflex. Therefore disrupting the normal release of oxytocin, subsequently interfering with the regular flow of milk and potentially reducing milk yield [11]. Reduced milk release

can also be attributed to insufficient stimulation, notably the absence of anterior breast massage [12]. Furthermore, unfavourable cow behaviour, stemming from fear, pain, or discomfort during milking, poses a significant challenge to animal welfare.

In order to monitor and prevent inflammatory udder diseases, commonly known as mastitis, which is the biggest problem in dairy farming, the following two parameters in milk, which are indicators of this disease, should be monitored. The first of these is the number of pathogenic bacteria that form colonies per millilitre of raw milk, and the other is the increase in the number of epithelial cells, that is, white blood cells, called the Somatic Cell Count (SCC) in raw milk. As these two indicators in milk increase, milk yield and quality loss occurs, and therefore economic losses also increase. In short, the increase in bacteria in milk indicates lack of hygiene; SCC shows milking machine and milker errors. In general, an SCC below 100,000 cells/ml indicates an uninfected cow; An SCC above 200,000 cells/ml indicates a cow possibly infected with mastitis. Cows infected with major pathogens have SCC greater than 300,000 cells/ml [13]. Table 1 below shows the relationship between SCC and the estimated daily milk loss per cow [14].

Table 1. Relationship between SCC and the estimated daily milk loss per cow (lbs)

SCC Score	SCC Range	Est. Daily Milk Loss Per Cow(lbs)
0	0–18,000	0
1	19,000–35,000	0
2	36,000–71,000	0
3	72,000–141,000	1.5
4	142,000–283,000	3.0
5	284,000–565,000	4.5
6	566,000–1,130,000	6.0
7	1,131,000–2,262,000	7.5
8	2,263,000–4,523,000	9.0
9	4,524,000–9,999,000	10.5

The main goal of this research was to reveal to what extent the milking duration, milk yield and quality are affected. While revealing this relationship, the known and expected effects on milk yield resulting from different fodder and concentrate feed's quantity and quality in the enterprises were removed through covariance analysis methods. Thus, as the milking machine moves away from the optimal operating values coupled with neglecting of major aspects of the milking routine, deteriorations in udder health, milk yield and quality will be more accurately associated. With these results, it will be possible to make the necessary adjustments in order to increase the amount of milk produced per cow to the highest possible values as well as minimize udder infections.

2 Methods

This research was conducted in four parts, each focusing on a different aspect of the study. The first part included observing and recording data based on the milking routine during the milking process, as well as collecting data on each enterprise. This data incorporated feeding and milking information, daily lactation yield information of the dairy cows, the total amount of milk milked into the tank during the morning and evening milking sessions, as well as the maintenance and repair data of the milking machines. Some of the stages and parameters recorded and evaluated in the milking routine research were: cleaning the udders of the cow before milking which included washing and/or cleaning the udders with a cloth, applying disinfectant to the udders before and after milking, using the delay method before milking to allow for the sufficient secretion of the oxytocin hormone and monitoring the milk flow to reduce blind milking [15]. The milking duration of each cow was recorded through a stopwatch as well which was evaluated as the time the milking cluster was attached to the time it was removed from the udders.

The second part of the research included conducting dry pulsation tests on the milking units and recording their results using the GEA brand Pulsotest Comfort model milking machine testing equipment. The vacuum levels, pulsation rate, pulsation ratio and pulsation cycle phases were measured in accordance with 6.2 of ISO 6690:2007.

The third part involved taking samples from the total raw milk milked on the working day (from the accumulating tank or cans) of each enterprise for the total bacteria count and somatic cell count. These samples were kept in cold containers (at ~ +4 °C in cold battery pack carrying bags) for analysis. The analysis for these parameters were conducted by the Scientific and Technology Application and Research Center in the Mehmet Akif Ersoy University in Burdur, Türkiye. The analysis methods were conducted in accordance with ISO 13366-2/AC:2008 [16] for the somatic cell count and TEMPO Total Viable Count (TVC) for the total mesophilic aerobic bacteria count. After collecting this information the next step, which is the fourth part, involved analysing the data statistically. Statistical methods were used to organize, summarize and interpret the collected data.

"The Generalized Linear Model" was the preferred method used in this research. GLM ANCOVA covariance analysis method were used for data entry and statistical evaluations, using EXCEL and MINITAB package programs, respectively. In cases where there was a high correlation between parameters regression analysis was applied. The independent discrete factors of this trial design included: the milking routine, the milking system, maintenance and repair, the milkline (level from the ground), the milking time (morning or evening), the number of milking units per milking person, the working vacuum, the pulsation rate, the pulsator ratio, limping, b (liner-open phase or suction phase) phase, d (massage phase) phase and the minimum massage phase duration. The responses used in this model were: the milking duration (second/cow), the milk yield per milking session (kg/cow) and the somatic cell count (cells/ml). The data on the total bacteria count was not analysed but its raw values are presented. Covariance data included: the daily average ration value (MJNEL/cow) and the average lactation day (day) of each individual enterprises.

The investigation into the milking routine concentrated on adherence to established milking routines across the different enterprises and the extent to which the parameters were followed and the duration taken to conduct. Additionally, an analysis of the maintenance of milking systems was conducted, including the frequency at which these systems were subjected to maintenance or repair. These assessments were categorized and evaluated using the Likert scale, ranging from 5 (very good) to 1 (very poor) [17].

3   Results

3.1   General Features of Enterprises

The collected data from each of the 20 enterprises visited and studied during this research were summarized to provide an overview of how each enterprise is structured. General details about each enterprise can be found in Table 2 below.

As shown in Table 2 above, the enterprises used various milking systems: three used the milking parlour system, two used the bucket milking system, and the majority (fifteen) used the can milking system. The enterprises also implemented different milkline systems: two used the highline milkline, sixteen used the midline milkline, and two used the lowline milkline. The table also provides details on the number of milking units used, the number of total milked cows, the number of milkers, the number of milking units per milking person, the total milked cows per milking person, the average lactation day, the average daily ration, the average recorded milking durations for each enterprise, the average daily milk yield per cow, the somatic cell count recorded and the total bacteria count. Shown as well are the minimum and maximum values, as well as the average values and the standard deviation values.

Table 3 above shows the average values of the measured pulsation characteristics of each enterprise. It presents the total number of pulsators used in each enterprise, the observed and recorded vacuum shown on the gauge as well as the measured working vacuum. The differences between these two values were calculated to show errors in its accuracy and are shown in the table as well. The pulsation rate, pulsator ratio, pulsation cycle phases (b suction phase, d massage phase), minimum massage phase duration, and limping values were also recorded and shown above. However, when it comes to the minimum, maximum, average and standard deviation values of this data, they were not determined from the enterprise average but from total individual pulsator values.

3.2   Milk Yield

The results of the variance analysis conducted to examine the effects of continuous variables including the average lactation day, average daily ration, working vacuum, pulsation rate, pulsator ratio, limping, b suction phase, d massage phase, minimum massage phase duration and categorical variables including the milking system, milkline, milking unit per milking person and the milking routine on the average milk yields obtained from the enterprises are presented in Table 4.

Parameters (sources) seen in Table 4 with a statistical P-Value ≤ 0.05 are significant in terms of their effects on milk yield. Continuous factors influencing milk yield are as

Table 2. General details of each enterprise

Entreprise No	Milking System	Milkline	Used Milking Units	Number of Milked Cows	Number of Milking Persons	Milking Unit/Milking Person	Avg Lactation Stage	Avg Daily Ration(MJNEL)	Avg Milking duration(sec)	Avg Daily Milk Yield((kg)	Tank Somatic Cell Count(cell/ml)	Total Mesophilic-Aerobic Bacteria Count(cfu/ml)
1	Bucket Milking	Midline	3	14	2	1.5	143	240	413	20,0	454000	>490000
2	Milking Parlour	Highline	8	17	2	4	164	146	446	16,5	212000	>490000
3	Can Milking	Lowline	4	10	1	4	220	117	302	11,0	339000	>490000
4	Milking Parlour	Lowline	16	10	2	8	48	127	389	19,2	117000	>490000
5	Can Milking	Midline	2	5	1	2	35	185	601	16,0	219000	71000
6	Can Milking	Midline	2	9	1	2	133	181	351	16,7	821000	>490000
7	Can Milking	Midline	2	9	1	2	169	118	316	10,8	828000	>490000
8	Bucket Milking	Midline	2	5	1	2	263	190	424	16,0	267000	>490000
9	Can Milking	Midline	2	6	1	2	377	157	280	10,5	202000	>490000
10	Can Milking	Midline	2	3	1	2	213	216	339	22,5	122000	>490000
11	Can Milking	Midline	2	9	1	2	94	154	410	13,1	1015000	>490000

(continued)

Table 2. (*continued*)

Entreprise No	Milking System	Milkline	Used Milking Units	Number of Milked Cows	Number of Milking Persons	Milking Unit/Milking Person	Avg Lactation Stage	Avg Daily Ration(MJNEL)	Avg Milking duration(sec)	Avg Daily Milk Yield((kg)	Tank Somatic Cell Count(cell/ml)	Total Mesophilic-Aerobic Bacteria Count(cfu/ml)
12	Can Milking	Midline	2	6	1	2	145	166	502	16,1	221000	>490000
13	Can Milking	Midline	2	10	1	2	106	177	619	23,5	783000	>490000
14	Can Milking	Midline	2	3	1	2	355	138	526	16,7	374000	>490000
15	Can Milking	Midline	2	9	1	2	212	204	424	20,4	1187000	>490000
16	Can Milking	Midline	2	6	1	2	377	157	280	10,5	215000	>490000
17	Can Milking	Midline	4	4	1	4	172	154	290	8,9	222000	>490000
18	Can Milking	Midline	2	5	1	2	130	112	386	11,8	163000	>490000
19	Can Milking	Midline	2	1	1	2	122	224	357	11,5	139000	>490000
20	Milking Parlour	Highline	10	35	1	10	173	202	496	11,4	230000	>490000
Min^T			2	1	1	1.5	35	111.9	280	8.875	117000	71000
Max^T			16	35	2	10	377	240.2	619	23.5	1187000	>490000
Mean^T			3.65	8.8	1.15	2.9	182.5	168.2	407.5	15.15	406500	>490000
SD^T			3.63	7.27	0.37	2.2	97.7	37.01	100.5	4.36	328047.4	~100000

Table 3. General milking machine configurations of the milking systems

Entreprise No	Vacuum on Gauge	Measured Working Vacuum	V gauge - V working	Avg Pulsation Rate	Avg Pulsator Ratio	Avg Limping	Avg Suction Phase	Avg Massage Phase	Avg Minimum Massage Phase Duration
1	42.9	41.9	1.0	101.9	58.6	1.2	37.7	27.1	162
2	44.0	43.8	0.2	72.0	58.8	2.5	31.8	24.6	209
3	44.0	37.1	6.9	112.0	56.9	3.0	34.3	27.3	152
4	51.5	49.1	2.4	78.4	55.3	1.7	28.5	23.9	186
5	55.0	43.4	11.6	61.2	51.5	2.1	35.8	28.7	282
6	55.0	42.5	12.5	76.3	59.3	2.5	35.0	26.6	212
7	54.0	46.0	8.0	108.6	59.1	1.6	31.8	21.8	112
8	42.0	51.0	−9.0	172.3	53	2.1	30.7	18.6	65
9	55.0	35.7	19.3	146.8	59.7	1.3	19.5	24.2	101
10	0.0	35.1	−35.5	110.1	56.5	4.4	31.9	31.8	176
11	53.0	52.6	0.4	71.5	60	4.5	37.5	22.8	196
12	51.0	45.5	5.5	102.8	56.9	4.3	28.4	20.1	118
13	48.0	46.5	1.5	87.5	53.4	3.8	31.1	23.1	159
14	48.0	42.5	5.5	94.9	59.8	3.9	29.8	18.9	127
15	46.0	48.3	−2.3	63.0	58.9	2.4	36.9	24.9	237
16	55.0	35.7	19.3	146.8	59.8	2.3	25.8	22.7	94
17	60.5	45.1	5.4	89.4	58.9	8.0	34.0	28.0	240
18	59.0	51.3	7.7	76.8	59.8	1.5	40.7	27.0	212
19	48.0	44.4	3.6	77.7	51.8	9.1	38.9	32.1	242
20	48.0	42.9	5.1	66.8	58.7	3.4	36.1	23.3	237
MinT	0.0	28.0	−42.2	49.5	47.8	0.0	24.7	0.0	49
MaxT	60.5	59.4	15.2	189.9	62.2	8.4	47.1	39.4	329
MeanT	47.0	45.2	1.8	84.0	57.5	2.8	34.9	23.7	193.0
SDT	9.4	4.7	8.6	28.4	3.1	2.2	4.6	5.1	70.7

Table 4. Analysis of variance for the average milk yield per milking session (kg)

Source	DF	Adj SS	Adj MS	F-Value	P-Value
Average Lactation Stage (day)	1	0.096	0.0957	0.24	0.623
Average Daily Ration (MJNEL)	1	11.546	11.5456	29.3	0.000
Working Vacuum (kPa)	1	18.586	18.5823	47.19	0.000
Pulsation Rate (min-1)	1	17.699	17.6988	44.95	0.000

Table 4. (*continued*)

Source	DF	Adj SS	Adj MS	F-Value	P-Value
Pulsator Ratio(%)	1	2.659	2.6590	6.75	0.011
Limping (%)	1	0.105	0.1047	0.27	0.0607
Suction Phase (%)	1	1.613	1.6133	4.10	0.045
Massage Phase (%)	1	14.406	14.4055	36.58	0.000
Minimum Massage Phase Duration (mS)	1	0.075	0.0750	0.19	0.663
Milking System	2	9.987	4.9937	12.68	0.000
Milkline	2	13.601	6.8005	17.27	0.000
Milking Time	1	3.247	3.2472	8.25	0.005
Milking Units per Milking Person	2	26,683	13.3413	33.88	0.000
Milking Routine	4	23.781	5.9452	15.10	0.000
Error	108	42.527	0.3938		
Lack of Fit	20	42.527	2.1263	*	
Pure Error	88	0.0000	0.0000		
Total	128	836.246			
Model Summary					

	S	R-sq	R-sq(adj)	R-sq(pred)	
	0.627506	94.91%	93.97%	*	

follows in order of significance level: The average milk yield obtained from the cows in the enterprises is highly significant ($P < 0.01$) with respect to the average daily ration values, the working vacuum, pulsation rate, massage phase (%). It is significantly affected by the pulsator ratio and the suction phase (b) ($P < 0.05$). Regarding the discrete factors indicating differences in the milking technique and the milking person, all of them have been found to be statistically significant ($P < 0.05$) on the average milk yield. Table 5 below presents the average values.

Table 5. Average values for the milk yield per milking session (kg).

Variable	Milking System	N	Mean	SE Mean	StDev	Minimum	Maximum
Avg Milk Yield per Milking Session (kg/cow)	1	34	5.18 b	0.129	0.755	5.0	8.824
	3	23	9.13 a	0.615	2.948	5.0	11.43
	4	72	8.46 a	0.251	2.129	5.0	11.00

**Milking system 1: Milking parlour, 2: Pipeline(Stanch barn), 3: Bucket milking, 4: Can milking

Table 5. (*continued*)

Variable	Milking System	N	Mean	SE Mean	StDev	Minimum	Maximum
Variable	Milkline	N	Mean	SE Mean	StDev	Minimum	Maximum
Avg Milk Yield per Milking Session (kg/cow)	1	16	10.80 a	0.437	1.749	5.5	11.43
	2	80	8.171 b	0.247	2.209	5.0	11.00
	3	33	5,116 c	0.116	0.666	5.0	8.824

**Milkline: Lowline, 2: Midline, 3: Highline

Variable	Milking Time	N	Mean	SE Mean	StDev	Minimum	Maximum
Avg Milk Yield per Milking Session (kg/cow)	1	60	9.280 a	0.244	1.893	5.5	11.43
	2	69	6.355 b	0.273	2.269	5.0	11.00

**Milking Time 1: Morning, 2: Evening

Variable	Milking Units per Milking Person	N	Mean	SE Mean	StDev	Minimum	Maximum
Avg Milk Yield per Milking Session (kg/cow)	2	76	8.338 b	0.245	2.136	5.0	11.00
	4	20	9.716 a	0.625	2.797	5.0	11.43
	5	33	5.070 c	0.070	0.400	5.0	7.300

**Milking Units/Milking Person 2: 1 or 2 units, 4: 3 or 4 units, 5: more than 4 units

Variable	Milking routine	N	Mean	SE Mean	StDev	Minimum	Maximum
Avg Milk Yield per Milking Session (kg/cow)	1	37	5.1351 d	0.0570	0.3466	5.0	6.000
	2	24	7.013 c	0.337	1.651	5.0	8.889
	3	13	7.397 c	0.614	2.212	5.4	10.83
	4	31	8.961 b	0.347	1.931	6.3	11.00
	5	24	10.958 a	0.265	1.296	5.0	11.43

**Likert Scale 1: Very poor, 2: Poor, 3: Moderate, 4: Good, 5: Very good

In Table 5 above, while there was no significant difference in the average raw values for the given independent categorical factor variables according to one-way variance analysis, based on GLM model variance analysis, it has been calculated that milk yields of cows, are higher in milking system 3 (bucket milking) than the other milking systems, lower in the highline milkline than in the midline and lowline milklines, higher in the group of milkers who milk more cows at once, up to a maximum of 4 cows and higher in the enterprises that follow the milking routine more accurately than those that neglect most essential parts of it. Additionally, it has been observed that there is a significant difference in milk yield between milking times, mainly due to the unequal time intervals

between morning and evening milking sessions. This resulted in a higher milk yield during the morning milking sessions than during the evening milking sessions.

3.3   Milking Duration

The results of the variance analysis conducted to examine the effects of continuous variables including the average lactation day, average daily ration, working vacuum, pulsation rate, pulsator ratio, limping, b suction phase, d massage phase, minimum massage phase and categorical variables including the milking system, milkline, milking unit per milking person and the milking routine on the milking duration obtained from the enterprises are presented in Table 6.

Table 6. Analysis of variance for the milking duration per milking session (sec).

Source	DF	Adj SS	Adj MS	F-Value	P-Value
Average Lactation Stage (day)	1	5375	5375	0.26	0.613
Average Daily Ration (MJNEL)	1	247	247	0.01	0.000
Working Vacuum (kPa)	1	80408	80408	3.84	0.000
Pulsation Rate (min-1)	1	147579	147579	7.05	0.000
Pulsator Ratio(%)	1	10041	10041	0.48	0.011
Limping (%)	1	28182	28182	1.35	0.0607
Suction Phase (%)	1	11651	11651	0.56	0.045
Massage Phase (%)	1	113141	113141	5.40	0.000
Minimum Massage Phase Duration (mS)	1	24	24	0.00	0.663
Milking System	2	7364	3682	0.18	0.000
Milkline	2	77966	38983	1.86	0.000
Milking Time	1	49946		2.39	0.005
Milking Units per Milking Person	2	87829	43910	2.10	0.000
Milking Routine	4	85419	21355	1.02	0.000
Error	108	2261276	20938		
Lack of Fit	20	520152	26008	1.31	0.192
Pure Error	88	1741125	19786		
Total	128	3161445			
Model Summary					
	S	R-sq	R-sq(adj)	R-sq(pred)	
	144.699	28.47%	15.23%	*	

According to the data in Table 6 above, among the continuous factors affecting the milking duration, the pulsation rate and the massage phase (%) are found to be

significant (P ≤ 0.05) while the working vacuum (P = 0,053) was found to be partially significant. All categorical factors indicating differences in machine and the milking person in the milking technique have been found to be statistically insignificant (P > 0.05) in their effects on the average milking duration. In Table 7 below, despite showing no significant effects on the milking duration, the average raw values for the given independent categorical factor variables according to one-way variance analysis have been shown.

Table 7. Average values for milking duration per milking session (sec)

Variable	Milking System	N	Mean	SE Mean	StDev	Minimum	Maximum
Milking Duration(sec)	1	34	491.4	22.1	128.9	268.0	737.0
	3	23	394.3	35.4	169.8	179.0	810.0
	4	72	438.9	19.0	161.2	191.0	1117.0

**Milking system 1: Milking parlour, 2: Pipeline(Stanch barn), 3: Bucket milking, 4: Can milking

Variable	Milkline	N	Mean	SE Mean	StDev	Minimum	Maximum
Milking Duration(sec)	1	16	404.9	41.7	167.0	179.0	810.0
	2	80	432.3	18.2	162.5	191.0	1117.0
	3	33	494.5	22.6	129.6	268.0	739.0

**Milkline: Lowline, 2: Midline, 3: Highline

Variable	Milking Time	N	Mean	SE Mean	StDev	Minimum	Maximum
Milking Duration(sec)	1	60	417.1	18.6	144.4	179.0	1015.0
	2	69	468.8	19.8	164.8	222.0	1117.0

**Milking Time 1: Morning, 2: Evening

Variable	Milking Units per Milking Person	N	Mean	SE Mean	StDev	Minimum	Maximum
Milking Duration(sec)	2	76	439.7 ab	18.7	163.2	191.0	1117.0
	4	20	384.9 b	35.1	156.9	179.0	810.0
	5	33	492.8 a	22.7	130.6	268.0	739.0

**Milking Units/Milking Person 2: 1 or 2units, 4: 3 or 4 units, 5: more than 4 units

Variable	Milking routine	N	Mean	SE Mean	StDev	Minimum	Maximum
Milking Duration(sec)	1	37	486.3 a	23.4	142.3	222.0	739.0
	2	24	365.5 b	14.0	68.4	241.0	504.0
	3	13	400.1 ab	30.1	108.7	240.0	628.0
	4	31	498.4 a	38.1	212.1	191.0	1117.0
	5	24	415.2 ab	29.6	144.9	179.0	810.0

**Likert Scale1: Very poor, 2: Poor, 3: Moderate, 4: Good, 5: Very good

It should be noted that conclusive results regarding the milking duration could not be obtained due to observed interruptions during the milking process. Milkers often

engaged in multiple tasks, such as feeding calves and cleaning, leading to delayed removal of milking clusters. Additionally, the issue of a few milkers handling too many cows simultaneously resulted in over-milking and, in some cases, incomplete milking.

3.4 Somatic Cell Count

The results of the variance analysis conducted to examine the effects of continuous variables including the average lactation day, working vacuum, pulsation rate, pulsator ratio, limping, b suction phase, d massage phase (%), minimum massage phase (mS) and categorical variables including the milking system, maintenance and repair, the milking routine, milkline, milking unit per milking person on the somatic cell count of each enterprise are presented in Table 8.

Table 8. Analysis of variance for the somatic cell count of each enterprise (per ml)

Source	DF	Adj SS	Adj MS	F-Value	P-Value
Average Lactation Stage (day)	1	30259304891	30259304891	3.74	0.056
Working Vacuum (kPa)	1	3.95540E + 11	3.95540E + 11	48.92	0.000
Pulsation Rate (min-1)	1	1.19328E + 11	1.19328E + 11	14.76	0.000
Pulsator Ratio(%)	1	351359473	351359473	0.04	0.835
Limping (%)	1	2730352515	2730352515	0.34	0.562
Suction Phase (%)	1	1.74354E + 11	1.74354E + 11	21.56	0.000
Massage Phase (%)	1	1.83870E + 11	1.83870E + 11	22.74	0.000
Minimum Massage Phase Duration (mS)	1	20939184471	20939184471	2.59	0.000
Milking System	2	8.92555E + 11	4.46277E + 11	55.19	0.111
Milkline	2	8.94951E + 11	4.47475E + 11	55.34	0.000
Milking Units per Milking Person	2	8.08338E + 11	4.04169E + 11	49.98	0.000
Milking Routine	4	1.53435E + 12	3.83587E + 11	57.44	0.000
Maintenance and Repair	4	1.81724E + 12	4.54310E + 11	56.18	0.000
Error	106	8.57137E + 11	8086199515		
Lack of Fit	18	8.57137E + 11	47618730475	*	*

(*continued*)

Table 8. (*continued*)

Source	DF	Adj SS	Adj MS	F-Value	P-Value
Pure Error	88	0	0		
Total	128	1.47360E + 13			
Model Summary					
	S	R-sq	R-sq(adj)	R-sq(pred)	
	89923.3	94.18%	92.98%	*	

Parameters seen in Table 8 with a statistical (P ≤ 0.01) have a highly significant effect on the somatic cell count. Continuous factors affecting milk yield, in order of importance based on significance levels, are as follows: the working vacuum, the pulsation rate, the massage phase (%) and the suction phase which have a highly significant effect on the milk yield. The average lactation day had a slight effect on the somatic cell count (P = 0,056). All the categorical factors showed a significant effect on the milk yield (P ≤ 0.01). These included the milking system, milkline, maintenance and repair, the number of milking units per milking person and the milking routine. Average values for the milk yield for each variable have been represented in Table 9 below.

Table 9. Average values for the somatic cell count (per ml).

Variable	Milking System	N	Mean	SE Mean	StDev	Minimum	Maximum
Somatic Cell Count(per ml)	1	34	226147 b	3350	19531	117000	230000
	3	23	373000 b	21744	104281	222000	454000
	4	72	668167 a	43171	366317	122000	1187000

**Milking system 1: Milking parlour, 2: Pipeline(Stanch barn), 3: Bucket milking, 4: Can milking

Variable	Milkline	N	Mean	SE Mean	StDev	Minimum	Maximum
Somatic Cell Count(per ml)	1	16	425750 b	21797	87188	117000	454000
	2	80	624900 a	41472	370941	122000	1187000
	3	33	229455 b	545	3133	212000	230000

**Milkline: Lowline, 2: Midline, 3: Highline

Variable	Maintenance and Repair	N	Mean	SE Mean	StDev	Minimum	Maximum
Somatic Cell Count(per ml)	1	10	1102200 a	84800	268161	339000	1187000
	2	25	347600 c	24704	123522	139000	454000

(*continued*)

Table 9. (*continued*)

Variable	Milking System	N	Mean	SE Mean	StDev	Minimum	Maximum
	3	29	785793 b	24175	130185	117000	828000
	4	57	340684 c	39207	296005	122000	1015000
	5	8	307125 c	19579	55378	267000	374000

**Milking Time 1: Morning, 2: Evening

Variable	Milking Units per Milking Person	N	Mean	SE Mean	StDev	Minimum	Maximum
Somatic Cell Count(per ml)	2	76	646105 a	42275	368541	122000	1187000
	4	20	389750 b	23200	103752	212000	454000
	5	33	226576 b	3424	19671	117000	230000

**Milking Units/Milking Person 2: 1 or 2units, 4: 3 or 4 units, 5: more than 4 units

Variable	Milking routine	N	Mean	SE Mean	StDev	Minimum	Maximum
Somatic Cell Count(per ml)	1	37	235000 b	2108	12824	230000	267000
	2	24	748458 b	63856	312830	212000	1015000
	3	13	209231 ab	27157	97914	122000	374000
	4	31	574839 a	52916	294622	177000	828000
	5	24	175750 ab	77208	378240	139000	1187000

**Likert Scale1: Very poor, 2: Poor, 3: Moderate, 4: Good, 5: Very good

The table above reveals that enterprises employing milking system 3 (can milking) and using milkline 2 (midline) had higher somatic cell counts (SCC) in their raw milk samples. Those closely adhering to maintenance and repair procedures exhibited lower SCC counts, while enterprises with minimal care for maintenance and repair had the highest SCC counts in their raw milk samples.

3.5 Total Bacteria Count

The aerobic mesophilic bacteria count (total bacteria count) is one of the most important factors affecting udder health and determining the milk quality [18]. Limits for somatic cell count (SCC) and total plate count (mesophilic micro-organisms) – TPC in cow's raw milk are given by Regulation (EC) No. 853/2004 of the European Parliament and of the Council, which lays down the count of micro-organisms at 30 °C $\leq 10^5$ CFU/ml and SCC at $\leq 4 \times 10^5$ /ml. For raw milk from other species, the limit for the TPC of micro-organisms at 30 °C is $\leq 1.5 \times 10^6$ CFU/ml [19].

All but one of the enterprises (5th enterprise) had a total mesophilic aerobic bacteria count (CFU/ml) above 490,000 (CFU/ml) while the remaining enterprise recorded a

significantly lower value of 100,000 (CFU/ml). This can be related to the storage of the raw milk after milking. It was observed that after milking the milk can/tank in the other enterprises would be left closed in the heat until the collecting tank would arrive. Where it could be exposed to both contamination and also lead to bacterial incubation. The 5th enterprise however, would store the milk can underneath a shady and cool area, as well as conduct the milking process closer to the milk collecting time. This is thought to be the reason for the difference in the total bacteria count.

3.6   Milking Routine

The milking routine which begins with cleaning the udders had nine out of twenty enterprises adhere to this practice. Only two of them dry the udders with a cloth after washing. The other two of the four enterprises that use a dry cloth only wipe the udders with a dry cloth without washing them. Of the 11 enterprises that clean the udders, two apply washing and drying, seven apply only wet washing, and two only clean the udders with a dry cloth. The other nine enterprises do not perform udder cleaning at all. 11 enterprises clean the udders then perform pre-massage on them. The other seven of the 18 enterprises that apply pre-massage start the milking routine directly with pre-massage, neglecting cleaning the udders. Two out of the total of 20 enterprises start milking by directly attaching the milking clusters, without doing any cleaning, pre-massage or applying any disinfectant, thus without applying the delay method (45–90 s) required for the release of the oxytocin hormone before attaching the milking cluster. Only 8 out of 20 farms attach the milking clusters correctly and 12 do so reversely (alternate milking pulse with front-back teat quarters, not right-left teat quarters). The most important milking routine procedures in farms are the pre-massage (18/20) and the removal of the last milk with the final massage (19/20). The most neglected milking routine operations are pre- and post-dipping. While no enterprise does pre-dipping, only 1 enterprise applies final dipping (1/20).

The milking routine was found to be significantly important ($P < 0,05$) according to one way variance analysis. Enterprises with a high Likert scale rating of 5 for milking routine achieved a milk yield of 10.96 kg/cow. In contrast, those with a low Likert scale rating of 1 yielded only 5.14 kg/cow. Enterprises with Likert scale ratings of 4, 3, and 2 obtained milk yields of 8.96 kg/cow, 7.4 kg/cow, and 7.01 kg/cow, respectively (Table 5 and Table 10). It should be noted that these values are not daily milk yield but milk yields obtained from one milking session.

3.7   Milking Machine Maintenance and Repair

Data collected from each enterprise during the first part of this research based on the maintenance and repair of the components of the milking system and to what frequency they were carried out are shown below in Table 11. Each component was classified according to the Likert scale (1- 5), 5 being very good and 1 being very poor. The classification of the cluster, liner, long and short milk and pulse tubes was based according to how often these components were changed while the classification of the pump, pulsator, vacuum gauge and regulator was based according to the frequency of repair and maintenance as well as to how often they are replaced. The evaluation of the maintenance

and repair of the pump included aspects such as honing, replacing the pallets and bearings of the pump and how frequent this was done. The evaluation of the pulsator included how often they were taken for maintenance, how often they were changed and/or configured. The same evaluation was conducted for the regulator and vacuum gauge. A general evaluation of the total maintenance and repair of each enterprise was given a classification according to each individual components maintenance and repair. However, according to the maintenance and repair data of the enterprises, no important relation was found to have a significant effect on the milk yield (P > 0,05).

Table 10. Milking routine evaluation criteria of the enterprises.

Entreprise No	Washing Udders	Drying With a Dry Cloth	Pre-Massage	Correct Cluster Attachment	Blind Milking Control	Delay Method Application	Final Dipping	Final Likert Value
1	+	−	+	+	+	+	−	5
2	−	−	+	−	+	−	−	2
3	−	−	+	−	+	−	−	2
4	−	+	+	−	+	+	−	4
5	+	−	+	+	+	−	−	4
6	−	−	+	−	+	−	−	2
7	+	−	+	+	+	−	−	4
8	−	−	-	−	+	−	−	1
9	−	−	+	+	+	−	−	3
10	+	−	+	−	+	−	−	3
11	−	−	+	−	+	−	−	2
12	−	+	+	+	+	−	−	4
13	+	−	+	−	+	+	−	4
14	+	−	+	−	+	−	−	3
15	+	+	+	+	+	−	+	5
16	−	−	+	+	+	−	−	3
17	−	−	+	−	+	−	−	2
18	+	−	+	−−	+	−	−	3
19	+	+	+	+	+	−	−	5
20	−	−	−	−	−	−	−	0

+: is applied or is done right -: is not applied or is done wrong
Likert Scale 0 & 1: Very Poor; 2: Poor; 3: Moderate; 4: Good; 5: Very Good

Table 11. Maintenance and repair evaluation criteria of the enterprises.

Entreprise No	Maintenance and Repair	Pump	Milking Cliusters	Pulsator	Maintenance Frequency	Blind Milking Control	Vacuum Gauge	Liner	Long milk and pulse tubes	Short milk and pulse tubes
1	2	1	2	2	5	1	1	4	1	1
2	2	1	3	3	1	1	1	4	1	1
3	1	2	2	1	1	1	1	1	1	1
4	3	3	4	3	3	3	3	5	3	3
5	2	1	3	3	1	1	1	4	4	1
6	3	3	4	3	3	3	3	4	3	3
7	3	2	4	3	1	1	1	5	4	4
8	5	4	4	5	4	4	4	5	4	5
9	4	4	4	4	4	4	4	3	3	4
10	4	5	4	4	4	4	4	5	4	4
11	4	5	4	3	3	3	3	4	3	3
12	4	3	4	5	3	3	3	2	3	5
13	3	5	1	1	3	1	1	5	1	5
14	5	5	5	5	4	5	5	5	4	5
15	1	1	4	3	3	1	1	2	1	1
16	4	4	4	4	3	4	4	3	3	4
17	2	4	3	2	1	1	1	2	1	1
18	4	4	4	5	3	4	4	3	3	4
19	2	2	3	2	1	4	1	1	2	2
20	4	5	5	5	4	5	4	4	3	3

Likert Scale 1: Very Poor; 2: Poor; 3: Moderate; 4: Good; 5: Very Good

4 Conclusion

Despite Türkiye having a large number of dairy farms, majority of the are small-family owned. However, there has been a shift in the number of dairy farms from small scale to large and more efficient farms [20]. This research aims to provide dairy farm owners with insights into the conformity of milking facilities and equipment with defined international standards, as well as to inform them about the correct and comprehensive implementation of milking machine configurations and milking routines required to achieve optimal milk yield and quality. Due to the lack of local literature, the original point of this research is to try to determine the current situation by addressing the issue of the "Milking Routine" and "Milking Machine". Determination of which steps in the machine milking routine are deviated from their proper order and values coupled with the determination of which technical parameters related to the milking machine deviate from international standards, gave an idea about the rates at which it may lead to loss of productivity, quality in udder health and raw milk production in some dairy cattle farms in the Bozanönü province. Thus, it will at least raise awareness in this sector, and the findings and comments made based on the literature will set an example for similar studies.

However, despite these findings, this research would have been made much better if each individual cow's milk yield and milk samples for the bacteria and somatic cell count was obtained and recorded separately and not as an enterprise average to more accurately relate the effects of the pulsator's working characteristics of the milking machine and the milking routine to the mentioned factors. Additionally, the pulsator's working characteristics would have been much better obtained if wet pulsator tests were conducted instead of dry pulsator tests. These factors will be taken into account in future related projects to further improve the precision of the results.

References

1. TÜİK Raw Milk Production Statistics Page, https://data.tuik.gov.tr/Bulten/Index?p=Cig-Sut-Uretim-Istatistikleri-2022-49699. Accessed 30 Sept 2023
2. Sinem D (2022) Livestock and Products Annual , Report No. TU2022–0037, United States Department of Agriculture, Foreign Agriculture Service
3. Dobson H, Smith R, Royal M, Knight Ch, Sheldon I (2007) The high-producing dairy cow and its reproductive performance. Reprod Domest Anim. **42**(Suppl 2):17–23. https://doi.org/10.1111/j.1439-0531.2007.00906.x. PMID: 17688598; PMCID: PMC2748269
4. Tančin V, Schams D, Mihina S, Bruckmaier RM (2001) Physiology of milk let-down during machine milking. ICAR Technical series No. 7, Physiological and technical aspects of machine milking. 26–27 June 2001, Nitra, Slovak Republic, 27–32. ISBN N
5. Jones GM (2006) The Role of Milking Equipment in Mastitis, Milk Quality & Milking Management, Virginia Tech
6. International Organization for Standardization [TS ISO 5707] (2007) Milking machine installations — Construction and performance
7. International Organization for Standardization [TS ISO 6690] (2007) Milking machine installations — Mechanical tests
8. International Organization for Standardization [TS ISO 3918] (2007) Milking machine installations — Vocabulary
9. Dairy NZ. Pulsation and vacuum systems Page. https://www.dairynz.co.nz/milking/the-milking-plant/pulsation-and-vacuum-systems/. Accessed 01 Oct 2023
10. NADIS Mastitis Part 9 - The Milking Machine page. https://www.nadis.org.uk/disease-a-z/cattle/mastitis/mastitis-part-9-the-milking-machine/. Accessed 09 Oct 2023
11. Temple D, Mainau E, Manteca X (2023) Cow's Welfare during Milking. https://www.fawec.org/en/practical-notes/63-cattle/297-cow-s-welfare-during-milking. Accessed 09 Oct 2023
12. ADHB a Dairy cow milking: milking routines page. https://ahdb.org.uk/knowledge-library/dairy-cow-milking-milking-routines. Accessed 01 Oct 2023
13. ADHB b Mastitis in cows: somatic cell counts (SCCs). https://ahdb.org.uk/knowledge-library/mastitis-in-cows-somatic-cell-counts-sccs. Accessed 01 Oct 2023
14. Smith JW, Chapa AM, Gilson WD, Ely LO Animal and Dairy Science Department , Somatic Cell Count Benchmarks (2009)
15. Emily K (2023) Timing the milking procedure. https://extension.umn.edu/dairy-milking-cows/timing-milking. Accessed 10 Oct 2023
16. International Organization for Standardization [TS EN ISO 13366–2] (2007) Milk - Enumeration of somatic cells - Part 2: Guidance on the operation of fluoro-opto-electronic counters
17. Likert R (1932). A technique for the measurement of attitudes

18. Orkun B (2021) Determination of the presence and antibiotic resistance of listeria species and aerobic mesophilic bacteria count of cow milks, Veteriner Hekimler Derneği Dergisi 92, 16–23. https://doi.org/10.33188/vetheder.714491
19. Kateřina B, Marcela V.K, Vladimír B, Libor K, Renáta KIK (2016) Microbiological quality of raw milk in the Czech Republic. Czech J Food Sci 34(3): 189–196. https://doi.org/10.17221/25/2016-CJFS
20. USK Discover Turkish Dairy Sector Page. https://ulusalsutkonseyi.org.tr/en/discover-turkish-dairy-sector/. Accessed 09 Oct 2023

Information Technologies, Sensors and Control Systems in Agriculture

Comparison and Evaluation of Vegetation Indices for Image Sensing Systems in Precision Agriculture

Ömer Barış Özlüoymak[✉] [ID]

Department of Agricultural Machinery and Technologies Engineering, Faculty of Agriculture,
Çukurova University, Adana, Turkey
`ozluoymak@cu.edu.tr`

Abstract. In precision agriculture, remote estimation processes such as the determination of the canopy area, the yield and plant volume are useful for the camera based observations. Especially, using accurate vegetation index for identifying the plants is very important in the remote image sensing systems. In this study, four frequently used Red Green Blue (RGB) vegetation indices were compared to the manually extracted plant region images of interest obtained in the ImageJ software by using Otsu thresholding method. Excess Green (ExG), Excess Green minus Excess Red (ExG-ExR), Green Percentage (G%) and Triangular Greenness Index (TGI) indices were used with digital color images of single artificial plants. A novel image processing algorithm was developed in LabVIEW software for determining the green area of artificial plants. Performances of mentioned RGB vegetation indices were also evaluated and compared with each other. The comparison of mentioned vegetation indices showed that the highest congruence ranking had been statistically obtained for the ExG and TGI indices at the estimations of the canopy areas according to the vegetative index. While both the ExG and TGI indices presented more proximities to the reference point (mean pixel values obtained by using ImageJ software), ExG-ExR and G% indices showed worse proximity performances to the referred mean pixel values obtained by using ImageJ software. According to the results, both ExG and TGI indices showed reliable separability and can be preferred for green canopy area estimation in image sensing systems.

Keywords: Canopy area · Image processing · Precision agriculture · Vegetative index

1 Introduction

Vegetation indices play a crucial role in the remote sensing of crops and weed plants within precision agriculture [1, 2]. As is well-known, precision agriculture has a positive impact on the environment by reducing waste, enhancing food security, and optimizing resource utilization [3]. Different spectral bands and vegetative index combinations have been used for crop and weed detection studies [4, 5]. Identifying plant biomass versus

soil and residue backgrounds is critical for automated remote sensing and machine vision applications like weed control, plant ecological assessments, and precision crop management systems. Using a precise vegetation index is highly significant in this context [1]. In addition to applications in crop mapping and identification, vegetation indices have found extensive use in crop monitoring studies. They serve as powerful indicators of stress, crop maturity, and various biophysical attributes [2]. Determining yield, plant volume and canopy area in camera-based observations relies on the identification of greenness or the green object in an image. While vegetation indices are usually computed over the entire remote-sensed area, spectral indices can serve as simply way how to calculate above-ground biomass [6].

While some vegetation indices such as Excess of Green Index (ExG), Excess Green minus Excess Red (ExG-ExR), Green Percentage (G%), Triangular Greenness Index (TGI), etc. utilize Red Green Blue (RGB) spectral bands, some vegetation indices such as Normalized Difference Red Edge Index (NDRE), Normalized Difference Vegetation Index (NDVI), Green Chlorophyll Index (GCI), Soil Adjusted Vegetation Index (SAVI), etc. utilize multispectral bands. Currently, many single or combined vegetation indices have been developed by using spectral bands and new sensors for specific purposes.

To determine the most suitable index for vineyard vegetation detection, [7] conducted a comparison of thirteen vegetation indices and computed a crop surface model. ExG, GBVI, RGBVI, GLI and G% indices were determined the best vegetation indices. [8] investigated the potential of airborne videography as a remote sensing tool for rapidly assessing crop conditions in an agricultural region, employing four vegetation indices. [5] studied, tested, and successfully identified weeds by using several indices of chromatic coordinates to distinguish living plant and a non-plant background. A modified hue was also preferred in differentiating weeds from non-plant surfaces. [9] conducted tests on ExG, NDI, and modified hue to separate plant material from various backgrounds. The ExG index was identified as superior to the other methods. Color information was used in the proposed algorithms in order to discriminate between background and plants. [10] studied fuzzy clustering methods and unsupervised color indices to determine their accuracy for classifying soil, plant and residue regions of interest. [11] used datasets acquired during the experiment to test the response of TGI to leaf chlorophyll content and to compare the results with other vegetation and chlorophyll indices. TGI was identified as the most effective spectral index for detecting crop nitrogen requirements.

Various RGB vegetation indices were compared to determine the most effective index for calculating canopy area in this study. Additionally, these RGB vegetation indices were compared with a well-accepted thresholding method (Otsu) to determine the proximity performances of these indices using image processing algorithms. A novel image processing algorithm was developed in LabVIEW software for processing images and determining the green area.

2 Materials and Methods

2.1 Materials

Image Acquisition System

The research was carried out at the automation laboratory of the Department of Agricultural Machinery and Technologies Engineering, Faculty of Agriculture, Çukurova University, Adana, Türkiye. An image capturing unit was constructed, comprising a black chamber, a CMOS GigE camera (Allied Vision, Mako, G-030C), a 9 mm focal length lens (Fujinon, HF9HA-1B), and a lighting system with 48 LED lamps (Cata, TL-4481). This unit was designed to capture images of artificial plant samples from a distance of 300 mm. The chamber was configured in the form of a cube and illumination intensity in the chamber was measured as 1390 lx. The GigE camera was operated with the help of a DC power supply (Pacific, 2305D+) to supply constant DC voltage. Image capturing unit was shown in Fig. 1.
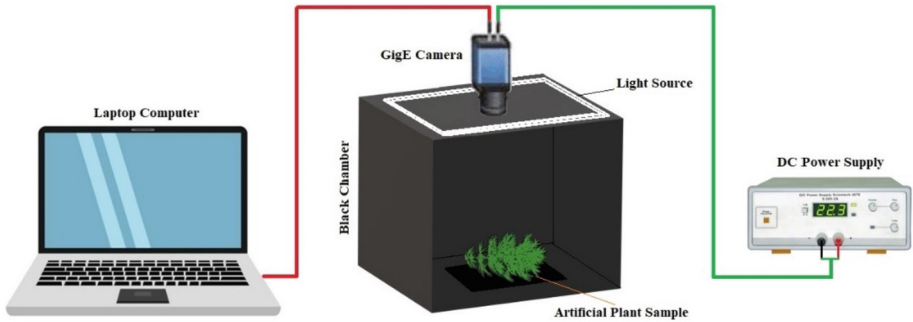
Fig. 1. Image capturing unit for transferring sample photos to the computer.

As shown in Fig. 1, photographs taken in JPEG format were captured through the aperture on the top of the black chamber. In the experiments, captured images were stored as 32-bit RGB image data and the resolution of the camera was 644×484 pixels. The image processing was performed using a laptop computer (Acer, Aspire, 4830TG) equipped with an Intel Core i5-5200U CPU and 4 GB RAM. For processing images and determining the green area of artificial plants, a novel image processing algorithm was developed in LabVIEW software (National Instruments Corporation, Austin-Texas-USA). Totally 5 artificial plant sample images were subjected to image analyses for vegetative index tests.

2.2 Methods

Digital Image Processing Method

After capturing process, the RGB images were segmented into their red (R), green (G), and blue (B) components. Following the application of image processing techniques, a grayscale image was initially generated, and subsequently, a binary image was obtained. The segmentation process isolated only the green objects corresponding to the artificial weed samples from the background. The segmented image is represented by Eq. (1) as provided below,

$$g(x, y) = \begin{cases} 1 \ if \ f(x, y) > T \\ 0 \ if \ f(x, y) \leq T \end{cases} \tag{1}$$

In the provided equation, *g(x, y)* represents the processed image, *f(x, y)* stands for the pixel value of the image at the xth column and y^{th} row, and *T* signifies the chosen threshold value [12].

Binary images for each vegetative index were generated by employing Otsu's threshold method [13]. This method is based on the analysis of the histogram of the tonal image resulting from the initial vegetative index image calculation [1], which was computed using LabVIEW software. The pixels are divided into two classes: C_0 and C_1, representing background and objects (or vice versa), using a threshold value at level k. C_0 includes pixels with levels [1,…, k], while C_1 includes pixels with levels [k + 1,…, L]. The probability of occurrence for each tonal class is given below [13]:

$$\Pr(C_0) = \sum_{i=1}^{k} P(i) \tag{2}$$

$$\Pr(C_1) = \sum_{i=k+1}^{L} P(i) \tag{3}$$

While the pixel values of artificial plants are defined as object, the remaining pixels are represented as background. Comparisons the developed image processing algorithms by using vegetative indices with manually derived by using ImageJ software are given in Fig. 2.

RGB Vegetation Indices

Vegetation indices were taken into consideration to enhance the robustness of the visual descriptor in distinguishing leaves from other objects. The vegetation index is a parameter used to measure plant photosynthesis (leaves generally exhibit a higher vegetation index value compared to soil and trunks) [3]. Greenness information were extracted according to the RGB vegetation indices and differentiated between vegetation and background. The formulation of the RGB-based vegetation indices is given in Table 1. The accuracies of RGB spectral indices were then compared to the binary vegetation images manually extracted using ImageJ software. The approximation error was found according to the formula as shown below;
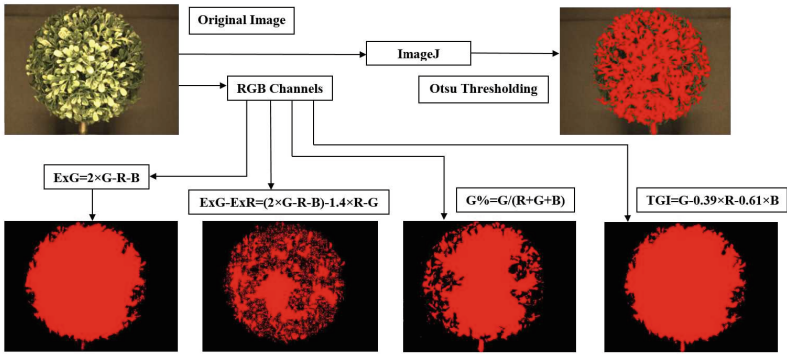
Fig. 2. Comparison of the developed software for vegetative indices with ImageJ software.

$$\%Error = \frac{|x - y|}{x} \times 100 \qquad (4)$$

where *% Error* is percent error; *x* is the pixel value obtained by ImageJ software; *y* is the pixel value calculated by the developed software.

Table 1. Vegetation indices based on RGB utilized in this study.

RGB Spectral Indices	Formulations	References
Excess Green	ExG = 2 × G-R-B	[5]
Excess Green-Excess Red	ExG-ExR = (2 × G-R-B)-1.4 × R-G	[1]
Green Percentage Index	G% = G/(R+G+B)	[14]
Triangular Greenness Index	TGI = G-0.39 × R-0.61 × B	[11]

Statistical Analysis Method

Imaging methods of RGB-based vegetation indices belong to the 5 artificial plant samples were statistically evaluated by using IBM SPSS statistical analysis software. To determine if there were any statistically significant differences between the means of two or more independent groups, the one-way analysis of variance (ANOVA) was employed. Post-hoc analysis was conducted using the Duncan test following the ANOVA. The post-hoc analysis is crucial in revealing the specific groups from which the observed difference originates when there is a significant difference between the groups as determined by the variance analysis.

3   Results and Discussion

3.1   Results

Comparisons of RGB Vegetative Indices

Otsu threshold method was used in image segmentation processes for all vegetative indices. To evaluate the proximity of the image sensing software, the accuracies of ExG, ExG-ExR, G%, and TGI were assessed in comparison to the manually extracted vegetation images obtained through ImageJ software. Measured proximity rates (%) for each RGB vegetation index across the ImageJ software are given in Table 2.

Table 2. Comparisons of vegetation indices based on RGB used in the image sensing system and ImageJ software based on the pixel values.

Plant	Pixel Values					Proximity (%)			
	ExG	ExG-ExR	G%	TGI	ImageJ	ExG	ExG-ExR	G%	TGI
P1	139767	48703	110091	140370	120902	15.60	59.72	8.94	16.10
P2	81102	44207	63030	82303	83731	3.14	47.20	24.72	1.71
P3	27706	15922	34434	26676	29086	4.74	45.26	18.39	8.29
P4	51457	47154	176178	51915	45316	13.55	4.06	288.78	14.56
P5	42533	11863	142484	43008	54021	21.27	78.04	163.76	20.39
			Mean Error (%)			**11.66**	**46.86**	**100.92**	**12.21**

As seen from the Table 2, the calculated pixel values of ExG as well as TGI indices, which are primarily dependent on the nitrogen and chlorophyll content, were very similar and closer to the pixel values obtained by the ImageJ software manually.

Statistical Analysis Based Classification

A basic comparison of vegetative indices was performed for determining groups on the obtained images. The greenness extraction process was provided by different vegetation indices. Both ExG and TGI indices discriminated vegetation more accurately and successfully than the ExG-ExR and Green Percentage indices.

According to the statistical results, the differences between the imaging methods were determined and a statistically significant difference between the groups according to the p value (Sig.) (p-level < 0.05) was found. Imaging methods used in the image sensing system were gathered in three sub groups. While both ExG and TGI indices were classified into a single group, ExG-ExR and Green Percentage indices were included in a separate subgroup, as indicated in Table 3.

Table 3. Duncan test analysis results for grouping imaging methods.

Plant	Imaging Method	Subset for alpha = 0.05		
		Group 1	Group 2	Group 3
Plant 1	ExG			139767.00
	ExG-ExR	48703.33		
	G%		110090.67	
	TGI			140370.00
Plant 2	ExG			81102.00
	ExG-ExR	44207.00		
	G%		63030.33	
	TGI			82303.67
Plant 3	ExG		27173.00	
	ExG-ExR	15922.33		
	G%			34434.33
	TGI		27009.67	
Plant 4	ExG		51457.00	
	ExG-ExR	47154.00		
	G%			176178.33
	TGI		51914.67	
Plant 5	ExG		42532.67	
	ExG-ExR	11863.33		
	G%			142483.67
	TGI		43008.33	

3.2 Discussion

Comparisons of vegetative index values for ExG, ExG-ExR, G% and TGI were conducted on the color images for green canopy area estimation in image sensing systems. According to the results, both ExG and TGI indices showed reliable separability with higher accuracy and can be preferred in precision agriculture systems. [6] found out similar results that both the TGI and ExG indices exhibited the highest consistency in the estimation of vegetation indices. Additionally, [11] demonstrated that the utilization of the TGI index produced the best results in later phenology stages when it was primarily influenced by leaf chlorophyll content.

4 Conclusion

This study contributes to the literature by advancing the development of a more flexible algorithm in digital image processing using in precision agriculture. Imaging methods of RGB-based vegetation indices belong to the 5 artificial plant samples were tested

and evaluated using a digital camera in order to differentiate plants from backgrounds under the controlled conditions. It was found that both ExG and TGI indices worked well for differentiating the artificial plant and the background when the accuracies of G%, ExG-ExR, TGI and ExG were compared. The calculated pixel values of both the ExG and TGI indices were very similar and closely aligned with the manually obtained pixel values. In plant area detection, both ExG and TGI indices yielded very similar results. The developed image sensing system demonstrated a high level of accuracy in estimating plant area when using the TGI and ExG vegetation indices.

RGB camera usage instead of using more expensive multispectral cameras is also possible for the estimation of plant area in machine vision systems for identification of plant canopies in the field conditions.

References

1. Meyer GE, Neto JC (2008) Verification of color vegetation indices for automated crop imaging applications. Comput Electron Agric 63:282–293

2. Yeom J et al (2019) Comparison of vegetation indices derived from UAV data for differentiation of tillage effects in agriculture. Remote Sens 11(1548):1–16. https://doi.org/10.3390/rs11131548

3. Baltazar AR, Santos FNd, Moreira AP, Valente A, Cunha BJ (2021) Smarter robotic sprayer system for precision agriculture. Electronics 10(2061). https://doi.org/10.3390/electronics10172061

4. Lamm RD, Slaughter DC, Giles DK (2002) Precision weed control for cotton. Trans ASAE 45:231–238

5. Woebbecke DM, Meyer GE, Bargen KV, Mortensen DA (1995) Color indices for weed identification under various soil, residue and lighting conditions. Trans ASAE 38:259–269

6. Starý K, Jelínek Z, Kumhálová J, Chyba J, Balážová K (2020) Comparing RGB - based vegetation indices from UAV imageries to estimate hops canopy area. Agron Res 18(4):2592–2601. https://doi.org/10.15159/AR.20.169

7. Pádua L et al (2018) Vineyard properties extraction combining UAS-based RGB imagery with elevation data. Int J Remote Sens 39(15–16):5377–5401. https://doi.org/10.1080/01431161.2018.1471548

8. Metternicht G (2003) Vegetation indices derived from high-resolution airborne videography for precision crop management. Int J Remote Sens 24(14):2855–2877. https://doi.org/10.1080/01431160210163074

9. Mao W, Wang Y, Wang Y (2003) Real-time detection of between-row weeds using machine vision. ASAE paper number: 031004. https://doi.org/10.13031/2013.15381

10. Meyer GE, Neto JC, Jones DD, Hindman TW (2004) Intensified fuzzy clusters for classifying plant, soil, and residue regions of interest from color images. Comput Electron Agric 42:161–180

11. Hunt ER Jr, Doraiswamy PC, McMurtrey JE, Daughtry CST, Perry EM, Akhmedov B (2013) A visible band index for remote sensing leaf chlorophyll content at the canopy scale. Int J Appl Earth Obs Geoinf 21:103–112. https://doi.org/10.1016/j.jag.2012.07.020

12. Gonzalez RC, Woods RE (2008) Digital image processing, 3rd edn. Prentice Hall, Hoboken

13. Otsu N (1979) A threshold selection method from gray-level histograms. IEEE Trans Syst Man Cybern 9(1):62–66
14. Richardson AD, Jenkins JP, Braswell BH, Hollinger DY, Ollinger SV, Smith ML (2007) Use of digital webcam images to track spring green-up in a deciduous broadleaf forest. Oecologia 152:323–334

Implementation and Assessment of an Autonomous Ground Vehicle (AGV) for On-Field Agricultural Operations

Gabriele Sara$^{(\boxtimes)}$, Giuseppe Todde , Daniele Pinna, Johnny Waked, and Maria Caria

Department of Agricultural Sciences, University of Sassari, Viale Italia 39A, 07100 Sassari, Italy
gsara@uniss.it

Abstract. In recent years, many studies have been focused on the development and implementation of autonomous ground vehicles (AGV) and teleoperated mobile robotic platforms capable of performing agricultural tasks (soil preparation, crop treatment, harvesting) with limited or no human intervention. The AGVs are emerging technologies where the availability of scientific evidence that clearly states the overall benefits of their implementation in the agricultural sector is still limited. Therefore, this study aims to customize a commercial AGV for specific use in agriculture and test its operating capabilities on-field to perform agricultural tasks coupled with different implements. The electric tracked AGV used in this study was a compact rover (1.30×1.05 m) powered by lead-acid batteries. The AGV was coupled to two self-propelled implements, a rotary flail mower and a rotary tiller. Considering the performance of the AGV and implements, the cutting efficiency (CE%), soil clumping, and bulk density (g cm^{-3}) were evaluated in relation to the towed load. In addition, the energy consumption (kWh) was measured while performing on-field tasks. The driving performance tests allowed to monitor the forward speeds where the maximum speed value corresponded to 0.77 m s^{-1}. In addition, the forward speed was significantly influenced by towed load but not by the time of use. The CE was 36.81% on average, and the rotary tiller operations improved the soil characteristics. The results of this study contribute to the implementation and use of AGV in agriculture to perform specific tasks in the field.

Keywords: Unmanned ground vehicle · Robot · Weed control · Soil tillage · Sustainable agriculture

1 Introduction

The agricultural sector has been faced with many challenges related to the environmental impacts of anthropogenic and farming practices. The increasing demand for world food production has been supported over the years by the improvement of the agricultural sector. Thanks to the introduction of new machinery e.g., tractors, automatic milking machines, and new management strategies e.g., genetic improvement, and the use of

fertilizers, it has been possible to increase production yields [1, 2]. Nowadays, the agricultural sector has the potential and responsibility to mitigate the environmental impacts of GHG emissions through sustainable actions and management strategies. This goal could be pursued with conservative approaches while improving yields and preserving soil fertility [3]. Furthermore, the introduction of smart technologies could be a powerful support tool for farmers to achieve this goal. The combination of precision agriculture practices, digital farming technologies, and robotic solutions could provide answers to these challenges as well as reduce the farmers' manual labor demand and increase their welfare [1, 4]. In the last years, many studies and manufacturers have been focused on the development and implementation of agricultural robots, autonomous ground vehicles (AGV), and teleoperated mobile platforms capable of carrying out agricultural tasks i.e., soil preparation, crop treatments, weed control, and harvest with limited or no human intervention [5, 6]. Despite AGVs and robotic solutions have been studied and tested in the agricultural context, equipped with sensors or implements, ready-to-market AGVs for farming applications are still rare. Moreover, AGVs are emerging technologies where the availability of scientific findings that clearly state the overall benefits deriving from their implementation in the agricultural sector are still limited. Additionally, despite the large quantity of robots applied in industry, few robots are effectively used by farmers as support for their activities [7]. Many challenges affect the implementation of AGV in the farming context since agricultural robots should operate in a dynamic and unstructured environment frequently producing insufficient results caused by integral uncertainties, unspecified operational settings, environmental conditions, and randomness of events [8]. Using robots in agricultural activities is complex because they must deal with living products like leaves and fruits creating high variability of parameters that would affect the robot's behavior, many of which cannot be controlled a priori [9].

This study aims to evaluate the performances of a tracked compact rover with autonomous navigation coupled with different implements accomplishing agricultural tasks in orchards and vineyards.

2　Materials and Methods

The AGV used in this study was produced by the Italian company "Niteko S.r.l." and was a fully electric tracked rover. The AGV was remote-controlled and was improved to perform autonomous navigation in the field. This AGV was 130 cm wide and 105 cm long, with rubber tracks of 33 cm each (Fig. 1) and powered by two lead acid batteries (200 Ah, 24 V). The components of the autonomous navigation system are real-time kinematics (RTK) GPS, composed by a receiver on the rover (u-blox, ANN-MB-00) and a base antenna to correct the signal. Moreover, the AGV was equipped with two ultrasonic bumper sensors as a security system to detect objects in front of the AGV, stopping it in case of obstacle detection (i.e., vine stock). The performances of the AGV coupled with towed implements were measured during on-field operations as well as the stand-alone AGV performance. The implements used are a rotary tiller (140 kg) and a flail mower AT120 (230 kg) produced by the "GEO Agric S.r.l" (GEO ITALY s.r.l., Italy). The working widths are respectively 90 cm and 120 cm, as well as the gasoline engine power of 4.8 kW and 11.8 kW for the tiller and mower, respectively.

The performances of the AGV towing implements were measured during soil and weed management operations in the iter-row of the vineyard and in the open field.
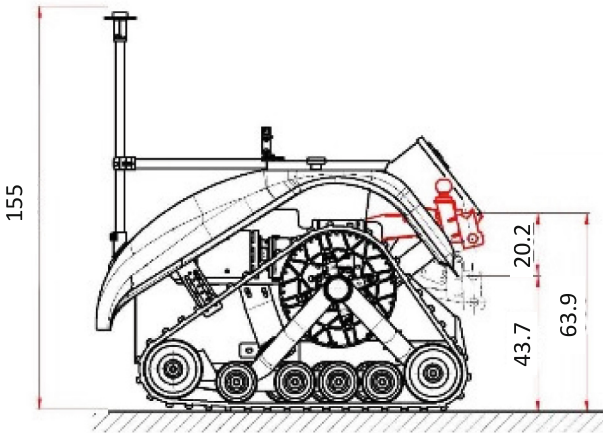
Fig. 1. Technical drawing of the customized autonomous ground vehicle (AGV) used in this study. Dimensions are in cm.

2.1 On-Field Operation Tests

The performances of the stand-alone AGV (Fig. 2a), and the AGV coupled with the rotary tiller (Fig. 2b), or with the flail mower (Fig. 2c) were tested. Specifically, the forward speed (m s^{-1}) and the energy uptake (kWh) to perform specific operations were considered. In addition, the influence of different towed weights on the performance of the AGV was investigated. The weights considered were the stand-alone AGV (W0), the rover coupled with rotary tiller (W140), and the rover coupled with the flail mower (W230). The forward speed was calculated by registering the time (s) to move the rover in a determined path of 100 m. The working efficiency of the towed implements was measured considering the tilling capacity of the AGV coupled with the rotary tiller as well as the cutting efficiency of the AGV coupled with the flail mower.

The tilling tests were done to evaluate the performance of the AGV while towing a tiller. The test simulated the operation of soil preparation for sowing. In plots of 1500 m^2, bulk density (g cm^{-3}) and amount of clumps (%) with different diameters were measured to evaluate the quality of the soil processing. The soil samples collected were six before tilling and nine after tilling. For the bulk density, a cylinder of a known volume of 130 cm^3 was used [10, 11], whereas to quantify the amount of clumps, two sieves with mesh sizes of 6x6 cm and 2x2 cm were used. The amount of clumps was measured weighing the total and residual fraction of each sieve. The humidity (%) of the soil samples was measured by weighting the samples before the drying process in an oven at a temperature of 105 °C until the weight of the sample became constant [11].

Fig. 2. Customized autonomous ground vehicle (AGV) and implements used in this study with different configurations. a) Stand-alone AGV, b) AGV coupled with rotary tiller, and c) AGV coupled with flail mower.

The mowing test was done to evaluate the performance of the AGV while towing a flail mower. Specifically, the cutting efficiency (%) was assessed. The data were collected in two different experimental plots during the winter season. A total of nine samples were randomly collected before mowing, in order to characterize the weed (height and diameter), and twenty-seven samples were collected after mowing. The sampling was randomly made inside each sub-plots using a 50x50 cm wood square. The cutting efficiency (CE) was determined using Eq. (1) and considering the ratio between weed dry matter (g) cut by a single passage of the flail mower towed by the AGV and the total biomass dry matter [12, 13]. The amount of cut weed was determined by the difference between the weed collected before mowing (DW_{pre}) and the residual weed uncut by the flail mower (DW_{post}) and collected using scissors.

$$CE = \left[(Dw_{pre} - Dw_{post})/Dw_{pre} \right] * 100 \tag{1}$$

Furthermore, the autonomous on-field navigation performances of the AGV were monitored. The autonomous navigation of the AGV was stressed to evaluate the capability of this system to autonomously navigate into the vine row. The data were collected in a vineyard with a slight slope of 0.4% in the forward direction of the row. The inter-row of the vineyard was not tilled but had spontaneous weed growth that homogeneously covered the soil. A total of five tests were conducted from April to May to collect data on the positions of the AGV.

3   Results and Discussion

Table 1 shows the results of the relationship between AGV towed weight (W0, W140, W230) and AGV performance in terms of forward speed (m s^{-1}). The maximum forward speed registered was 0.77 m s^{-1} considering the W0. Moreover, the results indicate that the towed weight has a significant effect on the forward speed of the AGV. In fact, the speed of W0 is higher than the speed of W140 and W230. Although the load tends to reduce the AGV's speed, differences in the order of 0.04 - 0.06 m s^{-1} are scarcely observable in practical terms on the field. However, this could have a different impact with implements of higher load of more than 300 kg, which may impact the AGV traction performance as well as the battery life and engine performances [14].

Considering the AGV towing capacity for a long time (2 h), it was observed that there are no significant differences in the forward speed and therefore in the performance of the AGV's electric engine. The speed remains constant from the start to end of the test for all loads considered. Furthermore, Table 1 reports the results of the AGV performances considering the energy absorption of the engines during the on-field trials. It was observed that the weight has no significant effect (*p-value* $= 0.736$) on the total amount of energy uptake by the AGV. Further analyses are needed to investigate if higher weight (more than 300 kg) could influence the total energy uptake of the AGV engines as well as the overall performance of the AGV.

Table 1. Average forward speed (m s^{-1}) and energy uptake (kWh) of the AGV considering different towed weights (kg). Values within rows with different superscript letters are statistically different (*p-value* < 0.05).

		Towed weight		
		W0	W140	W230
Speed (m s-1)	Max	0.77[a]	0.74[b]	0.71[b]
	Mean	0.57[a]	0.54[b]	0.52[b]
Energy (kWh)	Max	4.69[a]	4.10[a]	3.63[a]
	Mean	3.09[a]	2.75[a]	2.70[a]

Figure 3 shows the results of the tillage tests where an improvement of the seedbed was achieved. In fact, the clumps with higher sizes (between 2 cm and 6 cm) decreased after tilling the soil. In addition, the clumps with sizes higher than 6 cm were significantly reduced between pre- and post-tillage. Hence, the AGV showed the capability of towing a tiller to improve the soil quality regarding the subsequent sowing operations. Concerning bulk density of the soil, a reduction between pre-tillage and post-tillage of 1.02 g cm^{-3} and 0.92 g cm^{-3}, respectively, was observed.

These results underline how the system composed of AGV and rotary tiller provides a possible solution for managing the soil in vineyard inter-row or in areas where conventional tractors may not be able to pass due to their excessive sizes reducing also soil compaction than heavy tractors [15].
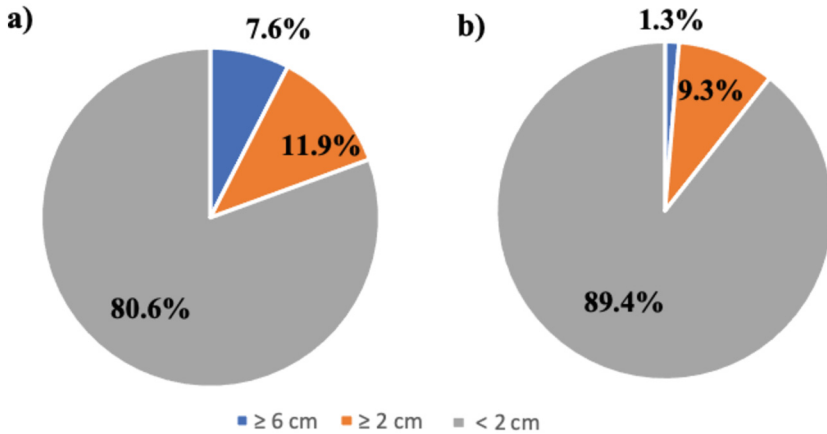
Fig. 3. Results of the tillage test performed with the AGV and rotary mower. a) Distribution of soil clumps according to size in the pre-tillage. b) Distribution of clumps post-tillage with the AGV average forward speed of 0.54 m s^{-1}.

The experimental plots of the mowing test were characterized by spontaneous vegetation on average with a dry matter content of 169.8 $\pm$ 46.65 g m^{-2}. The average height, average minimum, and average maximum of the weeds were 16.77 $\pm$ 8.94 cm, 10.47 $\pm$ 4.71 cm, and 33.81 $\pm$ 6.87 cm, respectively. Whereas the average diameters, average minimum and average maximum of the steams were 0.27 $\pm$ 0.2 cm, 0.11 $\pm$ 0.02 cm, and 0.42 $\pm$ 0.2 cm, respectively. The cutting efficiency of the flail mower towed by the AGV was on average 36.81 $\pm$ 10.22% in comparison with the total removal of the weed. This indicates how more than half of the weed biomass was not removed by a single passage of the AGV and mower. Other studies in which the agricultural robots' performance of weed removal was evaluated, an efficiency of more than 90% was observed and of 65% in the management of the vineyard inter-row [16, 17]. Moreover, a specific study on weed management in globe artichoke, showed that a small autonomous mower achieved a higher weed control effect, lower energy consumption and lower cost compared to the conventional system, suggesting the suitable implementation of these autonomous mowers in horticultural crops [18]. Despite the weeding removal efficiency result lower that 50%, the amount of residual weed does not represent a negative aspect, especially if farmers want to maintain a cover crop to avoid soil erosion.

In Fig. 4 are reported the coordinates registered by the AGV during autonomous navigation tests in the vineyard row. It was observed a deviation between the GPS points for the different replicates of the same path that are not overlayed as expected. This indicates that some errors occur in the autonomous navigation in comparison with the reference path. Nevertheless, the deviations from the reference path are not very large, in fact, the coefficient of determination (R^2) was high (Fig. 4). Moreover, the root mean square error is 53 cm. These deviations or errors may occur because of oscillation of the GPS antenna placed on the AGV during path recording caused by the vibrations of the AGV itself and the consequent trajectory adjustment automatically made by the AGV system software during autonomous navigation. Despite these errors,

the autonomous navigation allowed the AGV to move inside the vineyard row which in this case has a width of 2.5 m. The autonomous navigation system plays a critical role in AGVs. Research indicates that maintaining the correct route in agricultural settings poses significant challenges and allowing different autonomous driving performances [19, 20]. In addition, the measured forward speed of the rover in autonomous navigation was on average of 0.21 m s^{-1}, thus the rover needs 3.5 min to complete a single vineyard row of one hundred meters and this should be carefully considered when planning the AGV activities as this time could influence the operation management.
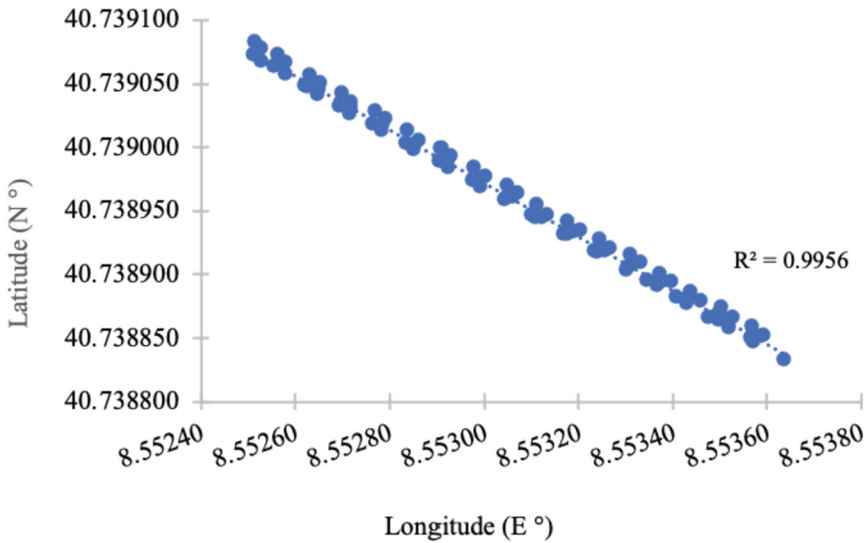
Fig. 4. Latitude (North decimal degrees) and longitude (East decimal degrees) measured by the AGV antenna during autonomous navigation in the vineyard row.

4   Conclusions

Autonomous robotic weed control systems hold promise toward the automation of this task [21, 22]. Robotic technology may also provide a means of reducing agriculture's current dependency on herbicides, improving its sustainability, and reducing its environmental impact [23]. In this study, the implementation of a commercial rover with Real Time Kinematic - GPS system was presented. Furthermore, the performances of the autonomous ground vehicle were measured by considering different configurations to accomplish agricultural tasks. Specifically, the AGV was coupled with a rotary tiller and a flail mower for soil and weed management evaluation tests, respectively. The results demonstrated the AGV's capability to efficiently tow implements up to 230 kg and 11.8 kW engine power for soil tillage and weed control.

The AGV coupled with the implements showed promising operative performances both in the vineyard inter-row and in the open field. Autonomous navigation tests were

positive, indicating an acceptable accuracy in the autonomous movement of the AGV in the vineyard, with errors in the order of 53 cm. In fact, the AGV was able to complete the path within the 2.5 m inter-row of the vineyard without hitting the vine rows. In the future, further studies will focus on the improvement of the autonomous navigation system as well as on the evaluation of the towing capacity and traction of the AGV. Moreover, other implementation of the AGV would be focused on the use of different batteries (i.e., lithium) to power the electric engines and evaluate the performance of the system.

Conflict of Interest. The Authors declare no competing interest.

References

1. Klerkx L, Jakku E, Labarthe P (2019) A review of social science on digital agriculture, smart farming and agriculture 4.0: new contributions and a future research agenda. NJAS-Wageningen J Life Sci 90:100315
2. Neethirajan S, Kemp B (2021) Digital livestock farming. Sens Bio-Sens Res 100408
3. Gancone A, Viznere R, Kaleja D, Pubule J, Blumberga D (2022) Towards climate neutrality via sustainable agriculture in soil management. Environ Clim Technol 26(1):535–547
4. Ghobadpour A, Monsalve G, Cardenas A, Mousazadeh H (2022) Off-road electric vehicles and autonomous robots in agricultural sector: trends, challenges, and opportunities. Vehicles 4(3):843–864
5. Xie D, Chen L, Liu L, Chen L, Wang H (2022) Actuators and sensors for application in agricultural robots: a review. Machines 10(10):913
6. Naio Technologies. http://www.naio-technologies.com/en/home/. Accessed 15 July 2023
7. Xiang R, Jiang H, Ying Y (2014) Recognition of clustered tomatoes based on binocular stereo vision. Comput Electron Agric 106:75e90
8. Bechar A, Vigneault C (2016) Agricultural robots for field operations: concepts and components. Biosys Eng 149:94–111. https://doi.org/10.1016/j.biosystemseng.2016.06.014
9. Bechar A, Vigneault C (2017) Agricultural robots for field operations. Part 2: operations and systems. Biosys Eng 153:110–128. https://doi.org/10.1016/j.biosystemseng.2016.11.004
10. Blake GR, Hartge KH (1986) Bulk density. In: Klute A (ed) Methods of soil analysis, part I. Physical and mineralogical methods, 2nd edn. ASA/SSSA, Madison, pp 363–375
11. de Lima RP, da Silva AP, Giarola NF, da Silva AR, Rolim MM (2017) Changes in soil compaction indicators in response to agricultural field traffic. Biosys Eng 162:1–10
12. Hossain MZ, Komatsuzaki M (2021) Weed management and economic analysis of a robotic lawnmower: a case study in a Japanese pear orchard. Agriculture 11(2):113
13. Hasan M, Mokhtar AS, Rosli AM, Hamdan H, Motmainna M, Ahmad-Hamdani MS (2021) Weed control efficacy and crop-weed selectivity of a new bioherbicide WeedLock. Agronomy 11(8):1488
14. Shafaei SM, Mousazadeh H (2023) On the power characteristics of an unmanned tracked vehicle for autonomous transportation of agricultural payloads. J Terrramech 109:21–36

15. Lagnelöv O, Larsson G, Nilsson D, Larsolle A, Hansson PA (2020) Performance comparison of charging systems for autonomous electric field tractors using dynamic simulation. Biosyst Eng 194:121–137

16. Bakker T, van Asselt K, Bontsema J, Müller J, van Straten G (2006) An autonomous weeding robot for organic farming. In: Field and service robotics: results of the 5th international conference. Springer, Heidelberg, pp 579–590

17. Reiser D, Sehsah ES, Bumann O, Morhard J, Griepentrog HW (2019) Development of an autonomous electric robot implement for intra-row weeding in vineyards. Agriculture 9(1):18

18. Gagliardi L et al (2021) Evaluation of autonomous mowers weed control effect in globe artichoke field. Appl Sci 2021(11):11658. https://doi.org/10.3390/app112411658

19. Nguyen P, Badenhorst PE, Shi F, Spangenberg GC, Smith KF, Daetwyler HD (2020) Design of an unmanned ground vehicle and LiDAR pipeline for the high-throughput phenotyping of biomass in perennial ryegrass. Remote Sens 2021(13):20. https://doi.org/10.3390/rs13010020

20. Kurita H, Oku M, Nakamura T, Yoshida T, Fukao T (2022) Localization method using camera and LiDAR and its application to autonomous mowing in orchards. J Robot Mechatron 34(4):877–886. https://doi.org/10.20965/jrm.2022.p0877

21. Slaughter DC, Giles DK, Downey D (2008) Autonomous robotic weed control systems: a review. Comput Electron Agric 61(1):63–78. https://doi.org/10.1016/j.compag.2007.05.008

22. Zhang W, Miao Z, Li N, He C, Sun T (2022) Review of current robotic approaches for precision weed management. Curr Robot Rep 3(3):139–151. https://doi.org/10.1007/s43154-022-00086-5. Epub 2022 Jul 22. PMID: 35891887; PMCID: PMC9305686

23. Todde G, Sara G, Pinna D, Sole S, Caria M (2023) Autonomous ground vehicle for weeding activities: preliminary sustainability assessments. In: Conference proceedings of Springer Publishing: "15th International Congress on Agricultural Mechanization and Energy in Agriculture – ANKAgEng'2023", in press

Autonomous Ground Vehicle for Field Activities: Preliminary Sustainability Assessments

Giuseppe Todde(✉) , Gabriele Sara , Daniele Pinna , Stefania Sole ,
and Maria Caria

Department of Agricultural Sciences, University of Sassari, Viale Italia 39a, 07100 Sassari, Italy
`gtodde@uniss.it`

Abstract. Currently, the use of agricultural machinery for on-field operations appears to be one of the most impactful activities in the food sector. The implementation by farmers of innovative solutions for improving farm efficiency and sustainability has been addressed in many ways. One of these solutions deals with the implementation of autonomous ground vehicles (AGVs) to carry out agricultural tasks, where the impacts associated with agricultural AGVs are still limited. Thus, this study aims to analyze the energy and environmental burdens of an AGV coupled with a mower. The life cycle assessment (LCA) methodology was adopted to analyze energy requirements and the associated environmental emissions. The fully electric AGV is equipped with two rubber tracks powered by 2000 W motors. The self-propelled rotary mower is powered by a 9 kW engine, weighs 230 kg, and has a working width of 120 cm. The results of the analysis showed that the embodied primary energy of both AGV plus Implement (AGV+I) accounted for 104 MJ kg^{-1}, while related emissions were found to be 6.86 kg CO_2e kg^{-1}. Moreover, analyzing the inputs of the AGV+I system, the battery pack and the iron materials accounted for the main portion of the total impacts. In conclusion, the outcomes of this study will strongly help to pursue the objectives and targets foreseen by the main strategic plans related to the reduction of environmental impacts, improvement of agricultural production efficiency, and increasing the digitization and innovation of the agricultural sector.

Keywords: Autonomous vehicles · On-field agricultural mechanization · Terrestrial vehicle · Carbon footprint

1 Introduction

The European Green Deal is a comprehensive plan approved by the European Commission in 2020 to transform the EU into a modern, resource-efficient, and competitive economy while addressing challenges such as climate change, energy security, and environmental degradation [1]. The agricultural sector faces the challenge of feeding a growing population while reducing its impact on the environment and human health. To achieve this, farms need to increase their efficiencies and capacities while minimizing labor use per cultivated hectare.

One way to achieve more sustainable and conservative farm practices is through the implementation of precision agriculture (PA) strategies. PA involves the use of advanced technologies, such as autonomous robots and fully connected systems, to optimize agricultural practices [2, 3]. This approach is considered a Smart Farming concept that represents a step forward from the automated farm into a fully connected and flexible system [4]. Achieving the precision agriculture principles and the smart farm concept is a long-term mission that will demand design modifications and further improvements on systems and components that are currently being used in agriculture [5]. In the last years, digital agricultural technologies have progressed in two broad classes: automated large tractors with driver-assistive systems and fully autonomous ground vehicles (AGVs) capable of carrying out agricultural tasks (soil preparation, crop treatments, weed control, harvest, etc.) with no human intervention [6, 7]. These technologies can contribute to reduce pesticide use [8], energy requirements and environmental emissions [9], soil compaction [10], workforce demand [11] and reduce the exposure of operators to hazard treatment [12]. However, the commercialization of fully robotic systems in agriculture remains restricted.

According to the European Standing Committee on Agricultural Research (2016) [13], further efforts should be made by both researchers and private companies to develop new solutions. In fact, AGVs are emerging technologies where the availability of scientific findings, that clearly state the overall benefits (related to energy, environmental and economic sustainability) deriving from their implementation in the agricultural sector, are still limited. As also suggested by Pradel et al., [14], there is an urgent need for accurate impact assessment to provide such quantitative values. This can be done by using Life Cycle Assessment (LCA), a method that enables to assess the above energy, environmental and economic impacts of using AGVs for agricultural activities. Under this context, for a further step into more sustainable and conservative farm practices, it is necessary to provide innovative and practical solutions for optimizing the implementation of AGVs in the agricultural sector and to improve the sustainability of food production. Thus, the main objective of this study was to analyze the energy and environmental impacts of a fully electric AGV coupled with a self-propelled rotary mower for the accomplishment of agricultural tasks.

2 Materials and Methods

The Life Cycle Assessment (LCA) methodology was adopted in this study to evaluate the energy and environmental impacts of an AGV coupled with a self-propelled mower [15–18]. The data used in the analysis was obtained through a reverse engineering approach of a fully electric and AGV and a self-propelled mower. The Xbot AGV was developed and built by the Niteko srl company, while the mower was built by the GEO-Agric srl company (Fig. 1). The fully electric AGV is equipped with two rubber tracks powered by 2000 W motors, while the autonomy is ensured by two 220 Ah lead-acid batteries. The self-propelled rotary flail mower is powered by a 9 kW engine, weighs 230 kg and has a working width of 120 cm (Table 1). The implement was coupled to the AGV through a standard tow hitch. The data adopted in this study were validated

and checked in accordance with the data quality parameters. Particularly, the data quality involved the time and geographical coverage, precision, consistency, completeness, representativeness, reproducibility, data sources, and information uncertainty.

Table 1. Main characteristics of the machines analyzed in this study.

Machine	Power (W)	Engine Type	Working width (cm)	Mass (kg)	Lifespan (hours)
AGV	2,000	Full electric	130	425	5,000
Mower	9,000	Gasoline	120	230	5,000

The material flows were determined for the AGV and the mower in the assembly and repair/maintenance phase. For the assembly phase, the material flows considered were those directly used as inputs. In the repair and maintenance phase, the material flows considered were inputs either directly and indirectly used for the standard maintenance of the machines.

Fig. 1. The electric autonomous ground vehicle (AGV) coupled with a self-propelled mower during weed control trials in vineyards.

The parts used in the machines were grouped by material classes, referring to the composition of the raw material of each piece, such as steel, aluminum, rubber, plastic, etc. In order to assess the embodied energy (MJ) and carbon footprint (CO_2e) of the machines studied, the amount of each machine input was multiplied by energy equivalent coefficients and emission factors, respectively. This procedure allowed us to assess the total energy and carbon footprint of the machine. After determining the total energy demand of the machine over the lifecycle, the energy and carbon indexes were expressed per unit of the time of the lifespan (h) and per mass of the machinery (kg). Due to the

low associated impacts, the industry infrastructure and labor were disregarded from the study [19]. Similarly, the impacts related to the machine use phase (gasoline and electricity consumption) were excluded since they may significantly differ due to operational characteristics.

In addition, the Monte Carlo analysis, using a 1000-run simulation, was accomplished to report uncertainty analysis of the parameters studied and to check the robustness of the Life Cycle Impact Assessment (LCIA). The Monte Carlo analysis uses random numbers to solve many calculation problems, it generates random variables with a certain probability distribution and estimates the numerical characteristics of the model with statistical methods to obtain the numerical solution of the actual problems [20, 21].

3 Results and Discussion

The data collected and the analysis carried out allowed us to quantify the amount of embodied energy and the carbon dioxide emissions that were linked to the machinery examined. Specifically, for the AGV the total embodied primary energy was about 30 GJ, corresponding to 70.73 MJ kg^{-1} and 5.41 MJ h^{-1} when referred to the functional units. The outcomes for the rotary mower highlighted an energy footprint of 7.8 GJ, which corresponded to 33.7 MJ kg^{-1} and 1.40 MJ h^{-1} when reported to the implement's weight and lifespan, respectively. For the climate change results, overall carbon dioxide emissions accounted for 1,920 and 540 kg CO_2e, respectively for the AGV and the mower. Observing the energy and environmental indexes assessed, for the AGV was found an emission factor per unit of life span accounted for 0.35 kg CO_2e h^{-1}, while the impact per unit of machinery mass was about 4.52 kg CO_2e kg^{-1}. Similarly, for the rotary mower, the emissions per functional unit accounted for 2.35 kg CO_2e kg^{-1} and 0.10 kg CO_2e h^{-1} (Table 2).

**Table 2.** Summary of the energy and carbon footprint results.

Machines	Energy Footprint		Carbon Footprint	
	MJ kg^{-1}	MJ h^{-1}	kg CO_2e kg^{-1}	kg CO_2e h^{-1}
AGV	70.73	5.41	4.52	0.35
Mower	33.67	1.40	2.35	0.10
AGV + Mower	104.40	6.81	6.86	0.44

Comparing the preliminary results found in this study for the AGV with conventional tractors, the requirements of primary energy per unit of AGV mass ranged from 12 to 28% less impacting. In fact, in the scientific literature, the energy demand for conventional tractors varies from 80 to 98 MJ kg^{-1} [22–24]. Greater results were obtained in the carbon emissions, where the AGV held about 0.35 kg CO_2e h^{-1} which is significantly less impacting of traditional agricultural machinery. In fact, recent studies found, for different tractor sizes, a life cycle emission indicator that ranged between 1 and 3 kg CO_2e h^{-1} [22, 25].

Nevertheless, the comparison between AGVs and traditional tractors must be underlined carefully as the two types of machinery have different characteristics, performance and farm utility. In any case, the AGV seems to be highly suited to accomplish specific on-field activities, especially for carrying out minimum tillage operations with conservative soil management practices or in small size areas for growing high-added value crops. The AGV might be particularly indicated to accomplish precision on-field tasks, thanks to the availability of autonomous driving systems.

Moreover, the application of AGVs in the agricultural field is associated with several advantages: increased cultivation surface; increased energy efficiency, due to the optimum torque of electric motors; reduced soil compaction; reduced requirements of workforce, and especially reduced phenomena of exploitation of the workforce; avoid human exposure to dangerous cultivation activities (cultivation on slopes, distribution of pesticides, etc.).
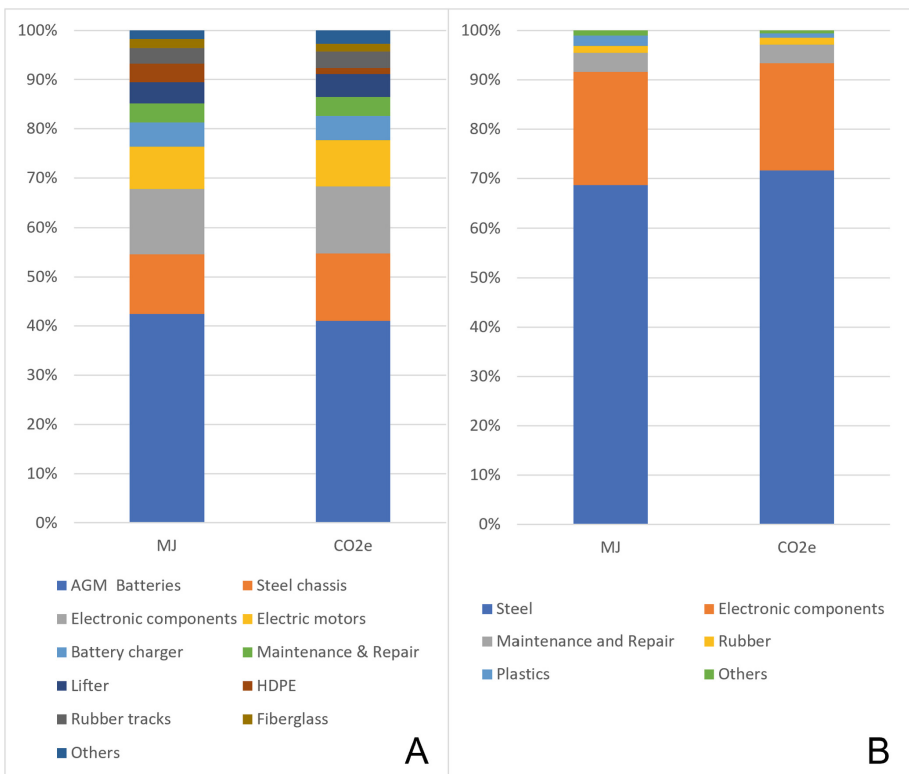

Fig. 2. Impacts (energy and carbon dioxide) distribution for the AGV (A) and for the rotary mower (B).

The results of the AGV's components (Fig. 2) highlighted that the battery pack represents over 42% of the total impacts followed by the electronic components (13%) and the steel chassis (12%). Negligible impacts were found for the fiberglass fairing and other small components.

For the mower, the distribution of the energy and environmental impacts among different components underlined that the carbon steel represents about 68% of total impacts, while less significant impacts were found for rubber parts and other small components.

In this circumstance, the adoption of recyclable materials as input for the production of agricultural machinery is a key factor in minimizing the material consumption and reducing the environmental loads, saving greenhouse gas emissions and the depletion of natural resources.

The Monte Carlo analysis for the examined machinery shows and confirms that the results, both for the energy and carbon footprint outcomes, related to the AGV and the rotary mower were robust (Fig. 3).
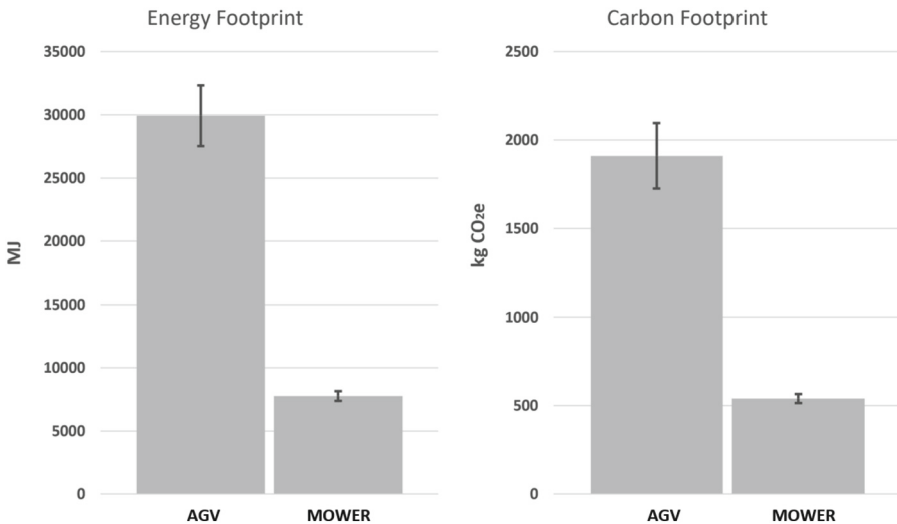
Fig. 3. Uncertainty analysis results from the Monte Carlo simulation for the AGV and mower, both for the energy and carbon footprint analysis.

4   Conclusions

This study analyzed the environmental impact, through an LCA methodology, of an autonomous ground vehicle implemented to accomplish agricultural operations. The main results are related to novel energy and environmental indicators of the AGV, where the embodied primary energy and the carbon emissions per functional unit resulted in lower than traditional agricultural machinery. The analysis showed that the embodied

primary energy of both AGV plus Implement (AGV+I) accounted for 104 MJ kg^{-1}, while related emissions were found to be 6.86 kg CO_2e kg^{-1}. Moreover, analyzing the inputs of the AGV+I system, the battery pack and the iron materials accounted for the main portion of the total impacts. The outcomes of this study represent a step forward a more sustainable and conservative farm practices, providing ground-breaking results for supporting the implementation of AGVs in the agricultural sector and improving the energy and environmental sustainability of food production. Additionally, this study will strongly help to pursue the objectives and targets foreseen by the main strategic plans related to the reduction of environmental impacts, improvement of agricultural production efficiency, and increasing the digitization and innovation of the agricultural sector.

Conflict of Interest. The authors declare no competing interest.

References

1. European Commission (2020) Communication from The Commission To The European Parliament, The European Council, The Council, The European Economic and Social Committee and The Committee Of The Regions, A Farm to Fork Strategy. For a fair, healthy and environmentally-friendly food system, COM (2020) 381 final, Brussels, 20.05.2020
2. Saiz-Rubio V, Rovira-Más F, Cuenca-Cuenca A, Alves F (2021) Robotics-based vineyard water potential monitoring at high resolution. Comput Electron Agric 187:106311
3. Medel-Jiménez F, et al (2022) Modelling soil emissions and precision agriculture in fertilization life cycle assessment - a case study of wheat production in Austria. J Clean Prod 380: 134841. https://doi.org/10.1016/j.jclepro.2022.134841
4. Burke R, Mussomeli A, Laaper S, Hartigan M, Sniderman B (2017) The smart factory: responsive, adaptive, connected manufacturing. Deloitte University Press. https://www2.deloitte.com/us/en/insights/focus/industry-4-0/smart-factory-connected-manufacturing.html
5. Gonzales De-Santos P, Fernández R, Sepúlveda D, Navas E, Armada M, (2019) Unmanned ground vehicles for smart farms. IntechOpen 6:73. https://doi.org/10.5772/intechopen.90683
6. Basu S, Omotubora A, Beeson M, Fox C (2020) Legal framework for small autonomous agricultural robots. AI & Soc 35(1):113–134
7. Pedersen SM, Fountas S, Have H, Blackmore BS (2006) Agricultural robots - system analysis and economic feasibility. Precis Agric 7(4):295–308
8. Fountas S, Mylonas N, Malounas I, Rodias E, Santos CH, Pekkeriet E, (2020) Agricultural robotics for field operations. Sensors 20(9): 2672
9. Gonzalez-de-Soto M, Emmi L, Benavides C, Garcia I, Gonzalez-de-Santos P (2016) Reducing air pollution with hybrid-powered robotic tractors for precision agriculture. Biosyst Eng 143:79–94
10. Vougioukas SG (2019) Agricultural robotics. In: Leonard NE (ed) Annual Review of Control, Robotics, and Autonomous Systems, vol 2, pp 365–392

11. Krishnan A, Swarna S, Balasubramanya HS (2020) Robotics, IoT, and AI in the automation of agricultural industry: a review. In: Proceedings of B-HTC 2020 - 1st IEEE Bangalore Humanitarian Technology Conference. 8 October 2020. Article number 9297856

12. Salcedo R, Zhu H, Ozkan E, Falchieri D, Zhang Z, Wei Z (2021) Reducing ground and airborne drift losses in young apple orchards with PWM-controlled spray systems. Comput Electron Agric 189:10638

13. European Standing Committee on Agricultural Research, 2016. Agricultural Knowledge and Innovation Systems Towards the Future – A Foresight Paper, Brussels. Luxembourg: Publications Office of the European Union

14. Pradel M, de Fays M, Seguineau C (2022) Comparative Life cycle assessment of intra-row and inter-row weeding practices using autonomous robot systems in French vineyards. Sci Total Environ 838:156441. https://doi.org/10.1016/j.scitotenv.2022.156441

15. ISO 14040 (2006). Environmental Management – Life Cycle Assessment – Principles and Framework. International Standard Organization

16. ISO 14044 (2006) Environmental management – Life cycle assessment – Requirements and guidelines. European Standard

17. ISO 14064-1 (2012) Greenhouse Gases – Part 1: Specification with Guidance at the Organization Level for Quantification and Reporting of Greenhouse Gas emissions and Removals. European Standard

18. ISO/TS 14067 (2013). Technical Specification. Greenhouse Gases – Carbon Footprint of Products – Requirements and Guidelines for Quantification and Communication. European Standard

19. Mantoam EJ, Mekonnen MM, Romanelli TL (2018) Energy demand and water footprint study of an agricultural machinery industry. AgricEngInt: CIGR J 20(3)

20. Rubinstein RY, Kroese DP (2016) Simulation and the Monte Carlo Method, 10. Wiley, Hoboken

21. Sun S, Ertz M (2020) Life cycle assessment and Monte Carlo simulation to evaluate the environmental impact of promoting LNG vehicles. MethodsX 7:101046

22. Mantoam EJ, Angnes G, Mekonnen MM, Romanelli TL (2020) Energy, carbon and water footprints on agricultural machinery. Biosyst Eng 198:304–322

23. Bowers W (1992) Agricultural field equipment. In: Fluck RC (ed) Energy in World Agriculture, p 117e129. Elsevier, New York

24. Hornacek M (1979) Application de l'analyse de energetique a 14 exploitation agricoles. Etudes du CNEEMA 457:1e120

25. Mantoam EJ, Romanelli TL, Gimenez LM (2016) Energy demand and greenhouse gases emissions in the life cycle of tractors. Biosyst Eng 151:158-170

Estimating Tall Fescue and Alfalfa Forage Biomass Using an Unmanned Ground Vehicle

Ali Bulent Koc[1]([envelope]) [ORCID], Curtis Erwin[1], Matias Jose Aguerre[2] [ORCID], and John P. Chastain[1] [ORCID]

[1] Department of Agricultural Sciences, Clemson University, 252 McAdams Hall, Clemson, SC 29634, USA
`bulent@clemson.edu`
[2] Department of Animal and Veterinary Sciences, Clemson University, 120 Poole Agricultural Center, Clemson, SC 29634, USA

Abstract. Improving the efficiency and utilization of forage crops is important for enhancing productivity. Precise assessments of biomass levels play a vital role in assisting producers of hay, silage, and grazers in determining the optimal harvest timing and achieving an efficient stocking rate. This study aimed to develop a pre-harvest biomass estimation method by utilizing crop height measurements obtained through a ski-shaped plate mounted on an unmanned ground vehicle (UGV). The research focused on evaluating the performance of the proposed method on tall fescue (*Schedonorus phoenix*) and alfalfa (*Medicago sativa*) trial plots. Measurements on the plots were made and then harvested at approximately 10, 20, and 30-day intervals. The ski-shaped plate, referred to as the "compression ski," was constructed and attached to a ground vehicle. Continuous height measurements of tall fescue and alfalfa were captured using an ultrasonic sensor and a microcontroller. Geotagged measurement locations were acquired through an RTK-GPS receiver mounted on the UGV. Plot boundaries were determined using aerial images processed in Agisoft Metashape and ArcGIS Pro. The compressed height indicators obtained were correlated with wet yield measurements, leading to the development of estimation models. Dry matter fractions (DMFs) of the crops were determined using oven drying method. The wet yield estimation models were combined with DMFs to create a prediction model for dry matter yield (kg DM/ha). The best-performing compression ski-based model achieved a standard error of 291 kg DM/ha for tall fescue and 491 kg DM/ha for alfalfa. The proposed pre-harvest biomass estimation method utilizing compressed height measurements with a UGV and a ski-shaped plate offers a promising approach to optimize efficiency and utilization in grassland management. This method holds potential for enhancing productivity and resource utilization in the aforementioned areas of forage production systems.

Keywords: Biomass yield · Tall fescue · Alfalfa · sensing · Unmanned ground vehicle

1 Introduction

Forage production systems involve either animal grazing or mechanical harvesting. In both scenarios, the integration of data collection and decision-making tools can significantly impact efficiency and profitability. In a mechanically harvested forage production system, the timing of harvest is among the most crucial short-term management decisions due to changes in the leaf-to-stem ratio across different plant maturity stages [1]. As plants mature and the leaf-to-stem ratio decreases, an optimal point emerges in the inverse relationship between biomass and nutritional quality. This point marks the maximum potential animal performance per area of harvested forages. Providing forage producers with a dependable method to accurately estimate standing forage biomass offers the advantage of identifying the optimal harvest time, ultimately leading to improved animal performance or enhanced forage quality.

In a rotational grazing system, precise estimation of biomass is essential, particularly in spring and fall. These seasons dictate the readiness of forage for summer and its stockpiling at the end of summer or during fall for winter grazing. However, biomass estimation for standing forage can be demanding. While experienced forage producers can visually assess small paddocks based on canopy height and growth stage, this becomes challenging with larger areas [2]. Apart from visual assessments, two primary methods are employed: destructive clip-and-weigh sampling and non-destructive measurements using canopy height and density. Destructive sampling involves cutting and weighing samples across the field, requiring careful attention due to labor and time intensity [3, 4].

Non-destructive or indirect estimations of canopy height are generally quicker and simpler. They require periodic calibration using destructive clip-and-weigh samples. The simplest non-destructive approach involves using a meter stick to measure the tallest parts of the canopy [4, 5]. Another technique, the falling plate meter or rising plate meter, applies uniform pressure to the canopy, measuring the resulting compressed height above the ground. The compression plate is lowered onto the forage canopy, which is commonly referred to as a "plonk." Plonk measurements are taken across the field and then averaged. Compressed height measurements consider stand density, plant turgidity, and vigor in biomass estimations [4, 6]. Non-destructive techniques like remote and proximal sensing eliminate the need for physical contact with plants. NDVI cameras and reflectance sensors gather data from forage canopies, calculating factors like canopy density [7]. Ultrasonic and laser sensors estimate height relative to a known ground point [8].

In practice, biomass estimation methods typically involve random selection of sample location in a grid to get representative samples for the field. This random selection could lead to operator bias and error. If geolocation beyond field identification is desired, the methods are further complicated by manually recording GPS locations. Depending on the size and variability of the paddock, large number of measurements may be required to achieve the spatial resolution necessary to draw statistically sound conclusions from the data [9].

Non-destructive and proximal sensing methods of forage biomass estimation have time savings up to a factor of 60 over the destructive "clip and weigh" method [8], but

currently still require a human operator to manually collect the data or drive a vehicle with attached sensors. Variability of species and plant uniformity/stand density are the most common reasons contributing to poor standing forage mass estimations via non-destructive methods [5, 6, 10–13]. Homogeneous forage stands are more accurately estimated than mixed stands [2, 8]. Growth stage and growing time has effects on the linearity of non-destructive estimation methods. During calibration, these methods should be conducted over all growth stages of the plant for higher accuracy. The correlations between non-destructive estimations and standing biomass deviate most at late growth stages and high biomass [10, 14–18]. Calibrations for non-destructive estimation methods can be improved by incorporating factors such as soil data, seasons, weather, presence of tillage, time of establishment, irrigation, and nutrient inputs [2, 16, 17, 19]. Other issues contributing to poor calibration includes too few samples, low sampling frequency, and low spatial, growth time, or seasonal calibration of the samples [11, 12, 16, 17, 20].

A common approach of non-destructive biomass estimation method development is correlating a form of canopy height measurement with harvested biomass samples. A perceived inaccuracy related to this approach is that the measured canopy height accounts for everything above the soil surface, while the harvested biomass samples leave several inches of stubble remaining on the ground. Harvested biomass samples also have variation such as differing heights of cut [8] and loss of material during handling of samples [18]. A potential solution could be a second height measurement of the forage sward after the biomass is removed. By subtracting the post-harvest measurement from the initial measurement, the resulting data is a change in height. When calibrated with the harvested biomass samples, the change in height could provide higher accuracy in pasture growth estimations [17, 20]. This approach is particularly interesting for use in grazing systems where the animals may consume the plants non-uniformly and trample a fraction of the forage which cannot be accounted for in pre-grazing estimations.

Compressed height measurements involve applying a uniform pressure onto the plant canopy. Stem deflection and canopy resistance are physical factors that play a role in the normal force applied to the compression surface. Researchers have also measured stem deflection without applying downward pressure to the plant canopy. This has been demonstrated with instruments such as pendulum meters and fixed impact plates. Using a pivoting cylindrical body, Ehlert et al. [21] measured the angle of deviation and compared it to dry plant mass. The correlation between pendulum angle and dry plant mass was also examined at varying pendulum masses, pendulum lengths, and pivot point heights as these parameters had to be adjusted based on the lowest plant height. Using a fixed "push bar" consisting of two parallel pipes with four load cells between them, Mathanker et al. [22] showed strong correlations between bending force and yield in Napier grass. A combination between the compressed height and pendulum deflection methods was described by Moyer and Schrock [9] in an experiment which involved a curved plate suspended by a pivoting arm. The apparatus was on a large sled with runners and towed by a vehicle.

Ultrasonic sensors are commonly used for measuring forage canopy height, but the acoustic properties require a smooth perpendicular surface to accurately measure distance. Issues have been cited regarding erratic and extraneous readings because of the

sound waves reflecting from non-perpendicular plant canopies and/or missing the plant canopy altogether and sensing the ground [12, 13, 17, 23]. Recently, more complex laser distance and ranging (LiDAR) sensors have become a feasible alternative to ultrasonic sensors due to decreasing cost and size. LiDAR sensors have been used to measure canopy height and volume [8, 11, 18, 20].

Advancements in technology offer unmanned ground vehicles and sensor alternatives for biomass estimation. The objective of this research is to develop and test a compressed canopy height measurement mechanism integrated with an unmanned ground vehicle for biomass estimation in tall fescue and alfalfa. The innovative aspects of this research includes the unique gliding mechanism mounted on a ground vehicle for compressed plant height measurements, featuring the use of an ultrasonic proximity sensor. Another important aspect of this research is the integration of geospatial data, which enhances the context for informed decision-making in pasture management, elevating the efficiency and sustainability of pastures.

2 Methods

2.1 Site Description

Experiments took place at Simpson Research and Education Center in Pendleton, SC, at an elevation of 230 m above sea level with approximately 127 cm annual rainfall. The field features Cecil sandy loam soil, sloping between 2–6%. Twelve 6.0 m × 1.2 m research plots of pure tall fescue (*Schedonorus phoenix*) and alfalfa (*Medicago sativa*) were planted at rates of 32.5 kg/ha and 37.8 kg/ha, respectively. Randomized block layout included three harvest intervals (10, 20, and 30 days) for each species (Fig. 1). Weather data was collected adjacent to the field containing the research trial plots using an IoT weather station (Tempest Weather Station, Santa Cruz, CA). The weather station transmitted data from the field via radio to the base station located within Wi-Fi range. The base station uploaded the weather data to the weather service (Weather Underground, San Francisco, CA). A Python script was used to extract the data in tabular form from the weather service using an application programming interface (API). Weather parameters acquired daily were average temperature, maximum temperature, minimum temperature, average relative humidity, maximum solar radiation, and accumulated precipitation.

2.2 Data Collection Procedure

At the beginning of each data collection campaign, an aerial cross-hatched survey was conducted using the DroneDeploy iOS application (DroneDeploy, San Francisco, CA) at an altitude of 20 m with a DJI Mavic Pro (DJI, Shenzhen, China) equipped with both Survey 3W RGB and Survey 3N NDVI cameras (MAPIR Inc., San Diego, CA). Twelve (12) ground control points (GCPs) were placed throughout the field for georeferencing. High-resolution orthomosaic photos were created in Agisoft Metashape (Agisoft LLC, St. Petersburg, Russia). Next, the research plots were measured with a compression ski mounted on an unmanned ground vehicle.

After the compressed height measurements, the plots were clipped to a height of 7.62 cm using a 24 V cordless hedge trimmer. PVC pipes with a diameter of 7.62 cm

**Fig. 1.** Completely randomized block design for the trial plot layout.

were used as a railing for the electric hedge trimmer to cut at a consistent height. Clipped samples were raked into 189 L bins and weighed in the field. The samples were sub-sampled for dry matter (DM) analysis in the laboratory where they were dried at 55 °C in a forced-air drying oven (Model 89511-414, VWR International, Radnor, PA) until constant weight was reached. The data collection procedure was planned to be repeated every 10 days. On day 30, the plots cut on days 10 and 20 were measured and sampled again as 20 and 10 days of regrowth, respectively. Overall, sixty-eight (68) tall fescue samples were collected, and forty-six (46) alfalfa samples were collected between May and September 2021. The reasons for reduced alfalfa samples were due to constant weed pressure and poor growth on plots 10, 11, and 12, which were marked with a red cross in Fig. 1.

2.3   Unmanned Ground Vehicle

The unmanned ground vehicle (UGV) with attached compression ski and ultrasonic proximity sensor were used to measure the canopy height at the center of each plot. A UGV with the dimensions of 82.9 cm × 78.2 cm × 86.6 cm was fabricated from 38 mm perforated galvanized square steel tube and used as the data acquisition platform (Fig. 2). The UGV consists of four 12–24 V 575 W DC gearmotors (Pride Mobility, Exeter, PA), driven by two 60 A motor drivers, powered by two 12 V 55 Ah batteries connected in series, controlled by a 2.4 GHz 9 channel RC and receiver (Turnigy 9X, Hong Kong, China).

For data collection, the UGV was instrumented with a 12 V 10 Ah battery, LM2596 voltage regulators to power Arduino, LCD display, and MB1634 ultrasonic sensor (Maxbotix, Brainerd, MN). Additionally, a laptop PC (HP, Palo Alto, CA) and Reach M2 RTK receiver (Emlid, Hong Kong, China) were mounted on the UGV. The Arduino system was connected to the laptop PC via USB.

The UGV was set up at the edge of the field. The compression ski was attached to the linear ball bearing sliders and a shade cloth was draped over the machine to avoid
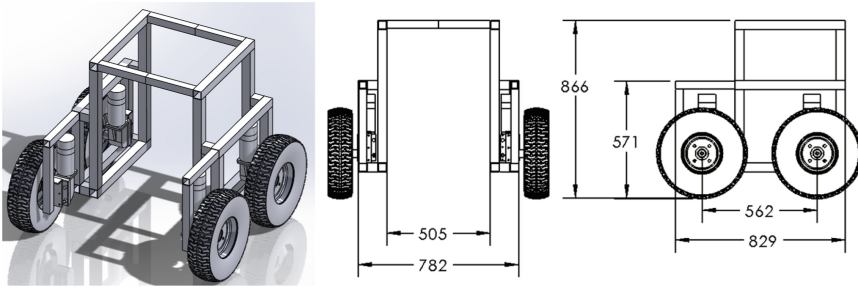
Fig. 2. UGV platform and its dimensions in mm.

extreme temperature spikes from solar radiation. The data collection program on the computer was begun and the human operator began driving the UGV over the plots using a remote control (RC). Using a Reach RS2 RTK GPS system, distance travelled by the vehicle was calculated in a Python code and the georeferenced compressed height measurements were recorded to a.csv file approximately every 30.5 cm travel distance (Fig. 3). Because the compressed height data was averaged over the length of the plot, it was important to collect the data points at equal intervals while moving over the plots. The UGV system was driven over the same plots again after the plots were harvested.
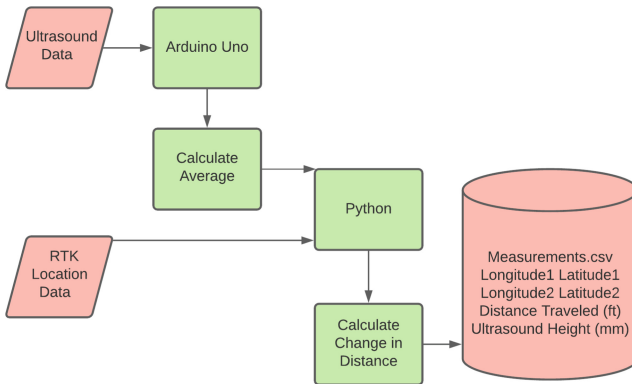
Fig. 3. Flow of data while making measurements in the field.

The compression ski was constructed with high impact acrylic and 3.175 mm × 12.700 mm aluminum bar (Fig. 4) [24]. The compression ski was attached to a pair of fixed ball bearing sliders which translate the normal force applied to the plate by the grass into vertical motion. According to reviewed literature, compression plates used by researchers typically have an applied pressure range of 2–10 kg/m^2 [3, 6, 14, 16, 25]. The mass (kg) and area (m^2) of the compression ski were designed to have an applied pressure of less than 7 kg/m^2 because mass can easily be added for a higher pressure if desired.
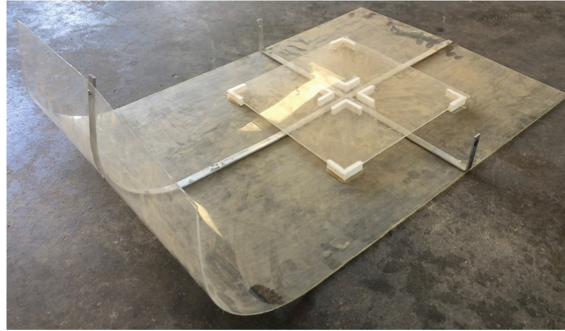
Fig. 4. Compression ski constructed for use with UGV.

The width of the compression ski was limited by the space in which it can operate within the UGV frame (width), approximately 50.8 cm. The optimal length of the compression ski was determined based on the mass of the materials used and mass of the extensions of the ball bearing sliders to which the compression ski was mounted. After construction, the compression ski mass was measured to be 1.75 kg, giving a pressure of 5.65 kg/m^2.

The MB1634 ultrasonic sensor was mounted fixed on the UGV frame, centered and parallel to the compression ski. The sensor mounting location was 0.597 m above the acrylic raised sensing surface when the compression ski was resting on flat and level concrete. Before each data collection campaign, the compression ski was placed on a flat and level surface, and the output from the data acquisition system (H) was confirmed to give a reading of zero (0). If the reading was not zero (0), the sensor mounting height factor (H$_0$) in the Arduino data acquisition system was adjusted to tare the distance output to zero. Over the course of this experiment, adjustment of the sensor mounting height factor (H$_0$) in the Arduino data acquisition system was not required. During data collection, 10 readings were taken from the sensor and averaged (H$_i$) to smooth the sensor output data. After setting up the compression ski, MB1634 sensor, and Arduino data acquisition system on the UGV, the function of the system was verified in a laboratory experiment using known heights.

2.4   Data Processing and Analysis

To process the data in ArcGIS Pro 2.8, a georeferenced RGB orthophoto of the research plots obtained from another concurrent study [26] was imported as a .tif file. The locations of the ground control points were imported to ArcGIS Pro (ESRI, Redlands, CA) and the orthophoto was further georeferenced if necessary. The .csv files containing the compressed height data points from the UGV system were imported and overlaid onto the RGB image. Boundary shapefiles were drawn around the plots of interest (Fig. 5). Using the *Summarize Within* tool in ArcGIS Pro, compressed height measurements within the boundaries of the plots were averaged, also the minimum value, maximum value, standard deviation, and point count of the plots were exported to Microsoft Excel to help identify outliers and undesired edge effects in the plots.

Fig. 5. RGB photo with ground control points (GCPs), data points, and plot boundaries overlayed in ArcGIS Pro 2.8 (blue teardrops show GCP's, yellow boundaries show reduced plot boundaries, green points show pre-harvest data points, and blue points show post-harvest data points).

2.5   Edge Effects and Data Reduction

Because the study was conducted on field plots, the compression ski was going to and from bare soil for each plot observation. Measurements taken near the edge of the plot boundaries were truncated due to edge effects that negatively affected the average compressed height. To standardize the data reduction method, preliminary tests were run to determine the appropriate number of data points to truncate from each end of the plots. Six tests were run to account for each species (tall fescue and alfalfa) and treatment (10, 20, or 30 days of growth). Compressed height data was plotted over distance travelled. For each plot, on both edges, three data points from bare soil outside the plot boundary were included. Based on visual assessment of the data points and the coefficient of variance for the data set after sequential reductions of the data, it was determined that removing one data point from inside each edge of the plot boundary would be sufficient to eliminate the edge effects. Physically, this stands to reason because the compression ski is 61 cm long, and the sensor is centered on the plate. With data points at 30.5 cm intervals, the entire length of the compression ski is guaranteed to be completely inside the plot on the second data point in from the edge of the plot.

2.6   Data Analysis

Microsoft Excel was used as the database for collecting, sorting, and analyzing the data. By excluding data points on the ends of the plots, compression ski data was reduced to eliminate edge effects. Compression ski data was exported as an average height (mm) for each plot observation from ArcGIS Pro 2.8 to Microsoft Excel. Plot yields and dry matter data were entered into Microsoft Excel. Regression analysis tools in Microsoft Excel were used to conduct statistical significance tests. Statistical significance was evaluated based on critical t-values and significant correlation coefficients. Compression ski data was analyzed using the pre- and post-harvest compressed height (CH_1 and CH_2) as well as the change in compressed height ($\Delta CH = CH_1 - CH_2$). Yield was calculated using the harvested biomass and measured area of each plot. Dry matter fraction (DMF) was

determined from the oven drying method and dry matter yield (DM yield) was calculated by multiplying the wet biomass yield of each plot with the dry matter fraction.

3 Results

3.1 Weather Data

The research plots used for this study were non-irrigated, therefore they were subjected to periods of low precipitation combined with high temperatures. The amount of precipitation and average daily temperature observed on each day is shown in Fig. 6. The total precipitation during the study was 693 mm. The maximum daily precipitation was 79.5 mm and observed on Julian date 229. Average daily temperature increased during the first quarter of the study, then stayed relatively constant between Julian dates 141 and 246. The maximum daily solar radiation decreased over the period of the study. Average daily relative humidity was 80% and it followed a similar trend as the average daily temperature.
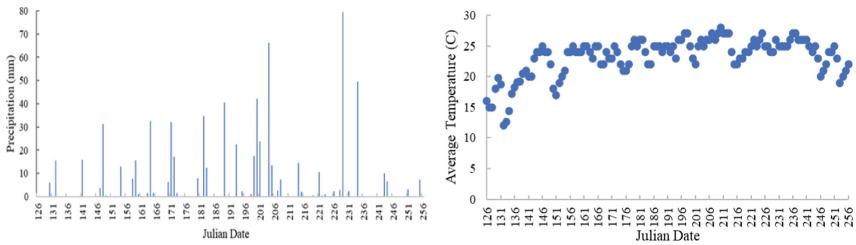
Fig. 6. Daily precipitation and temperature change during the growing season.

3.2 Tall Fescue

Tall fescue plots were sampled during 12 data collection campaigns for a total of 68 observations. The compression ski measured the tall fescue plots before (CH_1) and after (CH_2) they were harvested. Data was analyzed using the pre-harvest compressed height (CH_1) as well as the change in compressed height (ΔCH). The post-harvest measurements were not made on Julian date 165 due to thunderstorms, so $n = 61$ for all ΔCH data. Correlations were made for tall fescue wet yield (kg/ha) and compression ski compressed height indicators CH_1 and ΔCH (mm). Tall fescue dry matter fraction (DMF) was estimated independently. The final models combined tall fescue wet yield estimation models and tall fescue DMF estimation models to create tall fescue dry matter yield (DM yield) estimation models. A simple linear correlation was created for tall fescue wet yield (kg/ha) against mean compression ski height pre-harvest (CH_1) (mm). The significance of the simple linear correlation is summarized in Table 1.

   The plot of tall fescue wet yield by mean compression ski height pre-harvest (CH_1) was observed to be curvilinear, so a polynomial quadratic trendline was fit to the data

Table 1. Simple linear correlation analysis of indicator CH_1 with respect to tall fescue wet yield (r = correlation coefficient).

Indicator	n	r	Calculated t
CH_1	68	0.738*	8.885

* Highly significant correlation, |t-call, > $t_{0.001}$ = 3.444.

(Fig. 7a). The regression equation showing the quadratic trendline is shown in Table 2. The compressed height response to wet yield is not constant due to increased stem bending force and plant density with increased plant maturity and yield. The quadratic function is bound by the minimum and maximum compressed height values in the data set, and it should not be interpreted outside of those values.

The plot of tall fescue wet yield and ΔCH was modified by setting the y-intercept to zero (Fig. 7b). This stands to reason because if no biomass was removed, the ΔCH would be zero (0). Additionally, the 3 negative ΔCH values were truncated. They were interpreted as being below the practical limit for using the compression ski with the ΔCH method. At low yields and low heights, the mean post-harvest compressed height (CH_2) is subject to being higher than the mean pre-harvest compressed height (CH_1) due to irregularities in the field surface such as furrows, ant mounds, and large debris like rocks and sticks. The phenomenon of irregularities in the field surface is also applicable to large continuous pastures. Regression analysis was performed on the 2 models for tall fescue wet yield from compression ski heights (Table 2). The regression equations for tall fescue wet yield estimations based on the quadratic trendline using CH_1 and linear trendline using ΔCH are shown in Table 2.

Table 2. Regression analysis of compression ski tall fescue wet yield models.

| Function	n	R^2	SEy(kg/ha)	Regression Equation
CH_1	68	0.624*	1031	Yield = $1.067(CH_1)^2$ $- 90.587(CH_1) + 2368.343$
ΔCH	58	0.755**	1172	Yield = $99.663(\Delta CH)$

* Highly significant correlation, R^2 critical (0.01) = 0.160, error df = 65.
** Highly significant correlation, R^2 critical (0.01) = 0.111, error df = 57.

Based on the regression analysis, the quadratic pre-harvest compression ski height (CH_1) tall fescue wet yield model fit the data better than the linear ΔCH tall fescue wet yield model as indicated by the 141 kg/ha difference in standard error. This is a small difference in error, but considering that the ΔCH model requires twice as many data points, the extra field measurements do not yield any better results for tall fescue wet yield. Both models for compression ski tall fescue wet yield performed similarly in regression analysis, and they were both kept as candidates for the tall fescue DM yield models.
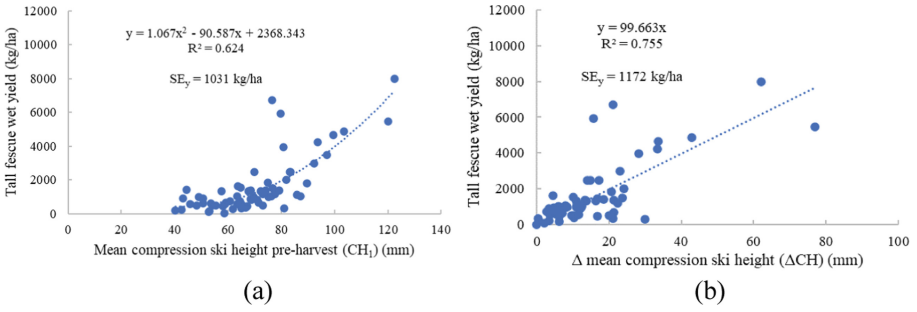
Fig. 7. (a) Quadratic function of tall fescue wet yields by mean compression ski height pre-harvest (CH_1), (b) Linear function of tall fescue wet yields by ΔCH mean compression ski height ($y = 0$).

Dry matter (DM) intake by animals is of high importance for animal performance. As a means of predicting dry matter yield (DM yield), dry matter fraction (DMF) must be incorporated into the yield predictions. The average tall fescue DMF over the entire experiment was 0.34. Multiplying the wet yield models by the DMF provides the DM yield. The DM yield equations are shown in Eqs. 1 and 2:

$$DM\ yield = \left(1.067(CH_1)^2 - 90.587(CH_1) + 2368.343\right) * DMF_{avg} \quad (1)$$

$$DM\ yield = 99.663(\Delta CH) * DMF_{avg} \quad (2)$$

Figure 8 shows the observed and predicted DM yield prediction equations for tall fescue when the $DMF_{avg} = 0.34$ was used with tall fescue quadratic trendline using CH_1 and linear trendline equation using ΔCH.
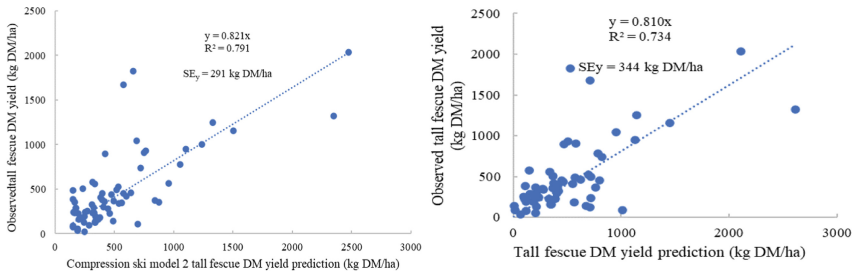
Fig. 8. Observed vs. predicted tall fescue DM yield using CH_1 and change in crop height (ΔCH) and average DMF_{avg} (0.34).

Based on the R^2 values and SE_y values, Eq. 1 seems to provide a slightly better fit to the data than Eq. 2, as it has a higher R^2 value and a lower SE_y value. However, both equations have relatively good fits to the data, suggesting that they can be useful for predicting tall fescue DM yield based on the pre-harvest height (CH_1) and change in crop height (ΔCH) with DMF_{avg}.

3.3 Alfalfa

Alfalfa plots were sampled during eleven data collection campaigns for a total of 46 observations. The compression ski measured the alfalfa plots before (CH_1) and after (CH_2) they were harvested. Data was analyzed using the pre-harvest compressed height (CH_1) as well as the change in compressed height (ΔCH). The post-harvest measurements were not made on Julian date 165 due to thunderstorms, so n = 40 for all ΔCH data.

Correlations were made for alfalfa wet yield (kg/ha) and compression ski compressed height indicators CH_1 and ΔCH (mm). Alfalfa dry matter fraction (DMF) was measured from oven drying method. The final models combined alfalfa wet yield estimation models and alfalfa DMF to create alfalfa dry matter yield (DM yield) estimation models. The plot of alfalfa wet yield by mean compression ski height pre-harvest (CH_1) was observed to be very scattered with a concentration of low-yield data points in the middle range of compressed height. Because the simple linear correlations of CH_1 did not realistically fit the alfalfa wet yield data, no further transformations were performed for this indicator.

The plot of alfalfa wet yield and ΔCH was modified by setting the y-intercept to zero (Fig. 9). This stands to reason because if no biomass was removed, the ΔCH would be zero. Additionally, the two negative ΔCH values were truncated. These negative ΔCH values were of greater magnitude than the 3 negative ΔCH values in the tall fescue compression ski data set. The negative values were interpreted as being below the practical limit for using the compression ski with the ΔCH method. At low yields and low heights, the mean post-harvest compressed height (CH_2) is subject to being higher than the mean pre-harvest compressed height (CH_1) due to irregularities in the field surface such as furrows, ant mounds, and large debris like rocks and sticks. The phenomenon of irregularities in the field surface is also applicable to large continuous pastures.
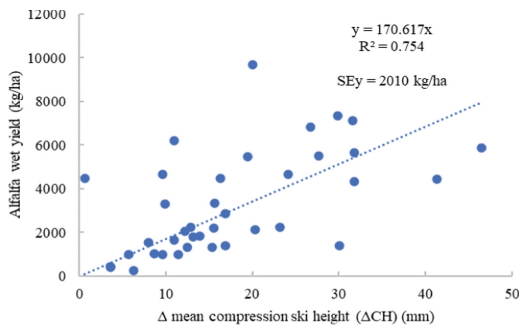

Fig. 9. Linear function of alfalfa wet yields by mean compression ski height (ΔCH) (y = 0).

Alfalfa DM yield model was developed from the linear ΔCH alfalfa wet yield prediction function and the average alfalfa DMF over the entire experiment. Average DMF of alfalfa for the growing season from the oven drying experiments was determined as 0.31. The alfalfa DM yield prediction (Eq. 3) was correlated with observed alfalfa DM

yield data (Fig. 10).

$$\text{Dry Matter yield} = 170.617(\Delta\text{CH}) * \text{DMF}_{\text{avg}} \tag{3}$$
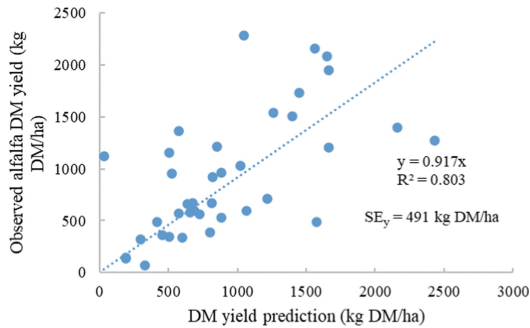
Fig. 10. Observed vs predicted alfalfa DM yield using the average seasonal dry matter fraction.

3.4 Discussions

Dry matter yields for tall fescue and alfalfa were developed using the measurements from the compression ski that was designed as an implement for an unmanned ground vehicle (UGV). Tall fescue DM yield estimation had much lower standard error than alfalfa. Coefficient of determination for tall fescue and alfalfa were in the range of 0.734 to 0.803. The compression ski best predicted tall fescue DM yield using a quadratic pre-harvest compressed height (CH_1) function, and best predicted alfalfa yield using a linear change in compressed height (ΔCH) function. Dry matter yields (DM) were estimated using the average dry matter fractions (DMFs) for tall fescue and alfalfa by adjusting the predicted wet yields. Table 3 shows the dry matter yield prediction equations based on the change in crop height measured with the compression ski mounted unmanned ground vehicle and the dry matter fraction values determined with oven drying.

Table 3. Summary of the compression ski DM yield prediction models.

Crop	Function	R^2	SE_y
Tall fescue	$0.821(1.067(CH_1)^2 - 90.587(CH_1) + 2368.343) * \text{DMF}_{\text{avg}}$	0.791	291
Alfalfa	$0.917(170.617 * \Delta CH_a * \text{DMF}_{\text{avg}-a})$	0.803	491

When correlated with observed yields, the compression ski models over-predicted DM yield by a range of 9–29%. The research plots were non-irrigated and subjected to some defoliation on alfalfa plots throughout the experiment, leading to a concentration of data points in the low range of compressed height and yield. Future work should

test the models on forage stands that are irrigated and/or subjected to lower defoliation pressure on alfalfa so more data can be captured for higher yielding situations.

Simple linear correlations of the pre-harvest compressed height measurements showed a curvilinear shape and had large negative y-intercepts, so polynomial functions were chosen to better fit the data. Regression analysis of the polynomial functions used in the final prediction model for tall fescue showed significantly better fit than linear functions, which suggests that the plant response to compressed height is not constant overall growth stages due to increased stem bending force and plant density with yield. The quadratic functions applied are bound by the minimum and maximum compressed height values in the data set and should not be interpreted outside those values. Post-harvest compressed height measurements (CH_2) were collected with the compression ski and subtracted from the pre-harvest compressed height measurements (CH_1) to give a change in compressed height (ΔCH). The ΔCH data provided more linear initial correlations with y-intercepts near zero, that were forced through the origin.

Tall fescue and alfalfa are morphologically different. Tall fescue is a relatively shallow rooting plant with a dense crown at the soil surface from which it grows long and wide leaves. Under stress, tall fescue rolls its leaves and concentrates biomass closer to the crown. Alfalfa has a deep tap root and grows jointing stems vertically from which the relatively small leaves grow. Under stress, alfalfa concentrates biomass in the stems and roots.

Creating ΔCH data points requires twice the number of data points, so pre-harvest compressed height data would be preferred when appropriate. Using the ΔCH method may be the only option for certain species, such as the alfalfa in this study. ΔCH data may also be more appropriate in fields with high variations of plant density and sporadic harvesting, such as in a low-pressure grazing scenario. Additionally, as technology is disseminated to forage production systems, automated systems and UGVs will eliminate the drudgery associated with collecting the number of data points, making the ΔCH method a more feasible option.

4   Conclusion

In this study, a compression plate with different directions of applied force was tested on two forage crop species of different morphology and demonstrated that the best yield predictions are dependent on these factors among others. A UGV mounted implement called a compression ski was developed for continuous compressed height measurement of forage crops. The compression ski was tested for pre-harvest DM yield prediction ability on pure trial plots of tall fescue and alfalfa. The compression ski was of simple construction partially because it was proximally sensed by an ultrasonic sensor which eliminated complex moving parts. The UGV platform was demonstrated to be a promising solution for increasing automation of geospatial data acquisition based on reliability, customizability, and ease of use. Variables of forage crop species, harvest type, defoliation pressure, and climate were examined to play a role in determining the best compressed height method and prediction model for a given forage production system.

This study brings innovative technology to benefit both researchers and producers in the field of pasture management and biomass estimation. For researchers, it introduces a precise canopy height measurement method which can be used for sustainable grazing studies. Producers gain practical solutions for optimizing pasture management based on an objective measurement method for increased productivity and sustainability. Additionally, the present work integrates geospatial data for location-specific decision-making, helping both researchers and producers with tools to enhance the agriculture industry. Future work will expand these methods to more forage crop species, larger areas, grazing systems, and different climates to further identify trends and ideal combinations of variables and develop best management practices for forage producers to optimize their ecological and financial efficiencies.

References

1. Ball DM et al (2001) Understanding forage quality 1(01):1–15 (2001)
2. Cho W et al (2019) Rising plate meter calibrations for forage mass of wheat and rye. Agric Environ Lett 4(1):180057
3. Earle D, McGowan A (1979) Evaluation and calibration of an automated rising plate meter for estimating dry matter yield of pasture. Aust J Exp Agric 19(98):337–343
4. Harmoney KR et al (1997) Determination of pasture biomass using four indirect methods. Agron J 89(4):665–672
5. Baxter LL et al (2017) Comparing nondestructive sampling techniques for predicting forage mass in Alfalfa-Tall wheatgrass pasture. Agron J 109(5):2097–2106
6. Rayburn EB et al (2017) Calibration of pasture forage mass to plate meter compressed height is a second-order response with a zero intercept. Crop Forage Turfgrass Manag 3(1):cftm2017.01.0003
7. Andersson K et al (2017) Estimating pasture biomass with active optical sensors. Adv Anim Biosci 8(2):754–757
8. Pittman JJ et al (2015) Estimation of biomass and canopy height in bermudagrass, alfalfa, and wheat using ultrasonic, laser, and spectral sensors. Sensors 15(2):2920–2943
9. Moyer JL, Schrock MD (2007) Automating measurement of forage mass in pasture. Forage Grazinglands 5(1):1–6
10. Boob M et al (2019) Harvest time determines quality and usability of biomass from lowland hay meadows. Agriculture 9(9):198
11. Ehlert D, Horn H-J, Adamek R (2008) Measuring crop biomass density by laser triangulation. Comput Electron Agric 61(2):117–125
12. Fricke T, Richter F, Wachendorf M (2011) Assessment of forage mass from grassland swards by height measurement using an ultrasonic sensor. Comput Electron Agric 79(2):142–152
13. Fricke T, Wachendorf M (2013) Combining ultrasonic sward height and spectral signatures to assess the biomass of legume–grass swards. Comput Electron Agric 99:236–247
14. Hakl J et al (2012) The use of a rising plate meter to evaluate lucerne (Medicago sativa L.) height as an important agronomic trait enabling yield estimation. Grass Forage Sci 67(4):589–596

15. Haultain J, Wigley K, Lee JM (2014) Rising plate meters and a capacitance probe estimate the biomass of chicory and plantain monocultures with similar accuracy as for ryegrass-based pasture. Proc New Zealand Grassland Assoc 76:67–74
16. Nakagami K, Itano S (2014) Improving pooled calibration of a rising-plate meter for estimating herbage mass over a season in cool-season grass pasture. Grass Forage Sci 69(4):717–723
17. Shannon KD et al (2013) Initial results utilizing a commercially available ultrasonic sensor for forage yield measurement, in 2013 Kansas City, Missouri, 21 July–24 July 2013. ASABE: St. Joseph, MI, p 1
18. Walter JDC et al (2019) Estimating biomass and canopy height with LiDAR for field crop breeding. Front Plant Sci 10:1145
19. Serrano J et al (2017) Proximal sensing for monitoring the productivity of a permanent Mediterranean pasture: influence of rainfall patterns. Adv Anim Biosci 8(2):796–801
20. Radtke PJ, Boland HT, Scaglia G (2010) An evaluation of overhead laser scanning to estimate herbage removals in pasture quadrats. Agric For Meteorol 150(12):1523–1528
21. Ehlert D, Hammen V, Adamek R (2003) On-line sensor pendulum-meter for determination of plant mass. Precision Agric 4(2):139–148
22. Mathanker SK et al (2015) Stem bending force and hydraulic system pressure sensing for predicting napiergrass yield during harvesting. Comput Electron Agric 111:174–178
23. Scotford IM, Miller PCH (2004) Combination of spectral reflectance and ultrasonic sensing to monitor the growth of winter wheat. Biosys Eng 87(1):27–38
24. Erwin C (2022) Unmanned ground vehicle proximal sensing for forage biomass production estimations, in agricultural sciences. Clemson University
25. Sanderson MA et al (2001) Estimating forage mass with a commercial capacitance meter, rising plate meter, and pasture ruler. Agron J 93(6):1281–1286
26. Koc AB et al (2023) Alfalfa biomass estimation using crop surface modeling and NDVI. Appl Eng Agric 39(2):251–264

Combining Digital Image Processing and Machine Learning is Useful for the Early Detection of Salinity and Drought Stresses in Cucumber

Parvin Mohammadi[1(✉)] [iD] and Keyvan Asefpour Vakilian[2] [iD]

[1] Department of Agrotechnology, College of Abouraihan, University of Tehran, Tehran, Iran
p.mohammadi68@ut.ac.ir

[2] Department of Biosystems Engineering, Gorgan University of Agricultural Sciences and Natural Resources, Gorgan, Iran

Abstract. Timely detection of plant abiotic stresses and their type and severity can be beneficial in order to prevent the loss of yield in crop production systems. This study introduces an image processing-based method to detect the type and severity of salinity and drought stress, as crucial abiotic stresses, in cucumber plants. Plants were cultivated in the greenhouse environment. Plant morphological features in the form of textural features were measured from the images captured from the plants. Sampling was performed five times at 3-day intervals beginning with applying the abiotic stresses. Measurements were conducted by transferring three leaves randomly selected from each pot to a chamber with artificial lighting equipped with a camera for image acquisition. The artificial neural network (ANN) was used based on the image textural features of the leaves as inputs and stress type and severity as output. The parameters of the network were optimized using a sophisticated optimization algorithm to achieve the most efficient machine. As a robust evolutionary method, the genetic algorithm was used to optimize the architecture of the ANNs. The results revealed that the image textural features for training ANNs optimized using the genetic algorithm could predict the type and severity of the plant abiotic stresses with MSE and R^2 values of 0.092 and 0.74, respectively. Since the machine was able to perform a reliable stress prediction within a short period after applying the stress, the proposed method can be used for the early detection of salinity and drought stresses in cucumber plants.

Keywords: Artificial neural networks · Severe stress conditions · Image textural features · Genetic algorithm · Optimization

1 Introduction

While the morphological, physiological, and biochemical attributes of plants undergo significant alterations due to biotic and abiotic stresses, these alterations are not exclusive to particular stressors [1]. To illustrate, distinct stress origins can lead to comparable alterations in characteristics such as plant height, as well as the weights of roots and

shoots, as morphological attributes of plants. To enhance the comprehension of plant responses within stress-related investigations, it is preferable to focus on traits at a molecular level that are almost exclusively associated with specific stress conditions. However, these methods are costly and time-consuming. Finding a reliable solution to determine the severity and type of the stresses based on the morphological traits of plants can be beneficial for farmers and plant pathologists since they are cost- and time-effective [2].

Abiotic stresses, including light, temperature, deficiency and excess of nutrients, drought, salinity, elevated carbon dioxide levels, and contamination by heavy metals, constitute some of the prevalent challenges encountered by crops [3]. Various types of stresses, such as salt and drought, are environmentally undesirable and can significantly impact successful crop production [4]. Elevated levels of salt and drought stress have a notable influence on the physiological and biochemical processes of numerous plant species [5]. The response of plants to drought stress can be assessed based on physiological indicators like relative water content, stomatal responses, active oxygen species, and the activation of antioxidative enzymes [6]. Salt stress can impede plant growth and development through mechanisms involving osmotic stress, ion toxicity, disrupted nutrient balance, and oxidative stress [7]. Cucumber (*Cucumis sativus* L.), particularly during its initial growth stages, is highly susceptible to both drought and salt stress [8]. Severe instances of drought and salinity stresses have adverse consequences on the growth, photosynthesis, biochemical composition, and textural attributes of cucumber fruits [9, 10].

Supervised and unsupervised machine learning algorithms are being used in plant science to model multivariate plant growth problems [11]. With the help of training data in the database, the machine learns the complex non-linear patterns between inputs and output [12–14]. When presented with a dataset that encompasses morphological characteristics of cucumber plants subjected to salt and drought stresses, a crucial question arises: Which specific features should be employed to train machine learning methods in order to ensure the accurate identification of stress type and severity? Consequently, this study undertakes the imposition of varying levels of salt and drought stresses on cucumber plants, both individually and concurrently. Throughout the experimental process, diverse attributes of the plants based on the images captured from the plant leaves are measured, contributing to the creation of an informative database that holds utility for the training of machine learning models. Subsequently, the artificial neural network (ANN) algorithm is employed, and its performance is amplified through the utilization of a metaheuristic optimization technique, namely the genetic algorithm (GA), to identify the category and intensity of stress based on the provided database.

The primary objectives of this research encompass: (a) assessing the performance of image-processing-based morphological traits in identifying salt and drought stresses in cucumber plants, and (b) determining a machine learning algorithm, honed through intricate evolutionary processes, tailored specifically for the accurate detection of stress conditions. A search in bibliographic databases reveals that a combination of image processing techniques and machine learning methods optimized with metaheuristic algorithms has not been studied so far. Therefore, the novelty of this work involves developing

sophisticated machines with performances improved with novel optimization methods to predict stress conditions in plants by having their images captured by RGB cameras.

2 Material and Methods

Figure 1 demonstrates the flowchart of the present study. Morphological attributes, encompassing energy, entropy, and local homogeneity, were extracted from images acquired from plant leaves using an image processing module. These attributes, as well as the sampling time, designated as machine inputs, were subsequently employed for the training of ANNs, with their parameters, including the number of hidden (learner) layers, the number of neurons in each layer, and their weight and bias parameters, fine-tuned through GA. The machine-generated outputs corresponded to the identification of stress type and quantification of its severity.

2.1 Plant Material and Experimental Design

Cucumber seeds were procured from a local vendor and subsequently subjected to surface sterilization using NaClO for a duration of 1 min, followed by thorough rinsing with distilled water. The seeds were initially cultivated in plug trays utilizing a growth medium comprising a blend of vermiculite, peat, and perlite in a ratio of 3:2:1. Upon reaching the 21st day of growth, the seedlings were transplanted into 5-L pots containing the same growth medium as that of the plug trays. Nutrient fertilization management, encompassing both macro- and micro-nutrients, was executed in accordance with the guidelines outlined in the literature. To sustain optimal growth conditions, the growth room's relative humidity was maintained at $70 \pm 5\%$, accompanied by a light intensity of $120 \, \mu molm^{-2} \, s^{-1}$.

A consistent and uniform irrigation regimen was upheld across all pots for a duration of 60 days. Subsequent to this period, the control group of plants received daily supplementation with tap water to sustain soil water potential at a level proximate to the field capacity. Contrastingly, plants subjected to drought treatment underwent water deprivation until the soil water potential diverged from the field capacity. Monitoring of soil moisture was carried out on a daily basis utilizing a time-domain reflectometry (TDR) device (PMS-714, LUTRON, Taiwan).

To explore various levels of drought stress severity, the soil moisture content was meticulously regulated to remain nonlethal and surpass the wilting point. Specifically, soil moisture was upheld at 100% (W_0, control), 80% (W_1), 60% (W_2), and 40% (W_3) of the field capacity. For plants undergoing salinity treatment, irrigation was administered using water containing distinct concentrations of NaCl: 0 (S_0, control), 20 mM (S_1), 40 mM (S_2), and 60 mM (S_3). Notably, concentrations exceeding 100 mM were deemed potentially lethal to young plants. Various studies have recommended similar drought and salinity levels to apply stresses to cucumber plants. It should be noted that both abiotic and biotic stresses can exert changes in various characteristics of cucumber plants [15].

Plant attributes were assessed five times, each separated by 3-day intervals, commencing from the initiation of the stress application. Experiments were done with four replications for each treatment. The total number of pots was $4 \times 4 \times 5 \times 3 = 240$.
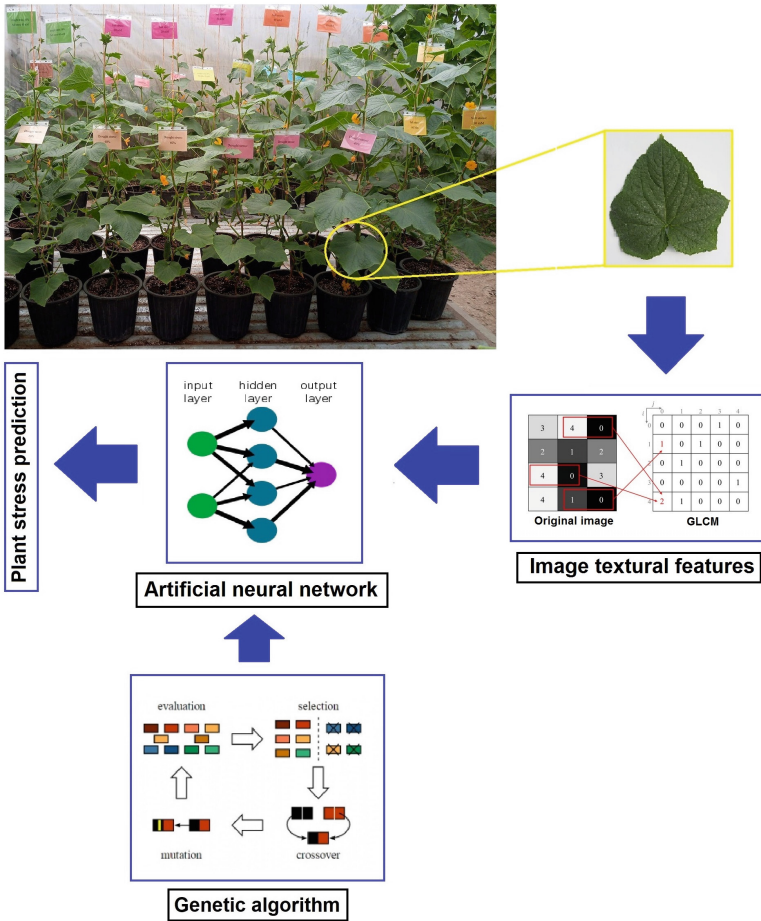
Fig. 1. Flowchart of the present study

2.2 Morphological Measurements

The digital image processing technique was employed to extract morphological attributes from leaf images. The image capture setup encompassed three components: a dark chamber, a CCD digital camera, and a 200-LED lighting array featuring a 70° viewing angle. This arrangement enhanced light uniformity within the area of interest. From each captured image, the leaf region of interest was isolated from the background through Canny edge detection, a process known as image segmentation [16]. Grayscale transformation was applied to convert the images into grayscale format by combining the weighted sums of the red (R), green (G), and blue (B) color components.

To capture the spatial correlation of gray-level values, a Gray-level Co-occurrence Matrix (GLCM) was utilized [17, 18]. Each element (i, j) within the GLCM denoted the frequency of occurrences where a pixel with value i was found horizontally adjacent to a pixel with value j. While a comprehensive set of 21 textural parameters was previously

identified, recent studies have indicated that the use of only three textural variables, adopted in this study, can effectively discern plant health: entropy (Eq. 1), energy (Eq. 2), and local homogeneity (Eq. 3), as established by Story et al. [19]

$$\text{Entropy} = -\sum_i \sum_j p(i,j) \log(p(i,j)) \tag{1}$$

$$\text{Energy} = \sum_i \sum_j p(i,j)^2 \tag{2}$$

$$\text{Local homogeneity} = \sum_i \sum_j \frac{p(i,j)}{1+(i-j)^2} \tag{3}$$

where $p(i,j)$ is the (i,j)-th element of the GLCM. The program for image processing was written with MATLAB R2018b programming environment.

2.3 Machine Learning Method

The obtained measurements of the various attributes under different stress conditions were compiled to form a database tailored for utilization in machine learning applications. Given that statistical analysis revealed insignificant effects of replication on the outcomes, mean values were employed in the preparation of the database. While statistical regression models offer mathematical equations for estimating the dependent variable based on input features, it's generally advisable to limit the number of input features to 2 due to the complexity of parameter estimation in high-dimensional problems. In contrast, machine learning techniques are capable of assimilating databases including hundreds of input features alongside corresponding dependent variables. In this study, ANN was employed to predict plant stress utilizing attribute values as inputs. For optimization purposes, GA, which is an evolutionary technique was employed to optimize the architecture of ANN during the training.

GA is a robust metaheuristic optimization approach that operates through a population comprising a collection of chromosomes, each representing a potential solution to the problem. Through an iterative process, termed generations, individuals yielding more favorable values for the objective function are allowed to persist and undergo crossover operations in subsequent iterations. In simpler terms, pairs of chromosomes acting as parents generate more dependable offspring in each generation by discarding weaker solutions associated with undesirable values of the objective function. Table 1 presents the parameters that were taken into consideration for the optimization methods in this study. The primary aim of these methods was to minimize the error associated with predicting stress levels utilizing the ANNs. In other words, the objective (fitness) function of GA during the optimization was to minimize the error of prediction performed by ANN. The optimization process ceased upon reaching the predefined maximum number of iterations. The parameters of the network that were optimized by GA to reach the lowest prediction error included the number of hidden (learner) layers, the number of neurons in each layer, and their weight and bias parameters.

In this study, a program was developed using the MATLAB programming environment to harness machine learning techniques based on the textural features extracted

Table 1. Parameters of the optimization algorithms

Optimization method	Parameter	Value
GA	Population size	100
	Maximum number of iterations	500
	Mutation rate	0.1
	Crossover percentage	0.5

from leaf images, as well as sampling time, as inputs and stress type and severity as outputs. The program encompassed the formulation of the ANN regression model designed to predict the model's output while utilizing the four input features (three textural features and one sapling time). The configuration of the ANN architecture, including the number of hidden (learner) layers (ranging from 1 to 3), the number of neurons within each layer (ranging from 5 to 15), and their corresponding weight and bias parameters, were systematically optimized employing advanced optimization algorithms. The aim was to attain the most efficient machine-learning model possible. The performance of the models was evaluated based on the mean squared error (MSE) (Eq. 4) and coefficient of determination (R^2) (Eq. 5)

$$\text{MSE} = \frac{1}{n} \sum_{i=1}^{n} (x_{\text{p}} - x_{\text{o}})^2 \tag{4}$$

$$R^2 = 1 - \frac{\sum_{i=1}^{n} (x_{\text{p}} - x_{\text{o}})^2}{\sum_{i=1}^{n} (x_{\text{o}} - \bar{x}_{\text{o}})^2} \tag{5}$$

where x_o is the severity level of the stress applied to the plants, x_p is the predicted value using ANNs, and n is the number of samples. The lower the MSE and higher the R^2, the better the performance of the machine learning model is.

3   Results and Discussion

Prior research has established the noteworthy impacts of both salinity and drought stress on the morphological attributes of cucumber plants. Nonetheless, accurately pinpointing the occurrence of these stresses poses a challenge due to the intricate and multifaceted nature of plant responses. These responses often exhibit delays in reacting to the underlying stress factors, rendering the process of pinpointing the exact source of stress highly intricate.

In control plants grown under optimal conditions, their leaves displayed robust health and vivid colors, resulting in elevated entropy levels. Conversely, plants subjected to salinity and drought treatments exhibited reduced surface structural complexity, leading to diminished entropy in their leaf images. As time progressed, the leaves of control

plants adopted a deeper green hue, causing a decline in image energy levels, as observed in previous studies [19]. On the contrary, the appearance of a yellowish tinge in treated plants contributed to an increase in image energy levels. Furthermore, the local homogeneity of images originating from control plants experienced a decrease as these plants evolved, displaying a spectrum of green shades and becoming more colorful during their growth. In contrast, treated plants, characterized by a uniform coloration, exhibited higher levels of homogeneity in their images. Similar results and findings are reported by Asefpour Vakilian and Massah [17, 20].

In alignment with the objectives outlined in this study, the utilization of machine learning techniques, in conjunction with morphological traits of cucumber plants, is pursued to enable the targeted identification of stress severity caused by abiotic factors. This approach aims to achieve accurate and specific detection of stress levels, particularly during the initial stages of stress imposition.

Table 2 presents the evaluation of morphological variables in their capacity to predict plant stress, as investigated within the scope of this study. The results indicate that the employed machine learning approach was proficient in identifying stress instances under conditions of severe salinity and drought. This capability holds particular significance for farmers, as the most substantial reduction in agricultural yield is observed when crops face severe abiotic stresses during their growth cycle.

Table 2. Performance evaluation of ANN and GA-ANN in the prediction of plant stress

	Training		Validation		Test	
ANN architecture	MSE	R^2	MSE	R^2	MSE	R^2
4-5-1	0.397	0.39	0.460	0.34	0.587	0.25
4-6-1	0.316	0.46	0.373	0.41	0.385	0.40
4-7-1	0.218	0.56	0.316	0.46	0.422	0.37
4-8-1	0.338	0.44	0.487	0.32	0.409	0.38
4-9-1	0.255	0.52	0.306	0.47	0.361	0.42
4-10-1	0.227	0.55	0.201	0.58	0.265	0.51
4-11-1	0.169	0.62	0.275	0.50	0.361	0.42
4-12-1	0.338	0.44	0.338	0.44	0.422	0.37
4-13-1	0.350	0.43	0.397	0.39	0.305	0.47
4-14-1	0.316	0.46	0.373	0.41	0.447	0.35
4-15-1	0.193	0.59	0.275	0.50	0.245	0.53
GA-ANN	0.087	0.75	0.083	0.76	0.092	0.74

Notably, the highest R^2 value for the test data achieved by the ANN machine in predicting both stresses simultaneously reached 0.74, achieved through an architecture featuring three hidden layers and optimized by GA. However, as Table 2 reveals, in the case of not using GA to optimize the structure of ANN, the R^2 values for test data did not

exceed 0.53. Proper determination of the weight and bias of the learner neurons and the number of hidden layer neurons is important since they affect not only the convergence of the network, but also the prediction performance. In order to understand the effect of the ANN parameters on the prediction, Table 2 shows the changes in the prediction performance due to the change of learner neurons in the hidden layer.

The morphological variables utilized in this study were image textural features, assessed through probability-density functions on GLCM. These features were extracted from leaf images obtained through an image acquisition system and subsequently transferred to a computer for in-depth analysis.

Furthermore, the utilization of GA as a metaheuristic optimization technique proved instrumental in enhancing the predictive capability of the machine learning model for plant stress detection. This improvement was evident from the significant decrease in MSE values, while a remarkable increase in R^2 values. The successful integration of GA optimization resulted in the development of an efficient machine learning approach, proficient in utilizing variables derived from the image processing technique to accurately predict and identify severe levels of abiotic stresses in cucumber plants. It should be noted that considering the size of the dataset investigated in this work, it was not possible to utilize deep learning for the prediction of stresses. Therefore, ANN, as a base regression model optimized by GA was used for the prediction.

In the context of other morphological attributes, such as plant height, shoot weight, and root weight, that were not considered in this study; while these traits generally showed susceptibility to increasing stress severity, they did not demonstrate specificity in terms of stress type. This aligns with findings from earlier studies [1, 21, 22] which highlighted that these traits' responses to stress were not unique to stress types and did not offer reliable discrimination between different types of stressors. Therefore, the use of image textural features as the only morphological features of the plants exerted acceptable results in predicting the outputs, i.e., type and severity of the stress.

4   Conclusions

An effort to introduce a promising image processing-based method to detect the type and severity of two main abiotic stresses, i.e., salinity and drought, in cucumber plants is reported in this paper. Treatments were selected in levels to apply a range of mild to rather severe stress conditions. The performance assessment of image-processing-based morphological traits showed that training these features to a machine such as ANN can identify the stress in the plants with acceptable efficiency. ANN, equipped with GA as an intricate evolutionary optimization technique can increase the MSE and R^2 values of the prediction up to 0.092 and 0.74, respectively. Due to the fact that the machine was capable of performing a reliable stress prediction within a short period after applying the stress, the proposed technique can be utilized for the early detection of abiotic stresses in cucumber plants.

Although physiological and biochemical features of plants such as enzymatic activities and microRNA regulation might provide us with higher prediction performance, they all require expensive laboratory equipment and time-consuming protocols [23].

Declaration of Competing Interest. The authors declare that they have no known competing financial interests or personal relationships that could have appeared to influence the work reported in this paper.

References

1. Asefpour Vakilian K (2019) Gold nanoparticles-based biosensor can detect drought stress in tomato by ultrasensitive and specific determination of miRNAs. Plant Physiol Biochem 145:195–204
2. Javidan SM, Banakar A, Asefpour Vakilian, K, Ampatzidis Y (2023) Tomato leaf diseases classification using image processing and weighted ensemble learning. Agronomy J (in Press)
3. Gong Z et al (2020) Plant abiotic stress response and nutrient use efficiency. Sci China Life Sci 63:635–674
4. Chandra S, Roychoudhury A (2020) Penconazole, paclobutrazol, and triacontanol in overcoming environmental stress in plants. In: Roychoudhury A, Tripathi DK (eds) Protective chemical agents in the amelioration of plant abiotic stress: biochemical and molecular perspectives. John Wiley & Sons, Hoboken, pp 510–534
5. Massonnet C, Costes E, Rambal S, Dreyer E, Regnard JL (2007) Stomatal regulation of photosynthesis in apple leaves: evidence for different water-use strategies between two cultivars. Ann Bot 100(6):1347–1356
6. Batool T et al (2020) Plant growth promoting rhizobacteria alleviates drought stress in potato in response to suppressive oxidative stress and antioxidant enzymes activities. Sci Rep 10:16975
7. Behera LM, Hembram P (2021) Advances on plant salinity stress responses in the postgenomic era: a review. J Crop Sci Biotechnol 24:117–126
8. Du C, Li H, Liu C, Fan H (2021) Understanding of the postgerminative development response to salinity and drought stresses in cucumber seeds by integrated proteomics and transcriptomics analysis. J Proteomics 232:104062
9. Ouzounidou G, Giannakoula A, Ilias I, Zamanidis P (2016) Alleviation of drought and salinity stresses on growth, physiology, biochemistry and quality of two *Cucumis sativus* L. cultivars by Si application. Br J Bot 39:531–539
10. Alsaeedi A, El-Ramady H, Alshaal T, El-Garawany M, Elhawat N, Al-Otaibi A (2019) Silica nanoparticles boost growth and productivity of cucumber under water deficit and salinity stresses by balancing nutrients uptake. Plant Physiol Biochem 139:1–10
11. Javidan SM, Banakar A, Asefpour Vakilian K, Ampatzidis Y (2023) Diagnosis of grape leaf diseases using automatic K-means clustering and machine learning. Smart Agric Technol 3:100081
12. Hashemi A, Asefpour Vakilian K, Khazaei J, Massah J (2014) An artificial neural network modeling for force control system of a robotic pruning machine. J Inf Organ Sci 38(1):35–41
13. Sarlaki E, Sharif Paghaleh A, Kianmehr MH, Asefpour Vakilian K (2021) Valorization of lignite wastes into humic acids: process optimization, energy efficiency and structural features analysis. Renew Energy 163:105–122
14. Esmaili M et al (2021) Assessment of adaptive neuro-fuzzy inference system (ANFIS) to predict production and water productivity of lettuce in response to different light intensities and CO_2 concentrations. Agric Water Manag 258:107201
15. Liao L, Hu Z, Liu S, Yang Y, Zhou Y (2021) Characterization of Germin-like proteins (GLPs) and their expression in response to abiotic and biotic stresses in cucumber. Horticulturae 7(10):412
16. Asefpour Vakilian K, Massah J (2013) An artificial neural network approach to identify fungal diseases of cucumber (*Cucumis sativus* L.) plants using digital image processing. Arch Phytopathol Plant Prot 46(13):1580–1588

17. Asefpour Vakilian K, Massah J (2017) A farmer-assistant robot for nitrogen fertilizing management of greenhouse crops. Comput Electron Agric 139:153–163
18. Javidan SM, Banakar A, Asefpour Vakilian K, Ampatzidis Y (2022) A feature selection method using slime mould optimization algorithm in order to diagnose plant leaf diseases. In: 2022 8th Iranian Conference on Signal Processing and Intelligent Systems (ICSPIS), pp. 1–5, Behshahr, Iran
19. Story D, Kacira M, Kubota C, Akoglu A, An L (2010) Lettuce calcium deficiency detection with machine vision computed plant features in controlled environments. Comput Electron Agric 74(2):238–243
20. Asefpour Vakilian K, Massah J (2012) Design, development and performance evaluation of a robot to early detection of nitrogen deficiency in greenhouse cucumber (*Cucumis sativus*) with machine vision. Int J Agric Res Rev 2:448–454
21. Schwarz D, Rouphael Y, Colla G, Venema JH (2010) Grafting as a tool to improve tolerance of vegetables to abiotic stresses: thermal stress, water stress and organic pollutants. Sci Hortic 127(2):162–171
22. Khan MM, Al-Mas'oudi RS, Al-Said F, Khan I (2013) Salinity effects on growth, electrolyte leakage, chlorophyll content and lipid peroxidation in cucumber (*Cucumis sativus* L.). In: International conference on food and agricultural sciences. IACSIT Press. Malaysia, pp 28–32
23. Lu XY, Huang XL (2008) Plant miRNAs and abiotic stress responses. Biochem Biophys Res Commun 368(3):458–462

Enabling Insecticide Spot Application on Boom Sprayer by Developing Machine Vision and Communcation Components

Ahmad Al-Mallahi[✉], Moammel Bin Motalab, Imran Hassan, and Travis Esau

Department on Engineering, Faculty of Agriculture, Dalhousie University, Truro, NS B2N 5E3, Canada
Ahmad.almallahi@dal.ca

Abstract. Despite its effectiveness in improving yield, uniform spraying has negative impacts on the environment and the use of resources. In this research project, we plan to contribute to the adaptation of spot spraying by developing electronic and mechanical components that allow boom sprayers of different size scales to adopt this technology. In this paper, we demonstrate the development of machine vision system that uses artificial intelligence to detect Colorado potato beetles based on YOLO v5 models, and the development of a communication to scheme to integrate the machine vision system with an open-source spraying mechanism via Controller Area Network. Using field images taken on-the-go from a camera mounted on a sprayer, the accuracy of detecting beetles reached 64%, which reveals a promising result given the possibility of enhancing image quality and the computation techniques moving forward. Also, the machine vision node, developed to integrate a machine vision system that consist of two neighbouring cameras, was able to flawlessly translate the detection results to a spraying system mounted on boom sprayer to control 6 nozzles individually. These results allow for scaling up the detection and spraying mechanisms to cover full booms which can reach to widths of 36 m. Beside building on the current developments on the detection and communication components, our next steps will include allowing for real-time spraying by introducing modifications on the pumping and nozzle components.

Keywords: Machine vision · ISOBUS · Nozzle control · Real-time spraying · Pest control

1 Introduction

In commercial crop production, spraying the entire field by agrochemicals uniformly using wide boom sprayers has been a common practice to protect crops from pests of all types – weeds, insects, and pathogens. This practice has continued despite the fact that not every inch of the field may require spraying as the distribution of any pest is most likely heterogenous. However, in the absence of methods to localize pest distribution and actuate spraying in a pace that matches the operational speed of a mechanical boom sprayer, uniform spraying has been the compromise to maximize yield despite

the environmental impacts it may cause [1]. Nevertheless, the continuous increase in the price of pesticides along with recent policies to encourage responsible use of resources (as depicted by the United Nation's Sustainable Development Goal 12) [2] has put pressure on stakeholders of crop production to investigate methods to optimize the use of pesticides. In addition, the recent developments in machine learning have made it possible to rapidly detect pests, especially weeds, on-the-go by mounting cameras on sprayers which opened the door for spot application of pesticides in a real-time manner [3].

However, most of these solutions are made for large-scale farms and scalability towards different sizes of farms or crops is not usually addressed. In addition, "studies about site-specific insecticide application are less prevalent than those about herbicides because the population dynamics of flying insects are very intense" [11]. Therefore, in this research project, our plan is to tackle the components needed to enable real-time spraying including the machine vision system (sensing component), and the communication between sensing and actuation (the communication component) for application on potato fields at regions in New Brunswick, Canada, where typically boom sprayers are 30–36 m wide and run in an operational forward speed of 4 m/s, usually constant. The farms size would range between 5–30 ha, so that the sprayer has forward runs in rows only as it would fold, turn, and unfold for the next run. Successful spot application would require sensing and actuation operating over the entire width of the sprayer which makes economical feasibility an extra challenge to the development, whose challenges include the ability to detect pests (typically small in size), the ability to handle data generated by the machine vision system and deliver it to the spraying nozzles, and the ability to actuate and accurately deliver pesticide to the target in real-time. In this paper, we present the progress we have made in developing the machine vision system to detect Colorado potato beetles [4] and its connection to the control system.

2 Methods

2.1 Sprayer

The sprayer used as an apparatus for this research work is Patriot 3240 (Case IH, Delaware, US) that operates at McCain Farms of the Future (Riverbank, Canada). It is a self-propelled machine with a boom that extends to 36 m carrying 60 nozzles. In average, the sprayer runs over the same spot once a week based on a pre-determined schedule and completes 12–15 runs during a one season. In this research, the sprayer is used as the platform to carry an imaging system to collect field data for training the machine vision system. Also it serves as the apparatus on which spot spraying will be enabled by deploying trained machine vision system on the control system to manipulate the sprayer nozzles at later stage of the project.

2.2 Imaging System

Firstly, an imaging system (Fig. 1) was built and mounted on the sprayer to collect data from the field during the 2021 growing season. It encompasses four principal components: a camera (RX0II, Sony, Tokyo, Japan) used for machine vision development,

a single-board computer (Latte-panda, Shanghai, China), an embedded device (AGX Xavier, Jetson, NVIDIA, Santa Clara CA, USA), and a frame grabber (Mypin, Mypin Electrical Co., Ltd., Zhongshan, China). While the single-board computer serves as a trigger to control the development camera, the embedded device receives the images of the camera via the frame grabber to select images of interest and train the machine vision models.
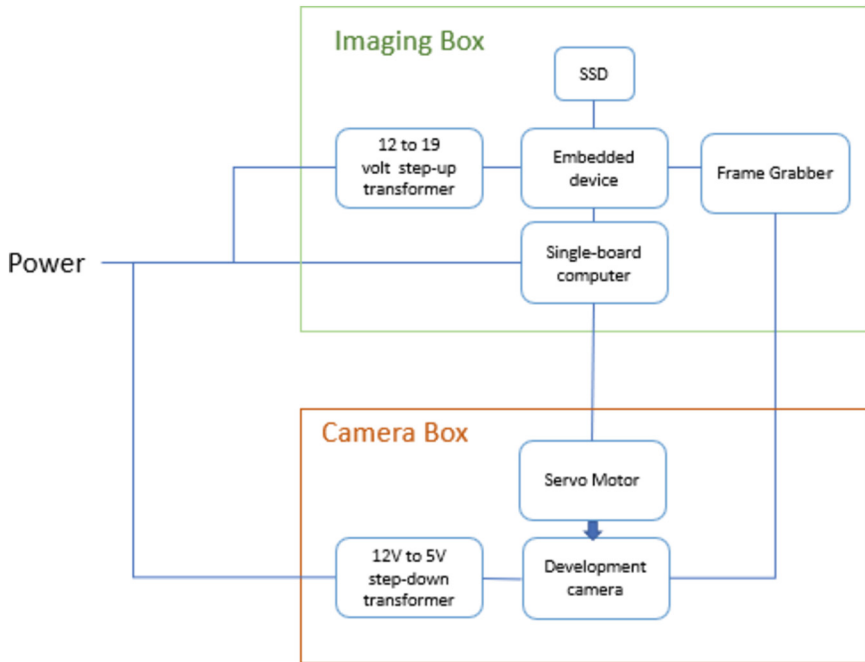
Fig. 1. Block Diagram of the imaging system mounted on sprayer for data collection

2.3 Training Machine Vision System

The imaging system deployed in 2021 was able to collect images during 7 runs which resulted in obtaining 43506 images out of which 800 included Colorado potato beetles.

A deep learning architecture known as "You Look Only Once version 5" (YOLOv5) [5] was then used to train a machine learning model to detect the insects, as small objects (as they appear in Fig. 2). The deep learning model was trained using cloud resources from the Digital Research Alliance, formerly known as Compute Canada, which functions as Canada's primary national high-performance computing (HPC) infrastructure [6]. This infrastructure provides users with access to both storage and computational resources, enhancing the efficiency of performing extensive data processing and analyses. To improve the success rate of detection a transfer learning technique was also implemented, for which a total of 389 images of higher resolution taken by a mobile

phone were added to the dataset. The dataset was divided into training (80%), validation (10%), and test (10%) datasets. To enable precise object detection, annotation was achieved by leveraging Robo-flow's online annotation tool, illustrating the presence of beetles denoted by bounding boxes.


Fig. 2. Top view of potato plants taken by the imaging system in which the insects are highlighted by the bounding boxes

2.4 Spray Control System

On the sprayer, numerous electronic components are interconnected and communicate with one another through Controller Area Network (CAN). The CAN bus is a serial communication protocol to ensure reliable transmission of data. One of these CAN buses operates according to the ISO 11783 protocol [7], it is commonly known as ISOBUS or the implement bus as it enables communication between a tractor and its propelled implement. While the primary aim of ISOBUS is to establish a standardized communication system for any combination of tractors, terminals and implements in a plug-and-play manner, it also accommodates communication via other compatible CAN protocols and other compatible proprietary messages [8].

Recognizing the growing demand for individual nozzle control, open-source nozzle control units have emerged in the market, offering ISOBUS-compliant individual nozzle control solutions, such as Hypro ProStop-E ISOBUS System (Pentair plc, London, UK) [9]. Opting for an open-source control unit alleviates the need for data logging and analysis since achieving the ISOBUS interface can be accomplished by adhering to
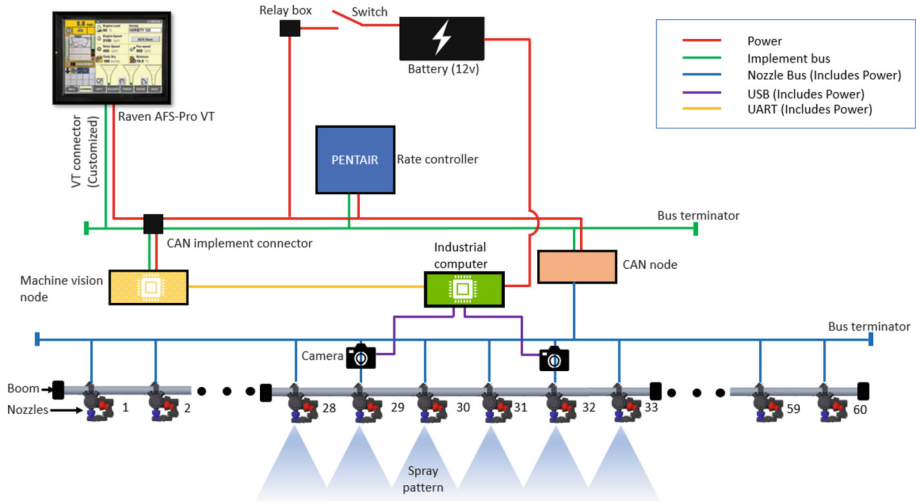
Fig. 3. MVS connected with an ISOBUS-compatible spraying system through the machine vision node

the publicly available guidelines provided by the manufacturer [10]. In order to enable control on the nozzles by the machine vision system, a communication architecture was built as shown in Fig. 3. In this design, we leverage a 12V DC battery from a tractor and incorporate a switch mechanism for activating the system as needed. Figure 3 also depicts the CAN communication diagram, indicated by green lines, outlining the CAN communication precisely implement bus within the system. An ISOBUS-compatible virtual terminal (Raven AFS-Pro 700, South Dakota, US) interfaces with the Hypro system. In this design one camera of the machine vision system controls 3 nozzles individually. Also, this design relies on a machine vision node which we built and implemented to convert insect detection results by the machine vision system to CAN messages understandable by the Hypro system.

3 Results

3.1 Detection of Beetles

Our experimental setup entailed a systematic upload of the datasets encompassing training, validation, and testing images, along with the YOLOv5 repository, to the Digital Research Alliance's Graham cloud infrastructure. Subsequently, the dataset served as input to the deep learning architecture, with multiple training configurations explored during this process. These configurations included variations in the learning rate, which ranged from 0.01 to 0.001, as well as the utilization of both Stochastic Gradient Descent (SGD) and the Adam optimizer.

The outcomes of our detection experiments underwent comprehensive analysis, with the principal evaluation metric being the confusion matrix. This matrix comprises several critical components, including true positives, false positives, and false negatives. Given

the central focus of our research on the accuracy of Colorado potato beetle detection, we define this accuracy metric as the ratio of true positives to the sum of true positives and false negatives. In the context of our research findings, the results are presented in terms of the performance of the YOLOv5 model for CPB detection. The following is a summary and explanation of the presented results in Table 1.

Table 1. Number of Colorado potato beetles detected on the test dataset

Type	Without Transfer learning	With Transfer learning
True Positive	25	32
False Positive	2	2
False Negative	24	16
Detection accuracy	49%	64%

In summary, the YOLOv5 model demonstrated a detection accuracy of 64% for the specific object of interest. While it correctly identified nearly half of the instances where these objects were present, it did miss a significant number of them. The presence of False Positives suggests an avenue for improvement in reducing incorrect detections, while the existence of False Negatives indicates a need to enhance the model's sensitivity to detect more of the target objects.

3.2   Practical Implementation of the Machine Vision Node

The Machine Vision Node, built to facilitate nozzle control for precise pest spraying by seamlessly connecting machine vision systems with boom spraying setups, comprises two single-board microcontrollers linked to a CAN transceiver and deploys two distinct algorithms to receive protocol messages from the machine vision system and identify pest-infested regions within the field of view (FOV) of each camera, dividing it into sections corresponding to individual nozzle spraying areas. The second algorithm processes these sections and generates CAN messages to control the nozzles, which are transmitted over the CAN bus, enabling instantaneous and synchronized control. In this specific scenario, the distance between these nozzles remains consistent along the entire length of the boom. In the protocol message, we considered the x-axis of the FOV, which runs parallel to the orientation of the boom. Conversely, we do not account for the y-axis of the FOV because the spray from the nozzles already covers the y-axis, aligning with the direction of travel.

The protocol message proposed format is encoded as strings, featuring a starting of the frame '{' and an end of the frame '}' to distinctly separate individual messages in the communication framework. In each FOV, the x-coordinate of the midpoint within this division is defined as the zero-point, serving as a critical reference for subsequent calculations and data interpretation.

In Fig. 4, both cameras share neighboring FOVs spanning one thousand millimeters, with the leftmost point designated as negative five hundred (–500) and the rightmost
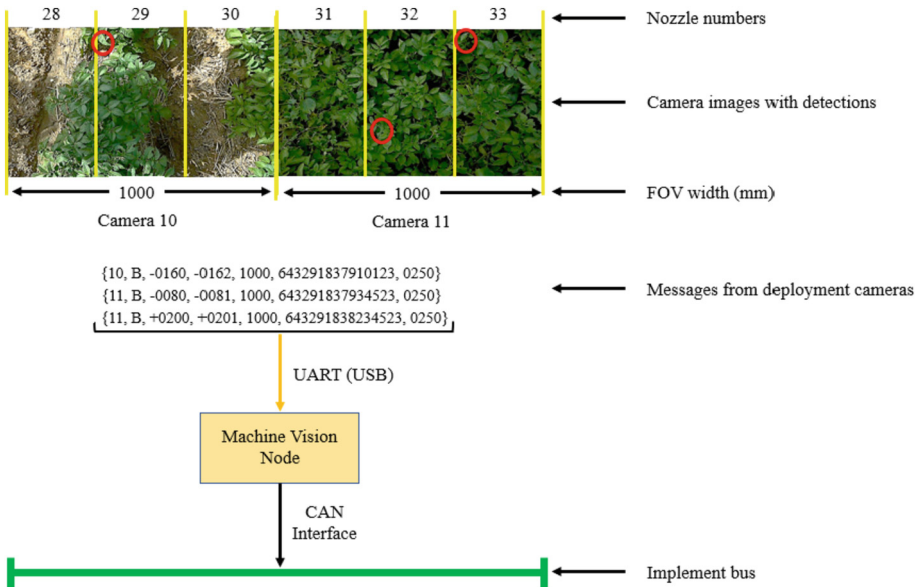
Fig. 4. Detection results of the deployment cameras in UART protocol converted to CAN messages via the machine vision node. Red circles show the location of the insects in field respective to the corresponding nozzle

point as positive five hundred (+500). For instance, if a potato beetle is detected near the leftmost point of the 2nd nozzle section under the first camera, we anticipate x-values like –0160 and –0162, indicating a two-millimeter width of the beetle. Our protocol message also includes timestamps for detection and time taken to identify anomalies. To meet these requirements effectively, we structured the protocol message format to be: {camera number, identified object, minimum x-value, maximum x-value, total x-range, detection timestamp, detection time}. Enabling spraying is achieved by using the information in the message while excluding time related information, which are intended for future development when mapping the performance of spraying becomes necessary.

4   Conclusion

This paper has demonstrated the development of a machine vision system to detect Colorado potato beetles on potato plants using images taken on-the-go of a camera mounted on the sprayer. The ability to get accuracy result of 64% on images taken under environmental conditions indicates a potential of improving detection by modifying the imaging techniques and the machine learning models. Scalability of the detection is tackled by developing the machine vision node which allows for a flexible integration of the machine vision systems with the control system of the nozzles by adopting Controller Area Network as the mean for data transportation and management within the sprayer. In addition to building on the current results in terms of accuracy and scalability, the next steps in development will include real-time spraying by introducing modifications to the hydraulic system that governs the sparying of the pesticide.

References

1. Kiley-Worthington M (1980) Problems of modern agriculture. Food Policy 5(3):208–215. https://doi.org/10.1016/0306-9192(80)90129-3
2. United Nations: TRANSFORMING OUR WORLD: THE 2030 AGENDA FOR SUSTAIN-ABLE DEVELOPMENT (A/RES/70/1), sustainabledevelopment.un.org (2015)
3. ASABE Staff: See & SprayTM select by John Deere Res. Mag. **29**(3), 7–8 (2022)
4. Fishel, F., et al.: Introduction to crop scouting (2018). https://mospace.umsystem.edu/xmlui/handle/10355/69211
5. Jocher, G., Changyu, L., Hogan, A., Yu, L., Changyu, R.P., Sullivan, T.: ultralytics/yolov5: Initial Release (v1.0) [Computer software]. Zenodo (2020). https://doi.org/10.5281/ZENODO.3908560
6. Government of Canada: Digital Research Alliance of Canada (2021). https://Alliancecan.ca/En
7. Salunkhe, A.A., Kamble, P.P., Jadhav, R.: Design and implementation of CAN bus protocol for monitoring vehicle parameters. In: 2016 IEEE International Conference on Recent Trends in Electronics, Information and Communication Technology (RTEICT) , pp. 301–304. IEEE (2016)
8. Schlingmann, N.: ISOBUS – standards and uses for data from farm machinery. In: Mottram, T. (Ed.), Digital Agritechnology: Robotics and Systems for Agriculture and Livestock Production, Academic Press, pp. 49–67. Elsevier (2022)
9. Al-Mallahi A, Natarajan M, Shirzadifar A (2023) Development of robust communication algorithm between machine vision and boom sprayer for spot application via ISO 11783. ISmart Agric. Technol. 4:100212. https://doi.org/10.1016/j.atech.2023.100212
10. Pentair Prostop-E ISOBUS Module System – Quick start guide. Pentair (2023a). https://www.pentair.com/content/dam/extranet/web/nam/hypro/quick-start-guide/hyp1101-prostop-e-isobus-qsg.pdf
11. Zanin ARA, Neves DC, Teodoro LPR et al (2022) Reduction of pesticide application via real-time precision spraying. Sci Rep 12:5638. https://doi.org/10.1038/s41598-022-09607-w

Emerging Smart Biosensors for the Specific and Ultrasensitive Detection of Plant Abiotic Stresses

Keyvan Asefpour Vakilian[(✉)]

Department of Biosystems Engineering, Gorgan University of Agricultural Sciences
and Natural Resources, Gorgan, Iran
keyvan.asefpour@gau.ac.ir

Abstract. The functionalities of microRNAs (miRNAs) and their target genes toward stress in plants have been revealed to humans due to the extensive work conducted in the last decade. A tissue-specific change in the regulation of miRNAs occurs as a result of plant stress. In this study, an optical biosensor has been used to measure the concentration of various miRNAs that involve plant stress response in tomatoes after applying drought, salinity, and temperature stresses to the plant. To carry out the experiments, plants were cultivated in a greenhouse environment. To apply drought conditions in plants, they were stressed by withholding water at various levels of field capacity. Saline irrigation water was used to apply salinity. Cold and heat stresses were applied to study the effects of temperature. The concentration of several plant miRNAs, including miRNA-167, miRNA-172, miRNA-393, and miRNA-396, in plant samples was measured after applying the stresses to the plants. After creating a database in which the plant miRNA concentrations were the inputs while the plant stress level was the model output, the artificial neural network was utilized to learn the patterns between the inputs and output. The results indicated that an artificial neural network with an architecture of 4-8-4 could predict the severity of the plant stress with the MSE and R^2 values of 0.070 and 0.94, respectively. This shows that combining optical biosensors and machine learning techniques could detect the stress level in stress conditions with acceptable specificity and sensitivity.

Keywords: Machine learning · Abiotic stress · miRNA biosensor · Tomato plants

1 Introduction

As single-stranded RNA molecules, microRNAs (miRNAs) are characterized by their limited protein-coding potential [1]. Despite the fact that miRNAs selectively target a very small fraction of mRNAs in plants, the significance of gene regulation due to the miRNAs is considerable [2]. A majority of these mRNAs are integral to various plant developmental processes. Moreover, substantial evidence underscores the correlations between plant stress responses and alterations in miRNA expression. Functioning as adverse post-transcriptional regulators, miRNAs exercise binding to their target mRNAs, thereby impeding the translation of these target mRNAs [3].

The crucial sources of abiotic stress in plants, namely salinity, temperature, drought, carbon dioxide, and heavy metal contamination, impose impacts on various morphological, physiological, and biochemical attributes of plants [4]. In response to the stressors, plants employ miRNA upregulation or downregulation mechanisms, consequently instigating a reconfiguration of gene expression to reinstate cellular homeostasis [5–7]. The modulation of plant miRNA expression during stress conditions exhibits a twofold specificity: it is contingent on the spatial distribution within plant tissues and the temporal progression through developmental/growth stages [8, 9].

The discernment of stress-responsive miRNAs offers valuable insights into their pivotal role in enhancing plants' mechanisms for stress tolerance [10]. An exploration of bibliographic databases indicates many studies on alterations in plant miRNA expression prompted by biotic and abiotic stressors [11]. This research has been carried out on a spectrum of plants including *Arabidopsis thaliana*, *Glycine max*, *Medicago truncatula*, *Triticum turgidum*, *Oryza sativa*, and *Zea mays* [12]. Investigations have demonstrated that certain miRNAs, such as miRNA-167, miRNA-172, miRNA-393, and miRNA-396, participate in diverse abiotic stress-related processes [5].

Certain abiotic stresses exert significant limitations on global agricultural productivity. Investigating miRNAs associated with these stresses and their role in plant responses is essential for understanding plant stress physiology [13]. Various techniques are developed to measure the expression (i.e., concentration) of miRNAs in plant samples [14]. Conventional techniques like northern blotting and polymerase chain reaction (PCR) have limitations, including restricted detection limits, linear response ranges, and low specificity. In this context, a reliable approach for the task of miRNA concentration measurement could involve the utilization of biosensors equipped with gold nanoparticles, functioning based on nanoparticle aggregation [15].

Utilizing machine learning methodologies, it is possible to determine the complex relationships between plant stress conditions and the expressions of miRNAs within plants [16]. The machine can learn these complex nonlinear patterns that connect inputs (specifically, miRNA expressions) to the desired output (namely, the presence of plant stress) [5]. Despite the broad spectrum of learning algorithms available, supervised learning emerges as a robust and efficient approach in the realm of plant sciences [17–19]. Artificial neural networks (ANNs), decision trees, support vector machines, fuzzy inference systems, adaptive neuro-fuzzy inference systems, and Naïve Bayes are examples of supervised learning methods widely utilized for recognizing patterns within databases [20]. The success of the machine's predictive performance, which is revealed through established performance evaluation criteria, essentially affirms the importance of the selected miRNA expressions used to train the machine in the process of plant responses to stress stimuli which is an essential concept in plant physiology and biology.

This study aims for (a) the assessment of the effects of various levels of common environmental stresses on the miRNA concentrations of tomato plants, and (b) the deployment of supervised learning techniques in predicting plant stress levels by having the miRNA expressions within plants as inputs. So far, no research has been reported about using machine learning to predict plant abiotic stresses in tomatoes based on their miRNA concentrations. The novelty of this work involves introducing a platform based

on miRNA concentration in tomato plants where machine learning can predict major plant abiotic stresses using data gathered by an optical miRNA biosensor.

2   Material and Methods

Figure 1 depicts the schematics of the present study. After applying the abiotic stresses, miRNA concentrations obtained by a smart optical biosensor were used to predict the stress levels using machine learning.

2.1   Plant Materials

Tomato (*Solanum lycopersicum*) seeds were procured from a local store in Gorgan, Golestan province, Iran. The seeds underwent a surface sterilization process involving exposure to NaClO for a duration of 1 min, followed by thorough rinsing with distilled water. Plug trays containing vermiculite, peat, and perlite in a ratio of 3:2:1 were used to grow seeds. On the 21st day, we transplanted the seedlings into 5-L pots of the same growth medium. Nutrient management for the nutrients followed the protocols outlined by Heeb et al. [21].

2.2   Stress Treatments

Uniform and complete irrigation was maintained for all pots until the plants reached the eighth true leaf stage, with water levels maintained at 100% of field capacity. Subsequently, for the control group of plants, daily tap water was supplied to sustain soil water potential at levels near the field capacity. Drought-treated plants were subjected to water stress by withholding water until the soil water potential diverged from field capacity, allowing for the examination of drought stresses with various severities, as outlined by Jafari et al. [22]. Six water treatment groups were studied in this work to cover a wide range of plant water stress, with soil water levels set at 100% (control), 90%, 80%, 70%, 60%, and 50% of field capacity.

   Moreover, four different levels of salinity (control at 1 dS/m, 2 dS/m, 3 dS/m, and 4 dS/m), four levels of cold exposure (control at 28 °C, 26 °C, 24 °C, and 22 °C), and four levels of heat exposure (control at 28 °C, 30 °C, 32 °C, and 34 °C) on various plant characteristics. These treatments were initiated once the plants reached the eighth true leaf stage. To achieve the desired soil salinity levels, varying amounts of NaCl were introduced into the irrigation water. Plant miRNA concentrations relevant to stress investigations were measured on three sampling times: at 45 days, 55 days, and 65 days after planting. In this research, all experiments were performed with four replications.

2.3   Determination of MiRNA Concentrations

The quantification of miRNAs, including miRNA-167, miRNA-172, miRNA-393, and miRNA-396, was executed as follows: Total RNA was extracted from five plant samples obtained from roots for each plant, utilizing a purification kit purchased from Norgen Biotek. The results were then averaged for these five samples and one value was recorded
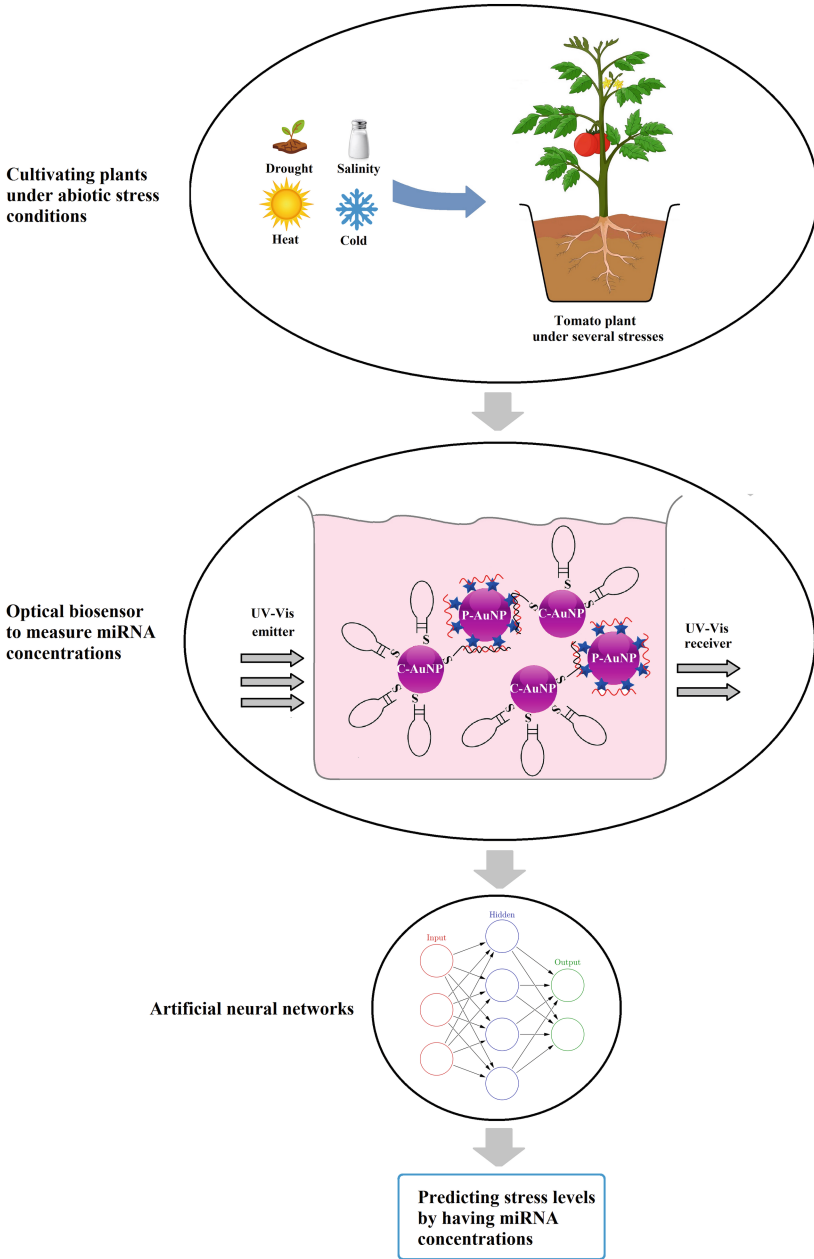
Fig. 1. The schematics of the present work.

for each miRNA concentration for each plant. The concentration of miRNAs implicated in plant stress responses within the samples was evaluated using a biosensor based on gold nanoparticles (AuNPs). The construction of the optical biosensor included a three-step process, as described in the brief below [23].

Step 1: A solution of polyethylenimine (PEI) (42 mM) was combined with $HAuCl_4$ (1.5 M) under rigorous agitation, sustaining a constant pH of 7.4 by the gradual addition of HCl to the mixture. Subsequently, the temperature of the solution was elevated. During this temperature change, the red color for the sample is achieved, indicating the reduction process. The produced solution that included PEI-AuNPs was stored at 4 °C for subsequent use. A 5 µL aliquot of the sample was then subjected to a 30-min incubation with 40 µL of synthesized PEI-AuNPs.

Step 2: Boiling $HAuCl_4$ solution was mixed with sodium citrate (1%) in a 21 mL volume, followed by vigorous stirring until a color transition was achieved. The solution was further stirred for 15 min and subsequently, 400 µL of it was combined with 2 µL of Tween-20 and 400 µL of each thiolated probe (1 µM). This mixture was centrifuged at 10,000 rpm for 15 min. The resulting supernatant was discarded, and the reddish precipitate was re-suspended in 200 µL of deionized water.

Step 3: Combining 5 µL of the products resulting from each of the steps described above induced a hybridization between the probe and the target miRNA, prompting inter-particle cross-linking aggregation and a consequent reduction in the distance between nanoparticles. Greater concentrations of the target miRNA led to increased aggregation. A reduction in absorption intensity at 530 nm served as the indicator of the reaction. The absorbance ratio of 750/530 nm was considered a measure of probe-target hybridization and, consequently, the concentration of the target miRNA. The UV-Vis spectra measurements during the experiments were performed using a multi-mode microplate reader.

The characteristics of the biosensor, including the limit of detection, linear range, sensitivity, specificity, repeatability, and reproducibility, in measuring miRNA concentrations are investigated in our previous work [15]. These characteristics were acceptable for miRNA analysis in plant tissue samples where the concentrations are in the range of femtomolar. In this situation, similar to the reports in the literature [24, 25], the results are reliable for investigating plant response toward biotic and abiotic stresses.

2.4 Machine-Learning Models

The concentrations of miRNAs studied in this work at different stress levels were utilized for the construction of a database reliable for machine learning purposes. Mean values of the replications were employed during the entering of measured values into the database. Each pattern encompassed the miRNA concentrations and the corresponding plant stress level.

While statistical regression models offer mathematical equations to predict dependent variables based on input features, their application is limited when input dimensions exceed two due to challenges in parameter estimation. In contrast, machine-learning methods are well-suited to learn from databases containing numerous input features. This study employed ANN as a learning-based regression model to predict the type and severity of stresses applied to the plants. ANN was implemented via a code written in the

MATLAB R2018b programming environment (Mathworks, MA, USA). For assessing model performance, a 5-fold cross-validation approach was adopted. The evaluation of model efficiency was conducted based on the coefficient of determination (R^2), and root mean squared error (RMSE) values.

3   Results and Discussion

Prior investigations have revealed the tissue-specific expression of miRNAs studied in this work in response to major abiotic stresses in tomato plants. This study seeks to establish a model wherein machine learning finds relationships between plant miRNA expression and stress conditions. It should be noted that a homogeneous miRNA concentration was observed in samples obtained from each plant, making it possible to consider one value for each miRNA concentration for each plant while creating the database for the machine learning procedure.

The miRNA contribution analysis in plant stress response in previous studies has unveiled a common pattern: stress-involved miRNAs imply a lack of specificity in their behavior concerning stress. This general non-specificity poses a challenge to predicting plant stress using a single miRNA's concentration, even when employing advanced computational tools. Some prior studies have identified specific miRNAs acting as indicators of particular biotic or abiotic stresses in certain plants [15]. However, this study demonstrated that miRNA concentration changes can be non-specific to individual stress types. Therefore, a combination of four miRNA concentrations studied in this work can be used to train ANN for predicting the type and severity of various tomato abiotic stresses.

Table 1 shows the RMSE and R^2 values for predicting the machine outputs by having the concentration of miRNAs as inputs. The table indicates that ANN was capable of accurately predicting the stress type and severity considering a suitable network architecture for ANN. The performance of the model in predicting stress levels varied among the architectures, with some outperforming others. The results indicate that ANN with the 4–8-4 architecture that includes eight neurons in the learner (hidden) layer outperformed other ANN methods in predicting plant stress. With an RMSE and R^2 value of 0.070 and 0.94, respectively, for test data, this architecture demonstrated a high accuracy, suggesting that measuring the concentrations of miRNA-167, miRNA-172, miRNA-393, and miRNA-396 in tomato plants could facilitate accurate stress prediction using ANN. Notably, kernel-based algorithms such as support vector machines were not employed as a learning algorithm in this study, primarily due to the limited understanding of complex behaviors between the model inputs and the outputs [26].

Consistent with prior findings, the results brought in Table 1 affirm that the studied miRNAs were markedly influenced by major abiotic stresses in plants [27]. The utilization of a gold nanoparticles-based optical biosensor for miRNA concentration determination is rationalized by the enhanced specificity of biosensor responses compared to conventional techniques like qRT-PCR, northern blot, and microarrays [28]. Although this study focuses on an optical biosensor, alternative methods such as electrochemical techniques are also proposed for miRNA analysis. It should be noted that electrochemical techniques demand extensive electrode pretreatments and expensive equipment. The limit of detection for the biosensor used in this study has been determined to be 0.5 fM in previous studies, with a resolution of 1 fM [5].

Table 1. Performance evaluation of the proposed ANN in the prediction of plant stress

ANN architecture	Training		Validation		Test	
	RMSE	R^2	RMSE	R^2	RMSE	R^2
4-5-4	0.260	0.64	0.260	0.64	0.324	0.57
4-6-4	0.269	0.63	0.305	0.59	0.234	0.67
4-7-4	0.243	0.66	0.287	0.61	0.343	0.55
4-8-4	0.066	0.95	0.063	0.96	0.070	0.94
4-9-4	0.066	0.95	0.066	0.95	0.130	0.82
4-10-4	0.243	0.66	0.286	0.61	0.296	0.60
4-11-4	0.167	0.76	0.243	0.66	0.324	0.57
4-12-4	0.260	0.64	0.374	0.52	0.314	0.58
4-13-4	0.1961	0.72	0.235	0.67	0.277	0.62
4-14-4	0.1746	0.75	0.154	0.78	0.203	0.71
4-15-4	0.131	0.82	0.211	0.70	0.277	0.62

During the experiments, certain miRNAs exhibited up-regulation under stress conditions, whereas others experienced down-regulation. This observation is consistent with expectations, given the dynamic nature of miRNA responses to stress. The selected stress levels in this study include mild, moderate, and severe stress scenarios within tomato plants [29]. Despite their low concentrations, caution must be exercised not to underestimate the biological significance of miRNA biomolecules. miRNAs target essential genes in plants, effective in various processes like root and leaf development, photochrome signaling, lateral organ polarity, meristem formation, vascular development, and stress response, as well as copper homeostasis, heavy metal tolerance, and oxidative stress.

While earlier studies have predominantly explored the impacts of severe stress conditions, the present findings illuminate the significant effects of even mild to moderate stress on miRNA concentrations. This intriguing observation highlights the potential utility of optical biosensors, similar to the one developed in this study, for early stress detection. It's essential to recognize that these findings are not limited to specific stress types, as demonstrated by the diversity of stress sources affecting a given miRNA, as reported in previous studies. During the last decade, the study of plant health status and its response to environmental stresses has included investigating the up/down-regulation of stress-involved miRNAs [30]. Although miRNAs are non-coding molecules, they function remarkably in regulating gene expression [31].

Moreover, during the last decade, biosensors and their application in various fields of plant science have become popular among plant scientists [5]. Biosensors benefit from several advantages, such as high specificity, rapid response, and reproducibility [32]. Researchers are able to overcome the limitations of traditional techniques by using optical and electrochemical biosensors to improve their capability of determining the

concentration of miRNAs in various plant tissues. The results prove the fact that combining optical biosensors and machine learning techniques could detect stress levels in stress conditions.

4   Conclusions

This study employs machine learning to explore the contributions of miRNAs in plant stress response. Despite the non-specific nature of miRNAs' responses to abiotic stresses like drought, salinity, and temperature, machine learning emerges as a valuable tool for the specific and ultrasensitive prediction of plant stress based on stress-involved miRNA concentrations. The ANN algorithm adopting four stress-involved miRNAs with the most significant contributions to plant response toward stress as inputs was used to predict the type and severity of the stress. The study outcomes confirm the hypothesis that machine learning serves as an efficient technique for enhancing our comprehension of the relationships between plant stress and miRNA expression.

As a limitation of this work, only four abiotic stresses were studied during the experiments. Investigating other abiotic stresses such as light and nutrient deficiency and toxicity as well as biotic stresses and considering their corresponding changes in miRNA concentration can be challenging for machine learning since the dimension of the database increases remarkably. This is an interesting idea that can be pursued in future studies.

Declaration of Competing Interest.   The author declares that he has no known competing financial interests or personal relationships that could have appeared to influence the work reported in this paper.

References

1. Cai Y, Yu X, Hu S, Yu J (2009) A brief review on the mechanisms of miRNA regulation. Genom. Proteom. Bioinform. 7(4):147–154
2. Budak H, Akpinar BA (2015) Plant miRNAs: biogenesis, organization and origins. Funct. Integr. Genom. 15:523–531
3. Sunkar R, Li YF, Jagadeeswaran G (2012) Functions of microRNAs in plant stress responses. Trends Plant Sci. 17(4):196–203
4. Chang YN, Zhu C, Jiang J, Zhang H, Zhu JK, Duan CG (2020) Epigenetic regulation in plant abiotic stress responses. J. Integr. Plant Biol. 62(5):563–580
5. Asefpour Vakilian K (2020) Machine learning improves our knowledge about miRNA functions towards plant abiotic stresses. Sci. Rep. 10:3041
6. Tiwari R, Rajam MV (2022) RNA-and miRNA-interference to enhance abiotic stress tolerance in plants. J. Plant Biochem. Biotechnol. 31(4):689–704
7. Mohammadi P, Asefpour Vakilian K (2023) Machine learning provides specific detection of salt and drought stresses in cucumber based on miRNA characteristics. Plant Methods 19:123
8. Begum Y (2022) Regulatory role of microRNAs (miRNAs) in the recent development of abiotic stress tolerance of plants. Gene 821:146283
9. Zhang Y, Zhou Y, Zhu W, Liu J, Cheng F (2022) Non-coding RNAs fine-tune the balance between plant growth and abiotic stress tolerance. Front Plant Sci 13:965745

10. Singh P, Dutta P, Chakrabarty D (2021) MiRNAs play critical roles in response to abiotic stress by modulating cross-talk of phytohormone signaling. Plant Cell Rep. 40(9):1617–1630

11. Singh DK, Mehra S, Chatterjee S, Purty RS (2020) In silico identification and validation of miRNA and their DIR specific targets in *Oryza sativa* Indica under abiotic stress. Non-coding RNA Res. 5(4):167–177

12. Sun X, Lin L, Sui N (2019) Regulation mechanism of microRNA in plant response to abiotic stress and breeding. Mol. Biol. Rep. 46:1447–1457

13. Singroha G, Sharma P, Sunkur R (2021) Current status of microRNA-mediated regulation of drought stress responses in cereals. Physiol. Plant 172(3):1808–1821

14. Jet T, Gines G, Rondelez Y, Taly V (2021) Advances in multiplexed techniques for the detection and quantification of microRNAs. Chem. Soc. Rev. 50(6):4141–4161

15. Asefpour Vakilian K (2019) Gold nanoparticles-based biosensor can detect drought stress in tomato by ultrasensitive and specific determination of miRNAs. Plant Physiol. Biochem. 145:195–204

16. Pradhan UK et al (2023) ASmiR: a machine learning framework for prediction of abiotic stress–specific miRNAs in plants. Funct. Integr. Genom. 23(2):92

17. Massah J, Asefpour Vakilian K, Torktaz S (2019) Supervised machine learning algorithms can predict penetration resistance in mineral-fertilized soils. Commun. Soil Sci. Plant Anal. 50(17):2169–2177

18. Ganjdoost M, Aboonajmi M, Mirsaeedghazi H, Asefpour Vakilian K (2021) Effects of power ultrasound treatment on the shelf life of button mushrooms: digital image processing and microbial counting can reveal the effects. Food Sci. Nutr. 9(7):3538–3548

19. Esmaili M et al (2021) Assessment of adaptive neuro-fuzzy inference system (ANFIS) to predict production and water productivity of lettuce in response to different light intensities and CO_2 concentrations. Agric. Water Manag. 258:107201

20. Javidan SM, Banakar A, Asefpour Vakilian K, Ampatzidis Y (2022) A feature selection method using slime mould optimization algorithm in order to diagnose plant leaf diseases. In: 2022 8th Iranian Conference on Signal Processing and Intelligent Systems (ICSPIS), Behshahr, Iran, pp 1–5

21. Heeb A, Lundegårdh B, Ericsson T, Savage GP (2005) Effects of nitrate-, ammonium-, and organic-nitrogen-based fertilizers on growth and yield of tomatoes. J. Plant Nutr. Soil Sci. 168(1):123–129

22. Jafari S, HashemiGarmdareh SE, Azadegan B (2019) Effects of drought stress on morphological, physiological, and biochemical characteristics of stock plant (*Matthiola incana* L.). Sci. Hortic. 253:128–133

23. Hakimian F, Ghourchian H, Hashemi AS, Arastoo MR, BehnamRad M (2018) Ultrasensitive optical biosensor for detection of miRNA-155 using positively charged Au nanoparticles. Sci. Rep. 8(1):2943

24. Crawford BM et al (2019) Plasmonic nanoprobes for in vivo multimodal sensing and bioimaging of microRNA within plants. ACS Appl. Mater. Interfaces 11(8):7743–7754

25. Nehra A, Kumar A, Ahlawat S, Kumar V, Singh KP (2022) Substrate-free untagged detection of miR393a using an ultrasensitive electrochemical biosensor. ACS Omega 7(6):5176–5189

26. Asefpour Vakilian K, Massah J (2016) An apple grading system according to European fruit quality standards using Gabor filter and artificial neural networks. Sci Study Res Chem Chem Eng Biotechnol Food Ind 17(1):75

27. Asefpour Vakilian K (2020) Determination of nitrogen deficiency-related microRNAs in plants using fluorescence quenching of graphene oxide nanosheets. Mol. Cell Probes 52:101576

28. Esmaeilzadeh AA, Yaseen MM, Khudaynazarov U, Al-Gazally ME, Opulencia MJC, Jalil AT (2022) Recent advances on electrochemical and optical biosensing strategies for monitoring of microRNA-21: a review. Anal. Methods 14:4449–4459

29. Shi X, Jiang F, Wen J, Zhen W (2019) Overexpression of solanum habrochaites microRNA319d (sha-miR319d) confers chilling and heat stress tolerance in tomato (*S. lycopersicum*). BMC Plant Biol. 19(1):214
30. Hashemi Shabankareh S, Asghari A, Azadbakht M, Asefpour Vakilian K (2023) Physical and physiological characteristics, as well as miRNA concentrations, are affected by the storage time of tomatoes. Food Chem. 429:136792
31. Varkonyi-Gasic E, Gould N, Sandanayaka M, Sutherland P, MacDiarmid RM (2010) Characterisation of miRNAs from apple (*Malus domestica* 'Royal Gala') vascular tissue and phloem sap. BMC Plant Biol. 10:159
32. Bazin I, Tria SA, Hayat A, Marty J-L (2017) New biorecognition molecules in biosensors for the detection of toxins. Biosens. Bioelectron. 87:285–298

A Method for Multispectral Images Alignment at Different Heights on the Crop

Sabina Laveglia(✉) ⬤ and Giuseppe Altieri ⬤

School SAFE, University of Basilicata, Viale dell'Ateneo Lucano 10, 85100 Potenza, Italy
`sabina.laveglia@unibas.it`

Abstract. Multispectral imaging (MSI) for agricultural applications is playing a key role in plant stress assessment. However, one of the main problems is the misalignment of spectral bands provided by these instruments. The approach proposed in this study considers various distances from the target (500 mm to 1500 mm with a step size of 100 mm) and applies corrective shifts to achieve accurate registration among bands. Through a comparative evaluation of two alignment methods, Checkerboard (CB) and Discrete Fourier Transform (FT), this research aims to provide an effective solution for accurate image registration by facilitating reliable spectral analysis. Specifically, the proposed method involved the analysis of alignment-related offsets among the tested methods. In addition, the study explored the extraction of vegetation spectral indices for vegetation analysis and discrimination between healthy and diseased plants and evaluated their relationship with the quality of alignment obtained at different heights. The results confirmed the trends in the changes in offsets as the target distance varies, showing satisfactory accuracy in the alignment of raw spectral images at different distances, with an error of about 1 pixel. Among the vegetation indices used, the Normalized Difference Vegetation Index (NDVI) proved to be capable of discriminating between healthy and nonhealthy leaves. The study aims to establish a framework applicable to remote sensing and agricultural monitoring, providing a valuable tool for monitoring plant health.

Keywords: Image alignment · Multispectral image · Image processing · Precision agriculture · Crop health status · Variable height

1 Introduction

Agriculture is a field that is an evolving field, especially in terms of employing more digital and information technology tools to increase its sustainability. One of the main goals of precision agriculture is to employ inputs rationally in conjunction with crop needs [1]; this requires monitoring techniques that are both rapid and reliable [2].

The growing need for rapid insight into the dynamics affecting plant development has led to the use of sensors based on non-destructive plant analysis. Spectral imaging (SI), being an integration of two modalities, namely imaging and point spectroscopy, is particularly emerging as a potential tool for both rapid and non-destructive assessment.

Two primary imaging approaches, i.e., multispectral imaging (MSI) and hyperspectral imaging (HSI), have proven successful in various agricultural applications, particularly in determining plant stress [3]. By seamlessly integrating spatial and spectral information, these techniques facilitate the simultaneous measurement of numerous physical attributes (such as size, shape, and colour) and chemical properties (including water, fat, and sugar content) within a targeted scene [4].

Spectral imaging data represent true three-dimensional space distribution maps (x, y) of spectral information at certain wavelengths (λ), i.e. the hypercubes (x, y, λ). While multispectral imaging involves the acquisition of a limited number of image layers of a scene, acquired in a specific segment (called a band) of the electromagnetic spectrum, hyperspectral imaging (HSI) acquires spectral images for narrow, contiguous spectral bands [5].

Most widely used multispectral sensors typically acquire 3 to 10 spectral bands per pixel within the resulting image hypercube. Their advantages in agricultural applications are significant, however, their utilization is hindered by the demand for advanced data processing expertise and high computational time [5]. Usually, the primary data processing procedures in imaging include the calibration, extraction of features, computation of vegetation indices, and classification of imagery. These processes facilitate accurate tracking of crop health and growth stages. Simultaneously, the dimensionality reduction simplifies intricate data while the deep learning reveals complex patterns. This seamless integration allows for informed decision-making through data-driven insights, enhancing agricultural practices for long-term sustainability [5].

Even so, there is considerable discussion about analytical approaches related to statistical processing techniques and, in particular, about the use and comparison of Machine Learning approach with traditional statistical processing techniques (e.g. PLS). Considerations of image analysis related to geometric features are often lacking, and are left to be performed using commercial software.

Many multispectral cameras use multiple physical sensors/lens assemblies to capture different spectral channels. When the camera is in motion, e.g. when mounted on a UAV, and the different sensors are not synchronized, the spatial misalignment among channels is not constant and a separate image registration step is further required for each captured image [6].

The close-range multispectral images are different from satellite images and UAV images. Indeed, close-range multispectral imaging is a challenging task and suffers technical complexities related to external factors (e.g., illumination effects) and vegetation-related factors (e.g., complex vegetation geometry) [7].

Multispectral cameras use often a physically different camera for each wavelength, most of the relatively low-cost commercial sensors available on the market, such as MicaSense Multispectral Sensors and Tetracam Micro-Miniature Multiple Camera Array System, they use several independent cameras with different filters to capture the different image bands, causing misalignment in image pixels for different image bands. This misalignment must be corrected before the analysis of a multiband image [6].

Misalignments between image bands are due to several reasons, such as the arrangement of sensors, movements during flight in the case of aerial vehicles, interference from the atmosphere, and so on [8, 9]. The small geometric misalignments between the

different image bands can be caused by the different thicknesses of the filters and by the vibration caused by the filter wheel [10]. Also, for imaging systems using beam splitters, image misalignment usually occurs due to various factors associated with imperfections in the system, such as lens distortions, positional tolerance of CCD sensors, different types of sensors and differences between the mechanical parts [11]. In addition, the unstable altitude of the airborne platform may cause a spatial error or a non-negligible image shift [12].

Like spectral information, calibration is also required for spatial metrics; image registration is the geometric alignment of two or more images of the same scene taken at different times, from different points of view, and/or different sensors [13].

Image registration is generally required to align two or more images. Typically, one image (the base image) is selected as the reference, against which the other images (input images) are compared. The image registration aims to align the input images with the base image by applying necessary spatial transformations, such as flipping, translating, rotating, cropping, resizing [11].

The process of image registration has been highly investigated [14]. Registration processes are usually divided into the following steps [14]: (i) feature detection, known in the literature as Control Points (CP's); (ii) feature matching; (iii) transformation model estimation; (iv) image resampling and transformation. The captured image is then mapped according to the mapping functions.

Feature matching is usually conducted by using either area-based methods (comparing and matching the images to a reference image without detecting features) or feature-based methods (where the image recording process relies on detecting the same control points in the images and in the reference image).

The distinction between the two methods lies in their different approaches. Area-based methods involve comparison of geometric shapes, like rectangles or circles, between reference and misaligned images. However, this method breaks down when complex geometric deformations are present. In contrast, feature-based methods focus on establishing pairwise correspondence between images by utilizing spatial relationships or feature descriptors. This approach aims to identify distinctive parts of the images as reliable matching points [14]. Several authors have combined the two approaches to overcome these limits [15, 16].

It has been observed that fewer control points can be found on images of certain channels. For example, Firmenichy et al. [17] observed a lack of sufficient control points to align infrared and red channels. Yasir et al. [6] have had difficulty registering near-infrared and visible channels. Other authors suggest a more rigorous method for electing the optimal band for feature matching [12].

In precision agriculture at short distances, automatic image recording is required for applications involving real-time monitoring and/or quick system response; for example, automatic image registration is needed for a robotic sprayer arm designed to work fully autonomously in a continuous operation mode [18].

The automatic image recording capability of a system using multispectral images is extremely important to ensure the accuracy of the collected data; moreover, due to the different arrangements occurring in precision agriculture remote sensing, usually, when

using images taken from far distances, the image misalignment is minimal and doesn't normally requires alignment registration of the images.

Although the use of satellite data is a well-established technology used in agriculture, and despite the improvements done in the spatial resolution offered by these systems, however, some topographic issues [19] need to be addressed along with consideration of atmospheric factors. Thus, the image alignment is considered as a minor problem. In addition, care is required in post-processing to evaluate temporal variations [20] as multi-temporal data may differ in their radiometric characteristics [21].

With regard to images from drones, the amount of information contained in the images per unit area is denser, being acquired at high altitudes of 10 to 60 m, and the images misalignment is negligible [22].

However, an approach allowing to align images is required when images are taken at short distances, but currently this is lacking in the literature, even if it is necessary to obtain accurate indices of the crop health status.

Other authors, in agreement with this work, consider that image misalignment and distortions represent a significant issue for data processing in proximal sensing applications [22]. Indeed, Krus A. et al. [22], using a commercial camera (Parrot Sequoia) mounted at a fixed height of 1.2 m on a crop field, showed that reference image suffered a significant 30% distortion due to multispectral lenses.

In proximal agricultural monitoring, images are acquired through the use of sensors with different spatial and spectral characteristics. Each sensor has different camera lenses, and, consequently, its intrinsic characteristics (i.e. the optical centre and focal length of the camera) and its extrinsic characteristics (i.e. the position of the camera in the scene) are also different.

Several authors [23–26] have used image calibration techniques based on algorithms taking into account the previously mentioned characteristics including both camera model [23] and lens distortion [24].

The method proposed by Scaramuzza D. et al. [27] requires the camera to observe a planar pattern using different orientations without any prior knowledge of the camera motion or the sensor pattern. The main idea is the automatic search for pattern edges through an image projection function. The application has proven to be performant during calibration, easy to implement in a specific Matlab toolbox [28], and has been further improved by Rufly M. et al. [29]. However, in accord with Geiger et al. [30], one obstacle of this application is the specificity of omnidirectional optical cameras; moreover, the beforementioned applications require a reference pattern for each camera orientation. As an alternative, the same authors have developed a simplified approach where the only assumption is that the image sensors share a common image using the same intensity, depth and field of view.

The main objective of this work is to develop a robust methodology for the automatic alignment of multispectral images for real-time applications. It is a systematic approach that considers several distances from the target and applies corrective shifts to achieve accurate registration across bands. By comparing and evaluating the performance of different methods, the study aims to provide an effective solution for accurate image alignment, enabling reliable spectral analysis across multiple bands. In addition,

the research seeks to establish a framework that can be applied to remote sensing and agricultural monitoring, providing a valuable monitoring aid.

2 Materials and Methods

A multispectral camera (Micasense RedEdge M, s/n: RX01-1908138-SC, AgEagle Aerial Systems Inc., Wichita, Kansas, USA) has been used to collect multispectral images. The camera is capable of acquiring five spectral bands (Blue (**B**) (475 nm $\pm$ 20 nm), Green (**G**) (560 nm $\pm$ 20 nm), Red (**R**) (668 nm $\pm$ 10 nm), Rededge (**RE**) (717 nm $\pm$ 10 nm), NIR (**NR**) (840 nm $\pm$ 40 nm)), the image size is 2.5 MB per each band. The acquired band images are misaligned, in the sense that their pixels don't correspond to each other.

The misalignment requires that each band images must be shifted along the X and Y direction in order to correctly analyze each pixel spectral content.

The operation is performed considering an image band as the fixed or reference band and then moving the other image bands in order to guarantee a satisfying alignment for each pixel.

Unfortunately, the X and Y offset to be considered change with respect to both the considered band and the distance from the target.

To resolve this issue, the following steps have been considered.

The images have been taken from different distances from the target (11 selected distances, ranging from 500 mm to 1500 mm with a step of 100 mm). At each distance, the target has been positioned centred in axis with respect to the camera and moved (out of axis) left, right, inside and outside, taking an overall of five images for each distance from the target (Fig. 1).
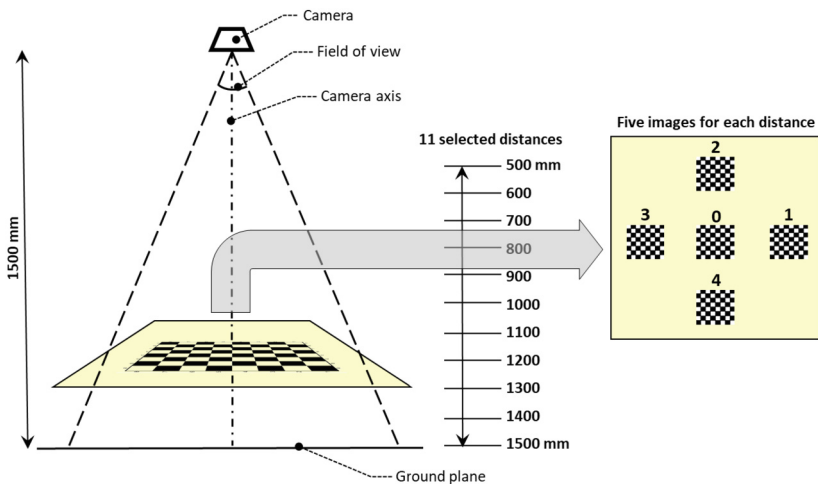
Fig. 1. Experimental design.

The target was constituted of a checkerboard pattern (9 rows × 7 columns), with squares of 35 mm, printed on an A3 sheet attached onto a rigid plywood sheet surface.

The checkerboard utilization arises from the alignment algorithm found in the **Image Processing Toolbox** of Matlab software. In particular, the function **detectCheckerboardPoints** allows for the measure of the points coordinates of a checkerboard pattern image based on the work of Geiger et al., 2012 [30].

The basic idea is very simple and refers to the class of so-called point-based methods.

Indeed, if a set of corresponding points pairs can be identified for a given set of image bands, then the alignment can be achieved by selecting some kind of transformation aligning these points. As these fiducial points must be reliable for the purposes of the alignment, they must have clearly identifiable features; therefore, the use of a checkerboard guarantees this characteristic. Indeed, the Matlab function **detectCheckerboardPoints** allows for the automatic identification of the checkerboard pattern fiducial points coordinates. The transformation must simply align the corresponding fiducial points for each image band.

Consequently, for each image band (at the same distance from the target) the detection algorithm is applied and, for each band, the algorithm outputs a series of 48 fiducial points (exactly where two black squares cross two white squares), an example is shown in Fig. 2.

Then, calculating the differences with reference to the image band considered as fixed (in our case, the Red band), 48 X offsets and 48 Y offsets are generated, the X offsets must be the same with low statistical noise, due to distortions induced by the lens, and the same must be valid for the Y offsets; thus, the average of these offsets, for each band, brings to the determination of the offsets that must be applied to align the bands along the X and Y dimensions.

The same happens when considering the images out of axis; even for these, the averaged X offsets and Y offsets are generated.
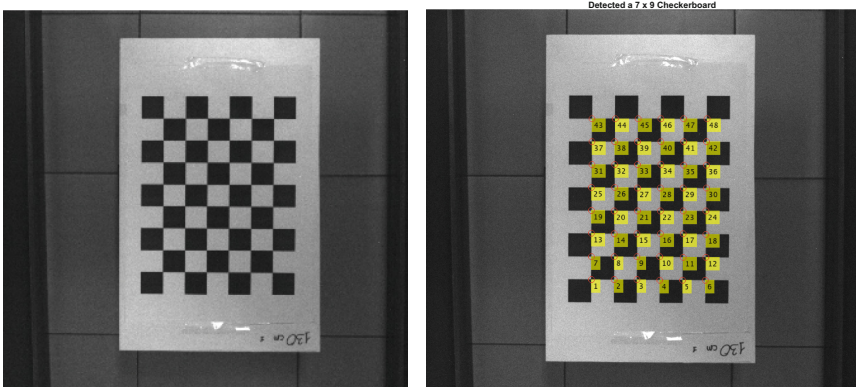
Fig. 2. Identification of the 48 points of the 9 × 7 checkerboard; the band B at 1300 mm distance (centred with the camera axis) is shown.

In addition, the offsets calculated for the five image bands at the same distance from the target must be the same, with only some statistical noise. Therefore, the final offsets that must be considered are the average of the offsets of the five image bands on the same plane (i.e. taken at the same distance). Indeed, as final result, the averaged offset is considered. However, these values are valid only for the considered distance.

Therefore, the previously exposed alignment method is repeated considering the images collected at different distances.

The described alignment method is a simple translation of the image bands.

The more general transformation to align two images (a moving image with reference to a fixed one) is an affine transformation. The affine transformation is a linear transformation preserving collinearity and ratios of distances. In general, an affine transformation is composed of four basic transformations, i.e. rotation, translation, dilation and shear. All these basic transformations are specified by 3×3 matrices in 2D space as the use of the augmented matrices technique allows for a simply matrix multiplication when composing the various listed basic transformations.

The **Image Processing Toolbox** of Matlab software contains a complete set of functions to handle this type of transformations. The preliminary calculation of the affine transformations on a series of test image bands confirmed that they are subject to translation only, with negligible rotation, dilation and shear.

The transformation matrices, related to each image band, depend on the distance from the target.

E.g., focusing on the X offset related to the Blue band (the fixed band is the Red), the data show how they change with respect to the distance from the target. These data have been successfully interpolated using as model the sum of two exponential functions: a*exp(b*distmm) + c*exp(d*distmm). Where a, b, c, d are parameters to be determined and distmm is the distance from the target in millimetres.

Because of this, the alignment procedure has been repeated at varying distances from the target in order to achieve a good modelling of the affine transformation matrices (Fig. 3).

Furthermore, considering the repetitive nature of the used checkerboard, the use of a bi-dimensional Fourier Transform has been positively tested. This algorithm arises from the work of Sicairos et al. [31]. In this case, for each image band, a single hot spot appears in the complex plane corresponding to checkerboard centre, and, therefore, a single offset value along the X and Y directions is generated, without the need to estimate the mean value on all the fiducial points as in the previous case of the checkerboard.

Therefore, two image alignment methods have been tested:

– **CB**: image band offsets measure based on the checkerboard method;
– **FT**: image band offsets measure based on the bi-dimensional Fourier transform.
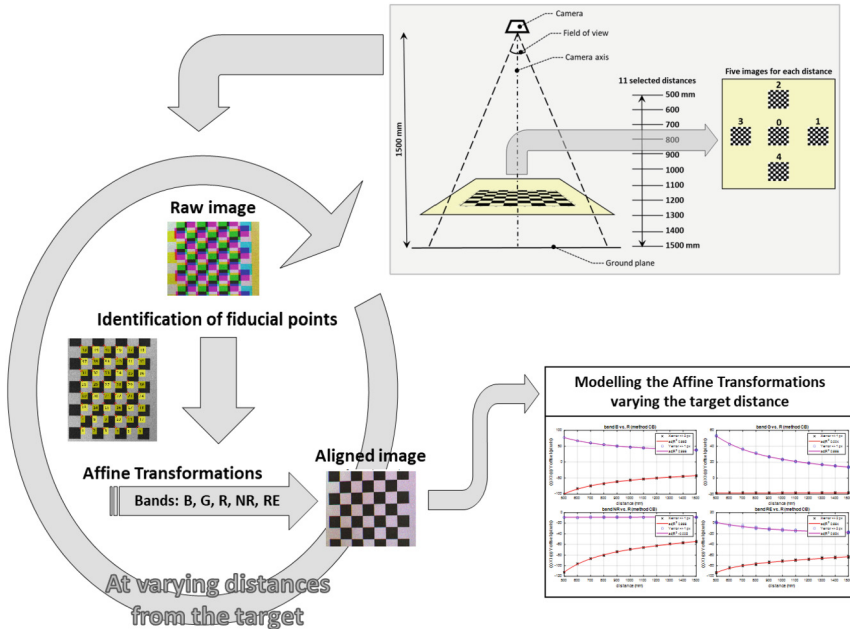
Fig. 3. The alignment procedure is repeated at varying distance from the target in order to achieve a good modelling of the affine transformation matrices.

3   Results and Discussion

Figure 4 shows the result of the obtained offsets with reference to R band, along X and Y directions, related, for simplicity, only to centred images, identified as 0 in Fig. 1, using the **CB** method. These offsets must be applied to B, G, NR and RE bands to align their pixels with those of the R band.

As it can see, the offset is changing with the target distance, however, the X offsets of G band and Y offsets of NR band are virtually constant with regard to the change in distance.

In addition, as the change occurring in offset mimic some kind of exponential curve, then, an exponential correlation has been investigated using the **Curve Fitting Toolbox** of Matlab software.

The best correlation with the experimental data is obtained using a sum of two exponential functions like the previously mentioned one: a*exp(b*distmm) + c*exp(d*distmm). Where a, b, c, d represent parameters to be determined and distmm is the distance from the target in millimetres.

This cannot be applied to X offsets of G band and Y offsets of NR band that, being virtually constant with regard to the change in distance, have been interpolated using a straight line (i.e. a degree 1 polynomial), so taking into account its mean value and the negligible slope value.

The performances of the correlation models, considering also the out of axis images, are reported in Table 1 for the **CB** method and in Table 2 for the **FT** method.
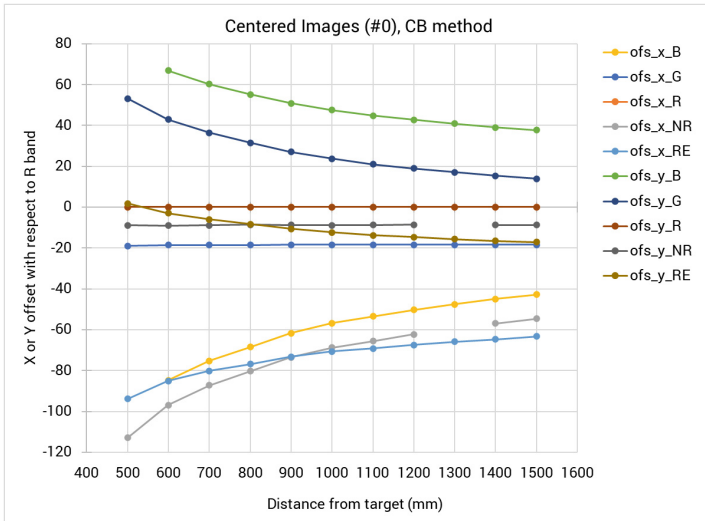
Fig. 4. Result of the offsets with respect to R band, along X and Y directions, considering the only the centred images, using the **CB** method.

In Fig. 5 are shown the results of the model interpolation of the experimental data when considering the offsets of B, G, NR, RE bands with reference to the R band, along X and Y directions, considering both the centred images and the four out of axis images, using the **CB** and **FT** method respectively.

The adjusted R^2 shows that the models reached a very high grade of correlation with the experimental data.

The Root Mean Square Error (RMSE) measures the error degree of the models. The value of 1.96*RMSE describes the error of the 95% confidence bounds for each model in terms of misaligned pixels. The error spans from ± 1 pixel to ± 2 pixels, to be noted that this error represents a very good result.

The presented results offer a comprehensive evaluation of correlation models employed in the alignment of spectral images using two distinct methods: the CB and FT method. For the CB method, the X offset models in the B vs. R and NR vs. R exhibit a robust fits, with an adjusted R^2 of approximately 0.995 and 0.998, respectively. This indicates that these models effectively account for a substantial portion of the data variability, supported by relatively low RMSE values. The Y offset models for both B vs. R and G vs. R demonstrate exceptional goodness of fit, boasting an adjusted R^2 of 0.996 and 0.998, respectively, demonstrating a high level of correlation and accuracy.

However, in the case of X offsets related to G vs. R, as expected, the linear model displays a weak correlation being the variables uncorrelated, implying that only a linear model can adequately capture the average value being the model slope negligible and showing, in addition, a relatively low RMSE. The same behavior is observed with regard to Y offsets related to NR vs. R, even here the linear model performs well showing a

Table 1. Performances of the correlation models, also considering the out of axis images, for the **CB** method. In round brackets are reported the 95% confidence bounds of the model parameters.

X offset MODEL, band B vs. R	Y offset MODEL, band B vs. R
y(x) = a*exp(b*x) + c*exp(d*x)	y(x) = a*exp(b*x) + c*exp(d*x)
a = −346.9 (−539.5, −154.2)	a = 167.7 (124.6, 210.8)
b = −0.004977 (−0.006446, −0.003508)	b = −0.003566 (−0.004493, −0.002639)
c = −91.79 (−105.1, −78.5)	c = 56.19 (44.69, 67.7)
d = −0.0005149 (−0.0006141, −0.0004157)	d = −0.0002801 (−0.0004056, −0.0001546)
adjrsquare: 0.9949	adjrsquare: 0.9963
rmse: 0.9700	rmse: 0.5802
X offset MODEL, band G vs. R	**Y offset MODEL, band G vs. R**
y(x) = p1*x + p2	y(x) = a*exp(b*x) + c*exp(d*x)
p1 = 0.0002558 (−0.0002205, 0.000732)	a = 170.3 (110.2, 230.4)
p2 = −18.78 (−19.31, −18.25)	b = −0.004385 (−0.005786, −0.002984)
	c = 53.46 (36.67, 70.25)
	d = −0.0009123 (−0.001114, −0.0007104)
adjrsquare: 0.0045	adjrsquare: 0.9979
rmse: 0.4669	rmse: 0.5155
X offset MODEL, band NR vs. R	**Y offset MODEL, band NR vs. R**
y(x) = a*exp(b*x) + c*exp(d*x)	y(x) = p1*x + p2
a = −340.3 (−449.9, −230.6)	p1 = 8.35e−05 (−0.0006478, 0.0008148)
b = −0.004872 (−0.005763, −0.003981)	p2 = −8.902 (−9.711, −8.093)
c = −101.4 (−109.5, −93.17)	
d = −0.0004169 (−0.0004719, −0.0003619)	
adjrsquare: 0.9982	adjrsquare: −0.0249
rmse: 0.6599	rmse: 0.6849
X offset MODEL, band RE vs. R	**Y offset MODEL, band RE vs. R**
y(x) = a*exp(b*x) + c*exp(d*x)	y(x) = a*exp(b*x) + c*exp(d*x)
a = −357.5 (−835.2, 120.2)	a = −12.96 (−26.53, 0.6019)
b = −0.006647 (−0.009726, −0.003569)	b = 0.0002194 (−0.0004157, 0.0008544)
c = −90.41 (−96.38, −84.45)	c = 71.81 (27.32, 116.3)
d = −0.00024 (−0.0002892, −0.0001907)	d = −0.003027 (−0.005457, −0.0005978)
adjrsquare: 0.9842	adjrsquare: 0.9539
rmse: 1.1065	rmse: 1.2363

Table 2. Performances of the correlation models, also considering the out of axis images, for the **FT** method. In round brackets are reported the 95% confidence bounds of the model parameters.

X offset MODEL, band B vs. R	Y offset MODEL, band B vs. R
y(x) = a*exp(b*x) + c*exp(d*x)	y(x) = a*exp(b*x) + c*exp(d*x)
a = −171.3 (−215.1, −127.6)	a = 122.5 (93.86, 151.2)
b = −0.002982 (−0.004305, −0.001658)	b = −0.002708 (−0.00408, −0.001336)
c = −67.72 (−97.91, −37.53)	c = 47.7 (22.28, 73.13)
d = −0.0003375 (−0.0005854, −8.958e−05)	d = −0.0001964 (−0.000485, 9.227e−05)
adjrsquare: 0.9967	adjrsquare: 0.9946
rmse: 0.7629	rmse: 0.6585
X offset MODEL, band G vs. R	**Y offset MODEL, band G vs. R**
y(x) = p1*x + p2	y(x) = a*exp(b*x) + c*exp(d*x)
p1 = 5.943e−05 (−0.0003575, 0.0004764)	a = 137.8 (83.93, 191.6)
p2 = −18.44 (−18.89, −17.98)	b = −0.004038 (−0.00575, −0.002326)
	c = 52.45 (30.15, 74.75)
	d = −0.0009115 (−0.001174, −0.000649)
adjrsquare: −0.0213	adjrsquare: 0.9964
rmse: 0.4079	rmse: 0.5644
X offset MODEL, band NR vs. R	**Y offset MODEL, band NR vs. R**
y(x) = a*exp(b*x) + c*exp(d*x)	y(x) = p1*x + p2
a = −165.6 (−186.2, −145.1)	p1 = −3.034e−05 (−0.0006243, 0.0005636)
b = −0.002514 (−0.003498, −0.00153)	p2 = −8.564 (−9.223, −7.904)
c = −65.5 (−95.2, −35.8)	
d = −0.0001637 (−0.0004024, 7.503e−05)	
adjrsquare: 0.9972	adjrsquare: −0.0411
rmse: 0.6949	rmse: 0.5691
X offset MODEL, band RE vs. R	**Y offset MODEL, band RE vs. R**
y(x) = a*exp(b*x) + c*exp(d*x)	y(x) = a*exp(b*x) + c*exp(d*x)
a = −78.29 (−109.4, −47.21)	a = −26.82 (−138.9, 85.23)
b = −0.002379 (−0.005748, 0.0009911)	b = −0.0001365 (−0.001952, 0.001679)
c = −68.19 (−118.3, −18.05)	c = 60.11 (−16.46, 136.7)
d = −7.048e−05 (−0.0004536, 0.0003127)	d = −0.001702 (−0.005504, 0.002099)
adjrsquare: 0.9659	adjrsquare: 0.9385
rmse: 1.2447	rmse: 1.2473

relatively low RMSE. With regard to RE vs. R comparison, both X and Y exponential correlation models present strong fit, showing their effectiveness in capturing a substantial portion of the data variability.
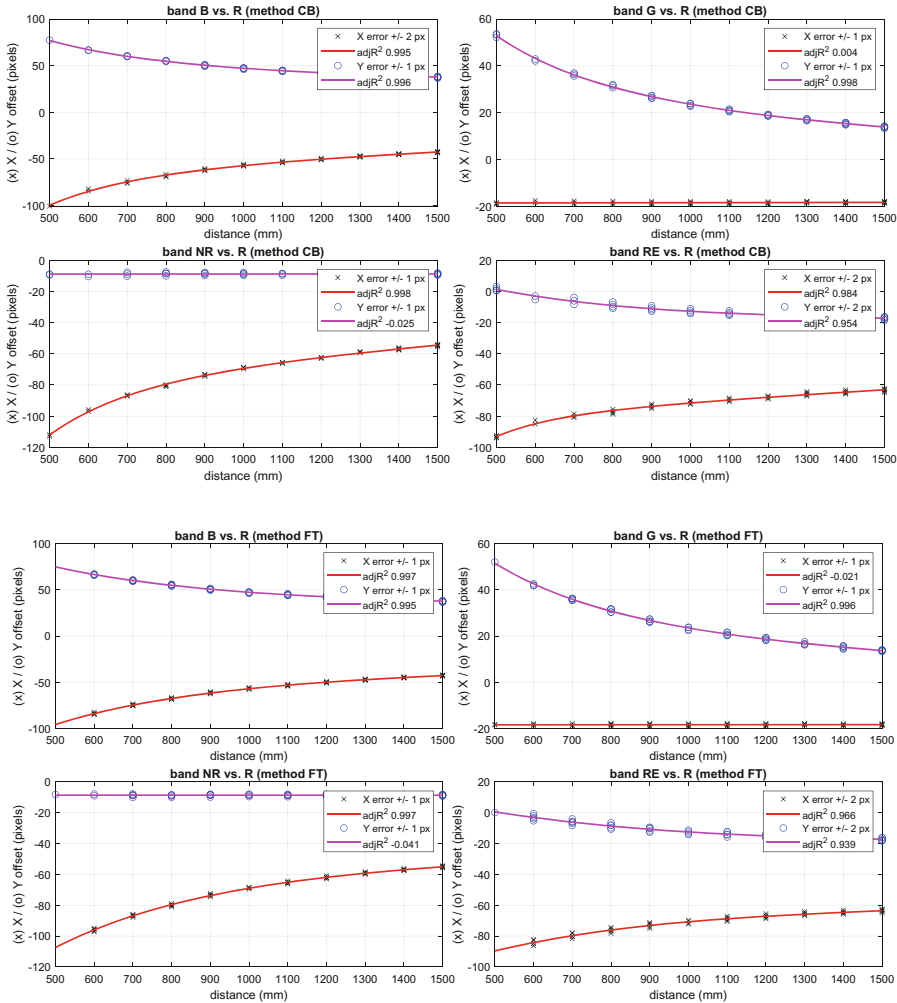
Fig. 5. Results of the model interpolation of the experimental data of the offsets of B, G, NR, RE bands with respect to the R band, along X and Y directions, considering both the centred images and the out of axis images, using the **CB** and **FT** method respectively.

Regarding to the FT method, the X offset models for B vs. R and NR vs. R comparisons similarly exhibit robust fit, showing an adjusted R^2 of 0.997. These models effectively explain a significant portion of the data variability with relatively low RMSE values. The Y offset models for B vs. R and G vs. R comparisons demonstrate high

adjusted R^2, exceeding 0.995 and 0.996, respectively. This emphasizes a strong degree of correlation and accuracy in these models.

However, in the case of X offsets related to G vs. R, the linear model displays a weak correlation, as expected, implying that only a linear model can adequately capture the average value, being the model slope negligible and showing a relatively low RMSE. The same happens for Y offsets related to NR vs. R. In the RE vs. R comparison, both X and Y exponential correlation models show a strong correlation fit.

Finally, the Fig. 6 shows the application of the two methods in order to align the raw spectral images at the distance of 1300 and 600 mm showing a very good achieved alignment.

Moreover, the extraction from image of well know spectral indices has been considered.

To this aim, the **Image Processing Toolbox Hyperspectral Imaging Library** has been considered for the calculation of some spectral indices (e.g. normalized difference vegetation index or NDVI) that subsequently have to be overlaid onto the aligned image in order to show useful information; this library is provided as a tools for the hyperspectral image processing and visualization, being an added value to the Image Processing Toolbox.
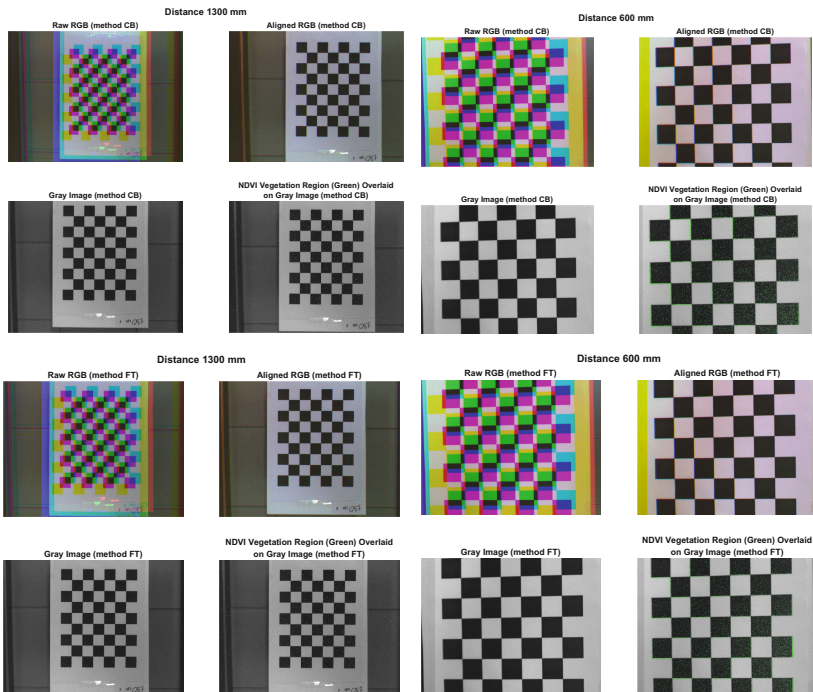
Fig. 6. Results of the models of interpolation applied to R, G, B bands of an image taken at a distance of 1300 and 600 mm from the camera, using the **CB** and **FT** method respectively. Moreover, the calculated NDVI index > 0.2 has been overlaid on the grey image with a green colour.

The library uses an HYPERCUBE object to make its calculations, being this constituted by the data cube of the image bands with added information regarding the bands centre wavelength value.

Considering the available bands in the images, the related spectral indices can be straightforwardly and effortlessly calculated by the Hyperspectral Imaging Library as reported in Fig. 7.

The available spectral indices are the following [32–34].

– Simple ratio (**SR**): that measures regions with green vegetation. A value greater than 3 indicates green vegetation.
– Normalized difference vegetation index (**NDVI**): that measures both the vegetation regions and the plant vigour. A value in the range of 0.2, 0.8 indicates vegetation presence.
– Enhanced vegetation index (**EVI**): this index measures the vegetation in regions with a high leaf area index. A value in the range of 0.2, 0.8 indicate a healthy vegetation.
– Optimized soil adjusted vegetation index (**OSAVI**): this index measures regions having sparse vegetation and high soil influence. A high value indicates a health and dense vegetation.
– Modified triangular vegetation index (**MTVI**): this index is used to estimate the leaf area. The calculation involves the determination of the area of a triangle in the spectral space connecting the minimum chlorophyll absorption, the near infrared edge, and the peak of the green reflectance.
– Modified chlorophyll absorption ratio index (**MCARI**): this index measures the relative abundance of chlorophyll being invariant with regard to both the illumination and the non-photosynthetic materials.
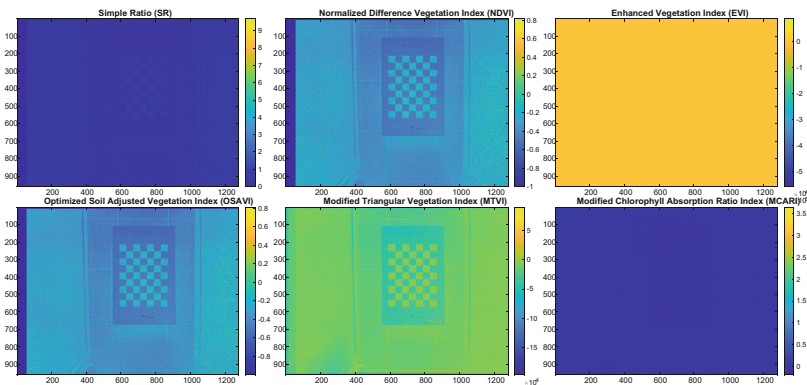
Fig. 7. Results of the calculation of some spectral indices on a test image taken from 1300 mm.

Finally, the setup methods have been used on images taken from lettuce plants (*Lactuga sativa L.*), also calculating NDVI and MCARI as spectral indices.

In Fig. 8 are shown the results of the alignment of images taken at a distance of 700 and 1400 on lettuce plants. After the alignment procedure, the NDVI [35] and MCARI

[36] indices have been calculated. These indices have been selected with regard to their current use in agriculture as methods of discrimination of the presence and vigour of the vegetation [23] and having the potential to identify the plant stress [37], respectively. They are shown overlaid as green colour on the grey scale image of the plants, after the choice of a threshold value of 0.40 and 17000 for NDVI and MCARI respectively. On three points (shown in Fig. 8), the chlorophyll content has been measured using an MC-100 Apogee Chlorophyll Meter (Apogee Instruments, Inc., 721 West 1800 North, Logan, Utah, 84321, USA). The measurement results were A $= 98.20$ umol.m^{-2}, B $= 32.50$ umol.m^{-2}, and C $= 5.30$ umol.m^{-2}, with 88.93 umol.m^{-2} as the mean value on the lettuce plants, as sampled on healthy (A and B) and diseased (C) leaves.
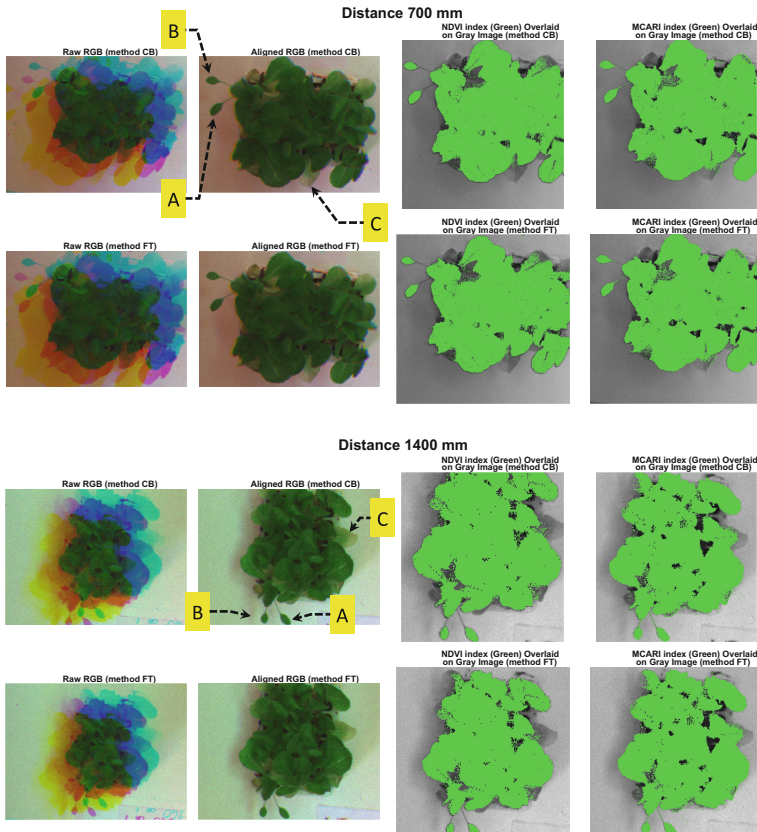
Fig. 8. Results of the alignment of images taken from 700 and 1400 distance on lettuce plants. The NDVI and MCARI indices have been calculated and shown overlaid (NDVI > 0.40, MCARI > 17000) as green colour on the grey scale image of the plants. On three points, the chlorophyll content has been measured using an Apogee Chlorophyll Meter (MC-100). (A $= 98.20$ umol.m^{-2}, B $= 32.50$ umol.m^{-2}, C $= 5.30$ umol.m^{-2}, being 88.93 umol.m^{-2} the mean value on the lettuce plants). Both alignment methods, at different distances, allow the NDVI index to correctly discriminate the not healthy C leaf.

Both alignment methods, CB and FT, at different distances, allowed the NDVI index to correctly discriminate the not healthy leaves.

In addition, it has been investigated the use of such two indices in order to identify problematic regions on the plant leaves.

To this aim, it has been used the logical Exclusive Or (XOR) between the logical matrices NDVI > 0.40 and MCARI > 17000 to identify a matrix logical mask showing regions with not healthy status but with some amount of chlorophyll content; this should identify the localization of the problematic regions belonging to the leaf.

The resulting logical mask matrix (UNHEALTHY) has been enhanced by erosion and dilation to reduce its false positive rate.

The image erosion was performed on the binary mask image using, as 2-D flat morphological structuring element, a disk-shaped element of size 2, then, an image dilation was performed on the previously eroded image with a disk-shaped element of size 3.

The Fig. 9 shows the results of such type of treatment carried out on the lettuce plants image from 700 mm distance.

The identification of the problematic regions is correctly handled, demonstrating how the considered spectral indices can be used for screening purposes.
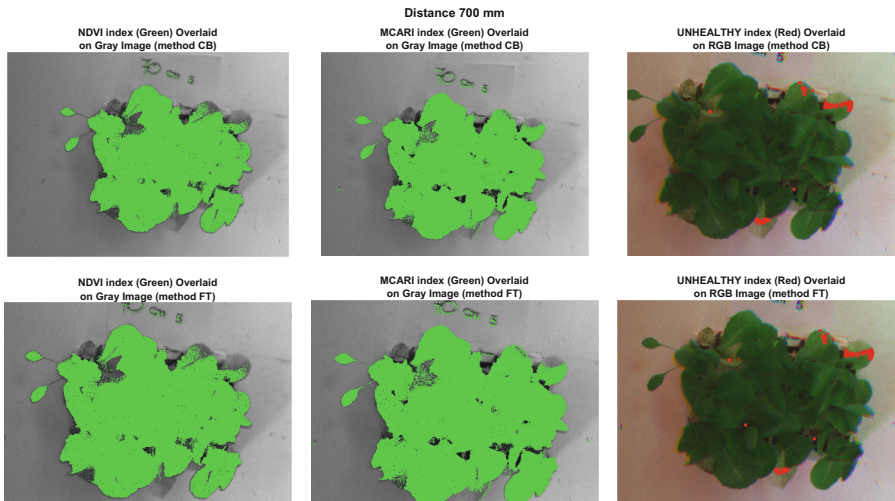
Fig. 9. Results of the calculation on images taken from 700 distance on lettuce plants. The NDVI and MCARI indices have been calculated and shown overlaid (NDVI > 0.40, MCARI > 17000) as green colour on the grey scale image of the plants. The UNHEALTHY mask has been overlaid in red colour on the RGB image of the lettuce plants. Both alignment methods, at different distances, allow the UNHEALTHY matrix logical mask to correctly identify the not healthy leaf regions.

4 Conclusions

In this study, an analysis of the offsets related to the alignment of multispectral images was conducted using two methodological approaches, CB and FT.

These were tested in both the X and Y directions with reference to the R-band of the images using the CB and FT method, focusing on centred and out-of-axis images. The investigation revealed interesting trends in offset variations as target distances varied. In particular, the G-band X offsets and the NR band Y offsets remained virtually constant regardless of distance variations. Comparatively, the FT method demonstrated correlation patterns with comparable performance to the CB method, especially in B vs. R and NR vs. A. Both methods provided valuable information for aligning spectral images, consistently achieving high R^2 values, demonstrating the effectiveness of the chosen modelling approaches.

To capture these trends, an exponential correlation model using the sum of two exponential functions was employed, resulting in a strong correlation with the experimental data. However, for the G-band X and NR-band Y offsets, which showed relative constancy, a linear interpolation method was applied. The performance of these correlation models has been rigorously evaluated, demonstrating their effectiveness even for out-of-axis images.

The practical application of these methods in aligning raw spectral images at varying distances has demonstrated good alignment accuracy. Furthermore, the study explored the extraction of spectral indices currently used in the literature, with the aim of extrapolating spectral information on vegetation and studying the relationship with respect to the alignment quality of the images obtained from the two methods studied.

In conclusion, this research has allowed to take a step forward in understanding the precise alignment of spectral images and the extraction of critical vegetation information. Although in its preliminary phase, this research establishes a basic framework for further applications in remote sensing and agricultural monitoring. The methodologies and results presented here promise an interesting resource for researchers and professionals in the field of multispectral imaging and data analysis.

Conflicts of Interest. The authors declare no conflict of interest.

References

1. Stafford JV (2000) Implementing precision agriculture in the 21st century. J Agric Eng Res 76(3):267–275
2. Saddik A, Latif R, El Ouardi A, Elhoseny M, Khelifi A (2022) Computer development based embedded systems in precision agriculture: tools and application. 72(1):589–611

3. Mahlein AK (2016) Plant disease detection by imaging sensors – parallels and specific demands for precision agriculture and plant phenotyping. Plant Disease. American Phytopathological Society

4. Xu J, Mishra P (2022) Combining deep learning with chemometrics when it is really needed: a case of real time object detection and spectral model application for spectral image processing. Anal Chim Acta 1202:339668

5. Omia E et al (2023) Remote sensing in field crop monitoring: a comprehensive review of sensor systems, data analyses and recent advances. Remote Sens 15(2):354

6. Yasir R, Eramian M, Stavness I, Shirtliffe S, Duddu H (2018) Data-driven multispectral image registration. In: Proceedings of 2018 15th conference on computer and robot vision, CRV 2018, pp 230–237

7. Mishra P, Asaari MSM, Herrero-Langreo A, Lohumi S, Diezma B, Scheunders P (2017) Close range hyperspectral imaging of plants: a review. Biosys Eng 164:49–67

8. Hassanpour M, Dadras Javan F, Azizi A (2019) Band to band registration of multi-spectral aerial imagery-relief displacement and miss-registration error. Int Arch Photogram Remote Sens Spat Inf Sci - ISPRS Arch 42(4/W18):467–474

9. Banerjee BP, Anuray S, Patrick R, Cullen J, Raval A, Cullen PJ (2018). Alignment of UAV-hyperspectral bands using keypoint descriptors in a spectrally complex environment. 9(6):524–533

10. Zhang A et al (2021) A handheld grassland vegetation monitoring system based on multispectral imaging. Agriculture 11(12):1262

11. Qin J, Chao K, Kim MS, Lu R, Burks TF (2013) Hyperspectral and multispectral imaging for evaluating food safety and quality. J Food Eng 118(2):157–171

12. Ren X, Sun M, Zhang X, Liu L (2017) A simplified method for UAV multispectral images mosaicking. Remote Sens 9(9):962

13. Hong G, Zhang Y (2007). Combination of feature-based and area-based image registration technique for high resolution remote sensing image. In: International geoscience and remote sensing symposium (IGARSS), pp 377–380

14. Zitová B, Flusser J (2003) Image registration methods: a survey. Image Vis Comput 21(11):977–1000

15. Feng R, Du Q, Li X, Shen H (2019) Robust registration for remote sensing images by combining and localizing feature- and area-based methods. ISPRS J Photogramm Remote Sens 151:15–26

16. Zhang X, Leng C, Hong Y, Pei Z, Cheng I, Basu A (2021) Multimodal remote sensing image registration methods and advancements: a survey. Remote Sens 13(24):5128

17. Firmenichy D, Brown M, Süsstrunk, S (2011) Multispectral interest points for RGB-NIR image registration, pp 181–184

18. Ron B, Ohad B-S, Yael E, Marko H (2014) Image registration for agricultural sensing tasks. cs.bgu.ac.ilB Ron, BS Ohad, E Yael, H Markocs.bgu.ac.il. Repéré à https://www.cs.bgu.ac.il/~obs/Publications/2014Berenstein_Ben_Shahar_Edan_Godesa_Hacevar-Image_Registration_for_Agriculture_Spraying_Tasks.pdf

19. Richter R, Kellenberger T, Kaufmann H (2009) Comparison of topographic correction methods. Remote Sens 1:184–196

20. Scaioni M, Barazzetti L, Gianinetto M (2018) Multi-image robust alignment of medium-resolution satellite imagery. Remote Sens 10(12):1969

21. Syrris V, Ferri S, Ehrlich D, Pesaresi M (2015) Image enhancement and feature extraction based on low-resolution satellite data. IEEE J Sel Top Appl Earth Obs Remote Sens 8:1986–1995

22. Krus A, Valero C, Ramirez J, Cruz C, Barrientos A, del Cerro J (2021) Distortion and mosaicking of close-up multi-spectral images. In: Precision agriculture 2021, pp. 33–46

23. Zhang Z (2000) A flexible new technique for camera calibration. IEEE Trans Pattern Anal Mach Intell 22(11):1330–1334
24. Heikkila J, Silven O (1997) A four-step camera calibration procedure with implicit image correction. In: IEEE international conference on computer vision and pattern recognition
25. Bouguet JY. Camera calibration toolbox for matlab. Computational Vision at the California Institute of Technology
26. Bradski G, Kaehler A (2008) Learning OpenCV: computer vision with the OpenCV library. O'Reilly, Sebastopol
27. Scaramuzza D, Martinelli A, Siegwart R (2006) A flexible technique for accurate omnidirectional camera calibration and structure from motion. In: Proceedings of IEEE international conference of vision systems (ICVS 2006), New York, 5–7 January
28. Scaramuzza D, Martinelli A, Siegwart R (2006) A toolbox for easy calibrating omnidirectional cameras. In: Proceedings to IEEE international conference on intelligent robots and systems (IROS 2006), Beijing China, 7–15 October
29. Rufli M, Scaramuzza D, Siegwart R (2008) Automatic detection of checkerboards on blurred and distorted images. In: Proceedings of the IEEE/RSJ international conference on intelligent robots and systems (IROS 2008), Nice, France, 22–26 September
30. Geiger A, Moosmann F, Car Ö, Schuster B (2012) Automatic camera and range sensor calibration using a single shot. In: Proceedings - IEEE international conference on robotics and automation, pp 3936–3943
31. Guizar-Sicairos M, Thurman ST, Fienup JR (2008) Efficient subpixel image registration algorithms. Opt Lett 33(2):156
32. Haboudane D, Miller JR, Pattey E, Zarco-Tejada PJ, Strachan IB (2004) Hyperspectral vegetation indices and novel algorithms for predicting green LAI of crop canopies: modeling and validation in the context of precision agriculture. Remote Sens Environ 90(3):337–352
33. Bannari A, Morin D, Bonn F, Huete AR (1995) A review of vegetation indices. Remote Sens Rev 13(1–2):95–120
34. Xue J, Su B (2017) Significant remote sensing vegetation indices: a review of developments and applications. J Sens 2017:1–17
35. Schell JA (1973) Monitoring vegetation systems in the great plains with ERTS. NASA Spec. Publ. 351:309
36. Daughtry CS, Walthall CL, Kim MS, De Colstoun EB, McMurtrey Iii JE (2000) Estimating corn leaf chlorophyll concentration from leaf and canopy reflectance. Remote Sens Environ 74:229–239
37. Zhang D, Wang Q, Lin F, Yin X, Gu C, Qiao H (2020) Development and evaluation of a new spectral disease index to detect wheat fusarium head blight using hyperspectral imaging. Sensors (Basel) 20(8):2260

Farm Management, Ergonomics, System Engineering, Health and Safety in Agriculture

Analysis of Factors Affecting Farmers' Intention to Use Autonomous Ground Vehicles

Johnny Waked[1], Gabriele Sara[1](✉) , Giuseppe Todde[1] , Daniele Pinna[1] ,
Georges Hassoun[2], and Maria Caria[1]

[1] Department of Agricultural Sciences, University of Sassari, Viale Italia 39A,
07100 Sassari, Italy
gsara@uniss.it

[2] Environmental and Natural Resources Department, Lebanese University, Dekwaneh, Lebanon

Abstract. In recent years, new autonomous ground vehicles (AGV) have been developed for the agricultural context to assist farmers and automate agricultural processes. Although there has been a high advancement in the development of AGV, this technology is not yet widely used on farms. Several factors may affect farmers' willingness to adopt an autonomous ground vehicle. Therefore, this study aims to investigate the factors that influence farmers' intentions to use AGV in agricultural activities. Based on previous studies that examine technology acceptance in the agricultural context, a model was developed. Based on Technology Acceptance Model (TAM) an extended version of the TAM was used including the Attitude of Confidence, Personal Innovativeness, Job Relevance, and Perceived Net Benefit. Sixty-eight farmers form various countries, mainly from Lebanon and Italy, completed a questionnaire to assess their intention to use AGV. Survey's answers were analyzed using partial least square structural equation modeling. The results of the measurement model indicated that all variables were valid except for the attitude of confidence. The structural analysis showed that personal innovativeness had a positive effect on perceived ease of use, while job relevance and perceived ease of use had a positive effect on perceived usefulness, which positively influenced attitude toward using AGV and perceived net benefit. It was also found that attitude and perceived net benefit had a positive effect on the farmers' intention to use AGV for field activities. Finally, the model outcomes underlined that neither farm size nor farmers' education level had any influence on their intention to use AGV in agriculture.

Keywords: Unmanned ground vehicles · Technology acceptance model · Robot · Agriculture · Agricultural robot · PLS-SEM

1   Introduction

In the twenty-first century, one of the significant challenges that humanity faces is to meet the rising demand for food while reducing wasted resources. Between 2005 and 2050 the worldwide food demand is expected to augment between 60 and 110%, meaning that there is a crucial need to adopt and apply precision agriculture management

techniques [1]. Agriculture is one of the main factors in reducing poverty and helps improve food security for around 80% of the world's impoverished people living in rural areas [2]. A crucial component of agriculture is irrigation water, which plays a vital role, especially in arid and semi-arid regions. Unfortunately, its availability is dwindling mainly because of population growth and climate change [2, 3]. Globally, around 70% of the total fresh-water resources are used in the agricultural sector [4] where irrigation has a share of 85% of the total water used in agriculture, generating about 40% of the total food production [1]. In addition to irrigation, fertilizer application can significantly increase crop yield, but it may also cause environmental pollution and soil hardening [5, 6]. Moreover, there is a global decline in arable-cultivated lands and a shortage of water resources. Therefore, optimizing fertilizer and irrigation strategies would help crop yield as well as save resources, reducing production costs, and protecting the environment. Precision agriculture (PA), also known as information-based management of agricultural production systems, was introduced in the mid-1980s to provide appropriate treatment at the right time [7]. PA is an agricultural management approach based on the collection, processing, and analysis of individual data to support management decisions on estimated variability. It enables farmers to make specific management decisions in both time and space to improve resource use efficiency, productivity, quality, profitability, and sustainability of agricultural production [8]. PA aims to reduce production inputs used in agriculture while improving overall the quality and quantity of agricultural productivity [7, 9].

Recently, new autonomous ground vehicles (AGV) have been developed for the agricultural context to assist farmers and automate agricultural processes. An AGV, also known as unmanned ground vehicle (UGV), is an autonomous or semi-autonomous terrestrial vehicle capable of performing specific operations supported by the RTK-GPS system that allows autonomous navigation in the field. Different vehicles have been developed with different dimensions, i.e., compact vehicles or large tractors, and different operating capabilities, i.e., towing implements, tilling, weeding, or spraying thanks to the implemented tools. Agricultural machinery manufacturers are developing a wide range of AGVs moving towards the use of electric engines and high-efficiency machines. In addition, the AGV market can be segmented based on various criteria including size, locomotion system, and purpose of use. UGVs can be used for several agricultural and farming practices, ranging from pruning, inspection, and disease detection to precise spraying of fertilizers, pesticides, and insecticides [10, 11]. Other activities that could be accomplished with the use of UGVs are cutting fruits [12], mowing [13], field scouting, weed control, harvesting [14], mapping, collecting soil and crop samples [15], monitoring animals [16, 17] and irrigation [18]. AGVs are promising technologies that could mark new agriculture characterized by automatic and autonomous systems. UGVs have the potential to provide a more sustainable agricultural production, which could aid in addressing the current challenges in agriculture. Although there has been a high advancement of AGV also for the agricultural context, this technology is not yet widespread on farms. In addition, several factors may affect farmers' willingness to adopt an autonomous ground vehicle.

Therefore, this study aimed to investigate the factors that influence farmers' intentions to use AGVs in agricultural activities by using an extended Technology Acceptance

Model (TAM) framework. Several studies are found related to the application of TAM for evaluating farmers' acceptance intention of specific smart technologies or precision agriculture technologies [19–21]. However, a limited number of studies have focused on the acceptance of unmanned ground vehicles in agriculture [22].

2   Technology Acceptance Model (TAM) Theoretical Background and Hypotheses

A model for technology acceptance was developed by Fred Davis in 1985 to explain the relationship between user motivation and actual system use. The model suggests that the user's motivation to use the system is influenced by an external motivation that includes the features and capabilities of the actual system. Davis also extended the model (Technology Acceptance Model) to include three motivation factors that are depicted in Fig. 1: Perceived Usefulness (PU), Perceived Ease of Use (PEOU), and attitude toward using [23].
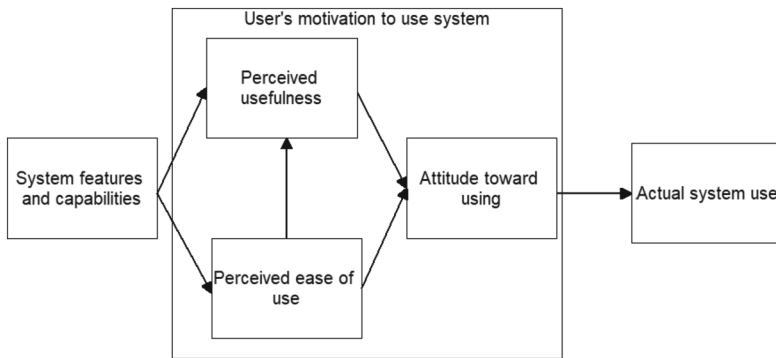
Fig. 1. Conceptual model for technology acceptance including TAM [20] (modified by the authors).

According to Davis [24], PU is defined as the extent to which a user believes that using the system will enhance job performance, while PEOU is described as the degree to which a user perceives that using the system is effortless. Both factors affect the user's attitude towards the system, which is a crucial element in determining whether the system will be accepted or rejected.

The TAM structure asserts that these factors determine a person's intention to use technology and, finally, the actual adoption. In addition, a system that is high in PU can lead the user to believe in the existence of a positive use-performance relationship [24]. Moreover, Adrian et al. [21], studied the influence of farmers' perceptions adopting precision agriculture technologies using this method. According to TAM a potential user is more probably to use a certain technology if he or she perceives it as useful [21]. Therefore, to analyze these aspects the following hypotheses were proposed:

H1: Perceived usefulness will influence the intentions to implement and use UGVs.

H2: Perceived usefulness will influence the attitude toward using UGVs in agriculture.

According to Davis in 1989 [24], if users don't realize an application that would fairly improve performance, they're not likely to use it, whereas Michels et al. [25] explained that a person who recognizes using technology as effortless also recognizes the technology as more helpful. As suggested by the TAM model, a farmer who sees using UGVs as simple has a higher intent to use it for agricultural practices. Additionally, if the farmer feels that the information given by the UGVs is helpful for the on-farm operations, there will be a higher intention for him or her to use an UGV. Furthermore, if a farmer believes that utilizing an UGV is simple, he or she also sees this tool as more helpful. Davis [24] also found mild proof that the PEOU could impact the intention to use (ITU) a technology through perceived usefulness. The following hypothesis were proposed evaluating that:

H3: Perceived ease of use will impact the perceived usefulness of UGVs.
H4: Perceived ease of use will affect attitude toward using UGVs in agriculture.

As already stated, as easily as the user finds the technology to use, he or she will find it useful and will most probably adopt it [21]. Meanwhile, ATU of a technology is a construct used in research for the measure of the positive or negative feelings of a certain user about the application of the target behavior. Attitude outlines a user's behavioral intention to use technology [26]. This is analyzed by the following hypothesis:

H5: Attitude toward using will influence the intention to use (ITU) and adopt UGVs, respectively.

In 2005, Adrian et al. [21] added a latent variable called attitude of confidence (AOC) in the extended TAM for adopting precision agriculture technologies. This variable was placed as "Precision agriculture technologies provide a vast amount of information and require new skills in using information systems" [21, 25]. The farmer to use this information must acquire new skills, therefore the latent variable "confidence subscale" measures "the confidence of a producer to learn and use precision agriculture technologies" [21, 25]. Experimental findings have demonstrated that the AOC, particularly the person's attitude to having the ability to use and learn technology, affects the perceived ease of use [21]. In addition, AGV provides large amounts of information for the farmers; to collect and use this information efficiently, the farmer requires new skills, like transforming the online data into maps to guide specific fertilizer applications. Thus, a positive effect of the AOC on the ITU of AGV, and PEOU is considered [25] and it was evaluated in this study by following proposed hypotheses:

H6: Attitude of confidence in using UGVs in agriculture has a positive effect on the perceived ease of use of UGVs.
H7: Individuals' attitude of confidence toward learning and using UGVs will affect their perception of the usefulness of these tools.
H8: Attitude of confidence in using UGVs in agriculture has a positive effect on the intention to use UGVs in agriculture.

Job relevance (JR) is the degree to which the technology applies to the user's job [23, 27]. A farmer may see that the UGV fits the tasks within the farm, he or she will see the

UGV as more useful and later will have a higher intention to use it [25]. Consequently, the subsequent hypotheses are investigated in this study:

H9: Job relevance of UGVs in agricultural activities has a positive effect on the perceived usefulness.
H10: Job relevance of UGVs in farming or agriculture has a positive effect on the intention to use and implement UGVs.

Adopting precision agriculture shows that some demographic factors could affect the adoption of the technologies and the technology profitability including tenure, location, farm size, age, farming experience, education, access to information, off-farm occupation, credit, and cultivated crops [21, 28]. Education level (El) affects the adoption of the technology, the highest the educational level is, the earliest technology is adopted. Among adopters, computer use is common due to higher educational degrees. While an increasing age lowers the probability of adopting technology because of factors fundamental to the aging process or the lowered probability of payback from a reduced planning perspective over which projected benefits can accumulate [28, 29]. Thus, this study analyzed the following hypothesis:

H11: Education level will affect the intentions to adopt UGVs.

Moreover, farm size (Fs) plays a crucial role in adopting farming technologies as AGV [29]. In fact, applying AGV needs a large investment in time, capital, and the learning process. This investment requires costs in transactions and information which will prevent small farms from investing in these technologies. Thus, this study analyzed the following hypothesis:

H12: Farm size will impact the intention to adopt UGVs.

Perceived net benefit (PNB) is the user's belief that the technology will offer him or her a benefit of more value than its cost. Within our study, this factor included the advantage of using AGV over current traditional practices considering the economic cost involved in implementing and adopting the technologies. Within the questionnaire, five items included the benefits of AGV: increased profits, increased yields, the cost-effectiveness of AGV, reduced costs, and information for more adequate decisions [21]. A farmer who perceives the potential net benefits when using AGV will more likely adopt them rather than a farmer who does not perceive the net benefit of these technologies. PNB is directly affected by perceived usefulness because PNB includes intrinsic usefulness [21]. Therefore, the subsequent hypotheses are investigated in this study:

H13: Perceived usefulness will affect the perceived net benefit of UGVs.
H14: Perceived net benefit will affect the intentions to use and adopt UGVs.

Personal innovativeness (PI) is a factor that describes the interest or willingness of a person to try new technology and determines a positive influence of the innovativeness of farmers to accept AGV postulated in hypotheses H15 and H16 as shown in Fig. 2. It is also hypothesized that personal innovativeness influences factors related to the farm where the farmer works or to the farmer himself [30]. These aspects, are analyzed in this study by the following proposed hypotheses:

H15: Farmer's personal innovativeness influences positively the perceived usefulness of UGVs.

H16: Farmer's personal innovativeness influences positively the perceived ease of use of UGVs.

Figure 2 allows us to better comprehend the adjustments and extensions made to the basic TAM along with the additional variables: personal innovativeness, attitude of confidence, job relevance, educational level, and farm size.
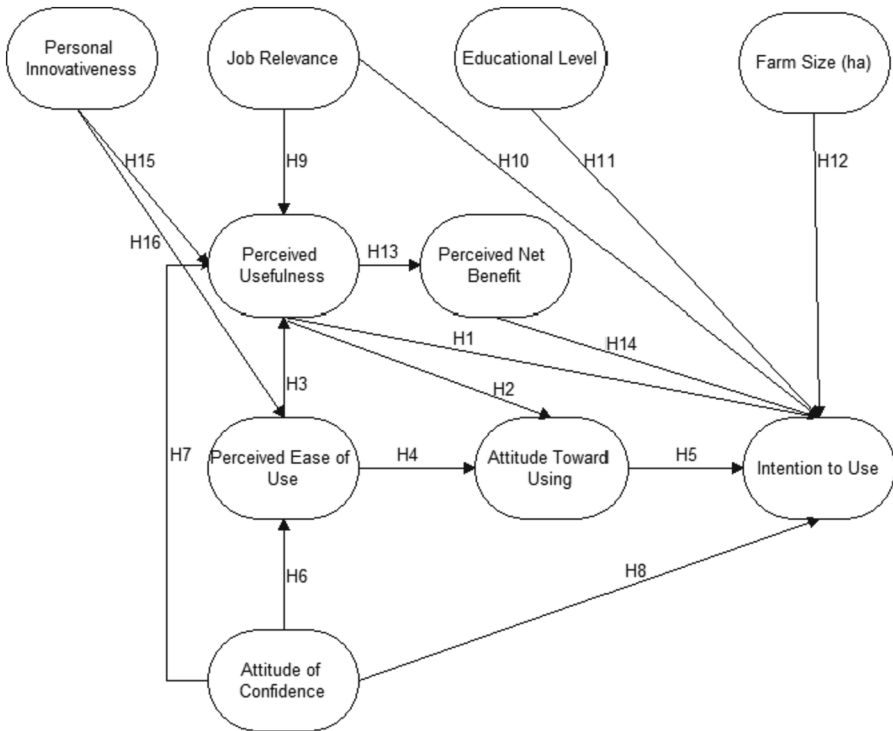

Fig. 2. Illustration of the proposed research model for UGVs' acceptance by the farmers. H1, H2… Hx = hypothesis to test.

3   Material and Methods

3.1   Survey Design and Analysis

This study involved a total of 68 farmers from different countries that answered to the submitted questionnaire. The first part of the survey concerns general questions, where the farmer provides sociodemographic (i.e., age, gender, education level) and farm-related information, i.e., size of the farm (ha), type tractors used, and type of farm (arable farm, hay farm, orchard). Then, in the second section of the questionnaire the

farmers were asked to assess 31 randomized statements (items) for the estimation of the extended TAM. The items serve as the indicators to estimate the corresponding latent variables and were measured by using a five-point Likert scale (1 = strongly disagree; 2 = disagree; 3 = neutral; 4 = agree; and 5 = strongly agree). To guarantee a reliable knowledge base about UGVs among the participating farmers, a one-minute, educational video on how UGVs work, and the probable extent of application were presented at the start of the questionnaire. All the items considered in this study were identified from proper literature and adjusted to match the context of this study about the use of autonomous ground vehicles in agriculture. The items used in the survey to assess the variables are presented in Table 1.

The questionnaire was originally developed in English and then translated into Italian and Arabic to spread out the sample of this survey. Moreover, before diffusing the questionnaire, it was pretested and implemented using Google Forms. For recruiting participants, several channels were used, such as e-mailing several farmers' associations and publishing the survey's link on the social media pages of many agricultural-related groups, alongside private contacts. To have complete-answered surveys, key questions have been set as mandatory, therefore there would be no incomplete datasets.

3.2 Statistical Data Analysis and Quality Criteria

The data collected with the questionnaires were analyzed using the partial least square-structural equation modeling (PLS-SEM) technique. PLS-SEM includes different multivariate statistical methods (factor analysis, multiple regression) that allow simultaneous inspection of the relationship between observed variables and latent variables as well as among latent variables. PLS-SEM is a nonparametric variance-based SEM that was selected since is less restrictive than other approaches which require normally distributed data and perform well also with a small sample size.

The model was analyzed using a two-step approach. First, the measurement model was inspected to test the relationship between the items and the latent variable. The quality criteria of the model considered were standardized factor loading (FL), average variance extracted (AVE), composite reliability (CR), and Cronbach's alfa. These quality criteria must accomplish a specific threshold that for FL, CR, and Cronbach's alfa is greater than 0.7, whereas AVE must be greater than 0.5 [31, 32]. In addition, the discriminant validity (DV), which indicates how different latent variables are from another one, was determined using the Fornell-Larcker criterion [33]. In the second step, the structural model was evaluated to test and determine the causal relationship between the latent variables. The developed model was tested by using standardized path coefficient (β) and t-statistics. The relevance and significance of the indicators are validated using a bootstrapping procedure with 5,000 subsamples. The "SEMinR" package in R software was used to perform the analysis.

3.3 Measures

The scale was developed from the literature review and previous studies. Table 1 presents the indicators correlated with the model constructs.

Table 1. References and indicators used.

Item	Statement	Reference
Factor "Perceived usefulness of UGVs in agriculture" (PU)		
Pu1	I think that with the help of UGVs, I will contribute to environmental protection with a more targeted application of fertilizer and pesticides and reduce production costs	[25, 34]
Pu2	I think using the UGVs, will increase on-farm productivity and income	[25, 35]
Pu3	Using the UGVs would enhance effectiveness on the on-farm job (mowing, tilling, spraying, and monitoring)	[36]
Pu4	Using the UGV would make it easier to do my on-farm job (mowing, tilling, spraying, and monitoring)	[25]
Pu5	I would find the UGV helpful in my on-farm job (mowing, tilling, spraying, and monitoring)	[25]
Factor "Perceived ease of use of UGVs in agriculture" (PEOU)		
Peou1	I think learning to use UGVs would be easy for me (piloting with remote control, setting autonomous mode, and using implements like a mower and tiller)	[25]
Peou2	I would find it easy to get the UGV to do what I want it to do (piloting with remote control, setting autonomous mode, and using implements like a mower and tiller)	[36]
Peou3	It would be easy for me to become skillful at using the UGV to perform specific on-field activities (mowing, tilling, spraying, and monitoring)	[36]
Peou4	I would find the UGV easy to use (piloting with remote control, setting autonomous mode, and using implements like a mower and tiller)	[36]
Peou5	Using UGVs (piloting with remote control, setting autonomous mode, and using attachments like a mower and tiller) seems understandable to me	[25]
Peou6	Learning to use UGVs (piloting with remote control, set autonomous mode, using attachments like a mower and tiller) is no problem for me	[25]
Factor "Attitude of confidence in using UGVs in agriculture" (AOC)		
Aoc1	I think I am not the type of farmer who is good at working with UGVs and other digital instruments	[25]
Aoc2	I don't think I would use UGVs since their use seems too complicated for me	[25]
Aoc3	I am no good with new technologies in precision agriculture	[21]
Factor "Job relevance of UGVs in agriculture" (JR)		
Jr1	Usage of UGVs is of high relevance for several operational procedures on my farm and field	[25]
Jr2	Usage of UGVs is important for my on-farm job	[25]

(*continued*)

Table 1. (*continued*)

Item	Statement	Reference
Jr3	Usage of UGVs is appropriate for my on-farm job and for my security	[37]
Intention to use UGVs in agriculture (ITU)		
Itu1	Assuming I have a UGV and the relative implements, I intend to use them for spraying, mowing, tilling and monitoring	[27]
Itu2	I will always try to use a UGV within my farm and/or field	[35]
Itu3	If I have a UGV, I will use it more often	[35]
Factor "Attitude toward using UGVs in agriculture" (ATU)		
Atu1	Using the UGV for mowing, tilling, spraying, and monitoring is a good idea	[36]
Atu2	The UGV makes work more interesting	[36]
Atu3	I would like to work with the UGV for mowing, tilling, spraying, and monitoring	[36]
Factor "Perceived net benefit of UGVs in agriculture" (PNB)		
Pnb1	I believe the use of UGVs can increase profits	[21]
Pnb2	I believe the use of UGVs can increase yields	[21]
Pnb3	I believe UGVs can provide information for better decision-making	[21]
Pnb4	I believe UGVs are cost-effective	[21]
Pnb5	I believe the use of UGVs can reduce production costs	[21]
Factor "Personal innovativeness of UGVs in agriculture" (PI)		
Pi1	I think I would like to explore on-field applications with the UGV (mowing, tilling, spraying, and monitoring)	[30]
Pi2	I enjoy being around people who are using and exploring new agricultural technologies like the UGV	[30]
Pi3	I often seek information on new agricultural technologies like the UGV	[30]

4   Results

4.1   Sample Description and Descriptive Results

The study had 68 participants, of whom 75% were male and 25% were female: most of them were from Lebanon 67% and the rest are from Italy, India, Iran, Jordan, Kenya, Kyrgyzstan, Pakistan, Palestine, South Africa, Trinidad and Tobago, Turkey, Uganda, and the United States of America. The average age range was 25–34 years (29%) followed by 35–44 years (28%), and 39% of the participants had a college degree. More than half of the applicants (52%) run a farm with a surface of less than five hectares of arable land, 42% of crops like wheat or vegetables, and 33% of fruit- or nut-producing trees. Only 12% of the participants don't use a tractor for earthworks, while 25% of the participants use utility tractors and 19% a two-wheel tractor.

4.2   Measurement Model Analysis

Before performing measurement model estimation, the multivariate normality distribution of the data was checked by computing multivariate skewness and kurtosis coefficients, which indicate the nonnormal distribution of the data. Therefore, considering the reduced sample size of the study and the nonnormality of the data a PLS-SEM technique was used. The results are evaluated using the two steps approach. The first step was measurement model testing to assess the relationship between the observed variables (items) and the corresponding latent variables (factors). In addition, convergent validity and internal consistency were evaluated by computing Cronbach's alfa, composite reliability (CR), and average variance extracted (AVE).

After the preliminary estimation of the measurement model, the items with a factor loading lower than 0.7 were removed (Pu1, Pu5, Peou1, Peou2, Pnb1, Pnb3, Aoc2, Aoc3) as these items' results were not enough correlated with the corresponding latent variables. Moreover, the AOC Cronbach's alfa resulted under the 0.7 threshold, thus this factor is removed from the model. The measurement model analysis, without low-loading items and AOC construct, was performed again and the descriptive statistics for items and factors are reported in Table 2. The mean value for the overall constructs is 4.01, which indicates that the respondent positively perceived the use of AGV for agricultural on-field activities.

Table 2. Measurement model analysis with reliability and validity index for items and constructs. Descriptive statistics with mean and standard deviation (SD) are reported for each item.

Construct/Item	Mean	Loadings[a]	Cronbah's alfa	CR[b]	AVE[c]
Perceived usefulness (PU)			0.873	0.922	0.798
Pu2	4.162	0.860			
Pu3	4.412	0.891			
Pu4	4.206	0.928			
Perceived ease of use (PEOU)			0.881	0.918	0.738
Peou2	4.088	0.906			
Peou3	4.309	0.817			
Peou4	4.176	0.862			
Peou5	4.088	0.848			
Job relevance (JR)			0.785	0.870	0.691
Jr1	3.985	0.830			
Jr2	3.471	0.834			
Jr3	3.471	0.829			
Attitude toward using (ATU)			0.835	0.901	0.752
Atu1	3.471	0.866			

(*continued*)

Table 2. (*continued*)

Construct/Item	Mean	Loadings[a]	Cronbah's alfa	CR[b]	AVE[c]
Atu2	3.471	0.838			
Atu3	3.985	0.896			
Perceived net benefit (PNB)			0.834	0.900	0.751
Pnb2	4.029	0.882			
Pnb4	3.941	0.862			
Pnb5	4.044	0.855			
Personal innovativeness (PI)			0.739	0.851	0.656
Pi1	4.250	0.843			
Pi2	4.338	0.809			
Pi3	3.971	0.775			
Intention to use (ITU)			0.825	0.895	0.741
Itu1	4.206	0.854			
Itu2	3.926	0.896			
Itu3	4.250	0.832			

[a]Standardized factor loadings
[b]Composite reliability
[c]Average variance extracted

Considering the readability and validity of the new measurement model (Table 2), all standardized factor loadings were higher than 0.7 and significant ($p < 0.001$), indicating a high correlation between items predicting the corresponding construct. Moreover, Cronbach's alfa, CR, and AVE of each construct were higher than the indicated thresholds, further confirming satisfactory convergent validity and internal consistency [31, 32]. The results of the discriminant validity are reported in Table 3 where no issues were observed among factors as the square root of AVE always exceeds the correlation between factors.

4.3   Structural Model Analysis

The structural model analysis allows for the investigation of the relationship among latent variables (constructs) of the model by estimating expected directional associations among variables. The summary of the hypothesis testing results was reported in Table 4, whereas the analysis of the relationship between the constructs is shown in Fig. 3, reporting standardized parameter estimates for the path coefficients and the statistical significance of each hypothesized path.

Table 3. Discriminant validity result considering the Fornell–Larcker criterion. The square roots of AVE are on the diagonal values (bold) and the correlation is on the off-diagonal values.

	PU	PEOU	ATU	PNB	JR	PI	ITU
PU	**0.893**						
PEOU	0.698	**0.859**					
ATU	0.842	0.672	**0.867**				
PNB	0.762	0.545	0.833	**0.866**			
JR	0.623	0.422	0.671	0.654	**0.831**		
PI	0.665	0.704	0.796	0.711	0.674	**0.810**	
ITU	0.749	0.623	0.853	0.821	0.708	0.777	**0.861**

Table 4. Results from the structural model.

Hypothesis	Results
H1: Perceived usefulness → Intention to use	not supported
H2: Perceived usefulness → Attitude toward using	supported
H3: Perceived ease of use → Perceived usefulness	supported
H4: Perceived ease of use → Attitude toward using	not supported
H5: Attitude toward using → Intention to use	supported
H6: Attitude of confidence → Perceived ease of use	–
H7: Attitude of confidence → Perceived usefulness	–
H8: Attitude of confidence → Intention to use	–
H9: Job relevance → Perceived usefulness	supported
H10: Job relevance → Intention to use	not supported
H11: Educational level → Intention to use	not supported
H12: Farm size → Intention to use	not supported
H13: Perceived usefulness → Perceived net benefit	supported
H14: Perceived net benefit → Intention to use	supported
H15: Personal innovativeness → Perceived usefulness	not supported
H16: Personal innovativeness → Perceived ease of use	supported

Considering the tested hypothesis, seven results were statistically significant ($p < 0.05$, $p < 0.001$) and six results were not supported (not statistically significant). It was not possible to test hypothesis 6, hypothesis 7, and hypothesis 8 due to the deletion of the AOC factor. Whereas it was observed that the intention to use (ITU) autonomous ground vehicle (AGV) was directly influenced by the farms' attitude toward their use

(ATU) supporting hypothesis 5, and by perceived net benefit (PNB) supporting hypothesis 14. Moreover, both PNB and ATU were influenced by perceived usefulness (PU) supporting hypothesis 13 and hypothesis 2, respectively. Whereas PU did not affect farmers' intention to use AGV since hypothesis 1 was not supported as well as farm size (hypothesis 12) and education level (hypothesis 11). Hypothesis 3 that perceived ease of use (PEOU) influenced PU was supported, but PEOU influence on farmers' attitudes was not supported (hypothesis 4). The factor of farmers' personal innovativeness (PI) only influences PEOU supporting (hypothesis 16) and not PU (hypothesis 15). Finally, job relevance (JR) had a direct effect only on PU (hypothesis 9), but not on the intention to use AGV (hypothesis 11).
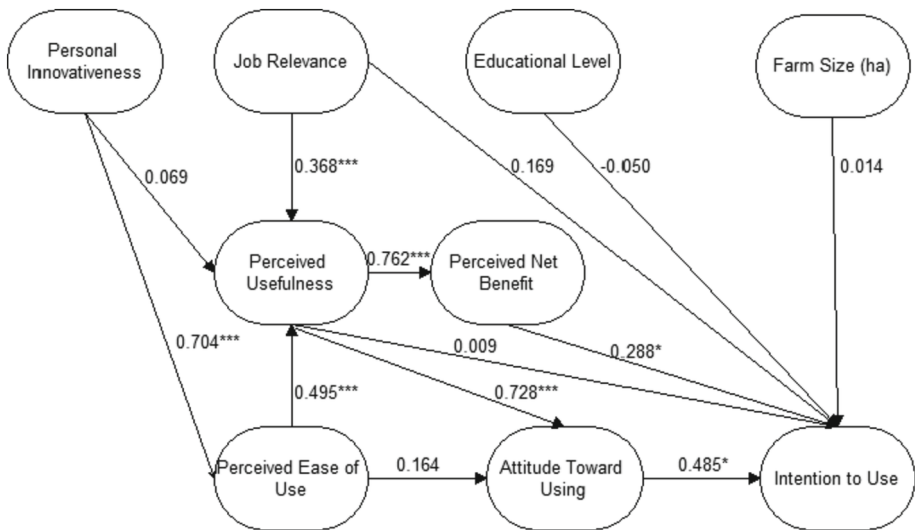
Fig. 3. The structural model analysis results with the hypothesis tested. Standardized parameter estimates for path coefficients are reported (***$p < 0.001$; **$p < 0.01$; *$p < 0.05$).

5 Discussion

In this study, a theoretical model was developed using the TAM to comprehend farmers' acceptance of autonomous ground vehicles in agriculture. The results showed that perceived usefulness (PU) and attitude toward using (ATU) AGVs positively affected the intention to use (ITU) and adopt UGVs in agriculture. Hence, based on the study findings, H2 was supported by the original and extended TAM structural models which is consistent with the findings of Rezaei et al. [32]. The construct of ATU had a significant positive impact on the ITU of UGVs in agriculture (supporting H5). This observation is consistent with the findings of many empirical studies in the setting of TAM-relevant research [26, 34, 38–40]. The study suggested that farmers who perceive AGVs as useful for their activities are more likely to have a positive attitude toward this technology

which will lead him or her to use it. However, none of the variables PU, JR, EL, and FS directly affected the ITU of UGVs in agriculture where the hypotheses H1, H10, H11, and H12 were rejected respectively. Despite the potential assistance provided by UGVs in various operational tasks, a farmer's Intention to Use of UGV tends to be lower, a finding that contradicts the results obtained by Michels et al. [25]. Our results also showed the acceptance of hypotheses H3, H9, H13, and H14, which suggested that PEOU has a positive effect on PU, which, in turn, positively impacts PNB, leading to the intention to use and adopt UGVs in agriculture. Both PEOU and JR had a positive effect on PU, meaning that farmers who perceive an AGV as easy to operate and suitable for their work will find this technology useful. PU affected PNB, which also had a positive impact on ITU indicating that a farmer perceives the AGV to be a beneficial investment, which makes them more likely to use it. Additionally, farmers who perceive AGVs as cost-effective are more likely to use them.

Specifically, PEOU is involved with the nature of a job and concerns the fundamental characteristics of technology, including clarity, flexibility, and ease of use. As the operation of technologies like UGVs gets easier, farmers tend to develop positive perceptions of their usage. When farmers are knowledgeable and confident in the robot's use, they are more likely to develop positive attitudes towards it.

This study also revealed a significant relationship between JR and PU. According to our results, farmers perceive an AGV as more useful if they recognize that its various functions are relevant to several on-farm tasks. This indicates that when the AGV provides relevant activities to farmers, it develops a sense of trust in the technology, leading to better-perceived usefulness, as shown in previous studies [25, 34]. Farmers who revealed the usefulness of using and learning unmanned ground vehicles and perceived a net benefit from using these robots showed a greater tendency to adopt these technologies [21].

The rejected hypothesis 15 suggested that PI did not directly affect PU, and thus did not impact the intention to use, as demonstrated in H1. Thus, PU is not correlated with the willingness of the farmer to try AGV.

Finally, the results supported hypothesis 16, suggesting that PI positively influences PEOU. According to these findings, innovative farmers with a positive attitude toward technology tend to appreciate and find useful the implication of unmanned vehicles in agriculture. Furthermore, such farmers might be more experienced in selecting suitable types of UGVs for their fields [41].

5.1   Limitation of the Study

This study about the farmers' intentions to use unmanned ground vehicles in agriculture, tried to broaden the sample of respondents by including farmers from different countries around the world, differently from Rübcke von Veltheim et al., [22] that involve only German farmers. However, this may lead to greater differences as they may have different economic conditions and agricultural farm structure. In any case, the main limitation of this study lies in the small number of responses, and therefore cannot reflect the entire farm's panorama. A larger and more balanced sample among different countries and including more female farmers would certainly be desirable for future research. Another

limitation is the fact that farmers do not currently use AGVs on their farms and therefore do not fully know what the real application of these vehicles could be.

6   Conclusions

This study used an extended Technology Acceptance Model to investigate the factors that influence the diffusion of autonomous ground vehicles in the agricultural domain. There is limited research on the acceptance of AGVs, a technology that can support farmers' activities and reduce the environmental impact of the agricultural sector. The novelty of this study was that it developed a survey in three different languages, Arabic, English, and Italian, expanding the dataset by considering both countries with emerging economies and countries with more stable economies. Furthermore, the study considered several factors such as educational level and farm size. In addition, external variables, including the attitude of confidence, personal innovativeness, and job relevance, were added to comprehend their impact on the attitude toward using AGVs and to provide a more comprehensive understanding of the factors that affect farmers' acceptance and adoption of technology. The research has confirmed the reliability of the TAM framework in describing intentions to adopt autonomous vehicles for farm activities. All the considered variables were validated during the analysis of the measurement model, except for the attitude of confidence, which was removed to improve the model fit. The results showed that the intention to use the AGV was directly affected by attitude towards its use and perceived net benefit, and indirectly influenced by personal innovativeness, job relevance, perceived usefulness, and perceived ease of use. These findings highlight that understanding farmers' attitudes and perceptions is important for the successful spread and implementation of AGVs in agriculture. Benefits and cost are key factors influencing the adoption decision. Therefore, efforts should be made to enhance farmers' understanding of the economic benefits and improve their perception of the effectiveness of using autonomous vehicles to accomplish on-farm tasks.

The study suggested that to spread and implement the usage of smart farming technologies such as AGVs among farmers, a farmer must believe that the AGV will provide more benefits than its cost and must feel positive about using this kind of technology.

Future research could focus on the efficiency and cost-effectiveness of using AGVs in farming practices to reduce costs and improve time management.

Conflict of Interest.   The Authors declare no competing interest.

References

1. Cheng D, Yao Y, Liu R, Li X, Guan B, Yu F (2023) Precision agriculture management based on a surrogate model assisted multiobjective algorithmic framework. Sci Rep 13(1):1–17. https://doi.org/10.1038/s41598-023-27990-w

2. Qamar T, Bawany NZ (2023) Agri-PAD a scalable framework for smart agriculture. Indonesian J Electr Eng Comput Sci 29(3):1597–1605. https://doi.org/10.11591/IJEECS.V29.I3.PP1597-1605

3. Kau AS, Gramlich R, Sewilam H (2023) Modelling land suitability to evaluate the potential for irrigated agriculture in the Nile region in Sudan. Sustain Water Resour Manag 9(1). https://doi.org/10.1007/S40899-022-00773-3

4. Bazzi H et al (2022) Detecting irrigation events over semi-arid and temperate climatic areas using sentinel-1 data: case of several summer crops. Agronomy, 12(11). https://doi.org/10.3390/AGRONOMY12112725

5. Bozal-Leorri A, Corrochano-Monsalve M, Arregui LM, Aparicio-Tejo PM, González-Murua C (2023) Evaluation of a crop rotation with biological inhibition potential to avoid N2O emissions in comparison with synthetic nitrification inhibition. J Environ Sci (China) 127:222–233. https://doi.org/10.1016/J.JES.2022.04.035

6. Kiani M et al (2022) Recycling eutrophic lake sediments into grass production: a four-year field experiment on agronomical and environmental implications. SSRN Electron J. https://doi.org/10.2139/ssrn.4238459

7. Gebbers R, Adamchuk VI (2010) Precision agriculture and food security. Science 327(5967):828–831. https://doi.org/10.1126/SCIENCE.1183899

8. ISPA, International Society of Precision Agriculture, https://www.ispag.org/about/definition. Accessed 26 Sept 2023

9. Raptis EK et al (2023) End-to-end precision agriculture UAV-based functionalities tailored to field characteristics. J Intell Robot Syst 107(2). https://doi.org/10.1007/S10846-022-01761-7

10. Fotio Tiotsop L, Servetti A, Masala E (2020) An integer linear programming model for efficient scheduling of UGV tasks in precision agriculture under human supervision. Comput Oper Res 114:104826. https://doi.org/10.1016/J.COR.2019.104826

11. Karthik M, Singh N, Sinha E, Anand B, SGowreesh SS (2018) Design and development of unmanned chemical spraying rover for agriculture application | request PDF. Int J Eng Adv Technol 8(2):18–21

12. Rakshitha N, Rekha HS, Sandhya S, Sandhya V, Sowndeswari S (2017) Pepper cutting UGV and disease detection using image processing. In: 2017 2nd IEEE international conference on recent trends in electronics, information & communication technology (RTEICT), 2018-January, pp 950–952. https://doi.org/10.1109/RTEICT.2017.8256738

13. Broderick JA, Tilbury DM, Atkins EM (2014) Optimal coverage trajectories for a UGV with tradeoffs for energy and time. Auton Robot 36(3):257–271. https://doi.org/10.1007/S10514-013-9348-X

14. Quaglia G, Visconte C, Scimmi LS, Melchiorre M, Cavallone P, Pastorelli S (2019) Design of the positioning mechanism of an unmanned ground vehicle for precision agriculture. Mech Mach Sci 73:3531–3540. https://doi.org/10.1007/978-3-030-20131-9_348/COVER

15. Botta A, Cavallone P (2021) Robotics applied to precision agriculture: the sustainable Agri.q rover case study. Mech Mach Sci 108:41–50. https://doi.org/10.1007/978-3-030-87383-7_5

16. Roure F et al (2018) GRAPE: ground robot for vineyard monitoring and protection. Adv Intell Syst Comput 693:249–260. https://doi.org/10.1007/978-3-319-70833-1_21

17. Usher C, Daley W, Webster B, Ritz C (2015) A study on quantitative metrics for evaluating animal behavior in confined environments. American Society of Agricultural and Biological Engineers Annual International Meeting, vol 6, no 1. https://doi.org/10.13031/AIM.20152190148

18. Srinivas A, Sangeetha J (2021) Smart irrigation and precision farming of paddy field using unmanned ground vehicle and internet of things system. Int J Adv Comput Sci Appl 12(12):407–414. https://doi.org/10.14569/IJACSA.2021.0121254

19. Caffaro F, Cremasco MM, Roccato M, Cavallo E (2020) Drivers of farmers' intention to adopt technological innovations in Italy: the role of information sources, perceived usefulness, and perceived ease of use. J Rural Stud 76:264–271
20. Rezaei-Moghaddam K, Salehi S (2010) Agricultural specialists' intention toward precision agriculture technologies: integrating innovation characteristics to technology acceptance model. Afr J Agric Res 5(11):1191–1199
21. Adrian AM, Norwood SH, Mask PL (2005) Producers' perceptions and attitudes toward precision agriculture technologies. Comput Electron Agric 48(3):256–271. https://doi.org/10.1016/j.compag.2005.04.004
22. Rübcke von Veltheim F, Theuvsen L, Heise H (2021) German farmers' intention to use autonomous field robots: a PLS-analysis. In: Precision agriculture, pp 1–28
23. Marangunić N, Granić A (2015) Technology acceptance model: a literature review from 1986 to 2013. Univ Access Inf Soc 14(1):81–95. https://doi.org/10.1007/S10209-014-0348-1/TABLES/3
24. Davis FD (1989) Perceived usefulness, perceived ease of use, and user acceptance of information technology. MIS Q: Manag Inf Syst 13(3):319–339. https://doi.org/10.2307/249008
25. Michels M, von Hobe CF, Weller von Ahlefeld PJ, Musshoff O (2021) The adoption of drones in German agriculture: a structural equation model. Precision Agric 22(6):1728–1748. https://doi.org/10.1007/S11119-021-09809-8
26. Zhu L, Xiong H, Ning Y, Lv M (2023) Addressing individual perception: extending the technology acceptance model to the interim payment method in construction projects. Sustainability (Switzerland) 15(9). https://doi.org/10.3390/su15097120
27. Venkatesh V, Davis FD (2000) A theoretical extension of the technology acceptance model: four longitudinal field studies. Manag Sci 46(2):186–204
28. Daberkow SG, McBride WD (2003) Farm and operator characteristics affecting the awareness and adoption of precision agriculture technologies in the US. Precision Agric 4(2):163–177. https://doi.org/10.1023/A:1024557205871
29. Caffaro F, Cavallo E (2019) The effects of individual variables, farming system characteristics and perceived barriers on actual use of smart farming technologies: evidence from the piedmont region, Northwestern Italy. Agriculture 9(5):111. https://doi.org/10.3390/agriculture9050111
30. Mohr S, Kühl R (2021) Acceptance of artificial intelligence in German agriculture: an application of the technology acceptance model and the theory of planned behavior. Precision Agric 22(6):1816–1844. https://doi.org/10.1007/S11119-021-09814-X/TABLES/13
31. Bagozzi RP, Yi Y (1988) On the evaluation of structural equation models. J Acad Market Sci 16(1):74–94
32. Nunnally JC, Bernstein IH (1994) Psychometric theory. McGraw-Hill, New York
33. Fornell C, Larcker DF (1981) Evaluating structural equation models with unobservable variables and measurement error. J Mark Res 18:39–50
34. Rezaei R, Safa L, Ganjkhanloo MM (2020) Understanding farmers' ecological conservation behavior regarding the use of integrated pest management - an application of the technology acceptance model. Glob Ecol Conserv 22:e00941. https://doi.org/10.1016/J.GECCO.2020.E00941
35. Sharifzadeh MS, Damalas CA, Abdollahzadeh G, Ahmadi-Gorgi H (2017) Predicting adoption of biological control among Iranian rice farmers: an application of the extended technology acceptance model (TAM2). Crop Prot 96:88–96. https://doi.org/10.1016/J.CROPRO.2017.01.014
36. Venkatesh V, Morris MG, Davis GB, Davis FD (2003) User acceptance of information technology: toward a unified view. MIS Q: Manag Inf Syst 27(3):425–478. https://doi.org/10.2307/30036540

37. Brar PS, Shah B, Singh J, Ali F, Kwak D (2022) Using modified technology acceptance model to evaluate the adoption of a proposed IoT-based indoor disaster management software tool by rescue workers. Sensors (Basel, Switzerland) 22(5). https://doi.org/10.3390/S22051866
38. Cheung R, Vogel D (2013) Predicting user acceptance of collaborative technologies: an extension of the technology acceptance model for e-learning. Comput Educ 63:160–175
39. Fathema N, Shannon D, Ross M (2015) Expanding the technology acceptance model (TAM) to examine faculty use of learning management systems (LMSs) in higher education institutions. J Online Learn Teach 11:210–232
40. Hussein Z (2017) Leading to intention: the role of attitude in relation to technology acceptance model in e-learning. Procedia Comput Sci 105:159–164
41. Khong H, Celik I, Le TTT, Lai VTT, Nguyen A, Bui H (2023) Examining teachers' behavioural intention for online teaching after COVID-19 pandemic: a large-scale survey. Educ Inf Technol 28(5):5999–6026

Rural Development Policy for Water Management Sustainability in Italy: Opportunities to Achieve Water Framework Directive Objectives

Ruberto Myriam(✉) , Chiappini Silvia , Ferrigno Marianna ,
Manganiello Veronica , Monteleone Alessandro , Pesce Alessandra ,
Zucaro Raffaella , and Pergamo Raffaella

Council for Agricultural Research and Economics (CREA), Research Centre for Agricultural Policies and Bioeconomy, Rome, Italy
`myriam.ruberto@crea.gov.it`

Abstract. Reg. (EU) 2021/2115 requires the integration between the Common Agriculture Policy (CAP) and the Water Framework Directive (WFD) in the 2021–2027 programming period, therefore the consistency between the National CAP Strategic Plan (CSP) and the River Basin Management Plans (RBMPs). To verify this consistency, a survey of River Basin District Authorities (RBDA) has been conducted in various steps along the CSP and RBMPs' programming process. The main objective of this work is to underline the approach adopted to verify whether and to what extent the macro interventions of CSP can contribute to the Key type of measures (KTM) of RBMP's and then to the priority identified at RBD level to achieve the WFD objectives. The result was that the interventions identified in the Italian CSP are quite appropriate for implementing the PoMs from a qualitative point of view, suggesting that about 70% of the proposed CSP interventions (30/43) are considered a tool for implementing the RBMPs. Furthermore, from a quantitative point of view, even if Rural Development resources provide a significant contribution to RBMPs, they must be considered together with other financing funds to provide an adequate cost recovery of PoMs measure. Weak points of integration may be important to understand which RBMPs needs cannot be met through the identified RD interventions, seeking other points of contact in the CSP, seeking other sources of funding, or rethinking RD regional strategies.

Keyword: Water framework directive · River basin district management plans · Water management · Common agricultural policy · Rural development policy

List of Abbreviations

CAP	Common Agricultural Policy
RD	Rural development
CSP	CAP Strategic Plan
RBD	River Basin District

PoM   Programme of Measures
RBMP   River Basin Management Plan
WFD   Water Framework Directive
ECA   European Court of Auditors RBDA: River Basin District Authority
KTM   Key Type of Measures

1 Introduction

Water is considered a scarce resource; for this reason, European Union started a complex legislative process in the 1990s, which ended with the issuance of the Water Framework Directive (WFD) in 2000 [1]. This measure introduces an ecosystem approach to water management; it becomes necessary to achieve quantitative as well as qualitative objectives, guaranteeing the maintenance and non-deterioration of groundwater levels, with the proactive participation of Member States in determining and preventing the impact of human activities on the available quantity of water [2].

The WFD institutionalises River Basin District (RBD), defined as "area of land and sea, made up of one or more neighbouring river basins together with their associated groundwaters and coastal waters, as the main unit for management of river basins" [3]. For each RBD, a River Basin Management Plan (RBMP) is required, as reference master plan on resource governance.

RBMPs must contain economic analysis of water uses (including agricultural water uses). Based on economic analysis, basic and supplementary measures are planned for filling the gap from good status of water bodies, forming the Program of Measures (PoM).

In accordance with the provisions of the WFD, in Italy seven RBD have been identified (Po, Northern Apennines, Eastern Alps, Central Apennines, Southern Apennines, Sardinia, Sicily), and a RBMP has been adopted for each RBD.

The agricultural sector is one of the main users of water and, at the same time, is also the one most in difficulty due to its scarcity [4]. As a result, for at least ten years now, the sustainable use of water resources in agriculture has been included in the strategic objectives of the Common Agricultural Policy (CAP) and in cross-compliance [5].

Since 2012, in the Communication from the European Commission "A Blueprint to Safeguard Europe's Water Resources" the need for better implementation and increased integration of WFD objectives into sectoral policy areas is highlighted [6]. The dominant belief is that the need for integration among policies is stronger in the agricultural sector [7].

The CAP represents, in fact, an important implementation tool of the WFD, both through the cross-compliance of direct payment (First Pillar) and by supporting, with the measures of Rural Development (Second Pillar), commitments for the rational use of water, the adoption of practices protecting water from polluting inputs, investments to promote the efficient use of water and the creation of ecological infrastructures.

Especially Rural Development (RD) is an important source of funding for measures that integrate water management with agricultural policy [8]. In some cases, this resulted

in effective integration that followed programming timelines [9]. In Denmark, for example, the Rural Development Program for 2006–2013 has been revised to provide funding to support the implementation of the Water Framework Directive [9].

For the agricultural sector, the evaluations carried out by the European Court of Auditors (ECA) in 2014 highlighted that only partially the integration of EU's water policy in CAP has been successful, in part due to the basic trade-off between the aims of the two policy objectives (food production vs good ecological health) [7]. They highlighted a limited impact of cross-compliance on water issues, as several important waters related issues are not covered by cross-compliance (i.e., the use of phosphorus), and a not fully exploitation of the potential of rural development to address water concerns [10].

Even in 2021, the ECA analysed the role of the CAP in the sustainable use of water resources, placing some recommendations in view of the new CAP to: improve water pricing levels for agriculture and authorisation for water abstraction; improve the use of RD and market support to push sustainable water use in agriculture; apply the post-2020 CAP rules so that funded irrigation projects contribute to the WFD objectives [11, 12].

So many expectations have been placed on the new post-2020 programming period and in the construction of the Green Architecture. In fact, a ring-fencing has been established that obliges Member States (MS) to allocate at least 25% of First Pillar resources (direct payments) to ecological schemes and a minimum percentage of 35% of Second Pillar expenditure (Rural Development) to agri-environmental measures.

The Regulation on the Strategic Plans for the CAP 2023–2027 [13] integrates the Water Framework Directives with a command-and-control approach [14]. The Regulation, considering ECA's recommendations about integration between the CAP and the environmental objectives of the WFD, also requires MSs to refer to how national environmental and climate plans acting EU policies, including the WFD, have been considered. In the described integration perspective, the irrigation investments financed by the CAP must be related to the areas identified by the RBDMPs and the related Programs of Measures (PoMs).

In the Italian CAP Strategic Plan (CSP) much emphasis has been placed on the integration of sustainable water use principles (Strategic Objective 5) with the funding mechanisms provided by the RD and direct payment, favouring the linkage with River Basin Management Plans (RBMPs).

The CSP defined by Italy encourages sustainable water management mostly within the RD interventions of Second Pillar. These interventions contribute to water protection objectives through investments (SRD), both at farm and off-farm level, environmental and climate commitments and other management commitments (SRA), exchange of knowledge and diffusion of information (SRH) [15]. The new CAP enhances environmental and climatic requirements to be met implementing agricultural practices, such as the crop rotation, safeguarding wetlands, and managing water resources in a sustainable manner [16]. Therefore, cross-compliance (statutory management requirements (SMR) and the maintenance of land in good agronomic and environmental condition (GAEC)) was strengthened even in relation to water issues. The issue of integration between the common agricultural policy and the Water Framework Directive is still under-addressed. Zucaro et al. (2017) conducted a geo spatial analysis method in order to assess if the measures foreseen in RBMPs and in the Rural Development Programmes (RDPs) 2014–2020

address agriculture pressure on water resources, in particular those linked to irrigation service [17].

More generally, the topic of policy integration has been addressed by several authors originally, in the context of environmental studies [18]. Peters (2018) examines limits of policy coordination problems. The author remarks the lack of a standardized method for addressing coordination problems, and the importance of the context for the success or failure of coordination attempts [19].

Alons (2017) investigates the limited scope of Environmental Policy Integration (EPI) in the CAP, through the multidimensional concept of EPI as a process, output and the outcome, finding that increased access of environmental actors to the decision-making process does not necessarily give them much influence, and that more mandatory policy instruments (output) do not guarantee more effective outcomes [20].

In Europe, useful coordination processes have been established, but they have difficulty in challenging existing institutional hierarchies and decision rules [21]. In this context, negative *coordination* (i.e. finding an agreement on how to avoid interference and conflict) should be overcome by *positive coordination*, which "involves multilateral negotiations that must jointly consider the policy options of all involved parties to agree on the contents of policies and resolve conflicts over distribution of resources" [21]. Urwin and Giordan (2008) recognize a good integration between agricultural policy and the water framework directive according to a top-down approach. Instead, using a bottom-up approach they track constraints on climate-adaptive planning that may arise from seemingly unrelated policies [22]. The objective of this work is to underline the approach for the integration between WFD and CAP, within the Italian policies implementation. Through the information provided by RBDAs, the correspondences between RD interventions planned in the CSP and the measures of the PoMs included in the RBMPs will be highlighted, to understand whether and to what extent the CAP resources can contribute to the achieving of the WFD objectives. For this work, the authorities (RBDA) were directly involved, which brought out the needs already expressed in their POM, highlighting which specific agricultural policy interventions they consider most useful for their territory among those available at national level. We aim to consider the strategies of the actors involved in the implementation of the policies, with a bottom-up approach, going beyond the investigation of the regulatory minimum-requirement for WFD integration in the CAP.

2 Materials and Methods

The analysis was carried out basing on PoMs of Italian RBMPs approved in December 2021 (Table 1), the draft of CSP notified to the European Commission on the 31/12/2021[1], and the final version of CSP approved in December 2022[2].

The analysis has been performed through a questionnaire submitted to each Italian RBDA from July to September 2022, in a tailored form (see Annex 1).

In these surveys the RBDAs were asked to indicate which RD interventions could potentially contribute to each measure of their PoM. To support the survey filling, the

---

[1] https://www.reterurale.it/downloads/Piano_Strategico_Nazionale_PAC_31-12-2021.pdf.
[2] https://www.reterurale.it/downloads/PSP_Italia_15112022.pdf.

Table 1. List of Italian RBMPs approved in December 2021

RBD	RBDMPs 2021–2027
Po	https://pianoacque.adbpo.it/piano-di-gestione-2021/
Northern Apennines	https://www.appenninosettentrionale.it/itc/?page_id=2904
Eastern Alps	https://distrettoalpiorientali.it/piano-gestione-acque/piano-gestione-acque-2021-2027/documentazione-e-cartografia/
Central Apennines	https://www.autoritadistrettoac.it/pianificazione/pianificazione-distrettuale/pgdac/pgdac3-secondo-aggiornamento-adottato-dalla-cip-del-20122021
Southern Apennines	https://www.distrettoappenninomeridionale.it/index.php/piano-iii-fase-2021-2027-menu/progetto-di-piano-di-gestione-acque-iii-ciclo-2021-2027-menu
Sardinia	https://pianogestionedistrettoidrografico.regione.sardegna.it/index.php?xsl=509&s=76&v=9&c=93824&tb=6695&st=7
Sicily	https://www.regione.sicilia.it/istituzioni/regione/strutture-regionali/presidenza-regione/autorita-bacino-distretto-idrografico-sicilia/pianificazione/piano-di-gestione-direttiva-2000-60/ciclo3

RBDAs were provided with a table with the list of the PoM measures mainly related to agricultural sector, and a selection of 43 interventions within the RD interventions of the CSP notified to the European Commission on the 31/12/2021, basing on their direct and indirect contribution to the protection of water and associated ecosystems) (see Annex 2).

Each RBMP's measures were associated by RBDA to one or multiple CSP interventions. Since each measure is linked to one or more KTM in the PoM, each CSP intervention was associated to one or more KTM[3] in the responses [23]. Therefore, the relationship between KTM and interventions is "many to many".

After collecting the responses, the correspondence between CSP interventions and RBMPs measures was checked to verify if the interventions could effectively contribute to the implementation of the identified measures, considering the specific financing rules of CSP and the detailed knowledge of intervention. Finally, the consistency between the CSP interventions and the KTM was verified, discarding the inappropriate or unfeasible links. Moreover, after the above-mentioned checks, a summary table was filled with all the data.

Initially, an analysis at national scale was performed. For a qualitative analysis, the data were reorganized to evaluate the types of interventions chosen by RBDAs to implement specific KTMs. More in detail, KTMs relevant to the agricultural sector, related to water quality, water quantity, hydro morphology an adaptation to climate change were considering for the current analysis (Table 2).

---

[3] KTM are groups of measures with a common purpose. KTMs are therefore containers of measures, independent even if not disconnected from each other, as the same individual action, due to the multiplicity of its objectives and characteristics, can be part of more than one KTM.

Table 2. List of Key Type of Measures considered

Code	Description
KTM 2	Reduce nutrient pollution from agriculture
KTM 3	Reduce pesticides pollution from agriculture
KTM 6	Improving hydromorphological conditions of water bodies other than longitudinal continuity
KTM 8	Water efficiency, technical measures for irrigation, industry, energy and households
KTM 24	Adaptation to climate change

Source 1. WFD Reporting guidance 2022

Particularly, the number of interventions correlated to each selected KTM, and the interventions more often chosen for the implementation of the PoM measures were evaluated. It is important to highlight that during the submission of the questionaries the CSP was in the draft stage and the final regional requirements were not defined. In fact, the CSP defines the complete list of interventions approved at national level, while each region can choose which to implement among them in relation to specific geographical needs and requirements. This choice was made after our survey. Therefore, after the approval of the CSP on December 2022, an in-depth check was performed to verify that in each RBDA at least one Region has adopted the RD intervention for which a link with RBMPs measure was previously identified.

Afterwards, a quantitative analysis was also performed to identify the contribution of RD intervention to the implementation of the RBMPs measures for selected KTMs from the economical point of view. The Regional planned expenditure amount from the CSP were considered and they were aggregated per RBD.

Finally, an analysis at RBD scale has been occurred to identify the contribution of the RD interventions in the cost recovery of the RBMPs measures. Specifically, for the Eastern Alps RBD a comparison between the planned expenditure for the RD interventions and the cost of the linked RBMPs measures was performed, since the relative PoM contains the cost of the planned measures even at the level of the individual Regions.

Considering the same KTM used for national scale analysis (Table 2), for the RBD scale analysis the following steps were applied:

1. from the PoM 2021–2027 of Eastern Alps RBMP 2021–2027 the amount of the cost of measures linked to the CSP interventions for all the regions included in the RBD were extract;
2. from the CSP approved in December 2022 the amount of planned expenditure for the interventions linked to RBMPs measures for all the Regions included in the RBD were obtained.
3. comparing the cost of the RBMPs measures and the planned expenditure for the related CSP interventions for the entire RBD, the financial contribution of RD to the implementation of the Eastern Alps RBMP measures was evaluated.

3   Results

3.1   National Analysis

The data analysis shows that 36 RD interventions can contribute to the implementation of the RBPMs measures. Specifically, the RBDAs identified 30 of the 43 RD interventions proposed in the questionnaire. Furthermore, they identified 6 RD interventions that were not present in the questionnaire, since the entire list of RD interventions was available (see Annex 2). Most of these interventions are related to the measures linked to KTM 6 and KTM 8. Moreover, a considerable number of interventions are connected to the KTMs 2 and 4, while only a few interventions are related to the KTM 3 (Fig. 1). As said, it is important to consider that a measure (and the related CSP intervention connected to it) can correspond to more than one KTMs so that the sum of the contributing interventions is major than the total number of CSP intervention (43).
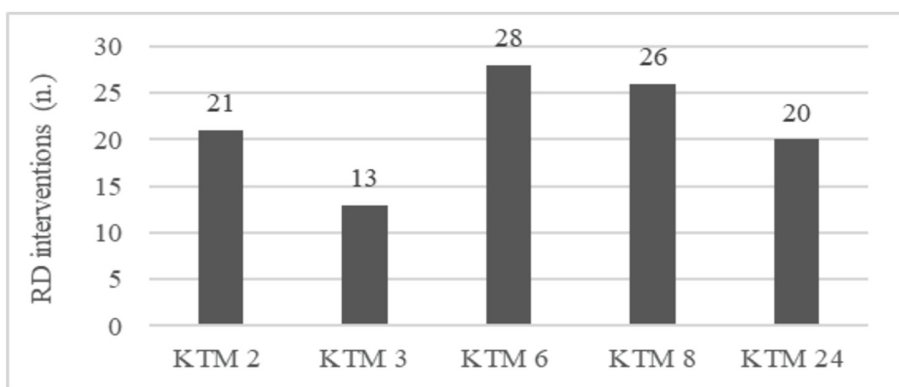
Fig. 1. Number of RD interventions linked to RBMPs measures for selected KTM. The relationship between KTM and interventions is "many to many". Source: our elaboration on RBDAs responses

Figures 2, 3, 4, and 5 show the number of RBDAs that have identified specific CSP interventions contributing to measures associated to selected KTMs.

Figure 2 shows the interventions that are identified for the implementation of the measures of the KTM 2. The highest number of interventions is under SRA24 (precision agriculture), which include commitments for the adoption of precision agriculture for the fertilization and phytosanitary treatments. These techniques will allow the optimization of the use of pollutant input. This type of intervention also includes the adoption of methods of precision irrigation that, by limiting the water excess on the field, reduces the leaching of nutrients and pesticides [24, 25].
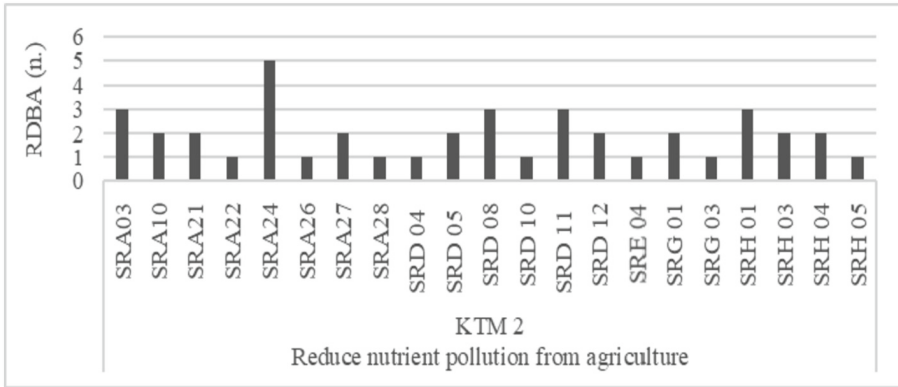
Fig. 2. Number of RBDAs identifying specific RD interventions linked to KTM2 measures (interventions are listed in Annex 2). Source: our elaboration on RBDAs responses
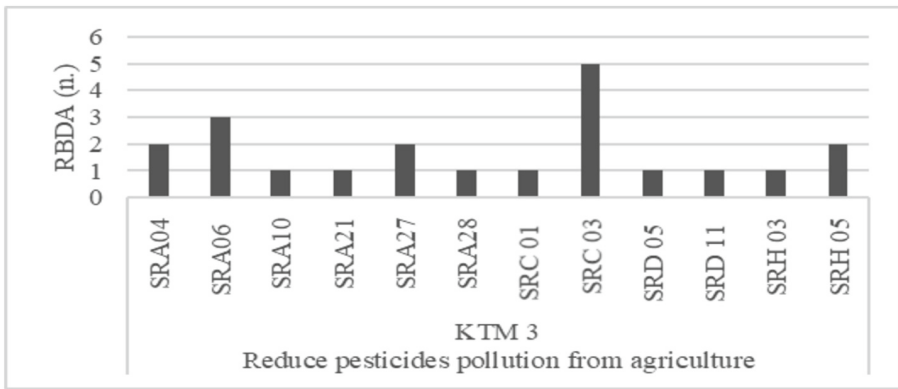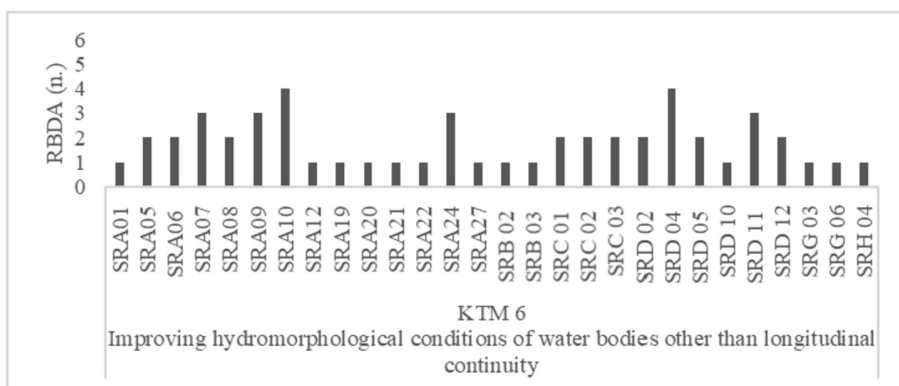

Fig. 3. Number of RBDAs identifying specific RD interventions linked to KTM3 measures (interventions are listed in Annex 2). Source: our elaboration on RBDAs responses

Figure 3 shows that the interventions more frequently chosen for the implementation of the measures linked to KTM 3 is SRC03 (Agricultural compensation for river basins), which compensates some disadvantages for the compliance of the WFD, such as limitation or prohibition of the use of pesticides and nutrients. This measure is important because it allows the economical sustainability in the compliance of the WFD, contributing to overcome the disagreements resulting by the joint implementation of the CAP and the WFD, in the case of conflicting environmental and economic objectives.

The interventions that were more frequently identified as contributing to KTM 6 are SRA10 (Management of ecological infrastructures) and SRD04 (Non-productive investments for environmental purposes) (Fig. 4). The intervention SRA10 contributes to the improving of the hydro morphological conditions of the aquatic systems such as wet meadows, wetlands and minor hydraulic network. These improvements are to be performed through the control of the maintenance of the bank vegetation, the reshaping of the banks and the maintaining of an adequate water level. The intervention SRD04 finances the investments for the realization and/or restoration of the ecological structures' functionalities related to the water systems, such as small lakes, wetlands meadows, resurgences, ditches etc. Moreover, this intervention finances the investment for the remediation or the implantation of the riverbed vegetation and along the banks (buffer strips-BS) in the irrigation ditches, and the realization of the wooded buffer strips (WBS).
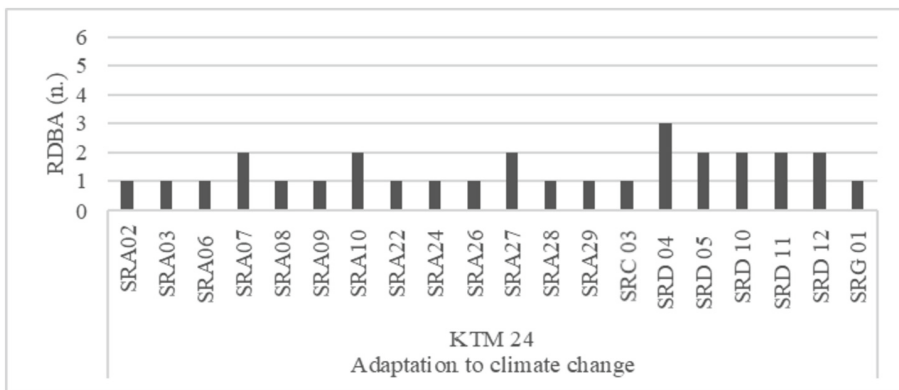

Fig. 4. Number of RBDAs identifying specific RD interventions linked to KTM6 measures (interventions are listed in Annex 2). Source: our elaboration on RBDAs responses
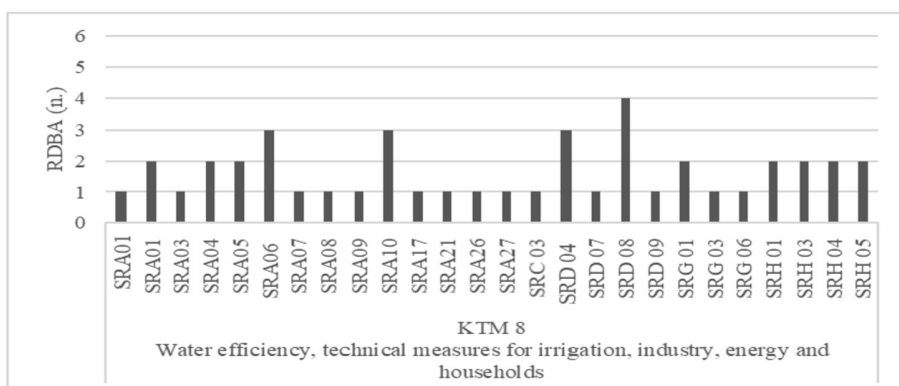
Fig. 5. Number of RBDAs identifying specific RD interventions linked to KTM8 measures (interventions are listed in Annex 2). Source: our elaboration on RBDAs responses

BS and WBS will contribute to reduce the waters pollution thanks to the potential of vegetation to absorb nutrients and pesticides from surface runoff.

The intervention with the highest occurrence for the KTM 8 and KTM 24 is SDR08 (Infrastructures for environmental purposes) (Fig. 5 and Fig. 6). This intervention finances the activities for the improvement, renewal and restoration of irrigation infrastructure, the creation and optimization of reservoirs and for the use of treated wastewater as additional water source for irrigation. These investments will allow to increase the efficiency of the water infrastructures (i.e., by reducing water losses from the irrigation network) and to reduce the water usage by promoting alternative water sources. For KTM 24 also SRA 02 "commitments for sustainable water use" has been selected, which offers payments for the optimization of volumes applied to the field, through the adoption of irrigation advisor methods based on soil/plant water balance.


Fig. 6. Number of RBDAs identifying specific RD interventions linked to KTM24 measures (interventions are listed in Annex 2). Source: our elaboration on RBDAs responses

In addition, as a result of this analysis, it was found that in some cases, no Regions included in the RBD have adopted the RD intervention for which the link with the measure of the PoM was identify. This emerged from the verification of the regional choices of RD interventions in the CSP. Figure 7 shows the number of interventions connected to the measures for which economic resources were allocated (adopted) or not (not adopted).

Figure 8 shows the total expenditure planned in the CSP for interventions related to KTM in Millions of euros. A greater amount of resources is referred to the measures linked to KTM 6 and KTM 8, for which the greatest number of interventions has also been identified (Fig. 1). As previously highlighted, since each intervention can contribute to more than one KTM, the amount of contribution to KTM could not be summarized. Hence, the amount contribution must be read individually for each KTM.
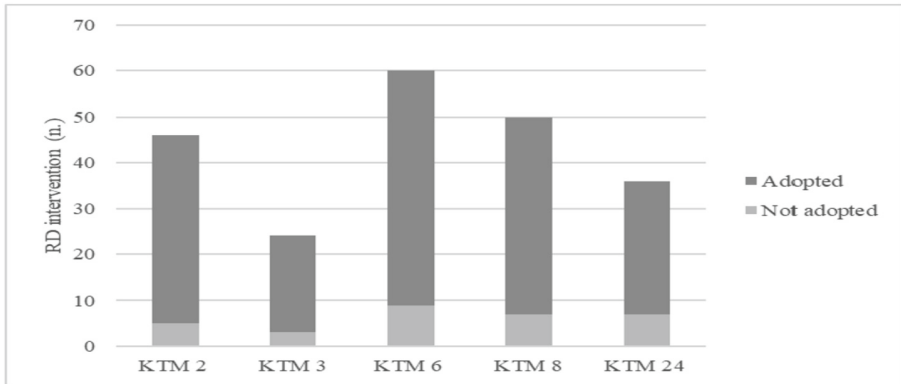
Fig. 7. Number of RD interventions connected to RBMPs measures, associated with the KTMs, for which economic resources were allocated (adopted) or not (not adopted). Source: our elaboration on RBDAs responses.
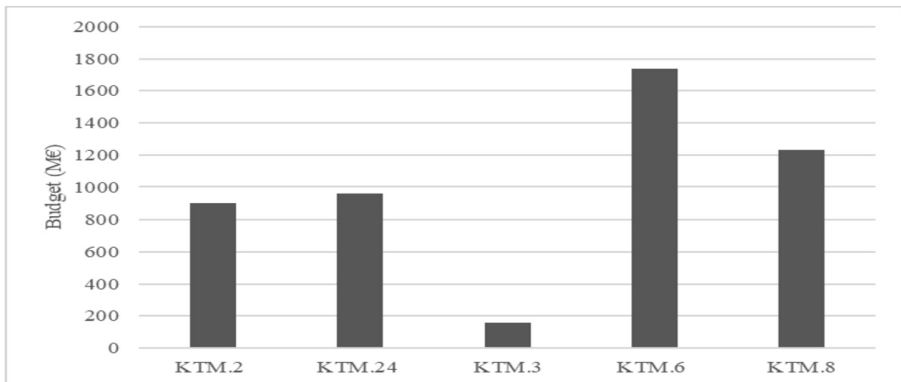

Fig. 8. Budget of RD interventions linked to RBMPs measures per KTM (M€). Source: our elaboration on RBDAs responses and CSP approved in December 2022.

3.2 River Basin District Analysis

The RBD analysis has been occurred for Eastern Alps River Basin District, including four Regions and Autonomous Provinces in North East of Italy (Fig. 9).

Figure 10 highlights the contribution of the RD interventions in the implementation of the KTMs of the Eastern Alps RBMP compared to the total cost of the linked measures. As can be observed in the graph below, the highest cost amounts are recorded for the KTM 2 and KTM 8. The highest contribution of RD planned resources is for the KTM 6, both in absolute terms and in relation to the cost of the measures. The budget of RD interventions linked to KTM3 measures covers the corresponding cost, exceeding the financing need.
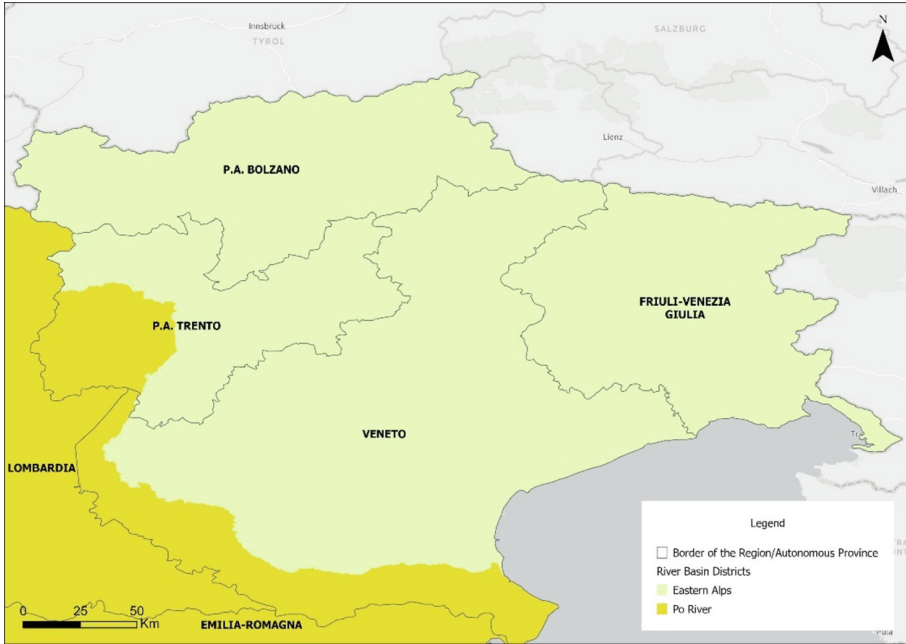
Fig. 9. Eastern Alps River Basin District: administrative limits. Source: our elaboration on SIGRIAN (National Information System for Agriculture Water Management) data
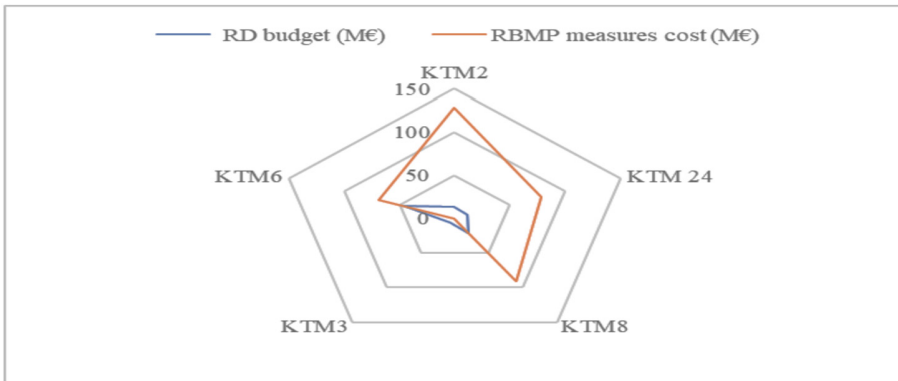
Fig. 10. Cost of Eastern Alps RBMP's measures for selected KTM compared to budget for RD linked interventions. Source: our elaboration on Eastern Alps RBDA responses and Eastern Alps RBMP

4 Discussion

The results show that CAP funds could have an important role in implementation of RBMP measures through many interventions that finance several and different good practices and investments for the sustainable management of water.

The CSP interventions identified by the RBDAs are quite appropriate with respect to the type of measures to be implemented. However, the lack of interventions more directly linked to water resources such as the SRA02 for some KTMs is controversial. This intervention, in fact, promoting the efficient water management fully responds to the KTM8 (Water efficiency, technical measures for irrigation, industry, energy and household) but this connection has not been highlighted by RBDAs and so not emerge from the results. Instead, SRA02 is identified as contributing to the KTM 24 (Adaptation to climate change). This suggests that the optimization of water used for field irrigation is seen mainly as a strategy to deal with the ever-decreasing water availability caused by the increasingly frequent and severe drought periods, rather than a measure for water use efficiency. This implies, also, that the attention is mainly given to face emergency issues, with less view to the improve a structural condition in long terms.

Furthermore, most of the interventions reported by the RBDAs were chosen by the Regions within their own RD strategy. However, some interventions identified by RBDA have not been adopted and funded by Regions belonging to them. This is a weakness of the integration process, as some PoMs measures cannot have potentially available resources from agricultural sector.

From the cost recovery point of view, the results show the availability of large resources in CSP for the implementation of the measures, especially for the KTM 6 and KTM 8. However, this amount must be compared with the cost of the PoM's measures. The analysis carried out for the Eastern Alps RBD demonstrates that, even if RD resources provide a significant contribution, they must be considered together with other financing funds to provide an adequate cost recovery.

The results obtained do not only provide a list of CSP interventions that generally have a positive impact on water resources. Rather, they provide an indication of the needs identified by the RBDAs, suggesting which CSP interventions have priority in their RBD, because they respond to RBMPs measures. This is a strong point of the adopted methodology of analysis.

5 Conclusion

The long policy-making and implementation process, from the adoption of the WFD to the integration of environmental objectives into the CAP, highlights a path that led to the definition of methods for quantifying the environmental cost generated by both the use of water and its recovery [26]. The process is still ongoing for the stated reasons, as well as shifting the objectives of the CAP from an economical (income support) to an environmental feature, requires effective strategies, which start from the integration of policies. This is a complex operation because it requires fitting together different planning processes. Specifically, the implementation of the WFD is based on water management planning at the RBD level, which leads to the planning of measures to

achieve the water-related environmental objectives, generating a financing requirement. The CAP, as a sectoral policy, is called upon to respond to this need, starting from the definition of the context and the objectives to be achieved.

The CSP, which includes the strategic choices of the regions to achieve various objectives, including the protection of water and related ecosystems, offers different opportunities. However, although an important source of funding, Rural Development financial resources must be accompanied by other National or European sources such as Recovery and Resilience Facility Plan, Cohesion Funds, national budget Law.

The points of lack of integration must be evaluated considering the different regulatory system of two programming tools - CSP and RBMPs. In fact, they follow different logics. The main difference is the type of objectives which they pursue. The RBMPs pursue purely environmental and water-specific objectives, albeit considering economic aspects through the socio-economic analysis required by the WFD. On the contrary, the CSP must respond not only to the WFD, but also to economic and social objectives, as well as other environmental policies. In fact, in addition to RBMPs, the CSP contains a list of other implementation tools for the national transposition of European Directives to which it is called upon to respond. Among these are the Regional Priority Action Plans for Natura 20000 for the implementation of Directive 2009/147/EC, the National Air Pollution Control Program for the implementation of Directive 2016/2284/EC, the National Integrated Plan for energy and climate 2030 (Directive 2009/28/EC) etc. Then, Regions must allocate their limited RD resources to meet several and different objectives. Consequently, some weaknesses in the integration were expected. However, weak points of integration may be important to understand which RBMPs needs cannot be met through the identified RD interventions, seeking other points of contact in the CSP, seeking other sources of funding, or rethinking RD regional strategies.

In any case, it's worth to note that the analysis shows a substantial consistency among policies and the absence of conflicts, even if in some case the objectives could be considered not entirely coincident. The results of the survey suggest that about 70% of the proposed CSP interventions (30/43) is considered as a tool for the implementation of the RBMPs. From this point of view, measures with a more transversal, such as technical assistance and extension services [27], represent an innovative border for the overall achievement of the objectives of efficient management of water resources. It deals with a more comprehensive integration of the material and immaterial investments devoted to environmental improvement and a more efficient management of natural resources at a territorial level. The analysis carried out represents an attempt to investigate the integration between CAP and WFD, emphasizing the context of the application of the policies and considering the lack of a standardized method for addressing coordination problems [19]. Furthermore, the involvement of the actors responsible for planning, through a bottom-up approach [22], allows us to overcome the just non-conflict logic between policies [21], seeking positive points of contact in terms of financial support for the implementation of the environmental policy for water.

Appendix

Annex 1. Format of the questionnaire submitted to the RBDAs - Eastern Alps sample

PoM Measures	RD Interventions																			
	SRA01	SRA02	[...]	SRA11	[...]	SRA29	[...]	SRC03	SRD02	SRD04	[...]	SRD11	[...]	SRE04	SRG01	[...]	SRG06	SRH01	[...]	SRH06
Measures to improve the ecological functionality of the watercourse																				
Projects for irrigation transformation from flow irrigation to pressurized irrigation																				
Projects for irrigation transformation from sprinkle to micro-irrigation																				
Specific Phytosanitary Defense Measures with low FP input																				
Construction of reservoirs and irrigation systems for the rationalization of water resources and the enhancement of valuable crops																				
Restructuring and adaptation of the irrigation supply network fed by surface water bodies for the purpose of saving water																				
Strengthening and adapting advisory services to farmers																				
[....]																				
River recovery and requalification for optimization of water resources																				
Standards and measures for water reuse																				
Interventions for the quantitative protection of water resources																				
Buffer distances from water bodies for the application of sewage sludge in agriculture																				

Annex 2. List of RD interventions potentially relevant to RBDMPs measures

Code	Name	Proposed to RBDAs	Selected by RBDAs
SRA 01	INTEGRATED PRODUCTION	X	X
SRA02	COMMITMENTS FOR SUSTAINABLE USE OF WATER	X	X
SRA03	REDUCED SOIL WORKING TECHNIQUES	X	X
SRA04	INTRODUCTION OF ORGANIC SUBSTANCE IN THE SOIL	X	X
SRA05	GRASSING OF TREE CROPS	X	X
SRA06	COVER CROPS	X	X
SRA07	CONVERSION OF ARABLE CROPS TO MEADOWS AND PASTURES	X	X
SRA08	PERMANENT MEADOWS AND PASTURE MANAGEMENT	X	X
SRA09	NATURA 2000 HABITAT MANAGEMENT	X	X
SRA10	ACTIVE MANAGEMENT OF ECOLOGICAL INFRASTRUCTURES	X	X
SRA11	*Not confimred in fial versione of CSP*	X	
SRA12	ECOLOGICAL CORRIDORS		X
SRA19	REDUCTION IN THE USE OF PESTAL PRODUCTS	X	X
SRA20	SUSTAINABLE USE OF NUTRIENTS	X	X

(continued)

Annex 2. (*continued*)

Code	Name	Proposed to RBDAs	Selected by RBDAs
SRA21	WASTE MANAGEMENT	X	X
SRA22	RICE FIELDS	X	X
SRA23	*Not confimred in fial versione of CSP*	X	
SRA24	PRECISION AGRICULTURE	X	X
SRA26	WITHDRAWAL OF ARABLE CROPS FROM PRODUCTION		X
SRA27	SILVO-ENVIRONMENTAL COMMITMENTS	X	X
SRA28	FORESTATION MAINTENANCE-FORESTATION		X
SRA29	ORGANIC PRODUCTION	X	X
SRB 02	SIGNIFICANT NATURAL DISADVANTAGES		X
SRB 03	AREAS WITH SPECIFIC CONSTRAINTS		X
SRC 01	NATURA 2000 AGRICULTURAL COMPENSATION	X	X
SRC 02	NATURA 2000 FORESTRY COMPENSATION	X	
SRC03	AGRICULTURAL COMPENSATION FOR RIVER BASINS	X	X
SRD 02	INVESTMENTS ENVIRONMENT CLIMATE ANIMAL WELFARE		X
SRD 04	NON-PRODUCTIVE INVESTMENTS FOR ENVIRONMENTAL PURPOSES		X
SRD 05	FORESTATION AND FORESTATION OF AGRICULTURAL LAND		X
SRD06	PREVENTION AND RESTORATION OF AGRICULTURAL PRODUCTIVITY	X	
SRD 07	INFRASTRUCTURES FOR AGRICULTURE AND SOCIO-ECONOMIC DEVELOPMENT	X	X
SRD 08	INFRASTRUCTURES FOR ENVIRONMENTAL PURPOSES	X	X

Annex 2. (*continued*)

Code	Name	Proposed to RBDAs	Selected by RBDAs
SRD 09	NON-PRODUCTIVE INVESTMENTS IN RURAL AREAS		X
SRD 10	FORESTATION AND FORESTATION OF NON-AGRICULTURAL LAND	X	X
SRD 11	NON-PRODUCTIVE FORESTRY INVESTMENTS	X	X
SRD 12	INVESTMENTS FOR THE PREVENTION AND RESTORATION OF FOREST DAMAGE	X	X
SRD14	NON-AGRICULTURAL PRODUCTIVE INVESTMENTS IN RURAL AREAS	X	
SRE 04	NON AGRICULTURAL START UP	X	X
SRF02	DAMAGES MUTUALITY FUND	X	
SRG 01	SUPPORT FOR EIP-AGRI OPERATIONAL GROUPS	X	X
SRG 03	PARTICIPATION IN QUALITY SCHEMES	X	X
SRG06	LEADER - IMPLEMENTATION OF LOCAL DEVELOPMENT STRATEGIES	X	
SRG10	PROMOTION OF QUALITY PRODUCTS	X	
SRH01	ADVISRORY SERVICES	X	
SRH03	TRAINING OF FARMERS	X	
SRH04	TRAINING ACTIONS	X	
SRH05	DEMONSTRATION ACTIONS	X	
SRH06	BACK OFFICE SERVICES FOR AKIS	X	

References

1. Kallis G (2001) The EU water framework directive: measures and implications. Water Policy 3:125–142
2. Vlachopoulou M, Coughlin D, Forrow D et al (2014) The potential of using the ecosystem approach in the implementation of the EU Water framework directive. Sci Total Environ 470–471:684–694
3. European Commission (2000) Directive 2000/60/EC of the European Parliament and of the Council of 23 October 20000 establishing a framework for community action in the field of water policy
4. Gruère G, Le Boëdec H (2019) Navigating pathways to reform water policies in agriculture

5. Matthews A (2013) Give to AgEcon search greening agricultural payments in the EU's common agricultural policy. Bio-Based Appl Econ 2:1–27

6. European Commission (2012) Communication from the commission to the European parliament, the council, the European economic and social committee and the committee of the regions. A Blueprint to Safeguard Europe's Water Resources

7. Carvalho L, Mackay EB, Cardoso AC et al (2019) Protecting and restoring Europe's waters: an analysis of the future development needs of the water framework directive. Sci Total Environ 658:1228–1238

8. Mohaupt V, Crosnier G, Todd R et al (2007) WFD and agriculture activity of the EU: first linkages between the CAP and the WFD at EU level. Water Sci Technol 56:163–170

9. Nielsen HØ, Frederiksen P, Saarikoski H et al (2013) How different institutional arrangements promote integrated river basin management. Evidence from the Baltic Sea Region. Land Use Policy 30:437–445

10. European Court of Auditors (2014) Integration of EU water policy objectives with the CAP: a partial success

11. European Court of Auditors (2021) Special Report Sustainable water use in agriculture: CAP funds more likely to promote greater rather than more efficient water use

12. Zucaro R, Manganiello V, Ruberto M et al (2021) L'uso sostenibile dell'acqua in agricoltura e integrazione delle politiche. PianetaPSR

13. European Commission (2021) Regulation (EU) 2021/2115 of the European Parliament and of the Council of 2 December 2021 establishing rules on support for strategic plans to be drawn up by Member States under the common agricultural policy (CAP Strategic Plans) and financed by the European Agricultural Guarantee Fund (EAGF) and by the European Agricultural Fund for Rural Development (EAFRD) and repealing Regulations (EU) No 1305/2013 and (EU) No 1307/2013

14. Rietig K (2013) Sustainable climate policy integration in the European union. Environ Policy Gov 23:297–310

15. Pergamo R, Ruberto M (2023) La gestione dell'acqua e delle risorse idriche nella politica di sviluppo rurale: un percorso in continuità tra diversi periodi di programmazione. PianetaPSR numero 123 aprile 2023

16. Doukas YE, Salvati L, Vardopoulos I (2023) Unraveling the European agricultural policy sustainable development trajectory. Land 12:1749

17. Zucaro R, Martello M, Antinoro C et al (2017) Mapping and analysis of pressures on water resources from agriculture to target water and agriculture policies. Chem Eng Trans 58:727–732

18. Trein P, Fischer M, Maggetti M et al (2023) Empirical research on policy integration: a review and new directions. Policy Sci 56:29–48

19. Peters BG (2018) The challenge of policy coordination. Policy Des Pract 1:1–11

20. Alons G (2017) Environmental policy integration in the EU's common agricultural policy: greening or greenwashing? J Eur Public Policy 24:1604–1622

21. Russel D, Castellari S, Capriolo A et al (2020) Policy coordination for national climate change adaptation in Europe: all process, but little power. Sustainability 12:5393

22. Urwin K, Jordan A (2008) Does public policy support or undermine climate change adaptation? Exploring policy interplay across different scales of governance. Glob Environ Chang 18:180–191

23. European Commission (2022) WFD Reporting Guidance 2022

24. Violino S, Figorilli S, Ferrigno M et al (2023) A data-driven bibliometric review on precision irrigation. Smart Agric. Technol 5:100320

25. Bwambale E, Abagale FK, Anornu GK (2022) Smart irrigation monitoring and control strategies for improving water use efficiency in precision agriculture: a review. Agric Water Manag 260:107324
26. Pergamo R, Ruberto M (2023) L'acqua tra agricoltura e ambiente: dalla Direttiva Quadro Acque alla nuova PAC, RRN Magazine n.18- febbraio 2023. RRN Magazine n18 11–12
27. Sequino V, Salerno C, Pesce A (2019) On innovation, cooperation and agriculture: some reflections on these topics. Rivista di Studi Sulla Sostenibilita' 2:125–150

Economic Analysis of Subsurface Drainage Systems in North Central Iowa

Kapil Arora[✉] and Kelvin Leibold

Department of Extension and Outreach, Iowa State University, Ames, IA 50011, USA
pbtiger@iastate.edu

Abstract. An economic analysis was performed for predicting the rate of return and payback period for installing subsurface drainage on Okoboji and Canisteo soil types for three different drain line spacings of 12.2, 18.3, and 24.4 m. DRAIN-MOD model predicted significant yield improvements for both soil types when compared with undrained conditions. With the parallel lateral drainage design and its installation, payback periods for the two soil types were analyzed for three different corn grain market prices. Analysis showed that the payback period was seven years or less for all the drain line spacings. For Canisteo soil type, the analysis showed an increase in rate of return with quicker payback as the drain line spacing was reduced from 24.4 m (80 feet) to 12.2 m (40 feet) for all three corn grain market prices. This was not the case for Okoboji soil type indicating that the spacing impacts payback period under different corn grain market prices. Caution should be used when interpreting the results from this analysis as drain line installation costs vary by project design and type of installation. Higher subsurface drainage project costs will increase the payback period.

Keywords: Subsurface · Drainage · Design · Yield · Economic · Analysis

1 Introduction

In the corn belt of United States and several areas around the world, subsurface drainage plays a critical role in making crop productivity profitable leading to better farm management. Subsurface drainage causes the excess soil water to leave the plant root zone resulting in better crop yields as the plant roots are not waterlogged for long time durations. In Iowa, subsurface drainage is fundamental to its agricultural economy. Farm operations of cultivation, planting, and pesticide applications on several farms are only feasible due to removal of excess soil water with subsurface drainage. As reported in 2019 by USDA-NASS [1], approximately 46.1% of Iowa's land in farms (over 5.7 million ha or over 14.1 million acres) is considered artificially drained with subsurface drains.

The economics of payback on a drainage system typically depends on drainage intensity (spacing and depth), drainage capacity (size and grade), water quality and quantity management (controlled drainage, shallow drainage, bioreactors, wetlands, etc.). Spacing and depth of subsurface drains are two key factors directly impacting the time it

takes for excess soil water removal after intense rainfall events. Soil types i.e., saturated hydraulic conductivity of the soil, also impacts how quickly the water will move through the soil to the subsurface drains. These three factors can be modelled for their impact on the soil water table and subsequently crop yields using a computer simulation model called DRAINMOD [2]. This model simulates the hydrology of poorly drained soils using climate data and predicts the effects of subsurface water management practices (drain spacing and depth) on water table depths and crop yields.

An economic analysis was then preformed using the cost of the subsurface system, its installation and maintenance costs, and increased revenue from improved crop yields on the return on investment. The Drain Spacing Tool [3] only estimates the optimum drain spacing that maximizes economic return on investment in the drainage system under corn-soybean rotation. This tool does not provide the return on investment as impacted by change in drain line spacings. A review of literature also did not show any other related work measuring return on investment as a function of drain line spacing. Secondly, economic information, based on yield improvements for different drain line spacings is currently not available currently to landowners and land tenants. This work can, therefore, help landowners and land tenants decide if it is beneficial to invest in subsurface drainage and the optimal drain spacings based on multiple pricing outcomes.

2 Methods

To perform economic analysis of the return on investment for the subsurface drainage system, the yield improvements were first predicted using the DRAINMOD computer model [2]. A drainage system with subsurface drains was then designed to calculate the drainage system costs. The increased revenue from improved yields at three difference corn commodity prices were then analyzed against subsurface drainage system costs to estimate the return-on-investment and payback periods.

2.1 DRAINMOD Modeling

Subsurface drain spacing is one of the key factors directly impacting the time it takes for excess soil water removal after intense rainfall events. Soil types i.e., saturated hydraulic conductivity of the soil, also impacts how quickly the water will move through the soil to the subsurface drains. These two factors were modelled for their impact on the soil water table and subsequently crop yields using a computer simulation model called DRAINMOD [2]. This model simulates the hydrology of poorly drained soils using climate data and predicts the effects of subsurface water management practices on water table depths and crop yields.

Three drain spacings of 12.2 m (40 ft), 18.3 m (60 ft), and 24.4 m (80 ft) were studied in this analysis using a drain depth of 0.9 m (3 ft). Different patterns of subsurface drains exist on the farmland which consist of parallel, herringbone, double main, and random. In this analysis, only the parallel subsurface drainage pattern was studied using DRAINMOD [2]. Subsurface drainage system design is explained in the next section. Two different poorly drained North Central Iowa soil types (Okoboji, and Canisteo) with saturated hydraulic conductivities of 3.3 and 10.1 mm/hr, respectively, were used in

DRANMOD [2] computer simulations to predict crop yields. These saturated hydraulic conductivities were obtained from Web Soil Survey [4].

2.2   Drainage System Design

For the purposes of the subsurface parallel drainage pattern, a 32.38-hectare (80 acres) farm field with a single uniform soil type was considered for design. A rectangular configuration of the field was considered with drainage laterals running parallel to each other with the main drainage line running perpendicular to the laterals (Fig. 1).
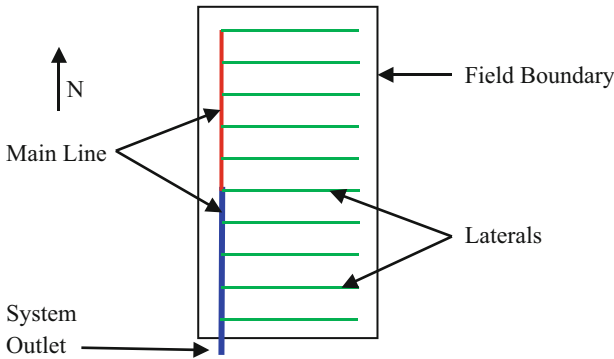
Fig. 1. A conceptual design (not to scale) of the parallel subsurface drainage system with green lines indicating laterals, blue line indicating the lower section of the main line with larger diameter, and the red line indicating the upper section of the main line with smaller diameter.

Field dimensions used in the design were 804.7 m by 402.3 m with the laterals running parallel to the shorter field boundary. The field was considered having a slope of 1% from northeast to southwest part of the field i.e., the laterals and main line were considered at 1% slope. Hooghoudt equation [5] for subsurface drain flow for steady state conditions was used to calculate the drainage coefficient for three different drain line spacings. Using these drainage coefficients, the main line was sized to ensure there was enough capacity in the main line to handle the flow rates being added to it from the laterals. ASABE [6] also explains Hooghoudt equation in its design standard for subsurface drainage.

Variables considered for completing calculations for the Hooghoudt equation [5] were depth to the drains from the surface (0.91 m or 3 ft.), depth to the impervious layer from the surface (2.44 m or 8 ft.), and depth to the water table midway between laterals after drawdown (0 m or ft.). Soil profile saturated hydraulic conductivity, both above and below the drain lines to the impervious layer, was considered to the same.

2.3   Drainage System Costs

Drainage system costs considered included cost of the drain line for different sizes, cost of installation using drain line plow equipped with Global Position System Real Time

Kinematics (GPS-RTK) and grade control, number of junctions, labor, fuel, and repairs and maintenance. A phone survey was also conducted to obtain market prices from three difference commercial drain line installers for the same configuration as provided in Fig. 1. These costs of drain lines, as installed, were averaged and the average cost of installation per meter of drain line installed was used in calculating the cost of the project as dollars per hectare or dollars per acre.

2.4 Rate of Return (ROR) Analysis

Continuous Corn crop for grain was selected for analysis in this paper. Corn grain yield improvements were calculated as a difference between the undrained yields and the anticipated yield as predicted by DRAINMOD model [2] for different drain line spacings. Yield potential of the different soil types, in metric tons per hectare (or bushels per acre) for corn was obtained from the 2017 Iowa Soil Properties and Interpretations Database [7].

The total length of laterals and main line (in meters) was calculated from the drainage design for the three different spacings. Using the drain line costs as dollar per meter installed, the total cost of the project was calculated and then converted to dollars per hectare using the area of the field drained.

Corn grain is a commodity in USA and its price fluctuates with the market. As such, a low price, a medium price, and a high price for the corn grain was used to calculate the increased revenue received for the three different spacings. This increased revenue was then used in the analysis to calculate the years it will take to pay off the drainage system costs paid at installation.

Rate of Return (ROR) Analysis was completed using the 2023 Farmland Tile Drainage Investment Analysis Spreadsheet available from Ag Decision Maker [8]. Number of years to pay back the investment cost was determined using in the annual increase in revenue but considering the annual cost for increased seed, fertilizer, grain handling, drying, and storage, as well as tile maintenance costs. These costs were assumed to be constant in the analysis irrespective of the corn grain market price.

3 Results

3.1 DRAINMOD Modeling

DRAINMOD model [2] predicted a significant increase in crop yields over the undrained conditions for both Okoboji and Canisteo soil types for three different drain line spacings as shown in Table 1 below. When compared with the undrained corn grain yields, the model showed significant improved yields for both soil types. For Canisteo soil type, corn grain yields were shown to have improved with closer spacings. For Okoboji soil type, the yield improvement was larger for 18.3 m (60 foot) spacing than for 12.2 m (40 foot) or 24.4 m (80 foot) spacing although the difference between 12.2 m (40 foot) and 18.3 m (60 foot) was small.

Table 1. Corn grain yields for three different drain line spacings.

Drain Line Spacing meters (feet)	ISPAID Maximum Yield MT/ha (bu./ac)	Undrained Yield MT/ha (bu./ac)	DRAINMOD Yield MT/ha (bu./ac)	Yield Improvement MT/ha (bu./ac)
Okoboji Soil Type				
12.2 (40)	11.8 (188)	7.08 (112.8)	11.67 (185.9)	4.59 (73.1)
18.3 (60)	11.8 (188)	7.08 (112.8)	11.68 (186.1)	4.60 (73.3)
24.4 (80)	11.8 (188)	7.08 (112.8)	11.56 (184.2)	4.48 (71.4)
Canisteo Soil Type				
12.2 (40)	14.06 (224)	9.84 (156.8)	13.92 (221.8)	4.08 (65.0)
18.3 (60)	14.06 (224)	9.84 (156.8)	13.89 (221.3)	4.04 (64.5)
24.4 (80)	14.06 (224)	9.84 (156.8)	13.77 (219.5)	3.93 (62.7)
Conversion: 1 bushel corn grain = 56 lb				

3.2 Drainage System Design

Total number of laterals and their total length, based on the subsurface drainage system as shown in Fig. 1, were calculated for the three different spacings and are shown in Table 2. Narrower spacings had more laterals, and therefore, more total length.

Table 2. Number of laterals and total lateral length for both soil types at three different drain line spacings.

Drain Line Spacing meters (feet)	Number of Laterals	Total Lateral Length meters (feet)
12.2 (40)	65	26,152 (85,800)
18.3 (60)	43	17,038 (55,900)
24.4 (80)	32	12,680 (41,600)

The diameter of the laterals (size) was determined to be 10.2 cm (4 inches) as this was the smallest size available in the market. Using Hooghoudt equation [5], the drainage coefficient was determined for both soil types and the three drainage spacings. The size of the main line was then determined to ensure main line had enough capacity to handle the flow rate. As the number of laterals in the upper part of the field were fewer, the upper main size was determined as a smaller diameter line. This size increased for the lower main line as the flow accumulated and thus a larger diameter was needed to handle the accumulated flow. The lower main line, upper main line, and lateral sizes (diameters) are shown below in Table 3.

Table 3. Lower main line, upper main line, and lateral sizes (diameters) for two different soil types at three different drain line spacings.

Drain Line Spacing meters (feet)	Lower Main Size cm (inches)	Upper Main Size cm (inches)	Lateral Size cm (inches)
Okoboji Soil Type			
12.2 (40)	15.2 (6)	10.2 (4)	10.2 (4)
18.3 (60)	10.2 (4)	10.2 (4)	10.2 (4)
24.4 (80)	10.2 (4)	10.2 (4)	10.2 (4)
Canisteo Soil Type			
12.2 (40)	25.4 (10)	20.3 (8)	10.2 (4)
18.3 (60)	20.3 (8)	15.2 (6)	10.2 (4)
24.4 (80)	15.2 (6)	(6)	10.2 (4)

3.3 Drainage System Costs

Installed drain line costs per meter, as determined from the survey, are listed in Table 4. The installed drain line costs increased as the drain line size (diameter) increased, however, this increase was not proportional to the drain line material cost for the respective sizes. As such, an installation cost factor was determined and is shown in Table 4. Installation cost factor was higher for smaller diameter drain lines than the larger drain lines, and its value decreased with increase in diameter. It should be noted that drain line material costs and installed costs are variable and change over time due to changes in labor, fuel, raw material costs, transportation, etc. Secondly, these surveyed costs are a sample of a subset of installers and drain line manufacturers.

Table 4. Average costs for drain lines as installed, drain line material cost, and installation factors for the different drain line sizes (diameter).

Drain Line Size cm (inches)	Installed Cost $/m ($/ft.)	Material Cost $/m ($/ft.)	Installation Factor
10.2 (4)	3.15 (0.96)	1.31 (0.40)	2.4
15.2 (6)	7.58 (2.31)	3.44 (1.05)	2.2
20.3 (8)	12.27 (3.74)	5.58 (1.70)	2.2
25.4 (10)	21.65 (6.60)	10.83 (3.30)	2
30.5 (12)	27.89 (8.50)	13.94 (4.25)	2
38.1 (15)	36.09 (11.00)	18.04(5.50)	2

3.4 Rate of Return (ROR) Analysis

Table 5 shows the Rate of Return (ROR) and the expected number of years to payback period for the investment amount spent of subsurface drainage system. For Canisteo soil type, the rate of return decreased, and payback period increased as the drain line spacing decreased from 24.4 m (80 feet) to 12.2 m (40 feet) for the three respective corn grain market prices used in the analysis. For the Okoboji soil type, this was true for the low corn grain market price. For the medium corn grain price, the rate of return and payback periods were similar. For the high corn grain price, the 18.3 m drain line spacing had the highest calculated rate of return and the lowest payback period amongst the three spacings.

Table 5. Rate of Return and Payback Period for three different corn grain prices, three different drain line spacings for the two soil types.

Drain Line Spacing m (feet)	Rate of Return percent	Pay Back Period years	Rate of Return percent	Pay Back Period years
	Okoboji Soil Type		Canisteo Soil Type	
Low Corn Grain Price ($137.80 / MT or $3.50 / bushel)				
12.2 (40)	16.1	7	20.5	5
18.3 (60)	24.5	5	30.3	4
24.4 (80)	31.8	4	34.4	3
Medium Corn Grain Price ($177.17 / MT or $4.50 / bushel)				
12.2 (40)	21.6	5	27.3	4
18.3 (60)	32.9	4	40.4	3
24.4 (80)	42.7	3	41.1	3
High Corn Grain Price ($216.54 / MT or $5.50 / bushel)				
12.2 (40)	27.1	4	34.2	3
18.3 (60)	41.3	3	50.6	2
24.4 (80)	53.6	2	47.8	3

4 Discussion and Conclusions

Yield improvements achieved with subsurface drainage have a significant impact of the profitability of a farming operation when compared with undrained conditions. In this analysis, the field layout was assumed to be a uniform soil type which is seldom the case. Typically, farm fields consist of several soil types and, thus, the yield improvements on a whole farm basis will not be as high as noted in this analysis. It will depend upon the weighted average of the area a particular soil type within a farm field and its respective yield improvement. Overall, the analysis showed an improvement in corn yields with subsurface drainage.

Drainage design used in this analysis is a parallel lateral design whereas in actual field conditions, a design may consist of a system which is herringbone, double main, or random. As such, the costs of drain line system will be different from what is presented in this analysis. Moreover, the cost of the drainage system can vary significantly on the size of the project. Typically, smaller projects (fewer hectares) cost more than larger projects which can also lead to differentiation in the economic analysis.

For Canisteo soil type, the analysis showed an increased rate of return with quicker payback as the drain line spacing was reduced from 24.4 m (80 feet) to 12.2 m (40 feet) for all three corn grain market prices. This was not the case for Okoboji soil type indicating that the spacing impacts payback period under different corn grain market prices.

References

1. USDA-NASS (2019). The 2017 Census of Agriculture for Iowa. U.S. Department of Agriculture's National Agricultural Statistics Service (NASS). USDA-NASS Report AC-17-A-15. Issued April 2019. USDA-NASS, Washington, D.C. https://www.nass.usda.gov/Publications/AgCensus/2017/Full_Report/Volume_1,_Chapter_1_State_Level/Iowa/iav1.pdf. Viewed: September 25, 2023

2. DRAINMOD (2013) Version 6.1 Build 105. NC State Agricultural Water Management, North Carolina State University, Raleigh, NC 27695 USA. Available online at https://www.bae.ncsu.edu/agricultural-water-management/drainmod/download/. Viewed: September 25, 2023

3. Drain Spacing Tool (2022). Extension Bulletin E3450. Michigan State University Extension, 446 W. Circle Drive, Room 409 Agriculture Hall, East Lansing, MI 48824 USA. https://www.canr.msu.edu/field_crops/uploads/files/E3450_Drain_Spacing_Tool_Rev.pdf. Viewed: September 25, 2023

4. Web Soil Survey (2019). Natural Resources Conservation Service, United States Department of Agriculture. https://websoilsurvey.nrcs.usda.gov/app/. Viewed: September 25, 2023

5. Hooghoudt SB (1940) (in Dutch) Algemene beschouwing van het probleem van de detailontwatering en de infiltratie door middel vanparallel loopende drains, greppels, slooten en kanalen. No. 7 in de serie: Bijdragen tot de kennis van eenige natuurkundigegrootheden van den grond. Bodemkundig Instituut te Groningen. Rijksuitgeverij Dienst van de Nderlandse Staatscourant. 's-Gravenhage, Algemeene Landsdrukkerij

6. ASABE (2019). Design and construction of subsurface drainage systems on agricultural lands in humid areas. ASABE Design Standard ASAE EP260.5. Released February 205, Reaffirmed November 2019. American Society of Agricultural and Biological Engineers. 2950 Niles Road, St. Joseph, Ml 49085–9659, USA. https://elibrary.asabe.org/abstract.asp?aid=45405&t=3&redir=aid=45405&redir=%5bconfid=s2000%5d&redirType=standards.asp&redirType=standards.asp. Viewed: September 25, 2023

7. ISPAID (2017) Iowa Soils Properties and Interpretations Database. Version 8.1.1. Iowa State University Extension and Outreach, Ames, IA 50011, USA. https://www.agron.iastate.edu/glsi/teaching/soil-and-land-use/soil-survey-digital-soil-data-ispaid/. Viewed: September 25, 2023

8. Ag Decision Maker (2023) Understanding the Economics of Tile Drainage – C2–90. Iowa State University Extension and Outreach, Ames, IA 50011, USA. https://www.extension.iastate.edu/agdm/wholefarm/html/c2-90.html. Viewed: September 25, 2023

Author Index